Frequency- and time-domain constrained control of linear systems Application to a flexible launch vehicle

Emmanuel Chambon

THÈSE

En vue de l'obtention du

DOCTORAT DE L'UNIVERSITÉ DE TOULOUSE

Délivré par : *l'Institut Supérieur de l'Aéronautique et de l'Espace (ISAE)*

Présentée et soutenue le *mardi 29 novembre 2016* **par :**

EMMANUEL CHAMBON

Frequency- and time-domain constrained control of linear systems
Application to a flexible launch vehicle

JURY

M. TURNER	Professor	University of Leicester	Rapporteur
M. ZASADZINSKI	Professeur	Université de Lorraine	Rapporteur
M. GANET	Ingénieure	Airbus Safran Launchers	Examinatrice
L. ZACCARIAN	Directeur de recherche	LAAS-CNRS	Examinateur
A. ZOLGHADRI	Professeur	Université de Bordeaux	Examinateur
P. APKARIAN	Directeur de recherche	Onera	Directeur de thèse
L. BURLION	Ingénieur de recherche	Onera	Directeur de thèse

École doctorale et spécialité :
EDSYS : Automatique 4200046

Unité de Recherche :
ONERA - The French Aerospace Lab
Centre de Toulouse
Département de Commande des Systèmes et Dynamique du Vol

Directeurs de Thèse :
Pierre APKARIAN (directeur de thèse)
Laurent BURLION (co-directeur de thèse)

To my family.

Acknowledgements

When reading a thesis manuscript, one could pretend to appreciate the work of a single person only. This is rarely – if ever – the case. This memoir is the result of personal work backed up by the knowledge and involvement of my advisors as well as by shared experiences.

First and foremost, I wish to thank you, Laurent and Pierre, for your active support, patience and availability. You have never failed to answer my questions – even the most incoherent ones. I hope to maintain contact with you in the future.

I would also like to thank Pr. Matthew Turner and Pr. Michel Zasadzinski for accepting to review this thesis manuscript. I appreciated their kind and interesting comments. Such discussion always helps to step back and appreciate the results as well as possible extensions or links with existing theories. Many thanks also go to Pr. Ali Zolghadri who accepted to preside the defence committee as well as to the remaining members of this committee, Martine Ganet and Dr. Luca Zaccarian, for the interesting questions session.

A PhD thesis is also about sharing experiences: Adrien, thanks for the involving political discussions, at the coffee breaks, after watching an engaged author film or at the restaurant. May these discussions always guide us in our citizen choices; Mathieu, it was a pleasure to share breaks and cycle along with you in our "unofficial" cycling club, as well as with Mathieu, Charles, Anthony, Claude, Xavier; Patrick, when is the next board game party? Sergio and Anne, thank you for the "franco-italian film" nights. *Arrivederci*! Élodie, that was a pleasure to share the office with you (see you at ASL!!). Jérémy (for the technical advice also), Alvaro, Matteo, Adèle, Mario, Marine, Lylia, Igor, Martin, Victor, Cédric, Pierre, Xavier, "the two Charles", Stéphanie, Guillaume, thanks for the joyful coffee breaks and after-works. And I almost certainly forget other PhD team-mates: Simon, Henri, Nicolas, Jean-Philippe, Yann ... Good luck to the new candidates: Pauline, Mehdi, Vincent, ... I also wish better health along with great success to Guillaume who deserves it more than any of us: I imagine few of us could endure the pain. Thank you for all the happy moments!

I wish also to thank the whole "Département de Commande des Systèmes et de Dynamique du Vol" staff, especially Catherine, Christelle and Valérie for their dedication to the PhD students. Not the least, I wish to thank Henry for supervising my master's thesis with Laurent and helping me realise there is never "no result at all", Fabrice for his help on IQCs (sorry for the lack of related results!!), Jean-Marc and Clément for their help with the SMAC Toolbox and Alexandre for the shared coffee breaks and up-to-date information on football matches results!! My thanks are also directed to *Onera* for the financial support.

Last but infinitely far from least, I wish to express my gratitude to my parents for their unquestioning support, at all times. I will always keep in mind the chance I had to grow and study in such stable, protective yet tolerant atmosphere. Maman, Papa, you are the footprints on the ground I shall try to follow. That being said, I cannot help but think of Mamie and Papy who never doubted of any of us. Your memory rests in my heart. Also, I wish to thank my sister and my close family for their support and their repeated efforts to improve my self-confidence, cooking and gardening skills.

Emmanuel

Résumé

Dans la plupart des applications actuelles, le cahier des charges pour la synthèse d'une loi de commande est un amalgame de contraintes fréquentielles et temporelles. Par exemple, la prise en compte de contraintes sur les fonctions de sensibilité s'accompagne souvent de contraintes temporelles sur les sorties qui doivent rester dans un intervalle prescrit au cours de l'évolution du système.

La synthèse d'une loi de commande satisfaisant aux contraintes fréquentielles est possible en utilisant les techniques de synthèse H_∞. Ces techniques reposent sur la détermination d'une solution optimale au problème de minimisation des normes H_∞ des fonctions de transfert de synthèse considérées. Les paramètres du contrôleur structuré considéré sont alors les variables de décision du problème. Des développements récents de ces méthodes de synthèse permettent désormais de formaliser des contraintes fréquentielles multiples et de natures variées sur des modèles de synthèse multiples. Un exemple d'application de cette nouvelle méthode est la détermination d'une loi de contrôle robuste stabilisant des configurations ou points de fonctionnements multiples.

En revanche, la formalisation de contraintes temporelles comme un ensemble de contraintes fréquentielles est complexe et requiert un réglage fastidieux de paramètres. Les contraintes fréquentielles qui en résultent peuvent par ailleurs entrer en conflit avec d'autres contraintes préexistantes et rendre le problème de synthèse plus complexe. L'exemple considéré de contrainte temporelle est l'appartenance d'une variable de sortie à un intervalle donné. Une approche possible pour prendre en compte simultanément des contraintes temporelles et fréquentielles est de synthétiser un contrôleur dit *nominal* satisfaisant seulement les contraintes fréquentielles. La sortie du contrôleur est ensuite modifiée de manière appropriée via une méthode dédiée dès que la contrainte temporelle n'est pas satisfaite. Ces techniques d'adaptation de la sortie du contrôleur sont regroupées sous le terme d'"approches évolutionnaires" dans une frange de la littérature dédiée au contrôle sous contraintes. Elles offrent une solution viable en pratique au problème du contrôle sous contraintes fréquentielles et temporelles mais n'offrent en principe pas de garantie sur la satisfaction de la contrainte temporelle et peuvent déstabiliser la boucle fermée si des précautions ne sont pas prises. D'autre part, la performance est souvent dégradée.

L'approche OIST (*Output to Input Saturations Transformation*) est l'une de ces "approches évolutionnaires". Elle a été proposée dans le but de garantir qu'une variable de sortie reste dans un intervalle prescrit au cours de l'évolution du système considéré. Son principe repose sur la transformation de la contrainte de sortie en saturations sur l'entrée de manière à contraindre l'évolution de la sortie contrainte sans trop impacter la performance du système. Cette méthode a été initialement proposée pour les systèmes non-linéaires. Elle ne peut cependant pas être appliquée sous sa forme actuelle aux systèmes incertains, aux systèmes dont l'état n'est pas entièrement mesuré et/ou ayant des sorties à non-minimum de phase à contraindre.

Ce travail de thèse propose une formulation de la méthode OIST dans le cas linéaire. Des résultats sont établis concernant le choix des paramètres de la méthode afin de garantir l'absence de chevauchement des bornes de la saturation. La satisfaction de la contrainte de sortie est ainsi garantie en cas d'application de la méthode. Dans le cas des systèmes à minimum de phase, la stabilité asymptotique de l'origine est démontrée en utilisant un compensateur anti-windup additionnel. Des résultats intéressants en terme de performance sont observés lors de l'utilisation d'un tel compensateur. La méthode est ensuite étendue pour prendre en compte la présence d'incertitudes et la méconnaissance de certains états. La satisfaction d'une contrainte sur une sortie en utilisant la méthode OIST alors que le vecteur d'état est mesuré seulement en partie nécessite de connaître des bornes garanties sur le vecteur d'état à chaque instant. Dans cette optique, la théorie des observateurs par intervalles est étudiée et utilisée dans ce travail.

En tant que problème annexe, une nouvelle approche est proposée pour la construction

d'observateurs par intervalles. Une approche par optimisation non-lisse directement inspirée du problème de synthèse de contrôleurs structurés est proposée afin de déterminer le changement de coordonnées invariant adéquat pour que la dynamique du système considéré soit coopérative dans les nouvelles coordonnées. Les résultats numériques obtenus sont comparés en simulation aux méthodes existantes.

Pour finir, les méthodes développées au cours de ce travail sont appliquées au contrôle atmosphérique d'un modèle simplifié de lanceur flexible. La variable contrainte dans ce problème est l'incidence du lanceur qui doit rester minimale afin de limiter les forces aérodynamiques et une possible destruction de la structure du lanceur. Ce problème s'avère être compliqué par la présence de rafales de vent qui est une entrée inconnue du système.

Mots-clés: contrôle sous contraintes de sortie, systèmes linéaires, systèmes incertains, observateur par intervalles, synthèse de contrôleur structuré

Abstract

In many real world applications, specifications related to the control design are a mixture of frequency- and time-domain requirements. For example, in addition to usual sensitivity-related constraints, it may be expected that output signals belong to prescribed intervals.

As far as frequency-domain constraints are concerned, solutions to the control design problem under this type of constraints can be obtained using H_∞-based techniques. These techniques rely on the minimization of the H_∞-norm of appropriately defined and weighted transfer functions in which the controller is a design parameter. Recent advances in this field of research allow the design of structured controllers such that multiple frequency-domain requirements are met for multiple models. This can for example be used to tackle problems where a single controller has to stabilize multiple working points or configurations.

However, time-domain constraints like admissible operating sets on a given state or output variable are difficult to formalize as frequency-domain constraints. This requires trial-and-error fine tuning design constraints through weightings selection which is a tricky task in most cases. Also, constraints conflicting with pure frequency-domain constraints may arise from such reformulation. Consequently, some output-constrained control approaches propose to neglect these time-domain constraints when designing the *nominal* controller. Then, the controller output is modified whenever the constraint is violated using an additional appropriately defined structure. These are called *evolutionary* strategies in the related literature. These techniques offer a viable solution to the output-constrained control design problem but often lack guarantees on the actual satisfaction of the constraint or even of the resulting closed-loop stability. Also, performance may be degraded.

The *Output to Input Transformation* (OIST) approach counts amongst these *evolutionary* techniques. It was proposed to enforce a time-domain constraint of the admissible operating set type on a single output variable. Using an appropriate transformation, saturations on the control input are formalized such that the considered output variable belongs to the expected operating interval. It was originally proposed for non-linear systems. However, in its current form, this approach cannot be applied to uncertain systems, to systems with incomplete state measurements or with non-minimum phase constrained outputs.

In this thesis, a reformulation of OIST in the linear framework is proposed. Results concerning the method design coefficients are obtained to guarantee satisfaction of the time-domain constraint. In the minimum phase case, guarantees on the global asymptotic stability of the closed-loop in the presence of the obtained control saturations are obtained using an anti-windup compensator. Next, extensions to the incomplete state measurements and uncertain cases are proposed. Enforcing an output constraint through the OIST technique when the full state is unmeasured is possible provided that each component of the state vector lies in a known interval at each time. Therefore, interval observers are studied and used here.

A new approach to the design of interval observers is also proposed as a side problem. A non-smooth optimization technique inspired by the structured controller synthesis problem is used to find a time-invariant state-coordinate transform such that the considered system is cooperative in the new coordinates. This is a key step in designing interval observers.

Finally, an application to the atmospheric flight control of a simplified flexible launch vehicle model is presented. The angle of attack of the launch vehicle is constrained to stay in a prescribed interval to avoid structural overload and potential damages. This proves to be a very challenging problem when extreme wind conditions are taken into consideration.

Keywords: output-constrained control, linear systems, uncertain systems, interval observer, structured controller design

Notations

blkdiag	Block-diagonal matrix of the considered matrices
diag	Diagonal matrix of the considered real parameters
dim	Dimension operator, e.g. $\dim(\mathbb{R}^n) = n$
d	Differential operator
eig	Vector of the eigenvalues of the considered matrix
$\mathcal{F}_l/\mathcal{F}_u$	Lower/Upper LFT
$\|\bullet\|_2$	H_2-norm
$\|\bullet\|_\infty$	H_∞-norm
$\mathbf{I}_n$	Identity matrix of size n
j	Imaginary unit
ker	Kernel operator, e.g. for $\mathbf{A} \in \mathbb{R}^n$ then $\ker(\mathbf{A}) = \{\boldsymbol{v} \in \mathbb{R}^n \text{ s.t. } \mathbf{A}\boldsymbol{v} = \mathbf{0}_n\}$
$\mathcal{L}_{\boldsymbol{f}}\sigma$	Lie derivative of σ in the direction of $\boldsymbol{f}$
rank	Rank of the considered matrix
s	Laplace transform variable
$\mathbf{A}$	Matrix notation
$\mathbf{A}^{-1}$	Matrix inverse (if it exists)
$\mathbf{A}^\top$	Matrix transpose
$\mathbf{A}_{m\times n}$	Matrix of $\mathbb{R}_{m\times n}$
$\mathbf{A}_{ij}$	Matrix $\mathbf{A} \in \mathbb{R}^{m\times n}$ element at row i and column j
$\mathbf{A}^+$	$\max(\mathbf{A}, \mathbf{0})$
$\mathbf{A}^-$	$\mathbf{A}^+ - \mathbf{A}$
$\mathbf{0}_{m\times n}$	Null matrix of size m by n
∂_i	Partial derivative operator with respect to the i-th element
Re	Real part of the considered complex number
$\mathcal{I}(\mathbb{R})$	Set of intervals of $\mathbb{R}$
$\mathbb{R}$	Set of real numbers
$\mathbb{R}^n$	Set of real vectors with dimension n
$\mathbb{R}^{m\times n}$	Set of real matrices with dimensions $m \times n$
$\mathbb{R}_+$	Set of positive real numbers
$\mathbb{R}_-$	Set of negative real numbers
$\mathbb{R}^\star$	Set of non-null real numbers
$\mathbb{Z}$	Set of integers
$\mathbb{Z}_+ = \mathbb{N}$	$\mathbb{Z} \cap \mathbb{R}_+$ (natural integers)
$(\mathbf{G})$	System notation
$\mathbf{T}_{\boldsymbol{u}\to\boldsymbol{y}}(s)$	Transfer function from input $\boldsymbol{u}$ to output $\boldsymbol{y}$ (MIMO)
$T^\star(s)$	Adjoint operator of SISO transfer function $T(s)$
z	Z-transform variable
$\boldsymbol{x}$	Vector notation

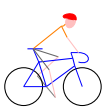

Acronyms

GES	Global Exponential Stability
GUAS	Global Uniform Asymptotic Stability
IPR	Internally Positive Representation
ISS	Input-to-State Stable
IQC	Integral Quadratic Constraints
LFR	Linear Fractional Representation
LFT	Linear Fractional Transformation
LMI	Linear Matrix Inequalities
LPV	Linear Parameter-Varying
LTI	Linear Time-Invariant
LTV	Linear Time-Varying
MPC	Model Predictive Control
MRAW	Model Recovery Anti-Windup
ODE	Ordinary Differential Equation
OIST	Output to Input Saturation Transformation
OISTeR	OIST extension for Robustness
SCT	State-Coordinate Transformation
SCorpIO	State-Coordinate transformation Optimisation for Interval Observers
SMAC	Systems Modeling, Analysis and Control

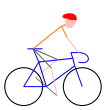

Legend

To improve the readability of this manuscript – which contains cumbersome equations in some of its chapters – icons are used to highlight the most important notions. While reading these parts only, it is possible to grasp the main contributions of this work. The icons are described below along with their intended meaning.

This is an important notion or result. Reading this statement is mandatory to understand the considered problem.

This is a key notion or result. Reading this statement is mandatory to understand the contributions.

This is a contribution of this thesis.

Contents

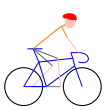

List of Publications

Journals & Books Chapters

[1] E. Chambon, P. Apkarian, and L. Burlion. Flexible launch vehicle control using robust observer-based controller obtained through structured H_∞ synthesis. In J. Bordeneuve-Guibé, C. Roos, and A. Drouin, editors, *Advances in Aerospace Guidance, Navigation and Control*, pages 23–38. Springer, Toulouse, France, 2015.

[2] E. Chambon, L. Burlion, and P. Apkarian. Détermination de matrice semblable Metzler par optimisation non lisse. *Journal Européen des Systèmes Automatisés (special issue)*. Accepted, to appear in 2017.

[3] E. Chambon, L. Burlion, and P. Apkarian. Time-response shaping using output to input saturation transformation. *International Journal of Control*. Accepted, under revision.

[4] E. Chambon, L. Burlion, and P. Apkarian. Overview of linear time-invariant interval observer design: towards a non-smooth optimisation-based approach. *IET Control Theory and Applications*, 10(11):1258–1268, July 2016.

International conferences with review committee

[1] E. Chambon, P. Apkarian, and L. Burlion. Metzler matrix transform determination using a non-smooth optimization technique with an application to interval observers. In *Proc. of the SIAM Conference on Control and its Applications*, pages 205–211, Paris, France, July 2015.

[2] E. Chambon, L. Burlion, and P. Apkarian. Output to input saturation transformation: demonstration and application to disturbed linear systems. In *Proc. of the 54th IEEE Conference on Decision and Control*, pages 7566–7571, Osaka, Japan, December 2015.

[3] E. Chambon, L. Burlion, and P. Apkarian. Robust output interval constraint using O/I saturation transformation with application to uncertain linear launch vehicle. In *Proc. of the 14th European Control Conference*, pages 1796–1801, Linz, Austria, July 2015.

National conferences

[1] E. Chambon, P. Apkarian, and L. Burlion. Détermination de matrice semblable Metzler par optimisation non lisse. In *Proc. of the 6th Journées Doctorales / Journées Nationales MACS, Bourges (France). Pre-selected for extended version submission in Journal Européen des Systèmes Automatisés (special issue)*, Bourges, France, June 2015.

[2] E. Chambon, L. Burlion, and P. Apkarian. Output– to input–saturation transformation: Application to a class of linear systems. In *Proc. of the 16th Congrès de l'Ecole Doctorale Systèmes*, Toulouse, France, May 2015.

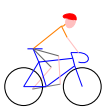

Part I

Introduction

Chapter 1

Constrained control of linear systems

This is the introductory chapter of this thesis work. The main problems considered in this manuscript are introduced. They are concerned with the atmospheric control of an uncertain flexible launch vehicle. More specifically, the difficulty comes from the time-domain constraint on the angle of attack which should remain below a critical value so as to ensure nominal performance of the launch vehicle. Also, specifications require that frequency-domain properties are satisfied for example on the closed-loop margins or flexible modes attenuation. Hence, the atmospheric control of the launch vehicle is a mixed frequency/time-domain constrained control problem. This type of problem is frequently met when designing a control law for any given linear system under time-domain constraints which motivates the proposition of generic results. A state of the art of the different fields of research involved is proposed and the major contributions of this thesis are introduced.

This chapter is organized in the following manner. First, a general introduction to the considered problem is proposed in 1.1. Then, a state of the art of the different problems involved is given in 1.2. The contributions of this thesis work are listed in 1.3 before detailing the manuscript outline in 1.4.

1.1 General introduction

Control systems have become a must in most applications with the increased complexity of processes and devices. For example, in spite of their own physiological complexity, using the human brains, nerves and muscles to guide a launch vehicle at hypersonic speed on the right trajectory is fanciful. This is however largely within the reach of an on-board computer controlling well-designed actuators. The design of control systems is a complex task. The objective of such system is to force the behaviour of the controlled process to behave in a nominal fashion. For example, it is expected that the barges represented in Fig. 1.4 do not collide with the waterway banks. This requires a precise modelling of the considered system and the formulation of clear specifications to be satisfied by the obtained closed-loop. As such, control design problems are most of the time dealing with constraints either in the frequency- or time-domain.

Frequency-domain constraints arise whenever a frequency-domain representation of the system is possible. This is the case when linear modelling of the system is obtained by linearising the "true" non-linear dynamics at a given working point. In the launch vehicle case, this corresponds to linearising the non-linear dynamics over a short period of time during which the mass and speed of the launch vehicle can be considered constant. Nonetheless, to account for the lack of measurements on these speed and mass parameters, a specific parameter-dependent modelling can be used to represent various situations which may arise at a given instant of the flight. Frequency-domain constraints are used whenever the control system should enforce specific frequency-domain properties such as closed-loop margins or closed-loop poles location. Of course, the designed control law should comply with the frequency-domain constraints for all possible values of the model parameters.

Time-domain constraints are generally an easier notion to grasp since they are directly related to simulation or experimentation depending on the development status of the system. Examples of time-domain constraints are plentiful, even in our very own life experience: for the ball and beam system, the constraint is to keep the ball on the beam; for your own bank account, the constraint is to never hit overdraft to avoid extra charges. According to Fig. 1.1, I seem to do it quite well or I do not seem to be in much of a caring or sparing mood over the considered period of time. From a control design point of view, time-domain constraints are however generally hard to satisfy since they directly depend on simulation results hence on the simulation parameters, most notably the considered class of disturbance inputs signals. In other words: different techniques than the ones used to enforce frequency-domain requirements are required and they highly depend on the designer choices: which signals are used in simulation, which ODE solver, etc.

As the title of this thesis suggests, we are concerned with control design problems subject to both types of constraints. Since the approaches dealing with each type of constraints are different, this requires some study to appropriately select each method and see how they can interact to enforce the considered constraints. An appropriate strategy to deal with mixed frequency-/time-domain constrained control design problems is first to design a controller which satisfies the frequency-domain requirements and then to modulate the resulting control input whenever the time-domain constraints are not met. This is the so-called *evolutionary* strategy [Goodwin 01] chosen in this work. More details on existing strategies are given in Chapter 3. In the following paragraphs, we introduce various realistic examples of constrained control to further detail the problematic.

Atmospheric control of a flexible launch vehicle The atmospheric control of a launch vehicle such as Ariane 5 (see Fig. 1.2) is quite a challenge. During the ascent, the structure of the launcher is exposed to an important aerodynamic stress culminating at the point of maximum dynamic pressure which occurs a few seconds after launch. This stress can be destructive or at least degrade the launcher performance in terms of trajectory. The amount of structural stress depends on the angle of attack which is the angle of the launch vehicle with respect to the incoming air flow. The angle of attack itself is possibly disturbed by wind gusts which are mostly unpredictable and which amplitude is not known with precision.

Moreover, due to its size and to the used materials (aluminium and composite), the launch vehicle structure is excited in the same way as a guitar string. More precisely, this results in the presence of flexible modes at rather low frequencies which act as disturbances on the output

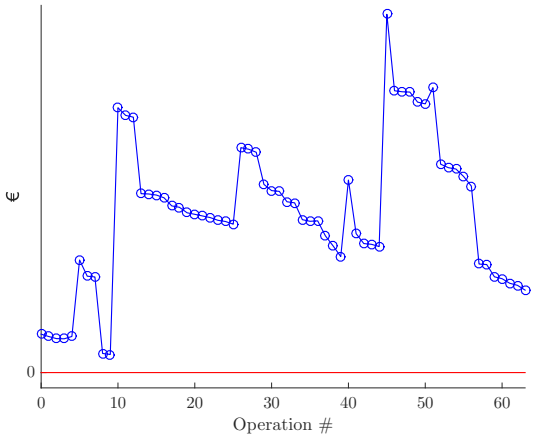

Figure 1.1: Balance of my bank account over 63 operations. Almost amplitude-constant cyclic events appear (salary and rent) and overdraft is nearly hit once. I do not seem to be currently in a sparing mood or I am perhaps expecting short-term expenses.

Figure 1.2: Ariane 5 launch vehicle before launch (left) and just after engines ignition (right). – *Credits*: DLR/Thilo Kranz (CC-BY 3.0) 2013.

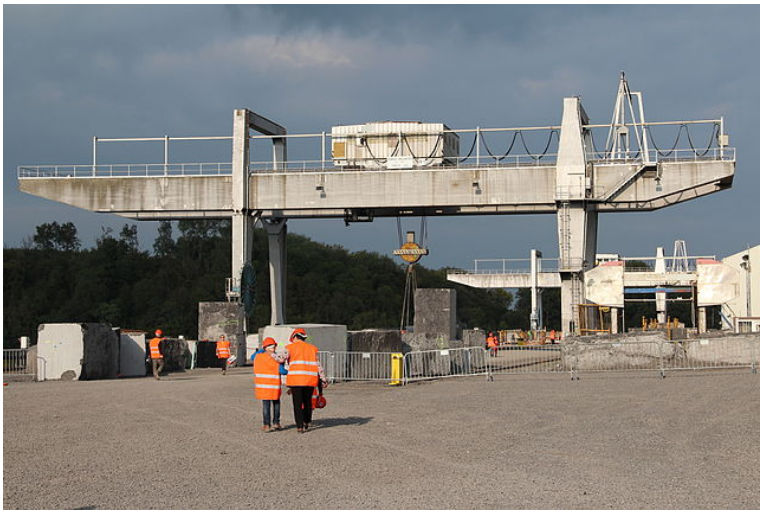

Figure 1.3: Example of an overhead crane in a quarry in Belgium. – *Credits*: Jean-Pol Grandmont (CC-BY 3.0) 2013.

measurements and can in turn be fed and excited by the control law if the designer is not careful. This results in a series of frequency-domain flexible modes roll-off specifications which add to the expected closed-loop stability and other requirements dealing for example with the sloshing of ergols. The time-domain constraint is obvious: since the aerodynamic stress on the structures is directly linked to the angle of attack, a maximal admissible value $\overline{\alpha}$ is set on the angle of attack α which should satisfy:

$$-\overline{\alpha}(t) \leq \alpha(t) \leq \overline{\alpha}(t), \forall t \in \mathbb{R}_+ \tag{1.1}$$

at all instants. Uncertainties are also introduced in the modelling to account for the difficulty to evaluate the mass as well as the aerodynamic and thrust performances of the launch vehicle. Also, the flexible modes dynamics are not exactly known and are approximated by uncertain 2-D systems for each flexible mode.

The designed controller should comply with the frequency- and time-domain constraints for all values of the uncertain parameters or at least for critical values of these parameters. This is covered in Chapters 2 and 6. Specifically, a robust controller is designed using an H_∞-based technique and its output is modulated through application of the extended OIST/OISTeR approach (see [Burlion 12] and Chapters 4 and 5). This results in both types of constraints being satisfied. Due to the complexity of the problem and the novelty of some of the involved approaches, simplified models of the launch vehicle are however used in this work.

Swaying mitigation strategy for overhead cranes Overhead cranes are commonly used whenever massive loads must be displaced by translation between two distant points. They are often used to unload/load containers in ports or sometimes in quarries as illustrated in Fig. 1.3. They can be composed of very high structures under which the load is suspended. Also, they may reach high speeds to minimize load or unload times so as to increase the rate of ships of reduce the docking fees for the shipowners. This can result in dangerous swaying or falling of the load transported under the overhead crane.

The objective is to displace a load from a point A to a point B. An appropriate tracking controller should comply with both frequency- and time-domain constraints. Frequency-domain constraints are formulated to attenuate the cable flexibilities which can be excited by the controller. Time-domain constraints are concerned with improving the tracking precision and speed or to ensure that the maximum swaying angle remains below a given value such that collisions are avoided especially during the phases of acceleration or deceleration.

A non-linear model of an overhead crane system is used in Chapter 3, 3.4 to illustrate the OIST approach in the non-linear case. In this example, the time-domain constraint is specified

Figure 1.4: Barges in tight waterways. – *Credits*: Pline (CC-BY 3.0) 2010[2] and F. Lamiot (CC BY 3.0) 2010.

on the angle between the load and the vertical axis and OIST is used to enforce the constraint.

Automated barge control Waterways have been used for centuries to move huge charges over long distances. The network is quite dense in Europe especially along rivers or even along completely artificial waterways such as the *Canal du Midi* in the South-West of France. The development of automated barges could be an interesting project to give a new birth to this decaying means of transportation which probably requires a reduced amount of fossil fuels in comparison with dozens of trucks. Within our introductory work however, this example is used to further illustrate the constrained control problem in a very meaningful manner.

In this case of application, the control problem is quite clear: the objective is to follow the banks of the river and eventually avoid collision with incoming barges. The first part of the objective is a typical time-domain constrained control problem: the part of the barge closest to one bank should never touch that bank! This is probably a more difficult problem than expected due to the inertia of such massive boats especially when loaded. Considering this system allows a physical interpretation of the OIST approach introduced in [Burlion 12], recalled in Chapter 3 and improved/extended in Chapters 4 and 5. Supposing that the barge can be reduced to a single point and that the existing controller proves to be efficient in terms of tracking performance but fails to enforce the time-domain constraint[3], the OIST approach consists in saturating the ship rudder angle such that the time-domain constraint is enforced[4] and the nominal tracking performance is not degraded much.

1.2 State of the art

First, a state of the art of the atmospheric control of a flexible launch vehicle is proposed. Then, reference is made to the chapters where the resources related to the involved theories are presented.

1.2.1 Atmospheric control of a flexible launch vehicle

Due to the complexity of the atmospheric control of launch vehicles, a rich literature is available on the subject. Most articles are concerned with robust control due to the presence of uncertainties in the modelling dynamics. As already mentioned in the general introduction, the complexity of the problem also depends on the presence of flexible modes which are likely to be excited by an ill-dimensioned control law.

[2] https://commons.wikimedia.org/w/index.php?curid=10981465
[3] In other words: the barge hits the bank.
[4] In other words: the barge does not hit the bank.

In [Knoblauch 12], H_∞-based synthesis is used in parallel with tuned elliptic filters to obtain a controller which satisfies the flexible modes roll-off requirement. The use of elliptic filters allows to filter the flexible modes dynamics on sufficiently large frequency intervals to account for the presence of uncertainties in those dynamics. This requires a good practical knowledge of the launch vehicle model as well as on elliptic filters. The authors in [Dubanchet 12] use guardian maps to analyse closed-loop stability and determine a set of admissible control gains such that the closed-loop dynamics satisfies to the prescribed requirements. The normalized co-prime factorization approach combined with LQG/LTR additions is exploited in [Abbas-Turki 07] to design a gain-scheduled controller for a time-varying model of the launch vehicle. In [Ganet 10], the design of the controller is performed using an LPV methodology with an illustration on an industrial benchmark of the flexible launch vehicle. Design techniques involving H_∞ criteria have been explored in various articles including [Alazard 03, Voinot 03b] and [Scorletti 10]. Robustness analysis – which can be useful to determine critical values of the uncertain parameters vector $\boldsymbol{\theta}$ – using μ-analysis techniques has been studied in [Imbert 01] and μ-synthesis in [Imbert 01].

1.2.2 Theoretical resources

As far as the control theories involved in this work are concerned, it has been chosen to present the related states of the art in the relevant chapters. Those are listed here for reference.

- *Output constrained control*: this is a major subject in this thesis work. A study of existing techniques is proposed in 3.2.2, Chapter 3. Especially, the differentiation between *cautious*, *evolutionary* and *tactical* strategies is documented and explained;
- *Interval observers*: the relevant resources are presented in details in B.2, Chapter B;
- *Robust control*: existing methods to the robust control of uncertain linear and non-linear systems are presented in 2.1.3, Chapter 2. The H_∞-based approaches are introduced in 2.1.4 to which the considered multi-models multi-objectives technique belongs.

1.3 Contributions

In this section, an overview of the different contributions of this thesis work is proposed. For complete details on each contribution please refer to the referenced chapters and literature.

1.3.1 Linear OIST formulation

In this thesis, the choice is made to first design a structured controller against frequency-domain requirements using H_∞-based control synthesis and then to consider an *evolutionary*[5] strategy to enforce (with guarantees) the time-domain constraint by acting on the controller output y_K. As explained in the introductory section of Chapter 4, it is chosen to consider the OIST strategy introduced in [Burlion 12] and presented in Chapter 3 which consists in saturating the controller output signal whenever the time-domain constraint is violated so as to restrict the admissible set of trajectories at each given instant of time:

$$u = \mathrm{sat}_{\underline{u}}^{\overline{u}}(y_K) \tag{1.2}$$

Another interest of the approach is that it remains applicable in the presence of bounded unknown input disturbances $\boldsymbol{d}$ with known bounds $\left[\underline{\boldsymbol{d}}, \overline{\boldsymbol{d}}\right]$. The OIST strategy is illustrated in Fig. 1.5.

The first major contribution of this thesis consists in applying the OIST strategy to the output-constrained control of linear time-invariant systems. This results in the formulation of explicit iterative expressions of the control saturations involved in this strategy. The current major limitations of the transformation are also formally identified, namely the risk of overlap of the obtained saturations and the lack of information on stability in the presence of saturations. This contribution is presented in the first part of Chapter 4 and has been covered in [Chambon 15c] and [Chambon b].

[5] In the sense of [Goodwin 01].

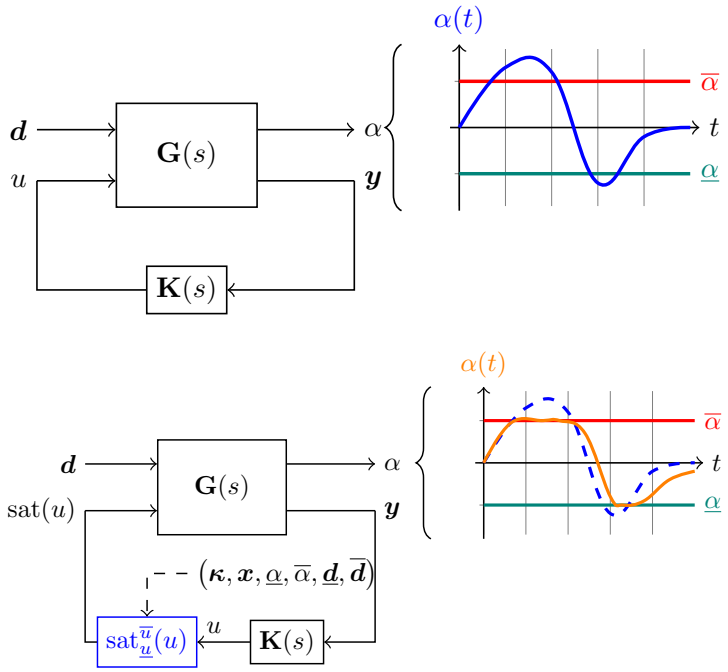

Figure 1.5: Informal illustration of the OIST *evolutionary* strategy. *Top*: nominal controller (no OIST); *Bottom*: with OIST saturations in the loop, the constraint is satisfied (in orange).

1.3.2 OIST saturations overlap mitigation and closed-loop stability analysis

The efficiency of the OIST approach depends on the fine selection of design parameters named $\boldsymbol{\kappa}$ and the closed-loop stability analysis in the presence of the proposed saturations. Following the formulation of explicit expressions in the linear case, the second contribution is the proposition of proven solutions to avoid saturations overlap and to ensure closed-loop stability.

As illustrated in Chapter 4, saturations overlap can lead to violating the time-domain constraint even when applying OIST. Also, stability of the resulting closed-loop is not ensured due to the presence of saturations. By appropriately selecting the coefficients $\boldsymbol{\kappa}$ and by introducing an anti-windup compensator, both problems are solved for minimum phase systems. This contribution is developed in Chapter 4 following the reformulation in the linear case. This was also covered in [Chambon 15c] and [Chambon b].

1.3.3 OIST extension for Robustness

OIST has been developed assuming that the considered system model is known and that its full state vector $\boldsymbol{x}$ is measured and perfectly known. A major contribution of this thesis is to extend OIST to systems with incomplete state vector measurements $\mathbf{C} \neq \mathbf{I}_n$ and for which the lack of knowledge on some parameters values are modelled by bounded uncertainties $\boldsymbol{\theta}$.

Using an appropriately designed interval observer, an extension of OIST – named OISTeR – is proposed to account for the presence of these uncertainties and to fill the lack of information on the state vector. In short, this so-called *extension for robustness* uses bounds $\underline{\boldsymbol{x}}$ and $\overline{\boldsymbol{x}}$ on the state vector $\boldsymbol{x}$ provided by the interval observer to obtain fully determined – yet more conservative – saturations such that the time-domain constraint is satisfied for all possible values of the vector of uncertainties θ. In this extension, saturations overlap is also avoided using appropriately defined parameters $\boldsymbol{\kappa}$ in a similar manner as in Chapter 4. This recent contribution was hinted in [Chambon 15a] and is detailed in Chapter 5.

1.3.4 Application to simplified models of the launch vehicle

The various contributions are illustrated on small theoretical models in each of the concerned chapters. In Chapter 6, those are illustrated on simplified models of the launch vehicle. First a robust observer-based controller is synthesized using H_∞-based control design to illustrate control law synthesis against frequency-domain requirements and in the presence of uncertainties. Next, OIST is applied to achieve the time-domain constraint on the angle of attack in the flexible launch vehicle case with no uncertainty. Finally, OISTeR is implemented on a rigid launch vehicle model with incomplete state measurements. Due to these models being non-minimum phase, specific measures are taken to avoid divergence upon saturation of the controller output. To increase performance of the interval observer, a reduced-order interval observer is also tested.

Details on the implementation of the contributions on the considered simplified launch vehicle models are given in Chapter 6 along with simulation results. Related publications include [Chambon 15a] and [Chambon 15d]. Due to the complexity of the problem, more complex models of the launch vehicle are not used but will be considered in future works. Especially, the use of the interval observer design technique detailed in Chapter 7 will be mandatory when considering additional flexible modes dynamics or in the presence of uncertain parameters.

1.3.5 Non-smooth optimization-based approach to linear interval observer design

The extension of OIST to the case of models containing uncertain parameters has been obtained by using an interval observer which is a dynamic system providing bounds $\underline{\boldsymbol{x}}$ and $\overline{\boldsymbol{x}}$ on the original system state $\boldsymbol{x}$. In the literature, interval observer are usually designed by starting from a classical observer and by expressing the resulting dynamics in new coordinates. The objective is to obtain a so-called cooperative system in the new coordinates. The change of coordinates is obtained through a transformation matrix $\mathbf{P}$ which determination is capital to obtain the cooperativity property. Existing determination methods provide either a time-varying or time-invariant transformation matrix.

In the case of a time-invariant state-coordinate transformation (SCT), existing methods are not very flexible and do not allow to include complex control-related constraints in the design of the interval observer or, more precisely, of the underlying classical observer. An additional contribution of this thesis is to propose a control-oriented SCT design approach. The resulting control design problem is solved using an appropriately chosen optimization algorithm. Extensions of the approach are proposed to simultaneously synthesize a structured controller and an interval observer on the resulting closed-loop.

This contribution is presented in Chapter 7. Related publications include [Chambon 16] and [Chambon 15b].

1.4 Dissertation outline

This manuscript is divided into three parts. Part II provides information on existing theories and required materiel to understand the contributions of this work. The main contributions of this thesis with regard to frequency- and time-domain constrained control of linear systems are exposed in Part III before concluding in Part IV.

Part II: Preliminaries

Chapter 2: Multi-models multi-objectives robust structured controller design

In this chapter, the multi-models multi-objectives structured controller design method introduced in [Apkarian 07, Apkarian 14] is applied to robust control. It is shown how to enforce frequency-domain requirements on a family of critical systems through the design of a structured controller. The critical systems are representative of the original system uncertainties. A specific controller structure based on a reduced-order classical observer and an estimated state feedback

is presented. An additional dynamic Youla parameter is used to account for the possibly limited number of degrees of freedom.

Chapter 3: Introduction to OIST

In this chapter, the *Output to Input Saturations Transformation* (OIST) theory introduced in [Burlion 12] is presented. This approach aims at enforcing a time-domain constraint on a non-linear system output. It relies on the introduction of well-defined saturations on the existing nominal control law such that the considered output signal belongs to the expected interval. The saturations are derived using the notion of relative degree of the constrained output with respect to the control input. The approach is illustrated on a simple non-linear crane model.

Part III: Frequency- and time-domain constrained control of linear systems

Chapter 4: Reformulation of OIST output constrained control approach in the linear framework

This chapter aims at describing the reformulation of the OIST approach when considering linear systems. As presented in Chapter 3, the OIST theory was originally introduced for non-linear systems. In this chapter, two undocumented problems of the OIST approach are also tackled, namely the possible saturations overlap problem as well as closed-loop stability analysis. Solutions are provided to both subjects. An appropriate definition of the OIST design parameters solves the overlap problem. In the case of minimum phase constrained outputs, asymptotic stability of the origin is obtained using an additional anti-windup compensator which also leads to improved performance. These results are then illustrated on the linear ball and beam model.

Chapter 5: Extension of OIST to the incomplete measurements and uncertain cases

An extension of the OIST approach as presented in Chapter 4 is introduced in this chapter to account for potential robustness issues. Original results were issued on known non-linear or linear systems with complete state measurements. In realistic applications however, the state vector is rarely known and uncertainties appear when modelling the dynamics. The purpose of *OIST extension for Robustness* (OISTeR) is to account for such cases. Using an appropriately defined interval observer, the notions of output constraint and propagated bounds are generalized. The output constraint is then enforced by applying the original OIST approach on these new concepts. A saturations overlap mitigation procedure is also proposed. Illustrations on theoretical examples are presented.

Chapter 6: Application to the atmospheric control of a linear uncertain flexible launch vehicle model

In this chapter, the main contributions of this thesis are applied to the atmospheric control of a simplified launch vehicle. The objective is to maintain the angle of attack of the launcher below a critical value. This is a challenging problem since the transfer to constrain is non-minimum phase.

First, a robust observer-based controller is synthesized using the multi-models multi-objectives synthesis technique described in Chapter 2. Then, the OIST approach to output-constrained control from Chapter 4 is applied to enforce the time-domain constraint in the absence of uncertain parameters. Last but not least, the OISTeR method from Chapter 5 is applied to enforce the considered time-domain constraint on the rigid launch vehicle in the absence of complete measurements of the state vector.

Satisfying results are obtained and some practical methods are presented to overcome the challenge caused by the non-minimum phase property. These methods are expected to offer valuable hints on how to improve both the OIST and OISTeR approaches in the near future.

Chapter 7: Development of a non-smooth optimisation-based approach to design linear interval observers

In this chapter, a new linear interval observer design method is introduced. Similarly to existing interval observer design methods[6], this relies on a time-invariant SCT. Using an appropriate reformulation of the SCT determination problem into a structured control design problem, the SCT can be numerically determined by solving an optimisation problem. Additional control-oriented requirements such as optimisation of the interval observer tightness $\overline{\boldsymbol{x}} - \underline{\boldsymbol{x}}$ can be formulated. The optimisation problem is solved using the same multi-model multi-objectives control design technique than in Chapter 2. This is illustrated on examples inspired by the existing literature. Comparatively to existing time-invariant SCT determination methods, our method performs better. Additionally, for a given unstable system, the same approach is applied to simultaneously design a controller and an interval observer of the closed-loop.

Part IV: Conclusion

Chapter 8: Discussion

The main contributions of this thesis are recalled here. Existing limitations of the results are highlighted and hints on possible improvements are given. Previously unmentioned possible cases of application of the contributions are discussed. Future works related to the frequency- and time-domain constrained control of linear systems are mentioned.

[6] See Chapter B for example.

Part II

Preliminaries

Chapter 2

Multi-models multi-objectives robust structured controller design

Many control design techniques exist to design an appropriate controller. In the case of robust control, the challenge is to design a stabilizing controller over a set Θ of uncertainties $\boldsymbol{\theta}$. Also, to reduce the problem complexity, use an existing satisfying structure or reduce the controller order, the controller may be chosen structured. The structured controller problem has been solved for H_∞-based control design using appropriate non-smooth non-convex optimisation methods in [Apkarian 06]. More recently [Apkarian 07], a multi-models multi-objectives approach has been proposed where the models and objectives can be considered independently when formulating the synthesis problem. In this chapter, the latter method is applied to the synthesis of a robust structured controller. A specific observer-based structure with Youla augmentation is considered. This chapter is based on results presented in [Chambon 15a].

An introduction to robust control is proposed in 2.1 with notations and a state of the art of existing robust control design techniques. The multi-models multi-objectives structured controller design approach introduced in [Apkarian 07, Apkarian 14] is then applied to the specific problem of robust control design in 2.2. In 2.3, an example of a possible structure for a robust controller is presented, namely the observer-based structure with Youla parameter augmentation. This is done in prevision of the examples in Chapter 6 where such structure is considered. Conclusions are then given in 2.4.

2.1 Introduction to robust control

The presence of uncertainties is inherent to any problem dealing with the representation of a real-world system. The purpose of inserting such uncertainties in the modelling of systems is to obtain a more faithful representation of the system state evolution. Also, unknown disturbances may be present which effects cannot be underestimated. As far as control design is considered, the presence of uncertainties and disturbances requires using specific approaches. These are numerous and based on various mathematical theories.

In this section, it is proposed to draw a state of the art of robust control theory, especially of the techniques dealing with the minimisation of H_∞ norms. Relevant notions related to linear systems theory are first recalled.

2.1.1 Linear systems theory prerequisites

2.1.1 (a) Representations of LTI systems

The dynamics of an LTI system can be represented in various ways. The more common representations are the state-space representation and the transfer function.

Time-domain representation Let $\boldsymbol{x} \in \mathbb{R}^n$ the vector of states, that is the vector of variables describing the system evolution. In most cases, the dynamics equation describing this evolution are non-linear in $\boldsymbol{x}$ and external variables acting on the system. For small intervals of variation of these variables and of the initial condition $\boldsymbol{x}_0$ (also called a *working point*) the dynamics can be often described by the following linear differential equation:

$$(\mathbf{G}) \begin{cases} \dot{\boldsymbol{x}}(t) &= \mathbf{A}\boldsymbol{x}(t) + \mathbf{B}\boldsymbol{u}(t) \\ \boldsymbol{y}(t) &= \mathbf{C}\boldsymbol{x}(t) + \mathbf{D}\boldsymbol{u}(t) \end{cases} \tag{2.1}$$

which is the state-space representation of the considered system $(\mathbf{G})$. The matrices $\mathbf{A}$, $\mathbf{B}$, $\mathbf{C}$ and $\mathbf{D}$ are called the state-space matrices and are of appropriate dimensions. The vectors $\boldsymbol{u} \in \mathbb{R}^l$ and $\boldsymbol{y} \in \mathbb{R}^m$ are respectively the vectors of inputs and outputs.

For better clarity, the inputs vector $\boldsymbol{u}$ is often divided between design inputs $\boldsymbol{w}$ (in control design problems), disturbance inputs $\boldsymbol{d}$ and control inputs $\boldsymbol{u}$ (abuse of notation). The outputs vector $\boldsymbol{y}$ is often divided between design outputs $\boldsymbol{z}$ (in control design problems) and measurements $\boldsymbol{y}$ (notation abuse).

The state-space representation is a time-domain representation in the sense it describes the evolution of the state variables $\boldsymbol{x}$ over a period of time. Using the Laplace transform, the state-space representation (2.2) can equivalently be expressed in the frequency-domain.

Sometimes, the state-space matrices may depend on unknown parameters, also called uncertainties. The uncertainties are represented by a vector $\boldsymbol{\theta}$ belonging to a subset Θ of $\mathbb{R}^q$. In this case, the state-space representation in (2.2) becomes

$$(\mathbf{G}) \begin{cases} \dot{\boldsymbol{x}}(t) &= \mathbf{A}(\boldsymbol{\theta})\boldsymbol{x}(t) + \mathbf{B}(\boldsymbol{\theta})\boldsymbol{u}(t) \\ \boldsymbol{y}(t) &= \mathbf{C}(\boldsymbol{\theta})\boldsymbol{x}(t) + \mathbf{D}(\boldsymbol{\theta})\boldsymbol{u}(t) \end{cases} \tag{2.2}$$

Frequency-domain representation Using the Laplace transform, the transfer function from $\boldsymbol{U}(s)$ to $\boldsymbol{Y}(s)$ is given by:

$$\mathbf{G}(s) = \frac{\boldsymbol{Y}(s)}{\boldsymbol{U}(s)} = \mathbf{D} + \mathbf{C}(s\mathbf{I} - \mathbf{A})^{-1}\mathbf{B} \tag{2.3}$$

where s is the Laplace transform variable. Equivalently, the transfer function can be denoted $\mathbf{G} = \left[\begin{array}{c|c} \mathbf{A} & \mathbf{B} \\ \hline \mathbf{C} & \mathbf{D} \end{array}\right]$ as in [Boyd 91]. The quadruplet $(\mathbf{A}, \mathbf{B}, \mathbf{C}, \mathbf{D})$ is called a realisation of $\mathbf{G}(s)$. This realisation is said to be minimal if $(\mathbf{A}, \mathbf{B})$ is controllable and $(\mathbf{C}, \mathbf{A})$ is observable (see 2.1.1 (c)).

Linear Fractional Transformation The Linear Fractional Transformation (LFT) is an operation used to connect two systems through feedback. This is particularly useful when designing controllers since the notion of *closing the loop* can be expressed as an LFT.

Let consider a system $(\mathbf{P})$ such that it describes the relation between input signals $\boldsymbol{w}$ and $\boldsymbol{u}$ and output signals $\boldsymbol{z}$ and $\boldsymbol{y}$:

$$\begin{bmatrix} \boldsymbol{Z}(s) \\ \boldsymbol{Y}(s) \end{bmatrix} = \mathbf{P}(s) \begin{bmatrix} \boldsymbol{W}(s) \\ \boldsymbol{U}(s) \end{bmatrix} = \begin{bmatrix} \mathbf{P_{11}}(s) & \mathbf{P_{12}}(s) \\ \mathbf{P_{21}}(s) & \mathbf{P_{22}}(s) \end{bmatrix} \begin{bmatrix} \boldsymbol{W}(s) \\ \boldsymbol{U}(s) \end{bmatrix} \tag{2.4}$$

Let also consider the following control law:

$$\boldsymbol{U}(s) = \mathbf{K}(s)\boldsymbol{Y}(s) \tag{2.5}$$

which acts as an output feedback where $\mathbf{K} = \left[\begin{array}{c|c} \mathbf{A_K} & \mathbf{B_K} \\ \hline \mathbf{C_K} & \mathbf{D_K} \end{array}\right]$. Then, the lower Linear Fractional Transformation of $(\mathbf{P})$ and $(\mathbf{K})$, denoted $\mathcal{F}_l(\mathbf{P}, \mathbf{K})$, is given by the transfer function from $\boldsymbol{W}(s)$ to $\boldsymbol{Z}(s)$:

$$\mathcal{F}_l(\mathbf{P}, \mathbf{K}) = \mathbf{P_{11}} + \mathbf{P_{12}}\mathbf{K}\left(\mathbf{I} - \mathbf{P_{22}}\mathbf{K}\right)^{-1}\mathbf{P_{21}} \tag{2.6}$$

If minimal realisations of $\mathbf{P}(s)$ and $\mathbf{K}(s)$ are given by:

$$\mathbf{P}(s) = \begin{bmatrix} \mathbf{P_{11}}(s) & \mathbf{P_{12}}(s) \\ \mathbf{P_{21}}(s) & \mathbf{P_{22}}(s) \end{bmatrix} = \begin{bmatrix} \mathbf{D_{11}} & \mathbf{D_{12}} \\ \mathbf{D_{21}} & \mathbf{D_{22}} \end{bmatrix} + \begin{bmatrix} \mathbf{C_1} \\ \mathbf{C_2} \end{bmatrix} (s\mathbf{I} - \mathbf{A})^{-1} \begin{bmatrix} \mathbf{B_1} & \mathbf{B_2} \end{bmatrix} \tag{2.7}$$

and

$$\mathbf{K}(s) = \mathbf{D_K} + \mathbf{C_K}\left(s\mathbf{I} - \mathbf{A_K}\right)^{-1}\mathbf{B_K} \tag{2.8}$$

then, a possible realisation[1] of $\mathcal{F}_l(\mathbf{P}, \mathbf{K})$ is:

$$\mathcal{F}_l(\mathbf{P}, \mathbf{K}) = \mathbf{D_{CL}} + \mathbf{C_{CL}}\left(s\mathbf{I} - \mathbf{A_{CL}}\right)^{-1}\mathbf{B_{CL}} \tag{2.9}$$

where

$$\begin{aligned} \mathbf{A_{CL}} &= \begin{bmatrix} \mathbf{A} + \mathbf{B_2}\left(\mathbf{I} - \mathbf{D_K}\mathbf{D_{22}}\right)^{-1}\mathbf{D_K}\mathbf{C_2} & \mathbf{B_2}\left(\mathbf{I} - \mathbf{D_K}\mathbf{D_{22}}\right)^{-1}\mathbf{C_K} \\ \mathbf{B_K}\left(\mathbf{I} - \mathbf{D_{22}}\mathbf{D_K}\right)^{-1}\mathbf{C_2} & \mathbf{A_K} + \mathbf{B_K}\left(\mathbf{I} - \mathbf{D_{22}}\mathbf{D_K}\right)^{-1}\mathbf{D_{22}}\mathbf{C_K} \end{bmatrix} \\ \mathbf{B_{CL}} &= \begin{bmatrix} \mathbf{B_1} + \mathbf{B_K}\left(\mathbf{I} - \mathbf{D_K}\mathbf{D_{22}}\right)^{-1}\mathbf{D_K}\mathbf{D_{21}} \\ \mathbf{B_K}\left(\mathbf{I} - \mathbf{D_{22}}\mathbf{D_K}\right)^{-1}\mathbf{D_{21}} \end{bmatrix} \\ \mathbf{C_{CL}} &= \begin{bmatrix} \mathbf{C_1} + \mathbf{D_{12}}\left(\mathbf{I} - \mathbf{D_K}\mathbf{D_{22}}\right)^{-1}\mathbf{D_K}\mathbf{C_2} & \mathbf{D_{12}}\left(\mathbf{I} - \mathbf{D_K}\mathbf{D_{22}}\right)^{-1}\mathbf{C_K} \end{bmatrix} \\ \mathbf{D_{CL}} &= \mathbf{D_{11}} + \mathbf{D_{12}}\left(\mathbf{I} - \mathbf{D_K}\mathbf{D_{22}}\right)^{-1}\mathbf{D_K}\mathbf{D_{21}} \end{aligned} \tag{2.10}$$

It can be noted that the internal stability of the closed-loop of $(\mathbf{P})$ with $(\mathbf{K})$ is equivalent to the stability of $\mathbf{A_{CL}}$. The upper LFT, denoted $\mathcal{F}_u$ is defined in a similar manner when considering an interconnection with the first inputs and outputs rather than the last ones.

As far as the notion of Linear Fractional Representation (LFR) is considered, it is mostly used in the presence of uncertainties where the objective is to obtain a $\boldsymbol{\theta}$-free minimal realisation $\mathbf{M}(s)$ of a given uncertain system $(\mathbf{G})$. In the case of parametric uncertainties and for a given vector $\boldsymbol{\theta}$ the LFT of LFR $\mathbf{M}$ and $\boldsymbol{\Delta} = \mathrm{diag}(\boldsymbol{\theta})$ equals $(\mathbf{G})$:

$$\mathbf{G}(\boldsymbol{\theta}, s) = \mathcal{F}_u(\mathbf{M}, \boldsymbol{\Delta}) \tag{2.11}$$

where $\mathbf{M}$ is a $\boldsymbol{\theta}$-free realisation. This is commonly referred to as an $\mathbf{M}$-$\boldsymbol{\Delta}$ modelling. LFRs can be computed using for example the *SMAC* Toolbox [Magni 06, Onera 16]. Commonly used upper and lower LFTs are illustrated in Fig. 2.1.

[1] Which is not necessarily a minimal realisation.

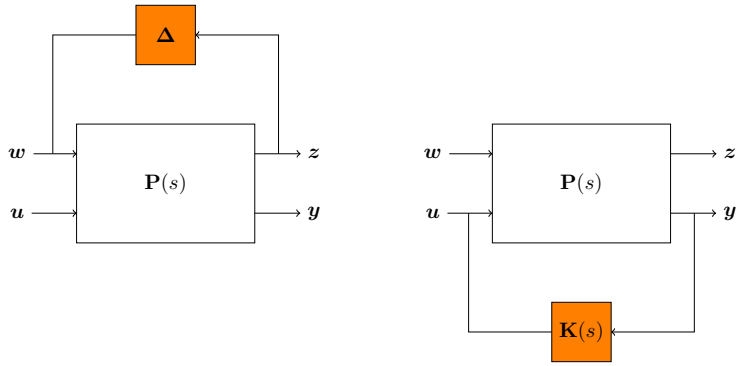

Figure 2.1: Examples of commonly used LFTs. *Left*: upper-LFT with a matrix parameter $\boldsymbol{\Delta}$ describing a fixed value of the vector of uncertainties $\boldsymbol{\theta}$. *Right*: lower-LFT with a dynamic controller structure for synthesis purposes.

2.1.1 (b) Control systems norms

The definitions of the H_2 and H_∞-norms of a system are presented here for future reference.

Signals norms Let consider a signal $\boldsymbol{x}$ with an analytic Laplace transform $\boldsymbol{X}(s)$ in $\mathrm{Re}(s) \geq 0$. If this Laplace transform is square-integrable (i.e. $\boldsymbol{X}(s) \in H_2$), the following norm can be defined:

$$\|\boldsymbol{X}\|_2 = \sqrt{\frac{1}{2\pi}\int_{-\infty}^{+\infty} \|\boldsymbol{X}(\mathrm{j}\omega)\|^2 \,\mathrm{d}\omega} \tag{2.12}$$

Also, let define the ∞-norm:

$$\|\boldsymbol{X}\|_\infty = \sup_{\mathrm{Re}(s)\geq 0} \|\boldsymbol{X}(s)\| = \sup_{\omega} \|\boldsymbol{X}(\mathrm{j}\omega\| \tag{2.13}$$

It is noted $\boldsymbol{X}(s) \in H_\infty$ if $\boldsymbol{X}(s)$ is analytic in $\mathrm{Re}(s) \geq 0$ such that $\|\boldsymbol{X}\|_\infty \leq \infty$.

Maximum singular value For a linear system with transfer function $\mathbf{G}(s)$, the singular values are defined as the square roots of the eigenvalues of the operator $\mathbf{G}^\star(\mathrm{j}\omega)\mathbf{G}(\mathrm{j}\omega)$ where $\mathbf{G}^\star(\mathrm{j}\omega)$ denotes the adjoint of $\mathbf{G}(\mathrm{j}\omega)$.

If $\mathbf{A} \in \mathbb{R}^{n\times n}$ is the state matrix obtained by using the state-space representation of this system, the maximum singular value equals the square root of the maximum eigenvalue of $\mathbf{A}\mathbf{A}^\top$:

$$\sigma_{\max}(\mathbf{A}) = \sqrt{\lambda_{\max}\left(\mathbf{A}\mathbf{A}^\top\right)} \tag{2.14}$$

H_2-norm Let consider a linear system with transfer function $\mathbf{G}(s)$. The H_2-norm is defined as:

$$\begin{aligned} \|\mathbf{G}(s)\|_2 &= \sqrt{\int_{-\infty}^{+\infty} \mathrm{tr}\left(\mathbf{G}^\star(\mathrm{j}\omega)\,\mathbf{G}(\mathrm{j}\omega)\right)\mathrm{d}\omega} \\ &= \sup_{\boldsymbol{U}(s)\in H_\infty} \frac{\|\boldsymbol{Y}(s)\|_2}{\|\boldsymbol{U}(s)\|_\infty} \end{aligned} \tag{2.15}$$

where tr is the trace operator. The H_2-norm provides information on the system output energy when disturbed by a white noise such that $\mathbf{U}^\star(\mathrm{j}\omega)\,\mathbf{U}(\mathrm{j}\omega) = \mathbf{I}$.

H_∞-norm Let consider a linear system with transfer function $\mathbf{G}(s)$. The H_∞-norm is defined as:

$$\begin{aligned} \|G(s)\|_\infty &= \sup_\omega \sigma_{\max}\left(\mathbf{G}\left(\mathrm{j}\omega\right)\right) \\ &= \sup_{\boldsymbol{U}(s)\in H_2} \frac{\|\boldsymbol{Y}(s)\|_2}{\|\boldsymbol{U}(s)\|_2} \end{aligned} \tag{2.16}$$

This norm is a measure of the maximal gain of the frequency response $\mathbf{G}\left(\mathrm{j}\omega\right)$.

2.1.1 (c) Control systems properties

In this section, some definitions related to control systems properties are introduced. Especially, before applying any control (resp. estimation) strategy, it is important to check that the system is controllable (resp. observable). Note that this is often taken for granted in this thesis that these verifications have been performed.

In the following, the linear system $(\mathbf{G})$ with the state-space representation in (2.2) is considered. In this case, $\boldsymbol{u}$ are the control inputs and $\boldsymbol{y}$ are the measurements outputs. The set of eigenvalues of $\mathbf{A} \in \mathbb{R}^{n\times n}$ is denoted $\mathrm{eig}(\mathbf{A})$.

Definition 2.1 (Controllability)**.**
$(\mathbf{G})$ is said to be controllable if the following matrix

$$\boldsymbol{\mathcal{C}} = \begin{bmatrix} \mathbf{B} & \mathbf{AB} & \mathbf{A}^2\mathbf{B} & \dots & \mathbf{A}^{n-1}\mathbf{B} \end{bmatrix} \tag{2.17}$$

has full row rank, i.e. $\mathrm{rank}\left(\boldsymbol{\mathcal{C}}\right) = n$.

A weaker notion than controllability is stabilizability. It is not used in this work. The observability is defined in a similar way except that the measurements matrix $\mathbf{C}$ is now considered.

Definition 2.2 (Observability)**.**
$(\mathbf{G})$ is said to be observable if the following matrix

$$\boldsymbol{\mathcal{O}} = \begin{bmatrix} \mathbf{C} \\ \mathbf{CA} \\ \mathbf{CA}^2 \\ \vdots \\ \mathbf{CA}^{n-1} \end{bmatrix} \tag{2.18}$$

has full row rank, i.e. $\mathrm{rank}\left(\boldsymbol{\mathcal{O}}\right) = n$.

A weaker notion than observability is detectability. It allows to formulate results even in the presence of unobservable states.

Definition 2.3 (Detectability)**.**
$(\mathbf{G})$ is said to be detectable if all the unobservable states are stable.

In practice, the detectability property can be proven using the following lemma.

Lemma 2.4 (Popov-Belevitch-Hautus detectability lemma)**.**
Let $\mathbf{A} \in \mathbb{R}^{n\times n}$ and $\mathbf{C} \in \mathbb{R}^{m\times n}$ respectively the state and measurements matrices of a linear system. The pair $(\mathbf{A}, \mathbf{C})$ is detectable if and only if $\forall \lambda \in \mathbb{C}$ such that $\lambda \in$ eig$(\mathbf{A})$ and $\mathrm{Re}\left(\lambda\right) \geq 0$*:*

$$\mathit{rank}\left(\begin{bmatrix} \left(\lambda\mathbf{I} - \mathbf{A}\right)^\top & \mathbf{C}^\top \end{bmatrix}\right) = n \tag{2.19}$$

2.1.2 Relevant notations for robust control

In this chapter, we consider uncertain linear time-invariant systems with disturbance inputs. A typical state-space representation for such system is given by:

$$(\mathbf{G}) \begin{cases} \dot{\boldsymbol{x}} &= \mathbf{A}(\boldsymbol{\theta})\boldsymbol{x} &+ \mathbf{B_u}(\boldsymbol{\theta})\boldsymbol{u} &+ \mathbf{B_w}(\boldsymbol{\theta})\boldsymbol{w} \\ \boldsymbol{y} &= \mathbf{C_y}(\boldsymbol{\theta})\boldsymbol{x} &+ \mathbf{D_{y,u}}(\boldsymbol{\theta})\boldsymbol{u} &+ \mathbf{D_{y,w}}(\boldsymbol{\theta})\boldsymbol{w} \\ \boldsymbol{z} &= \mathbf{C_z}(\boldsymbol{\theta})\boldsymbol{x} &+ \mathbf{D_{z,u}}(\boldsymbol{\theta})\boldsymbol{u} &+ \mathbf{D_{z,w}}(\boldsymbol{\theta})\boldsymbol{w} \\ \boldsymbol{x}(0) &= \boldsymbol{x}_0 \end{cases} \tag{2.20}$$

where $\boldsymbol{x} \in \mathbb{R}^n$, $\boldsymbol{y} \in \mathbb{R}^m$, $\boldsymbol{z} \in \mathbb{R}^N$, $\boldsymbol{u} \in \mathbb{R}^l$ is the control input and $\boldsymbol{w} \in \mathbb{R}^N$ is the combination of unknown disturbance and design inputs. Note these inputs are possibly repeated such that $\boldsymbol{z}$ and $\boldsymbol{w}$ have the same dimension. It is common in the control design community to make the distinction between the actual measurements vector $\boldsymbol{y}$ and the design outputs $\boldsymbol{z}$. The design transfer functions $T_{\boldsymbol{w}\to\boldsymbol{z}}(s)$ are then used to formulate control design requirements as explained later. The considered disturbances are either state or measurements disturbances depending on the definitions of $\mathbf{B_w}$ and $\mathbf{D_{y,w}}$. The vector of uncertainties is denoted $\boldsymbol{\theta} \in \Theta$ where Θ is a subset of $\mathbb{R}^q$. The uncertain parameters $\boldsymbol{\theta}$ are considered to be time-invariant in the entire manuscript. For a given $\boldsymbol{\theta} \in \Theta$, the equivalent transfer function for the state-space representation in (2.20) is obviously given by:

$$\begin{aligned} \begin{bmatrix} \boldsymbol{Z}(s) \\ \boldsymbol{Y}(s) \end{bmatrix} &= \begin{bmatrix} \mathbf{D_{z,w}}(\theta) + \mathbf{C_z}(\theta)\left[s\mathbf{I} - \mathbf{A}(\theta)\right]^{-1}\mathbf{B_w}(\theta) & \mathbf{D_{z,u}}(\theta) + \mathbf{C_z}(\theta)\left[s\mathbf{I} - \mathbf{A}(\theta)\right]^{-1}\mathbf{B_u}(\theta) \\ \mathbf{D_{y,w}}(\theta) + \mathbf{C_y}(\theta)\left[s\mathbf{I} - \mathbf{A}(\theta)\right]^{-1}\mathbf{B_w}(\theta) & \mathbf{D_{y,u}}(\theta) + \mathbf{C_y}(\theta)\left[s\mathbf{I} - \mathbf{A}(\theta)\right]^{-1}\mathbf{B_u}(\theta) \end{bmatrix} \begin{bmatrix} \boldsymbol{W}(s) \\ \boldsymbol{U}(s) \end{bmatrix} \\ &= \mathbf{T}(s,\boldsymbol{\theta}) \begin{bmatrix} \boldsymbol{W}(s) \\ \boldsymbol{U}(s) \end{bmatrix} \end{aligned} \tag{2.21}$$

If a more specific structure is not specified, dynamic controllers are given by the following state-space representation:

$$(\mathbf{K}) \begin{cases} \dot{\boldsymbol{x}}_K &= \mathbf{A_K}\boldsymbol{x}_K + \mathbf{B_K}\boldsymbol{u}_K \\ \boldsymbol{y}_K &= \mathbf{C_K}\boldsymbol{x}_K + \mathbf{D_K}\boldsymbol{u}_K \end{cases} \tag{2.22}$$

where $\boldsymbol{x} \in \mathbb{R}^{n_K}$, $\boldsymbol{u}_K \in \mathbb{R}^m$ and $\boldsymbol{y}_K \in \mathbb{R}^l$. This quite generic controller is structured in the sense of the fixed order n_K chosen for the state vector $\boldsymbol{x}_K$. More precise structures can be specified as is notably done in 2.3. The notation $\mathbf{K}(s,\boldsymbol{p})$ is also used where $\boldsymbol{p}$ is a vector of design parameters. For example:

$$\mathbf{K}(s,\boldsymbol{p}) = \mathbf{K}(s,\mathbf{A_K},\mathbf{B_K},\mathbf{C_K},\mathbf{D_K}) = \mathbf{D_K} + \mathbf{C_K}\left(s\mathbf{I} - \mathbf{A_K}\right)^{-1}\mathbf{B_K} \tag{2.23}$$

The loop is then closed using the following relations as also illustrated in Fig. 2.2:

$$\begin{cases} \boldsymbol{u}_K &= \boldsymbol{y} \\ \boldsymbol{u} &= \boldsymbol{y}_K \end{cases} \tag{2.24}$$

In this chapter, the notation $\|\bullet\|$ refers to the H_∞ or H_2-norm. In case these norms are limited on a prescribed frequency interval Ω, these are denote $\|\bullet\|_\Omega$.

2.1.3 State of the art

The notion of robust control refers to the control design approaches which are *robust* – i.e. which performance is not degraded more than a predefined level of expectation – to the presence of uncertainties and/or unknown disturbances in the modelling of the considered control system. The most common hypothesis coming with such approaches is that the uncertainties and disturbances are found within a given set. For example, it is often supposed that an uncertain

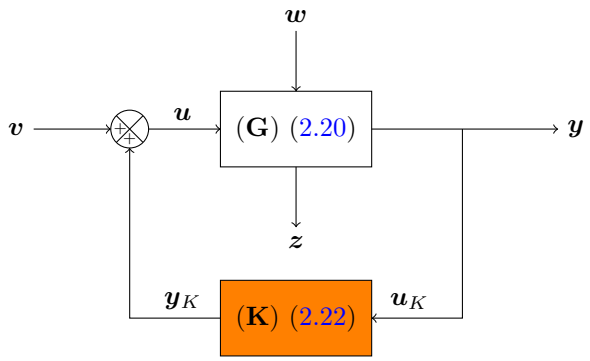

Figure 2.2: Closed-loop of (2.20) with (2.22) resulting from the relations in (2.24).

parameter θ lies within the interval $[\underline{\theta}, \overline{\theta}]$. In this section, a non-exhaustive list of robust control design methods is proposed. As far as H_∞-based control design techniques are concerned, they are tackled in the next section.

Sliding mode control is a non-linear control technique which consists in applying a discontinuous input signal to the considered non-linear system. Literature involved with describing this concept include [Utkin 92, Utkin 93, Lu 97]. The sliding mode approach is robust to parametric uncertainties since it is basically a switching control law and does not require precise information on the system dynamics. The LQG/LTR (Linear Quadratic Gaussian/Loop-Transfer Recovery) control approach introduced in [Kwakernaak 69] and rediscovered in [Doyle 81, Stein 87] was proposed as a remedy to the lack of robustness of the traditional LQG optimal control design method. However, the main drawback of traditional LQG/LTR control design is that it can overly degrade performance. A procedure was proposed in [Ravanbod 12] which improves performance and allows to tune PID structures. More recently, passivity-based control (PBC) as been introduced and developed in [Ortega 01, Ortega 02, Rodríguez 03]. It is aimed at considering the system energy in the control design procedure rather than the input and output signals nature and properties. Other approaches include Lyapunov Function Redesign. As explained in [Khalil 02], this consists in using a Lyapunov function on the nominal model ($\boldsymbol{\theta} = \mathbf{0}$) to derive a Lyapunov function for the uncertain dynamics ($\boldsymbol{\theta} \neq \mathbf{0}$).

As far as the robust control of LPV systems is concerned, interesting resources include the works in [Poussot-Vassal 08] where the robust control of an LPV automotive model is explored and [Briat 15] which stands as an extensive source of information on LPV and time-delay systems. Note that a quite extensive bibliographical study on robust control is available in [Poussot-Vassal 08].

2.1.4 H_∞-based approaches

In the linear case, robust control techniques involving H_∞-norm optimization of given transfers has been a buzzing field of research since the 1980's. First works [Zames 81, Francis 84b, Francis 84a] considered the use of the sensitivity functions and led to the definition of the robustness principle. The mixed sensitivity problem was introduced in [Kimura 84]. It introduced additional weightings in the H_∞ norms of the sensitivity function which allowed to consider broader classes of systems namely those with pure integrators. The standard H_∞ problem, which is basically a disturbance rejection problem in its simplest form, was introduced in [Doyle 84]. A solution using a state-space approach was provided. The standard problem theory was then unified in [Francis 87]. Solutions to this problem were proposed and successively improved in [Glover 88, Doyle 89]. They are based on the resolution of Riccati equations and lead to controllers with the same order as the controlled system. Additional works proposed more practical approaches such as the loop-shaping procedure in [McFarlane 92] or proposed to exploit the structure of the uncertainties such as the singular structured value method in [Doyle 82].

In most of these works, a solution to the problem was generally obtained by solving high-order Riccati equations. The article [Doyle 89] provided a solution to the H_∞ and H_2 standard problem

for MIMO systems based on the resolution of an Algebraic Riccati equation (ARE). Alternatives to the Riccati equations were later introduced in the form of LMIs-based techniques [Gahinet 94, Iwasaki 94]. Complete references on the subject include [Boyd 94] and [Zhou 96].

In practice, structured controller with limited order in regard of the original system are often sought for. This leads to an optimisation problem for which the cost functional is non-smooth non-convex. In spite of the existence of approaches based on LMIs [El Ghaoui 97] or benefiting from the separation principle inherent to the observer-based structure [Zasadzinski 07], more recent methods [Apkarian 06, Burke 06] focus on finding a local optimal solution using non-smooth optimisation-based algorithms. In [Apkarian 07], the approach proposed in [Apkarian 06] has been extended to account for the presence of H_∞-norm requirements on limited frequency intervals only. These works led to [Apkarian 15] where the set of critical models for robust controller synthesis is dynamically generated in the case of parametric uncertainties. The multi-models multi-objectives technique described and used in this Chapter has been proposed in [Apkarian 13, Apkarian 14].

2.2 Multi-models multi-objectives structured controller design approach

In this section, the multi-model multi-objective H_∞-based approach introduced in [Apkarian 07] is exposed. After formulating the usual control design problem using LFTs, it is shown that it is equivalent to an optimization problem. In the case where the controller is structured and multiple models and requirements are considered, this optimization problem is non-linear, non-convex and non-smooth. Using existing works, a local solution to this optimization problem can be found.

2.2.1 Considered multi-models multi-objectives synthesis problem

The problem considered in this chapter is to design a structured controller ($\mathbf{K}$) (2.22) for the system ($\mathbf{G}$) (2.20) against some control requirements formulated to constrain the closed-loop dynamics as well as some prescribed transfers norms. Robustness with respect to the uncertainties $\boldsymbol{\theta} \in \Theta$ and disturbances in $\boldsymbol{w} \in \mathbb{R}^N$ must be ensured. Informally speaking, this means that the control requirements should be enforced for all uncertainties $\boldsymbol{\theta}$ in the subset $\Theta \subset \mathbb{R}^q$ and for the considered class of input disturbance signals. In the case of uncertain systems, the necessity to consider multiple models can easily be grasped.

To begin with, let consider a LFR of ($\mathbf{G}$). Such linear fractional representation corresponds to a minimal representation of the considered model where the dependency in the uncertainties can be eliminated. These uncertainties are then gathered in a specific external $\boldsymbol{\Delta}$ block. Linear Fractional Representations can be computed using for example the *SMAC* Toolbox [Magni 06, Onera 16]. Let consider the following LFR:

$$\begin{aligned}\begin{bmatrix}\boldsymbol{Z_\Delta}(s)\\ \boldsymbol{Z}(s)\\ \boldsymbol{Y}(s)\end{bmatrix} &= \begin{bmatrix}\mathbf{P_{11}}(s) & \mathbf{P_{12}}(s) & \mathbf{P_{13}}(s)\\ \mathbf{P_{21}}(s) & \mathbf{P_{22}}(s) & \mathbf{P_{23}}(s)\\ \mathbf{P_{31}}(s) & \mathbf{P_{32}}(s) & \mathbf{P_{33}}(s)\end{bmatrix}\begin{bmatrix}\boldsymbol{W_\Delta}(s)\\ \boldsymbol{W}(s)\\ \boldsymbol{U}(s)\end{bmatrix}\\ &= \mathbf{P}(s)\begin{bmatrix}\boldsymbol{W_\Delta}(s)\\ \boldsymbol{W}(s)\\ \boldsymbol{U}(s)\end{bmatrix}\end{aligned} \tag{2.25}$$

where $\boldsymbol{\Delta} \in \mathbb{R}^{n_\Delta \times n_\Delta}$ – with $n_\Delta \geq q$ – is such that the upper-LFT $\mathcal{F}_u(\mathbf{P}(s), \boldsymbol{\Delta})$ equals $\mathbf{T}(s, \boldsymbol{\theta})$ in (2.21) for a given $\boldsymbol{\theta} \in \Theta$. The corresponding $\boldsymbol{\Delta}$ block is thus denoted $\boldsymbol{\Delta}_{\boldsymbol{\theta}}$. Note that using appropriate transformations, it can be ensured that

$$\overline{\sigma}(\boldsymbol{\Delta}_{\boldsymbol{\theta}}) \leq 1 \tag{2.26}$$

We denote $\mathcal{B}(\boldsymbol{\Delta}) = \{\boldsymbol{\Delta}_{\boldsymbol{\theta}} : \overline{\sigma}(\boldsymbol{\Delta}_{\boldsymbol{\theta}}) \leq 1\}$. Then, using the LFT framework, "closing the loop" for a fixed $\boldsymbol{\theta}$ as in (2.24) is performed using the lower-LFT of $\mathcal{F}_u(\mathbf{P}(s), \boldsymbol{\Delta}_{\boldsymbol{\theta}})$ and $\mathbf{K}(s, \boldsymbol{p})$:

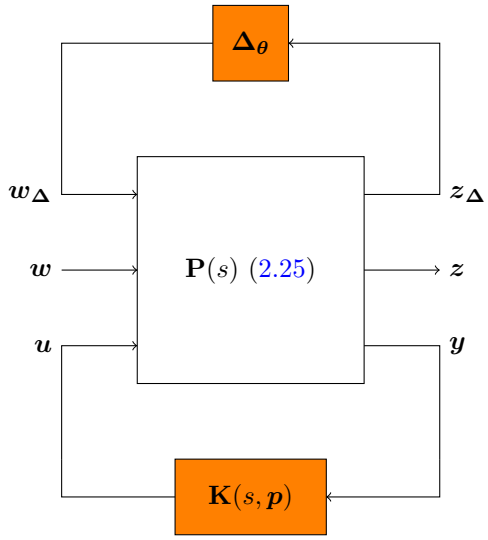

Figure 2.3: Illustration of the upper and lower LFTs as considered in (2.27). Variable blocks for different values of $\boldsymbol{\theta}$ and different controller state-space matrices are represented in orange color.

$$\mathbf{Z}(s) = \mathcal{F}_l\left(\mathcal{F}_u\left(\mathbf{P}(s), \boldsymbol{\Delta_\theta}\right), \mathbf{K}(s,\boldsymbol{p})\right)\mathbf{W}(s) \tag{2.27}$$

These successive transformations are illustrated in Fig. 2.3 for $\boldsymbol{\Delta_\theta}$ corresponding to a given $\boldsymbol{\theta} \in \Theta$. In control design problems, the block $\mathbf{K}(s,\boldsymbol{p})$ is the one to compute or "tune" against control requirements.

Any control design problem corresponds to tuning $\mathbf{K}(s,\boldsymbol{p})$ such that some specifications are satisfied. In the presence of uncertainties, these specifications should also be enforced for all $\boldsymbol{\theta} \in \Theta$. In the following, two types of constraints are considered: the ones which can be expressed as common constraints on the H_2 or H_∞-norm of prescribed transfers and the ones which cannot.

2.2.1 (a) Transfer norm constraints and priorities

When using H_∞-based approaches, specifications are expressed as frequency-domain constraints on the H_2 of H_∞-norms of user-defined design transfers $T_{\boldsymbol{w}_i \to \boldsymbol{z}_i}(s, \mathbf{K}(s,\boldsymbol{p}), \boldsymbol{\Delta_\theta})$ for $i \in \mathbb{N}^\star$ with $i \leq N$. A typical feasibility problem is to find $\boldsymbol{p}$ such that a set of constraints on the H_2 or H_∞-norms of considered design transfers are satisfied:

$$\|T_{\boldsymbol{w}_i \to \boldsymbol{z}_i}(s, \mathbf{K}(s,\boldsymbol{p}), \boldsymbol{\Delta_\theta})\| \leq 1,\ \forall i \in \mathbb{N}^\star \text{ s.t. } i \leq N \tag{2.28}$$

However, more specific and complex problems are sometimes considered where priority is given to some constraints. The norm constraint may also be expressed on a limited frequency range Ω. The following terminology is used whether the norm should be minimized (objective) or driven below the unit (constraint):

$$\begin{aligned} \text{Objective}: &\quad \min_{\boldsymbol{p}} \max_{i,\boldsymbol{\theta}\in\Theta} \left\{\|T_{\boldsymbol{w}_i \to \boldsymbol{z}_i}(s, \mathbf{K}(s,\boldsymbol{p}), \boldsymbol{\Delta_\theta})\|_\Omega\right\} \\ \text{Constraint}: &\quad \max_{i,\boldsymbol{\theta}\in\Theta} \left\{\|T_{\boldsymbol{w}_i \to \boldsymbol{z}_i}(s, \mathbf{K}(s,\boldsymbol{p}), \boldsymbol{\Delta_\theta})\|_\Omega\right\} \leq 1 \end{aligned} \tag{2.29}$$

Using works in [Apkarian 07, Apkarian 13, Apkarian 14], it appears that aggregating these objectives is not necessary as would be required using conventional H_∞-based design techniques. Hence, we can speak of a *multi-objectives* approach. As far as the vector of uncertainties is concerned, it can be argued that the number of considered objectives and constraints in (2.31) is potentially infinite due to $\boldsymbol{\theta} \in \Theta$, with Θ a subset of $\mathbb{R}^q$. This results in the impossibility to formalize the conditions in an optimization algorithm.

A possible approach is to use the notion of *critical* case. Using a limited number of so-called *critical* cases, the constraints in (2.31) can be formalized in an optimization program

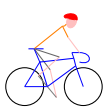

at the cost of losing any guarantee on the whole subset Θ. In the presence of uncertainties, *critical* cases correspond to values of $\boldsymbol{\theta}$ (hence of $\boldsymbol{\Delta}_{\boldsymbol{\theta}}$) for which H_∞ worst-case performance $\max_{\boldsymbol{\Delta}_{\boldsymbol{\theta}} \in \mathcal{B}(\boldsymbol{\Delta})} \|\mathcal{F}_u\left(\mathbf{P}(s), \boldsymbol{\Delta}_{\boldsymbol{\theta}}\right)\|_\infty$ is achieved. Since the following equality stands [Roos 10]:

$$\max_{\boldsymbol{\Delta}_{\boldsymbol{\theta}} \in \mathcal{B}(\boldsymbol{\Delta})} \|\mathcal{F}_u\left(\mathbf{P}(s), \boldsymbol{\Delta}_{\boldsymbol{\theta}}\right)\|_\infty = \max_{\boldsymbol{\Delta}_{\boldsymbol{\theta}} \in \mathcal{B}(\boldsymbol{\Delta}),\ \omega \in \mathbb{R}_+} \overline{\sigma}\left(\mathcal{F}_u\left(\mathbf{P}\left(\mathrm{j}\omega\right), \boldsymbol{\Delta}_{\boldsymbol{\theta}}\right)\right) \tag{2.30}$$

then multiple critical models are obtained for given ranges of the frequency ω. A solution to this optimisation problem was obtained and is detailed in [Roos 10]. It is based on results from the μ-analysis field which are not detailed here, this being out of scope. Good references to μ-analysis theory include [Packard 93, Ferreres 99].

As a consequence, only a limited number of *critical* cases $\Theta_c = \{\boldsymbol{\theta}_1, \ldots, \boldsymbol{\theta}_r\}$ can be considered, corresponding to H_∞ *worst-case* performance over certain ranges of frequencies. Using these critical models for the considered critical $\boldsymbol{\theta}$ values, a limited number of objectives and constraints is obtained:

$$\begin{aligned} \text{Objective}: &\quad \min_{\boldsymbol{p}} \max_{i,j} \left\{ \left\| T^j_{\boldsymbol{w}_i \to \boldsymbol{z}_i}\left(s, \mathbf{K}(s, \boldsymbol{p})\right) \right\|_\Omega \right\} \\ \text{Constraint}: &\quad \max_{i,j} \left\{ \left\| T^j_{\boldsymbol{w}_i \to \boldsymbol{z}_i}\left(s, \mathbf{K}(s, \boldsymbol{p})\right) \right\|_\Omega \right\} \leq 1 \end{aligned} \tag{2.31}$$

where $1 \leq j \leq r$ and $T^h_{\boldsymbol{w}_i \to \boldsymbol{z}_j}\left(s, \mathbf{K}(s, \boldsymbol{p})\right)$ denotes the transfer function from input $\boldsymbol{w}_i$ to output $\boldsymbol{z}_i$ for $\boldsymbol{\theta} = \boldsymbol{\theta}_j$ and a given design parameters vector $\boldsymbol{p}$. Multiple critical models are hereby considered hence the denomination of *multi-models* design technique.

2.2.1 (b) Other constraints

Other types of constraints can also be considered when designing a controller. These constraints cannot always be expressed as conditions on the norms of given transfer functions. They include constraints on:

- closed-loop stability;
- Controller dynamics stability;
- Margins at specified loop openings.

Finding appropriate design parameters $\boldsymbol{p}$ such that the constraints in (2.31) and 2.2.1 (b) are fulfilled is an optimization problem. It is formalizin the following section.

2.2.2 Final formulation as an optimization problem

In the previous section, the notion of multi-objectives multi-models structured controller synthesis problem has been clarified in the case of uncertain systems. The resulting optimization problem is now formally presented.

Problem 2.5 (Multi-objectives multi-models structured controller design optimization problem [Apkarian 07, Apkarian 15])**.**
Let $\boldsymbol{p}$ the vector of design parameters. Solve:

$$\begin{aligned} &\text{minimize} && f(\boldsymbol{p}) \\ &\text{subject to} && g(\boldsymbol{p}) \leq c, \quad c \in \mathbb{R} \end{aligned} \tag{2.32}$$

where $f(\boldsymbol{p}) = \max_i f_i(\boldsymbol{p})$, $g(\boldsymbol{p}) = \max_j g_j(\boldsymbol{p})$ are aggregates of either transfer norms constraints 2.2.1 (a) (possibly on frequency-limited ranges) or other constraints 2.2.1 (b).

This is the most generic way of representing the structured controller design problem taking multiple models and multiple requirements into account. By construction, f and g are non-smooth functions of the design parameters $\boldsymbol{p}$ due to the presence of the max aggregating function. Also, the constraints f_i and g_j for given indices i and j can be non-smooth as is the

case with constraints on the H_∞-norm of design transfers. Moreover, as already tackled in [Apkarian 06], the optimization Problem 2.5 is non-convex as soon as a structured controller $\mathbf{K}(s, \boldsymbol{p})$ is considered in stead of a full-order controller. In conclusion, Problem 2.5 is a non-smooth non-convex program. Theoretical approaches to provide a local solution to this problem have been proposed notably in [Apkarian 06, Apkarian 07, Apkarian 15] and are not detailed here. Based on these works, a dedicated solver was implemented in [MATLAB 14]. Examples of application of this technique include [Gahinet 13].

2.3 Introduction to observer-based controllers with Youla parameter augmentation

In this section, an example of a viable structure for the controller is presented, namely the observer-based controller structure. After enumerating the pros for such structure, it is shown how to obtain a proper formulation of this controller structure fit for synthesis. In case more degrees of freedom are required, it is shown how to introduce a so-called Youla parameter which adds dynamics to the pre-existing classical observer dynamics. This structure will be used in 6.2 to illustrate the multi-models multi-requirements design technique on the uncertain flexible launch vehicle example.

2.3.1 Choosing an observer-based structure for the controller

As mentioned in the previous section 2.2, any controller structure can be considered for synthesis against the considered requirements. The advantages of structuring the controller are numerous:

- this reduces the order of the controller thus facilitating its implementation;
- This can provide a precise physical interpretation to the controller internal signals instead of a black-box interpretation of the synthesized controller;
- This allows the use of existing structures which have proven satisfying based on experience and testing;
- This is expected to facilitate further operations required on the synthesized controller.

As far as the aerospace application in 6.2, Chapter 6 is concerned, the choice is made to consider an observer-based structure. Similarly to many aerospace problems, the considered linear models representing the launch vehicle are obtained from linearising the original non-linear model at prescribed working points. The control law covering the evolution of the dynamics between these working points is then obtained through interpolation which results in the control law being gain-scheduled [Voinot 03a]. An observer-based structure is expected to facilitate the interpolation of the structuring observer and feedback gains as mentioned in [Alazard 03, Stilwell 97]. Also, it gives a physical interpretation to the controller internal signal since the rigid body dynamics of the launch vehicle is observed and can be interpreted.

2.3.2 Presentation of the observer-based structure

In this section, the observer-based structure is presented. From a nominal model obtained for nominal value $\boldsymbol{\theta}_n$ of the uncertain parameters in (2.20), a reduced-order classical observer is first designed. Then, a feedback gain fed by the observed reduced-order state is designed. Finally, to anticipate the lack of degrees of freedom in the resulting structure, an augmentation by a dynamic Youla parameter is considered.

2.3.2 (a) Considered nominal model

To design the dynamics of the classical observer, it is decided to consider nominal values of the uncertain parameters in $\boldsymbol{\theta}$. The system dynamics in (2.20) is then evaluated for this nominal vector of parameters $\boldsymbol{\theta}_n$. The choice for the nominal vector $\boldsymbol{\theta}_n$ depends on the considered

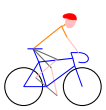

problem. In the general case, if the vector of uncertain parameters can be bounded by two quantities $\underline{\boldsymbol{\theta}}$ and $\overline{\boldsymbol{\theta}}$ such that

$$\underline{\boldsymbol{\theta}} \leq \boldsymbol{\theta} \leq \overline{\boldsymbol{\theta}}$$

then a possible choice for $\boldsymbol{\theta}_n$ is

$$\boldsymbol{\theta}_n = \frac{\overline{\boldsymbol{\theta}} - \underline{\boldsymbol{\theta}}}{2}$$

As proposed, let evaluate the considered uncertain system in (2.20) for $\boldsymbol{\theta} = \boldsymbol{\theta}_n$. This results in the following state-space representation for the nominal model:

$$(\mathbf{G_n}) \left\{ \begin{array}{rcl} \dot{\boldsymbol{x}}_n &=& \mathbf{A_n}\boldsymbol{x}_n + \mathbf{B_{n,u}}\boldsymbol{u} + \mathbf{B_{n,w}}\boldsymbol{w} \\ \boldsymbol{y}_n &=& \mathbf{C_{n,y}}\boldsymbol{x}_n + \mathbf{D_{n,u}}\boldsymbol{u} + \mathbf{D_{n,w}}\boldsymbol{w} \end{array} \right. \tag{2.33}$$

where $\mathbf{A_n} = \mathbf{A}(\boldsymbol{\theta}_n)$, $\mathbf{B_{n,u}} = \mathbf{B_u}(\boldsymbol{\theta}_n)$, $\mathbf{B_{n,w}} = \mathbf{B_w}(\boldsymbol{\theta}_n)$, $\mathbf{C_{n,y}} = \mathbf{C_y}(\boldsymbol{\theta}_n)$, $\mathbf{D_{n,u}} = \mathbf{B_u}(\boldsymbol{\theta}_n)$ and $\mathbf{D_{n,w}} = \mathbf{D_w}(\boldsymbol{\theta}_n)$. This can be equally obtained using the upper-LFT of $\mathbf{P}(s)$ with $\boldsymbol{\Delta}_{\boldsymbol{\theta}_n}$: $\mathcal{F}_u(\mathbf{P}(s), \boldsymbol{\Delta}_{\boldsymbol{\theta}_n})$.

A note on rigid/flexible dynamics In aerospace/aeronautical applications, recent advances have allowed the use of new, lighter, materials. Also, the considered structures size have increased as is the case with wings or deployable solar panels. This has resulted in an increased impact of the flexibilities on the structures and especially on the control of the systems featuring such structures.

In the launch vehicle case, as will be detailed in 6.2, the flexible modes do not impact the rigid body dynamics of the system, that is its trajectory in the considered frame. However, they act as a disturbance on the measurements through the $\mathbf{C_y}$ matrix. From a dynamics representation point of view, this means that the matrix $\mathbf{A_n}$ is block-diagonal:

$$\mathbf{A_n} = \begin{bmatrix} \mathbf{A_n^1} & \mathbf{0} \\ \mathbf{0} & \mathbf{A_n^2} \end{bmatrix} \tag{2.34}$$

From an observer-based controller point of view, observing the flexible modes would be equivalent to re-injecting the disturbances in the control loop with is not desired. The determining dynamics is of course the rigid body dynamics which models the trajectory of the system in the considered frame. This motivates using a reduced-order classical observer rather than a full-order observer in the design of the considered observer-based controller. Hence, only the following dynamics is observed and serves as the nominal model on which the classical observer is built:

$$\dot{\boldsymbol{x}}_n^1 = \mathbf{A_n^1}\boldsymbol{x}_n^1 + \mathbf{B_{n,u}^1}\boldsymbol{u} + \mathbf{B_{n,w}^1}\boldsymbol{w} \tag{2.35}$$

where $\boldsymbol{x}_n^1 \in \mathbb{R}^{n_1}$. In the launch vehicle case, the vector $\boldsymbol{y} \in \mathbb{R}^m$ gives a measure of the rigid-body variables disturbed by the bending modes dynamics. This vector is used as an input to the classical observer considered in the next section. Additional synthesis requirements can be considered to reject the measurements noises and improve the control performance of the closed-loop.

2.3.2 (b) Reduced-order classical observer

As already mentioned, only the part of the state related to rigid body dynamics (2.35) is observed. The following reduced-order classical observer is thus considered:

$$\left(\widehat{\mathbf{G_n}}\right) \left\{ \begin{array}{rcl} \dot{\widehat{\boldsymbol{x}}}_n^1 &=& \left(\mathbf{A_n^1} - \mathbf{L}\mathbf{C_{n,y}^1}\right)\widehat{\boldsymbol{x}_n^1} + \mathbf{B_{n,u}^1}\boldsymbol{u} + \mathbf{L}\boldsymbol{y} \\ \widehat{\boldsymbol{y}} &=& \mathbf{C_{n,y}^1}\widehat{\boldsymbol{x}_n^1} \end{array} \right. \tag{2.36}$$

where $\mathbf{L} \in \mathbb{R}^{n_1 \times m}$ is the observer-gain to be designed and $\mathbf{C_{n,y}^1}$ represents the n_1 first columns of $\mathbf{C_{n,y}}$. In the following section, the observer state $\boldsymbol{x}_n^1$ is used in the feedback-loop to stabilize the system.

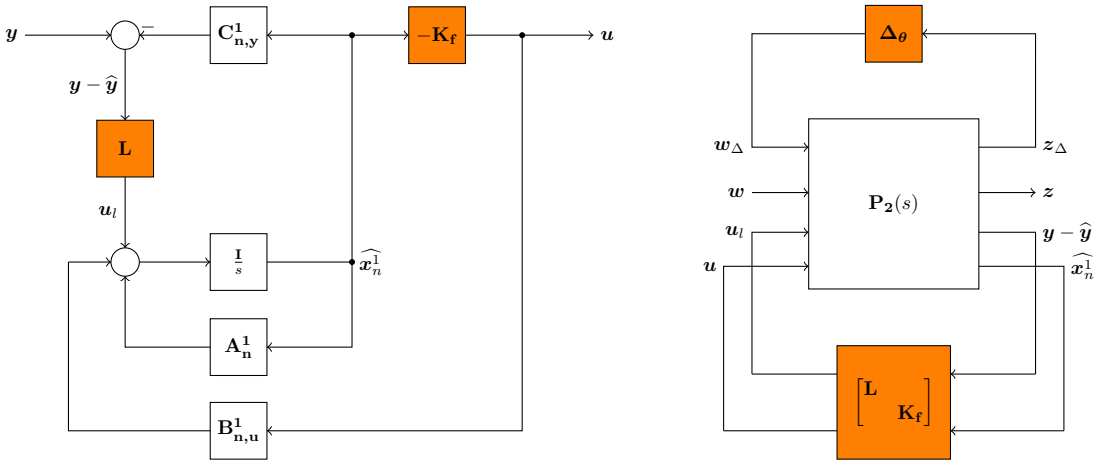

Figure 2.4: *Left*: observer-based controller structure; *Right*: LFT used for structured controller synthesis purposes

2.3.2 (c) Resulting observer-based structure

In the previous section, a classical observer was built on top of the uncertain disturbed plant measurements $\boldsymbol{y}$. Only part of the dynamics, the rigid body part to be precise, is observed. As a consequence, the vector $\widehat{\boldsymbol{x}^1_n}$ is an estimate of the true rigid body state $\boldsymbol{x}^1$. This estimate is based on a nominal model corrected by the uncertain disturbed plant measurements.

The observer-based structure then uses this estimate to obtain the feedback loop considering a static-state feedback gain $\mathbf{K_f} \in \mathbb{R}^{l \times n_1}$:

$$\boldsymbol{u} = -\mathbf{K_f}\widehat{\boldsymbol{x}^1_n} \tag{2.37}$$

Similarly to the observer gain $\mathbf{L}$, the feedback gain $\mathbf{K_f}$ is a design parameter. The controller structure resulting from the classical observer in (2.36) and the feedback gain in (2.37) is represented on the left side of Fig. 2.4. The considered design parameters $\mathbf{L}$ and $\mathbf{K_f}$ are highlighted in orange. From a controller synthesis perspective, these parameters are externalized using the following LFR for the inner controller structure:

$$(\mathbf{P_K}) \quad \left[\begin{array}{c|c} \mathbf{A^1_n} & \begin{bmatrix}\mathbf{0}_{n_1\times m} & \mathbf{I}_{n_1} & \mathbf{B^1_{n,u}}\end{bmatrix} \\ \hline \begin{bmatrix}\mathbf{0}_{l\times n_1} \\ -\mathbf{C^1_{n,y}} \\ \mathbf{I}_{n_1}\end{bmatrix} & \begin{bmatrix}\mathbf{0}_{l\times m} & \mathbf{0}_{l\times n_1} & \mathbf{I}_l \\ \mathbf{I}_m & \mathbf{0}_{m\times n_1} & \mathbf{0}_{m\times l} \\ \mathbf{0}_{n_1\times m} & \mathbf{0}_{n_1\times n_1} & \mathbf{0}_{n_1\times l}\end{bmatrix} \end{array}\right] \tag{2.38}$$

where we have used the common state-space partitioning representation of [Boyd 91]. The inputs to $(\mathbf{P_K})$ are respectively $\boldsymbol{y}$, $\boldsymbol{u}_l$ and $\boldsymbol{y}_K = \boldsymbol{u}$. Its outputs are respectively $\boldsymbol{u}$, $\boldsymbol{y}-\widehat{\boldsymbol{y}}$ and $\widehat{\boldsymbol{x}^1_n}$. Using the LFR in (2.38), the controller structure in Fig. 2.4 is obtained through two successive lower-LFTs (or equivalently through one LFT after applying an appropriately defined block diagonal operator on the design parameters):

$$\begin{aligned} \mathbf{K}(s,\boldsymbol{p}) \;=\; \frac{\mathbf{U}(s)}{\mathbf{Y}(s)} \;&=\; \mathcal{F}_l\left(\mathcal{F}_l\left(\mathbf{P_K}(s),\mathbf{K_f}\right),\mathbf{L}\right) \\ &=\; \mathcal{F}_l\left(\mathbf{P_K}(s),\mathrm{blkdiag}\left(\mathbf{L},\mathbf{K_f}\right)\right) \end{aligned} \tag{2.39}$$

where $\boldsymbol{p} = \begin{bmatrix}\mathbf{L} & \mathbf{K_f}\end{bmatrix}$. From a multi-model synthesis approach and with slight modifications of the LFR in (2.25) and LFT in Fig. 2.3 using $\mathbf{K}(s,\boldsymbol{p})$ as in (2.39), the synthesis models for different values of $\boldsymbol{\theta} \in \Theta_c$ can be obtained via LFT as illustrated on the right side of Fig. 2.4.

2.3.2 (d) Reduced-order vs. degrees of freedom: the Youla augmentation

In the previous section, the structure for a typical observer-based controller has been detailed. Two static gains, respectively the observer gain $\mathbf{L} \in \mathbb{R}^{n_1\times m}$ and $\mathbf{K_f} \in \mathbb{R}^{l\times n_1}$ have been intro-

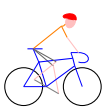

duced. These are the design parameters which will be tuned against multiple requirements on multiple synthesis models. The total number of variables considered in this control synthesis problem is thus equal to $(m+l)\,n_1$ where m is the number of measurements outputs, l the number of control inputs and n_1 the order of the classical observer (or, practically speaking, of the considered system rigid body dynamics).

Depending on the original system order, the number of variables mentioned above may be insufficient in terms of degrees of freedom. For example, requirements related to attenuating the bending modes may be hard to fulfil without giving more degrees of freedom than the $(m+l)\,n_1$ variables resulting from choosing static observer and feedback gains. A solution to enrich the dynamics of the studied controller is to consider an augmented controller based on the original observer-based controller and a dynamic Youla parameter $\mathbf{Q}(s)$. The Youla-Kučera parametrization was originally introduced for transfer functions in [Youla 76a, Youla 76b, Kučera 80] to parametrize the whole set of stabilizing controllers for a given plant. Formulations were later proposed using state-space representations [Nett 84]. Modern resources on the subject include [Kučera 11, Colaneri 97, Antsaklis 05].

In our case, based on a stabilizing controller for two given gains $\mathbf{L}$ and $\mathbf{K_f}$, the Youla dynamic parameter $\mathbf{Q}(s)$ can be used to increase the considered observer-based controller without destabilizing the closed-loop. Hence, the number of degrees of freedom increases without changing the core structure or introducing undesired instabilities in the closed loop.

Similarly to any dynamic system, the Youla parameter can be represented by the following state-space representation:

$$(\mathbf{Q})\begin{cases} \dot{\boldsymbol{x}}_Q &= \mathbf{A_Q}\boldsymbol{x}_Q + \mathbf{B_Q}\boldsymbol{u}_Q \\ \boldsymbol{y}_Q &= \mathbf{C_Q}\boldsymbol{x}_Q + \mathbf{D_Q}\boldsymbol{u}_Q \end{cases} \tag{2.40}$$

where $\boldsymbol{x}_Q \in \mathbb{R}^{n_Q}$ is the selected order for the Youla parameter. In the considered case, the following interconnections are considered:

$$\begin{aligned} \boldsymbol{u}_Q &= \boldsymbol{y} - \widehat{\boldsymbol{y}} \\ \boldsymbol{u} &= \boldsymbol{y}_Q - \mathbf{K_f}\widehat{\boldsymbol{x}_n^1} \end{aligned} \tag{2.41}$$

The controller structure resulting from the classical observer in (2.36), the feedback gain in (2.37) and the Youla dynamic parameter $(\mathbf{Q})$ is represented on the left side of Fig. 2.5. Similarly to the static gains $\mathbf{L}$ and $\mathbf{K_f}$, $(\mathbf{Q})$ is a design parameter and is highlighted in orange on the figure. For synthesis purposes, it can be externalized using an appropriate LFR for the inner controller structure:

$$\left(\mathbf{P_K^Q}\right) \quad \left[\begin{array}{c|cccc} \mathbf{A_n^1} & \begin{bmatrix}\mathbf{0}_{n_1\times m} & \mathbf{I}_{n_1} & -\mathbf{B_{n,u}^1} & \mathbf{B_{n,u}^1}\end{bmatrix} \\ \hline \begin{bmatrix}\mathbf{0}_{l\times n_1} \\ -\mathbf{C_{n,y}^1} \\ \mathbf{I}_{n_1} \\ -\mathbf{C_{n,y}^1}\end{bmatrix} & \begin{bmatrix}\mathbf{0}_{l\times m} & \mathbf{0}_{l\times n_1} & -\mathbf{I}_l & \mathbf{I}_l \\ \mathbf{I}_m & \mathbf{0}_{m\times n_1} & \mathbf{0}_{m\times l} & \mathbf{0}_{m\times l} \\ \mathbf{0}_{n_1\times m} & \mathbf{0}_{n_1\times n_1} & \mathbf{0}_{n_1\times l} & \mathbf{0}_{n_1\times l} \\ \mathbf{I}_m & \mathbf{0}_{m\times n_1} & \mathbf{0}_{m\times l} & \mathbf{0}_{m\times l}\end{bmatrix} \end{array}\right] \tag{2.42}$$

where we have used the same state-space partitioning representation as previously. The inputs to $\left(\mathbf{P_K^Q}\right)$ are respectively $\boldsymbol{y}$, $\boldsymbol{u}_l$, $\boldsymbol{y}_K = \boldsymbol{u}$ and $\boldsymbol{y}_Q$. Its outputs are respectively $\boldsymbol{u}$, $\boldsymbol{y} - \widehat{\boldsymbol{y}}$, $\widehat{\boldsymbol{x}_n^1}$ and $\boldsymbol{u}_Q = \boldsymbol{y} - \widehat{\boldsymbol{y}}$. Using the LFR in (2.42), the controller structure in Fig. 2.5 is obtained through three successive lower-LFTs:

$$\begin{aligned} \mathbf{K}(s,\boldsymbol{p}) = \frac{\mathbf{U}(s)}{\mathbf{Y}(s)} &= \mathcal{F}_l\left(\mathcal{F}_l\left(\mathcal{F}_l\left(\mathbf{P_K^Q}(s),(\mathbf{Q})\right),\mathbf{K_f}\right),\mathbf{L}\right) \\ &= \mathcal{F}_l\left(\mathcal{F}_l\left(\mathbf{P_K^Q}(s),(\mathbf{Q})\right),\mathrm{blkdiag}\left(\mathbf{L},\mathbf{K_f}\right)\right) \end{aligned} \tag{2.43}$$

where $\boldsymbol{p} = \begin{bmatrix}\mathbf{A_Q} & \mathbf{B_Q} & \mathbf{C_Q} & \mathbf{D_Q} & \mathbf{K_f} & \mathbf{L}\end{bmatrix}$. From a multi-models synthesis approach and with slight modifications of the LFR in (2.25) and LFT in Fig. 2.3 using $\mathbf{K}(s,\boldsymbol{p})$ as in (2.43), the synthesis models for different values of $\boldsymbol{\theta} \in \Theta_c$ can be obtained via LFT as illustrated on the right side of Fig. 2.5.

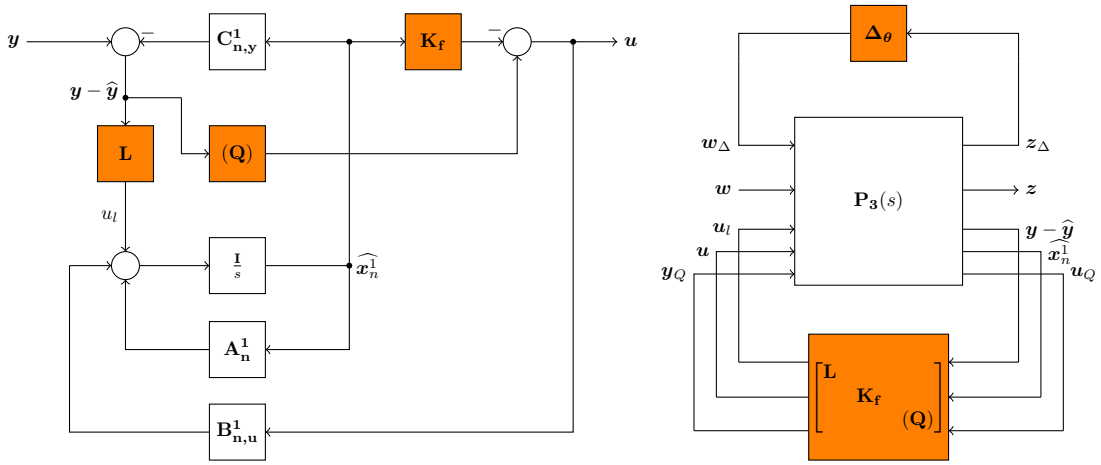

Figure 2.5: *Left*: observer-based controller structure with Youla parameter **Q** augmentation; *Right*: LFT used for structured controller synthesis purposes

2.3.3 Conclusions on the augmented observer-based structure

In this section, the observer-based structure with Youla parameter augmentation has been presented. This structure has been chosen in order to give a physical meaning to the control signals and especially to the controller state. Also, it is expected to simplify the development of gain-scheduled controllers. The Youla dynamic parameter is used to increase the number of decision variables in the optimisation problem resulting from the formulation of control design requirements.

The controller obtained depends on three design parameters $\mathbf{L}$, $\mathbf{K_f}$ and $(\mathbf{Q})$. Using appropriate Linear Fractional Representations, these parameters can be externalized as illustrated in Figs. 2.4 and 2.5. They can then be optimised solving a multi-models multi-requirements optimization problem as presented in 2.2.

In 6.2, Chapter 6 the problem of designing a control law for a flexible launch vehicle against frequency- and time-domain specifications is tackled. The observer-based structure is used and optimized through a multi-models multi-requirements approach.

2.4 Concluding remarks

In this chapter, the structured controller design method proposed in [Apkarian 07, Apkarian 14] has been applied to the robust control of an uncertain linear system. Multiple models obtained for critical values of the vector of uncertainties $\boldsymbol{\theta}$ are considered for synthesis on which multiple frequency-domain requirements are expressed. The resulting optimization problem is then solved using non-smooth optimization-based techniques. In the recent work [Apkarian 15], the same approach is used but where the critical models are determined automatically within the optimization loop. This further reduces the involvement of the designer in the challenging task of determining these critical models.

The observer-based controller structure with a Youla parameter has also been detailed. In the launch vehicle control problem, a reduced-order observer is used upon noticing that the only useful dynamics to be observed is the rigid body dynamics. The proposed controller structure takes this into account. Application to the atmospheric control of the uncertain flexible launch vehicle is considered in Chapter 6 where it is shown that achieving a time-domain constraint on the angle of attack is tedious task when tuning frequency-domain requirements only. This motivates considering an additional output-constraint control technique. Using such *evolutionary* technique, it is possible to use the synthesized structured controller obtained through the synthesis described in this chapter and yet achieve the expected output constraint. This is detailed in the following chapter and in Chapters 4 and 5.

Chapter 3

Introduction to OIST

In this chapter, the Output to Input Saturation Transformation (*OIST*) introduced in [Burlion 12] for non-linear systems is presented. This transformation is used to enforce a time-domain constraint on a considered system output. It proposes to introduce a saturation on a pre-existing control law. Here, a specific class of non-linear minimum phase systems is considered where the state derivative depends linearly on the input. The notion of relative degree is used to derive the expressions of the time-varying saturations to apply to the control.

The required notations and definitions are recalled in 3.1. The motivations for saturating the control signal to enforce an output constraint are identified in 3.2 using a simplified non-linear crane model. The transformation is then formally introduced in 3.3 and applied to the crane control problem in 3.4.

3.1 Notations and definitions

In this section, generic notations and definitions are introduced. Let $\boldsymbol{x} \in \mathbb{R}^n$ and $1 \leq i \leq n$. The partial derivative operator with respect to the i-th element of $\boldsymbol{x}$ is denoted $\partial_i = \frac{\partial}{\partial \boldsymbol{x}_i}$.

Definition 3.1 ($\mathcal{C}^1$-class form)**.**
Let σ a mapping from $\mathbb{R}^n$ to $\mathbb{R}$. It is said to be of class $\mathcal{C}^1$ if $\forall i \in \mathbb{N}^\star$ s.t. $i \leq n$, $\partial_i \sigma$ exists and is continuous.

In the following, the notation $\sigma \in \mathcal{C}^1(\mathbb{R}^n, \mathbb{R})$ for a $\mathcal{C}^1$ form is used.

Definition 3.2 ($\mathcal{C}^k$-class mapping)**.**
Let $\boldsymbol{f}$ a mapping from $\mathbb{R}^n$ to $\mathbb{R}^m$ and $k \geq 1$. It is said to be of class $\mathcal{C}^k$ if $\forall (i,j) \in \mathbb{N}^\star \times \mathbb{N}^\star$ s.t. $i \leq m$, $j \leq k$, $\mathrm{d}^j \boldsymbol{f}_i$ exists and is continuous, where d denotes the differential operator. In case this is true for any $k \geq 1$, $\boldsymbol{f}$ belongs to $\mathcal{C}^\infty(\mathbb{R}^n, \mathbb{R}^m)$.

Let now introduce the definition of the Lie derivative.

Definition 3.3 (Lie derivative of a $\mathcal{C}^1$ form)**.**
Given $\sigma \in \mathcal{C}^1(\mathbb{R}^n, \mathbb{R})$ and $\boldsymbol{f} \in \mathcal{C}^\infty(\mathbb{R}^n, \mathbb{R}^n)$, the Lie derivative of σ in the direction of $\boldsymbol{f}$ is denoted $\mathcal{L}_{\boldsymbol{f}}\sigma$ and is defined by

$$\mathcal{L}_{\boldsymbol{f}}\sigma = \sum_{i=1}^{n} \boldsymbol{f}_i \partial_i \sigma$$

The definition of the Lie derivative is used to define the relative degree of a variable with respect to the input of a dynamic non-linear system.

Definition 3.4 (Relative degree)**.**
Let consider the following non-linear dynamics

$$\dot{\boldsymbol{x}} = \boldsymbol{f}(\boldsymbol{x}) + \boldsymbol{g}(\boldsymbol{x})u$$

where $\boldsymbol{x} \in \mathbb{R}^n$, $u \in \mathbb{R}$ and $(\boldsymbol{f}, \boldsymbol{g}) \in \mathcal{C}^\infty(\mathbb{R}^n, \mathbb{R}^n)$. Let $\alpha = \sigma(\boldsymbol{x})$ where $\sigma \in \mathcal{C}^k(\mathbb{R}^n, \mathbb{R})$ with $k \in \mathbb{Z}_+^\star$. The variable α is said to be of relative degree k with respect to u if $\forall \boldsymbol{x} \in \mathbb{R}^n$, $\forall i \in \mathbb{Z}_+$ s.t. $1 < i \leq k$,

$$\mathcal{L}_{\boldsymbol{g}}\mathcal{L}_{\boldsymbol{f}}^{k-i}\sigma(\boldsymbol{x}) = 0 \text{ and } \mathcal{L}_{\boldsymbol{g}}\mathcal{L}_{\boldsymbol{f}}^{k-1}\sigma(\boldsymbol{x}) \neq 0$$

The set of intervals of $\mathbb{R}$ is denoted $\mathcal{I}(\mathbb{R})$.

3.2 Motivations for a new approach to output-constrained control

The control of dynamic systems under constraints is a challenging task. Constraints may be expressed in the frequency- or time-domain on the system inputs, state or outputs. In this chapter and section, light is shed on the output-constrained control problem. More specifically, to ensure a non-linear system remains in a nominal operating mode, it may be necessary to ensure that some of its outputs remain in a given interval over time.

Example 3.5. In the ball-and-beam example, the nominal operating mode is characterized by the ball rolling on the beam. If one measures the position of the ball on the beam, a reasonable output constraint to remain in this operating mode is to ensure the ball position belongs to the interval defined by the beam length. ♣

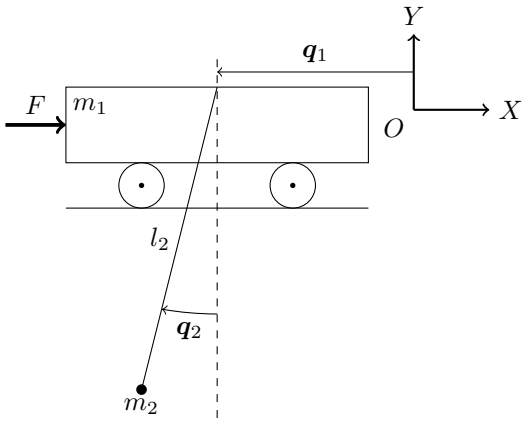

Figure 3.1: Simplified crane viewed as a pendulum on a cart.

In this section, an example is introduced in 3.2.1 to highlight the necessity to introduce such constraints in some control problems. A review of the state of the art of state- and output-constrained control is presented in 3.2.2. Finally, reasons for proposing a new approach to handle such constraints are detailed in 3.2.3.

3.2.1 An example: non-linear crane control

A simple non-linear crane model is considered in this section. This illustrates the motivations of designing new approaches to consider output constraints. The crane model and notations are inspired from the cart-pole examples in [Olfati-Saber 01, Section 5.4, p. 136] and [Spong 96].

Equations of motion The considered system is represented in Fig. 3.1. The notations and their numerical values are recorded in Table 3.1.

Notation	Description	Numerical value
$(O; X, Y)$	Inertial frame of reference	-
m_1	Cart mass	0.5 kg
m_2	Pendulum mass	0.4 kg
l_2	Pendulum length (center of mass)	0.6 m
I_2	Pendulum mass moment of inertia	0.006 kg.m^2
$\boldsymbol{q}_1$	Cart position abscissa	$q_1(0) = -10$ m
$\boldsymbol{q}_2$	Pendulum angle	$q_2(0) = 0$
F	External force to set the cart in motion	-

Table 3.1: Description of the notations in Fig. 3.1 and numerical values used in simulation.

The mass of the pendulum is supposed to be located in one point. A no-slip hypothesis is also made. It is supposed that the whole state is measured (positions and velocities). Using the laws of motion, the following relations are obtained, where $(\mathbf{G})$ denotes the system:

$$(\mathbf{G}) \begin{cases} (m_1 + m_2)\,\ddot{\boldsymbol{q}}_1 + m_2 l_2 \cos(\boldsymbol{q}_2)\ddot{\boldsymbol{q}}_2 - m_2 l_2 \sin(\boldsymbol{q}_2)\dot{\boldsymbol{q}}_2^2 &= F \\ m_2 l_2 \cos(\boldsymbol{q}_2)\ddot{\boldsymbol{q}}_1 + \left(I_2 + m_2 l_2^2\right)\ddot{\boldsymbol{q}}_2 + m_2 g l_2 \sin(\boldsymbol{q}_2) &= 0 \end{cases} \tag{3.1}$$

Using results in [Olfati-Saber 01, Section A.5, p. 291], the crane system inertia matrix

$$\mathbf{M} = \begin{bmatrix} \mathbf{M}_{11} & \mathbf{M}_{12}(q_2) \\ \mathbf{M}_{12}(q_2) & \mathbf{M}_{22} \end{bmatrix}$$

components are given by

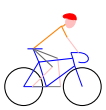

$$\begin{aligned} \mathbf{M}_{11} &= m_1 + m_2 \\ \mathbf{M}_{12}(\boldsymbol{q}_2) &= m_2 l_2 \cos(\boldsymbol{q}_2) \\ \mathbf{M}_{22} &= m_2 l_2^2 + I_2 \end{aligned} \tag{3.2}$$

The inertia matrix only depends on $\boldsymbol{q}_2$, hence $\boldsymbol{q}_1$ is said to be the external variable and $\boldsymbol{q}_2$ the shape variable of the system. This allows to rewrite (3.1) in the following form

$$(\mathbf{G}) \begin{cases} \mathbf{M}_{11}\ddot{\boldsymbol{q}}_1 + \mathbf{M}_{12}(\boldsymbol{q}_2)\ddot{\boldsymbol{q}}_2 + h_1(\boldsymbol{q}, \dot{\boldsymbol{q}}) &= F \\ \mathbf{M}_{12}(\boldsymbol{q}_2)\ddot{\boldsymbol{q}}_1 + \mathbf{M}_{22}\ddot{\boldsymbol{q}}_2 + h_2(\boldsymbol{q}, \dot{\boldsymbol{q}}) &= 0 \end{cases} \tag{3.3}$$

where $\boldsymbol{q} = \begin{bmatrix} \boldsymbol{q}_1 & \boldsymbol{q}_2 \end{bmatrix}^\top$ is called the vector of generalized coordinates and

$$\begin{aligned} h_1(\boldsymbol{q}, \dot{\boldsymbol{q}}) &= -m_2 l_2 \sin(\boldsymbol{q}_2)\dot{\boldsymbol{q}}_2^2 \\ h_2(\boldsymbol{q}, \dot{\boldsymbol{q}}) &= m_2 g l_2 \sin(\boldsymbol{q}_2) \end{aligned} \tag{3.4}$$

Partial feedback linearization Using a similar approach to [Chung 95, Spong 96], a partial feedback linearization is now performed using adequate rewriting of (3.3). Let consider the following partially linearizing feedback law

$$F = \left(\mathbf{M}_{11} - \frac{\mathbf{M}_{12}(\boldsymbol{q}_2)^2}{\mathbf{M}_{22}} \right) u - \frac{\mathbf{M}_{12}(\boldsymbol{q}_2)}{\mathbf{M}_{22}} h_2(\boldsymbol{q}, \dot{\boldsymbol{q}}) + h_1(\boldsymbol{q}, \dot{\boldsymbol{q}}) \tag{3.5}$$

where u is the new control input. Using this feedback law, the dynamics in (3.3) may be rewritten in the following form [Spong 96]:

$$(\mathbf{G_l}) \begin{cases} \dot{\boldsymbol{q}}_1 &= \boldsymbol{p}_1 \\ \dot{\boldsymbol{p}}_1 &= u \\ \dot{\boldsymbol{q}}_2 &= \boldsymbol{p}_2 \\ \dot{\boldsymbol{p}}_2 &= -\gamma_1 \sin(\boldsymbol{q}_2) - \gamma_2 \cos(\boldsymbol{q}_2) u \end{cases} \tag{3.6}$$

where $\gamma_1 = \frac{m_2 l_2 g}{I_2 + m_2 l_2^2}$ and $\gamma_2 = \frac{m_2 l_2}{I_2 + m_2 l_2^2}$. In the existing literature [Chung 95, Spong 96], this form is used to design a control law $u(\boldsymbol{q}, \dot{\boldsymbol{q}})$.

Considered nominal control law The typical case study suggested in [Burlion 12] supposes that a control law – which will be called *nominal* – has already been designed and stabilizes the studied system. In this section, the nominal control law is introduced on the partially linearized form in (3.6). The following control law is considered:

$$u = -k_1 \boldsymbol{q}_1 - k_2 \boldsymbol{p}_1 + k_3 \cos(\boldsymbol{q}_2) \boldsymbol{p}_2 \tag{3.7}$$

where the parameters k_i, $i \in [1 \dots 3]$ are positive real numbers and are set to the following values for simulations:

$$k_1 = 0.25,\ k_2 = 1,\ k_3 = 1 \tag{3.8}$$

The control law in (3.7) is a slight adaptation of the control laws used in [Chung 95, Spong 96] to stabilize an unstable cart-pole system to the origin. In [Chung 95], local exponential stability is proved as well as convergence of the system energy to some fixed design value. The purpose being illustrative only, these results are not detailed here.

Note that more complex control strategies could be figured out using approaches in [Spong 96, Olfati-Saber 01]. This is not covered here since a simple control strategy is convenient enough to illustrate the new proposed approach to output-constrained control.

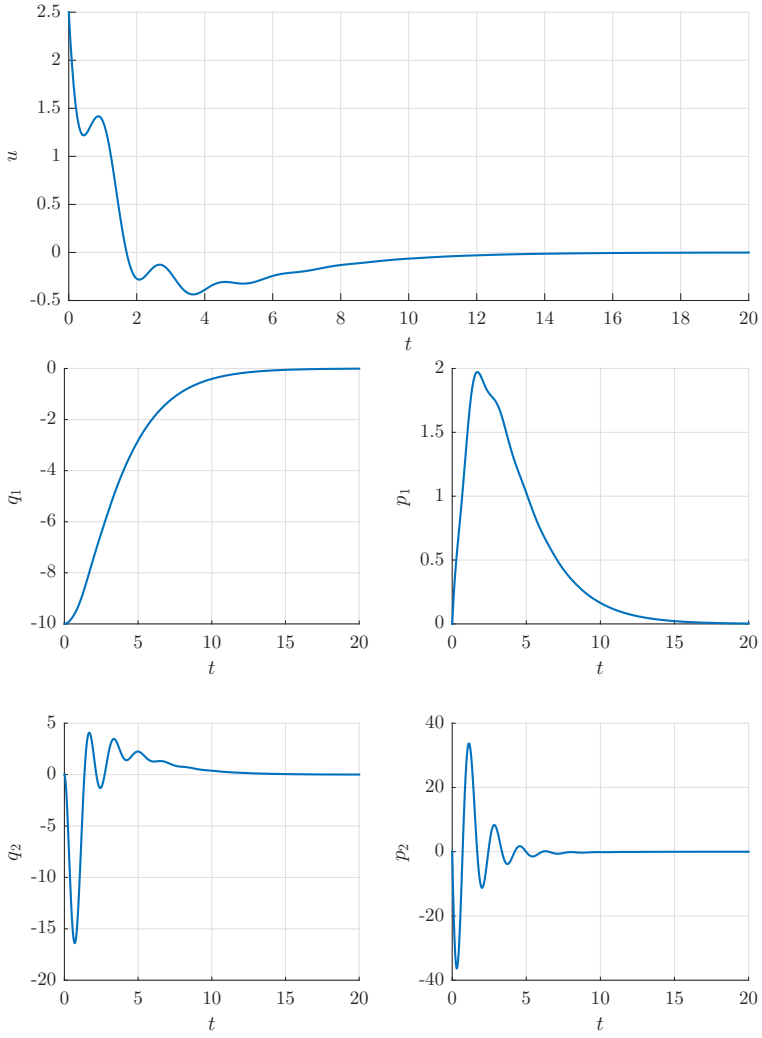

Figure 3.2: non-linear crane model simulation results using the *nominal* control law. *Top*: nominal control law, see (3.7); *Bottom*: ($\mathbf{G_l}$) state, see (3.6).

Simulation results The system ($\mathbf{G_l}$) in (3.6) is now simulated in closed-loop with the control law proposed in (3.7). The numerical values are given in Table 3.1 and (3.8). The initial condition is set to $(\boldsymbol{q}_1, \boldsymbol{p}_1, \boldsymbol{q}_2, \boldsymbol{p}_2) = \begin{bmatrix} -10 & 0 & 0 & 0 \end{bmatrix}$ and the system is simulated over 20s. The simulation results are shown in Fig. 3.2. It can be observed that the control law stabilizes the system to the origin. The oscillations of the pendulum may however be considered important with a maximum angle of 15°. It may be off-specifications for some applications for example if the load is an open tank containing a fluid.

Introducing an output constraint Considering the crane control example, control law design specifications may require to limit the reachable set of a system output. This can be formulated as a time-domain constraint on the considered output which will be denoted $\alpha = \sigma(\boldsymbol{x}) \in \mathbb{R}$. Examples of such constraints have been represented in Fig. 3.3:

- in the top figure, a time-invariant constraint is set on $\alpha = \boldsymbol{p}_1$ which corresponds to a speed limit profile. Mathematically speaking, the following should be ensured:

$$0 \leq \alpha = \sigma(x) = \boldsymbol{p}_1 \leq \overline{\boldsymbol{p}_1}, \, \forall t$$

  where $\overline{\boldsymbol{p}_1}$ describes the maximum allowable speed. This constrains the maximum allowable speed of the cart;

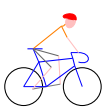

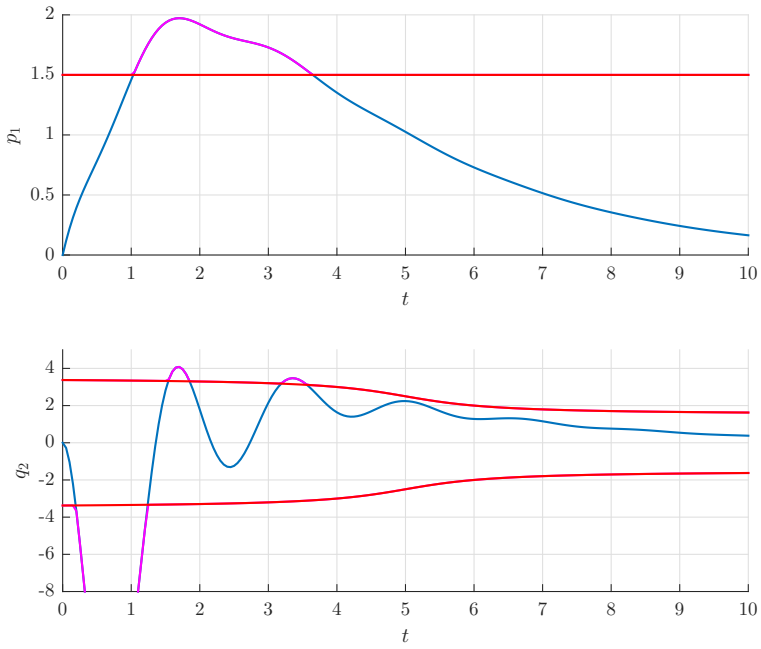

Figure 3.3: Illustration of the type of considered constraints (in red). Signals values violating the constraint are represented in magenta.

- in the bottom figure, a time-varying constraint is set on $\alpha = \boldsymbol{q}_2$. Mathematically speaking, the following should be ensured:

$$\underline{\boldsymbol{q}_2}(t) \leq \alpha = \sigma(x) = \boldsymbol{q}_2 \leq \overline{\boldsymbol{q}_2}(t), \forall t$$

  where $\underline{\boldsymbol{q}_2}(t)$ and $\overline{\boldsymbol{q}_2}(t)$ describe the bounds set on $\boldsymbol{q}_2$. This constrains the pendulum admissible inclinations.

Other constraints on other variables could also be imagined. Note that in these examples, the output constraint is also a state constraint. Using the control law in (3.7), the constraints informally specified in Fig. 3.3 are violated as simulation shows. Still informally, three control philosophies can be considered to achieve satisfaction of the considered time-domain constraints:

- *Cautious*: modify the control law so as not to reach the constraints;
- *Evolutionary*: keep the already designed control law and use an additional signal to compensate for the overly demanding control signal in case the constraints are violated;
- *Tactical*: design a new control law using techniques which handle time-domain constraints;

A more formal state of the art is now presented to review the existing techniques which take state or output constraints into account.

3.2.2 State of the art of output-constrained control

Because of their direct influence on the closed-loop stability, input constraints are a well-studied subject in control theory. Also, non-linear constraints like input saturations are often faithful representations of real-world phenomena which must be considered when designing a control law. This is for example the case of planes elevators which tilt is limited due to physical constraints. Different strategies have been considered to account for such constraints in the control design. In [Goodwin 01, Rojas 02, De Dona 02], the authors classified the possible strategies in three major categories:

- *Cautious* strategies which consist in designing the control law such that the constraints are not triggered.

  Example 3.6. In the saturated control case, a *cautious* control law is designed such that the saturations are never reached. ♣

  Despite being easy to implement, such strategies often result in a loss of control performance and efficiency, the control law not being allowed to linger on the saturation;

- *Evolutionary*[1] approaches which are based on a control law violating the constraints but which bring additional information to mitigate the consequences of this violation.

  Example 3.7. In the saturated control case, an example of an *evolutionary* approach is the anti-windup design which consists in augmenting the controller dynamics whenever the saturations are met. ♣

  Such strategies are harder to implement but have been widely studied in the literature during the past few years due to their practical interest;

- *Tactical* strategies which consider the constraints in the design of the control law. They are tightly related to the optimisation field.

  Example 3.8. In the saturated control case, a *tactical* strategy would minimize some performance criteria (e.g. the steady-state tracking error) subject to the presence of saturations on the actuators. ♣

  Such strategies are widely documented but are in general more complex to use than the other strategies.

As far as the output-constrained problem is concerned, the same families of strategies can be identified. In [Gilbert 91, Rojas 02] the relationship between a constrained output and an induced constrained input was studied in the case of known discretized linear systems. Consequently, a time-domain constraint on an output can be achieved by acting on the control input using the aforementioned approaches.

Cautious strategies Such strategies include the so-called low-gain control strategy presented in [Lin 93] in the linear framework. Since global asymptotic stability cannot be obtained in non-degenerated cases whatever the control, the authors propose to achieve semi-global exponential stability only. The existence of control feedbacks achieving this type of stability is then shown. As already mentioned however, such approaches can lead to control laws showing poor performance.

Evolutionary strategies Anti-windup design for saturated systems is the most representative example of such evolutionary strategies. The presence of saturations is a well-tackled problem in linear control design since a saturated control law may induce divergence of the loop. Recovering from such a degraded situation is fanciful in most cases without additional tools to avoid divergence. An overview of anti-windup techniques and remaining challenges is proposed in [Tarbouriech 09] while modern anti-windup synthesis is extensively covered in [Zaccarian 01]. An LMI-based approach is presented in [Grimm 03] for both analysis and synthesis of the anti-windup closed-loop. In the case of non-linear systems, the literature is less abundant, as also underlined in [Tarbouriech 09]. In the case of the specific class of Euler-Lagrange systems, an anti-windup scheme is proposed in [Morabito 04]. A more general approach is presented in [Teo 09] where the authors propose to use gradient projection to modify the controller update law whenever a constraint is active on the control.

The anti-windup design has also been used to enforce state and output constraints through its action on the control input. In [Rojas 02], a limiting circuit with a predicting stage is introduced between the controller output and the control input. A saturation and non-linear

[1] The term has nothing to do with the class of evolutionary algorithms in optimisation. Aside note: the use of such algorithms in control would rather fit in a *tactical* approach.

mapping function are used to compute an allowed control action whenever the state-constraint is violated. In [Turner 02], an output violation compensator is used in an additional feedback loop to satisfy the output constraint as far as possible. LMI-based theorems inspired from the existing anti-windup synthesis literature are also proposed. However, the use of anti-windup in the state/output-constrained case does not offer guarantees to the effective satisfaction of the constraints.

In the case of non-linear tracking systems, reference governors can be considered [Gilbert 02]. The basic idea is to modify the tracking reference so as to satisfy the state constraints whenever getting near the boundary of the admissible set.

The approach proposed in [Burlion 12] and presented in this chapter for non-linear systems is of the *evolutionary* type. It is based on the transformation of an output constraint into saturations on the control input using information on the output relative degree with respect to the control input. It was applied to a sub-problem of the image-based automatic landing of an UAV[2] in [Burlion 13]. The authors used the technique to maintain points of interest in the camera field of view during the approach and landing phases of the UAV. Reformulation in the linear case with a closed-loop stability proof was performed in [Chambon 15c] and [Chambon b] and is presented in Chapter 4. An extension of OIST to account for uncertainties and incomplete state measurements is proposed in Chapter 5.

Tactical strategies This family of strategies is closely related to optimal control problems. In [De Dona 02], a distinction is made between fixed horizon optimal control and receding horizon optimal control, also called model predictive control (MPC). Fixed horizon approaches are not very robust to unmodelled events while receding horizon ones are more robust by dynamically determining the optimal control over a finite amount of time. The underlying optimisation problem can consider constraints on the state and outputs of the system. The MPC research field has been very active in the last years in the non-linear world also [Findeisen 07] and real world applications are already reported [Qin 03]. These methods can however be heavier to implement than anti-windup.

A more exotic approach is presented in [Tee 09] for non-linear SISO systems in strict feedback form. The authors use a specific type of Lyapunov functions, called Barrier Lyapunov functions, which have the property to grow towards infinity when the system state approaches a pre-defined set of finite values. This helps to design a control law enforcing state constraints.

For linear systems, other tactical approaches exist like iterative feedback tuning [Gevers 02] or simulation-based non-smooth optimisation [Apkarian 11]. They optimise the controller performance under state or output constraints. Fulfilment of the constraints is checked using time-domain response with respect to a class of input and/or disturbance signals. Like the anti-windup approach, such strategies do not offer certificates on the actual satisfaction of the considered time-domain constraints for any type of input signal.

3.2.3 A new approach to the output-constrained control problem

The crane control problem presented in 3.2.1 illustrated that, given a control law, additional time-domain constraints considered later in the synthesis may not be achieved. From an application point of view, this may occur when the control law is designed according to some specifications which are later updated or which are prioritized in the control design.

This motivates using either a *cautious* or *evolutionary* strategy to refine the control law actually used. A study of the available literature on constrained control in 3.2.2 has shown that *cautious* strategies can lead to degraded performance in comparison with *evolutionary* approaches. As far as *evolutionary* strategies are concerned, a big proportion of the literature is dedicated to linear systems. Also, there does not seem to exist approaches which certifies that the time-domain constraint will actually be satisfied whatever the input or disturbance signals.

This motivates the work in [Burlion 12]. A new *evolutionary* approach is proposed to the output-constrained problem of non-linear systems.

[2] Unmanned Aerial Vehicle

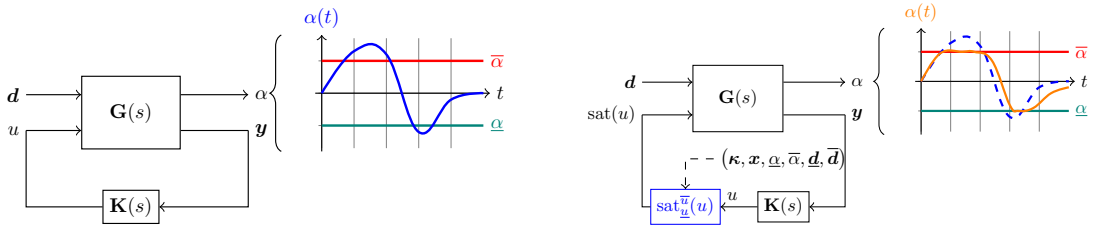

Figure 3.4: Informal illustration of the OIST *evolutionary* strategy. *Left*: nominal controller (no OIST); *Right*: with OIST saturations in the loop, the constraint is satisfied (in orange).

3.3 Output to input saturation transformation

In this section, the new approach proposed in [Burlion 12] to enforce an output constraint is presented in the non-linear case. This approach is called *Output to Input Saturation Transformation* and will be referred to using the acronym *OIST*.

The approach belongs to the class of *evolutionary* strategies [Goodwin 01]. A control law is used to enforce specific properties on the unconstrained closed-loop. Whenever the output constraint is violated, saturations are activated on the control input as illustrated in Fig. 3.4. This is an attempt to retrieve in the non-linear framework a relationship between a constrained output and a constrained input as unveiled in [Gilbert 91].

3.3.1 Considered class of non-linear systems and constraints

Let consider the following single-input continuous-time non-linear system:

$$(\mathbf{G}) \begin{cases} \dot{\boldsymbol{x}} &= \boldsymbol{f}(\boldsymbol{x}) + \boldsymbol{g}(\boldsymbol{x})u \\ \boldsymbol{y} &= \boldsymbol{x} \\ \boldsymbol{x}(0) &= \boldsymbol{x}_0 \end{cases} \tag{3.9}$$

where $\boldsymbol{x} \in \mathbb{R}^n$, $u \in \mathbb{R}$ and $(\boldsymbol{f}, \boldsymbol{g}) \in \mathcal{C}^\infty(\mathbb{R}^n, \mathbb{R}^n) \times \mathcal{C}^\infty(\mathbb{R}^n, \mathbb{R}^n)$. The crane model used in 3.2 belongs to this class of non-linear models since its partially linearized dynamics in (3.6) can easily be expressed in the form of (3.9). Another example of such model is the basic flight combat aircraft model considered in [Burlion 12].

Considering the control of the system in (3.9), the design of an appropriate control signal u is subject to fulfilling specific objectives. Local stability, time-response performance or overshoot limitation are examples of constraints the control should satisfy. In [Burlion 12], an additional type of constraint, generically called *output constraint* and denoted $\mathcal{K}$ is introduced:

Definition 3.9 (Output constraint)**.**
Let denote $\alpha := \sigma(\boldsymbol{x})$ the considered system output where $\sigma \in \mathcal{C}^k(\mathbb{R}^n, \mathbb{R})$[a]. Let $\Omega_\alpha(t) = [\underline{\alpha}(t), \overline{\alpha}(t)] \in \mathcal{I}(\mathbb{R})$ where $\underline{\alpha}(t)$ and $\overline{\alpha}(t)$ are sufficiently smooth[b] time-varying unidimensional signals satisfying

$$\underline{\alpha}(t) < \overline{\alpha}(t),\ \forall t \in \mathbb{R}_+$$

The considered output α is said to satisfy the constraint $\mathcal{K}(\Omega_\alpha)$ if

$$\alpha(t) \in \Omega_\alpha(t),\ \forall t \in \mathbb{R}_+$$

[a] The integer k is the relative degree with respect to u, see Assumption 3.13.
[b] This notion will be specified later on.

Further, the system in (3.9) is supposed to be minimum phase [Isidori 95]. This allows to state global results as far as stability in the presence of saturations is concerned. The non-minimum-phase case is discussed in 3.3.5.

Assumption 3.10 (Minimum-phase system)**.**
The non-linear system

$$\begin{cases} \dot{\boldsymbol{x}} &= \boldsymbol{f}(\boldsymbol{x}) + \boldsymbol{g}(\boldsymbol{x})u \\ \alpha &= \sigma(\boldsymbol{x}) \end{cases}$$

is supposed to be minimum-phase.

The definition of *nominal control law* is now introduced. The concept of nominality is used to remain coherent with its interpretation in the saturated control case. Hence, the notion refers to the control law applied when the output constraint is satisfied.

Definition 3.11 (Nominal control law)**.**
The control law $u(\boldsymbol{y})$ is said to be nominal if it achieves the desired control design objectives (including closed-loop stability) to the exception of $\mathcal{K}(\Omega_\alpha)$. In other words, there may exist $t \in \mathbb{R}_+$ s.t.

$$\alpha(t) = \sigma(\boldsymbol{x}) \notin \Omega_\alpha(t)$$

The values taken by the output signal α using the nominal control law are not certified to belong to the interval Ω_α at all times. This motivates developing an *evolutionary* approach to enforce the time-domain constraint while keeping the considered nominal control law.

3.3.2 Output constraint to input saturation problem formulation

In [Burlion 12], it is proposed to enforce an output constraint as described in Definition 3.9 by introducing time-varying saturations on the system input signal u. The idea is to constrain the set of admissible control signal values to consequently restrict the resulting set of output signal values. The problem of finding the adequate saturations is now formally introduced.

Problem 3.12 (Output constraint to input saturation problem)**.**
Let consider system (**G**) in (3.9) with $\alpha = \sigma(\boldsymbol{x}) \in \mathbb{R}$ the constrained output. Let $\mathcal{K}(\Omega_\alpha)$ a time-domain constraint and u a known nominal control law. Design two signals $\underline{u}$ and $\overline{u}$ such that the closed-loop

$$\begin{cases} \dot{\boldsymbol{x}} &= \boldsymbol{f}(\boldsymbol{x}) + \boldsymbol{g}(\boldsymbol{x})u \\ \boldsymbol{y} &= \boldsymbol{x} \\ \boldsymbol{x}(0) &= \boldsymbol{x}_0 \\ \alpha &= \sigma(\boldsymbol{x}) \\ u &\in \left[\underline{u}\left(\boldsymbol{x}, \Omega_\alpha(t), \dot{\Omega}_\alpha(t), \ldots\right), \overline{u}\left(\boldsymbol{x}, \Omega_\alpha(t), \dot{\Omega}_\alpha(t), \ldots\right)\right] \end{cases} \tag{3.10}$$

satisfies $\mathcal{K}(\Omega_\alpha)$, i.e.

$$\alpha(t) \in \Omega_\alpha(t),\ \forall t \in \mathbb{R}_+$$

The *transformation* of the output constraint $\mathcal{K}(\Omega_\alpha)$ into saturations $(\underline{u}, \overline{u})$ fulfilling the constraint relies on the knowledge of the system dynamics, the expected bounds $\Omega_\alpha(t)$ and the form σ. Such transformation is now proposed.

3.3.3 Proposed transformation (OIST)

The ability to derive control saturations from a constraint impacting an output clearly depends on how this output variable depends on the control input. In the following, such dependence is ensured by making an assumption on the relative degree of α with respect to u.

Assumption 3.13 (Assumption on the relative degree of α wrt. u)**.**
The constrained output $\alpha = \sigma(\boldsymbol{x})$ with $\sigma \in \mathcal{C}^k(\mathbb{R}^n, \mathbb{R})$ is supposed to be of relative degree $k \in \mathbb{Z}_+^\star$ with respect to the control input u.

Hence, according to Definition 3.4, the k-th differential of $\alpha = \sigma(\boldsymbol{x})$ is given by

$$\alpha^{(k)}(t) = \mathcal{L}_{\boldsymbol{f}}^k \sigma(\boldsymbol{x}) + \mathcal{L}_{\boldsymbol{g}} \mathcal{L}_{\boldsymbol{f}}^{k-1} \sigma(\boldsymbol{x}) u \tag{3.11}$$

where $\mathcal{L}_{\boldsymbol{g}} \mathcal{L}_{\boldsymbol{f}}^{k-1} \sigma(\boldsymbol{x}) \neq 0$, $\forall \boldsymbol{x} \in \mathbb{R}^n$. This dependence in u of the k-th differential of α will be used to derive the expressions of the saturations to apply to the control input. Prior to this, a new definition is introduced to pave the way for a constructive lemma which will be used to obtain those expressions.

Definition 3.14 (Propagated bounds)**.**
Let $\boldsymbol{\kappa} = \begin{bmatrix} \kappa_1 & \dots & \kappa_k \end{bmatrix} \in \mathbb{R}_+^k$ a vector of positive constants and let suppose the output constraint bounds $(\underline{\alpha}(t), \overline{\alpha}(t))$ are functions of $\mathcal{C}^k(\mathbb{R}_+, \mathbb{R})$. Let define $\underline{\alpha}_0(t) = \underline{\alpha}(t)$, $\overline{\alpha}_0(t) = \overline{\alpha}(t)$ and, $\forall i \in \mathbb{N}^\star$ s.t. $i \leq k$:

$$\begin{aligned} \underline{\alpha}_i(t) &= \kappa_i \left(\underline{\alpha}_{i-1}(t) - \alpha^{(i-1)}(t) \right) + \dot{\underline{\alpha}}_{i-1}(t) \\ \overline{\alpha}_i(t) &= \kappa_i \left(\overline{\alpha}_{i-1}(t) - \alpha^{(i-1)}(t) \right) + \dot{\overline{\alpha}}_{i-1}(t) \end{aligned} \tag{3.12}$$

These are called *propagated bounds* in the sense they propagate the expected bounds $\underline{\alpha}(t)$ and $\overline{\alpha}(t)$ up to the k-th differential of α.

The coefficients in $\boldsymbol{\kappa}$ are degrees of freedom which selection is discussed later. Prior to using the propagated bounds to achieve the time-domain constraint, it is required that the considered output signal α derivatives initially satisfy these bounds:

Assumption 3.15 (Assumption on the initial satisfaction of the propagated bounds)**.**
It is assumed that

$$\forall i \in \mathbb{N} \text{ s.t. } i \leq k,\ \alpha^{(i)}(0) \in \Omega_\alpha^i(0)$$

where $\Omega_\alpha^i(t) = \left[\underline{\alpha}_i(t), \overline{\alpha}_i(t) \right]$, $\forall t$.

The definition of propagated bounds is used in the following lemma which is the true backbone of the transformation:

Lemma 3.16 (Propagated bounds lemma)**.**
Let suppose Assumptions 3.13 and 3.15 are satisfied. Let define propagated bounds as in Definition 3.14, $\forall i \in \mathbb{N}$ s.t. $i \leq k$. Then,

$$\alpha^{(k)}(t) \in [\underline{\alpha}_k(t), \overline{\alpha}_k(t)] = \Omega_\alpha^k(t),\ \forall t \in \mathbb{R}_+ \Rightarrow \alpha(t) \in [\underline{\alpha}(t), \overline{\alpha}(t)] = \Omega_\alpha(t),\ \forall t \in \mathbb{R}_+$$

Proof. The proof is performed iteratively for a fixed k. Let j such that $1 \leq j \leq k$. Suppose that $\alpha^{(k)}(t) \in \left[\underline{\alpha}_k(t), \overline{\alpha}_k(t) \right]$, $\forall t \Rightarrow \alpha^{(j)}(t) \in \left[\underline{\alpha}_j(t), \overline{\alpha}_j(t) \right]$, $\forall t$ where the propagated bounds are defined as in Definition 3.14. It is also supposed that Assumption 3.15 is satisfied. Only the lower bound is considered. The demonstration is similar in the upper bound case. Suppose

$$\exists t_2 > 0,\ \alpha^{(j-1)}(t_2) < \underline{\alpha}_{j-1}(t_2) \tag{3.13}$$

then, since $\alpha^{(j-1)}(0) \in \Omega_\alpha^{j-1}(0)$ and, by continuity of $\alpha^{(j-1)}$ and $\underline{\alpha}_{j-1}$

$$\exists t_1,\ 0 < t_1 < t_2,\ \begin{cases} & \alpha^{(j-1)}(t_1) = \underline{\alpha}_{j-1}(t_1) \\ \forall t \in [t_1, t_2], & \alpha^{(j-1)}(t) \leq \underline{\alpha}_{j-1}(t) \end{cases} \tag{3.14}$$

But, using the recurrence hypothesis, the definition of $\underline{\alpha}_j(t)$ and the fact that $\forall t$, $\kappa_j(t) \geq 0$, one obtains, $\forall t \in [t_1, t_2]$,

$$\begin{aligned} \alpha^{(j)}(t) &\geq \underline{\alpha}_j(t) \\ &\geq \kappa_j(t)\left(\underline{\alpha}_{j-1}(t) - \alpha^{(j-1)}(t)\right) + \dot{\widehat{\underline{\alpha}_{j-1}}}(t) \\ &\geq \dot{\widehat{\underline{\alpha}_{j-1}}}(t) \end{aligned} \tag{3.15}$$

hence, using the property of integrals,

$$\begin{aligned} \int_{t_1}^{t_2} \alpha^{(j)}(\lambda)\mathrm{d}\lambda &\geq \int_{t_1}^{t_2} \dot{\widehat{\underline{\alpha}_{j-1}}}(\lambda)\mathrm{d}\lambda \\ \alpha^{(j-1)}(t_2) - \alpha^{(j-1)}(t_1) &\geq \underline{\alpha}_{j-1}(t_2) - \underline{\alpha}_{j-1}(t_1) \end{aligned} \tag{3.16}$$

which contradicts (3.13). In other words

$$\forall t > 0,\ \alpha^{(j-1)}(t) \geq \underline{\alpha}_{j-1}(t) \tag{3.17}$$

which proves the lemma, by recursion. □

Hence, by enforcing constraints on the k-th differential of α, which depends on the control input u as shown in (3.11), the constraint $\mathcal{K}(\Omega_\alpha)$ can be enforced. Supposing that $\mathcal{L}_{\boldsymbol{g}}\mathcal{L}_{\boldsymbol{f}}^{k-1}\sigma(\boldsymbol{x}) > 0$, $\forall \boldsymbol{x}$, the k-th propagated bound expression is then used to derive saturations on u, using (3.11) and Lemma 3.16:

$$\underline{u}(\boldsymbol{x}) = \frac{\underline{\alpha}_k(t) - \mathcal{L}_{\boldsymbol{f}}^k\sigma(\boldsymbol{x})}{\mathcal{L}_{\boldsymbol{g}}\mathcal{L}_{\boldsymbol{f}}^{k-1}\sigma(\boldsymbol{x})},\ \overline{u}(\boldsymbol{x}) = \frac{\overline{\alpha}_k(t) - \mathcal{L}_{\boldsymbol{f}}^k\sigma(\boldsymbol{x})}{\mathcal{L}_{\boldsymbol{g}}\mathcal{L}_{\boldsymbol{f}}^{k-1}\sigma(\boldsymbol{x})} \tag{3.18}$$

where $\mathcal{L}_{\boldsymbol{g}}\mathcal{L}_{\boldsymbol{f}}^{k-1}\sigma(\boldsymbol{x})$ is certified to be non-null by Definition 3.4.

Remark 3.17. In case $\mathcal{L}_{\boldsymbol{g}}\mathcal{L}_{\boldsymbol{f}}^{k-1}\sigma(\boldsymbol{x}) < 0$, $\forall \boldsymbol{x}$ then the expressions of $\underline{u}$ and $\overline{u}$ are exchanged in (3.18). ◇

Remark 3.18. In case $k = 0$ and supposing α can be expressed as $\alpha(t) = \sigma(\boldsymbol{x}) + \sigma_u(\boldsymbol{x})u$ with $\sigma_u(\boldsymbol{x}) > 0$, $\forall \boldsymbol{x}$ and $\alpha(0) \in \Omega_\alpha(0)$ then applying the transformation gives

$$\underline{u}(\boldsymbol{x}) = \frac{\underline{\alpha}(t) - \sigma(\boldsymbol{x})}{\sigma_u(\boldsymbol{x})},\ \overline{u}(\boldsymbol{x}) = \frac{\overline{\alpha}(t) - \sigma(\boldsymbol{x})}{\sigma_u(\boldsymbol{x})} \tag{3.19}$$

In case $\sigma_u(\boldsymbol{x}) < 0$, $\forall \boldsymbol{x}$ then Remark 3.17 applies. ◇

3.3.4 A solution to the output-constrained problem using OIST

In the previous section, a transformation of the output constraint into input saturations has been performed. The notion of propagated bounds in Definition 3.14 introduces design parameters $\boldsymbol{\kappa}$ which selection is however not detailed. In this section, this parameters selection is commented. Also, a solution to Problem 3.12 using OIST is formally stated.

First, the notion of *overlapping signals* used later in the chapter is introduced.

Definition 3.19 (Overlapping signals)**.**
Two unidimensional signals $\underline{s}(t)$ and $\overline{s}(t)$ are said to overlap if $\exists t_1 > 0$, $\delta > 0$ such that $\forall t < t_1$, $\underline{s}(t) \leq \overline{s}(t)$ and $\forall t \in [t_1, t_1 + \delta[$, $\underline{s}(t) > \overline{s}(t)$.

Example 3.20. The notion of overlap is illustrated in Fig. 3.5 for two unidimensional signals $\underline{s}(t)$ and $\overline{s}(t)$. ♣

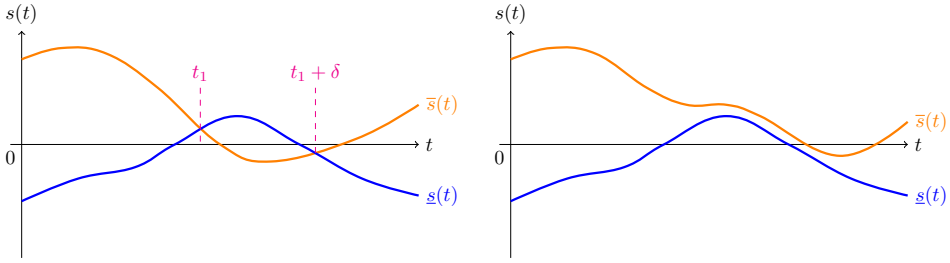

Figure 3.5: *Left*: example of two overlapping signals, overlap starts at time t_1 and stops at $t_1+\delta$. *Right*: the represented signals do not overlap over the represented interval of time.

For Lemma 3.16 to be applicable, the propagated bounds signals must not overlap. In our case, saturations overlap occurs when considering non-symmetrical time-varying constraints $\underline{\alpha}(t)$ and $\overline{\alpha}(t)$ or in the presence of unknown disturbances as described later in Pb. 3.26.

For now, it must be ensured that $\forall i \in \mathbb{N}$ s.t. $i \leq k$, $\underline{\alpha}_i(t) < \overline{\alpha}_i(t)$. This can be obtained by choosing the constant coefficients in $\boldsymbol{\kappa}$ "big enough". Prior to this thesis work, this was the only constructive rule to obtain these coefficients. More precisions on that aspect are given in Chapter 4.

Remark 3.21. It was mentioned in [Burlion 12] that choosing a time-varying $\boldsymbol{\kappa}$ may help to avoid propagated bounds overlap. However, no constructive rules were elaborated in this case. A thorough study on the subject is performed in Chapter 4 where time-varying expressions are derived for the first time in the linear case, thus ensuring no propagated bounds overlap. ◇

Remark 3.22. In the case $k = 0$, saturations do no overlap if $\underline{\alpha}(t) < \overline{\alpha}(t)$, $\forall t$. There is no degree of freedom. Hence, the designer should define the expected bounds on α carefully especially if they depend on external variables. ◇

The main result in [Burlion 12] is now stated. This offers a solution to Problem 3.12 in the case of an undisturbed certain system with fully measured state.

Theorem 3.23 (A solution to Problem 3.12)**.**
Let assume 3.13 and 3.15 are satisfied with $k \geq 1$. Let define propagated bounds as in Definition 3.14 where the constant design parameters $\boldsymbol{\kappa}$ are chosen big enough such that propagated bounds overlap does not occur. If one chooses

$$\underline{u}(t,\boldsymbol{x}) = \frac{\underline{\alpha}_k(t) - \mathcal{L}_{\boldsymbol{f}}^k\sigma(\boldsymbol{x})}{\mathcal{L}_{\boldsymbol{g}}\mathcal{L}_{\boldsymbol{f}}^{k-1}\sigma(\boldsymbol{x})},\ \overline{u}(t,\boldsymbol{x}) = \frac{\overline{\alpha}_k(t) - \mathcal{L}_{\boldsymbol{f}}^k\sigma(\boldsymbol{x})}{\mathcal{L}_{\boldsymbol{g}}\mathcal{L}_{\boldsymbol{f}}^{k-1}\sigma(\boldsymbol{x})} \tag{3.20}$$

then $\alpha(t) \in \Omega_\alpha(t)$, $\forall t$ if u is forced to stay in $[\underline{u}, \overline{u}]$.

Proof. Straightforward using the definition of propagated bounds (3.12) and Lemma 3.16. □

Remark 3.24. This is important to note that no stability result is stated in this theorem. More precisely, if Assumption 3.10 is not satisfied, then the system internal state may diverge. This is discussed in 3.3.5. ◇

Remark 3.25. In case $k = 0$, the control saturations are adapted as mentioned in Remark 3.18. ◇

3.3.5 Remarks on the proposed approach

In this section, a few hints are given on how more complex problems could be considered in the non-linear case. Note that these problems are considered more thoroughly in the linear framework in Chapter 4.

A warning on stability It is well-known in control systems stability analysis that the introduction of saturations in the control loop, even time-invariant and decorrelated from the system state, can destabilise the closed-loop in most cases. As far as OIST is concerned and in the case of non-minimum phase systems, the internal zero dynamics will diverge upon saturation of the control input. This is exposed in 4.6.2 for linear systems.

Consequently, no general stability result was provided in this chapter. In the case of minimum phase systems, global asymptotic stability can be proved using appropriate anti-windup loops. This is done in Chapter 4 for linear minimum phase systems. As far as non-linear systems are concerned, evaluating the zero dynamics is more tricky and no general result can be stated.

Robust output-constrained problem In [Burlion 12], another problem, called *robust output constraint problem* is formulated. This considers the case where the system is disturbed by an unknown input signal:

$$(\mathbf{G})\begin{cases} \dot{\boldsymbol{x}} &= \boldsymbol{f}(\boldsymbol{x}) + \boldsymbol{g}(\boldsymbol{x})u + \boldsymbol{g}_2(\boldsymbol{x})\boldsymbol{d} \\ \boldsymbol{y} &= \boldsymbol{x} \\ \boldsymbol{x}(0) &= \boldsymbol{x}_0 \end{cases} \tag{3.21}$$

where $\boldsymbol{d} \in \mathbb{R}^m$ is an unknown disturbance and $\boldsymbol{g}_2 \in \mathcal{C}^\infty(\mathbb{R}^m, \mathbb{R}^n)$. It is supposed that $\boldsymbol{d}(t)$ is bounded by known sufficiently smooth vectors $\underline{\boldsymbol{d}}(t)$ and $\overline{\boldsymbol{d}}(t)$ at all times. Problem 3.12 reformulates into

Problem 3.26 (Robust output constraint to input saturation problem)**.**
Let consider the system $(\mathbf{G})$ in (3.21) with $\alpha = \sigma(\boldsymbol{x}) \in \mathbb{R}$ the constrained output. Let $\mathcal{K}(\Omega_\alpha)$ a time-domain constraint and u a known nominal control law. Design two signals $\underline{u}$ and $\overline{u}$ such that the closed-loop

$$\begin{cases} \dot{\boldsymbol{x}} &= \boldsymbol{f}(\boldsymbol{x}) + \boldsymbol{g}(\boldsymbol{x})u + \boldsymbol{g}_2(\boldsymbol{x})\boldsymbol{d} \\ \boldsymbol{y} &= \boldsymbol{x} \\ \boldsymbol{x}(0) &= \boldsymbol{x}_0 \\ \alpha &= \sigma(\boldsymbol{x}) \\ u &\in \left[\underline{u}\left(\boldsymbol{x}, \Omega_\alpha(t), \dot{\Omega}_\alpha(t), \ldots, \underline{\boldsymbol{d}}(t), \overline{\boldsymbol{d}}(t), \underline{\boldsymbol{d}}^{(1)}(t), \overline{\boldsymbol{d}}^{(1)}(t), \ldots\right), \right. \\ & \qquad \left. \overline{u}\left(\boldsymbol{x}, \Omega_\alpha(t), \dot{\Omega}_\alpha(t), \ldots, \underline{\boldsymbol{d}}(t), \overline{\boldsymbol{d}}(t), \underline{\boldsymbol{d}}^{(1)}(t), \overline{\boldsymbol{d}}^{(1)}(t), \ldots\right)\right] \end{cases} \tag{3.22}$$

satisfies $\mathcal{K}(\Omega_\alpha)$ i.e.

$$\alpha(t) \in \Omega_\alpha(t),\ \forall t \in \mathbb{R}_+$$

A solution to this problem is proposed in the linear case in Chapter 3.

The output-feedback case The OIST approach has been presented in the case where the whole state is known. This allows to determine the control saturations which are functions of the state as shown in (3.18).

In case the whole state is not measured, the author suggests to use a specific form of observer namely framers (also called interval observers). Framers are used to obtain certified bounds on the system state which would then be used in the propagated bounds expressions. Typically, they provide two signals $\underline{\boldsymbol{x}}(t)$ and $\overline{\boldsymbol{x}}(t)$ such that

$$\underline{\boldsymbol{x}}(t) \leq \boldsymbol{x}(t) \leq \overline{\boldsymbol{x}}(t),\ \forall t \tag{3.23}$$

where $\boldsymbol{x}$ is the considered system state. In the non-linear case, building framers is non-trivial. Consequently, most works [Raïssi 12, Efimov 13f, Efimov 13d] consider specific classes of non-linear systems. As far as the linear framework is concerned, designing interval observers is now

well documented as shown in Chapter B. A solution to the output-constrained output-feedback problem is provided in Chapter 5 in the linear case.

3.4 Illustration on the crane problem

In this section, application of OIST is illustrated on the crane example presented in 3.2. The model in (3.6) is considered in closed-loop with the control law in (3.7). The whole state is supposed to be measured. The system is considered to be undisturbed and with known parameters.

Considered time-domain constraint A time-domain constraint is set on the pendulum angle, i.e. $\alpha = \boldsymbol{q}_2$. The reason for considering such constraint is to avoid dangerous swaying of the load modelled by the pendulum. This is representative of real life applications: the load could be an open tank containing some liquid. Let define

$$\begin{aligned} \underline{\alpha}(t) &= -\beta_1 + \tfrac{2\beta_2}{\pi}\arctan(t-\beta_3) \\ \overline{\alpha}(t) &= \beta_1 - \tfrac{2\beta_2}{\pi}\arctan(t-\beta_3) \end{aligned} \tag{3.24}$$

with $\beta_1 = 0.0436$, $\beta_2 = 0.0175$ and $\beta_3 = 5$ for simulation. This constraint is equal to the one used to illustrate a time-varying constraint in Fig. 3.3. Using the control law in (3.7), one can see that the constraint is not enforced. Hence, implementing the OIST approach is proposed. Note that the constraints specified in (3.24) are symmetric, satisfy to the required smoothness assumptions and can be easily differentiated:

$$\begin{aligned} \dot{\underline{\alpha}}(t) &= \tfrac{2\beta_2}{\pi}\tfrac{1}{1+(t-\beta_3)^2} \\ \dot{\overline{\alpha}}(t) &= -\dot{\underline{\alpha}}(t) \\ \ddot{\underline{\alpha}}(t) &= -\tfrac{2\beta_2}{\pi}\tfrac{2(t-\beta_3)}{(1+(t-\beta_3)^2)^2} \\ \ddot{\overline{\alpha}}(t) &= -\ddot{\underline{\alpha}}(t) \end{aligned} \tag{3.25}$$

Relative degree and assumptions Considering Definition 3.4 and (3.6), the constrained output $\alpha = \boldsymbol{q}_2$ is of relative degree 2 with respect to u. Also, Assumption 3.15 is fulfilled when using the initial condition $\boldsymbol{x}_0 = \begin{bmatrix} -10 & 0 & 0 & 0 \end{bmatrix}^\top$.

Propagated bounds and design parameters Let $\underline{\alpha}_0(t) = \underline{\alpha}(t)$, $\overline{\alpha}_0(t) = \overline{\alpha}(t)$ and, using Definition 3.14, one obtains the following propagated bounds

$$\begin{aligned} \underline{\alpha}_1(t) &= \kappa_1\left(\underline{\alpha}(t) - q_2\right) + \dot{\underline{\alpha}}(t) \\ \overline{\alpha}_1(t) &= \kappa_1\left(\overline{\alpha}(t) - q_2\right) + \dot{\overline{\alpha}}(t) \\ \underline{\alpha}_2(t) &= \kappa_2\kappa_1\left(\underline{\alpha}(t) - q_2\right) + \left[\kappa_1+\kappa_2\right]\left(\dot{\underline{\alpha}}(t) - p_2\right) + \ddot{\underline{\alpha}}(t) \\ \overline{\alpha}_2(t) &= \kappa_2\kappa_1\left(\overline{\alpha}(t) - q_2\right) + \left[\kappa_1+\kappa_2\right]\left(\dot{\overline{\alpha}}(t) - p_2\right) + \ddot{\overline{\alpha}}(t) \end{aligned} \tag{3.26}$$

where the constant parameters κ_1 and κ_2 are chosen "big enough" to avoid saturations overlap as explained in 3.3.4.

Resulting saturations Before formulating the control saturations similarly to what was obtained in (3.18), it must be ensured that $\mathcal{L}_{\boldsymbol{g}}\mathcal{L}_{\boldsymbol{f}}^{k-1}\sigma(\boldsymbol{x}) \neq 0$, $\forall \boldsymbol{x}$:

Assumption 3.27 (OIST saturations validity)**.**
It is supposed that the pendulum angle value satisfies to

$$\boldsymbol{q}_2(t) \in \left]-\frac{\pi}{2}, \frac{\pi}{2}\right[, \forall t$$

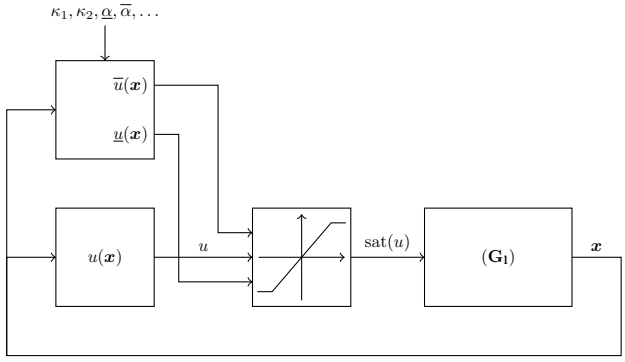

Figure 3.6: Simplified representation of the interconnection used in simulation

Considering the initial simulation results in Fig. 3.2 which were obtained with the control law in Eq. (3.7), the assumption is already satisfied. Under Assumption 3.27, the following saturations are obtained:

$$\begin{aligned} \underline{u}(\boldsymbol{x}) &= -\frac{\overline{\alpha}_2 + \gamma_1 \sin(\boldsymbol{q}_2)}{\gamma_2 \cos(\boldsymbol{q}_2)} \\ \overline{u}(\boldsymbol{x}) &= -\frac{\underline{\alpha}_2 + \gamma_1 \sin(\boldsymbol{q}_2)}{\gamma_2 \cos(\boldsymbol{q}_2)} \end{aligned} \tag{3.27}$$

where, according to Remark 3.17, the fact that $-\gamma_2 \cos(\boldsymbol{q}_2) < 0$, $\forall \boldsymbol{q}_2 \in \left]-\frac{\pi}{2}, \frac{\pi}{2}\right[$ has been considered.

Simulation results The model in (3.6) is simulated over $20s$ in closed-loop with the control law in (3.7) and the time-varying saturations in (3.27). The design parameters $\boldsymbol{\kappa}_1$ and $\boldsymbol{\kappa}_2$ are respectively set to 5 and 10. A simplified representation of the interconnection is drawn in Fig. 3.6.

The simulation results are represented in blue in Fig. 3.7 to 3.9. The results obtained without inserting the saturations in the loop are represented in magenta. The lower (resp. upper) bounds and saturations are represented in green (resp. red).

The results in Fig. 3.9 show that it is possible to constrain the pendulum angle in the time-domain using the presented *Output to Input Saturation Transformation*. It is interesting to note in Fig. 3.8 that the introduction of saturations on the control law increases the time-response of the system. This is a well-known behaviour of saturated systems. A trade-off can be identified: for less restrictive bounds on the considered output, a better time-response can be achieved and vice versa. Also, for a given constraint, better time-responses can be achieved by appropriately selecting $\boldsymbol{\kappa}$. Figure 3.7 shows that the control law is saturated whenever its value would result in violating the output constraint.

Influence of $\boldsymbol{\kappa}$ Choosing the appropriate values for the design constants $\boldsymbol{\kappa}$ can be tricky. These parameters were introduced in Definition 3.14. Apart from having to choose them strictly positive, not much was said. This comes from the fact that this choice is quite problem-dependent. In the crane control problem, what is observed is that, for a fixed $\boldsymbol{\kappa}_1$, the bigger $\boldsymbol{\kappa}_2$ the shorter the time-response for α. This comes from the fact that more magnitude is allowed to the control. Similar results are observed for a fixed $\boldsymbol{\kappa}_2$. This is illustrated in Fig. 3.10 where each parameter is varied while the other is kept constant. A color scale is used to identify the value chosen for the considered coefficient in each simulation.

3.5 Conclusion

The *Output to Input Saturation Transformation* initially introduced in [Burlion 12] has been presented in this chapter. This is a new approach to design a control law which satisfies a time-domain output constraint. In comparison with the existing literature, this method belongs to

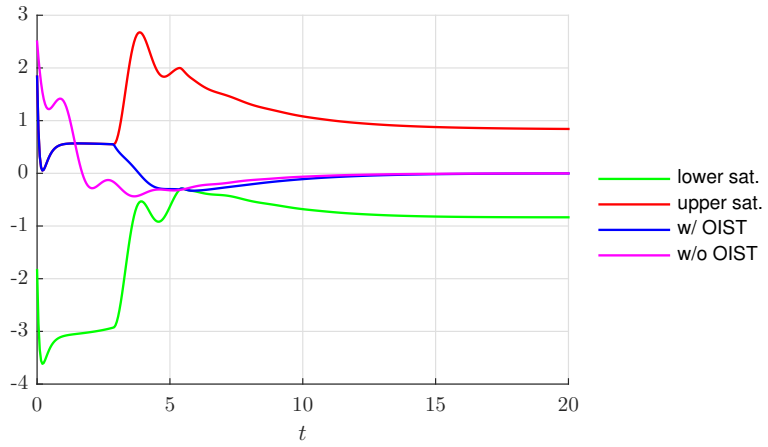

Figure 3.7: Control law obtained in simulation along with considered saturations (obtained through OIST).

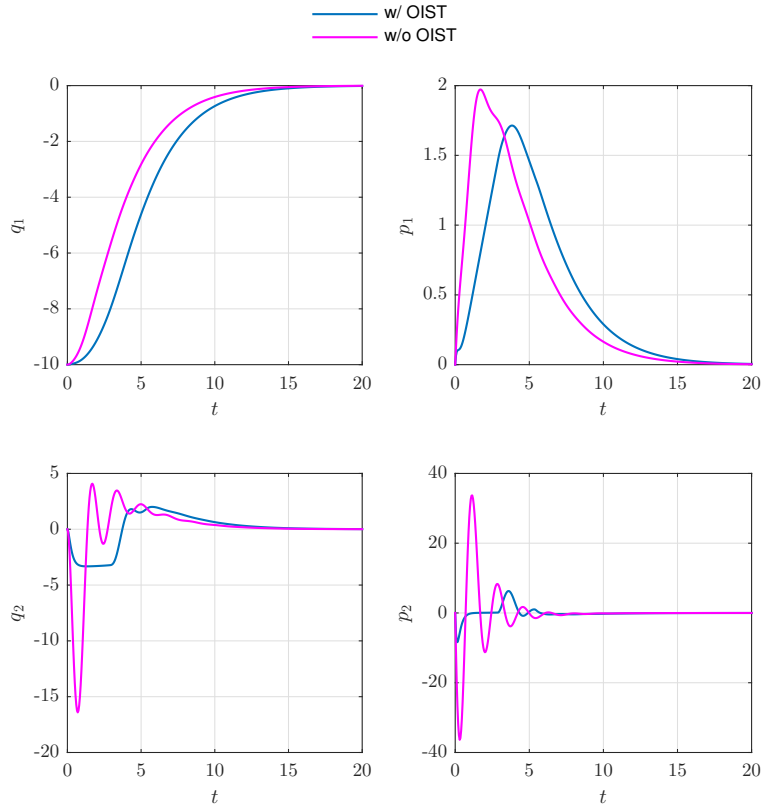

Figure 3.8: System state simulation.

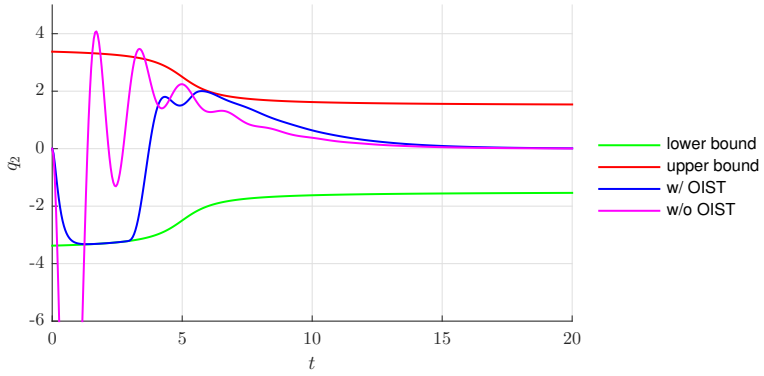

Figure 3.9: Focus on $\alpha = \boldsymbol{q}_2$; the output constraint is represented.

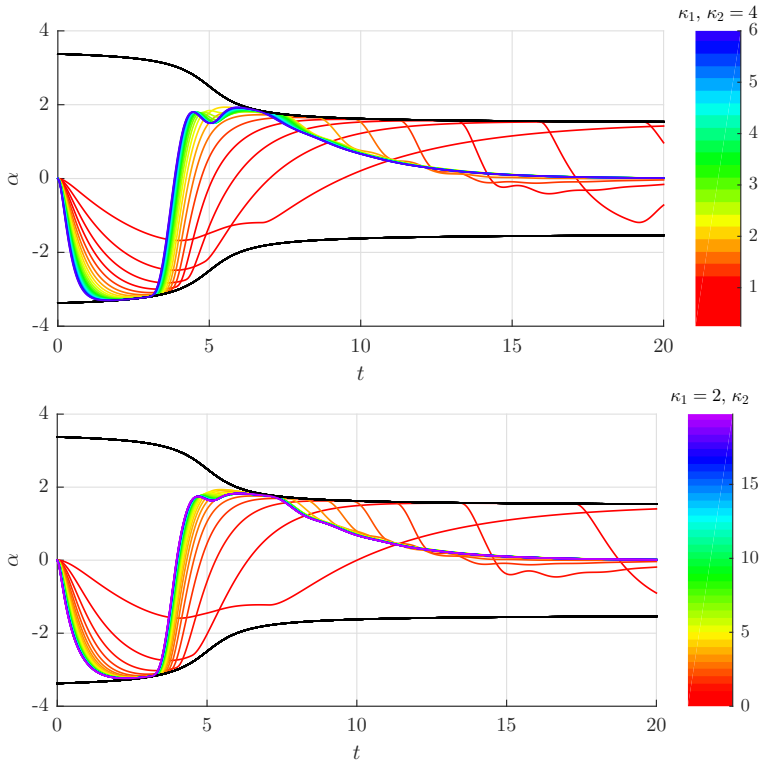

Figure 3.10: Informal study of the influence of $\boldsymbol{\kappa}_1$ and $\boldsymbol{\kappa}_2$ values; Each parameter is varied for a constant value of the other.

the *evolutionary* strategies class [Goodwin 01]. Using an assumption on the relative degree of the considered output with respect to the control input, time-varying saturations are obtained and applied to a pre-existing stabilizing control law. Some remarks have been made on the type of stability achieved and hints have been formulated on how to solve more complex problems. The whole approach has been applied to a simplified non-linear crane control problem with a constraint on the admissible pendulum angle. A brief study of the impact of the design parameters on the time-response has been performed on this example.

This chapter concludes the preliminary part of this thesis. The contributions are now presented starting with the reformulation of the *evolutionary* OIST approach in the linear framework.

Part III

Contributions to frequency- and time-domain constrained control of linear systems

Chapter 4

Reformulation of OIST output constrained control approach in the linear framework

As illustrated in Chapter 2, a non-smooth optimization-based technique can be used to synthesize an appropriate structured controller with respect to prescribed frequency-domain requirements. Enforcing time-domain constraints is more difficult and requires trial-and-error tuning of the frequency-domain requirements. OIST was introduced for non-linear systems in [Burlion 12] to enforce a time-domain constraint on an output variable. However, the closed-loop stability in the presence of the designed saturations needs to be studied and an inappropriate choice of the design parameters $\boldsymbol{\kappa}$ can lead to saturations overlap. After reformulating the approach in the linear framework, these problems are tackled with theoretical guarantees. This chapter is based on results presented in [Chambon 15c] and [Chambon b].

Reasons are given in 4.1 for choosing the OIST evolutionary approach. Notations and definitions are introduced in 4.2. A case study is used in 4.3 to illustrate the existing problems of the original formulation. Then, the reformulation of OIST in the linear framework is proposed in 4.4 along with solutions to the aforementioned problems. The approach is illustrated on a simple example in 4.5. Then, some miscellaneous remarks are made in 4.6 before concluding in 4.7.

4.1 Selection of an output-constrained control approach

The different strategies to deal with output or state constraints through an appropriate definition or modification of the control law have been presented in 3.2.2. Three main strategies have been identified, following the classification proposed in [Goodwin 01]:

- *Cautious*: the control law is designed using trial-and-error such that the constraints are satisfied;
- *Evolutionary*: the nominal control law is compensated using an additional structure whenever the constraints are violated;
- *Tactical*: the constraints are formalized in the control law design procedure.

The reasons for considering the evolutionary OIST approach introduced in [Burlion 12] and presented in Chapter 3 are now detailed. The primary reason for not considering a *cautious* strategy has been mentioned in Chapter 3: such strategies often lead to a loss of performance and efficiency of the control law since they forbid the constrained output (or state) to actually linger on the constraint.

In the previous chapter, an efficient procedure for designing structured controller against frequency-domain requirements has been presented. This procedure can be used to solve many control problems, especially those met in the aerospace industry. However, time-domain constraints on an output or state cannot be easily enforced using such H_∞-based techniques. Hence an additional *evolutionary* strategy needs to be considered where the nominal control law satisfies the frequency-domain constraints and is compensated whenever the time-domain output/state constraint is violated. Within the *evolutionary* strategies mentioned in 3.2.2, the OIST approach is expected to offer guarantees on the actual satisfaction of the constraint contrary to the anti-windup-based techniques [Turner 02]. In comparison with the *cautious* strategies, the obtained performance is expected to be much better especially when considering the addition of an anti-windup compensator [Herrmann 10].

Considering a *tactical* strategy such as MPC would required reformulating the frequency-domain specifications of the H_∞ control design problem in an appropriate cost functional. This is not the purpose of this thesis work which considers a specific family of control design approaches adapted to the considered specifications. Also, using ad hoc techniques such as [Apkarian 11] only offers guarantees on the families of input signals considered in the simulation-based non-smooth optimization.

In this work, it is chosen to consider an *evolutionary* approach to the output-constrained control problem. More precisely, the OIST approach [Burlion 12] is considered since it offers guarantees on the satisfaction of the considered output constraint. Also, it can be used on top of existing control design strategies such as the one presented in Chapter 2. The works originating in the OIST approach have mainly considered non-linear systems. In the linear case, detailed expressions of the considered saturations can be obtained. Also, open problems were left undocumented such as the potential saturations overlap or the closed-loop stability analysis problems. The purpose of this chapter is thus twofold: first, the OIST approach is reformulated in the linear case and second, solutions to the existing undocumented problems are theorised for the first time.

4.2 Notations and definitions

The notion of overlap of two signals has been introduced in Definition 3.19. The same definition holds in this chapter. The notion of cyclic permutation is used to shorten the iterative expressions obtained later in this chapter. It is defined as follows:

Definition 4.1 (Cyclic permutation of length k on the elements of a vector $\boldsymbol{s} \in \mathbb{R}^k$)**.**
Let $\boldsymbol{s} = \begin{bmatrix} \boldsymbol{s}_1 & \dots & \boldsymbol{s}_k \end{bmatrix} \in \mathbb{R}^k$. The cyclic permutation of length k on the elements of $\boldsymbol{s}$ is denoted $\boldsymbol{\sigma}$ and defined as:

$$\begin{aligned} \boldsymbol{\sigma}: \quad \mathbb{R}^k &\to \mathbb{R}^k \\ \boldsymbol{v} &\mapsto \boldsymbol{\sigma}(\boldsymbol{v}) \end{aligned} \tag{4.1}$$

where $\boldsymbol{\sigma}(\boldsymbol{v}) = \begin{bmatrix} \sigma(\boldsymbol{s}_1) & \dots & \sigma(\boldsymbol{s}_k) \end{bmatrix}$ and

$$\sigma(\boldsymbol{s}_i) = \begin{cases} \boldsymbol{s}_{i-1} & \text{if} \quad 1 < i \leq k \\ \boldsymbol{s}_k & \text{if} \quad i = 1 \end{cases} \tag{4.2}$$

As a reminder, the saturation and deadzone functions applied to a variable $\boldsymbol{x} \in \mathbb{R}^n$ and respectively denoted $\mathrm{sat}_{\underline{\boldsymbol{x}}}^{\overline{\boldsymbol{x}}}(\boldsymbol{x})$ and $\mathrm{Dz}_{\underline{\boldsymbol{x}}}^{\overline{\boldsymbol{x}}}(\boldsymbol{x})$ for two saturations $\underline{\boldsymbol{x}}$ and $\overline{\boldsymbol{x}}$ in $\mathbb{R}^n$ are related by:

$$\mathrm{sat}_{\underline{\boldsymbol{x}}}^{\overline{\boldsymbol{x}}}(\boldsymbol{x}) = \boldsymbol{x} - \mathrm{Dz}_{\underline{\boldsymbol{x}}}^{\overline{\boldsymbol{x}}}(\boldsymbol{x}) \tag{4.3}$$

In the following, we define functions which will be used as differentiable approximates of non-differentiable functions such as the absolute value or max functions. Some properties of these approximates are also derived. First the Lambert function is defined:

Definition 4.2 (Lambert function)**.**
Let F the function defined by $F(x) = xe^x, \forall x \in \mathbb{R}$. The inverse function of F is the Lambert function denoted $W_0(y)$ which fulfils $F(W_0(y)) = W_0(y)\, e^{W_0(y)} = y$.

The Lambert function is used to define the following constants:

$$\begin{aligned} c_1 &= \tfrac{1}{2} W_0\left(\tfrac{1}{e}\right) + \tfrac{1}{2} \\ c_2 &= c_1 - \tanh(c_1)\, c_1 \end{aligned} \tag{4.4}$$

Using these constants, let define the following functions:

$$\begin{aligned} f_{\mathrm{abs}}: \quad \mathbb{R} &\to \mathbb{R} \\ x &\mapsto \tanh(x)\, x + c_2 \\ f_{\max}: \quad \mathbb{R} \times \mathbb{R} &\to \mathbb{R} \\ (x, y) &\mapsto \tfrac{1}{2}\left[x + y + f_{\mathrm{abs}}(x + y)\right] \\ g: \quad \mathbb{R} \times \mathbb{R} &\to \mathbb{R} \\ (x, y) &\mapsto f_{\max}\left(f_{\mathrm{abs}}(x), f_{\mathrm{abs}}(y)\right) \end{aligned} \tag{4.5}$$

It is observed that these functions satisfy to ordering properties with respect to the functions they approximate. This is summed up in the following proposition.

Proposition 4.3 (Approximating functions (4.5) properties)**.**
The functions defined in (4.5) satisfy the following properties:

- f_{abs} *and* f_{max} *are differentiable over* $\mathbb{R}$*;*
- g *is differentiable over* $\mathbb{R} \times \mathbb{R}$*;*
- $f_{abs}(x) \geq |x|, \forall x \in \mathbb{R}$*;*
- $f_{max}(x, y) \geq \max(x, y), \forall (x, y) \in \mathbb{R} \times \mathbb{R}$.

Proof. First, let $f(x) = (2x - 1)\mathrm{e}^{2x}$. Then, $f(c_1) = W_0\left(\frac{1}{\mathrm{e}}\right) \mathrm{e}^{W_0\left(\frac{1}{\mathrm{e}}\right)} \mathrm{e} = \frac{1}{\mathrm{e}} \times \mathrm{e} = 1$ by definition of the Lambert function. Second, using the basics of real analysis on the function $h(x)$ defined by $\forall x$, $h(x) = f_{\mathrm{abs}}(x) - |x|$, the inequalities in Proposition 4.3 are achieved. As far as the function $f_{\max}$ is concerned, the same study is performed using the following equality: $\forall (x, y)$, $\max(x, y) = \frac{1}{2}\left[x + y + |x - y|\right]$. □

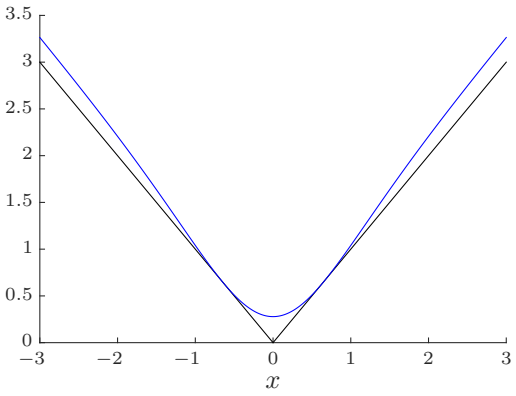

Figure 4.1: Representation of the absolute value function (in black) and its differentiable approximate f_{abs} (in blue) over the interval $[-3, 3]$.

The functions definitions in (4.5) are extended to the multidimensional case $\boldsymbol{x} \in \mathbb{R}^n$ in an element-wise manner. Proposition 4.3 remains valid in that case. The absolute value function and its approximate f_{abs} are represented in Fig. 4.1.

4.3 Case study: an illustration of existing problems

To introduce the considered output-constrained problem and the OIST approach, a simple linearised ball and beam system is considered in this section. The objective is to maintain the ball on the beam even in the presence of disturbances. A linear controller has been synthesized but does not achieve the mentioned output constraint. Violation of the considered time-domain constraint motivates the use of a dedicated *evolutionary*[1] method. In this case, guarantees on the constraint satisfaction are expected whichever the considered state disturbance signal and the OIST approach is selected. However, previously undocumented problems related to the direct application of the method as presented in [Burlion 12] or Chapter 3 arise which motivates bringing guarantees to the OIST method.

4.3.1 Considered ball and beam model

The considered problem is the position tracking of a ball on a beam in the presence of heavy disturbance. The considered system and notations are illustrated in Fig. 4.2.

The beam is actuated using a lever arm and the objective is to drive the system from $r_0 = 0.5$m to the setpoint $r_s = 0.6$m. An unknown disturbance force d is eventually applied to the ball acceleration. The disturbance signal used in simulation is represented in plain blue in Fig. 4.3(a). It is supposed that bounds are known for this disturbance at each time. The state vector of the system is given by $\boldsymbol{x} = \begin{bmatrix} r \\ \dot{r} \end{bmatrix}$ and the measurements vector by $\boldsymbol{y} = \boldsymbol{x}$. The constrained output is given by:

$$\alpha = \mathbf{C}_{\boldsymbol{\alpha}} \boldsymbol{y} = \mathbf{C}_{\boldsymbol{\alpha}} \boldsymbol{x} \tag{4.6}$$

with $\mathbf{C}_{\boldsymbol{\alpha}} = \begin{bmatrix} 1 & 0 \end{bmatrix}$. It corresponds to the ball position on the beam.

The reason for monitoring this variable is quite obvious. The beam length is limited to $L = 1$m which means that even a theoretically stabilizing control law can result in the ball falling off the beam especially in the presence of a disturbance. An example of a time-domain requirement to avoid such behaviour is to satisfy $0.1 \leq \alpha(t) \leq 0.9$ (in meters), $\forall t$. More exotic time-varying requirements can also be considered as illustrated below. The system state-space representation is given by:

[1] See the definition of an *evolutionary* approach in Chapter 3, 3.2.

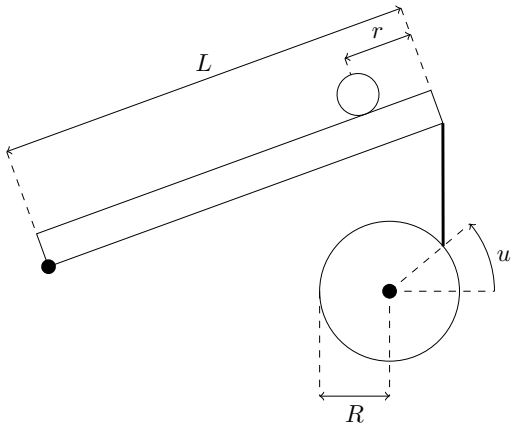

Figure 4.2: Ball and beam system representation. Thick dots indicate fixed axes of rotation.

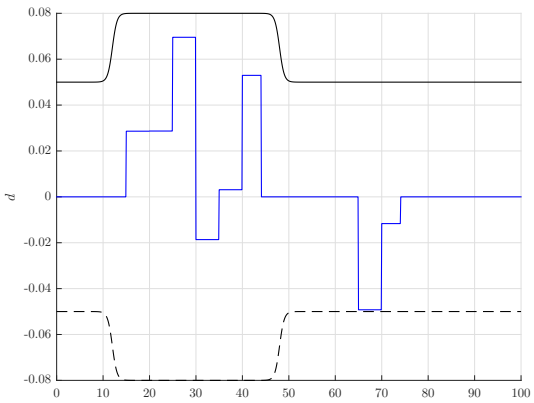

(a) In blue, considered state disturbance d (in simulation). Known bounds $\underline{d}$ and $\overline{d}$ on this signal are represented in black.

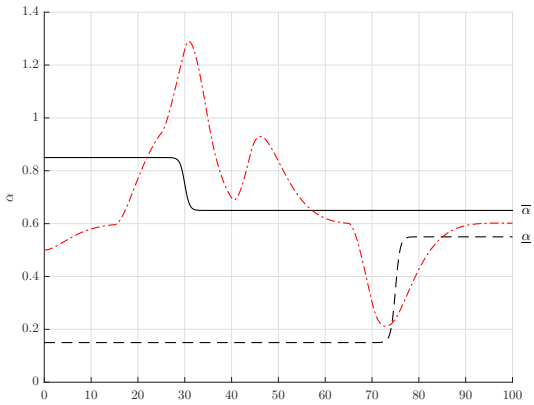

(b) Simulation results for the considered constrained variable α when the time-domain requirement (in black) is not considered during the controller synthesis.

Figure 4.3: Considered disturbance signal and constrained output initial simulation.

$$\mathbf{A} = \begin{bmatrix} 0 & 1 \\ 0 & 0 \end{bmatrix}, \mathbf{B} = \begin{bmatrix} 0 & 0 \\ -0.21 & 1 \end{bmatrix}, \mathbf{C} = \mathbf{I_2}, \mathbf{D} = \begin{bmatrix} 0 & 0 \\ 0 & 0 \end{bmatrix} \tag{4.7}$$

where the inputs are respectively the control input u and the disturbance input d. As far as the nominal control design is concerned, a state-feedback controller with integral action is implemented to achieve steady-state accuracy. The considered controller state-space matrices are given by

$$\mathbf{A_K} = -1.5779, \mathbf{B_K} = \begin{bmatrix} 0.0322 & 0.2339 \end{bmatrix}, \mathbf{C_K} = -0.0644, \mathbf{D_K} = \begin{bmatrix} -0.3156 & -2.0937 \end{bmatrix} \tag{4.8}$$

where $\boldsymbol{u}_K = \boldsymbol{y}_s - \boldsymbol{y}$ with $\boldsymbol{y}_s = \begin{bmatrix} r_s & 0 \end{bmatrix}^\top$.

This dynamic controller stabilizes the system and yields good results on r_s-setpoint tracking. However, using this controller, the ball position represented in dashed-dotted red line in Fig. 4.3(b) violates the time-varying time-domain requirement represented in black lines. In practice, the ball falls off the beam.

4.3.2 Application of the original OIST method

Since the controller has already been designed, an *evolutionary* approach is proposed to enforce the considered time-domain requirement illustrated in Fig. 4.3(b). Guarantees on the actual satisfaction of the requirement are expected for any disturbance signal with known bounds and the OIST approach as presented in [Burlion 12] and Chapter 3 is thus chosen.

4.3.2 (a) Study of the relative degree

The relative degree Definition 3.4 still holds in the linear case. A brief study of the constrained output α expression shows that it is of relative degree $k = 2$ with respect to the control input u and $l = 2$ with respect to the disturbance input d. This means that the second derivative of α, denoted $\alpha^{(2)}$, depends on both u and d, see (3.11):

$$\alpha^{(2)} = \mathbf{C_\alpha A}^2 \boldsymbol{x} + \mathbf{C_\alpha A B_u} u + \mathbf{C_\alpha A B_d} d \tag{4.9}$$

4.3.2 (b) Propagated bounds definition

Using Definition 3.14 of the propagated bounds and considering constant design parameters κ_1 and κ_2, the following expressions are obtained:

$$\begin{aligned}
\underline{\alpha}_0 &= \underline{\alpha} \\
\overline{\alpha}_0 &= \overline{\alpha} \\
\underline{\alpha}_1 &= \kappa_1 \left(\underline{\alpha} - \mathbf{C_\alpha} \boldsymbol{x} \right) + \dot{\underline{\alpha}} \\
\overline{\alpha}_1 &= \kappa_1 \left(\overline{\alpha} - \mathbf{C_\alpha} \boldsymbol{x} \right) + \dot{\overline{\alpha}} \\
\underline{\alpha}_2 &= \kappa_1 \kappa_2 \left(\underline{\alpha} - \mathbf{C_\alpha} \boldsymbol{x} \right) + (\kappa_1 + \kappa_2) \left(\dot{\underline{\alpha}} - \mathbf{C_\alpha A} \boldsymbol{x} \right) + \ddot{\underline{\alpha}} \\
\overline{\alpha}_2 &= \kappa_1 \kappa_2 \left(\overline{\alpha} - \mathbf{C_\alpha} \boldsymbol{x} \right) + (\kappa_1 + \kappa_2) \left(\dot{\overline{\alpha}} - \mathbf{C_\alpha A} \boldsymbol{x} \right) + \ddot{\overline{\alpha}}
\end{aligned} \tag{4.10}$$

4.3.2 (c) Resulting control saturations

The control saturations are coherent with the expressions given in (3.18). Using (4.9), the control saturations which allow to satisfy the necessary condition in Lemma 3.16 are given by:

$$\begin{aligned}
\underline{u} &= \frac{1}{\mathbf{C_\alpha A B_u}} \left[\underline{\alpha}_k - \mathbf{C_\alpha A} \boldsymbol{x} + |\mathbf{C_\alpha A B_d}| \max \left(|\underline{d}|, |\overline{d}| \right) \right] \\
\overline{u} &= \frac{1}{\mathbf{C_\alpha A B_u}} \left[\overline{\alpha}_k - \mathbf{C_\alpha A} \boldsymbol{x} - |\mathbf{C_\alpha A B_d}| \max \left(|\underline{d}|, |\overline{d}| \right) \right]
\end{aligned} \tag{4.11}$$

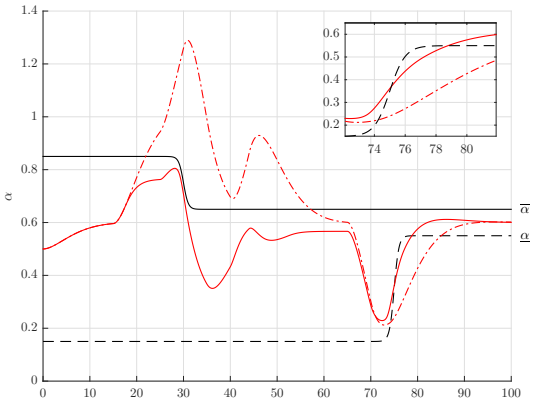

(a) Time-domain requirement (in black) and simulation results for the regulated variable α. The dashed-dotted red line is obtained when using the nominal controller and the plain red line is obtained when using OIST as in [Burlion 12] and Chapter 3.

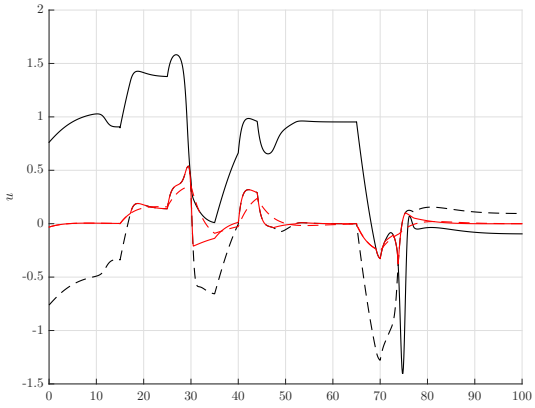

(b) Control signal (in red) and control saturations obtained using OIST as in [Burlion 12] and Chapter 3. Overlap starts around $t_1 = 73$s.

Figure 4.4: Case study: simulation results w/ (plain red) or w/o (dashed-dotted red) OIST in the loop, with $\kappa_1 = 1$ and $\kappa_2 = 0.6$.

4.3.2 (d) Design parameters selection

As mentioned in Chapter 3, it was proposed in [Burlion 12] to choose the coefficients κ_1 and κ_2 in (4.10) as constants. In the presence of a time-varying requirement or disturbances, it was also hinted that choosing them "big enough" was preferable to avoid control saturations overlap[2]. For illustrative purposes, the values $\kappa_1 = 1$ and $\kappa_2 = 0.6$ are used in simulation.

4.3.2 (e) Simulation results and conclusions

A simulation of the system in closed-loop with the controller in (4.8) and the saturations expressions in (4.11) (i.e. $u = \text{sat}_{\underline{u}}^{\overline{u}}(y_K)$) is performed over 100s. The disturbance profile in Fig. 4.3(a) and the time-domain constraint in Fig. 4.3(b) are considered. The simulation results are shown in Fig. 4.4 where the dashed-dotted red line refers to the results without using OIST and the plain red line refers to the results when introducing the saturations in the feedback loop.

At first, it seems that the constrained output satisfies the requirement. However, when paying closer attention, it appears that violation of this constraint occurs at time $t = 75$s. This results from the two control saturations overlap starting at time t_1 as illustrated in Fig. 4.4(b). Such behaviour could be avoided by increasing the values of κ_1 and κ_2 as illustrated in plain blue line in Fig. 4.5 where the simulation was performed using $\kappa_1 = 1$ and $\kappa_2 = 10$. Another solution is to consider time-varying coefficients as hinted in [Burlion 12] and Chapter 3. The first solution is fast to implement in practice but may lead to exceedingly demanding control saturations and offers no guarantee if a different requirement or disturbance signal is considered. The second solution is safer and offers guarantees but is harder to implement. Also, guarantees on the closed-loop stability in the presence of saturations are expected. These previously undocumented subjects are discussed in this chapter as main contributions.

4.4 Reformulation of OIST in the linear framework

In this thesis work, the considered systems are linear. The OIST approach was initially introduced in [Burlion 12] for non-linear systems and could be used straightforwardly without much modification. However, in the linear case, iterative expressions on the system matrices as well as interesting results related for example to the closed-loop stability, can be obtained. This

[2]Refer to Definition 3.19 for a precise definition of the notion.

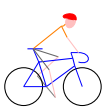

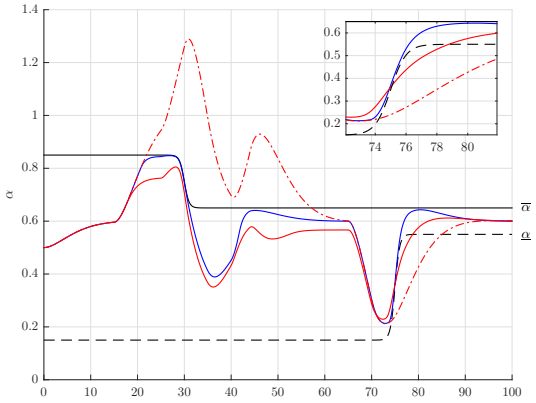

Figure 4.5: In plain blue line: additional simulation with $\kappa_1 = 1$ and $\kappa_2 = 10$. The considered requirement is enforced at all times but with no guarantee.

motivates a complete reformulation of the OIST approach despite the core principle remaining identical. This reformulation was initiated in [Chambon 15c] and [Chambon b] and is detailed in this section.

4.4.1 Considered class of linear systems and requirement

In this section, we consider a known linear time-invariant system $(\mathbf{G})$ described by the following state-space representation:

$$(\mathbf{G}) \begin{cases} \dot{\boldsymbol{x}} &= \mathbf{A}\boldsymbol{x} &+ \mathbf{B_u}u &+ \mathbf{B_d}\boldsymbol{d} \\ \boldsymbol{y} &= \boldsymbol{x} & &+ \mathbf{D_d}\boldsymbol{d} \end{cases} \tag{4.12}$$

where $\mathbf{A} \in \mathbb{R}^{n\times n}$, $\mathbf{B} = \begin{bmatrix}\mathbf{B_u} & \mathbf{B_d}\end{bmatrix} \in \mathbb{R}^{n\times m}$ and $\mathbf{D} = \begin{bmatrix}\mathbf{0}_{n\times 1} & \mathbf{D_d}\end{bmatrix} \in \mathbb{R}^{n\times m}$. The state vector is denoted $\boldsymbol{x} \in \mathbb{R}^n$ and the measurements vector is denoted $\boldsymbol{y} \in \mathbb{R}^n$. The input vector concatenates the single control input $u \in \mathbb{R}$ and the unknown inputs which are denoted $\boldsymbol{d} \in \mathbb{R}^{m-1}$. These unknown inputs can be used to model either state or measurements disturbances. Since no particular assumption has been made on the state-matrix $\mathbf{A}$, $(\mathbf{G})$ might be an unstable system. Let consider it is stabilized using the following dynamic controller $(\mathbf{K})$:

$$(\mathbf{K}) \begin{cases} \dot{\boldsymbol{x}}_K &= \mathbf{A_K}\boldsymbol{x}_K + \mathbf{B_K}\boldsymbol{u}_K \\ y_K &= \mathbf{C_K}\boldsymbol{x}_K + \mathbf{D_K}\boldsymbol{u}_K \end{cases} \tag{4.13}$$

where $\boldsymbol{x}_K \in \mathbb{R}^{n_K}$, $\boldsymbol{u}_K = \boldsymbol{y} - \boldsymbol{y}_s$ for $\boldsymbol{y}_s$ an optional set-point vector and $u = y_K$ in the nominal case, that is before introducing any saturation or anti-windup compensator as is the consequence of using the OIST approach. Note that the closed-loop consisting of system $(\mathbf{G})$ and controller $(\mathbf{K})$ is well-posed in any case since it is supposed that $\mathbf{D_u} = \mathbf{0}$. To illustrate the purpose of the OIST methodology selected in 4.1, the considered controller is supposed to have been designed prior to considering any time-domain requirement on an output variable. This is typical of an *evolutionary* approach as already highlighted in Chapter 3. If needed, other types of approaches are referenced in 3.2.2.

The objective in this chapter is to enforce a time-domain constraint on a given output variable. This may be an element of the output vector $\boldsymbol{y}$ or a combination of such elements. To consider the more general case, let introduce the matrix $\mathbf{C_\alpha} \in \mathbb{R}^{1\times n}$. The considered constrained output is denoted α and is defined by

$$\begin{aligned} \alpha &= \mathbf{C_\alpha}\boldsymbol{y} \\ &= \mathbf{C_\alpha}\boldsymbol{x} + \mathbf{C_\alpha}\mathbf{D_d}\boldsymbol{d} \\ &= \mathbf{C_\alpha}\boldsymbol{x} + \mathbf{D_\alpha}\boldsymbol{d} \end{aligned} \tag{4.14}$$

where $\mathbf{D_\alpha} = \mathbf{C_\alpha D_d} \in \mathbb{R}^{1\times m-1}$. Note that the case $\mathbf{D_\alpha} \neq \mathbf{0}$ is very conservative, hence, the application of OIST to such case may be very difficult. This is discussed in Chapter 6 where a practical solution is also proposed. The output constraint considered on α is similar in every way to the Definition 3.9 given in Chapter 3. It is named $\mathcal{K}(\Omega_\alpha)$ where $\Omega_\alpha(t) = [\underline{\alpha}(t), \overline{\alpha}(t)]$ is an interval of $\mathbb{R}$ for two time-varying design signals $\underline{\alpha}(t)$ and $\overline{\alpha}(t)$ such that

$$\underline{\alpha}(t) \leq \overline{\alpha}(t),\ \forall t \in \mathbb{R}_+ \tag{4.15}$$

These two design signals are also supposed to be sufficiently smooth where this notion will be specified later. Enforcing the time-domain constraint $\mathcal{K}(\Omega_\alpha)$ consists in keeping α in Ω_α at all times. This is formalized in 4.4.2. However, prior to stating the considered problems, some assumptions were made which were necessary to obtain guarantees on the reformulated OIST approach. Using these assumptions, a solution was obtained and is detailed in 4.4.3. Subsequent works aim at reducing the number and conservativeness of these assumptions.

Assumption 4.4 (Converging requirement signals)**.**
The time-domain requirement signals $\underline{\alpha}$ and $\overline{\alpha}$ are supposed to converge towards constant values denoted by:

$$\lim_{t\to+\infty} \underline{\alpha}(t) = \underline{\alpha}^\star,\ \lim_{t\to+\infty} \overline{\alpha}(t) = \overline{\alpha}^\star \tag{4.16}$$

where $\underline{\alpha}^\star \leq \overline{\alpha}^\star$.

This assumption is used to study the system equilibrium reachability when proving the asymptotic stability of the closed-loop. In practice, this assumption means that the output constraint can be considered static after some time. This is realistic since either the expected requirement should be given during a limited amount of time as is the case with the atmospheric flight of a launch vehicle or the expected requirement is already constant to mitigate the effects of a perturbation during the whole "lifetime" of the considered system.

The following assumption defines how the considered constrained output relates to the inputs u and $\boldsymbol{d}$. This is determining in the application of OIST.

Assumption 4.5 (Relative degree of the constrained output wrt inputs)**.**
Let $(k, l_1, \ldots, l_q) \in \mathbb{N}^{q+1}$ such that $0 \leq l_i \leq k$, for $1 \leq i \leq q$ and $q \leq m-1$. It is supposed the constrained output variable α is of relative degree k (resp. l_i) with respect to u (resp. the disturbance input $\boldsymbol{d}_i$).

Note that for a given index i, the relative degree l_i may be null. This corresponds to the case of measurements disturbances in case the matrix $\mathbf{D_\alpha}$ in (4.14) is non-null. State disturbances are thus characterized by $l_i \geq 1$. Also, the disturbances with a relative degree greater than k are not considered since they will not impact the method, hence $q \leq m-1$.

The next assumption is done to obtain simpler expressions in 4.6. It is not mandatory and mostly considered for presentation purposes.

Assumption 4.6 (Relation satisfied by the relative degrees)**.**
It is supposed that the non-null relative degrees considered in Assumption 4.5 satisfy to the relation

$$2l_i > k,\ \forall i \text{ s.t. } 1 \leq i \leq q \tag{4.17}$$

Also, it is supposed that measurement disturbances ($l_i = 0$) do not impact the state dynamics. This means that $\mathbf{B_{d}}_i = \mathbf{0_n}$ where $\mathbf{B_{d}}_i$ denotes the i-th column of $\mathbf{B_d}$.

Let, $\forall i$ s.t. $1 \leq i \leq q$: $\boldsymbol{\mathcal{D}}_i = \begin{bmatrix} \boldsymbol{d}_i & \dot{\boldsymbol{d}}_i & \ldots & \boldsymbol{d}_i^{(k-l_i)} \end{bmatrix}^\top \in \mathbb{R}^{k-l_i+1}$.

These vectors are supposed to be bounded by known bounds and, similarly to Assumption 4.4, these bounds are supposed to converge.

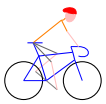

Assumption 4.7 (Bounded disturbances with known converging bounds)**.**
Let $i \in \mathbb{N}$ such that $1 \leq i \leq q$. There exists known time-varying continuous vectors $\underline{\boldsymbol{\mathcal{D}}_i}$ and $\overline{\boldsymbol{\mathcal{D}}_i}$ in $\mathbb{R}^{k-l_i+1}$ such that

$$\underline{\boldsymbol{\mathcal{D}}_i}(t) \leq \boldsymbol{\mathcal{D}}_i(t) \leq \overline{\boldsymbol{\mathcal{D}}_i}(t), \forall t \tag{4.18}$$

or, more precisely,

$$\underline{\boldsymbol{d}_i^{(j)}}(t) = \underline{\boldsymbol{\mathcal{D}}_i}_j(t) \leq \boldsymbol{d}_i^{(j)}(t) \leq \overline{\boldsymbol{\mathcal{D}}_i}_j(t) = \overline{\boldsymbol{d}_i^{(j)}}(t), \forall j \text{ s.t. } 0 \leq j \leq k - l_i, \forall t \tag{4.19}$$

Also, these vectors are supposed to converge towards vectors $\underline{\boldsymbol{\mathcal{D}}_i}^\star$ and $\overline{\boldsymbol{\mathcal{D}}_i}^\star$:

$$\lim_{t\to+\infty} \underline{\boldsymbol{\mathcal{D}}_i}(t) = \underline{\boldsymbol{\mathcal{D}}_i}^\star, \ \lim_{t\to+\infty} \overline{\boldsymbol{\mathcal{D}}_i}(t) = \overline{\boldsymbol{\mathcal{D}}_i}^\star \tag{4.20}$$

where $\underline{\boldsymbol{\mathcal{D}}_i}^\star = \begin{bmatrix}\underline{\boldsymbol{d}_i}^\star & 0 & \dots & 0\end{bmatrix}$ and $\overline{\boldsymbol{\mathcal{D}}_i}^\star = \begin{bmatrix}\overline{\boldsymbol{d}_i}^\star & 0 & \dots & 0\end{bmatrix}$.

This assumption brings information on the disturbance which may be conservative if the disturbance is not modelled very well. In practice, the most common considered bounds are of the form $\underline{\boldsymbol{\mathcal{D}}_i}^\star$ and $\overline{\boldsymbol{\mathcal{D}}_i}^\star$ since not much is usually known on the variations of the disturbances.

The next assumptions are concerned with the closed-loop stability of the saturated system. They are extensively used in 4.4.4.

Assumption 4.8 (Finite energy disturbance)**.**
The disturbance $\boldsymbol{d}$ is supposed to be of finite energy: $\|\boldsymbol{d}\| < +\infty$.

This will mainly be used to prove asymptotic stability. The controller (**K**) was introduced to stabilize the considered system. The type of stability as well as the equilibrium are specified in the following assumption.

Assumption 4.9 (Stabilizing controller (**K**))**.**
The controller (**K**) in (4.13) is supposed to asymptotically (resp. exponentially) stabilize (**G**) in (4.12) to the origin $\boldsymbol{x}^\star = 0$, under Assumption 4.8 (resp. $\boldsymbol{d} = 0$). The controller state at the equilibrium is denoted $\boldsymbol{x}_K^\star$ and $\boldsymbol{x}_K^\star = 0$.

Note that in this assumption, it is supposed that the asymptotic equilibrium is the origin. This is not conservative in the sense that a translation of this equilibrium can easily be performed when considering a non-null set-point.

The next assumption is the most conservative. It restricts the class of systems on which the approach can be applied *with guarantees*. This considered class of systems is the class of minimum phase systems:

Assumption 4.10 (Minimum phase system (**G**))**.**
The zeros of the SISO transfer function $T_{u\to\alpha}(s)$ from the control input u to the constrained output variable α are supposed to be with strictly negative real part.

Of course, the transformation can still be applied on non-minimum-phase systems but with unexpected results and at the cost of the global guarantee on the closed-loop stability or satisfaction of the constraint. Due to the unstable zeros, the system state may diverge upon saturation of the control input. For slowly unstable zeros, stability may be preserved but violation of the requirement will undoubtedly occur. This results from Proposition 4.32 not being satisfied in the non-minimum phase case. This is illustrated and studied in 4.6.2.

In this section, we described the considered system and made some assumptions which will be necessary to reformulate the OIST approach as well as to demonstrate stability results. In the following section, the considered problems are formally introduced to which the OIST approach is proposed as a solution.

4.4.2 Considered problems statements

The main problem tackled in this chapter is an output-constrained control problem using a new *evolutionary* approach [De Dona 02] based on introducing saturations on the stabilizing controller output [Burlion 12]. However, it was stated in the conclusions of 4.3 that applying this transformation does not come with guarantees on the actual satisfaction of the constraint or worse, on the resulting closed-loop stability. The formulation of the considered problems reflects these aspects:

Problem 4.11 (Output constrained control problem using OIST)**.**
Find two saturating signals $[\underline{u}(t), \overline{u}(t)]$ and a domain $\mathcal{C}_0$ such that for two given design signals $\underline{\alpha}(t)$ and $\overline{\alpha}(t)$ fulfilling $\underline{\alpha}(t) \leq \overline{\alpha}(t)$, $\forall t \in \mathbb{R}_+$, the constrained output α satisfies the constraint $\mathcal{K}(\Omega_\alpha)$:

$$\alpha(t) \in \Omega_\alpha(t) = [\underline{\alpha}(t), \overline{\alpha}(t)], \forall t \in \mathbb{R}_+ \tag{4.21}$$

for the system (**G**) in (4.12) in closed-loop with controller (**K**) in (4.13) and the saturations:

$$\begin{cases} \dot{\boldsymbol{x}}(t) &= \mathbf{A}\boldsymbol{x}(t) + \mathbf{B_u}u(t) + \mathbf{B_d}\boldsymbol{d}(t) \\ \boldsymbol{y}(t) &= \boldsymbol{x}(t) + \mathbf{D_d}\boldsymbol{d}(t) \\ \alpha(t) &= \mathbf{C_\alpha}\boldsymbol{x}(t) + \mathbf{D_\alpha}\boldsymbol{d}(t) \\ \dot{\boldsymbol{x}}_K(t) &= \mathbf{A_K}\boldsymbol{x}_K(t) + \mathbf{B_K}\boldsymbol{y}(t) \\ y_K(t) &= \mathbf{C_K}\boldsymbol{x}_K(t) + \mathbf{D_K}\boldsymbol{y}(t) \\ u(t) &= \mathrm{sat}_{\underline{u}(t)}^{\overline{u}(t)}(y_K(t)) \\ \boldsymbol{x}_0 &\in \mathcal{C}_0 \end{cases} \tag{4.22}$$

where it is supposed that Assumptions 4.4 to 4.10 are satisfied.

One may note that the problem of saturations overlap which was raised in 4.3 has not been addressed. This motivates the following remark.

Remark 4.12 (Saturations overlap mitigation subproblem)**.** As commented in 4.3.2 (e), finding a solution to Problem 4.11 implicitly requires that this solution guarantees the absence of saturations overlap. ◇

The purpose of the *Output to Input Saturation Transformation* (OIST) approach is to find the expressions of $\underline{u}(t)$ and $\overline{u}(t)$ such that the constraint on the output α is actually enforced. In practice, the "saturation" on the output α is *transformed* into a saturation on the control input. However, as mentioned in 4.3, the introduction of saturations in the closed-loop can lead to instabilities since saturating the input is equivalent to opening the stabilizing loop. Thus, another problem must be considered when applying OIST:

Problem 4.13 (Closed-loop stability using OIST)**.**
Guarantee that the origin of the saturated closed-loop in (4.22) is asymptotically stable.

A solution to Problem 4.11 is proposed in the next section where the reformulation of OIST in the linear framework along with results on saturations overlap mitigation are proposed. Problem 4.13 is tackled in 4.4.4. A solution is obtained which proves the global asymptotic stability of the system in (4.22) using the control saturations obtained in 4.4.3.

4.4.3 OIST with saturations overlap avoidance

The OIST approach introduced in [Burlion 12] for non-linear systems is now reformulated in the linear case for systems of the form (4.12) and fulfilling to Assumptions 4.4 to 4.10. This approach brings a solution to Problem 4.11 with guarantees on non-overlapping of the saturations as highlighted in Remark 4.12. For the first time, this thesis work describes in details how to choose the OIST design parameters time-varying such that saturations overlap is avoided.

4.4.3 (a) From the constrained output to the input: using the relative degree

Using Assumption 4.5, the dependency of the constrained output α with respect to u and $\boldsymbol{d}$ can be highlighted. Under Assumption 4.6, the expression of the k-th derivative of α is given by:

$$\alpha^{(k)}(t) = \mathbf{C}_{\boldsymbol{\alpha}}\mathbf{A}^k\boldsymbol{x}(t) + \mathbf{C}_{\boldsymbol{\alpha}}\mathbf{A}^{k-1}\mathbf{B}_{\mathbf{u}}u(t) + \sum_{i=1,l_i=0}^{q} \mathbf{D}_{\boldsymbol{\alpha}i}d_i^{(k)}(t) + \sum_{i=1,l_i\neq 0}^{q}\sum_{j=l_i}^{k} \mathbf{C}_{\boldsymbol{\alpha}}\mathbf{A}^{j-1}\mathbf{B}_{\mathbf{d}i}d_i^{(k-j)}(t) \tag{4.23}$$

where $\mathbf{B}_{\mathbf{d}i}$ refers to the i-th column of $\mathbf{B}_{\mathbf{d}}$. Note that due to the matrix $\mathbf{D}_{\boldsymbol{\alpha}}$ the k-th α-derivative depends on the k-th derivatives of the elements of $\boldsymbol{d}$ with respect to which it has a null relative degree. Hence, indicating $l_i = 0$ is in fact superfluous. By Definition 3.4 of the relative degree, the k-th derivative of α hence depends on the control input u.

Example 4.14 (Application to a simple example)**.** Let consider a stable system of the form (4.12) with $\boldsymbol{d} = \begin{bmatrix} d_1 & d_2 \end{bmatrix}^\top$ and $\alpha = \mathbf{C}_{\boldsymbol{\alpha}}\boldsymbol{x} + \mathbf{D}_{\boldsymbol{\alpha}}\boldsymbol{d} \in \mathbb{R}$ is of relative degree $k = 2$ with respect to u, $l_1 = 0$ with respect to d_1 (measurement disturbance) and $l_2 = 1$ with respect to d_2 (state disturbance). It is supposed that $\mathbf{C}_{\boldsymbol{\alpha}} = \begin{bmatrix} 1 & 0 \end{bmatrix}$ and, in coherence with Assumption 4.6, $\mathbf{B}_{\mathbf{d}1} = \mathbf{0}_{\mathbf{n}}$. Using (4.12), determination of the expression of $\ddot{\alpha}$ is straightforward:

$$\ddot{\alpha} = \mathbf{C}_{\boldsymbol{\alpha}}\mathbf{A}^2\boldsymbol{x} + \mathbf{C}_{\boldsymbol{\alpha}}\mathbf{A}\mathbf{B}_{\mathbf{u}}u + \ddot{d}_1 + \mathbf{C}_{\boldsymbol{\alpha}}\mathbf{A}\mathbf{B}_{\mathbf{d}2}d_2 + \mathbf{C}_{\boldsymbol{\alpha}}\mathbf{B}_{\mathbf{d}2}\dot{d}_2 \tag{4.24}$$

which is consistent with (4.23). ♣

In the next section, we show how the time-domain constraint expressed on the output α can be translated into a necessary condition on $\alpha^{(k)}$ using (4.23). Since the latter depends on the control input u, that necessary condition is in turn expressed as saturations on u in 4.4.3 (c).

4.4.3 (b) Propagated bounds: definition and a lemma

Considering Problem 4.11, the objective is to ensure that the constrained variable α satisfies $\alpha(t) \in \Omega_\alpha(t)$, $\forall t$. We now show how adequate constraints on the successive derivatives of α can be used to fulfil this requirement. Let consider a vector of known positive time-varying signals

$$\boldsymbol{\kappa}(t) = \begin{bmatrix} \kappa_1(t) & \dots & \kappa_k(t) \end{bmatrix}^\top \in \mathbb{R}_+^k \tag{4.25}$$

These signals will be the design parameters of the method. Contrary to what was considered in Chapter 3, these coefficients are now considered time-varying by default. The notion of propagated bounds was already defined in 3.3.3, Definition 3.14. These propagated bounds are used to *propagate* the interval constraint $\Omega_\alpha(t)$ to the successive derivatives of α. The definition is recalled here where time-varying design parameters $\boldsymbol{\kappa}(t)$ are now used.

Definition 4.15 (Propagated bounds)**.**
Let $\boldsymbol{\kappa}(t) = \begin{bmatrix} \kappa_1(t) & \dots & \kappa_k(t) \end{bmatrix} \in \mathbb{R}_+^k$ a vector of adequately smooth[a] positive time-varying signals and let suppose the output constraint signals $(\underline{\alpha}(t), \overline{\alpha}(t))$ are functions of $\mathcal{C}^k(\mathbb{R}_+, \mathbb{R})$. Let define $\underline{\alpha}_0(t) = \underline{\alpha}(t)$, $\overline{\alpha}_0(t) = \overline{\alpha}(t)$ and, $\forall i \in \mathbb{N}^\star$ s.t. $i \leq k$:

$$\begin{aligned} \underline{\alpha}_i(t) &= \kappa_i(t)\left(\underline{\alpha}_{i-1}(t) - \alpha^{(i-1)}(t)\right) + \dot{\underline{\alpha}}_{i-1}(t) \\ \overline{\alpha}_i(t) &= \kappa_i(t)\left(\overline{\alpha}_{i-1}(t) - \alpha^{(i-1)}(t)\right) + \dot{\overline{\alpha}}_{i-1}(t) \end{aligned} \tag{4.26}$$

These are called *propagated bounds* in the sense they propagate the expected bounds $\underline{\alpha}(t)$ and $\overline{\alpha}(t)$ up to the k-th differential of α.

[a] See Remark 4.16.

Remark 4.16. By *adequately smooth*, it is understood that, $\forall i \in \mathbb{N}_+$ s.t. $i \leq k$, $\kappa_i(t) \in \mathcal{C}^{k-i}(\mathbb{R}_+, \mathbb{R}_+)$. ◇

Prior to recalling the core lemma and for the OIST approach to be applicable, Assumption 3.15 still needs to be satisfied. Basically, satisfying this assumption means that the initial value of the constrained output and its derivatives should belong to the intervals composed by the propagated bounds:

$$\forall i \in \mathbb{N} \text{ s.t. } i \leq k,\ \alpha^{(i)}(0) \in \Omega_\alpha^i(0) \tag{4.27}$$

where $\Omega_\alpha^i(t) = [\underline{\alpha}_i(t), \overline{\alpha}_i(t)]$, $\forall t$. Fulfilling this assumption provides a solution for the initial admissible domain $\mathcal{C}_0$ introduced in Problem 4.11. This can be considered an aside problem but should not be underestimated. Failing to satisfy this assumption can lead to unexpected results even in the absence of implementation error.

Lemma 3.16 remains applicable. For the sake of clarity, it is recalled here:

Lemma 4.17 (Propagated bounds lemma)**.**
Let suppose Assumptions 4.5 and 3.15 are satisfied. Let define propagated bounds as in Definition 4.15, $\forall i \in \mathbb{N}$ s.t. $i \leq k$. Then,

$$\alpha^{(k)}(t) \in [\underline{\alpha}_k(t), \overline{\alpha}_k(t)] = \Omega_\alpha^k(t),\ \forall t \in \mathbb{R}_+ \Rightarrow \alpha(t) \in [\underline{\alpha}(t), \overline{\alpha}(t)] = \Omega_\alpha(t),\ \forall t \in \mathbb{R}_+$$

Proof. See the proof of Lemma 3.16 in 3.3.3. □

Remark 4.18. Note this Lemma is still valid when introducing more conservative bounds $\underline{\beta}_j(t)$ and $\overline{\beta}_j(t)$ on $\alpha^{(j)}(t)$, i.e. satisfying for any given i such that $1 \leq i \leq k$:

$$\underline{\alpha}_i(t) \leq \underline{\beta}_i(t),\ \overline{\beta}_i(t) \leq \overline{\alpha}_i(t),\ \forall t \tag{4.28}$$

Also note these more conservative bounds are not necessarily defined by an iterative relation as in (4.26). ◇

This lemma was directly inspired by Assumption 4.5 which led to (4.23) where the dependence on u is highlighted. It provides a necessary condition to enforce the time-domain constraint on the considered constrained output α. Since $\alpha^{(k)}$ depends on the control input, this condition is equivalent to keeping u in the interval $[\underline{u}(t), \overline{u}(t)]$, $\forall t$ where $\underline{u}$ and $\overline{u}$ are appropriately-defined saturations. Of course, this is subject to knowing the system state as well as bounds on the disturbance signals, which is supposed in the whole section as by the definition of the output signal $\boldsymbol{y}$ and Assumption 4.7. The deduction of the control saturations from (4.23) and Lemma 4.17 is performed in the next section.

4.4.3 (c) Resulting expressions of the control saturations

Using the relative degree Definition 3.4, an expression of $\alpha^{(k)}$ in function of the control input u has been obtained in (4.23). Also, it was shown that satisfying a necessary condition on $\alpha^{(k)}$ leads to fulfilling the time-domain constraint $\alpha(t) \in \Omega_\alpha(t)$, $\forall t$. With a slight transformation, this necessary condition can thus be expressed in the form of saturations to apply to the control input u.

First, under Assumption 4.5, there is $\mathbf{C_\alpha A}^{k-1}\mathbf{B_u} \neq 0$. For the time-being, let also suppose that $\mathbf{C_\alpha A}^{k-1}\mathbf{B_u} > 0$. Considering Lemma 4.17 and (4.23), and supposing that the expressions of $\underline{\alpha}_k(t)$ and $\overline{\alpha}_k(t)$ as defined in (4.26) for $i = k$ are known $\forall t$, the saturations to apply to the control input u such that the necessary condition is satisfied can be obtained. In this undisturbed case, i.e. for $\boldsymbol{d} = 0$, these saturations are given by:

$$\begin{aligned} \underline{u}(t) &= \frac{1}{\mathbf{C_\alpha A}^{k-1}\mathbf{B_u}} \left[\underline{\alpha}_k(t) - \mathbf{C_\alpha A}^k \boldsymbol{x}(t)\right] \\ \overline{u}(t) &= \frac{1}{\mathbf{C_\alpha A}^{k-1}\mathbf{B_u}} \left[\overline{\alpha}_k(t) - \mathbf{C_\alpha A}^k \boldsymbol{x}(t)\right] \end{aligned} \tag{4.29}$$

In the more general case where $\boldsymbol{d} \neq 0$, the saturations expressions depend on the disturbance and cannot be determined straightforwardly. However, using Assumption 4.7 which supposes

that the disturbance vector $\boldsymbol{d}$ and its derivatives[3] are bounded with known bounds, the following saturations are obtained:

$$\begin{aligned}
\underline{u}(t) &= \frac{1}{\mathbf{C_\alpha A^{k-1} B_u}} \Big[\underline{\alpha}_k(t) - \mathbf{C_\alpha A}^k \boldsymbol{x}(t) + \textstyle\sum_{i=1,l_i=0}^{q} |\mathbf{D}_{\boldsymbol{\alpha}i}| \max\left(\left|\underline{\boldsymbol{d}_i^{(k)}}(t)\right|, \left|\overline{\boldsymbol{d}_i^{(k)}}(t)\right| \right) \\
&\qquad + \textstyle\sum_{i=1,l_i\neq 0}^{q} \sum_{j=l_i}^{k} \left|\mathbf{C_\alpha A}^{j-1}\mathbf{B_d}\right| \max\left(\left|\underline{\boldsymbol{d}_i^{(k-j)}}(t)\right|, \left|\overline{\boldsymbol{d}_i^{(k-j)}}(t)\right| \right) \Big] \\
\overline{u}(t) &= \frac{1}{\mathbf{C_\alpha A^{k-1} B_u}} \Big[\overline{\alpha}_k(t) - \mathbf{C_\alpha A}^k \boldsymbol{x}(t) - \textstyle\sum_{i=1,l_i=0}^{q} |\mathbf{D}_{\boldsymbol{\alpha}i}| \max\left(\left|\underline{\boldsymbol{d}_i^{(k)}}(t)\right|, \left|\overline{\boldsymbol{d}_i^{(k)}}(t)\right| \right) \\
&\qquad - \textstyle\sum_{i=1,l_i\neq 0}^{q} \sum_{j=l_i}^{k} \left|\mathbf{C_\alpha A}^{j-1}\mathbf{B_d}\right| \max\left(\left|\underline{\boldsymbol{d}_i^{(k-j)}}(t)\right|, \left|\overline{\boldsymbol{d}_i^{(k-j)}}(t)\right| \right) \Big]
\end{aligned} \tag{4.30}$$

Note that by definition of $\mathbf{D}_{\boldsymbol{\alpha}}$, bounds on the k-th derivatives of the elements of $\boldsymbol{d}$ are only required for the elements $\boldsymbol{d}_i$ with $l_i = 0$.

Example 4.19 (Illustration of the resulting control saturation)**.** Let consider the model introduced in Example 4.14 under Assumption 4.7. Let find a solution to Pb. 4.11 for two given design signals $\underline{\alpha}(t)$ and $\overline{\alpha}(t)$. Using the expression of $\ddot{\alpha}$ in (4.24), Definition 4.15 of the propagated bounds and applying the transformation of the output constraint into control saturations, the following expressions are obtained:

$$\begin{aligned}
\underline{u} &= \frac{1}{\mathbf{C_\alpha AB_u}} \Big[\underline{\alpha}_2 - \mathbf{C_\alpha A}^2 \boldsymbol{x} + \max\left(\left|\underline{d_1^{(2)}}\right|, \left|\overline{d_1^{(2)}}\right| \right) + |\mathbf{C_\alpha AB_{d2}}| \max\left(|\underline{d_2}|, |\overline{d_2}| \right) \\
&\qquad + |\mathbf{C_\alpha B_{d2}}| \max\left(|\underline{\dot{d}_2}|, |\overline{\dot{d}_2}| \right) \Big] \\
\overline{u} &= \frac{1}{\mathbf{C_\alpha AB_u}} \Big[\underline{\alpha}_2 - \mathbf{C_\alpha A}^2 \boldsymbol{x} - \max\left(\left|\underline{d_1^{(2)}}\right|, \left|\overline{d_1^{(2)}}\right| \right) - |\mathbf{C_\alpha AB_{d2}}| \max\left(|\underline{d_2}|, |\overline{d_2}| \right) \\
&\qquad - |\mathbf{C_\alpha B_{d2}}| \max\left(|\underline{\dot{d}_2}|, |\overline{\dot{d}_2}| \right) \Big]
\end{aligned} \tag{4.31}$$

where $\mathbf{C_\alpha AB_u} \neq 0$ by definition of the relative degree with $k = 2$ and $\mathbf{C_\alpha AB_u}$ is supposed to be positive. The obtained expressions are coherent with (4.30). ♣

To be appropriately defined, the saturations in both (4.29) and (4.29) should not overlap, i.e. they should satisfy $\overline{u}(t) > \underline{u}(t)$, $\forall t$. Saturations overlap can be caused by choosing non-symmetrical time-varying constraint signals $\underline{\alpha}(t)$ and $\overline{\alpha}(t)$ and/or due to the presence of bounded unknown disturbances as is the case in Problem 4.11. The presence of bounded unknown disturbances effectively led to more conservative saturations as shown in (4.30).

Saturations overlap can be avoided using appropriately defined time-varying design parameters $\boldsymbol{\kappa}(t)$. This was mentioned in Chapter 3, Remark 3.21. It was also mentioned that no constructive rules existed on how to choose these parameters. New results on that subject are presented in 4.4.3 (e).

Remark 4.20. In case $\mathbf{C_\alpha A}^{k-1}\mathbf{B_u} < 0$ and to avoid loss of generality, proper re-ordering of $\underline{u}(t)$ and $\overline{u}(t)$ is required. For a given signal y_K, the saturating operator can be defined as follows:

$$\mathrm{sat}_{\underline{u}(t)}^{\overline{u}(t)}(y_K)(t) = \max(\min(\underline{u}(t), \overline{u}(t)), \min(y_K(t), \max(\underline{u}(t), \overline{u}(t)))) \tag{4.32}$$

◇

Before tackling the overlap problem, it can be noted that the saturations expressions in (4.30) depend on the quantities $\underline{\alpha}_k(t)$ and $\overline{\alpha}_k(t)$ which expression has not be specified yet. This is presented in the next section.

[3] Up to the relative degree l_i for element d_i.

4.4.3 (d) Explicit formulation of the propagated bounds

The control input saturations obtained in (4.30) depend on the propagated bounds $\underline{\alpha}_k(t)$ and $\overline{\alpha}_k(t)$ as defined in (4.26) for $i = k$. Since the relative degrees of α with respect to the components of $\boldsymbol{d}$ are supposed to be smaller than k in Assumption 4.5 this means that the propagated bounds can depend on $\boldsymbol{d}$ which is an unknown quantity. This motivates a more thorough study of the propagated bounds expressions. We start by considering the case in Example 4.14 to show that explicit expressions can be derived from the iterative propagated bounds definition:

Example 4.21 (Explicit expressions of the propagated bounds)**.** Let consider the case introduced in Example 4.14. Considering the iterative definition of the propagated bounds in (4.26), we obtain, for the lower propagated bounds:

$$\begin{aligned}
\underline{\alpha}_0 &= \underline{\alpha} \\
\underline{\alpha}_1 &= \kappa_1 \left(\underline{\alpha} - \mathbf{C}_{\boldsymbol{\alpha}}\boldsymbol{x} - d_1\right) + \dot{\underline{\alpha}} \\
\underline{\alpha}_2 &= \kappa_2 \left(\underline{\alpha}_1 - \mathbf{C}_{\boldsymbol{\alpha}}\mathbf{A}\boldsymbol{x} - \mathbf{C}_{\boldsymbol{\alpha}}\mathbf{B}_{\mathbf{d}2}d_2 - \dot{d}_1\right) + \dot{\underline{\alpha}}_1 \\
&= \left(\kappa_1\kappa_2 + \dot{\kappa}_1\right)\left(\underline{\alpha} - \mathbf{C}_{\boldsymbol{\alpha}}\boldsymbol{x} - d_1\right) + \left(\kappa_1 + \kappa_2\right)\left(\dot{\underline{\alpha}} - \mathbf{C}_{\boldsymbol{\alpha}}\mathbf{A}\boldsymbol{x} - \dot{d}_1\right) + \ddot{\underline{\alpha}} - \left(\kappa_1 + \kappa_2\right)\mathbf{C}_{\boldsymbol{\alpha}}\mathbf{B}_{\mathbf{d}2}d_2
\end{aligned} \tag{4.33}$$

where the time-varying design parameters κ_1 and κ_2 are defined in a later section. Similar expressions are obtained for the upper bounds. As expected, $\underline{\alpha}_2$ and $\overline{\alpha}_2$ depend on the unknown signals d_1 and d_2. This makes the determination of the control input saturations in (4.31) impossible to apply in their current form.

Before introducing more conservative expressions in place of the propagated bounds, note that the expressions in (4.33) can be written as

$$\begin{aligned}
\underline{\alpha}_1 &= u_0^1\left(\underline{\alpha} - \mathbf{C}_{\boldsymbol{\alpha}}\boldsymbol{x} - d_1\right) + \left(\dot{\underline{\alpha}} - \mathbf{C}_{\boldsymbol{\alpha}}\mathbf{A}\boldsymbol{x} - \dot{d}_1\right) + \mathbf{C}_{\boldsymbol{\alpha}}\mathbf{A}\boldsymbol{x} + \dot{d}_1 \\
&= U^1\left\{\underline{\boldsymbol{\mathcal{A}}} - \boldsymbol{\mathcal{O}}\boldsymbol{x} - \boldsymbol{\mathcal{D}}_1\right\} + \mathbf{C}_{\boldsymbol{\alpha}}\mathbf{A}\boldsymbol{x} + \dot{d}_1 - \boldsymbol{V}_2^1\boldsymbol{\mathcal{D}}_2 \\
\underline{\alpha}_2 &= u_0^2\left(\underline{\alpha} - \mathbf{C}_{\boldsymbol{\alpha}}\boldsymbol{x} - d_1\right) + u_1^2\left(\dot{\underline{\alpha}} - \mathbf{C}_{\boldsymbol{\alpha}}\mathbf{A}\boldsymbol{x} - \dot{d}_1\right) + \left(\ddot{\underline{\alpha}} - \mathbf{C}_{\boldsymbol{\alpha}}\mathbf{A}^2\boldsymbol{x} - \ddot{d}_1\right) + \mathbf{C}_{\boldsymbol{\alpha}}\mathbf{A}^2\boldsymbol{x} \\
&\qquad\qquad + \ddot{d}_1 - v_0^2 d_2 \\
&= U^2\left\{\underline{\boldsymbol{\mathcal{A}}} - \boldsymbol{\mathcal{O}}\boldsymbol{x} - \boldsymbol{\mathcal{D}}_1\right\} + \mathbf{C}_{\boldsymbol{\alpha}}\mathbf{A}^2\boldsymbol{x} + \ddot{d}_1 - \boldsymbol{V}_2^2\boldsymbol{\mathcal{D}}_2
\end{aligned} \tag{4.34}$$

where

$$\begin{aligned}
\underline{\boldsymbol{\mathcal{A}}} &= \begin{bmatrix}\underline{\alpha} & \dot{\underline{\alpha}} & \ddot{\underline{\alpha}}\end{bmatrix}^\top \\
\boldsymbol{\mathcal{O}} &= \begin{bmatrix}\mathbf{C}_{\boldsymbol{\alpha}} & \mathbf{C}_{\boldsymbol{\alpha}}\mathbf{A} & \mathbf{C}_{\boldsymbol{\alpha}}\mathbf{A}^2\end{bmatrix}^\top \\
\boldsymbol{\mathcal{D}}_1 &= \begin{bmatrix}d_1 & \dot{d}_1 & \ddot{d}_1\end{bmatrix}^\top \in \mathbb{R}^3 \\
\boldsymbol{\mathcal{D}}_2 &= \begin{bmatrix}d_2 & \dot{d}_2\end{bmatrix}^\top \in \mathbb{R}^2 \\
\boldsymbol{U}^1 &= \begin{bmatrix}u_0^1 & 1 & 0\end{bmatrix} \\
&= \begin{bmatrix}\kappa_1 & 1 & 0\end{bmatrix} \\
\boldsymbol{U}^2 &= \begin{bmatrix}u_0^2 & u_1^2 & 1\end{bmatrix} \\
&= \begin{bmatrix}\kappa_1\kappa_2 + \dot{\kappa}_1 & \kappa_1 + \kappa_2 & 1\end{bmatrix} \\
\boldsymbol{V}_2^1 &= \begin{bmatrix}0 & 0\end{bmatrix} \\
\boldsymbol{V}_2^2 &= \begin{bmatrix}v_{2,0}^2 & 0\end{bmatrix} \\
&= \begin{bmatrix}u_1^2\mathbf{C}_{\boldsymbol{\alpha}}\mathbf{B}_{\mathbf{d}2} & 0\end{bmatrix}
\end{aligned} \tag{4.35}$$

As will be highlighted hereafter, iterative expressions link the row vectors $\boldsymbol{U}^2$ and $\boldsymbol{U}^1$ and the vectors $\boldsymbol{V}_2^2$ and $\boldsymbol{V}_2^1$. Also, using the resulting explicit expressions and Assumption 4.7 and considering Remark 4.18, more conservative expressions of the propagated bounds will be derived to account for the unknown signals in $\boldsymbol{\mathcal{D}}_1$ and $\boldsymbol{\mathcal{D}}_2$. ♣

Following a similar procedure than in Example 4.21, for any $j \in \mathbb{N}^\star$ such that $j \leq k$, let introduce the following vectors:

$$\begin{array}{rcl} \boldsymbol{U}^j & = & \begin{bmatrix} u_0^j & \dots & u_k^j \end{bmatrix} \in \mathbb{R}^{1\times(k+1)} \\ \boldsymbol{V}_i^j & = & \begin{bmatrix} v_{i,0}^j & \dots & v_{i,k-l_i}^j \end{bmatrix} \in \mathbb{R}^{1\times(k-l_i+1)}, \forall i \in \mathbb{N}^\star \text{ s.t. } i \leq q \text{ and } l_i \neq 0 \end{array} \tag{4.36}$$

where

- $u_j^j = 1$;
- $\forall m > j$, $u_m^j = 0$;
- $\forall m > \max(-1, j - l_i - 1)$, $v_{i,m}^j = 0$;
- $v_{i,0}^{l_i+1} = u_{l_i-1}^{l_i} \mathbf{C}_{\boldsymbol{\alpha}} \mathbf{A}^{l_i-1} \mathbf{B}_{\mathbf{d}i}$.

Interestingly enough, it is also obtained that since $u_0^1 = \kappa_1$ then $u_j^{j+1} = \sum_{w=1}^{j+1} \kappa_w$, $\forall j$ s.t. $0 \leq j < k$. Let also consider the following matrices:

$$\begin{array}{rcl} \underline{\boldsymbol{\mathcal{A}}} & = & \begin{bmatrix} \underline{\alpha} & \dot{\underline{\alpha}} & \dots & (\underline{\alpha})^{(k)} \end{bmatrix}^\top \in \mathbb{R}^{k+1} \\ \overline{\boldsymbol{\mathcal{A}}} & = & \begin{bmatrix} \overline{\alpha} & \dot{\overline{\alpha}} & \dots & (\overline{\alpha})^{(k)} \end{bmatrix}^\top \in \mathbb{R}^{k+1} \\ \boldsymbol{\mathcal{O}} & = & \begin{bmatrix} \mathbf{C}_{\boldsymbol{\alpha}} & \mathbf{C}_{\boldsymbol{\alpha}}\mathbf{A} & \dots & \mathbf{C}_{\boldsymbol{\alpha}}\mathbf{A}^k \end{bmatrix}^\top \in \mathbb{R}^{(k+1)\times n} \end{array} \tag{4.37}$$

The expressions in (4.34) are then generalized and the following explicit expressions are obtained for the propagated bounds $\underline{\alpha}_j$ and $\overline{\alpha}_j$ at step j:

$$\begin{array}{rcl} \underline{\alpha}_j & = & \boldsymbol{U}^j \left\{ \underline{\boldsymbol{\mathcal{A}}} - \boldsymbol{\mathcal{O}}\boldsymbol{x} - \sum_{i=1,l_i=0}^{q} \mathbf{D}_{\boldsymbol{\alpha}i} \boldsymbol{\mathcal{D}}_i \right\} + \mathbf{C}_{\boldsymbol{\alpha}} \mathbf{A}^j \boldsymbol{x} + \sum_{i=1,l_i=0}^{q} \mathbf{D}_{\boldsymbol{\alpha}i} \boldsymbol{d}_i^{(j)} - \sum_{i=1,l_i\neq 0}^{q} \boldsymbol{V}_i^j \boldsymbol{\mathcal{D}}_i \\ \overline{\alpha}_j & = & \boldsymbol{U}^j \left\{ \overline{\boldsymbol{\mathcal{A}}} - \boldsymbol{\mathcal{O}}\boldsymbol{x} - \sum_{i=1,l_i=0}^{q} \mathbf{D}_{\boldsymbol{\alpha}i} \boldsymbol{\mathcal{D}}_i \right\} + \mathbf{C}_{\boldsymbol{\alpha}} \mathbf{A}^j \boldsymbol{x} + \sum_{i=1,l_i=0}^{q} \mathbf{D}_{\boldsymbol{\alpha}i} \boldsymbol{d}_i^{(j)} - \sum_{i=1,l_i\neq 0}^{q} \boldsymbol{V}_i^j \boldsymbol{\mathcal{D}}_i \end{array} \tag{4.38}$$

Using this formulation of the propagated bounds coupled to their iterative definition in (4.26), the vectors $\boldsymbol{U}^j$ and $\boldsymbol{V}_i^j$ (for $i \in \mathbb{N}^\star$, $i \leq q$) are given by the following iterative expressions:

$$\begin{array}{lrcl} & \boldsymbol{U}^0 & = & \begin{bmatrix} 1 & 0 & \dots & 0 \end{bmatrix} \\ \forall j \text{ s.t. } 1 \leq j \leq k, & \boldsymbol{U}^j & = & \kappa_j \boldsymbol{U}^{j-1} + \dot{\boldsymbol{U}}^{j-1} + \boldsymbol{\sigma}\left(\boldsymbol{U}^{j-1}\right) \\ \forall j \text{ s.t. } 0 \leq j \leq l, & \boldsymbol{V}_i^j & = & \begin{bmatrix} 0 & \dots & 0 \end{bmatrix} \\ \forall j \text{ s.t. } l < j \leq k & \boldsymbol{V}_i^j & = & \kappa_j \left(\boldsymbol{V}_i^{j-1} + \mathbf{C}_{\boldsymbol{\alpha}} \mathbf{A}^{j-l_i-1} \begin{bmatrix} \mathbf{A}^{l_i-1}\mathbf{B}_{\mathbf{d}i} & \dots & \mathbf{A}^{2l_i-j}\mathbf{B}_{\mathbf{d}i} & 0 & \dots & 0 \end{bmatrix} \right) \\ & & & + \dot{\boldsymbol{V}}_i^{j-1} + \boldsymbol{\sigma}\left(\boldsymbol{V}_i^{j-1}\right) + \begin{bmatrix} \sum_{w=0}^{j-l_i-1} u_{l_i-1-w}^{j-1} \mathbf{C}_{\boldsymbol{\alpha}} \mathbf{A}^{l_i-1+w} \mathbf{B}_{\mathbf{d}i} & 0 & \dots & 0 \end{bmatrix} \end{array} \tag{4.39}$$

where $\boldsymbol{\sigma}$ is the cyclic permutation of length $k+1$ on the elements of $\boldsymbol{U}^{j-1}$ (resp. $\boldsymbol{V}_i^{j-1}$), as defined in Definition 4.1.

As illustrated in Example 4.21, the explicit expressions of the propagated bounds in (4.38) depend on the unknown but bounded[4] quantities $\boldsymbol{\mathcal{D}}_i$. The consequence is that the control saturations detailed in (4.30) cannot be made explicit and implemented in a control algorithm.

However, as mentioned in Remark 4.18, the propagated bounds Lemma 4.17 is still applicable in the case more conservative bounds $\underline{\beta}_j$ and $\overline{\beta}_j$ are considered:

$$\underline{\alpha}_j \leq \underline{\beta}_j, \ \overline{\alpha}_j \geq \overline{\beta}_j, \ \forall j \in \mathbb{N}^\star \text{ s.t. } j \leq k, \forall t \tag{4.40}$$

[4] See Assumption 4.7.

Contrary to the original propagated bounds, these new bounds $\underline{\beta}_j$ and $\overline{\beta}_j$ are however not defined iteratively but deduced from the original propagated bounds expressions. Using Assumption 4.7, the following is obtained for a given $j \in \mathbb{N}^\star$:

$$\begin{aligned}
\underline{\beta}_j &= \boldsymbol{U}^j \{\underline{\boldsymbol{\mathcal{A}}} - \boldsymbol{\mathcal{O}}\boldsymbol{x}\} + \left|\boldsymbol{U}^j\right| \textstyle\sum_{i=1,l_i=0}^{q} |\mathbf{D}_{\boldsymbol{\alpha}i}| \max\left(\left|\underline{\boldsymbol{\mathcal{D}}_i}\right|, \left|\overline{\boldsymbol{\mathcal{D}}_i}\right|\right) + \mathbf{C}_{\boldsymbol{\alpha}}\mathbf{A}^j\boldsymbol{x} \\
&\quad + \textstyle\sum_{i=1,l_i=0}^{q} |\mathbf{D}_{\boldsymbol{\alpha}i}| \max\left(\left|\underline{\boldsymbol{d}_i^{(j)}}\right|, \left|\overline{\boldsymbol{d}_i^{(j)}}\right|\right) + \textstyle\sum_{i=1,l_i\neq 0}^{q} \left|\boldsymbol{V}_i^j\right| \max\left(\left|\underline{\boldsymbol{\mathcal{D}}_i}\right|, \left|\overline{\boldsymbol{\mathcal{D}}_i}\right|\right) \\
\overline{\beta}_j &= \boldsymbol{U}^j \{\overline{\boldsymbol{\mathcal{A}}} - \boldsymbol{\mathcal{O}}\boldsymbol{x}\} - \left|\boldsymbol{U}^j\right| \textstyle\sum_{i=1,l_i=0}^{q} |\mathbf{D}_{\boldsymbol{\alpha}i}| \max\left(\left|\underline{\boldsymbol{\mathcal{D}}_i}\right|, \left|\overline{\boldsymbol{\mathcal{D}}_i}\right|\right) + \mathbf{C}_{\boldsymbol{\alpha}}\mathbf{A}^j\boldsymbol{x} \\
&\quad - \textstyle\sum_{i=1,l_i=0}^{q} |\mathbf{D}_{\boldsymbol{\alpha}i}| \max\left(\left|\underline{\boldsymbol{d}_i^{(j)}}\right|, \left|\overline{\boldsymbol{d}_i^{(j)}}\right|\right) - \textstyle\sum_{i=1,l_i\neq 0}^{q} \left|\boldsymbol{V}_i^j\right| \max\left(\left|\underline{\boldsymbol{\mathcal{D}}_i}\right|, \left|\overline{\boldsymbol{\mathcal{D}}_i}\right|\right)
\end{aligned} \tag{4.41}$$

By convention, it is also chosen $\underline{\beta}_0 = \underline{\alpha}_0 = \underline{\alpha}$ and $\overline{\beta}_0 = \overline{\alpha}_0 = \overline{\alpha}$. Note these expressions are not differentiable. In the next section, it will be required to obtain differentiable design coefficients $\boldsymbol{\kappa}$ motivating the use of differentiable over-approximating functions of max and $|\bullet|$. These new expressions are now illustrated on the example.

Example 4.22 (Illustration of the new – conservative – propagated bounds)**.** From the expressions of the propagated bounds in (4.33), the following more conservative expressions are obtained:

$$\begin{aligned}
\underline{\beta}_0 &= \underline{\alpha} \\
\underline{\beta}_1 &= \kappa_1 (\underline{\alpha} - \mathbf{C}_{\boldsymbol{\alpha}}\boldsymbol{x}) + \underline{\dot{\alpha}} + |\kappa_1| \max\left(\left|\underline{d_1}\right|, \left|\overline{d_1}\right|\right) \\
\underline{\beta}_2 &= (\kappa_1\kappa_2 + \dot{\kappa}_1)(\underline{\alpha} - \mathbf{C}_{\boldsymbol{\alpha}}\boldsymbol{x}) + (\kappa_1 + \kappa_2)(\underline{\dot{\alpha}} - \mathbf{C}_{\boldsymbol{\alpha}}\mathbf{A}\boldsymbol{x}) + \underline{\ddot{\alpha}} + |\kappa_1\kappa_2 + \dot{\kappa}_1| \max\left(\left|\underline{d_1}\right|, \left|\overline{d_1}\right|\right) \\
&\qquad |\kappa_1 + \kappa_2| \max\left(\left|\underline{\dot{d}_1}\right|, \left|\overline{\dot{d}_1}\right|\right) + |\kappa_1 + \kappa_2| \left|\mathbf{C}_{\boldsymbol{\alpha}}\mathbf{B}_{\mathbf{d}2}\right| \max\left(\left|\underline{d_2}\right|, \left|\overline{d_2}\right|\right)
\end{aligned} \tag{4.42}$$

which is consistent with (4.41). Similar expressions are obtained for the upper bounds. Note that bounds on d_1 and d_2 were supposedly known in Example 4.19 under Assumption 4.7. ♣

Using these new expressions for the propagated bounds, the control input saturations are redefined. Using a slight abuse of notation where $\underline{u}$ and $\overline{u}$ now refer to the new saturations, the following is obtained:

$$\begin{aligned}
\underline{u}(t) &= \tfrac{1}{\mathbf{C}_{\boldsymbol{\alpha}}\mathbf{A}^{k-1}\mathbf{B}_{\mathbf{u}}} \Big[\underline{\beta}_k(t) - \mathbf{C}_{\boldsymbol{\alpha}}\mathbf{A}^k\boldsymbol{x}(t) + \textstyle\sum_{i=1,l_i=0}^{q} |\mathbf{D}_{\boldsymbol{\alpha}i}| \max\left(\left|\underline{\boldsymbol{d}_i^{(k)}}(t)\right|, \left|\overline{\boldsymbol{d}_i^{(k)}}(t)\right|\right) \\
&\qquad + \textstyle\sum_{i=1,l_i\neq 0}^{q} \sum_{j=l_i}^{k} \left|\mathbf{C}_{\boldsymbol{\alpha}}\mathbf{A}^{j-1}\mathbf{B}_{\mathbf{d}i}\right| \max\left(\left|\underline{\boldsymbol{d}_i^{(k-j)}}(t)\right|, \left|\overline{\boldsymbol{d}_i^{(k-j)}}(t)\right|\right)\Big] \\
\overline{u}(t) &= \tfrac{1}{\mathbf{C}_{\boldsymbol{\alpha}}\mathbf{A}^{k-1}\mathbf{B}_{\mathbf{u}}} \Big[\overline{\beta}_k(t) - \mathbf{C}_{\boldsymbol{\alpha}}\mathbf{A}^k\boldsymbol{x}(t) - \textstyle\sum_{i=1,l_i=0}^{q} |\mathbf{D}_{\boldsymbol{\alpha}i}| \max\left(\left|\underline{\boldsymbol{d}_i^{(k)}}(t)\right|, \left|\overline{\boldsymbol{d}_i^{(k)}}(t)\right|\right) \\
&\qquad - \textstyle\sum_{i=1,l_i\neq 0}^{q} \sum_{j=l_i}^{k} \left|\mathbf{C}_{\boldsymbol{\alpha}}\mathbf{A}^{j-1}\mathbf{B}_{\mathbf{d}i}\right| \max\left(\left|\underline{\boldsymbol{d}_i^{(k-j)}}(t)\right|, \left|\overline{\boldsymbol{d}_i^{(k-j)}}(t)\right|\right)\Big]
\end{aligned} \tag{4.43}$$

Now that the saturations expressions have been fully detailed, one has to ensure that there is no overlap. Saturations overlap is a consequence of considering conservative bounds on the unknown disturbances and the possible variations of the output constraint. Consequences of saturations overlap was highlighted in the case study in 4.3. It was shown that the time-domain requirement cannot be enforced with guarantees in the presence of saturations overlap. A solution to mitigate this phenomenon and obtain guarantees on the solution to Problem 4.11 is described in the next section.

4.4.3 (e) Saturations overlap mitigation

To mitigate propagated bounds and saturations overlap, the quantities $\overline{\beta}_j - \underline{\beta}_j$ can be considered. It is shown that factorization by κ_j in these expressions is possible. Through proper definition

of the design coefficients in $\boldsymbol{\kappa}$, overlap can thus be avoided. In the case $j = k$, additional terms also appear as a consequence of the saturations expressions obtained in (4.43).

A formal study of saturations overlap is now proposed. Let $\Delta_0 = \overline{\beta}_0 - \underline{\beta}_0 = \overline{\alpha} - \underline{\alpha}$ and, $\forall j \in \mathbb{N}^\star$ s.t. $j \leq k$, $\Delta_j = \overline{\beta}_j - \underline{\beta}_j$. Using (4.41), the following expression is obtained for Δ_j:

$$\begin{aligned}\Delta_j = \boldsymbol{U}^j \left\{\overline{\boldsymbol{\mathcal{A}}} - \underline{\boldsymbol{\mathcal{A}}}\right\} - 2\left|\boldsymbol{U}^j\right| \sum_{i=1,l_i=0}^{q} |\mathbf{D}_{\boldsymbol{\alpha} i}| \max\left(\left|\underline{\boldsymbol{\mathcal{D}}_i}\right|, \left|\overline{\boldsymbol{\mathcal{D}}_i}\right|\right) \\ - 2\sum_{i=1,l_i=0}^{q} |\mathbf{D}_{\boldsymbol{\alpha} i}| \max\left(\left|\underline{\boldsymbol{d}_i^{(j)}}\right|, \left|\overline{\boldsymbol{d}_i^{(j)}}\right|\right) - 2\sum_{i=1,l_i\neq 0}^{q} \left|\boldsymbol{V}_i^j\right| \max\left(\left|\underline{\boldsymbol{\mathcal{D}}_i}\right|, \left|\overline{\boldsymbol{\mathcal{D}}_i}\right|\right)\end{aligned} \tag{4.44}$$

In its current state, this expression cannot be factorized by κ_j nor is differentiable. However, let suppose $\kappa_j \geq 0$, $\forall t$ and let use the following inequalities where the function f_{abs} is defined in (4.5):

$$\begin{aligned}\left|\kappa_j \boldsymbol{U}^{j-1} + \dot{\boldsymbol{U}}^{j-1} + \boldsymbol{\sigma}\left(\boldsymbol{U}^{j-1}\right)\right| &\leq \kappa_j \left|\boldsymbol{U}^j\right| + \left|\dot{\boldsymbol{U}}^{j-1} + \boldsymbol{\sigma}\left(\boldsymbol{U}^{j-1}\right)\right| \\ &\leq \kappa_j f_{\text{abs}}\left(\boldsymbol{U}^j\right) + f_{\text{abs}}\left(\dot{\boldsymbol{U}}^{j-1} + \boldsymbol{\sigma}\left(\boldsymbol{U}^{j-1}\right)\right)\end{aligned} \tag{4.45}$$

and similar inequalities in the case of $\boldsymbol{V}_i^j$. Using these inequalities, a conservative differentiable under-approximation of Δ_j is obtained which can be factorized by κ_j:

$$\Delta_j \geq \widehat{\Delta}_j = \kappa_j \lambda_j^d + \lambda_j^n \tag{4.46}$$

where λ_j^d and λ_j^n only depend on the coefficents κ_l such that $1 \leq l < j$:

$$\begin{aligned}\lambda_j^d &= \boldsymbol{U}^{j-1}\left\{\overline{\boldsymbol{\mathcal{A}}} - \underline{\boldsymbol{\mathcal{A}}}\right\} - 2 f_{\text{abs}}\left(\boldsymbol{U}^{j-1}\right) \textstyle\sum_{i=1,l_i=0}^{q} |\mathbf{D}_{\boldsymbol{\alpha} i}|\, g\left(\underline{\boldsymbol{\mathcal{D}}_i}, \overline{\boldsymbol{\mathcal{D}}_i}\right) \\ &\qquad -2\textstyle\sum_{i=1,l_i\neq 0}^{q} f_{\text{abs}}\left(\boldsymbol{V}_i^{j-1} + \mathbf{C}_{\boldsymbol{\alpha}} \mathbf{A}^{j-l_i-1} \mathbf{H}_{\mathbf{1}}\right) g\left(\underline{\boldsymbol{\mathcal{D}}_i}, \overline{\boldsymbol{\mathcal{D}}_i}\right) \\ \lambda_j^n &= \left[\dot{\boldsymbol{U}}^{j-1} + \boldsymbol{\sigma}\left(\boldsymbol{U}^{j-1}\right)\right]\left\{\overline{\boldsymbol{\mathcal{A}}} - \underline{\boldsymbol{\mathcal{A}}}\right\} - 2 f_{\text{abs}}\left(\dot{\boldsymbol{U}}^{j-1} + \boldsymbol{\sigma}\left(\boldsymbol{U}^{j-1}\right)\right) \textstyle\sum_{i=1,l_i=0}^{q} |\mathbf{D}_{\boldsymbol{\alpha} i}|\, g\left(\underline{\boldsymbol{\mathcal{D}}_i}, \overline{\boldsymbol{\mathcal{D}}_i}\right) \\ &\qquad -2\textstyle\sum_{i=1,l_i=0}^{q} |\mathbf{D}_{\boldsymbol{\alpha} i}|\, g\left(\underline{\boldsymbol{d}_i^{(j)}}, \overline{\boldsymbol{d}_i^{(j)}}\right) \\ &\qquad -2\textstyle\sum_{i=1,l_i\neq 0}^{q} f_{\text{abs}}\left(\dot{\boldsymbol{V}}_i^{j-1} + \boldsymbol{\sigma}\left(\boldsymbol{V}_i^{j-1}\right) + \mathbf{H}_{\mathbf{2}i}\right) g\left(\underline{\boldsymbol{\mathcal{D}}_i}, \overline{\boldsymbol{\mathcal{D}}_i}\right) \\ \mathbf{H_1} &= \begin{bmatrix}\mathbf{A}^{l_i-1}\mathbf{B}_{\mathbf{d}i} & \dots & \mathbf{A}^{2l_i-j}\mathbf{B}_{\mathbf{d}i} & 0 & \dots & 0\end{bmatrix} \\ \mathbf{H_{2}}_i &= \begin{bmatrix}\sum_{w=0}^{j-l_i-1} u_{l_i-1+w}^{j-1} \mathbf{C}_{\boldsymbol{\alpha}} \mathbf{A}^{l_i-1+w} \mathbf{B}_{\mathbf{d}i} & 0 & \dots & 0\end{bmatrix}\end{aligned} \tag{4.47}$$

where f_{abs} and g are the differentiable approximates defined in (4.5). Propagated bounds and saturations overlap does not occur if the quantities Δ_j remain positive which is satisfied if $\widehat{\Delta}_j$ is itself positive, $\forall j \leq k-1$. For $j = k$, one has to consider the difference $\overline{u} - \underline{u}$. This is recalled in the following lemma:

Lemma 4.23 (Propagated bounds/Saturations overlap avoidance)**.**
Propagated bounds and saturations overlap is avoided if

- $\forall j \in \mathbb{N}$ *such that* $j \leq k-1$, $\widehat{\Delta}_j > 0$, $\forall t$*;*
- *For* $j = k$, $\forall t$*:*

$$\widehat{\Delta}_k > 2 \sum_{i=1,l_i=0}^{q} |\mathbf{D}_{\boldsymbol{\alpha}i}| \max\left(\left|\underline{d_i^{(k)}}\right|, \left|\overline{d_i^{(k)}}\right|\right) + 2 \sum_{i=1,l_i\neq 0}^{q} \sum_{j=l_i}^{k} \left|\mathbf{C}_{\boldsymbol{\alpha}} \mathbf{A}^{j-1} \mathbf{B}_{\mathbf{d}i}\right| \max\left(\left|\underline{\boldsymbol{d}_i^{(k-j)}}(t)\right|, \left|\overline{\boldsymbol{d}_i^{(k-j)}}(t)\right|\right) \quad (4.48)$$

Considering the expression of $\widehat{\Delta}_j$ in (4.46), the necessary condition exposed in Lemma 4.23 to avoid propagated bounds and saturations overlap can be achieved by appropriately choosing the coefficients κ_j in $\boldsymbol{\kappa}$. Since the vectors $\boldsymbol{U}^j$ and $\boldsymbol{V}_i^j$ depend on time-derivatives of these design coefficients $\boldsymbol{\kappa}$, the fact that $\widehat{\Delta}_j$ up to $j = k-1$ is differentiable is capital. This was also illustrated in Example 4.21. Note however that the coefficient κ_k needs not be differentiable which is the case in Theorem 4.24.

In the following theorem, a suitable expression of the design coefficients in $\boldsymbol{\kappa}$ is presented. This is a main contribution of this thesis work: for the first time, time-varying coefficients are defined to bring guarantees to the OIST approach.

Theorem 4.24 (Design coefficients selection guaranteeing saturations overlap avoidance)**.** *Let $\breve{\boldsymbol{\kappa}} = \begin{bmatrix}\breve{\kappa}_1 & \dots & \breve{\kappa}_k\end{bmatrix}^\top \in \mathbb{R}_+^{\star k}$ a vector of strictly positive constants. Propagated bounds and saturations overlap is avoided if*

- *$\underline{\alpha} < \overline{\alpha}$, $\forall t$ (as assumed in Problem 4.11) and $\lambda_1^d \neq 0$, $\forall t$;*
- *$\forall j \in \mathbb{N}^\star$ such that $j \leq k-1$, $\widehat{\Delta}_j > 0$ is satisfied by choosing, $\forall t$:*

$$\kappa_j = \frac{\breve{\kappa}_j - \lambda_j^n}{\lambda_j^d} \quad (4.49)$$

  where $\breve{\kappa}_j$ is chosen such that $\kappa_1 > \frac{1}{2}$, $\forall j > 1$: $\kappa_j > 1$ and $\lambda_{j+1}^d \neq 0$, $\forall t$;

- *For $j = k$, one ensures $\overline{u} - \underline{u} > 0$ by choosing, $\forall t$:*

$$\kappa_k = \frac{1}{\lambda_k^d}\left[\breve{\kappa}_k - \lambda_k^n + 2 \sum_{i=1,l_i=0}^{q} |\mathbf{D}_{\boldsymbol{\alpha}i}| \max\left(\left|\underline{d_i^{(k)}}\right|, \left|\overline{d_i^{(k)}}\right|\right) + 2 \sum_{i=1,l_i\neq 0}^{q} \sum_{j=l_i}^{k} \left|\mathbf{C}_{\boldsymbol{\alpha}} \mathbf{A}^{j-1} \mathbf{B}_{\mathbf{d}i}\right| \max\left(\left|\underline{\boldsymbol{d}_i^{(k-j)}}(t)\right|, \left|\overline{\boldsymbol{d}_i^{(k-j)}}(t)\right|\right)\right] \quad (4.50)$$

  where $\breve{\kappa}_k$ is chosen such that $\kappa_k > \frac{1}{2}$, $\forall t$.

Remark 4.25. Note that this theorem is more conservative than the original Problem 4.11 as far as $\underline{\alpha}$ and $\overline{\alpha}$ are concerned. Indeed $\underline{\alpha}$ and $\overline{\alpha}$ should be chosen such that $\lambda_1^d \neq 0$ otherwise κ_1 in (D.7) may be undefined. This is completely related to the way the coefficients are defined in the proposed theorem. This is the reason why no stronger assumption is considered in Problem 4.11. ◇

Remark 4.26. To derive the inequalities in (4.45), it was supposed that $\kappa_j \geq 0$. The necessary conditions proposed in Theorem 4.24 are however more strict since it is prescribed that $\breve{\boldsymbol{\kappa}}$ is chosen such that $\kappa_1 > \frac{1}{2}$, $\kappa_k > \frac{1}{2}$ and $\kappa_j > 1$ for any other j. This has to do with guaranteeing closed-loop stability. This is discussed in the proof of Proposition 4.32 in 4.4.4. ◇

Proof. Proving Theorem 4.24 is straightforward using Lemma 4.23 and considering (4.46) and (4.43). □

The design procedure introduced in Theorem 4.24 for the coefficients in $\boldsymbol{\kappa}$ is now illustrated on Example 4.22.

Example 4.27 (Time-varying design coefficients $\boldsymbol{\kappa}$ for overlap mitigation)**.** Considering the more conservative propagated bounds defined in (4.42) and using the inequalities in (4.45), expressions of the form (4.46) are obtained:

$$\begin{aligned}
\widehat{\Delta}_0 &= \overline{\alpha} - \underline{\alpha} \\
\widehat{\Delta}_1 &= \kappa_1 \left(\overline{\alpha} - \underline{\alpha} - 2g\left(\underline{d_1}, \overline{d_1}\right)\right) + \dot{\overline{\alpha}} - \dot{\underline{\alpha}} \\
\widehat{\Delta}_2 &= \kappa_2 \lambda_2^d + \lambda_2^n \\
\lambda_2^d &= \kappa_1 \left(\overline{\alpha} - \underline{\alpha}\right) + \dot{\overline{\alpha}} - \dot{\underline{\alpha}} - 2\kappa_1 \max\left(\left|\underline{d_1}\right|, \left|\overline{d_1}\right|\right) - 2\max\left(\left|\underline{\dot{d}_1}\right|, \left|\overline{\dot{d}_1}\right|\right) \\
&\qquad -2\left|\mathbf{C}_{\boldsymbol{\alpha}}\mathbf{B}_{\mathbf{d}2}\right| \max\left(\left|\underline{d_2}\right|, \left|\overline{d_2}\right|\right) \\
\lambda_2^n &= \dot{\kappa}_1 \left(\overline{\alpha} - \underline{\alpha}\right) - 2\kappa_1 \left(\dot{\overline{\alpha}} - \dot{\underline{\alpha}}\right) + \overline{\alpha}^{(2)} - \underline{\alpha}^{(2)} - 2\left|\dot{\kappa}_1\right| \max\left(\left|\underline{d_1}\right|, \left|\overline{d_1}\right|\right) - 2\kappa_1 \max\left(\left|\underline{\dot{d}_1}\right|, \left|\overline{\dot{d}_1}\right|\right) \\
&\qquad -2\kappa_1 \left|\mathbf{C}_{\boldsymbol{\alpha}}\mathbf{B}_{\mathbf{d}2}\right| \max\left(\left|\underline{d_2}\right|, \left|\overline{d_2}\right|\right)
\end{aligned} \tag{4.51}$$

Supposing $\overline{\alpha}$ and $\underline{\alpha}$ are such that $\overline{\alpha} - \underline{\alpha} - 2g\left(\underline{d_1}, \overline{d_1}\right) \neq 0$, the following design coefficients can be used to avoid saturations overlap:

$$\begin{aligned}
\kappa_1 &= \frac{\breve{\kappa}_1 - \dot{\overline{\alpha}} + \dot{\underline{\alpha}}}{\overline{\alpha} - \underline{\alpha} - 2g\left(\underline{d_1}, \overline{d_1}\right)} \\
\kappa_2 &= \frac{\breve{\kappa}_2 - \lambda_2^n + 2\max\left(\left|\underline{d_1^{(2)}}\right|, \left|\overline{d_1^{(2)}}\right|\right) + 2\sum_{j=1}^{2} \left|\mathbf{C}_{\boldsymbol{\alpha}}\mathbf{A}^{j-1}\mathbf{B}_{\mathbf{d}2}\right| \max\left(\left|\underline{d_2^{(2-j)}}\right|, \left|\overline{d_2^{(2-j)}}\right|\right)}{\lambda_2^d}
\end{aligned} \tag{4.52}$$

where $\breve{\kappa}_1$ and $\breve{\kappa}_2$ are constants chosen such $\kappa_1 > \frac{1}{2}$, $\lambda_2^d \neq 0$ and $\kappa_2 > \frac{1}{2}$. ♣

In this section a saturations overlap mitigation procedure was proposed for the first time. In the case study 4.3 it was shown that applying the OIST approach as proposed in [Burlion 12] without precautions in the choice of the design parameters could lead to a loss of guarantees on the constraint satisfaction. This results from the lack of knowledge on the disturbances and output constraint signals $\underline{\alpha}$ and $\overline{\alpha}$ variations. The same consequences would be witnessed when applying the control saturations obtained in (4.43) with poorly chosen coefficients $\boldsymbol{\kappa}$.

In Theorem 4.24, the coefficients $\boldsymbol{\kappa}$ were thus precisely defined such that saturations overlap does not occur. They are time-varying by construction. The new design parameters $\breve{\boldsymbol{\kappa}}$ are constants and easier to choose. They could be determined using optimization techniques. This is tackled later in this chapter, see 4.6.1.

In the next section, a solution to Problem 4.11 is formally stated. Potential limits to this solution are also raised which motivates studying closed-loop stability with more details in 4.4.4.

4.4.3 (f) Conclusion: a solution to Problem 4.11

The problem of satisfying a time-domain constraint $\mathcal{K}\left(\Omega_\alpha\right)$ on a considered output α was formalized in Problem 4.11. A solution to this problem was developed for non-linear systems in [Burlion 12]. In 4.4.3, the extension to linear systems was detailed – which is characterized by more explicit expressions – following works in [Chambon 15c] and [Chambon b].

It was shown that by using the relative degree of the considered constrained output α with respect to the control input u and by defining so-called *propagated bounds* then saturations on the control are obtained such that the time-domain constraint is fulfilled. However, due to the conservativeness introduced by considering the bounds on the disturbance signal $\boldsymbol{d}$ and to the possibly time-varying constraint signals $\underline{\alpha}$ and $\overline{\alpha}$, saturations overlap can occur as illustrated in the case study 4.3. This results in losing any guarantees obtained through the method. Using appropriate expressions for the method's coefficients $\boldsymbol{\kappa}$ as detailed in Theorem 4.24, it was shown that saturations overlap can be avoided.

Theorem 4.28 (Output constrained control Problem 4.11 guaranteed solution using OIST)**.** *Let consider the system* (**G**) *in* (4.12) *in closed-loop with the controller* (**K**) *in* (4.13)*. Let* α *the constrained output and* $\mathcal{K}(\Omega_\alpha)$ *the considered time-domain constraint. Let suppose Assumptions 4.4 to 4.10 are satisfied.*

If the control input u *is such that*

$$u = sat_{\underline{u}}^{\overline{u}}(y_K)\,,\ \forall t \tag{4.53}$$

where

- $\underline{u}$ *and* $\overline{u}$ *are given in* (4.43)*;*
- *The propagated bounds expressions are detailed in* (4.41)*;*
- *The design parameters* $\boldsymbol{\kappa}$ *are chosen as in Theorem 4.24,*

then $\alpha \in \Omega_\alpha$, $\forall t$.

This theorem is a solution to Problem 4.11 using the *Output to Input Saturation Transformation* approach. However, inserting saturations in the control loop is known to be unsafe as far as closed-loop stability is concerned [Tarbouriech 11] since saturating the control input corresponds to "opening" the loop.

Remark 4.29 (Closed-loop stability in the presence of OIST saturations)**.** In Theorem 4.28, the proposed solution does not guarantee the system closed-loop stability. It may happen that the time-domain constraint is actually satisfied but the system state diverges. This depends on the open-loop behaviour of the system and its controller. In this case, additional structures like anti-windup compensators are often considered to recover from such degraded situation. This is the purpose of the next section. ◇

4.4.4 Guaranteed closed-loop stability using OIST

In the previous section, a solution to Problem 4.11 was proposed. Using appropriately defined control saturations, the time-domain constraint $\mathcal{K}(\Omega_\alpha)$ was enforced. However, as mentioned in Remark 4.29, the introduction of saturations in the closed-loop could potentially lead to the controller or system state divergence.

This was formalized in Problem 4.13. Obviously, the proposed solution to Problem 4.11 does not fulfil the expected guarantees of Problem 4.13. Additional theories are thus considered in this section to propose a common solution to both Problems 4.11 and 4.13.

4.4.4 (a) Miscellaneous results on the control saturations

Prior to studying the closed-loop stability, miscellaneous results are presented. First, it may be noted that the control saturations in (4.43) depend on the system state $\boldsymbol{x}$. Thus, it may be difficult to prove any stability result in the presence of such saturations. However, it is shown that this dependency can be removed using an appropriate transformation. Second, a study of the reachability of the system origin is proposed. It is indeed expected that the desired equilibrium can be reached in the presence of the considered control saturations.

State-free saturations Considering the expressions of the control saturations in (4.43) and of the propagated bounds in (4.41) for $j = k$, it is interesting to note that only one term depends on the state-vector $\boldsymbol{x}$. Let denote this term $\boldsymbol{K}_{\text{oist}}$. It is defined by

$$\boldsymbol{K}_{\text{oist}} = \frac{\boldsymbol{U}^k \boldsymbol{\mathcal{O}}}{\mathbf{C}_{\boldsymbol{\alpha}} \mathbf{A}^{k-1} \mathbf{B}_{\mathbf{u}}} \in \mathbb{R}^{1\times n},\ \forall t \tag{4.54}$$

Then, let define the two following saturating signals:

$$\begin{array}{rcl} \underline{v} & = & \underline{u} + \boldsymbol{K}_{\text{oist}}\boldsymbol{x} + \sum_{i=1,l_i=0}^{q} |\boldsymbol{K}_{\text{oist}}\mathbf{D}_{\mathbf{d}i}| \max\left(\left|\underline{\boldsymbol{d}_i}\right|, \left|\overline{\boldsymbol{d}_i}\right|\right) \\ \overline{v} & = & \overline{u} + \boldsymbol{K}_{\text{oist}}\boldsymbol{x} - \sum_{i=1,l_i=0}^{q} |\boldsymbol{K}_{\text{oist}}\mathbf{D}_{\mathbf{d}i}| \max\left(\left|\underline{\boldsymbol{d}_i}\right|, \left|\overline{\boldsymbol{d}_i}\right|\right) \end{array} \tag{4.55}$$

Using the following equality (with $\boldsymbol{x} = \boldsymbol{y}$ by assumption):

$$\text{sat}_{\underline{u}}^{\overline{u}}(y_K) = \text{sat}_{\underline{u}+\boldsymbol{K}_{\text{oist}}\boldsymbol{y}}^{\overline{u}+\boldsymbol{K}_{\text{oist}}\boldsymbol{y}}(y_K + \boldsymbol{K}_{\text{oist}}\boldsymbol{y}) - \boldsymbol{K}_{\text{oist}}\boldsymbol{y} \tag{4.56}$$

and noting that $\underline{v} \geq \underline{u} + \boldsymbol{K}_{\text{oist}}\boldsymbol{y}$, $\overline{v} \leq \overline{u} + \boldsymbol{K}_{\text{oist}}\boldsymbol{y}$, applying state-free saturations through the following input signal:

$$v = \text{sat}_{\underline{v}}^{\overline{v}}(y_K + \boldsymbol{K}_{\text{oist}}\boldsymbol{y}) \tag{4.57}$$

still allows to satisfy the necessary condition in Lemma 4.17. Since the term $\boldsymbol{K}_{\text{oist}}\boldsymbol{x}$ compensates the state-dependent quantity in $\underline{u}$ (resp. $\overline{u}$), the saturations are state-free and only depend on design parameters and signals. Thus, closed-loop stability analysis is expected to be easier to perform.

Remark 4.30 (New saturations overlap mitigation)**.** To mitigate the overlap of the new saturations, the coefficient κ_k is adapted accordingly in Th. 4.24. In particular, it must be ensured that $\overline{v} - \underline{v} > 0$, $\forall t$, i.e.

$$\overline{u} - \underline{u} - 2\sum_{i=1,l_i=0}^{q} |\boldsymbol{K}_{\text{oist}}\mathbf{D}_{\mathbf{d}i}| \max\left(\left|\underline{d_i}\right|, \left|\overline{d_i}\right|\right) > 0 \tag{4.58}$$

from which κ_k is deduced. ◇

Using the original formulation and saturations, the closed-loop system dynamics was given by

$$\dot{\boldsymbol{x}} = \mathbf{A}\boldsymbol{x} + \mathbf{B}_{\mathbf{u}}\text{sat}_{\underline{u}}^{\overline{u}}(y_K) + \mathbf{B}_{\mathbf{d}}\boldsymbol{d} \tag{4.59}$$

Using the newly define signal v and the corresponding saturations in (4.55), the closed-loop system dynamics becomes

$$\dot{\boldsymbol{x}} = \left[\mathbf{A} - \mathbf{B}_{\mathbf{u}}\boldsymbol{K}_{\text{oist}}\right]\boldsymbol{x} + \mathbf{B}_{\mathbf{u}}\text{sat}_{\underline{v}}^{\overline{v}}(y_K + \boldsymbol{K}_{\text{oist}}\boldsymbol{y}) - \mathbf{B}_{\mathbf{u}}\boldsymbol{K}_{\text{oist}}\mathbf{D}_{\mathbf{d}}\boldsymbol{d} + \mathbf{B}_{\mathbf{d}}\boldsymbol{d} \tag{4.60}$$

These new state-free saturating signals $\underline{v}$ and $\overline{v}$ are considered in the following sections to obtain guarantees on the closed-loop stability.

Admissible asymptotic equilibrium In the previous sections, expressions have been obtained for the control saturations and design parameters $\boldsymbol{\kappa}$. Under Assumptions 4.4, 4.7 and 4.9, it can be shown that these quantities converge towards constant values. Studying these final values gives information on the admissible asymptotic equilibrium. In practice, whenever an equilibrium is not reachable, this is a result of the control input sticking to a saturation. In this section, expressions of the limits of the aforementioned quantities are derived.

Considering Theorem 4.24 along with Assumptions 4.4 and 4.7, it can be observed that the time-varying design signals $\boldsymbol{\kappa}$ in (D.7) converge towards constant values. This results in the vectors $\boldsymbol{U}^j$ and $\boldsymbol{V}_i^j$ defined in (4.39) (for $i \in \mathbb{N}^\star$, $i \leq q$ and $j \in \mathbb{N}$, $j \leq k$) and $\boldsymbol{K}_{\text{oist}}$ to converge to constant finite values $\boldsymbol{U}^{j,\star}$, $\boldsymbol{V}_i^{j,\star}$ and $\boldsymbol{K}_{\text{oist}}^\star$. Consequently, as far as the saturations in (4.55) are concerned and using Assumption 4.9, they tend towards finite values $\underline{v}^\star$ and $\overline{v}^\star$ (supposing that $k > 0$):

$$
\begin{aligned}
\underline{v}^\star &= \frac{1}{\mathbf{C_\alpha A}^{k-1}\mathbf{B_u}}\left[\underline{\beta}_k^\star + \sum_{i=1,l_i\neq 0}^{q}\left|\mathbf{C_\alpha A}^{k-1}\mathbf{B_d}_i\right|\max\left(\left|\underline{\boldsymbol{d}_i}^\star\right|,\left|\overline{\boldsymbol{d}_i}^\star\right|\right)\right] \\
&\quad + \sum_{i=1,l_i=0}^{q}\left|\boldsymbol{K}_{\text{oist}}^\star\mathbf{D_d}_i\right|\max\left(\left|\underline{\boldsymbol{d}_i}^\star\right|,\left|\overline{\boldsymbol{d}_i}^\star\right|\right) \\
\overline{v}^\star &= \frac{1}{\mathbf{C_\alpha A}^{k-1}\mathbf{B_u}}\left[\overline{\beta}_k^\star - \sum_{i=1,l_i\neq 0}^{q}\left|\mathbf{C_\alpha A}^{k-1}\mathbf{B_d}_i\right|\max\left(\left|\underline{\boldsymbol{d}_i}^\star\right|,\left|\overline{\boldsymbol{d}_i}^\star\right|\right)\right] \\
&\quad - \sum_{i=1,l_i=0}^{q}\left|\boldsymbol{K}_{\text{oist}}^\star\mathbf{D_d}_i\right|\max\left(\left|\underline{\boldsymbol{d}_i}^\star\right|,\left|\overline{\boldsymbol{d}_i}^\star\right|\right) \\
\underline{\beta}_k^\star &= \boldsymbol{U}^{j,\star}\underline{\boldsymbol{\mathcal{A}}}^\star + \left|\boldsymbol{U}^{j,\star}\right|\sum_{i=1,l_i=0}^{q}\left|\mathbf{D_\alpha}_i\right|\max\left(\left|\underline{\boldsymbol{\mathcal{D}}_i}^\star\right|,\left|\overline{\boldsymbol{\mathcal{D}}_i}^\star\right|\right) \\
&\quad + \sum_{i=1,l_i\neq 0}^{q}\left|\boldsymbol{V}_i^{j,\star}\right|\max\left(\left|\underline{\boldsymbol{\mathcal{D}}_i}^\star\right|,\left|\overline{\boldsymbol{\mathcal{D}}_i}^\star\right|\right) \\
\overline{\beta}_k^\star &= \boldsymbol{U}^{j,\star}\overline{\boldsymbol{\mathcal{A}}}^\star - \left|\boldsymbol{U}^{j,\star}\right|\sum_{i=1,l_i=0}^{q}\left|\mathbf{D_\alpha}_i\right|\max\left(\left|\underline{\boldsymbol{\mathcal{D}}_i}^\star\right|,\left|\overline{\boldsymbol{\mathcal{D}}_i}^\star\right|\right) \\
&\quad - \sum_{i=1,l_i\neq 0}^{q}\left|\boldsymbol{V}_i^{j,\star}\right|\max\left(\left|\underline{\boldsymbol{\mathcal{D}}_i}^\star\right|,\left|\overline{\boldsymbol{\mathcal{D}}_i}^\star\right|\right)
\end{aligned}
\tag{4.61}
$$

The unsaturated control converges towards

$$
v^\star = \mathbf{C_K}{\boldsymbol{x}_K}^\star + \mathbf{D_K}\left(\boldsymbol{x}^\star + \mathbf{D_d}\boldsymbol{d}^\star\right) = 0 \tag{4.62}
$$

under the previously mentioned assumptions. In the following assumption, it is given under which conditions this equilibrium $v^\star = 0$ is an admissible asymptotic equilibrium.

Proposition 4.31 (Admissible asymptotic equilibrium)**.**
Let suppose Assumptions 4.4, 4.7 and 4.9 are satisfied. In the non-restrictive case where $\boldsymbol{x}^\star = 0$*, this is an admissible asymptotic equilibrium if*

$$
v^\star = 0 \in [\underline{v}^\star, \overline{v}^\star] \tag{4.63}
$$

For the practitioner, note that the expressions of $\underline{v}^\star$ and $\underline{v}^\star$ in (4.61) can be determined when applying the transformation since they depend on known design parameters only.

Now we have tackled the admissible equilibrium problem, the problem of guaranteeing closed-loop stability can be studied. First, the closed-loop representation is detailed using the state-free saturations obtained in (4.55). Second, an anti-windup loop is considered in addition to the feedback loop to guarantee the closed-loop asymptotic stability.

4.4.4 (b) Closed-loop representation

The system (4.12) in closed-loop with controller (4.13) and state-free saturations (4.55) is given by the following state-space representation:

$$
\begin{cases}
\dot{\boldsymbol{x}}(t) &= \left[\mathbf{A} - \mathbf{B_u}\boldsymbol{K}_{\text{oist}}(t)\right]\boldsymbol{x}(t) + \mathbf{B_u}v(t) + \left(\mathbf{B_d} - \mathbf{B_u}\boldsymbol{K}_{\text{oist}}(t)\mathbf{D_d}\right)\boldsymbol{d}(t) \\
\boldsymbol{y}(t) &= \boldsymbol{x}(t) + \mathbf{D_d}\boldsymbol{d}(t) \\
\dot{\boldsymbol{x}}_K(t) &= \mathbf{A_K}\boldsymbol{x}_K(t) + \mathbf{B_K}\boldsymbol{y}(t) \\
y_K(t) &= \mathbf{C_K}\boldsymbol{x}_K(t) + \mathbf{D_K}\boldsymbol{y}(t) \\
v(t) &= \text{sat}_{\underline{v}(t)}^{\overline{v}(t)}\left(y_K(t) + \boldsymbol{K}_{\text{oist}}(t)\boldsymbol{y}(t)\right) \\
\alpha(t) &= \mathbf{C_\alpha}\boldsymbol{x}(t) + \mathbf{D_\alpha}\boldsymbol{d}(t)
\end{cases}
\tag{4.64}
$$

The stability of this system is studied in the next section.

4.4.4 (c) Guaranteeing the closed-loop stability with an anti-windup approach

Due to the presence of a dynamic controller and saturations, unexpected closed-loop behaviour is expected. Anti-windup techniques have been widely studied and used to avoid behaviours like

controller state divergence. Some of these techniques are presented in [Kapoor 98, Tarbouriech 09, Grimm 03]. The approach proposed in [Menon 06] and [Herrmann 10] deals with a specific class of non-linear systems to which the system presented in (4.64) belongs. In this article, the anti-windup framework is used to enforce the closed-loop stability of the system in (4.64) where the time-varying gain $\boldsymbol{K}_{\text{oist}}$ and saturations are respectively given by (4.54) and (4.55). This provides an answer to Problem 4.13.

Similarly to [Herrmann 10], the function $f(\boldsymbol{x},t) = \boldsymbol{K}_{\text{oist}}(t)\boldsymbol{x}(t)$ which is linear in our case is the main difficulty in proving the stability in the presence of saturations. First, as in [Herrmann 10, Assumption 1, p. 1470], the stability of the open-loop system $\dot{\boldsymbol{x}} = [\mathbf{A} - \mathbf{B_u}\boldsymbol{K}_{\text{oist}}(t)]\,\boldsymbol{x}$ is studied.

Proposition 4.32 (Open-loop stability)**.**
The open-loop system described by

$$\dot{\boldsymbol{x}} = [\mathbf{A} - \mathbf{B_u}\boldsymbol{K}_{oist}(t)]\,\boldsymbol{x} \tag{4.65}$$

is GES.

Proof. The proof is inspired by [Herrmann 10]. A complete proof is presented in A.1. □

The following Lemma will be used in the proof of the main Theorem 4.34 which brings a solution to Problem 4.13.

Lemma 4.33 ($f(\boldsymbol{x},t)$ is Lipschitz)**.**
$\forall \boldsymbol{x}(t) \in \mathbb{R}^n$, $\forall t$, the function $f(\boldsymbol{x},t) = -\boldsymbol{K}_{oist}(t)\boldsymbol{x}(t)$ is Lipschitz (with respect to $\boldsymbol{x}$). Moreover, $-\boldsymbol{K}_{oist}(t)\boldsymbol{x}(t)$ is K_1-Lipschitz, where $K_1 = \max_t \|\boldsymbol{K}_{oist}(t)\| \in \mathbb{R}$.

Proof. Let $\forall \boldsymbol{x} \in \mathbb{R}^n$, $\forall t$, $f(\boldsymbol{x},t) = -\boldsymbol{K}_{\text{oist}}(t)\boldsymbol{x}(t)$. Then, $\forall \boldsymbol{x} \in \mathbb{R}^n$, $\frac{\partial f}{\partial \boldsymbol{x}}(\boldsymbol{x},t) = -\boldsymbol{K}_{\text{oist}}(t)$. Since $\boldsymbol{K}_{\text{oist}}(t)$ is continuous $\forall t$ by definition of the coefficients $\boldsymbol{\kappa}$ and continuity of the vectors $\underline{\boldsymbol{\mathcal{D}}_i}(t)$ and $\overline{\boldsymbol{\mathcal{D}}_i}(t)$ for $i \in \mathbb{N}^\star$, $i \leq q$ (see Assumption 4.7), the function f is continuously differentiable with respect to the state $\boldsymbol{x}$. This implies that $\boldsymbol{K}_{\text{oist}}(t)\boldsymbol{x}(t)$ is a Lipschitz continuous function with respect to $\boldsymbol{x}$. □

To ensure asymptotic stability of the saturated closed-loop, it is necessary to use an additional anti-windup loop. Considering the system in (4.64), the following anti-windup compensator with state $\boldsymbol{x}_a \in \mathbb{R}^n$ is introduced:

$$(G_a)\begin{cases} \dot{\boldsymbol{x}}_a(t) &= \mathbf{A}\boldsymbol{x}_a(t) + \mathbf{B_u}u_a(t) \\ \boldsymbol{y}_a(t) &= \boldsymbol{x}_a(t) \\ u_a(t) &= -\boldsymbol{K}_{\text{oist}}(t)\boldsymbol{y}_a(t) - \text{Dz}_{\underline{v}(t)}^{\overline{v}(t)}\left(y_K(t) + \boldsymbol{K}_{\text{oist}}(t)\boldsymbol{y}(t)\right) \\ \dot{\boldsymbol{x}}_K^1(t) &= \mathbf{A_K}\boldsymbol{x}_K^1(t) + \mathbf{B_K}\boldsymbol{y}_a(t) \\ v_1(t) &= -\mathbf{C_K}\boldsymbol{x}_K^1(t) - [\mathbf{D_K} + \boldsymbol{K}_{\text{oist}}(t)]\,\boldsymbol{y}_a(t) \end{cases} \tag{4.66}$$

The control v is then modified into

$$\begin{aligned} v(t) &= \text{sat}_{\underline{v}(t)}^{\overline{v}(t)}\left(u(t) + \boldsymbol{K}_{\text{oist}}(t)\boldsymbol{y}(t) + v_1(t)\right) \\ &= \text{sat}_{\underline{v}(t)}^{\overline{v}(t)}\left(\mathbf{C_K}\boldsymbol{x}_K^2(t) + \mathbf{D_K}\left(\boldsymbol{y}(t) - \boldsymbol{y}_a(t)\right) + \boldsymbol{K}_{\text{oist}}(t)\left(\boldsymbol{y}(t) - \boldsymbol{y}_a(t)\right)\right) \end{aligned} \tag{4.67}$$

where $\dot{\boldsymbol{x}}_K^2 = \mathbf{A_K}\boldsymbol{x}_K^2 + \mathbf{B_K}(\boldsymbol{y} - \boldsymbol{y}_a)$. The main result of this section is the following theorem which ensures stability of the origin of the system in closed-loop with the saturated nominal controller and the anti-windup compensator (4.66). Both this theorem and its proof are inspired by [Menon 06] and [Herrmann 10].

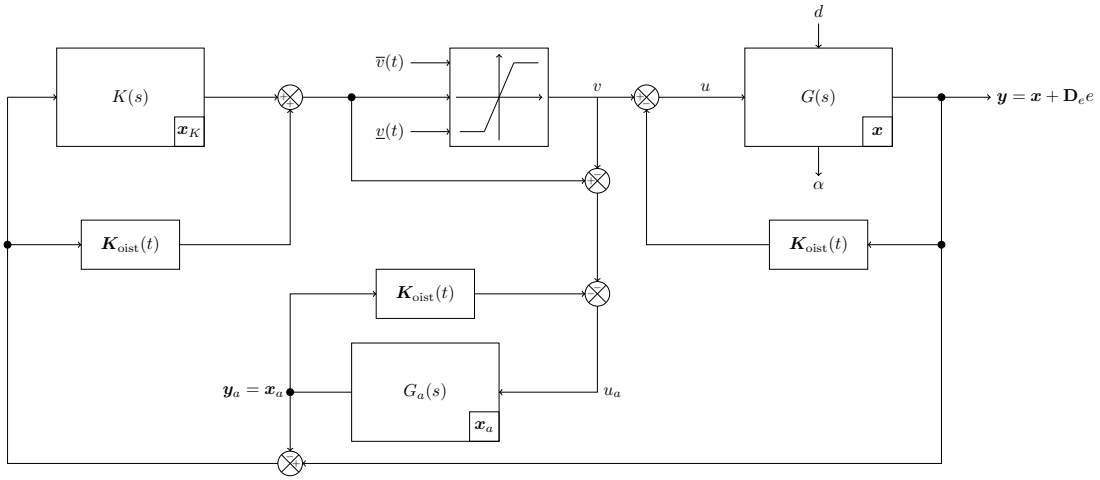

Figure 4.6: Illustration of the closed-loop with anti-windup compensator where $\underline{v}$ and $\overline{v}$ are obtained through application of OIST. Global asymptotic stability is guaranteed under the considered assumptions.

Theorem 4.34 (Guaranteed closed-loop stability, Problem 4.13)**.**
If Assumptions 4.4 to 4.10 are satisfied[a] *(resulting in Theorem 4.24 and Proposition 4.32), the origin of the closed-loop system consisting of the following system*

$$\dot{\boldsymbol{x}} = [\mathbf{A} - \mathbf{B_u}\boldsymbol{K}_{oist}]\,\boldsymbol{x} + \mathbf{B_u}v + [\mathbf{B_d} - \mathbf{B_u}\boldsymbol{K}_{oist}\mathbf{D_d}]\,\boldsymbol{d} \tag{4.68}$$

where the time-varying saturations are given in (4.55) – the control law v in (4.67) and the anti-windup compensator given in (4.66) is GAS.

[a] And excluding the pathological case where $\boldsymbol{d}$ is a non-converging finite energy distribution, which is not a realistic physical case.

Proof. A complete proof is available in A.2. □

Following works in [Herrmann 10], an additional anti-windup compensator was considered. This allowed to obtain results on the closed-loop stability in the presence of the saturations obtained applying OIST. An illustration of the system in closed-loop with the anti-windup compensator and saturating block is given in Fig. 4.6. This is the typical structure obtained when implementing OIST on a linear system.

Remark 4.35 (In practice: an anti-windup compensator is not mandatory!)**.** In Theorem 4.34, the use of an anti-windup compensator is theoretically necessary to obtain guarantees on the stability of the origin. However, in practice, such compensator is not always required when applying OIST. In that case, slightly different performance results may be observed. A comparison of the performance results obtained using an anti-windup compensator or not is performed on the application, see 4.5. Informally speaking, it appears that when using an anti-windup compensator then the constrained output is "allowed" to linger on the constraint such that the nominal behaviour is recovered "as much as possible". ◇

It may appear that Theorem 4.34 is obtained at the cost of many conservative assumptions. However, the most critical one is Assumption 4.10 which is directly related to the system dynamics and not to external signals such as disturbances. In the presence of a non-minimum phase system, global asymptotic stability cannot be achieved. This is discussed in 4.6.2.

4.4.5 Conclusions on the reformulation

In this section, the reformulation of the OIST approach initially introduced to enforce time-domain constraints on non-linear systems has been proposed. The considered system must satisfy Assumptions 4.4 to 4.10. The limitations of the transformation which were raised in 4.3 have been tackled. More precisely:

- using appropriate expressions of the design coefficients $\boldsymbol{\kappa}$ in Theorem 4.24, saturations overlap can be avoided;
- This allowed to formulate a solution to the constrained output control Problem 4.11 in Theorem 4.28;
- Using an anti-windup compensator, the global asymptotic stability of the origin of the considered systems was guaranteed in Theorem 4.34.

Of course, some problems remain open. First, it was supposed all along the reformulation that the whole state is measured and known. Second, the system model was supposed to be known with no uncertain parameters or dynamics. Also, we only considered the case where $T_{u\to\alpha}(s)$ is a minimum-phase transfer. This allowed to obtain an interesting result as far as asymptotic stability is considered. However, closed-loop stability cannot be guaranteed in the case of non-minimum phase transfers and it is expected that only local stability can be achieved for such systems. This motivates the study in 4.6.2.

Before switching to extensions of the OIST approach, the theoretical results obtained in this chapter are applied to the ball and beam model which served as a case study.

4.5 Application to the ball and beam model

The ball and beam example which served as a case study in 4.3 to illustrate existing limitations to the OIST approach is considered again. This time, the results obtained in Theorem 4.28 are used to avoid saturations overlap and guarantee satisfaction of the time-domain constraint on the ball position. The state-space representation in (4.7) is considered. Prior to the application of the method, a formal review of the assumptions is performed.

4.5.1 Formal review of the assumptions

The assumptions in 4.4.1 are reviewed in the case of the ball and beam system introduced in 4.3.1:

- the considered time-domain requirement signals $\underline{\alpha}$ and $\overline{\alpha}$ are represented in Fig. 4.3(b) converge towards $\underline{\alpha}^\star = 0.55\text{m}$ and $\overline{\alpha}^\star = 0.65\text{m}$ respectively. Assumption 4.4 is satisfied;
- The constrained output variable is of relative degree $k = 2$ with respect to the control input u and $l = 2$ with respect to the disturbance d. Assumption 4.5 is satisfied;
- Assumption 4.6 is obviously satisfied since $2l > k$;
- The disturbance d is known to be bounded by the signals $\underline{d}$ and $\overline{d}$ represented in black in Fig. 4.3(a) which converge towards $\underline{d}^\star = -0.05$ and $\overline{d}^\star = -\underline{d}^\star$. Hence, Assumption 4.7 is satisfied;
- The disturbance signal used in simulation converges towards zero and takes finite values. Assumption 4.8 is satisfied in simulation;
- The controller ($\mathbf{K}$) considered in (4.8) asymptotically stabilizes the unconstrained ball and beam system. Assumption 4.9 is fulfilled;
- Last but not least, the transfer between the control input u and the constrained output α (ball position) is minimum phase since

$$T_{u\to\alpha}(s) = -\frac{0.21}{s^2} \tag{4.69}$$

Assumption 4.10 is thus satisfied.

Remark 4.36. Note that the set-point $r_s = 0.6$ m (and $\dot{r}_s = 0$ m/s) is not the origin of the system (it is still a feasible equilibrium). However, using some transformation equivalent to a translation and choosing a non-null initial condition, one can obtain a set-point on the origin of the system. Hence Theorem 4.34 and its proof are still valid if using an appropriately designed anti-windup compensator. ◇

The approach detailed in 4.4 is now applied to this system.

4.5.2 OIST implementation, guaranteed with no overlap

Using the results developed in 4.4 and considering $\underline{\alpha} = 0.1$ m, $\overline{\alpha} = 0.9$ m, the following expressions are obtained for the successive $\widehat{\Delta}_i(t)$:

$$\forall t, \begin{cases} \widehat{\Delta}_0(t) &= 0.8 \\ \widehat{\Delta}_1(t) &= \kappa_1(t)\lambda_1^d(t) + \lambda_1^n(t) \\ \widehat{\Delta}_2(t) &= \kappa_2(t)\lambda_2^d(t) + \lambda_2^n(t) \end{cases} \tag{4.70}$$

where

$$\begin{aligned} \lambda_1^d(t) &= \overline{\alpha}(t) - \underline{\alpha}(t) \\ \lambda_1^n(t) &= \dot{\overline{\alpha}} - \dot{\underline{\alpha}} \\ \lambda_2^d(t) &= \begin{bmatrix}\kappa_1(t) & 1 & 0\end{bmatrix}\left\{\overline{\boldsymbol{\mathcal{A}}}(t) - \underline{\boldsymbol{\mathcal{A}}}(t)\right\} \\ \lambda_2^n(t) &= \begin{bmatrix}\dot{\kappa}_1(t) & \kappa_1(t) & 1\end{bmatrix}\left\{\overline{\boldsymbol{\mathcal{A}}}(t) - \underline{\boldsymbol{\mathcal{A}}}(t)\right\} \end{aligned} \tag{4.71}$$

Then, the values of the design signals $\kappa_i(t)$ are deduced from these expressions and Theorem 4.24:

$$\begin{aligned} \kappa_1(t) &= \frac{\breve{\kappa}_1 - \lambda_1^n(t)}{\lambda_1^d(t)} \\ \kappa_2(t) &= \frac{\breve{\kappa}_2 - \lambda_2^n(t) + 2|\mathbf{C_\alpha AB_d}|\max\left(|\underline{d}(t)|, |\overline{d}(t)|\right)}{\lambda_2^d(t)} \end{aligned} \tag{4.72}$$

where $\breve{\boldsymbol{\kappa}} = \begin{bmatrix}\breve{\kappa}_1 & \breve{\kappa}_2\end{bmatrix} = \begin{bmatrix}0.5 & 5\end{bmatrix}$ are chosen such that the conditions in Th. 4.24 are satisfied. It is then possible to obtain saturations on the control signal. Note that $\mathbf{C_\alpha AB_u} = -0.21 < 0$ in this example so the operator in (4.32) is used to obtain the adequate saturations.

4.5.3 Guaranteed closed-loop stability

In this example, the controller is stable and using an anti-windup compensator is not necessary. For illustrative purposes and to illustrate the action of such structure, an anti-windup is however designed following results in 4.4.4. The time-varying coefficient $\boldsymbol{K}_{\text{oist}}(t)$ is defined as follows:

$$\boldsymbol{K}_{\text{oist}}(t) = \frac{\boldsymbol{U}^2(t)\boldsymbol{\mathcal{O}}}{\mathbf{C_\alpha AB_u}} \tag{4.73}$$

where $\boldsymbol{U}^2(t) = \begin{bmatrix}\kappa_2(t)\kappa_1(t) + \dot{\kappa}_1(t) & \kappa_1(t) + \kappa_2(t) & 1\end{bmatrix}$ and $\boldsymbol{\mathcal{O}} = \begin{bmatrix}\mathbf{C_\alpha} & \mathbf{C_\alpha A} & \mathbf{C_\alpha A}^2\end{bmatrix}^\top$. The simulation results w/ or w/o an anti-windup structure in the loop are compared in 4.5.4 (b).

4.5.4 Simulations and results

Using the data in 4.5.2, simulations are performed over 100s. The disturbance signal used in simulation is shown in Fig. 4.3(a).

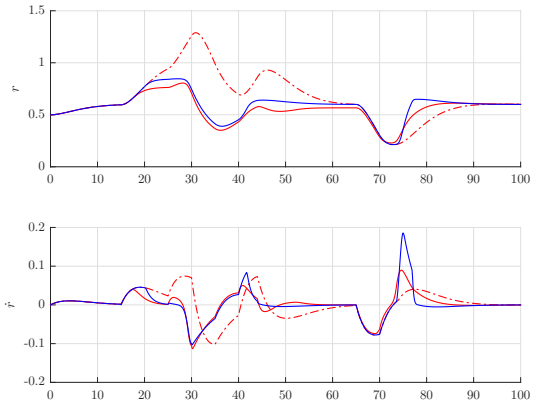

(a) System state using time-varying coefficients (in blue), using constant coefficients (plain red), or, without using OIST (dashed-dotted red).

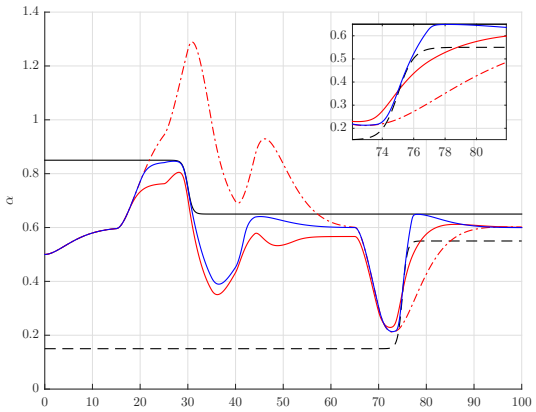

(b) Regulated variable using time-varying coefficients (in blue), using constant coefficients (plain red), or, without using OIST (dashed-dotted red). A zoom is performed for $72 \leq t \leq 82$s. In the time-varying coefficients case, the requirement is guaranteed.

Figure 4.7: System state and regulated variable $\alpha = r$ simulation results.

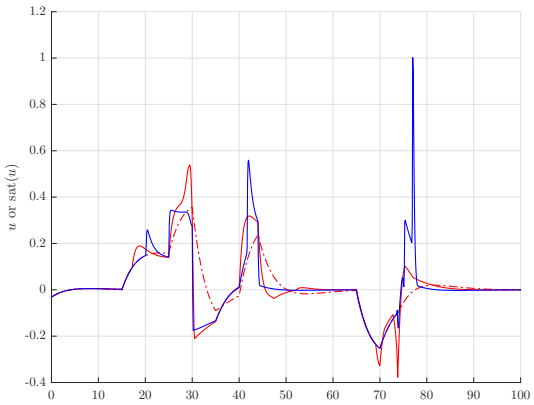

(a) Control signal obtained using time-varying coefficients (in blue), using constant coefficients (plain red), or, without using OIST (dashed-dotted red).

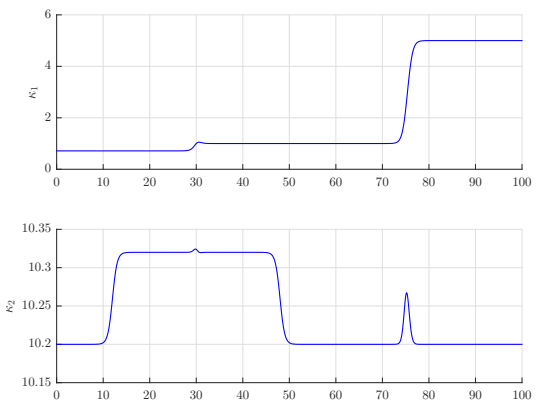

(b) OIST design parameters $\boldsymbol{\kappa}(t)$ obtained (time-varying case only) through application of Theorem 4.24.

Figure 4.8: Control signal and OIST design parameters $\boldsymbol{\kappa}(t)$ simulation results.

4.5.4 (a) Simulation results w/o anti-windup compensation

The simulation results are represented in Figs. 4.7 and 4.8. The data are represented in dashed-dotted red when considering the nominal control law only (no saturations), in plain red when considering OIST with constant coefficients (see the case study in 4.3) and in plain blue when the saturations obtained using OIST are introduced in the closed-loop *and* the OIST coefficients are chosen time-varying as in Theorem 4.24, see (4.72). As mentioned in 4.3, the synthesized controller is not efficient enough and the ball falls off the beam. Using OIST and the knowledge on the disturbances bounds, the time-domain constraint is satisfied and nominal performance is recovered whenever the constraint is not violated. Note that the proposed approach leads to some conservatism due to the lack of knowledge on d, especially around $t = 45$s. Also, some conservatism could be introduced by using differentiable upper-approximates of the absolute value and maximum functions.

Contrary to the constant coefficients case, it can be noted in Fig. 4.7(b) that the use of time-varying coefficients as defined in Theorem 4.24 offers guarantees on the time-domain requirement satisfaction at all times. This results from the saturations not overlapping in this case, whatever the choice of $\breve{\boldsymbol{\kappa}}$.

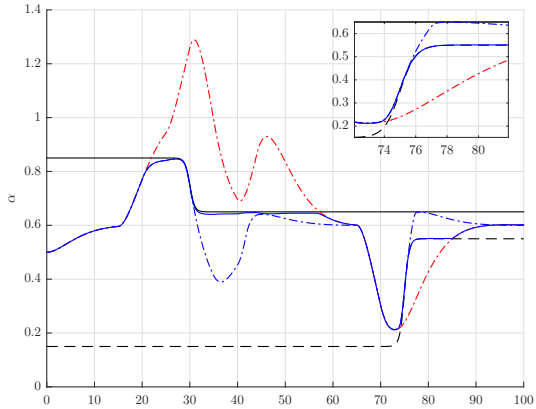

(a) Comparison of the regulated variable simulation results.

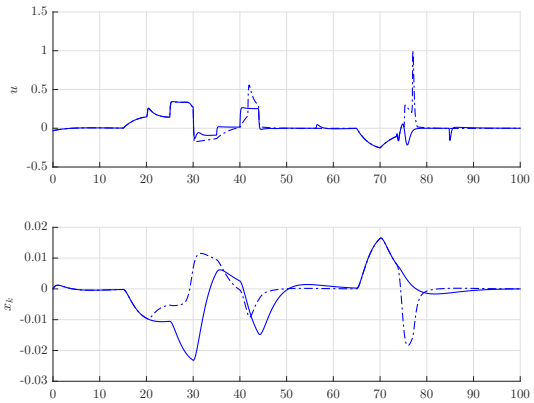

(b) Comparison of the control signal u and controller state x_K.

Figure 4.9: Comparison of the simulation results obtained w/ (plain blue) or w/o (dashed-dotted blue) an anti-windup.

It appears in Fig. 4.8(a) that the control law variations are much sharper in the saturated cases. This is a trade-off required for complying with the time-domain requirement. Optimization of the constants $\check{\boldsymbol{\kappa}}$ may help to obtain less demanding although satisfying control laws, see 4.6.1.

4.5.4 (b) Comparison of simulation results w/ or w/o anti-windup compensation

In the previous section, satisfying results were obtained without using an anti-windup structure in the feedback loop. The influence of such structure is illustrated in Fig. 4.9. The simulation results obtained with (resp. without) the anti-windup in the feedback loop are represented in plain (resp. dashed-dotted) blue. It appears that the use of an anti-windup allows the control law to stay longer on the saturations. This results in the regulated variable sticking to the time-domain requirement limits. In an informal way, this means that the nominal performance is less degraded since the control law tries to copy the original control as much as possible. In a more formal way, this means that the anti-windup compensator improves performance.

4.5.4 (c) Conclusions on the simulation results

The results obtained in simulation are highly satisfactory. Using time-varying design parameters in the OIST approach as proposed in Theorem 4.24, a time-domain requirement on a given regulated variable can be fulfilled *with guarantees*. Moreover, the closed-loop stability is ensured as demonstrated in 4.4.4. In practice, using an anti-windup compensator is not mandatory. However, it has been observed in the illustrating example that the regulated variable sticks to the requirement bounds to copy the original system response as much as possible when using such compensator. As a conclusion, using an anti-windup compensator improves performance.

4.6 Miscellaneous remarks

In this section, miscellaneous remarks on the OIST method are presented. It is shown how the design parameters $\check{\boldsymbol{\kappa}}$ can be optimized with respect to a pre-defined cost function. Also, the consequence of applying OIST on non-minimum phase systems is illustrated.

4.6.1 An approach to OIST design coefficients optimization

Choosing the design coefficients in $\boldsymbol{\kappa}$ can be tricky. On simple examples (like the double integrator), a trade-off appears between performance and control energy. For big values of the design

coefficients, performance is improved (the constrained output is allowed to linger on the saturations) but this can result in demanding control inputs with inappropriate swaying. Considering an optimization procedure for these coefficients can be a good option to avoid such behaviours.

In this thesis work we have tested the AMPL modelling language [Fourer 02] coupled to the IPOPT optimizer [Wächter 06] to find an optimal value of the coefficients in $\boldsymbol{\kappa}$ with respect to a prescribed cost functional. The IPOPT package can be used to find a local solution $\boldsymbol{x}_s$ to the following type of problems:

$$\begin{array}{ll} \min & f(\boldsymbol{x}) \\ \boldsymbol{x} \in \mathbb{R}^n & \\ \text{s. t.} & \underline{\boldsymbol{g}} \leq \boldsymbol{g}(\boldsymbol{x}) \leq \overline{\boldsymbol{g}} \\ & \underline{\boldsymbol{x}} \leq \boldsymbol{x} \leq \overline{\boldsymbol{x}} \end{array} \tag{4.74}$$

where $\underline{\boldsymbol{g}}$ and $\overline{\boldsymbol{g}}$ denote the bounds on the constraints function $\boldsymbol{g}(\boldsymbol{x})$ and $\underline{\boldsymbol{x}}$ and $\overline{\boldsymbol{x}}$ denote the bounds on the variable. The cost functional is denoted f. In this dissertation, the considered illustrating model is the disturbed double integrator:

$$\begin{aligned} \dot{\boldsymbol{x}}_1 &= \boldsymbol{x}_2 \\ \dot{\boldsymbol{x}}_2 &= u + d \end{aligned} \tag{4.75}$$

where d is the disturbance and u the control input. For simulations, the signal $d(t) = e^{-0.25t}\sin(2t)$ is used as the disturbance. Bounds $\underline{d}$ and $\overline{d}$ on this disturbance are supposed to be known. They are given by:

$$\underline{d}(t) = -e^{-0.25t},\ \overline{d}(t) = e^{-0.25t} \tag{4.76}$$

The system is initialised at $\boldsymbol{x}_0 = \begin{bmatrix} 1 \\ 0 \end{bmatrix}$. The nominal control law is given by $u = -\boldsymbol{x}_1 - \boldsymbol{x}_2$. A time-domain constraint is set on $\boldsymbol{x}_2$: this state variable should belong to the interval $[\underline{\alpha} = -0.3, \overline{\alpha} = 0.3]$. Application of OIST as detailed in 4.4 leads to the following saturations:

$$\begin{aligned} \underline{u}(t) &= \kappa(t)\left(\underline{\alpha} - \boldsymbol{x}_2(t)\right) + \max\left(\left|\underline{d}(t)\right|, \left|\overline{d}(t)\right|\right) \\ \overline{u}(t) &= \kappa(t)\left(\overline{\alpha} - \boldsymbol{x}_2(t)\right) - \max\left(\left|\underline{d}(t)\right|, \left|\overline{d}(t)\right|\right) \end{aligned} \tag{4.77}$$

and the control input signal is modified accordingly: $u = \mathrm{sat}_{\underline{u}}^{\overline{u}}(-\boldsymbol{x}_1 - \boldsymbol{x}_2)$. To avoid saturations overlap, the design coefficient $\kappa \in \mathbb{R}$ is chosen as follows:

$$\kappa(t) = \frac{\breve{\kappa} + 2\max\left(\left|\underline{d}(t)\right|, \left|\overline{d}(t)\right|\right)}{\overline{\alpha} - \underline{\alpha}} \tag{4.78}$$

where $\breve{\kappa}$ is a strictly positive constant to determine. It is decided to optimize this constant $\breve{\kappa}$ with respect to the following cost functional:

$$f(\boldsymbol{x}_u, \boldsymbol{x}_c, u_c) = W_1 \frac{T}{N} \sum_{i=0}^{N-1} (\boldsymbol{x}_{c,i} - \boldsymbol{x}_{u,i})^\top (\boldsymbol{x}_{c,i} - \boldsymbol{x}_{u,i}) + W_2 \frac{T}{N} \sum_{i=0}^{N-1} u_{c,i}^2 \tag{4.79}$$

where W_1 and W_2 are appropriate weightings, T is the simulation final time, N is the number of samples ($0 \leq i \leq N-1$), $\boldsymbol{x}_u$ is the state of the system in closed-loop with the nominal law $u_u = -\boldsymbol{x}_{u,1} - \boldsymbol{x}_{u,2}$ and $\boldsymbol{x}_c$ is the state of the system in closed-loop with $u_c = \mathrm{sat}_{\underline{u}}^{\overline{u}}(-\boldsymbol{x}_{c,1} - \boldsymbol{x}_{c,2})$. Another constraint is set on the saturated control u_c so as to eliminate fast variations of the input signal: $-10 \leq \frac{N}{T}(u_{c,i} - u_{c,i-1}) \leq 10$ for $1 \leq i \leq N-1$. The following numerical values are chosen before optimization of $\breve{\kappa}$ – $N = 2000$, $T = 20$s, $W_1 = W_2 = 1$ – and the Euler integration scheme is selected to formulate the dynamical constraints. The resulting code expressed in the AMPL formalism is presented in C.1. The problem is then solved using the IPOPT optimizer and the following result is obtained:

$$\breve{\kappa}_{\mathrm{opt}} = 14.225 \tag{4.80}$$

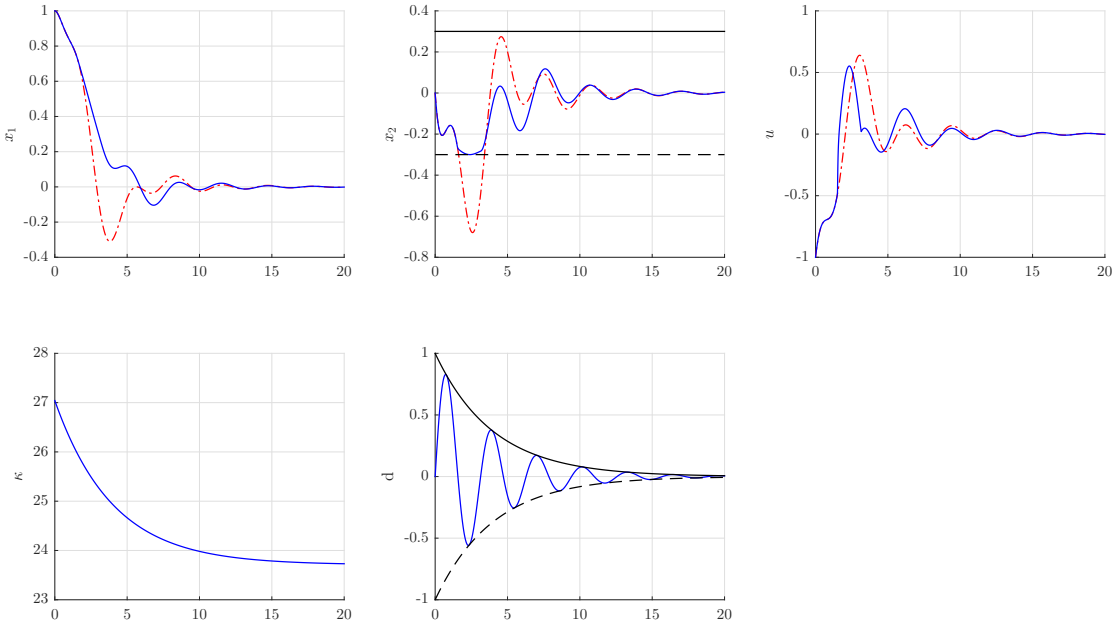

Figure 4.10: OIST applied to the double integrator using the optimal value of $\breve{\kappa}$ returned by AMPL/IPOPT as described in 4.6.1.

Using this optimal value for the design coefficient $\breve{\kappa}$, the double integrator is simulated over 20s in closed-loop with the unconstrained nominal law (in dashed-dotted red) and the saturated law (in blue). The simulation results are represented in Fig. 4.10.

Using AMPL/IPOPT, an optimal value of the OIST design coefficient $\breve{\kappa}$ considering a specific cost functional has been obtained for the double integrator example. Satisfying simulation results are obtained since the output constraint is satisfied and the control input is not too demanding. This illustrative example shows that the OIST design parameters can be optimized using existing optimal control design techniques. This augurs future works in optimal automated tuning of the OIST coefficients.

4.6.2 A challenge: the non-minimum phase case

The reformulation of OIST in the linear framework was possible thanks to some assumptions. Especially, the difficult case of a non-minimum transfer between the control input u and the constrained output α was set aside in Assumption 4.10. In this section, two non-minimum phase systems are considered to illustrate the consequences of applying OIST without considering the zero dynamics. Especially, in that case, the achieved stability is local only but two behaviours are identified depending on the speed of the unstable zero dynamics.

Let consider the following stable transfer between the control input u and the constrained output α:

$$T_{u\to\alpha}^{\text{slow}}(s) = \frac{-3.9\,(s-0.1)}{s^2+s+0.26} = \frac{K\,(s-z_1)}{s^2+s+0.26} \tag{4.81}$$

This transfer zero dynamics is unstable. However, this is a slow dynamics since its zero equals $z_1 = 0.1$. The second system zero dynamics is also unstable but has a fast zero dynamics with $z_1 = 10$:

$$T_{u\to\alpha}^{\text{fast}}(s) = \frac{-0.039\,(s-10)}{s^2+s+0.26} \tag{4.82}$$

Both systems have a DC gain of 1.5. In simulation, they are excited with the following input signal:

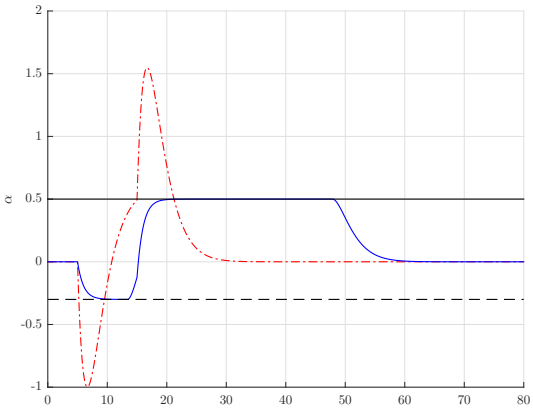

(a) In blue: constrained output α simulation and, in dashed-dotted red, unconstrained simulation.

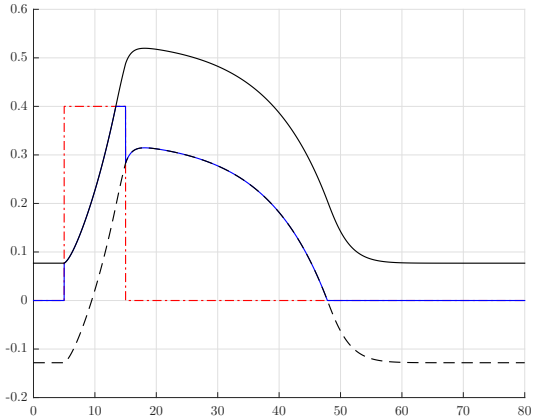

(b) System control input u simulation, when using OIST in the loop (in blue) and without OIST (in dashed-dotted red). In the second case, the input equals the exciting step signal.

Figure 4.11: OIST applied to the NMP system in (4.81) with a slow zero dynamics.

$$u(t) = \begin{cases} 0.4 & \text{if } t \in [5, 15] \\ 0 & \text{otherwise} \end{cases} \tag{4.83}$$

and are initialized at $\boldsymbol{x}_0 = 0$. The output α is constrained to stay in $[\underline{\alpha}, \overline{\alpha}]$ where $\underline{\alpha} = -0.3$ and $\overline{\alpha} = 0.5$. Application of the *Output to Input Saturation Transformation* leads to

$$\begin{aligned} \underline{u} &= \tfrac{1}{K}\left[\kappa_1\left(\overline{\alpha} - \alpha\right) - \dot{\alpha}\right] \\ \overline{u} &= \tfrac{1}{K}\left[\kappa_1\left(\underline{\alpha} - \alpha\right) - \dot{\alpha}\right] \end{aligned} \tag{4.84}$$

where it is supposed that the state $\boldsymbol{x}$ is known hence $\dot{\alpha} = \mathbf{C}_{\boldsymbol{\alpha}}\mathbf{A}\boldsymbol{x}$ is known. Also, it is chosen $\kappa_1 = 1$. Note that $K < 0$ which explains the actual expressions of the saturations in (4.84). Let $\boldsymbol{K}_{\text{oist}} = \frac{1}{K}\left(\kappa_1\alpha + \dot{\alpha}\right)$. Using the interconnection in Fig. 4.6, note that $\mathbf{A} - \mathbf{B}\boldsymbol{K}_{\text{oist}}$ has positive eigenvalues which theoretically explains the observed divergence.

The simulation results are represented in Fig. 4.11 (resp. Fig. 4.12) for $T^{\text{slow}}_{u\to\alpha}(s)$ (resp. $T^{\text{fast}}_{u\to\alpha}(s)$). The simulated signals are represented in blue when OIST is used to limit the control input and in dashed-dotted red in the unconstrained case. The bounds are represented in black (dashed line for the lower bound).

The simulation results in Fig. 4.11 show that when the zero dynamics is slow then the stability of the saturated closed-loop is ensured on a quite large set of constrained trajectories. Of course, divergence still occurs if greater values of the input signal are selected like $u(t) = 0.5$ for $t \in [5, 15]$.

On the contrary, when the zero dynamics is fast, divergence occurs even for small violations of the constraint. This is illustrated in Fig. 4.12 where only parts of the signals are represented.

In this section, we have illustrated the influence of unstable zero dynamics when solving the constrained-output problem using OIST. Informally, two behaviours have been identified: if the zero dynamics is slow then the stability of the closed-loop can be ensured on a quite large set of trajectories. In the other case, if the zero dynamics is fast, divergence occurs even for small violations of the time-domain constraint.

In practice, this means that OIST is still applicable "as is" in the presence of slow unstable zeros. Of course, the stability can only be local. This can be studied using common stability analysis techniques which are left for future works.

4.7 Conclusions

In this chapter, the OIST approach to output constrained control design introduced in [Burlion 12] for non-linear systems has been reformulated for linear systems. Existing problems such as the

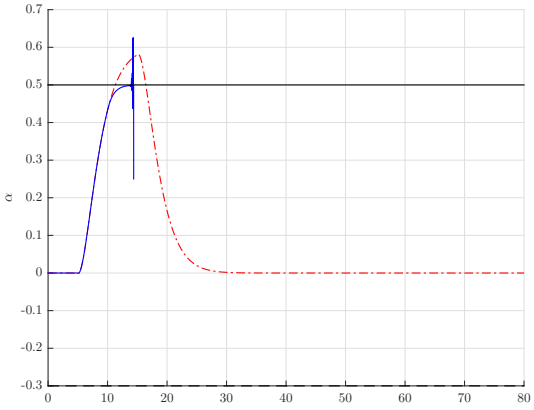

(a) In blue: constrained output α simulation and, in dashed-dotted red, unconstrained simulation.

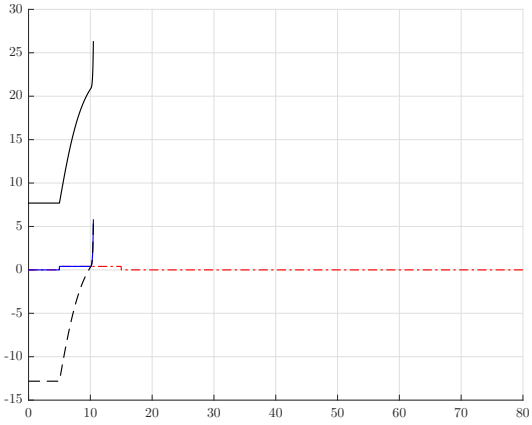

(b) System control input u simulation, when using OIST in the loop (in blue) and without OIST (in dashed-dotted red).

Figure 4.12: OIST applied to the NMP system in (4.82) with a fast zero dynamics.

risk of saturations overlap have been detailed in 4.3. In 4.4, the reformulation in the linear framework has been described. Considering this type of systems has allowed to formulate iterative expressions to determine the different parameters used in the transformation. Details have been brought on how to appropriately select the method design coefficients $\boldsymbol{\kappa}$ so as to avoid saturations overlap. Another major contribution of this chapter is the demonstration of global asymptotic stability of the origin for minimum phase transfers $T_{u\to\alpha}(s)$ when using an additional anti-windup compensator. The *Output to Input Saturation Transformation* has been successfully applied to the ball and beam example, preventing the ball from falling off the beam.

In 4.6, some additional subjects have been tackled. Notably, it has been illustrated on a simple example that techniques commonly used amongst the optimal control community can be implemented to optimally tune the method design coefficients $\boldsymbol{\kappa}$ against a cost functional and additional constraints. This is promising as far as the applicability of the method to real-life constrained control problems is concerned. A clear perspective of this work is to consider more complex cases of application as well as the use of other optimizers to compare their performance on the considered problem. In the same section, the impact of non-minimum phase behaviours has also been illustrated for the unaccustomed reader.

As far as the perspectives of the method itself are concerned, an automated design of the saturations could be of interest. The involvement required to be familiar with the method as well as the complexity of the expressions currently hinders its applicability quite a bit.

In the next chapter, the OIST approach is extended to the case of uncertain systems with incomplete state measurements. This problem is complex and the expressions of the saturations obtained in 4.4 can no longer be applied due to the lack of knowledge on $\boldsymbol{x}$. This requires the use of additional theories to provide sufficient information on the system state hence on the considered constrained output.

Chapter 5

Extension of OIST to the incomplete measurements and uncertain cases

In the previous chapter, the OIST approach to enforce a time-domain constraint on a given output, initially introduced for non-linear systems in [Burlion 12] has been reformulated in the linear framework. Additional results related to saturations overlap mitigation and closed-loop stability analysis have been detailed. However, the considered class of system, namely LTI systems with full state measurements, is rather limited in view of the problems encountered in practice.

In this chapter, the *OIST extension for Robustness* (OISTeR) is presented to account for the possible presence of uncertainties in the considered model. Also, the case of systems for which the whole state is not measured is considered. The extension is based on the use of interval observers. The reader unfamiliar with such systems may find useful information in Chapter B. This work is quite novel and has not yet been published. However, hints on how to propose an extension to the original OIST approach for linear systems were already proposed in [Chambon 15d] as well as in the perspectives of [Chambon 15c].

The chapter is organised as follows. The motivations for extending the OIST approach as proposed in Chapter 4 are detailed in 5.1. Then, the problem of enforcing a time-domain constraint on a considered uncertain LTI system output is stated in 5.2. To solve this problem, the OIST extension for Robustness is introduced in 5.3. The approach is then applied on various examples in 5.4 before concluding in 5.5 on future perspectives for this extension.

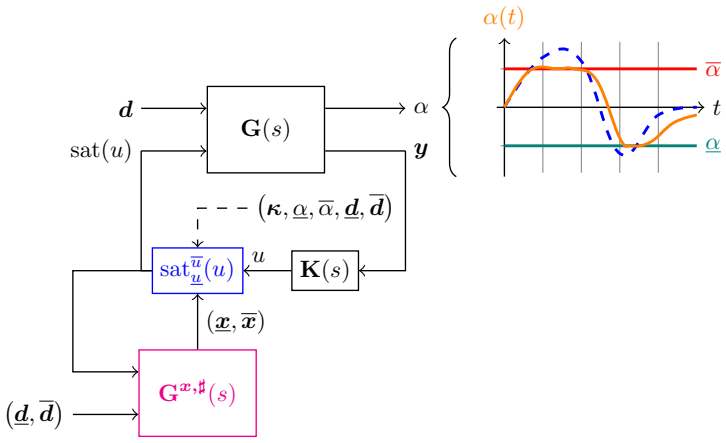

Figure 5.1: Illustration of OISTeR strategy. An interval observer $\left(\mathbf{G}^{\boldsymbol{x},\sharp}\right)$ is introduced to complement for the lack of knowledge on the system and controller state vectors.

5.1 Motivations for an extension of OIST

The *Output to Input Saturation Transformation* (OIST) approach was introduced in [Burlion 12] as a new *evolutionary* technique to enforce a time-domain constraint on a non-linear system output α with pre-existing control law u. This approach has been presented in details in Chapter 3 for non-linear systems only as in the originating works.

In Chapter 4, the approach has been reformulated in the case of linear systems. Additional contributions have been proposed amongst which guarantees on the absence of overlap for the obtained saturations $\underline{u}$ and $\overline{u}$ to apply to the pre-existing so-called nominal control law. Using an additional anti-windup compensator, global asymptotic stability of the origin was also proved in the case of minimum phase systems.

In both the originating works and first contributions of this thesis however, the state $\boldsymbol{x} \in \mathbb{R}^n$ of the original system (4.12) has been supposed to be measured. Eventually, the measurements $\boldsymbol{y} = \boldsymbol{x} + \mathbf{D_d}\boldsymbol{d}$ have at worst been supposed to be disturbed by an external unknown signal $\boldsymbol{d}$. It remains that the state vector current value $\boldsymbol{x}$ is directly accessible for use in the OIST approach as detailed in both Chapters 3 and 4. In Chapter 4, this knowledge of the possibly disturbed system state vector $\boldsymbol{x}$ resulted in the expressions for the saturations to depend in $\boldsymbol{x}$ as made evident in (4.41) and (4.43).

However, when considering more practical cases, the state vector $\boldsymbol{x}$ is rarely entirely measured. Also, most systems dynamics depend on uncertain parameters which have not been taken into account in the current OIST approach. This motivates extending OIST to these complex cases where fewer information on the system dynamics are available. A solution is to compensate for the lack of knowledge on the state vector value by using an observer. More precisely, an interval observer is introduced to provide guaranteed bounds $\underline{\boldsymbol{x}}$ and $\overline{\boldsymbol{x}}$ on the state vector value $\boldsymbol{x}$. This is illustrated in Fig. 5.1.

5.2 Extended problem statement: taking robustness into account

In Chapter 4, robustness with respect to uncertainties was not considered. The considered class of systems in 4.4.1 was the class of known linear time-invariant systems with full-measured state. In this section, this considered class is broadened to uncertain linear time-invariant systems with partially measured state. This is a more realistic representation of systems commonly met in practice. The OIST problems initially formulated for linear systems in 4.4.2 is then updated to apply to this broader class of systems.

5.2.1 Extension of the considered class of linear systems

In this chapter, uncertain linear time-invariant systems are considered in the continuous-time framework. The following generic state-space representation is considered throughout this chapter:

$$(\mathbf{G})\begin{cases} \dot{\boldsymbol{x}} &= \mathbf{A}(\boldsymbol{\theta})\,\boldsymbol{x} &+ \mathbf{B_u} u &+ \mathbf{B_d}(\boldsymbol{\theta})\,\boldsymbol{d} \\ \boldsymbol{y} &= \mathbf{C}(\boldsymbol{\theta})\,\boldsymbol{x} &+ \mathbf{D_u}(\boldsymbol{\theta})\,u &+ \mathbf{D_d}(\boldsymbol{\theta})\,\boldsymbol{d} \\ \boldsymbol{x}(0) &= \boldsymbol{x}_0 & & \end{cases} \tag{5.1}$$

where $\boldsymbol{x} \in \mathbb{R}^n$, $y \in \mathbb{R}^l$, $u \in \mathbb{R}$ is the control input and $\boldsymbol{d} \in \mathbb{R}^{m-1}$ is the unknown vector of disturbances inputs. In comparison with the class considered in the initial formulation of OIST, see (4.12) in Chapter 4, this representation now includes uncertainties through vector $\boldsymbol{\theta} \in \Theta$ where $\Theta \subset \mathbb{R}^q$. This vector of uncertainties is supposed to be bounded as guaranteed by the following assumption made for future introduction of an interval observer:

Assumption 5.1 (Bounded vector of uncertainties $\boldsymbol{\theta}$)**.**
There exist two known vectors $\underline{\boldsymbol{\theta}}$ and $\overline{\boldsymbol{\theta}}$ in $\Theta \subset \mathbb{R}^q$ such that

$$\underline{\boldsymbol{\theta}} \leq \boldsymbol{\theta} \leq \overline{\boldsymbol{\theta}} \tag{5.2}$$

Also, for $\boldsymbol{\theta} \in \Theta$, it is supposed that the system (5.1) is well-posed, i.e. its state-space matrices are well-defined:

Assumption 5.2 (Well-posed system (5.1))**.**
System (5.1) state-space matrices are well-defined $\forall \boldsymbol{\theta} \in \Theta$.

Remark 5.3. Under Assumptions 5.1 and 5.2, there exist appropriately defined bounding matrices such that:

$$\begin{array}{rcccl} \underline{\mathbf{A}} & \leq & \mathbf{A}(\boldsymbol{\theta}) & \leq & \overline{\mathbf{A}} \\ \underline{\mathbf{B_d}} & \leq & \mathbf{B_d}(\boldsymbol{\theta}) & \leq & \overline{\mathbf{B_d}} \\ \underline{\mathbf{C}} & \leq & \mathbf{C}(\boldsymbol{\theta}) & \leq & \overline{\mathbf{C}} \\ \underline{\mathbf{D_u}} & \leq & \mathbf{D_u}(\boldsymbol{\theta}) & \leq & \overline{\mathbf{D_u}} \\ \underline{\mathbf{D_d}} & \leq & \mathbf{D_d}(\boldsymbol{\theta}) & \leq & \overline{\mathbf{D_d}} \end{array}, \forall \boldsymbol{\theta} \in \left[\underline{\boldsymbol{\theta}}, \overline{\boldsymbol{\theta}}\right] \tag{5.3}$$

◇

As far as the initial condition $\boldsymbol{x}_0$ is concerned, it is not necessarily known however, similarly to Assumption B.10, bounds $\underline{\boldsymbol{x}_0}$ and $\overline{\boldsymbol{x}_0}$ are supposed to be known for this vector. Also, as in Assumption 4.7, the unknown vector of disturbance inputs $\boldsymbol{d}$ is supposed to be bounded by known bounds $\underline{\boldsymbol{d}}$ and $\overline{\boldsymbol{d}}$.

Depending on the properties of the state matrix $\mathbf{A}(\boldsymbol{\theta})$, system $(\mathbf{G})$ might be unstable or its performance may fall short of the designer expectations. To solve these control problems, a dynamic controller $(\mathbf{K})$ with fixed order n_K is introduced:

$$(\mathbf{K})\begin{cases} \dot{\boldsymbol{x}}_K &= \mathbf{A_K}\boldsymbol{x}_K + \mathbf{B_K}\boldsymbol{u}_K \\ y_K &= \mathbf{C_K}\boldsymbol{x}_K + \mathbf{D_K}\boldsymbol{u}_K \\ \boldsymbol{x}_K(0) &= \mathbf{0} \end{cases} \tag{5.4}$$

where $\boldsymbol{x}_K \in \mathbb{R}^n$, $\boldsymbol{u}_K \in \mathbb{R}^m$ and the state-space matrices are of appropriate dimensions. The design of this structured controller is discussed later on in this chapter. It was also discussed in Chapter 2 where the synthesis was performed against multiple requirements on multiple models to account for critical values the vector of uncertainties $\boldsymbol{\theta}$. The nominal loop is closed using the conventional relations:

$$\begin{cases} \boldsymbol{u}_K &= \boldsymbol{y} \\ u &= y_K + v \end{cases} \tag{5.5}$$

where v is an external control input signal which use will be highlighted later on. Let make the following assumption which ensures that $1 - \mathbf{D_K D_u} \neq 0$ and is thus invertible:

Assumption 5.4 (Closed-loop well-posedness)**.**
The closed-loop consisting of the uncertain LTI system (5.1), the structured dynamic controller (5.4) and the interconnection (5.5) is supposed to be well-posed. In other words, the following real quantity is invertible:

$$1 - \mathbf{D_K D_u}(\boldsymbol{\theta}) \neq 0, \forall \boldsymbol{\theta} \in \Theta \tag{5.6}$$

This results in the following state-space representation for the closed-loop:

$$\begin{aligned} \dot{\boldsymbol{X}} &= \begin{bmatrix} \mathbf{A}(\boldsymbol{\theta}) + \mathbf{B_u}\Delta_u(\boldsymbol{\theta})\mathbf{D_K C}(\boldsymbol{\theta}) & \mathbf{B_u}\Delta_u(\boldsymbol{\theta})\mathbf{C_K} \\ \mathbf{B_K C}(\boldsymbol{\theta}) + \mathbf{B_K D_u}(\boldsymbol{\theta})\Delta_u(\boldsymbol{\theta})\mathbf{D_K C}(\boldsymbol{\theta}) & \mathbf{A_K} + \mathbf{B_K D_u}(\boldsymbol{\theta})\Delta_u(\boldsymbol{\theta})\mathbf{C_K} \end{bmatrix} \boldsymbol{X} \\ &\quad + \begin{bmatrix} \mathbf{B_u} & \mathbf{B_d}(\boldsymbol{\theta}) + \mathbf{B_u}\Delta_u(\boldsymbol{\theta})\mathbf{D_K D_d}(\boldsymbol{\theta}) \\ \mathbf{0} & \mathbf{B_K D_d}(\boldsymbol{\theta}) + \mathbf{B_K D_u}(\boldsymbol{\theta})\Delta_u(\boldsymbol{\theta})\mathbf{D_K D_d}(\boldsymbol{\theta}) \end{bmatrix} \begin{bmatrix} v \\ \boldsymbol{d} \end{bmatrix} \\ &= \mathbf{A_X}(\boldsymbol{\theta})\boldsymbol{X} + \mathbf{B_{X,v}}v + \mathbf{B_{X,d}}(\boldsymbol{\theta})\boldsymbol{d} \end{aligned} \tag{5.7}$$

where $\boldsymbol{X} = \begin{bmatrix} \boldsymbol{x} \\ \boldsymbol{x}_K \end{bmatrix}$ and $\Delta_u(\boldsymbol{\theta}) = [1 - \mathbf{D_K D_u}(\boldsymbol{\theta})]^{-1}$. The initial condition is set to $\boldsymbol{X}_0 = \begin{bmatrix} \boldsymbol{x}_0 \\ \mathbf{0} \end{bmatrix}$. This representation will be used when designing an interval observer on the closed-loop as explained in 5.3 and 7.4.

Similarly to the problem tackled in Chapters 3 and 4, the objective is to satisfy a time-domain requirement $\mathcal{K}(\Omega_\alpha)$ on a given output $\alpha = \mathbf{C_\alpha}\boldsymbol{x}$. Note that this time it may not be possible to evaluate α depending on what is unmeasured. Given two possibly time-varying signals $\underline{\alpha}(t)$ and $\overline{\alpha}(t)$ such that $\underline{\alpha}(t) \leq \overline{\alpha}(t)$, $\forall t \in \mathbb{R}_+$ and $\Omega_\alpha(t) = [\underline{\alpha}(t), \overline{\alpha}(t)]$, the objective is to fulfil:

$$\alpha(t) \in \Omega_\alpha(t), \forall t \in \mathbb{R}_+ \tag{5.8}$$

Using the closed-loop state $\boldsymbol{X}$, let define $\mathbf{C_{X\alpha}} = \begin{bmatrix} \mathbf{C_\alpha} & \mathbf{0}_{1\times n_K} \end{bmatrix}$. The constrained output is equivalently defined by $\alpha = \mathbf{C_{X\alpha}}\boldsymbol{X}$ and the time-domain constraint $\mathcal{K}(\Omega_\alpha)$, see Definition 3.9 corresponds to satisfying

$$\underline{\alpha}(t) \leq \mathbf{C_{X\alpha}}\boldsymbol{X} \leq \overline{\alpha}(t), \forall t \in \mathbb{R}_+ \tag{5.9}$$

Satisfying Assumptions 4.4 to 4.9 is still relevant. Small adjustment is however made for Assumption 4.9 where the controller should stabilize a family of models rather than only one model due to the presence of uncertainties $\boldsymbol{\theta}$:

Assumption 5.5 (Updated Assumption 4.9 on controller $(\mathbf{K})$)**.**
The controller $(\mathbf{K})$ in (5.4) is supposed to asymptotically (resp. exponentially) stabilize $(\mathbf{G})$ in (5.1) for any $\boldsymbol{\theta} \in \Theta$ to the origin $\boldsymbol{x}^\star = 0$, under Assumption 4.8 (resp. $\boldsymbol{d} = 0$). The controller state at the equilibrium is denoted $\boldsymbol{x_K}^\star$ and $\boldsymbol{x_K}^\star = 0$.

Remark 5.6. In practice, the controller $(\mathbf{K})$ is designed to stabilize a limited number of critical models, which is discussed in Chapter 2. ◇

Remark 5.7. Assumption 5.5 basically means that $\mathbf{A_X}(\theta)$ is Hurwitz $\forall\theta$. ◇

More precisions on these assumptions will be given in 5.3. In the next section, the original output constrained OIST-based control Problem 4.11 is updated in consideration of the broader class of systems (5.1).

5.2.2 Extended OIST problem statement

The OIST approach is an *evolutionary* approach [De Dona 02] based on introducing saturations on the controller output such that the values taken by the constrained output α remain in an admissible set. The problem of finding the adequate saturations has been formalized as Problem 4.11. This formulation is now updated to account for the broader class of considered systems, namely uncertain linear time-invariant systems with no specific constraint on the measurements matrix $\mathbf{C}(\boldsymbol{\theta})$. Comments are made below for this rather different formulation in comparison with Problem 4.11.

Problem 5.8 (System (5.1) output constrained control problem using OISTeR)**.**
Find two saturating signals $[\underline{v}(t), \overline{v}(t)]$ and a domain $\mathcal{C}_0$ such that for two given design signals $\underline{\alpha}(t)$ and $\overline{\alpha}(t)$ satisfying $\underline{\alpha}(t) \leq \overline{\alpha}(t)$, $\forall t \in \mathbb{R}_+$, the constrained output α satisfies the constraint $\mathcal{K}(\Omega_\alpha)$:

$$\alpha(t) \in \Omega_\alpha(t) = [\underline{\alpha}(t), \overline{\alpha}(t)], \forall t \in \mathbb{R}_+ \tag{5.10}$$

for the system $(\mathbf{G})$ in (5.1) in well-posed[a] closed-loop with controller $(\mathbf{K})$ in (5.4) and the saturations obtained with OISTeR:

$$\begin{cases} \dot{\boldsymbol{x}}(t) &= \mathbf{A}(\boldsymbol{\theta})\boldsymbol{x}(t) + \mathbf{B_u}u(t) + \mathbf{B_d}(\boldsymbol{\theta})\boldsymbol{d}(t) \\ \boldsymbol{y}(t) &= \mathbf{C}(\boldsymbol{\theta})\boldsymbol{x}(t) + \mathbf{D_u}(\boldsymbol{\theta})u(t) + \mathbf{D_d}(\boldsymbol{\theta})\boldsymbol{d}(t) \\ \alpha(t) &= \mathbf{C_\alpha}\boldsymbol{x}(t) \\ \dot{\boldsymbol{x}}_K(t) &= \mathbf{A_K}\boldsymbol{x}_K(t) + \mathbf{B_K}\boldsymbol{y}(t) \\ y_K(t) &= \mathbf{C_K}\boldsymbol{x}_K(t) + \mathbf{D_K}\boldsymbol{y}(t) \\ u(t) &= y_K(t) + v(t) \\ v(t) &= \mathrm{sat}_{\underline{v}(t)}^{\overline{v}(t)}(0) \\ \boldsymbol{x}_0 &\in \mathcal{C}_0 \end{cases} \tag{5.11}$$

where it is supposed that Assumptions 4.4 to 4.10 and in 5.2.1 are satisfied.

[a] See Assumption 5.4.

This formulation is different from the original formulation in Problem 4.11. It can be noted that the output y_K of the controller is no longer saturated. The external input v introduced in (5.5) is used as the new saturated input. This comes from the choice to consider the closed-loop in the application of OIST rather than just the original system for which the controller output is saturated. When the conditions on α are met, the input v is set to 0 and the closed-loop behaves nominally. A corrective signal is otherwise applied. This new formulation is a contribution of this thesis. As highlighted later in 5.3.3, $\underline{v}(t)$ and $\overline{v}(t)$ depend on the closed-loop state hence are part of this closed-loop.

Similarly to Problem 4.11, this statement implicitly requires the designed saturating signals $\underline{v}(t)$ and $\overline{v}(t)$ not to overlap. Also, the stability Problem 4.13 is still critical since the introduction in the closed-loop of saturations depending on the system state can lead to instabilities. However, in the newly considered problem, stability must be ensured over a family of systems rather than on one system only, due to the presence of uncertainties:

Problem 5.9 (Closed-loop stability using extended OIST)**.**
Guarantee that the origin of the saturated closed-loop in (D.21) is asymptotically stable $\forall \boldsymbol{\theta} \in \Theta$.

The OIST approach initially described for known LTI systems in Chapter 4 is extended to uncertain LTI systems with incomplete state vector measurements following a similar explanation path. A solution to Problem 5.8 is thereby provided. It makes use of interval observers which are described in Chapter B and additional results from Chapter 7 are used. Finding a solution

to Problem 5.9 is still a perspective for future works at the time of writing. However, in the case of systems with incomplete measurements and no uncertainty, the proof of stability is expected to be quite similar to the one in A.2.

5.3 OIST extension for Robustness (*OISTeR*)

In this section, the *Output to Input Saturation Transformation* presented in Chapters 3 and 4 is extended to the case of uncertain LTI systems (5.1) with incomplete measurements of their state vector $\boldsymbol{x}$. Contrary to the previously studied case, the considered constrained output expression $\alpha = \mathbf{C}_{\boldsymbol{\alpha}}\boldsymbol{x}$ can no longer be differentiated. The obtained expression (4.23) would indeed depend on $\boldsymbol{x}$ which cannot be evaluated.

Interestingly enough, the proposed framework is quite similar in its assumptions to the interval observer theory. Assumption 4.7 is reminiscent of assumptions made to evaluate bounds on a given system state vector. Also, obtaining such guaranteed bounds on the state vector is interesting within the OIST approach since it allows to bound the quantity $\mathbf{C}_{\boldsymbol{\alpha}}\boldsymbol{x}$ and to formalize the time-domain constraint on these bounds rather than on the unknown quantity α. This is the core of the OIST generalization which is now described in details.

5.3.1 Interval observer of the closed-loop and differentiability issues

In this section, an interval observer is introduced on the closed-loop dynamics obtained in (D.19). Differentiability issues related to the chosen structure for the interval observer are tackled. They are critical within the OIST framework since successive differentiations of the time-domain constraint are required (see Chapter 4). Also, some details are given on why the interval observer is designed on top of the closed-loop rather than on the initial system.

5.3.1 (a) Interval observer of the closed-loop

Let consider the following system which was obtained in (D.19) by considering system (5.1) in closed-loop with the controller (5.4) and (5.5):

$$\dot{\boldsymbol{X}} = \mathbf{A}_{\mathbf{X}}(\boldsymbol{\theta})\,\boldsymbol{X} + \mathbf{B}_{\mathbf{X},\mathbf{v}}v + \mathbf{B}_{\mathbf{X},\mathbf{d}}(\boldsymbol{\theta})\,\boldsymbol{d} \tag{5.12}$$

Considering Assumption 5.1, it appears that the vector of uncertainties $\boldsymbol{\theta}$ is bounded. Let consider a fixed nominal value $\boldsymbol{\theta}_n \in [\underline{\boldsymbol{\theta}}, \overline{\boldsymbol{\theta}}] \subset \Theta$ for this vector. For example, $\boldsymbol{\theta}_n = \frac{\overline{\boldsymbol{\theta}}-\underline{\boldsymbol{\theta}}}{2}$ is an admissible nominal value. The system in (5.12) can be rewritten as:

$$\begin{aligned} \dot{\boldsymbol{X}} &= \mathbf{A}_{\mathbf{X},\mathbf{n}}\boldsymbol{X} + \boldsymbol{\Delta}\mathbf{A}_{\mathbf{X}}(\boldsymbol{\theta})\,\boldsymbol{X} + \mathbf{B}_{\mathbf{X},\mathbf{v}}v + \mathbf{B}_{\mathbf{X},\mathbf{d}}(\boldsymbol{\theta})\,\boldsymbol{d} \\ &= \mathbf{A}_{\mathbf{X},\mathbf{n}}\boldsymbol{X} + \mathbf{B}_{\mathbf{X},\mathbf{v}}v + \boldsymbol{f}(\boldsymbol{X},\boldsymbol{d},\theta) \end{aligned} \tag{5.13}$$

where $\mathbf{A}_{\mathbf{X},\mathbf{n}} = \mathbf{A}_{\mathbf{X}}(\boldsymbol{\theta}_n)$, $\boldsymbol{\Delta}\mathbf{A}_{\mathbf{X}}(\boldsymbol{\theta}) = \mathbf{A}_{\mathbf{X}}(\boldsymbol{\theta}) - \mathbf{A}_{\mathbf{X},\mathbf{n}}$ and

$$\boldsymbol{f}(\boldsymbol{X},\boldsymbol{d},\theta) = \boldsymbol{\Delta}\mathbf{A}_{\mathbf{X}}(\boldsymbol{\theta})\,\boldsymbol{X} + \mathbf{B}_{\mathbf{X},\mathbf{d}}(\boldsymbol{\theta})\,\boldsymbol{d} \tag{5.14}$$

Using the notations in Remark 5.3, the definitions of matrices $\mathbf{A}_{\mathbf{X}}$ and $\mathbf{B}_{\mathbf{X},\mathbf{d}}$ in (D.19), Assumption 4.7 and Lemma 1 in [Efimov 13e], the quantity in (5.14) can be bounded:

$$\underline{\boldsymbol{f}}(\underline{\boldsymbol{X}},\overline{\boldsymbol{X}},\underline{\boldsymbol{d}},\overline{\boldsymbol{d}}) \leq \boldsymbol{f}(\boldsymbol{X},\boldsymbol{d},\theta) \leq \overline{\boldsymbol{f}}(\underline{\boldsymbol{X}},\overline{\boldsymbol{X}},\underline{\boldsymbol{d}},\overline{\boldsymbol{d}}) \tag{5.15}$$

where the bounding quantities are given by:

$$\begin{aligned} \underline{\boldsymbol{f}}(\underline{\boldsymbol{X}},\overline{\boldsymbol{X}},\underline{\boldsymbol{d}},\overline{\boldsymbol{d}}) &= \underline{\boldsymbol{\Delta}\mathbf{A}_{\mathbf{X}}}^{+}\underline{\boldsymbol{X}}^{+} - \overline{\boldsymbol{\Delta}\mathbf{A}_{\mathbf{X}}}^{+}\underline{\boldsymbol{X}}^{-} - \underline{\boldsymbol{\Delta}\mathbf{A}_{\mathbf{X}}}^{-}\overline{\boldsymbol{X}}^{+} + \overline{\boldsymbol{\Delta}\mathbf{A}_{\mathbf{X}}}^{-}\overline{\boldsymbol{X}}^{-} \\ &\quad + \underline{\mathbf{B}_{\mathbf{X},\mathbf{d}}}^{+}\underline{\boldsymbol{d}}^{+} - \overline{\mathbf{B}_{\mathbf{X},\mathbf{d}}}^{+}\underline{\boldsymbol{d}}^{-} - \underline{\mathbf{B}_{\mathbf{X},\mathbf{d}}}^{-}\overline{\boldsymbol{d}}^{+} + \overline{\mathbf{B}_{\mathbf{X},\mathbf{d}}}^{-}\overline{\boldsymbol{d}}^{-} \\ \overline{\boldsymbol{f}}(\underline{\boldsymbol{X}},\overline{\boldsymbol{X}},\underline{\boldsymbol{d}},\overline{\boldsymbol{d}}) &= \overline{\boldsymbol{\Delta}\mathbf{A}_{\mathbf{X}}}^{+}\overline{\boldsymbol{X}}^{+} - \underline{\boldsymbol{\Delta}\mathbf{A}_{\mathbf{X}}}^{+}\overline{\boldsymbol{X}}^{-} - \overline{\boldsymbol{\Delta}\mathbf{A}_{\mathbf{X}}}^{-}\underline{\boldsymbol{X}}^{+} + \underline{\boldsymbol{\Delta}\mathbf{A}_{\mathbf{X}}}^{-}\underline{\boldsymbol{X}}^{-} \\ &\quad + \overline{\mathbf{B}_{\mathbf{X},\mathbf{d}}}^{+}\overline{\boldsymbol{d}}^{+} - \underline{\mathbf{B}_{\mathbf{X},\mathbf{d}}}^{+}\overline{\boldsymbol{d}}^{-} - \overline{\mathbf{B}_{\mathbf{X},\mathbf{d}}}^{-}\underline{\boldsymbol{d}}^{+} + \underline{\mathbf{B}_{\mathbf{X},\mathbf{d}}}^{-}\underline{\boldsymbol{d}}^{-} \end{aligned} \tag{5.16}$$

The interval observer structure is now properly introduced. Using Assumption 5.5, it can be observed that $\mathbf{A_{X,n}}$ is Hurwitz by evaluating $\mathbf{A_X}(\boldsymbol{\theta})$ at $\boldsymbol{\theta} = \boldsymbol{\theta}_n$. Also, let consider the following assumption which is reminiscent of Assumption B.17:

Assumption 5.10 (Known SCT to ensure cooperativity of (D.19))**.**
Let $\mathbf{A_{X,n}} = \mathbf{A_X}(\boldsymbol{\theta}_n)$ where $\mathbf{A_X}(\boldsymbol{\theta})$ is defined in (D.19). There exists $\mathbf{P} \in \mathbb{R}^{(n+n_K)\times(n+n_K)}$ such that $\mathbf{P}\mathbf{A_{X,n}}\mathbf{P}^{-1}$ is Metzler. This matrix is Hurwitz by construction[a].

[a] $\mathbf{A_X}(\boldsymbol{\theta})$ evaluated at $\boldsymbol{\theta} = \boldsymbol{\theta}_n$ is Hurwitz.

In practice, such matrix $\mathbf{P}$ is rarely known or is hard to determine by hand. The simultaneous design of the controller $(\mathbf{K})$ and appropriate SCT matrix $\mathbf{P}$ is discussed in 5.3.2 based on the approach initiated in [Chambon 16], see Chapter 7. Let denote $\mathbf{M_Z} = \mathbf{P}\mathbf{A_{X,n}}\mathbf{P}^{-1}$. The state-coordinate change $\boldsymbol{Z} = \mathbf{P}\boldsymbol{X}$ is considered. Under Assumption 5.10 and using Definition B.11, the following system is proposed as a candidate interval observer for (D.19):

$$\begin{array}{rcl}
\dot{\underline{\boldsymbol{Z}}} & = & \mathbf{M_Z}\underline{\boldsymbol{Z}} + \mathbf{P}\mathbf{B_{X,v}}v + \underline{\boldsymbol{g}}\left(\underline{\boldsymbol{Z}}, \overline{\boldsymbol{Z}}, \underline{\boldsymbol{d}}, \overline{\boldsymbol{d}}\right) \\
\dot{\overline{\boldsymbol{Z}}} & = & \mathbf{M_Z}\overline{\boldsymbol{Z}} + \mathbf{P}\mathbf{B_{X,v}}v + \overline{\boldsymbol{g}}\left(\underline{\boldsymbol{Z}}, \overline{\boldsymbol{Z}}, \underline{\boldsymbol{d}}, \overline{\boldsymbol{d}}\right) \\
\underline{\boldsymbol{Z}_0} & = & \mathbf{P}^{+}\underline{\boldsymbol{X}_0} - \mathbf{P}^{-}\overline{\boldsymbol{X}_0} \\
\overline{\boldsymbol{Z}_0} & = & \mathbf{P}^{+}\overline{\boldsymbol{X}_0} - \mathbf{P}^{-}\underline{\boldsymbol{X}_0} \\
\underline{\boldsymbol{X}} & = & \mathbf{T}^{+}\underline{\boldsymbol{Z}} - \mathbf{T}^{-}\overline{\boldsymbol{Z}} \\
\overline{\boldsymbol{X}} & = & \mathbf{T}^{+}\overline{\boldsymbol{Z}} - \mathbf{T}^{-}\underline{\boldsymbol{Z}}
\end{array} \tag{5.17}$$

where $\mathbf{T} = \mathbf{P}^{-1}$, $\underline{\boldsymbol{X}_0} = \begin{bmatrix} \boldsymbol{x}_0 \\ \mathbf{0} \end{bmatrix}$, $\overline{\boldsymbol{X}_0} = \begin{bmatrix} \overline{\boldsymbol{x}_0} \\ \mathbf{0} \end{bmatrix}$ and

$$\begin{array}{rcl}
\underline{\boldsymbol{g}}\left(\underline{\boldsymbol{Z}}, \overline{\boldsymbol{Z}}, \underline{\boldsymbol{d}}, \overline{\boldsymbol{d}}\right) & = & \mathbf{P}^{+}\underline{\boldsymbol{f}}\left(\mathbf{T}^{+}\underline{\boldsymbol{Z}} - \mathbf{T}^{-}\overline{\boldsymbol{Z}}, \mathbf{T}^{+}\overline{\boldsymbol{Z}} - \mathbf{T}^{-}\underline{\boldsymbol{Z}}, \underline{\boldsymbol{d}}, \overline{\boldsymbol{d}}\right) \\
& & -\mathbf{P}^{-}\overline{\boldsymbol{f}}\left(\mathbf{T}^{+}\underline{\boldsymbol{Z}} - \mathbf{T}^{-}\overline{\boldsymbol{Z}}, \mathbf{T}^{+}\overline{\boldsymbol{Z}} - \mathbf{T}^{-}\underline{\boldsymbol{Z}}, \underline{\boldsymbol{d}}, \overline{\boldsymbol{d}}\right) \\
\overline{\boldsymbol{g}}\left(\underline{\boldsymbol{Z}}, \overline{\boldsymbol{Z}}, \underline{\boldsymbol{d}}, \overline{\boldsymbol{d}}\right) & = & \mathbf{P}^{+}\overline{\boldsymbol{f}}\left(\mathbf{T}^{+}\underline{\boldsymbol{Z}} - \mathbf{T}^{-}\overline{\boldsymbol{Z}}, \mathbf{T}^{+}\overline{\boldsymbol{Z}} - \mathbf{T}^{-}\underline{\boldsymbol{Z}}, \underline{\boldsymbol{d}}, \overline{\boldsymbol{d}}\right) \\
& & -\mathbf{P}^{-}\underline{\boldsymbol{f}}\left(\mathbf{T}^{+}\underline{\boldsymbol{Z}} - \mathbf{T}^{-}\overline{\boldsymbol{Z}}, \mathbf{T}^{+}\overline{\boldsymbol{Z}} - \mathbf{T}^{-}\underline{\boldsymbol{Z}}, \underline{\boldsymbol{d}}, \overline{\boldsymbol{d}}\right)
\end{array} \tag{5.18}$$

This interval observer is a candidate only since condition (3) in Definition B.11 may not be satisfied even if $\mathbf{P}$ and $(\mathbf{K})$ comply with (1) and (2).

5.3.1 (b) Differentiability issues

Due to the presence of the max function in the definitions of $\underline{\boldsymbol{f}}$ and $\overline{\boldsymbol{f}}$ in (5.16), the dynamics in (5.17) are not differentiable. This will be crucial in 5.3.3 when differentiation of the constraints will be required. In 4.2, the functions f_{abs} and $f_{\max}$ have been introduced as approximates of the absolute value and max functions respectively. By definition, for a given vector $\boldsymbol{X} \in \mathbb{R}^n$, $\boldsymbol{X}^{+} = \max(\boldsymbol{X}, \mathbf{0})$. Using both f_{abs} and $f_{\max}$, bounding approximates of $\max(\boldsymbol{X}, \mathbf{0})$ can be obtained. Let consider the two following $\mathcal{C}^{\infty}(\mathbb{R}, \mathbb{R})$ functions:

$$\begin{array}{rcl}
f_m(x) & = & \frac{1}{2}\left(x + x\tanh(x)\right) \\
f_p(x) & = & \frac{1}{2}\left(x + x\tanh(x) + c_2\right)
\end{array}, \forall x \in \mathbb{R} \tag{5.19}$$

where c_2 is defined in 4.4. Let consider the element-wise $\mathcal{C}^{\infty}(\mathbb{R}^n, \mathbb{R}^n)$ counterparts $\boldsymbol{f}_m(\boldsymbol{x})$ and $\boldsymbol{f}_p(\boldsymbol{x})$ for $\boldsymbol{x} \in \mathbb{R}^n$:

$$\begin{array}{rcl}
\left[\boldsymbol{f}_m(\boldsymbol{x})\right]_i & = & f_m(\boldsymbol{x}_i) \\
\left[\boldsymbol{f}_p(\boldsymbol{x})\right]_i & = & f_p(\boldsymbol{x}_i)
\end{array}, \forall \boldsymbol{x} \in \mathbb{R}^n, \forall i \in \mathbb{N}^{\star} \text{ s.t. } i \leq n \tag{5.20}$$

Then, it is observed that the function $\max(\boldsymbol{x}, \mathbf{0})$ which is $\mathcal{C}^0$ only can be bounded by two $\mathcal{C}^{\infty}$ functions.

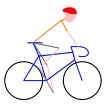

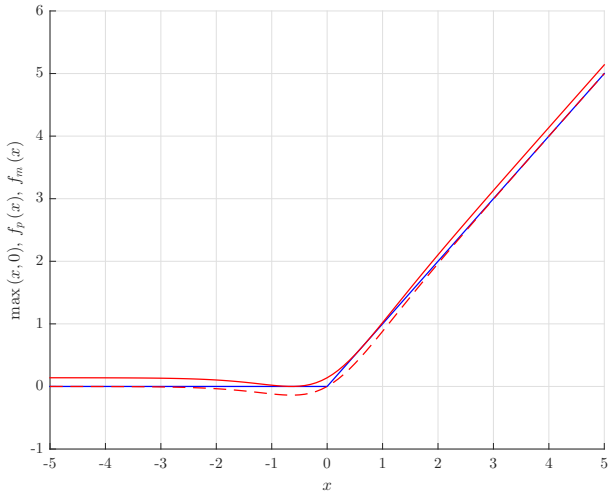

Figure 5.2: In red, the differentiable functions f_m and f_p defined in (5.19) are appropriate bounds of the $\max(x, 0)$ non-differentiable function (in blue).

Proposition 5.11 ($\mathcal{C}^\infty$ bounds of the $\mathcal{C}^0$ function $\max(\boldsymbol{x}, \boldsymbol{0})$)**.**
Let $\boldsymbol{x} \in \mathbb{R}^n$. Then the operator $\boldsymbol{x}^+ = \max(\boldsymbol{x}, \boldsymbol{0})$ can be bounded by the two following $\mathcal{C}^\infty$ functions:

$$\boldsymbol{f}_m(\boldsymbol{x}) \leq \boldsymbol{x}^+ \leq \boldsymbol{f}_p(\boldsymbol{x}) \tag{5.21}$$

where $\boldsymbol{f}_m(\boldsymbol{x})$ and $\boldsymbol{f}_p(\boldsymbol{x})$ are defined in (5.20). Consequently, by definition of $\boldsymbol{x}^- = \boldsymbol{x}^+ - \boldsymbol{x}$, the following inequalities are also satisfied:

$$\boldsymbol{f}_m(\boldsymbol{x}) - \boldsymbol{x} \leq \boldsymbol{x}^- \leq \boldsymbol{f}_p(\boldsymbol{x}) - \boldsymbol{x} \tag{5.22}$$

Proof. Straightforward using real analysis on $\mathbb{R}^\star_+$ and $\mathbb{R}^\star_-$. □

This proposition and especially the inequalities in (5.21) are illustrated in Fig. 5.2. The bounds are represented in red while the non-differentiable function $\max(x, 0)$ is represented in blue.

Using the functions $\boldsymbol{f}_m$ and $\boldsymbol{f}_p$ applied to $\underline{\boldsymbol{Z}}$, $\overline{\boldsymbol{Z}}$, $\underline{\boldsymbol{d}}$ or $\overline{\boldsymbol{d}}$, it is possible to obtain differentiable approximates of the non-differentiable functions $\underline{\boldsymbol{g}}$ and $\overline{\boldsymbol{g}}$ in (5.16). Let denote $\underline{\boldsymbol{g}}^\infty$ and $\overline{\boldsymbol{g}}^\infty$ these functions which are $\mathcal{C}^\infty$ by property of the hyperbolic tangent function. It can be straightforwardly verified that the following inequalities are satisfied:

$$\begin{array}{rcl} \underline{\boldsymbol{g}}^\infty(\underline{\boldsymbol{Z}}, \overline{\boldsymbol{Z}}, \underline{\boldsymbol{d}}, \overline{\boldsymbol{d}}) & \leq & \underline{\boldsymbol{g}}(\underline{\boldsymbol{Z}}, \overline{\boldsymbol{Z}}, \underline{\boldsymbol{d}}, \overline{\boldsymbol{d}}) \\ \overline{\boldsymbol{g}}^\infty(\underline{\boldsymbol{Z}}, \overline{\boldsymbol{Z}}, \underline{\boldsymbol{d}}, \overline{\boldsymbol{d}}) & \geq & \overline{\boldsymbol{g}}(\underline{\boldsymbol{Z}}, \overline{\boldsymbol{Z}}, \underline{\boldsymbol{d}}, \overline{\boldsymbol{d}}) \end{array}, \forall (\underline{\boldsymbol{Z}}, \overline{\boldsymbol{Z}}, \underline{\boldsymbol{d}}, \overline{\boldsymbol{d}}) \tag{5.23}$$

With a small abuse of notation where we use $\underline{\boldsymbol{Z}}$ and $\overline{\boldsymbol{Z}}$ as the new system state, this leads to a new candidate interval observer for the closed-loop (D.19):

$$\begin{array}{rcl} \dot{\underline{\boldsymbol{Z}}} & = & \mathbf{M}_{\mathbf{X}} \underline{\boldsymbol{Z}} + \mathbf{B}_{\mathbf{Z},\mathbf{v}} v + \underline{\boldsymbol{g}}^\infty(\underline{\boldsymbol{Z}}, \overline{\boldsymbol{Z}}, \underline{\boldsymbol{d}}, \overline{\boldsymbol{d}}) \\ \dot{\overline{\boldsymbol{Z}}} & = & \mathbf{M}_{\mathbf{X}} \overline{\boldsymbol{Z}} + \mathbf{B}_{\mathbf{Z},\mathbf{v}} v + \overline{\boldsymbol{g}}^\infty(\underline{\boldsymbol{Z}}, \overline{\boldsymbol{Z}}, \underline{\boldsymbol{d}}, \overline{\boldsymbol{d}}) \end{array} \tag{5.24}$$

where $\mathbf{B}_{\mathbf{Z},\mathbf{v}} = \mathbf{P}\mathbf{B}_{\mathbf{X},\mathbf{v}}$. This interval observer is more conservative in the sense that less precise bounds on $\boldsymbol{g}$ in (5.14) are used. Also, this is a candidate interval observer since condition (3) in Definition B.11 may be even harder to satisfy than for the original candidate (5.17). This time however, the dynamics is differentiable which is required in theory to apply OIST. Of course, the dynamics remains non-linear. This motivates using a more compact notation for this candidate interval observer (5.24). More precisely, it can be noted that the functions $\underline{\boldsymbol{g}}^\infty$ and $\overline{\boldsymbol{g}}^\infty$ depend

in $(\underline{\boldsymbol{Z}}, \overline{\boldsymbol{Z}})$ and $(\underline{\boldsymbol{d}}, \overline{\boldsymbol{d}})$ in an independent fashion. This comes from (5.16) where we have isolated in blue the quantities in $\underline{\boldsymbol{f}}$ and $\overline{\boldsymbol{f}}$ which depend on $\underline{\boldsymbol{X}}$ and $\overline{\boldsymbol{X}}$ and in red the quantities which depend on $\underline{\boldsymbol{d}}$ and $\overline{\boldsymbol{d}}$. This allows us to write:

$$\dot{\boldsymbol{\zeta}} = \boldsymbol{h}_1(\boldsymbol{\zeta}) + \mathbf{B}_{\mathbf{Z},\mathbf{v}} v + \boldsymbol{h}_2(\boldsymbol{\mathcal{D}}) \tag{5.25}$$

where $\boldsymbol{\zeta} = \begin{bmatrix} \underline{\boldsymbol{Z}} \\ \overline{\boldsymbol{Z}} \end{bmatrix}$, $\boldsymbol{\mathcal{D}} = \begin{bmatrix} \underline{\boldsymbol{d}} \\ \overline{\boldsymbol{d}} \end{bmatrix}$ and $\boldsymbol{h}_1$ and $\boldsymbol{h}_2$ are non-linear although $\mathcal{C}^\infty$ functions defined as the following mappings:

$$\boldsymbol{h}_1 : \mathbb{R}^{2(n+n_K)} \to \mathbb{R}^{2(n+n_K)}, \ \boldsymbol{h}_2 : \mathbb{R}^{2(m-1)} \to \mathbb{R}^{2(n+n_K)} \tag{5.26}$$

This is formalised in the following proposition.

Proposition 5.12 (Candidate non-linear differentiable interval observer of (D.19))**.** *The following non-linear system*

$$(\mathbf{G}^{\mathbf{z},\sharp}) \begin{cases} \dot{\boldsymbol{\zeta}} &= \boldsymbol{h}_1(\boldsymbol{\zeta}) + \mathbf{B}_{\mathbf{Z},\mathbf{v}} v + \boldsymbol{h}_2(\boldsymbol{\mathcal{D}}) \\ \boldsymbol{\zeta}_0 &= \begin{bmatrix} \underline{\boldsymbol{Z}_0} & \overline{\boldsymbol{Z}_0} \end{bmatrix}^\top \end{cases} \tag{5.27}$$

where $\boldsymbol{\zeta} \in \mathbb{R}^{2(n+n_K)}$, $\boldsymbol{\mathcal{D}} = \begin{bmatrix} \underline{\boldsymbol{d}} \\ \overline{\boldsymbol{d}} \end{bmatrix}$ *and* $\boldsymbol{h}_1$ *and* $\boldsymbol{h}_2$ *are* $\mathcal{C}^\infty$ *mappings is a candidate interval observer of the closed-loop (D.19) with*

$$\begin{aligned} \underline{\boldsymbol{Z}} &= \begin{bmatrix} \mathbf{I}_{n+n_K} & \mathbf{0}_{(n+n_K)\times(n+n_K)} \end{bmatrix} \boldsymbol{\zeta} \\ \overline{\boldsymbol{Z}} &= \begin{bmatrix} \mathbf{0}_{(n+n_K)\times(n+n_K)} & \mathbf{I}_{n+n_K} \end{bmatrix} \boldsymbol{\zeta} \\ \underline{\boldsymbol{X}} &= \mathbf{T}^+ \underline{\boldsymbol{Z}} - \mathbf{T}^- \overline{\boldsymbol{Z}} \\ \overline{\boldsymbol{X}} &= \mathbf{T}^+ \overline{\boldsymbol{Z}} - \mathbf{T}^- \underline{\boldsymbol{Z}} \end{aligned} \tag{5.28}$$

for $\mathbf{T} = \mathbf{P}^{-1}$ *where* $\mathbf{P}$ *is such that* $\mathbf{P}\mathbf{A}_{\mathbf{X},\mathbf{n}}\mathbf{P}^{-1}$ *is Metzler (see Assumption 5.10).*

The problem of satisfying condition (3) in Definition B.11 is discussed in 5.3.2 where the synthesis of the structured dynamic controller and the appropriate SCT is considered.

5.3.1 (c) Justification of the choice of an interval observer on the closed-loop

Up to now, the choice for considering an interval observer on the closed-loop has not be explained. A conventional interval observer on the original system could indeed be designed as in B.3. However, such interval observer would depend on the original system measurements vector $\boldsymbol{y}$ and potentially on successive derivatives of this vector. This would invariably lead to the unknown components of the state to be re-injected in the expressions of the OIST saturations as detailed in 5.3.3. This is illustrated in the following example.

Example 5.13. Let consider the following simple system for illustrative purposes:

$$\begin{cases} \dot{\boldsymbol{x}}_1 &= -\boldsymbol{x}_1 + \boldsymbol{x}_2 \\ \dot{\boldsymbol{x}}_2 &= -2\boldsymbol{x}_2 + d + u \end{cases} \tag{5.29}$$

where d is an unknown disturbance such that $\underline{d} \leq d \leq \overline{d}, \forall t \in \mathbb{R}_+$ where $\underline{d}$ and $\overline{d}$ are known signals. Only $\boldsymbol{x}_1$ is supposed to be measured hence $\mathbf{C} = \begin{bmatrix} 1 & 0 \end{bmatrix}$. Let suppose $\alpha = \boldsymbol{x}_1$ hence $\mathbf{C}_{\boldsymbol{\alpha}} = \mathbf{C}$. Note that this system is cooperative hence a trivial interval observer could be designed. In most cases however, an additional degree of freedom is required to be able to constrain the convergence speed of the observer. Hence, let consider the conventional approach exposed in B.3 for interval observer design. Let $\mathbf{L}$ the classical observer gain such that:

$$\dot{\widehat{\boldsymbol{x}}} = (\mathbf{A} - \mathbf{L}\mathbf{C})\,\widehat{\boldsymbol{x}} + \mathbf{L}y \tag{5.30}$$

is stable and cooperative or, in other words, such that $(\mathbf{A}-\mathbf{LC})$ is Hurwitz Metzler. The observation error dynamics is thus given by:

$$\dot{\boldsymbol{e}} = (\mathbf{A}-\mathbf{LC})\,\boldsymbol{e} + \mathbf{B_d} d \tag{5.31}$$

and an interval observer of this system is trivially obtained as:

$$\begin{aligned} \dot{\underline{e}} &= (\mathbf{A}-\mathbf{LC})\,\underline{e} + \mathbf{B_d}\underline{d} \\ \dot{\overline{e}} &= (\mathbf{A}-\mathbf{LC})\,\overline{e} + \mathbf{B_d}\overline{d} \end{aligned} \tag{5.32}$$

Consequently, bounds on the original state vector $\boldsymbol{x}$ are respectively given by $\underline{\boldsymbol{x}} = \widehat{\boldsymbol{x}} + \underline{\boldsymbol{e}}$ and $\overline{\boldsymbol{x}} = \widehat{\boldsymbol{x}} + \overline{\boldsymbol{e}}$. In section 5.3.3, the notion of generalized propagated bounds will be introduced to account for the fact that $\boldsymbol{x}$ is no longer known contrary to guaranteed bounds $[\underline{\boldsymbol{x}}, \overline{\boldsymbol{x}}]$. Similarly to the original OIST approach detailed in 4, these generalized propagated bounds are iteratively defined and depend on the following quantities:

$$\beta_m = \mathbf{C}_{\boldsymbol{\alpha}}\underline{\boldsymbol{x}},\ \beta_p = \mathbf{C}_{\boldsymbol{\alpha}}\overline{\boldsymbol{x}} \tag{5.33}$$

and their successive derivatives. Noting that

$$\ddot{\underline{\boldsymbol{x}}} = \ddot{\underline{\boldsymbol{e}}} + (\mathbf{A}-\mathbf{LC})^2\,\widehat{x} + (\mathbf{A}-\mathbf{LC})\,\mathbf{L}y + \mathbf{LC}\dot{\boldsymbol{x}} \tag{5.34}$$

it may happen for systems with $k \geq 2$ that the propagated bounds depend on the original system state and especially on its unmeasured components (red term). On the contrary, the state vector of an interval observer on the closed-loop[1] does not depend on the measurements vector $\boldsymbol{y}$. ♣

Considering an interval observer on the closed-loop requires to simultaneously design the controller and an appropriate time-invariant SCT such that the closed-loop state matrix is Metzler in the new coordinates. This is considered in the next section.

5.3.2 Simultaneous structured controller/time-invariant SCT synthesis

The simultaneous design of a dynamic structured controller and an interval observer on the resulting closed-loop is discussed in 7.4. However, in the current case, the considered interval observer is non-linear as highlighted in Proposition 5.12. Using (5.24) results in the following tightness $\boldsymbol{E}_d$ dynamics, where $\boldsymbol{E}_d = \frac{1}{2}\left(\overline{\boldsymbol{Z}} - \underline{\boldsymbol{Z}}\right)$:

$$\dot{\boldsymbol{E}}_d = \mathbf{M}_{\mathbf{X}}\boldsymbol{E}_d + \frac{1}{2}\left[\overline{\boldsymbol{g}}^{\infty}\left(\underline{\boldsymbol{Z}}, \overline{\boldsymbol{Z}}, \underline{\boldsymbol{d}}, \overline{\boldsymbol{d}}\right) - \underline{\boldsymbol{g}}^{\infty}\left(\underline{\boldsymbol{Z}}, \overline{\boldsymbol{Z}}, \underline{\boldsymbol{d}}, \overline{\boldsymbol{d}}\right)\right] \tag{5.35}$$

The functions $\underline{\boldsymbol{g}}^{\infty}$ and $\overline{\boldsymbol{g}}^{\infty}$ are non-linear in $\underline{\boldsymbol{Z}}$ and $\overline{\boldsymbol{Z}}$. In practice, this means that this model cannot be used as a synthesis model in the approach presented in Chapter 7. More precisely, contrary to the known case, no constraint can be set on the interval $\left[\underline{\boldsymbol{Z}}, \overline{\boldsymbol{Z}}\right]$ in the considered uncertain case. The condition (3) to qualify (5.27) as an interval observer can thus only be verified during the analysis and not during the synthesis.

5.3.3 Description of the OIST extension

In this section, the extension of the OIST theory to be applicable to systems of the form (5.1) is considered. Using the interval observer in Proposition 5.12 and synthesized in 5.3.2, the time-domain constraint on the unknown quantity $\alpha = \mathbf{C}_{\mathbf{X}\boldsymbol{\alpha}}$ is translated into two time-domain constraints on known quantities depending on the bounding variables $\underline{\boldsymbol{X}}$ and $\overline{\boldsymbol{X}}$. The saturations $\underline{v}$ and $\overline{v}$ are then determined using a similar transformation as the original OIST.

It appears that this new approach is in fact a generalization of the existing OIST as presented in Chapter 4. For systems with a fully measured state, the expressions derived in the current chapter can be simplified into their counterparts in Chapter 4.

[1] A design method of interval observers on closed-loops is proposed in Chapter 7.

5.3.3 (a) Generalized time-domain constraint

As extensively mentioned at the beginning of this chapter and in previous chapters dealing with OIST, the objective is to enforce a time-domain constraint as defined in Definition 3.9 on a given output $\alpha = \mathbf{C_\alpha} \boldsymbol{x}$. In (5.9), the considered output has been appropriately redefined to refer to the closed-loop state $\boldsymbol{X}$. The time-domain constraint is thus to ensure $\mathbf{C_{X\alpha}} \boldsymbol{X} \in [\underline{\alpha}, \overline{\alpha}]$.

However, it has been argued that this quantity cannot be evaluated in most cases since $\mathbf{C}(\boldsymbol{\theta}) \neq \mathbf{I_n}$. As a consequence, the approach proposed in Chapter 4 cannot be applied in this case. The solution is to express the time-domain constraint on known guaranteed bounds of $\mathbf{C_{X\alpha}} \boldsymbol{X}$. Such bounds can be obtained using the interval observer proposed in Proposition 5.12 and designed in 5.3.2. Indeed, using such observer, the following is obtained:

$$\mathbf{C_{X\alpha}}^+ \underline{\boldsymbol{X}} - \mathbf{C_{X\alpha}}^- \overline{\boldsymbol{X}} \leq \mathbf{C_{X\alpha}} \boldsymbol{X} \leq \mathbf{C_{X\alpha}}^+ \overline{\boldsymbol{X}} - \mathbf{C_{X\alpha}}^- \underline{\boldsymbol{X}} \tag{5.36}$$

where $\underline{\boldsymbol{X}}$ and $\overline{\boldsymbol{X}}$ are determined from the known interval observer state vector $\boldsymbol{\kappa}$.

Remark 5.14. In most cases where the constraint concerns an element of the state vector $\boldsymbol{X}$, the matrix $\mathbf{C_{X\alpha}}$ is either non-negative or negative. Consequently, simpler expressions are often obtained in (5.36) since $\mathbf{C_{X\alpha}}^- = \mathbf{0}$ (respectively $\mathbf{C_{X\alpha}}^+ = \mathbf{0}$) in that case. ◇

Using the guaranteed bounds obtained in (5.36), it is observed that by enforcing two constraints on these guaranteed bounds then the initial constraint can be satisfied:

$$\begin{cases} \mathbf{C_{X\alpha}}^+ \underline{\boldsymbol{X}} - \mathbf{C_{X\alpha}}^- \overline{\boldsymbol{X}} & \geq & \underline{\alpha} \\ \mathbf{C_{X\alpha}}^+ \overline{\boldsymbol{X}} - \mathbf{C_{X\alpha}}^- \underline{\boldsymbol{X}} & \leq & \overline{\alpha} \end{cases}, \forall t \in \mathbb{R}_+ \Rightarrow \underline{\alpha} \leq \mathbf{C_{X\alpha}} \boldsymbol{X} \leq \overline{\alpha}, \forall t \in \mathbb{R}_+ \tag{5.37}$$

which motivates the following definition of a generalized time-domain output constraint, inspired by Definition 3.9:

Definition 5.15 (Generalized output constraint $\mathcal{K}(\Omega_\alpha)$)**.**
Let $\alpha = \mathbf{C_{X\alpha}} \boldsymbol{X}$ the considered system (5.1) constrained output. Let $\Omega_\alpha(t) = [\underline{\alpha}(t), \overline{\alpha}(t)]$ where $\underline{\alpha}(t)$ and $\overline{\alpha}(t)$ are sufficiently smooth time-varying unidimensional signals satisfying

$$\underline{\alpha}(t) \leq \overline{\alpha}(t), \forall t \in \mathbb{R}_+ \tag{5.38}$$

Let suppose an interval observer has been designed from the candidate system in Proposition 5.12 such that bounds are known on the system state vector $\boldsymbol{X} \in \left[\underline{\boldsymbol{X}}, \overline{\boldsymbol{X}}\right]$. The considered output $\alpha = \mathbf{C_{X\alpha}} \boldsymbol{X}$ is said to satisfy the constraint $\mathcal{K}(\Omega_\alpha)$ if

$$\begin{cases} \mathbf{C_{X\alpha}}^+ \underline{\boldsymbol{X}} - \mathbf{C_{X\alpha}}^- \overline{\boldsymbol{X}} & \geq & \underline{\alpha} \\ \mathbf{C_{X\alpha}}^+ \overline{\boldsymbol{X}} - \mathbf{C_{X\alpha}}^- \underline{\boldsymbol{X}} & \leq & \overline{\alpha} \end{cases}, \forall t \in \mathbb{R}_+ \tag{5.39}$$

This is called a generalization of Definition 3.9 since in case the state vector $\boldsymbol{X}$ is known then the initial definition is retrieved.

Remark 5.16. Note that the generalized output constraint in (5.39) is infeasible in case the signals $\underline{\alpha}$ and $\overline{\alpha}$ are chosen such that

$$\overline{\alpha} - \underline{\alpha} \leq \left(\mathbf{C_{X\alpha}}^+ + \mathbf{C_{X\alpha}}^-\right)\left(\overline{\boldsymbol{X}} - \underline{\boldsymbol{X}}\right) \tag{5.40}$$

which can be conservative especially in case α depends on unmeasured states. On the contrary, the condition $\overline{\alpha} - \underline{\alpha} > 0$ is retrieved if α depends on measured states only. ◇

5.3.3 (b) Generalized propagated bounds and Lemma

As extensively covered in Chapters 3 and 4, the OIST approach relies on the relative degree (see Definition 3.4) of the regulated variable α with respect to the control input. Upon differentiation of the constraints and constrained output α, the dependency in the control input is

uncovered from which the saturations are deduced. The same procedure is applied here with slight differences however.

Let define $\beta_m = \sigma_m(\boldsymbol{\zeta})$ and $\beta_p = \sigma_p(\boldsymbol{\zeta})$ where $\boldsymbol{\zeta}$ is the state vector from the interval observer in Proposition 5.12 and the functions σ_m and σ_p are defined as the following mappings:

$$\sigma_m : \mathbb{R}^{2(n+n_K)} \to \mathbb{R},\ \sigma_p : \mathbb{R}^{2(n+n_K)} \to \mathbb{R} \tag{5.41}$$

with their expressions given by:

$$\begin{aligned}
\sigma_m(\boldsymbol{\zeta}) &= \mathbf{C_{X\alpha}}^{+}\underline{\boldsymbol{X}} - \mathbf{C_{X\alpha}}^{-}\overline{\boldsymbol{X}} \\
&= \left(\mathbf{C_{X\alpha}}^{+}\mathbf{T}^{+} + \mathbf{C_{X\alpha}}^{-}\mathbf{T}^{-}\right)\underline{\boldsymbol{Z}} - \left(\mathbf{C_{X\alpha}}^{+}\mathbf{T}^{-} + \mathbf{C_{X\alpha}}^{-}\mathbf{T}^{+}\right)\overline{\boldsymbol{Z}} \\
&= \left[\mathbf{C_{X\alpha}}^{+}\mathbf{T}^{+} + \mathbf{C_{X\alpha}}^{-}\mathbf{T}^{-} \quad -\mathbf{C_{X\alpha}}^{+}\mathbf{T}^{-} - \mathbf{C_{X\alpha}}^{-}\mathbf{T}^{+}\right]\boldsymbol{\zeta} \\
&= \mathbf{\Sigma_m}\boldsymbol{\zeta} \\
\sigma_p(\boldsymbol{\zeta}) &= \mathbf{C_{X\alpha}}^{+}\overline{\boldsymbol{X}} - \mathbf{C_{X\alpha}}^{-}\underline{\boldsymbol{X}} \\
&= \left(\mathbf{C_{X\alpha}}^{+}\mathbf{T}^{+} + \mathbf{C_{X\alpha}}^{-}\mathbf{T}^{-}\right)\overline{\boldsymbol{Z}} - \left(\mathbf{C_{X\alpha}}^{+}\mathbf{T}^{-} + \mathbf{C_{X\alpha}}^{-}\mathbf{T}^{+}\right)\underline{\boldsymbol{Z}} \\
&= \left[-\mathbf{C_{X\alpha}}^{+}\mathbf{T}^{-} - \mathbf{C_{X\alpha}}^{-}\mathbf{T}^{+} \quad \mathbf{C_{X\alpha}}^{+}\mathbf{T}^{+} + \mathbf{C_{X\alpha}}^{-}\mathbf{T}^{-}\right]\boldsymbol{\zeta} \\
&= \mathbf{\Sigma_p}\boldsymbol{\zeta}
\end{aligned} \tag{5.42}$$

where different notations are used. Using the work in 5.3.1 (b) dealing with differentiability issues affecting the dynamics of the interval observer, it appears that the functions σ_m and σ_p are $\mathcal{C}^\infty$ functions of the variable $\boldsymbol{\zeta}$. As a reminder, the dynamics of the interval observer is given by:

$$\dot{\boldsymbol{\zeta}} = \boldsymbol{h}_1(\boldsymbol{\zeta}) + \mathbf{B_{Z,v}}v + \boldsymbol{h}_2(\boldsymbol{\mathcal{D}}) \tag{5.43}$$

where $\boldsymbol{h}_1$ and $\boldsymbol{h}_2$ are $\mathcal{C}^\infty$ functions. Before detailing the expressions of the successive derivatives of β_m and β_p, Assumption 4.5 must be reviewed in view of the considered generalized constraints. Since α is not directly considered anymore, the important information is not its relative degree with respect to v but rather the relative degree of β_m and β_p with respect to v. The relative degree with respect to $\underline{\boldsymbol{d}}$ and $\overline{\boldsymbol{d}}$ is also studied. As a result, it is observed that the newly obtained assumption is less demanding in terms of knowledge on the unknown disturbance input $\boldsymbol{d}$. Especially, Assumption 4.7 can be heavily simplified as a result.

Assumption 5.17 (Relative degree of the generalized output constraint wrt the control input v)**.**
Let $k \in \mathbb{N}$. It is supposed the generalized output constraint functions β_m and β_p are of relative degree k with respect to v.

Contrary to the case considered in Chapter 4, the generalized output constraint functions do not depend on $\boldsymbol{d}$ but on its bounds $\underline{\boldsymbol{d}}$ and $\overline{\boldsymbol{d}}$. This comes from the fact that these functions are determined from the interval observer dynamics. In Chapter 4, the bounds were defined in function of the original system dynamics. Consequently, Assumption 4.7 is no longer required. This new formulation based on an interval observer can also be used when the knowledge on the disturbance is very limited and Assumption 4.7 is not satisfied.

The expressions of the k-th derivative and i-th derivatives of β_m and β_p for the natural integer $i < k$ are now detailed under Assumption 5.17. They are used in the definition of the so-called generalized propagated bounds which is reminiscent of Definition 4.15. Finding an explicit expression for these derivatives is hard but some resources [Daoutidis 89] [Isidori 95, Chapter 5] give a hint on how to formalise such problems using relative degree properties and Lie derivatives. For $i \in \mathbb{N}$ such that $i < k$, we have:

$$\begin{aligned}
\beta_m^{(i)} &= \mathcal{L}^i_{\boldsymbol{h}_1}\sigma_m(\boldsymbol{\zeta}) + \sum_{j=0}^{i-1}\frac{\mathrm{d}^j}{\mathrm{d}t^j}\left(\mathcal{L}_{\mathbf{I}}\mathcal{L}^{i-1-j}_{\boldsymbol{h}_1}\sigma_m(\boldsymbol{\zeta})\,\boldsymbol{h}_2(\boldsymbol{\mathcal{D}})\right) \\
\beta_p^{(i)} &= \mathcal{L}^i_{\boldsymbol{h}_1}\sigma_p(\boldsymbol{\zeta}) + \sum_{j=0}^{i-1}\frac{\mathrm{d}^j}{\mathrm{d}t^j}\left(\mathcal{L}_{\mathbf{I}}\mathcal{L}^{i-1-j}_{\boldsymbol{h}_1}\sigma_p(\boldsymbol{\zeta})\,\boldsymbol{h}_2(\boldsymbol{\mathcal{D}})\right)
\end{aligned} \tag{5.44}$$

and, for $i = k$ where k is the relative degree of β_m and β_p wrt v (see Assumption 5.17):

$$\begin{array}{rcl} \beta_m^{(k)} & = & \mathcal{L}_{\boldsymbol{h}_1}^k \sigma_m(\boldsymbol{\zeta}) + \mathcal{L}_{\mathbf{B_{Z,v}}} \mathcal{L}_{\boldsymbol{h}_1}^{k-1} \sigma_m(\boldsymbol{\zeta})\, v + \sum_{j=0}^{k-1} \frac{\mathrm{d}^j}{\mathrm{d}t^j} \left(\mathcal{L}_{\mathbf{I}} \mathcal{L}_{\boldsymbol{h}_1}^{k-1-j} \sigma_m(\boldsymbol{\zeta})\, \boldsymbol{h}_2(\boldsymbol{\mathcal{D}}) \right) \\ \beta_p^{(k)} & = & \mathcal{L}_{\boldsymbol{h}_1}^k \sigma_p(\boldsymbol{\zeta}) + \mathcal{L}_{\mathbf{B_{Z,v}}} \mathcal{L}_{\boldsymbol{h}_1}^{k-1} \sigma_p(\boldsymbol{\zeta})\, v + \sum_{j=0}^{k-1} \frac{\mathrm{d}^j}{\mathrm{d}t^j} \left(\mathcal{L}_{\mathbf{I}} \mathcal{L}_{\boldsymbol{h}_1}^{k-1-j} \sigma_p(\boldsymbol{\zeta})\, \boldsymbol{h}_2(\boldsymbol{\mathcal{D}}) \right) \end{array} \tag{5.45}$$

where $\mathcal{L}_f \sigma$ is the notation for the Lie derivative of σ in the direction f as defined in Definition 3.3. The original Definition 4.15 of the propagated bounds assumed that the quantity α was known and that its derivatives could be expressed in function of the known system state vector $\boldsymbol{x}$ as in (4.23). This is not the case here which motivates the following definition of so-called generalized propagated bounds. Note that the original definition is retrieved if the state vector $\boldsymbol{X}$ is known. Similarly to the original definition, the introduction of design parameters $\boldsymbol{\kappa}$ is also considered.

Definition 5.18 (Generalized propagated bounds)**.**
Let $\boldsymbol{\kappa}(t) = \begin{bmatrix} \kappa_1(t) & \dots & \kappa_k(t) \end{bmatrix} \in \mathbb{R}_+^k$ a vector of adequately smooth[a] positive time-varying signals and let suppose the output constraint signals $(\underline{\alpha}(t), \overline{\alpha}(t))$ are functions of $\mathcal{C}^k(\mathbb{R}_+, \mathbb{R})$. Let define $\underline{\beta}_0(t) = \underline{\alpha}(t)$, $\overline{\beta}_0(t) = \overline{\alpha}(t)$ and, $\forall i \in \mathbb{N}^\star$ s.t. $i \leq k$:

$$\begin{array}{rcl} \underline{\beta}_i(t) & = & \kappa_i(t) \left(\underline{\beta}_{i-1}(t) - \beta_m^{(i-1)}(t) \right) + \dot{\widehat{\underline{\beta}_{i-1}}}(t) \\ \overline{\beta}_i(t) & = & \kappa_i(t) \left(\overline{\beta}_{i-1}(t) - \beta_p^{(i-1)}(t) \right) + \dot{\widehat{\overline{\beta}_{i-1}}}(t) \end{array} \tag{5.46}$$

where $\beta_m = \sigma_m(\boldsymbol{\zeta})$ and $\beta_p = \sigma_p(\boldsymbol{\zeta})$ (5.42). These are called *generalized propagated bounds* in the sense they generalize the Definition 4.15 of propagated bounds to the case where the state vector $\boldsymbol{X}$ is not fully measured.

[a] See Remark (4.16).

Originally (see Chapter 4) the propagated bounds are determined to obtain a reformulated time-domain constraint on the k-th derivative of α. In the current case, α is not known contrary to the guaranteed bounds β_m and β_p furnished by the interval observer considered in Proposition 5.12. Consequently, the propagated bounds are used to enforce the reformulated time-domain constraint respectively on the k-th derivatives of β_m and β_p. Since these are guaranteed bounds on the value of α, the original time-domain constraint $\mathcal{K}(\Omega_\alpha)$ is enforced. This is the informal explanation of the content of the following Lemma.

Lemma 5.19 (Generalized propagated bounds lemma)**.**
Let define the generalized propagated bounds as in Definition 5.18. Let suppose Assumption 5.17 is satisfied and that $\forall i \in \mathbb{N}$ *such that* $i \leq k$, $\beta_m^{(i)}(0) \geq \underline{\beta}_i(0)$ *and* $\beta_p^{(i)}(0) \leq \overline{\beta}_i(0)$. *Then,*

$$\left\{ \begin{array}{rcl} \beta_m^{(k)} & \geq & \underline{\beta}_k \\ \beta_p^{(k)} & \leq & \overline{\beta}_k \end{array} \right., \forall t \in \mathbb{R}_+ \Rightarrow \left\{ \begin{array}{rcl} \beta_m & \geq & \underline{\beta}_0 = \underline{\alpha} \\ \beta_p & \leq & \overline{\beta}_0 = \overline{\alpha} \end{array} \right., \forall t \in \mathbb{R}_+$$
$$\Rightarrow \underline{\alpha} \leq \mathbf{C}_{\mathbf{X}\boldsymbol{\alpha}} \boldsymbol{X} \leq \overline{\alpha},\ \forall t \in \mathbb{R}_+ \Rightarrow \alpha(t) \in \Omega_\alpha(t),\ \forall t \in \mathbb{R}_+ \tag{5.47}$$

Proof. The proof is similar to the proof of Lemma 4.17 but considering two different expressions for the upper and lower bounds expressions. In fact, the proof can be achieved by stating that β_m should lie in $\left[\underline{\beta}_0, +\infty\right[$ and β_p in $\left]-\infty, \overline{\beta}_0\right]$ and by applying Lemma 4.17 on each constraint. □

Using this Lemma, the dependence on v highlighted in (5.45) can be used to achieve the generalized time-domain constraint $\mathcal{K}(\Omega_\alpha)$ defined in Definition 5.15. Using the first necessary condition in (5.47), saturations $\underline{v}(t)$ and $\overline{v}(t)$ can be derived respectively from the inequality

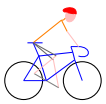

$\beta_m^{(k)} \geq \underline{\beta}_k$ and $\beta_p^{(k)} \leq \overline{\beta}_k$. Since these expressions depend on known quantities only, the resulting saturations are fully determined. The expressions of these saturations are detailed in the next section.

5.3.3 (c) Resulting control saturations on the external control input v

Using Lemma 5.19 and the dependence on v[2] of the k-th derivatives of β_m and β_p (see (5.45)), the saturations $\underline{v}$ and $\overline{v}$ which are used to compensate for the violation of the time-domain constraint $\mathcal{K}(\Omega_\alpha)$ in (D.21) are given in (5.48) for positive values of $\mathcal{L}_{\mathbf{B_{z,v}}}\mathcal{L}_{\boldsymbol{h}_1}^{k-1}\sigma_m(\boldsymbol{\zeta})$ and $\mathcal{L}_{\mathbf{B_{z,v}}}\mathcal{L}_{\boldsymbol{h}_1}^{k-1}\sigma_p(\boldsymbol{\zeta})$. To explicitly determine these expressions, it is supposed that $\sum_{j=0}^{k-1}\frac{\mathrm{d}^j}{\mathrm{d}t^j}\left(\mathcal{L}_{\mathbf{I}}\mathcal{L}_{\boldsymbol{h}_1}^{k-1-j}\sigma_m(\boldsymbol{\zeta})\,\boldsymbol{h}_2(\boldsymbol{\mathcal{D}})\right)$ and $\sum_{j=0}^{k-1}\frac{\mathrm{d}^j}{\mathrm{d}t^j}\left(\mathcal{L}_{\mathbf{I}}\mathcal{L}_{\boldsymbol{h}_1}^{k-1-j}\sigma_p(\boldsymbol{\zeta})\,\boldsymbol{h}_2(\boldsymbol{\mathcal{D}})\right)$ do not depend on v.

$$\begin{aligned}\underline{v} &= \frac{1}{\mathcal{L}_{\mathbf{B_{z,v}}}\mathcal{L}_{\boldsymbol{h}_1}^{k-1}\sigma_m(\boldsymbol{\zeta})}\left[\underline{\beta}_k - \mathcal{L}_{\boldsymbol{h}_1}^{k}\sigma_m(\boldsymbol{\zeta}) - \sum_{j=0}^{k-1}\frac{\mathrm{d}^j}{\mathrm{d}t^j}\left(\mathcal{L}_{\mathbf{I}}\mathcal{L}_{\boldsymbol{h}_1}^{k-1-j}\sigma_m(\boldsymbol{\zeta})\,\boldsymbol{h}_2(\boldsymbol{\mathcal{D}})\right)\right]\\ \overline{v} &= \frac{1}{\mathcal{L}_{\mathbf{B_{z,v}}}\mathcal{L}_{\boldsymbol{h}_1}^{k-1}\sigma_p(\boldsymbol{\zeta})}\left[\overline{\beta}_k - \mathcal{L}_{\boldsymbol{h}_1}^{k}\sigma_p(\boldsymbol{\zeta}) - \sum_{j=0}^{k-1}\frac{\mathrm{d}^j}{\mathrm{d}t^j}\left(\mathcal{L}_{\mathbf{I}}\mathcal{L}_{\boldsymbol{h}_1}^{k-1-j}\sigma_p(\boldsymbol{\zeta})\,\boldsymbol{h}_2(\boldsymbol{\mathcal{D}})\right)\right]\end{aligned} \tag{5.48}$$

where $\mathcal{L}_{\mathbf{B_{z,v}}}\mathcal{L}_{\boldsymbol{h}_1}^{k-1}\sigma_m(\boldsymbol{\zeta}) \neq 0$ and $\mathcal{L}_{\mathbf{B_{z,v}}}\mathcal{L}_{\boldsymbol{h}_1}^{k-1}\sigma_p(\boldsymbol{\zeta}) \neq 0$ under Assumption 5.17. The saturations depend on the k-th derivatives of the generalized propagated bounds β_m and β_p. Note this is very difficult to determine a general explicit expression of these propagated bounds in the considered extended case. This can be done on a case-by-case basis only.

Remark 5.20. The saturations expressions have been obtained in (5.48) for positive values of the quantities $\mathcal{L}_{\mathbf{B_{z,v}}}\mathcal{L}_{\boldsymbol{h}_1}^{k-1}\sigma_m(\boldsymbol{\zeta})$ and $\mathcal{L}_{\mathbf{B_{z,v}}}\mathcal{L}_{\boldsymbol{h}_1}^{k-1}\sigma_p(\boldsymbol{\zeta})$. In case these quantities are negative, the easiest approach is to adapt the definition of the constrained output α such that they become positive. This is considered in the example proposed in 5.4.1 where α is chosen equal to $-\boldsymbol{x}_1$ such that $\mathbf{C_{X\alpha}TM_XPB_{X,v}}$ is positive. ◇

The problem of saturations overlap raised in 4.3 is still present in the considered case. For known LTI systems with full state measurements, the problem has been solved in 4.4.3 (e) and more precisely in Theorem 4.24. A similar result in proposed in the next section for the considered extended case. The results are expressed in a slightly more generic form due to the lack of explicit expressions as highlighted above.

5.3.3 (d) Control saturations overlap mitigation

As in Chapter 4, let consider the quantity $\Delta_j = \overline{\beta}_j - \underline{\beta}_j$ for $j \in \mathbb{N}$ such that $j \leq k$. Using the Definition 5.18 of the generalized propagated bounds, the following is obtained:

$$\Delta_j = \kappa_i\left(\overline{\beta}_{j-1} - \underline{\beta}_{j-1} - \beta_p^{(i-1)} + \beta_m^{(i-1)}\right) + \dot{\overline{\beta}}_{i-1} - \dot{\underline{\beta}}_{i-1} \tag{5.49}$$

Contrary to the case studied in Chapter 4 where the propagated bounds depend both on $\beta^{(j-1)} = \alpha^{(j-1)}$, the upper and lower propagated bounds are not defined in a "symmetric" way, that is, $\underline{\beta}_j$ depends on $\beta_m^{(j-1)}$ and $\overline{\beta}_j$ on $\beta_p^{(j-1)}$. For Lemma 5.19 to be applicable, this means that Δ_j should satisfy to the following inequalities:

$$\Delta_j > \beta_p^{(j)} - \beta_m^{(j)},\ \forall j \in \mathbb{N} \text{ s.t. } j \leq k \tag{5.50}$$

This is formalized in the following lemma. More attention is dedicated to the specific case of $j = k$ where it should be ensured that $\overline{v} - \underline{v} \geq 0$ for the saturations expressions in (5.48).

Lemma 5.21 (Propagated bounds/Saturations overlap mitigation)**.**
Propagated bounds and saturations overlap is mitigated if:

- $\forall j \in \mathbb{N}$ *such that* $j \leq k-1$, $\Delta_j > \beta_p^{(j)} - \beta_m^{(j)}$, $\forall t$;

[2] Under the relative degree Assumption 5.17.

- *For $j = k$, $\forall t$:*

$$\Delta_k \geq \max \left(\beta_p^{(k)} - \beta_m^{(k)}, \mathcal{L}_{\boldsymbol{h}_1}^k \sigma_p(\boldsymbol{\zeta}) - \mathcal{L}_{\boldsymbol{h}_1}^k \sigma_m(\boldsymbol{\zeta}) + \sum_{j=0}^{k-1} \frac{\mathrm{d}^j}{\mathrm{d}t^j} \left(\mathcal{L}_{\mathbf{I}} \mathcal{L}_{\boldsymbol{h}_1}^{k-1-j} \sigma_m(\boldsymbol{\zeta}) \boldsymbol{h}_2(\boldsymbol{\mathcal{D}}) \right) - \sum_{j=0}^{k-1} \frac{\mathrm{d}^j}{\mathrm{d}t^j} \left(\mathcal{L}_{\mathbf{I}} \mathcal{L}_{\boldsymbol{h}_1}^{k-1-j} \sigma_p(\boldsymbol{\zeta}) \boldsymbol{h}_2(\boldsymbol{\mathcal{D}}) \right) \right) \tag{5.51}$$

Note that Lemma 4.23 is retrieved if the original system is supposed to be known with full state measurements since in that case $\beta_p^{(j)} - \beta_m^{(j)} = 0$. Considering the generic expression of Δ_j in (5.49), the necessary condition exposed in Lemma 5.21 to avoid generalized propagated bounds and saturations overlap can be achieved by appropriately choosing the coefficients κ_j in $\boldsymbol{\kappa}$. Since $\boldsymbol{h}_1$ and $\boldsymbol{h}_2$ are differentiable following the transformations in 5.3.1 (b), all quantities in Δ_j are differentiable.

In the following theorem, a suitable expression is obtained for the design coefficients in $\boldsymbol{\kappa}$. Similarly to Theorem 4.24, this is a main contribution of this thesis work which allows to enforce a time-domain constraint with guarantees on the resulting saturations overlap mitigation.

Theorem 5.22 (Design coefficients selection guaranteeing saturations overlap mitigation)**.** *Let $\breve{\boldsymbol{\kappa}} = \begin{bmatrix} \breve{\kappa}_1 & \dots & \breve{\kappa}_k \end{bmatrix}^\top \in \mathbb{R}_+^{\star k}$ a vector of strictly positive constants. Generalized propagated bounds (5.46) and saturations (5.48) overlap is mitigated if*

- *$\overline{\alpha} - \underline{\alpha} > \beta_p - \beta_m$, $\forall t$ or, in a more explicit form: $\overline{\alpha} - \underline{\alpha} > \left(\mathbf{C}_{\mathbf{X}\boldsymbol{\alpha}}{}^+ + \mathbf{C}_{\mathbf{X}\boldsymbol{\alpha}}{}^- \right) \left(\overline{\boldsymbol{X}} - \underline{\boldsymbol{X}} \right)$, $\forall t$ which was already mentioned in Remark 5.16*
- *$\forall j \in \mathbb{N}^\star$ such that $j \leq k-1$, $\Delta_j > \beta_p^{(j)} - \beta_m^{(j)}$ is satisfied by choosing, $\forall t$:*

$$\kappa_j = \frac{\breve{\kappa_j} - \dot{\overline{\beta}}_{j-1} + \dot{\underline{\beta}}_{j-1} + \beta_p^{(j)} - \beta_m^{(j)}}{\overline{\beta}_{j-1} - \underline{\beta}_{j-1} - \beta_p^{(j-1)} + \beta_m^{(j-1)}} \tag{5.52}$$

- *For $j = k$, ones ensures $\overline{v} - \underline{v} \geq 0$ by choosing, $\forall t$:*

$$\kappa_k = \frac{\breve{\kappa_k} - \dot{\overline{\beta}}_{k-1} + \dot{\underline{\beta}}_{k-1} + \Pi}{\overline{\beta}_{k-1} - \underline{\beta}_{k-1} - \beta_p^{(k-1)} + \beta_m^{(k-1)}} \tag{5.53}$$

where

$$\Pi = \max \left(\beta_p^{(k)} - \beta_m^{(k)}, \mathcal{L}_{\boldsymbol{h}_1}^k \sigma_p(\boldsymbol{\zeta}) - \mathcal{L}_{\boldsymbol{h}_1}^k \sigma_m(\boldsymbol{\zeta}) + \sum_{j=0}^{k-1} \frac{\mathrm{d}^j}{\mathrm{d}t^j} \left(\mathcal{L}_{\mathbf{I}} \mathcal{L}_{\boldsymbol{h}_1}^{k-1-j} \sigma_m(\boldsymbol{\zeta}) \boldsymbol{h}_2(\boldsymbol{\mathcal{D}}) \right) - \sum_{j=0}^{k-1} \frac{\mathrm{d}^j}{\mathrm{d}t^j} \left(\mathcal{L}_{\mathbf{I}} \mathcal{L}_{\boldsymbol{h}_1}^{k-1-j} \sigma_p(\boldsymbol{\zeta}) \boldsymbol{h}_2(\boldsymbol{\mathcal{D}}) \right) \right) \tag{5.54}$$

Proof. Straightforward considering Lemma 5.21 and the expression of Δ_j in (5.49). □

The saturations overlap procedure exposed for the first time in 4.4.3 (e) has been extended to the more complex considered case. Appropriate definitions of the design coefficients in $\boldsymbol{\kappa}$ has been proposed to mitigate the occurrence of saturations overlap. This offers guarantees on the satisfaction of the considered time-domain output constraint $\mathcal{K}(\Omega_\alpha)$ when applying OIST.

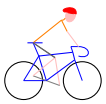

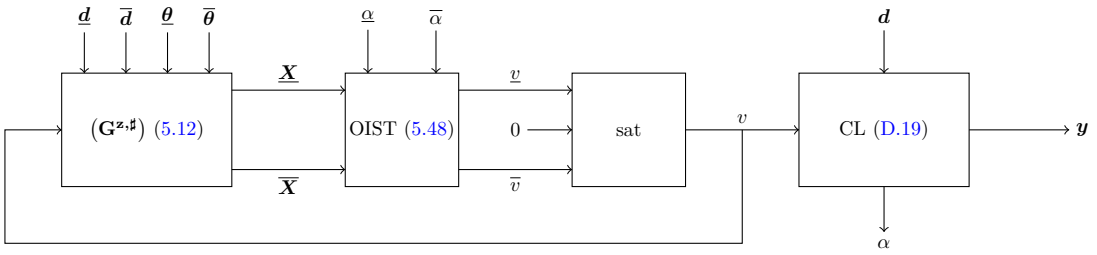

Figure 5.3: Systems interconnection resulting from the solution to Problem 5.8 proposed in Theorem 5.23.

In the next section, the solution to Problem 5.8 is formally stated.

5.3.3 (e) Conclusion: a solution to Problem 5.8

In the certain LTI case with full state measurements, a solution to the output constrained control problem have been proposed in Theorem 4.28. In this chapter and more precisely in 5.3, the OIST approach has been extended to account for uncertain LTI systems with partial state measurements.

It has been shown that by using an interval observer of a specific form (see Proposition 5.12) then the unknown constrained output signal α can be bounded by known certified quantities. By extending the definition of propagated bounds (see Definition 5.18) and considering an updated *propagated bounds lemma* (see Lemma 5.19), it has been shown that the time-domain constraint $\mathcal{K}(\Omega_\alpha)$ can be enforced. Expressions of design coefficients ensuring no saturations overlap have also been obtained in Theorem 5.22. These results are summed up in the following theorem.

Theorem 5.23 (Output constrained control Problem 5.8 guaranteed solution using OIST)**.** *Let consider the well-posed*[a] *closed-loop in* (D.19) *where v is an external input signal. Let $\alpha = \mathbf{C}_{\mathbf{X}\boldsymbol{\alpha}}\boldsymbol{X}$ the constrained output and $\mathcal{K}(\Omega_\alpha)$ the considered time-domain constraint. Let suppose Assumptions 4.4, 4.8, 5.1, 5.5 and 5.17 are satisfied.*

If the external control input v is chosen such that

$$v = sat_{\underline{v}}^{\overline{v}}(0)\ ,\ \forall t \tag{5.55}$$

where

- *$\underline{v}$ and $\overline{v}$ are given in* (5.48)*;*
- *The generalized propagated bounds expressions are detailed in* (5.46)*;*
- *The design parameters in $\boldsymbol{\kappa}$ are chosen as in Theorem 5.22;*
- *The bounds on the state $\boldsymbol{X}$ are obtained using the interval observer in Proposition 5.12,*

then $\alpha \in \Omega_\alpha$, $\forall t$.

[a] See Assumptions 5.2 and 5.4.

The resulting interconnection of the considered systems is represented in Fig. 5.3. On this figure, the dependence of the interval observer dynamics on $\boldsymbol{\theta}_n$ and the bounding matrices in (5.3) is illustrated by the vectors $\underline{\boldsymbol{\theta}}$ and $\overline{\boldsymbol{\theta}}$ bounding the vector of uncertainties $\boldsymbol{\theta}$.

5.3.3 (f) A note on closed-loop stability

In the chapter dedicated to reformulating the original OIST approach in the linear framework[3], new results were stated as far as closed-loop stability is concerned. In Theorem 4.34, it has been

[3] See Chapter 4.

stated that the origin of the considered constrained system in closed-loop with the considered controller and the saturations provided by OIST is globally asymptotically stable.

In this chapter, the facts that the considered system is perfectly modelled by the dynamics and that the state vector $\boldsymbol{x}$ is completely known have been dismissed. This has led to a generalisation of the original OIST theory based on the introduction of an additional system qualified as an interval observer. According to Theorem 5.23 and Fig. 5.3, the main problem is now to demonstrate the stability of this interval observer in closed-loop with the corrective input signal $v = \text{sat}_{\underline{v}}^{\overline{v}}(0)$ (see Problem 5.9). Since the interval observer copies the dynamics of the original system for a nominal $\boldsymbol{\theta}_n$ value of the uncertain parameters, the case of non-minimum phase control input to constrained output transfers remains unchanged: global asymptotic stability cannot be obtained for such systems. Also, a precise analysis of the interval observer stability is required as per Definition B.11.

These are left as perspectives for future works.

5.3.4 Conclusions on the OIST extension

In this section, an extension to the OIST approach has been proposed, resulting in Theorem 5.23. The initial OIST theory was proposed in [Burlion 12] and reformulated for LTI systems in Chapter 4 following works in [Chambon 15c] and [Chambon 16]. However, the reformulation supposed that the considered system state was fully measured and did not consider the case of uncertain systems.

The purpose of the *OIST extension for Robustness* (OISTeR) is to propose a generalisation of OIST in the case of uncertain systems with partially measured states. The notion of "generalization" has been extensively used in the development of the new method. This is indeed interesting to note that in case the system state vector is known and the system is certain then similar results to the ones proposed in Chapter 4 are obtained.

In the new approach, a quite innovative way (within the OIST theory) of integrating the saturations obtained through OIST application has been considered. Typically, a new input signal v has been considered and defined as $v = \text{sat}_{\underline{v}}^{\overline{v}}(0)$ where $\underline{v}$ and $\overline{v}$ are the saturations obtained through OISTeR. The system input is then defined by $u = y_K + v$. Also, due to the fact that the measurements vector $\boldsymbol{y}$ derivatives may depend on unmeasured states, the closed-loop has been considered in the design of the introduced interval observer rather than the original system. To simultaneously design the controller and the interval observer on the closed-loop, the numerical approach proposed in 7.4[4] has been used.

As mentioned in introduction, the approach is quite recent. Perspectives to improve the method and obtain theoretical guarantees are listed in 5.5. Before that, in the next section, the OISTeR approach is applied to various theoretical examples to illustrate how a time-domain constraint can be enforced on an output even in the presence of uncertainties or partially measured state.

5.4 Examples

The *OIST extension for Robustness* approach introduced in 5.3 is applied on two theoretical examples specially built to satisfy some structural hypotheses. A more realistic application is considered in Chapter 6 where the launch vehicle model is non-cooperative and subject to incomplete state vector measurements.

5.4.1 Second-order LTI system with incomplete state measurements

In this example, the OISTeR approach is illustrated on a known non-cooperative system with incomplete state measurements, that is a system for which $\mathbf{C} \neq \mathbf{I_n}$. First, a stabilizing dynamic controller ($\mathbf{K}$) is determined along with the appropriate SCT matrix $\mathbf{P}$ such that the system is cooperative in the new coordinates. Then, OISTeR is applied to enforce a given time-domain constraint on an output α.

[4] See Chapter 7.

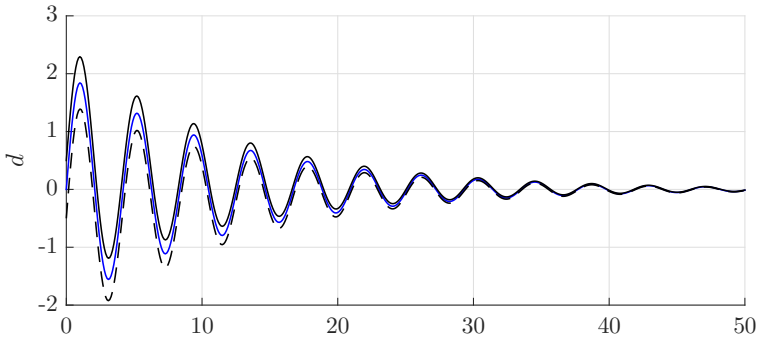

Figure 5.4: In blue: disturbance signal d used in simulation, in black: known bounds $\underline{d}$ and $\overline{d}$.

Considered model Let consider a known LTI non-cooperative system described by the following state-space representation:

$$(\mathbf{G}) \begin{cases} \dot{\boldsymbol{x}} &= \mathbf{A}\boldsymbol{x} + \mathbf{B_u}u + \mathbf{B_d}d \\ y &= \mathbf{C}\boldsymbol{x} \\ \boldsymbol{x}_0 &= \mathbf{0} \end{cases} \tag{5.56}$$

where the considered matrices are defined by:

$$\mathbf{A} = \begin{bmatrix} -1 & -\frac{1}{2} \\ 0 & 0 \end{bmatrix}, \mathbf{B_u} = \begin{bmatrix} 0 \\ 1 \end{bmatrix}, \mathbf{B_d} = \begin{bmatrix} 0 \\ 1 \end{bmatrix}, \mathbf{C} = \begin{bmatrix} 1 & 0 \end{bmatrix} \tag{5.57}$$

Note that $\mathbf{A}$ is not Metzler[5] hence $(\mathbf{G})$ is non-cooperative. The initial system state is supposed to be known hence $\underline{\boldsymbol{x}_0}$ and $\overline{\boldsymbol{x}_0}$ equal $\boldsymbol{x}_0$.

In simulation, the system is initialized at $\boldsymbol{x}_0 = \mathbf{0}$. The disturbance input d is supposed to be bounded by two known signals $\underline{d}$ and $\overline{d}$ represented in black color in Fig. 5.4. In simulation, the signal d represented in blue in the same figure is used.

The considered constrained output is initially defined by $\alpha = \boldsymbol{x}_1 = \mathbf{C_\alpha}\boldsymbol{x}$ with $\mathbf{C_\alpha} = \begin{bmatrix} 1 & 0 \end{bmatrix}$. It is expected that the output signal α should remain within $[-0.1, 0.8]$. However, this further leads to the quantity $\mathbf{C_{X\alpha}A_XB_{X,v}}$ being negative, where the matrices are defined in the following paragraph. This would make the application of Lemma 5.19 difficult in the determination of the saturations $\underline{v}$ and $\overline{v}$ expressions. Hence, it chosen to consider $\alpha = -\boldsymbol{x}_1$ i.e. $\mathbf{C_\alpha} = \begin{bmatrix} -1 & 0 \end{bmatrix}$ and the time-domain constraint is modified in consequence: $\underline{\alpha} = -0.8$ and $\overline{\alpha} = 0.1$.

Stabilizing controller and transformation matrix synthesis A dynamic controller $(\mathbf{K})$ with $n_K = 1$ is chosen in this example. The corresponding state-space representation is given in (5.4) and the loop is closed using the following relations:

$$u = y_K + v,\ u_K = y \tag{5.58}$$

where v is the new control input which will be driven in the OIST methodology to enforce the considered time-domain constraint on α. The closed-loop dynamics is defined by:

$$\begin{aligned} \dot{\boldsymbol{X}} &= \begin{bmatrix} \mathbf{A} + \mathbf{B_u D_K C} & \mathbf{B_u C_K} \\ \mathbf{B_K C} & \mathbf{A_K} \end{bmatrix} \boldsymbol{X} + \begin{bmatrix} \mathbf{B_u} \\ 0 \end{bmatrix} v + \begin{bmatrix} \mathbf{B_d} \\ 0 \end{bmatrix} \\ &= \mathbf{A_X}\boldsymbol{X} + \mathbf{B_{X,v}}v + \mathbf{B_{X,d}}d \end{aligned} \tag{5.59}$$

which is coherent with the dynamics obtained in (D.19) for a well-posed known system with $\mathbf{D_u} = 0$. Note that the matrix $\mathbf{A_X}$ is still not Metzler. Supposing there exists $\mathbf{P}$ such that $\mathbf{M_X} = \mathbf{PA_XP}^{-1}$ is Metzler, an interval observer can easily be found on the following system where $\boldsymbol{Z} = \mathbf{P}\boldsymbol{X}$:

[5] See Definition B.1.

$$\dot{\boldsymbol{Z}} = \mathbf{M}_{\mathbf{X}}\boldsymbol{Z} + \mathbf{PB}_{\mathbf{X},\mathbf{v}}v + \mathbf{PB}_{\mathbf{X},\mathbf{d}}d \tag{5.60}$$

Using Lemma B.12, the unknown quantity $\mathbf{PB}_{\mathbf{X},\mathbf{d}}d$ is bounded by the following vectors:

$$(\mathbf{PB}_{\mathbf{X},\mathbf{d}})^{+}\,\underline{d} - (\mathbf{PB}_{\mathbf{X},\mathbf{d}})^{-}\,\overline{d} \leq \mathbf{PB}_{\mathbf{X},\mathbf{d}}d \leq (\mathbf{PB}_{\mathbf{X},\mathbf{d}})^{+}\,\overline{d} - (\mathbf{PB}_{\mathbf{X},\mathbf{d}})^{-}\,\underline{d} \tag{5.61}$$

Note that due to the fact that the original system is known then the interval observer is a linear system. As per Proposition 5.12, it is given by:

$$\begin{array}{rcl}
\dot{\underline{\boldsymbol{Z}}} & = & \mathbf{M}_{\mathbf{X}}\underline{\boldsymbol{Z}} + \mathbf{PB}_{\mathbf{X},\mathbf{v}}v + (\mathbf{PB}_{\mathbf{X},\mathbf{d}})^{+}\,\underline{d} - (\mathbf{PB}_{\mathbf{X},\mathbf{d}})^{-}\,\overline{d} \\
\dot{\overline{\boldsymbol{Z}}} & = & \mathbf{M}_{\mathbf{X}}\overline{\boldsymbol{Z}} + \mathbf{PB}_{\mathbf{X},\mathbf{v}}v + (\mathbf{PB}_{\mathbf{X},\mathbf{d}})^{+}\,\overline{d} - (\mathbf{PB}_{\mathbf{X},\mathbf{d}})^{-}\,\underline{d} \\
\underline{\boldsymbol{Z}}(0) & = & \mathbf{P}^{+}\underline{\boldsymbol{X}_0} - \mathbf{P}^{-}\overline{\boldsymbol{X}_0} \\
\overline{\boldsymbol{Z}}(0) & = & \mathbf{P}^{+}\overline{\boldsymbol{X}_0} - \mathbf{P}^{-}\underline{\boldsymbol{X}_0} \\
\underline{\boldsymbol{X}} & = & \mathbf{T}^{+}\underline{\boldsymbol{Z}} - \mathbf{T}^{-}\overline{\boldsymbol{Z}} \\
\overline{\boldsymbol{X}} & = & \mathbf{T}^{+}\overline{\boldsymbol{Z}} - \mathbf{T}^{-}\underline{\boldsymbol{Z}}
\end{array} \tag{5.62}$$

where $\underline{\boldsymbol{X}_0} = \begin{bmatrix}\boldsymbol{x}_0 \\ 0\end{bmatrix}$, $\overline{\boldsymbol{X}_0} = \begin{bmatrix}\overline{\boldsymbol{x}_0} \\ 0\end{bmatrix}$ and $\mathbf{T} = \mathbf{P}^{-1}$. The determination of the transformation matrix $\mathbf{P}$ is discussed below. The tightness of the interval $\left[\underline{\boldsymbol{Z}}, \overline{\boldsymbol{Z}}\right]$ as provided by the interval observer in (5.62) can be evaluated by considering the dynamics of $\boldsymbol{E}_d = \frac{1}{2}\left(\overline{\boldsymbol{Z}} - \underline{\boldsymbol{Z}}\right)$:

$$\dot{\boldsymbol{E}}_d = \mathbf{M}_{\mathbf{X}}\boldsymbol{E}_d + \frac{1}{2}\left[(\mathbf{PB}_{\mathbf{X},\mathbf{d}})^{+} + (\mathbf{PB}_{\mathbf{X},\mathbf{d}})^{-}\right]\left(\overline{d} - \underline{d}\right) \tag{5.63}$$

From a design point of view, this dynamics is not linear in the design parameter $\mathbf{P}$ since it depends on the quantities $(\mathbf{PB}_{\mathbf{X},\mathbf{d}})^{+}$ and $(\mathbf{PB}_{\mathbf{X},\mathbf{d}})^{-}$. An additional synthesis constraint (see below) can be considered such that $(\mathbf{PB}_{\mathbf{X},\mathbf{d}})^{-} = \mathbf{0}$. In that case, the dynamics of $\boldsymbol{E}_d$ is characterized by:

$$\dot{\boldsymbol{E}}_d = \mathbf{M}_{\mathbf{X}}\boldsymbol{E}_d + \frac{1}{2}\mathbf{PB}_{\mathbf{X},\mathbf{d}}\left(\overline{d} - \underline{d}\right) \tag{5.64}$$

As far as the controller synthesis is concerned, the approach presented in Chapter 7, 7.4 is applied. The following numerical results are obtained:

$$(\mathbf{K})\begin{cases} \dot{x}_K = -5.698x_K + -2.975y \\ y_K = 22.15x_K + 13.5y \end{cases} \tag{5.65}$$

and

$$\mathbf{P} = \begin{bmatrix} -0.1875 & 0.3281 & -0.7139 \\ -0.2268 & 0.1776 & 0.2497 \\ 0.3485 & 0.0458 & 0.5366 \end{bmatrix} \tag{5.66}$$

OISTeR application With the addition of the controller state variable, the output variable α can be defined as $\alpha = \mathbf{C}_{\mathbf{X}\boldsymbol{\alpha}}\boldsymbol{X}$ where $\mathbf{C}_{\mathbf{X}\boldsymbol{\alpha}} = \begin{bmatrix}-1 & 0 & 0\end{bmatrix}$. Then, considering that ${\mathbf{C}_{\mathbf{X}\boldsymbol{\alpha}}}^{+} = \mathbf{0}$ and ${\mathbf{C}_{\mathbf{X}\boldsymbol{\alpha}}}^{-} = |\mathbf{C}_{\mathbf{X}\boldsymbol{\alpha}}|$, the interval observer in (5.62) provides the following bounds for α:

$$\mathbf{C}_{\mathbf{X}\boldsymbol{\alpha}}\overline{\boldsymbol{X}} \leq \mathbf{C}_{\mathbf{X}\boldsymbol{\alpha}}\boldsymbol{X} \leq \mathbf{C}_{\mathbf{X}\boldsymbol{\alpha}}\underline{\boldsymbol{X}} \tag{5.67}$$

or, in the new coordinates:

$$\mathbf{C}_{\mathbf{X}\boldsymbol{\alpha}}\left(\mathbf{T}^{+}\overline{\boldsymbol{Z}} - \mathbf{T}^{-}\underline{\boldsymbol{Z}}\right) \leq \mathbf{C}_{\mathbf{X}\boldsymbol{\alpha}}\boldsymbol{X} \leq \mathbf{C}_{\mathbf{X}\boldsymbol{\alpha}}\left(\mathbf{T}^{+}\underline{\boldsymbol{Z}} - \mathbf{T}^{-}\overline{\boldsymbol{Z}}\right) \tag{5.68}$$

Let $\beta_m = \mathbf{C}_{\mathbf{X}\boldsymbol{\alpha}}\left(\mathbf{T}^{+}\overline{\boldsymbol{Z}} - \mathbf{T}^{-}\underline{\boldsymbol{Z}}\right)$ and $\beta_p = \mathbf{C}_{\mathbf{X}\boldsymbol{\alpha}}\left(\mathbf{T}^{+}\underline{\boldsymbol{Z}} - \mathbf{T}^{-}\overline{\boldsymbol{Z}}\right)$. These quantities are of relative degree $k = 2$ with respect to v. Using Definition 5.18 of generalized propagated bounds and Lemma 5.19 where

$$
\begin{aligned}
\dot{\beta}_m &= \mathbf{C_{X\alpha}}\left(\mathbf{T}^{+}\mathbf{M_X}\overline{\boldsymbol{Z}} - \mathbf{T}^{-}\mathbf{M_X}\underline{\boldsymbol{Z}}\right) + \mathbf{C_{X\alpha}}\left(\mathbf{T}^{+}\mathbf{PB_{X,d}}\overline{d} - \mathbf{T}^{-}\mathbf{PB_{X,d}}\underline{d}\right)\\
\dot{\beta}_p &= \mathbf{C_{X\alpha}}\left(\mathbf{T}^{+}\mathbf{M_X}\underline{\boldsymbol{Z}} - \mathbf{T}^{-}\mathbf{M_X}\overline{\boldsymbol{Z}}\right) + \mathbf{C_{X\alpha}}\left(\mathbf{T}^{+}\mathbf{PB_{X,d}}\underline{d} - \mathbf{T}^{-}\mathbf{PB_{X,d}}\overline{d}\right)\\
\ddot{\beta}_m &= \mathbf{C_{X\alpha}}\left(\mathbf{T}^{+}{\mathbf{M_X}}^2\overline{\boldsymbol{Z}} - \mathbf{T}^{-}{\mathbf{M_X}}^2\underline{\boldsymbol{Z}}\right) + \mathbf{C_{X\alpha}}\mathbf{A_X}\mathbf{B_{X,v}}v\\
&\quad + \mathbf{C_{X\alpha}}\left(\mathbf{T}^{+}\mathbf{M_X}\mathbf{PB_{X,d}}\overline{d} - \mathbf{T}^{-}\mathbf{M_X}\mathbf{PB_{X,d}}\underline{d}\right) + \mathbf{C_{X\alpha}}\left(\mathbf{T}^{+}\mathbf{PB_{X,d}}\dot{\overline{d}} - \mathbf{T}^{-}\mathbf{PB_{X,d}}\dot{\underline{d}}\right)\\
\ddot{\beta}_p &= \mathbf{C_{X\alpha}}\left(\mathbf{T}^{+}{\mathbf{M_X}}^2\underline{\boldsymbol{Z}} - \mathbf{T}^{-}{\mathbf{M_X}}^2\overline{\boldsymbol{Z}}\right) + \mathbf{C_{X\alpha}}\mathbf{A_X}\mathbf{B_{X,v}}v\\
&\quad + \mathbf{C_{X\alpha}}\left(\mathbf{T}^{+}\mathbf{M_X}\mathbf{PB_{X,d}}\underline{d} - \mathbf{T}^{-}\mathbf{M_X}\mathbf{PB_{X,d}}\overline{d}\right) + \mathbf{C_{X\alpha}}\left(\mathbf{T}^{+}\mathbf{PB_{X,d}}\dot{\underline{d}} - \mathbf{T}^{-}\mathbf{PB_{X,d}}\dot{\overline{d}}\right)
\end{aligned}
\tag{5.69}
$$

the following saturations are obtained and applied to the nominally null input signal v:

$$
\begin{aligned}
\underline{v} &= \tfrac{1}{\mathbf{C_{X\alpha}}\mathbf{A_X}\mathbf{B_{X,v}}}\Big[\underline{\beta}_2 - \mathbf{C_{X\alpha}}\left(\mathbf{T}^{+}{\mathbf{M_X}}^2\overline{\boldsymbol{Z}} - \mathbf{T}^{-}{\mathbf{M_X}}^2\underline{\boldsymbol{Z}}\right)\\
&\quad - \mathbf{C_{X\alpha}}\left(\mathbf{T}^{+}\mathbf{M_X}\mathbf{PB_{X,d}}\overline{d} - \mathbf{T}^{-}\mathbf{M_X}\mathbf{PB_{X,d}}\underline{d}\right) - \mathbf{C_{X\alpha}}\left(\mathbf{T}^{+}\mathbf{PB_{X,d}}\dot{\overline{d}} - \mathbf{T}^{-}\mathbf{PB_{X,d}}\dot{\underline{d}}\right)\Big]\\
\overline{v} &= \tfrac{1}{\mathbf{C_{X\alpha}}\mathbf{A_X}\mathbf{B_{X,v}}}\Big[\overline{\beta}_2 - \mathbf{C_{X\alpha}}\left(\mathbf{T}^{+}{\mathbf{M_X}}^2\underline{\boldsymbol{Z}} - \mathbf{T}^{-}{\mathbf{M_X}}^2\overline{\boldsymbol{Z}}\right)\\
&\quad - \mathbf{C_{X\alpha}}\left(\mathbf{T}^{+}\mathbf{M_X}\mathbf{PB_{X,d}}\underline{d} - \mathbf{T}^{-}\mathbf{M_X}\mathbf{PB_{X,d}}\overline{d}\right) - \mathbf{C_{X\alpha}}\left(\mathbf{T}^{+}\mathbf{PB_{X,d}}\dot{\underline{d}} - \mathbf{T}^{-}\mathbf{PB_{X,d}}\dot{\overline{d}}\right)\Big]
\end{aligned}
\tag{5.70}
$$

As far as OISTeR design parameters κ_1 and κ_2 are concerned, they are chosen according to Theorem 5.22 to avoid saturations overlap as exposed in Lemma 5.19. The constants $\breve{\kappa}_1$ and $\breve{\kappa}_2$ are chosen such that $\breve{\kappa}_1 = 2$ and $\breve{\kappa}_2 = 10$.

Simulation results The system in (5.56) is simulated in closed-loop with (5.65) and the saturations obtained in the previous paragraph applied to the corrective input signal v as described in the OISTeR theory. The simulation is performed over 30s. Simulation results are shown in Figs. 5.5 and 5.6.

The closed-loop system (5.59) state is represented in Fig. 5.5(a) either in the presence of the saturated corrective input signal v (plain blue line) or not (dashed blue line). The output constraint is represented in red in Fig. 5.5(b) along with the constrained output signal $\alpha = -\boldsymbol{x}_1$ in blue (plain: w OISTeR, dashed: w/o OISTeR). It can be observed that the corrective signal $v = \mathrm{sat}_{\underline{v}}^{\overline{v}}(0)$ produced by OISTeR and represented in blue in Fig. 5.6(a) allows to satisfy the output constraint. As expected, this signal equals zero when the constraint is satisfied and is modified by the OISTeR saturations in the other case. In conclusion, it can be said that the output constraint is enforced through using Lemma 5.19 but at the cost of a very precise knowledge of bounds on the disturbance d.

The OISTeR design parameters are represented in Fig. 5.6(b). Using these parameters defined as in Th. 5.22 saturations overlap is avoided.

Conclusions The OISTeR approach has been successfully applied to the LTI model with incomplete state measurements in (5.56). Using an appropriately defined corrective input signal $v = \mathrm{sat}_{\underline{v}}^{\overline{v}}(0)$, the output constraint has been enforced despite the lack of knowledge on state $\boldsymbol{x}_2$. As illustrated in Fig. 5.5(b), the output constraint is enforced on the bounds provided by the interval observer hence on all possible trajectories for the disturbance signals d such that $\underline{d} \leq d \leq \overline{d}$.

These are interesting results. However, the approach is quite conservative: it requires a very tight interval $\left[\underline{\boldsymbol{X}}, \overline{\boldsymbol{X}}\right]$ which is achieved either by an appropriate SCT design method or by reducing the interval $\left[\underline{d}, \overline{d}\right]$ which is representative of the knowledge on the disturbance. Future works will be dedicated to reducing the conservatism of the approach.

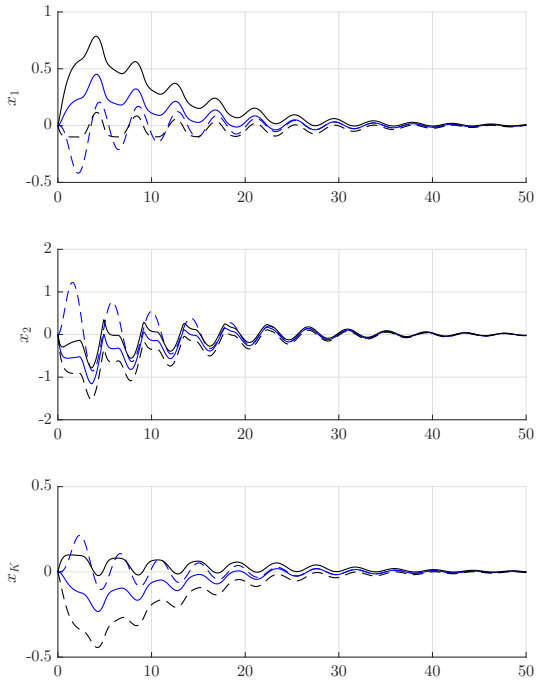

(a) System (5.59) state simulation in closed-loop with OISTeR saturations (in plain blue line) and without saturations (in dashed blue line). The interval observer estimates are represented in black.

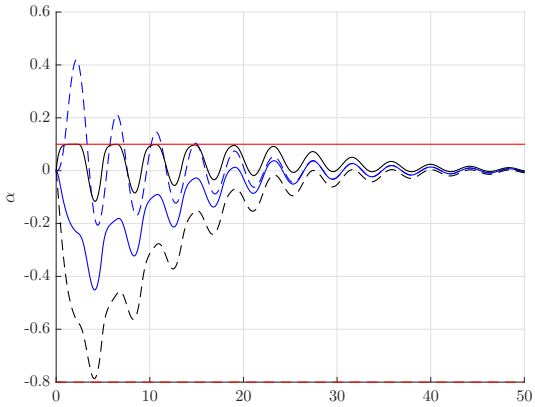

(b) Constrained output $\alpha = -\boldsymbol{x}_1$ simulation results, w (plain blue line) or w/o (dashed blue line) OISTeR saturations. Interval observer bounds for $-\boldsymbol{x}_1$ are represented in black.

Figure 5.5: State and constrained output α simulation results.

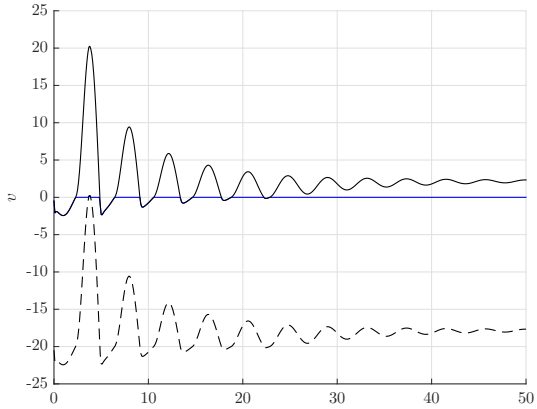

(a) Control input v (in blue) and saturations obtained through application of OISTeR (in black).

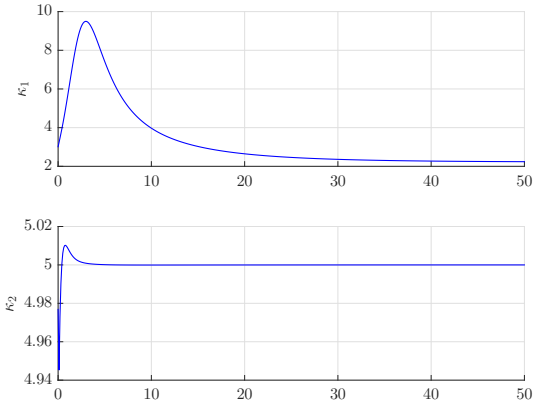

(b) OISTeR time-varying design parameters chosen as in 5.22 to avoid saturations overlap.

Figure 5.6: Corrective input v and OISTeR design parameters simulation results.

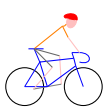

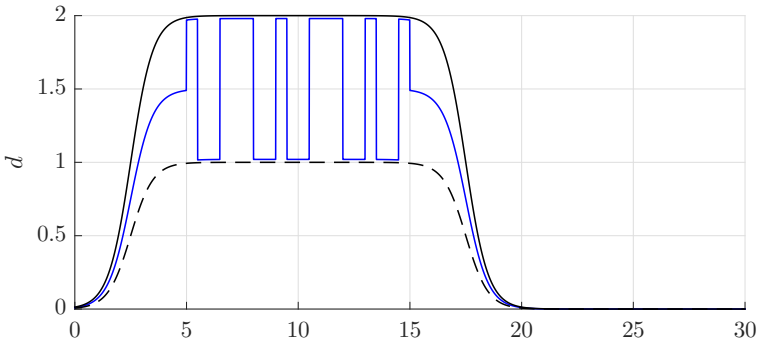

Figure 5.7: In blue: disturbance signal d used in simulation, in black: known bounds $\underline{d}$ and $\overline{d}$.

5.4.2 Second-order uncertain cooperative LTI system

This example illustrates the method on a cooperative uncertain LTI system. The cooperativity hypothesis allows to consider $\mathbf{P} = \mathbf{I}$ in Assumption 5.10 for an appropriately defined controller. This is detailed below.

Considered model Let consider an uncertain LTI cooperative[6] system characterized by the following state-space representation:

$$(\mathbf{G}) \begin{cases} \dot{\boldsymbol{x}} &= \mathbf{M}(\theta)\,\boldsymbol{x} + \mathbf{B_u} u + \mathbf{B_d} d \\ y &= \mathbf{C}\boldsymbol{x} \\ \boldsymbol{x}_0 &= \mathbf{0} \end{cases} \tag{5.71}$$

where the state-space matrices are given by:

$$\mathbf{M}(\theta) = \begin{bmatrix} 0.1 & 1 \\ 2+\theta & -3 \end{bmatrix}, \mathbf{B_u} = \begin{bmatrix} 1 \\ 0 \end{bmatrix}, \mathbf{B_d} = \begin{bmatrix} 0 \\ 1 \end{bmatrix}, \mathbf{C} = \begin{bmatrix} 1 & 0 \end{bmatrix} \tag{5.72}$$

where $\theta \in [-1, 1]$ is the only uncertain parameter. The matrix $\mathbf{M}(\theta)$ is Metzler (see Definition B.1) but is not Hurwitz for some values of θ, for example $\theta = 0$. The disturbance signal d considered in simulation is represented in blue in Fig. 5.7 along with the known bounds $\underline{d}$ and $\overline{d}$ which are represented in black.

As indicated in (5.71), the system initial condition is set to $\mathbf{0}$ in simulation. It is supposed to be known hence the bounding vectors $\underline{\boldsymbol{x}_0}$ and $\overline{\boldsymbol{x}_0}$ both equal $\mathbf{0}$.

The considered constrained output is given by $\alpha = \boldsymbol{x}_2 = \mathbf{C}_{\boldsymbol{\alpha}}\boldsymbol{x}$ with $\mathbf{C}_{\boldsymbol{\alpha}} = \begin{bmatrix} 0 & 1 \end{bmatrix}$. The objective is to maintain this output signal in the interval $[\underline{\alpha}, \overline{\alpha}]$ with $\underline{\alpha} = -0.3$ and $\overline{\alpha} = 0.5$.

Since the system is unstable, a controller is first designed to stabilize it for all possible values of the uncertainty θ. A multi-models multi-requirements approach as presented in Chapter 2 for uncertain linear systems is used. Since the original system is already cooperative, note that building an interval observer for this system is trivial and does not require more specific attention. Especially, no additional matrix $\mathbf{P}$ needs to be synthesized.

Stabilizing controller synthesis After some trial and error, a static controller $D_K \in \mathbb{R}$ is chosen. Considering a dynamic controller with $n_K = 1$ does not improve the synthesis results much and is thus discarded. This results in the following control law:

$$u = y_K + v = D_K y + v \tag{5.73}$$

The closed-loop dynamics is thus given by:

$$\begin{aligned} \dot{\boldsymbol{X}} &= \left[\mathbf{M}(\theta) + \mathbf{B_u} D_K \mathbf{C}\right] \boldsymbol{X} + \mathbf{B_u} v + \mathbf{B_d} d \\ &= \mathbf{M_X} \boldsymbol{X} + \boldsymbol{\Delta}\mathbf{M_X}(\theta)\,\boldsymbol{X} + \mathbf{B_u} v + \mathbf{B_d} d \end{aligned} \tag{5.74}$$

[6] See Def. B.3 of a cooperative system (continuous-time).

where $\boldsymbol{X} = \boldsymbol{x}$ and $\mathbf{\Delta M_X}(\theta) = \begin{bmatrix} 0 & 0 \\ \theta & 0 \end{bmatrix}$. Note that there exists $\overline{\mathbf{\Delta M_X}} = \begin{bmatrix} 0 & 0 \\ 1 & 0 \end{bmatrix}$ such that $-\overline{\mathbf{\Delta M_X}} \leq \mathbf{\Delta M_X} \leq \overline{\mathbf{\Delta M_X}}$. Using [Efimov 13e, Lemma 1], the quantity $\mathbf{\Delta M_X}(\theta)\boldsymbol{X}$ can thus be bounded in the following manner:

$$-\overline{\mathbf{\Delta M_X}}\left(\overline{\boldsymbol{X}}^{+} + \underline{\boldsymbol{X}}^{-}\right) \leq \mathbf{\Delta M_X}(\theta)\boldsymbol{X} \leq \overline{\mathbf{\Delta M_X}}\left(\overline{\boldsymbol{X}}^{+} + \underline{\boldsymbol{X}}^{-}\right) \tag{5.75}$$

It can be noted that the dynamics in (5.74) is cooperative $\forall\theta \in [-1, 1]$, $\forall D_K \in \mathbb{R}$. Building an interval observer on such cooperative systems is trivial. According to [Efimov 13e], the following system is an interval observer for (5.74):

$$\begin{aligned} \dot{\underline{\boldsymbol{X}}} &= \mathbf{M_X}\underline{\boldsymbol{X}} - \overline{\mathbf{\Delta M_X}}\left(\overline{\boldsymbol{X}}^{+} + \underline{\boldsymbol{X}}^{-}\right) + \mathbf{B_u}v + \mathbf{B_d}\underline{d} \\ \dot{\overline{\boldsymbol{X}}} &= \mathbf{M_X}\overline{\boldsymbol{X}} + \overline{\mathbf{\Delta M_X}}\left(\overline{\boldsymbol{X}}^{+} + \underline{\boldsymbol{X}}^{-}\right) + \mathbf{B_u}v + \mathbf{B_d}\overline{d} \\ \underline{\boldsymbol{X}}(0) &= \boldsymbol{x}_0 \\ \overline{\boldsymbol{X}}(0) &= \boldsymbol{x}_0 \end{aligned} \tag{5.76}$$

where it is used that $\mathbf{B_d}^{-} = \mathbf{0}$. Using the results in 5.3.1 (b), a differentiable version of this interval observer can be obtained by noting that:

$$\begin{aligned} \overline{\mathbf{\Delta M_X}}\left(\overline{\boldsymbol{X}}^{+} + \underline{\boldsymbol{X}}^{-}\right) &\leq \overline{\mathbf{\Delta M_X}}\left(\boldsymbol{f}_p\left(\overline{\boldsymbol{X}}\right) + \boldsymbol{f}_p\left(\underline{\boldsymbol{X}}\right)\right) - \overline{\mathbf{\Delta M_X}}\underline{\boldsymbol{X}} \\ -\overline{\mathbf{\Delta M_X}}\left(\overline{\boldsymbol{X}}^{+} + \underline{\boldsymbol{X}}^{-}\right) &\geq -\overline{\mathbf{\Delta M_X}}\left(\boldsymbol{f}_p\left(\overline{\boldsymbol{X}}\right) + \boldsymbol{f}_p\left(\underline{\boldsymbol{X}}\right)\right) + \overline{\mathbf{\Delta M_X}}\underline{\boldsymbol{X}} \end{aligned} \tag{5.77}$$

This results in more conservative yet differentiable bounds being obtained on $\mathbf{\Delta M_X}(\theta)\boldsymbol{X}$. With a slight abuse of notation where $\boldsymbol{X}$ is the state of the newly defined differentiable dynamics, the following is an interval observer for the closed-loop dynamics in (5.74):

$$\begin{aligned} \dot{\underline{\boldsymbol{X}}} &= \mathbf{M_X}\underline{\boldsymbol{X}} - \overline{\mathbf{\Delta M_X}}\left(\boldsymbol{f}_p\left(\overline{\boldsymbol{X}}\right) + \boldsymbol{f}_p\left(\underline{\boldsymbol{X}}\right)\right) + \overline{\mathbf{\Delta M_X}}\underline{\boldsymbol{X}} + \mathbf{B_u}v + \mathbf{B_d}\underline{d} \\ \dot{\overline{\boldsymbol{X}}} &= \mathbf{M_X}\overline{\boldsymbol{X}} + \overline{\mathbf{\Delta M_X}}\left(\boldsymbol{f}_p\left(\overline{\boldsymbol{X}}\right) + \boldsymbol{f}_p\left(\underline{\boldsymbol{X}}\right)\right) - \overline{\mathbf{\Delta M_X}}\underline{\boldsymbol{X}} + \mathbf{B_u}v + \mathbf{B_d}\overline{d} \end{aligned} \tag{5.78}$$

The tightness of the interval $\left[\underline{\boldsymbol{X}}, \overline{\boldsymbol{X}}\right]$ which bounds $\boldsymbol{X}$ can be evaluated by considering the following non-linear dynamics, where $\boldsymbol{E}_d = \frac{1}{2}\left(\overline{\boldsymbol{X}} - \underline{\boldsymbol{X}}\right)$:

$$\dot{\boldsymbol{E}}_d = \mathbf{M_X}\boldsymbol{E}_d + \overline{\mathbf{\Delta M_X}}\left(\boldsymbol{f}_p\left(\overline{\boldsymbol{X}}\right) + \boldsymbol{f}_p\left(\underline{\boldsymbol{X}}\right)\right) - \overline{\mathbf{\Delta M_X}}\underline{\boldsymbol{X}} + \frac{1}{2}\mathbf{B_d}\left(\overline{d} - \underline{d}\right) \tag{5.79}$$

As far as the controller synthesis is concerned, nine "critical" models are considered. Values θ_i of θ for these critical models are chosen in the following set:

$$\Theta_c = \{\theta_i | \theta_i = -1 + 0.25i,\ 0 \leq i \leq 8\} \tag{5.80}$$

The static controller synthesis is performed over these critical models such that the closed-loop is stable, the H_2-norm $\left\|\frac{1}{0.3}T_{d\to\boldsymbol{X}}(s)\right\|_2$ is less than the unity and $\mathbf{M_X}$ is Metzler. Since the matrix $\mathbf{B_u}D_K\mathbf{C}$ only impacts $\mathbf{M_X}_{11}$, the latter condition is trivial. Nonetheless, the approach presented in Chapter 7, 7.4 is used to perform the synthesis. The following numerical value is obtained for the controller gain:

$$D_K = -13.8978 \tag{5.81}$$

OISTeR application The objective is to keep $\boldsymbol{x}_2$ in the interval $[\underline{\alpha}, \overline{\alpha}]$. Note that since $\mathbf{C_\alpha} = \begin{bmatrix} 0 & 1 \end{bmatrix}$ then $\mathbf{C_\alpha}^{+} = \mathbf{C_\alpha}$ and $\mathbf{C_\alpha}^{-} = \mathbf{0}$. Also, as mentioned in the previous paragraph, since the system is cooperative for all values of θ then bounds $\underline{\boldsymbol{X}}$ and $\overline{\boldsymbol{X}}$ on the closed-loop state are trivially computed using the interval observer in (5.78). Hence:

$$\mathbf{C_\alpha}\underline{\boldsymbol{X}} \leq \mathbf{C_\alpha}\boldsymbol{X} \leq \mathbf{C_\alpha}\overline{\boldsymbol{X}} \tag{5.82}$$

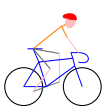

According to 5.3.3 (a) and Definition 5.15, the output constraint can be satisfied by fulfilling the following generalized output constraint:

$$\begin{cases} \mathbf{C}_{\boldsymbol{\alpha}}\underline{\boldsymbol{X}} \geq \underline{\alpha} \\ \mathbf{C}_{\boldsymbol{\alpha}}\overline{\boldsymbol{X}} \leq \overline{\alpha} \end{cases}, \forall t \in \mathbb{R}_+ \tag{5.83}$$

Let $\beta_m = \mathbf{C}_{\boldsymbol{\alpha}}\underline{\boldsymbol{X}}$ and $\beta_p = \mathbf{C}_{\boldsymbol{\alpha}}\overline{\boldsymbol{X}}$. These quantities are of relative degree $k = 2$ with respect to v. Using the Definition 5.18 of generalized propagated bounds and Lemma 5.19 where

$$\begin{aligned}
\dot{\beta}_m &= \mathbf{C}_{\boldsymbol{\alpha}}\mathbf{M}_{\mathbf{X}}\underline{\boldsymbol{X}} - \mathbf{C}_{\boldsymbol{\alpha}}\boldsymbol{\Delta}\mathbf{M}_{\mathbf{X}}\left(\boldsymbol{f}_p\left(\overline{\boldsymbol{X}}\right) + \boldsymbol{f}_p\left(\underline{\boldsymbol{X}}\right)\right) + \mathbf{C}_{\boldsymbol{\alpha}}\boldsymbol{\Delta}\mathbf{M}_{\mathbf{X}}\underline{\boldsymbol{X}} + \mathbf{C}_{\boldsymbol{\alpha}}\mathbf{B}_{\mathbf{d}}\underline{d} \\
\dot{\beta}_p &= \mathbf{C}_{\boldsymbol{\alpha}}\mathbf{M}_{\mathbf{X}}\overline{\boldsymbol{X}} + \mathbf{C}_{\boldsymbol{\alpha}}\boldsymbol{\Delta}\mathbf{M}_{\mathbf{X}}\left(\boldsymbol{f}_p\left(\overline{\boldsymbol{X}}\right) + \boldsymbol{f}_p\left(\underline{\boldsymbol{X}}\right)\right) - \mathbf{C}_{\boldsymbol{\alpha}}\boldsymbol{\Delta}\mathbf{M}_{\mathbf{X}}\underline{\boldsymbol{X}} + \mathbf{C}_{\boldsymbol{\alpha}}\mathbf{B}_{\mathbf{d}}\overline{d} \\
\ddot{\beta}_m &= \gamma_{m,2} + \mathbf{C}_{\boldsymbol{\alpha}}\left[\mathbf{M}_{\mathbf{X}} - \boldsymbol{\Delta}\mathbf{M}_{\mathbf{X}}\left(\nabla\boldsymbol{f}_p\left(\overline{\boldsymbol{X}}\right) + \nabla\boldsymbol{f}_p\left(\underline{\boldsymbol{X}}\right)\right) + \boldsymbol{\Delta}\mathbf{M}_{\mathbf{X}}\right]\mathbf{B}_{\mathbf{u}}v \\
&= \gamma_{m,2} + \mathbf{C}_{\boldsymbol{\alpha}}\mathbf{V}_m\left(\underline{\boldsymbol{X}}, \overline{\boldsymbol{X}}\right)\mathbf{B}_{\mathbf{u}}v \\
\ddot{\beta}_p &= \gamma_{p,2} + \mathbf{C}_{\boldsymbol{\alpha}}\left[\mathbf{M}_{\mathbf{X}} + \boldsymbol{\Delta}\mathbf{M}_{\mathbf{X}}\left(\nabla\boldsymbol{f}_p\left(\overline{\boldsymbol{X}}\right) + \nabla\boldsymbol{f}_p\left(\underline{\boldsymbol{X}}\right)\right) - \boldsymbol{\Delta}\mathbf{M}_{\mathbf{X}}\right]\mathbf{B}_{\mathbf{u}}v \\
&= \gamma_{p,2} + \mathbf{C}_{\boldsymbol{\alpha}}\mathbf{V}_p\left(\underline{\boldsymbol{X}}, \overline{\boldsymbol{X}}\right)\mathbf{B}_{\mathbf{u}}v
\end{aligned} \tag{5.84}$$

the following saturations are obtained and applied to the nominally null input signal v:

$$\begin{aligned}
\underline{v} &= \frac{1}{\mathbf{C}_{\boldsymbol{\alpha}}\mathbf{V}_m\left(\underline{\boldsymbol{X}}, \overline{\boldsymbol{X}}\right)\mathbf{B}_{\mathbf{u}}}\left(\underline{\beta}_2 - \gamma_{m,2}\right) \\
\overline{v} &= \frac{1}{\mathbf{C}_{\boldsymbol{\alpha}}\mathbf{V}_p\left(\underline{\boldsymbol{X}}, \overline{\boldsymbol{X}}\right)\mathbf{B}_{\mathbf{u}}}\left(\overline{\beta}_2 - \gamma_{p,2}\right)
\end{aligned} \tag{5.85}$$

where $\gamma_{m,2}$ and $\gamma_{p,2}$ are defined in (5.86) and $\underline{\beta}_2$, $\overline{\beta}_2$ are the propagated bounds expressions for $k = 2$. As far as OISTeR design parameters κ_1 and κ_2 are concerned, they are chosen according to Theorem 5.22 to avoid saturations overlap as exposed in Lemma 5.21. The constants $\check{\kappa}_1$ and $\check{\kappa}_2$ are chosen such that $\check{\kappa}_1 = 1$ and $\check{\kappa}_2 = 6$.

$$\begin{aligned}
\gamma_{m,2} &= \mathbf{C}_{\boldsymbol{\alpha}}{\mathbf{M}_{\mathbf{X}}}^2\underline{\boldsymbol{X}} - \mathbf{C}_{\boldsymbol{\alpha}}\mathbf{M}_{\mathbf{X}}\boldsymbol{\Delta}\mathbf{M}_{\mathbf{X}}\left(\boldsymbol{f}_p\left(\overline{\boldsymbol{X}}\right) + \boldsymbol{f}_p\left(\underline{\boldsymbol{X}}\right)\right) + \mathbf{C}_{\boldsymbol{\alpha}}\mathbf{M}_{\mathbf{X}}\boldsymbol{\Delta}\mathbf{M}_{\mathbf{X}}\underline{\boldsymbol{X}} + \mathbf{C}_{\boldsymbol{\alpha}}\mathbf{M}_{\mathbf{X}}\mathbf{B}_{\mathbf{d}}\underline{d} \\
&\quad -\mathbf{C}_{\boldsymbol{\alpha}}\boldsymbol{\Delta}\mathbf{M}_{\mathbf{X}}\nabla\boldsymbol{f}_p\left(\overline{\boldsymbol{X}}\right)\left[\mathbf{M}_{\mathbf{X}}\overline{\boldsymbol{X}} + \boldsymbol{\Delta}\mathbf{M}_{\mathbf{X}}\left(\boldsymbol{f}_p\left(\overline{\boldsymbol{X}}\right) + \boldsymbol{f}_p\left(\underline{\boldsymbol{X}}\right)\right) - \boldsymbol{\Delta}\mathbf{M}_{\mathbf{X}}\underline{\boldsymbol{X}} + \mathbf{B}_{\mathbf{d}}\overline{d}\right] \\
&\quad -\mathbf{C}_{\boldsymbol{\alpha}}\boldsymbol{\Delta}\mathbf{M}_{\mathbf{X}}\nabla\boldsymbol{f}_p\left(\underline{\boldsymbol{X}}\right)\left[\mathbf{M}_{\mathbf{X}}\underline{\boldsymbol{X}} - \boldsymbol{\Delta}\mathbf{M}_{\mathbf{X}}\left(\boldsymbol{f}_p\left(\overline{\boldsymbol{X}}\right) + \boldsymbol{f}_p\left(\underline{\boldsymbol{X}}\right)\right) + \boldsymbol{\Delta}\mathbf{M}_{\mathbf{X}}\underline{\boldsymbol{X}} + \mathbf{B}_{\mathbf{d}}\overline{d}\right] \\
&\quad +\mathbf{C}_{\boldsymbol{\alpha}}\boldsymbol{\Delta}\mathbf{M}_{\mathbf{X}}\mathbf{M}_{\mathbf{X}}\underline{\boldsymbol{X}} - \mathbf{C}_{\boldsymbol{\alpha}}\boldsymbol{\Delta}{\mathbf{M}_{\mathbf{X}}}^2\left(\boldsymbol{f}_p\left(\overline{\boldsymbol{X}}\right) + \boldsymbol{f}_p\left(\underline{\boldsymbol{X}}\right)\right) + \mathbf{C}_{\boldsymbol{\alpha}}\boldsymbol{\Delta}{\mathbf{M}_{\mathbf{X}}}^2\underline{\boldsymbol{X}} \\
&\quad +\mathbf{C}_{\boldsymbol{\alpha}}\boldsymbol{\Delta}\mathbf{M}_{\mathbf{X}}\mathbf{B}_{\mathbf{d}}\underline{d} + \mathbf{C}_{\boldsymbol{\alpha}}\mathbf{B}_{\mathbf{d}}\dot{\underline{d}} \\
\gamma_{p,2} &= \mathbf{C}_{\boldsymbol{\alpha}}{\mathbf{M}_{\mathbf{X}}}^2\overline{\boldsymbol{X}} + \mathbf{C}_{\boldsymbol{\alpha}}\mathbf{M}_{\mathbf{X}}\boldsymbol{\Delta}\mathbf{M}_{\mathbf{X}}\left(\boldsymbol{f}_p\left(\overline{\boldsymbol{X}}\right) + \boldsymbol{f}_p\left(\underline{\boldsymbol{X}}\right)\right) - \mathbf{C}_{\boldsymbol{\alpha}}\mathbf{M}_{\mathbf{X}}\boldsymbol{\Delta}\mathbf{M}_{\mathbf{X}}\underline{\boldsymbol{X}} + \mathbf{C}_{\boldsymbol{\alpha}}\mathbf{M}_{\mathbf{X}}\mathbf{B}_{\mathbf{d}}\overline{d} \\
&\quad +\mathbf{C}_{\boldsymbol{\alpha}}\boldsymbol{\Delta}\mathbf{M}_{\mathbf{X}}\nabla\boldsymbol{f}_p\left(\overline{\boldsymbol{X}}\right)\left[\mathbf{M}_{\mathbf{X}}\overline{\boldsymbol{X}} + \boldsymbol{\Delta}\mathbf{M}_{\mathbf{X}}\left(\boldsymbol{f}_p\left(\overline{\boldsymbol{X}}\right) + \boldsymbol{f}_p\left(\underline{\boldsymbol{X}}\right)\right) - \boldsymbol{\Delta}\mathbf{M}_{\mathbf{X}}\underline{\boldsymbol{X}} + \mathbf{B}_{\mathbf{d}}\overline{d}\right] \\
&\quad +\mathbf{C}_{\boldsymbol{\alpha}}\boldsymbol{\Delta}\mathbf{M}_{\mathbf{X}}\nabla\boldsymbol{f}_p\left(\underline{\boldsymbol{X}}\right)\left[\mathbf{M}_{\mathbf{X}}\underline{\boldsymbol{X}} - \boldsymbol{\Delta}\mathbf{M}_{\mathbf{X}}\left(\boldsymbol{f}_p\left(\overline{\boldsymbol{X}}\right) + \boldsymbol{f}_p\left(\underline{\boldsymbol{X}}\right)\right) + \boldsymbol{\Delta}\mathbf{M}_{\mathbf{X}}\underline{\boldsymbol{X}} + \mathbf{B}_{\mathbf{d}}\overline{d}\right] \\
&\quad -\mathbf{C}_{\boldsymbol{\alpha}}\boldsymbol{\Delta}\mathbf{M}_{\mathbf{X}}\mathbf{M}_{\mathbf{X}}\underline{\boldsymbol{X}} + \mathbf{C}_{\boldsymbol{\alpha}}\boldsymbol{\Delta}{\mathbf{M}_{\mathbf{X}}}^2\left(\boldsymbol{f}_p\left(\overline{\boldsymbol{X}}\right) + \boldsymbol{f}_p\left(\underline{\boldsymbol{X}}\right)\right) - \mathbf{C}_{\boldsymbol{\alpha}}\boldsymbol{\Delta}{\mathbf{M}_{\mathbf{X}}}^2\underline{\boldsymbol{X}} \\
&\quad -\mathbf{C}_{\boldsymbol{\alpha}}\boldsymbol{\Delta}\mathbf{M}_{\mathbf{X}}\mathbf{B}_{\mathbf{d}}\underline{d} + \mathbf{C}_{\boldsymbol{\alpha}}\mathbf{B}_{\mathbf{d}}\dot{\overline{d}}
\end{aligned} \tag{5.86}$$

Simulation results The system in (5.71) is simulated in closed-loop with (5.81) and the saturations obtained in the previous paragraph applied to the corrective input signal v as described in the OISTeR theory. The simulation takes place over 30s and the uncertain parameter θ is chosen in Θ_c as defined in (5.80). Simulation results are shown in Figs. 5.8 and 5.9.

The closed-loop system (5.74) state is represented in Fig. 5.8(a) either in the presence of the saturated corrective input signal v (plain line) or not (dashed line). It can be observed that the output-constraint on $\boldsymbol{x}_2$ (in red) is satisfied whichever the value of $\theta \in \Theta_c$. The corrective input v is represented in Fig. 5.8(b) along with the applied saturations. As already noted, this signal equals 0 whenever the output constraint is satisfied. In this case, the closed-loop behaves nominally. Whenever the output constraint is violated, the OISTeR saturations introduce a

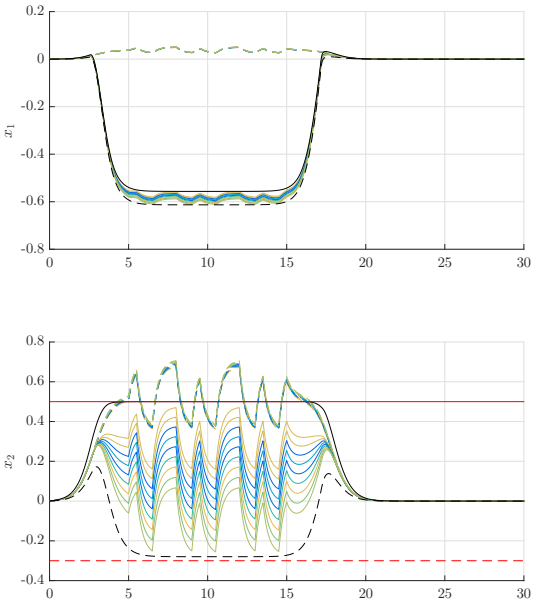

(a) System (5.74) state simulation in closed-loop with OISTeR saturations (in plain line) and without saturations (in dashed line). The time-domain constraint on $\boldsymbol{x}_2$ is represented in red and the interval observer estimates in black.

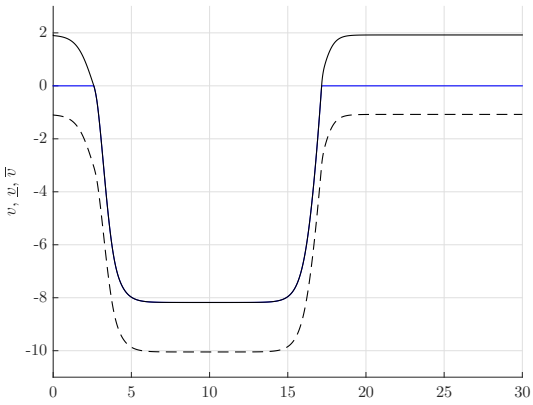

(b) Control input v (in blue) and saturations obtained through application of OISTeR (in black).

Figure 5.8: State and control input v simulation results for $\theta \in \Theta_c$.

corrective signal on the controller output. Using the notion of generalized propagated bounds and Lemma 5.19, the bounds on the state provided by the interval observer are guaranteed to satisfy the output constraint as illustrated in Fig. 5.8(a). Hence, the constraint is satisfied for all values of $\theta \in [-1, 1]$.

The generalized propagated bounds and design parameters obtained using OISTeR are represented in Fig. 5.9. It can be checked in simulation that the following relations are satisfied as required to avoid saturations overlap (see Lemma 5.21): $\overline{\beta_1} - \underline{\beta_1} > \dot{\beta}_p - \dot{\beta}_m$ and $\overline{\beta_2} - \underline{\beta_2} > \ddot{\beta}_p - \ddot{\beta}_m$.

Conclusions In conclusion, OISTeR has been successfully applied to the cooperative uncertain LTI model in (5.71) with incomplete state measurements. Using an appropriately defined corrective input signal $v = \text{sat}_{\underline{v}}^{\overline{v}}(0)$, the output constraint has been enforced for all values of θ in $[-1, 1]$. In fact, the constraint is enforced on the interval observer state which provides guaranteed bounds on the closed-loop state vector $\boldsymbol{X}$. Through this application, it appears that applying OISTeR is roughly equivalent to applying OIST on an interval observer of the closed-loop.

Despite these interesting results, it appears that the approach is quite conservative. The interval observer interval $\left[\underline{\boldsymbol{X}}, \overline{\boldsymbol{X}}\right]$ should be very tight. A good knowledge of the disturbance can help improve the tightness. On the contrary, a poor definition of the bounds can lead to the output constraint being violated from the beginning. OISTeR cannot be applied in this case.

These observations result from the novelty of the proposed results. Future works should focus on reducing the conservatism.

5.5 Comments on the extension and perspectives

In this chapter, an extension of the *Output to Input Saturation Transformation* has been proposed to account for the possible presence of uncertainties in the considered model and the lack of information on the state vector value. This is based on the interval observer theory presented in Chapter B and on the numerical method presented in Chapter 7 to simultaneously design a

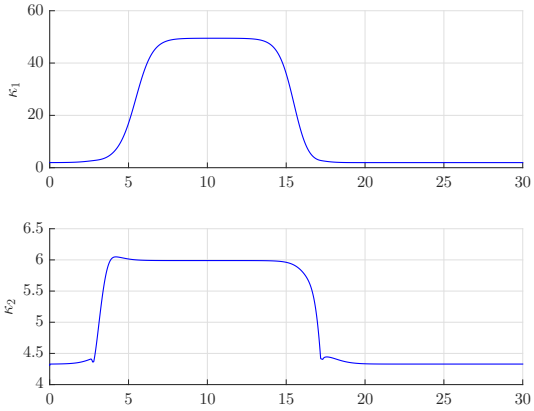

(a) OISTeR time-varying design parameters chosen as in 5.22 to avoid saturations overlap.

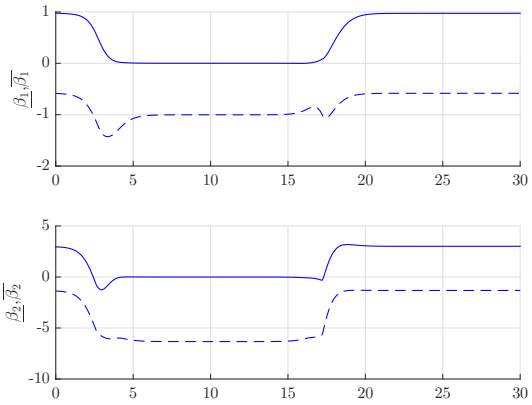

(b) OISTeR generalized propagated bounds chosen as in 5.18.

Figure 5.9: OISTeR design parameters and generalized propagated bounds simulation results.

structured controller along with such interval observer on the resulting closed-loop.

As already mentioned, the results presented in this chapter are new and the OISTeR approach should be considered as work in progress. More precisely, a rigorous stability analysis of the resulting system in Theorem 5.23 is a clear short term perspective for future works. The solution provided for minimum phase systems in Chapter 4 to bring guarantees to closed-loop stability by considering an anti-windup compensator should be updated to account for these new results. It is expected to be quite straightforward in the absence of uncertain parameters. Moreover systems with $\mathbf{B}_{\mathbf{X},\mathbf{v}}$ depending on $\boldsymbol{\theta}$ could be considered, which was not the case in this study.

Longer-term works should focus on reducing the conservatism of the method. As illustrated in the examples in 5.4, the method requires the interval observer to provide an interval $\left[\underline{\boldsymbol{X}}, \overline{\boldsymbol{X}}\right]$ as tight as possible of the expected value of the state vector $\boldsymbol{X}$. This also depends on the knowledge of the input disturbance d: if the known bounds $\underline{d}$ or $\overline{d}$ are not close enough to the actual value of the disturbance signal then the method may not be applicable. Maybe considering stochastic approaches to estimate the interval $\left[\underline{\boldsymbol{X}}, \overline{\boldsymbol{X}}\right]$ with a certain degree of confidence would help reduce this conservatism at the cost of theoretical guarantees, though achieving more satisfying results in practice. Considering time-varying SCT (see B.4.1) rather than time-invariant SCT (see B.4.2) should improve the tightness of the interval but lead to more complex expressions due to the dependence of the transformation matrix $\mathbf{P}$ on time. Another long-term extension of OISTeR is to provide a similar approach to output-constrained control in the case of LTV and LPV systems.

Chapter 6

Application to the atmospheric control of a linear uncertain flexible launch vehicle model

In this chapter, the main contributions of this thesis work are applied to simplified models of the longitudinal motion of a flexible launch vehicle. Depending on the considered contribution, flexible modes, uncertainties and knowledge of the state vector value may or may not be considered. Note that some numerical values may be missing in this chapter for confidentiality purposes. This chapter is based on results presented in [Chambon 15a] and [Chambon 15d].

The launch vehicle model is introduced in 6.1. The equations of the longitudinal motion are presented along with the flexible modes dynamics and uncertain parameters. A state-space representation is deduced. Then, a robust observer-based controller is synthesized in 6.2 following works in Chapter 2. The problem of output-constrained control is then considered in 6.3 where the contributions in Chapters 4 and 5 are successively applied. Conclusions and perspectives are drawn in 6.4.

6.1 Linear launch vehicle model

The longitudinal launch vehicle model used in this chapter is based on existing models commonly used for the design of control laws during atmospheric flight. This model is extensively described in [Ganet 10] prior to investigating LPV control techniques. Other interesting resources using this model include [Renault 08, Saunois 09, Scorletti 10]. A similar model was used within the PIROLA initiative dedicated to evaluating robust control approaches for the control of launch vehicles and resulting from a cooperation between the CNES, ONERA and other partners [Clément 01, Imbert 03, Voinot 03b]. The model and notations are described in the next section. For reference, a simplified representation of the launch vehicle is represented in Fig. 6.1.

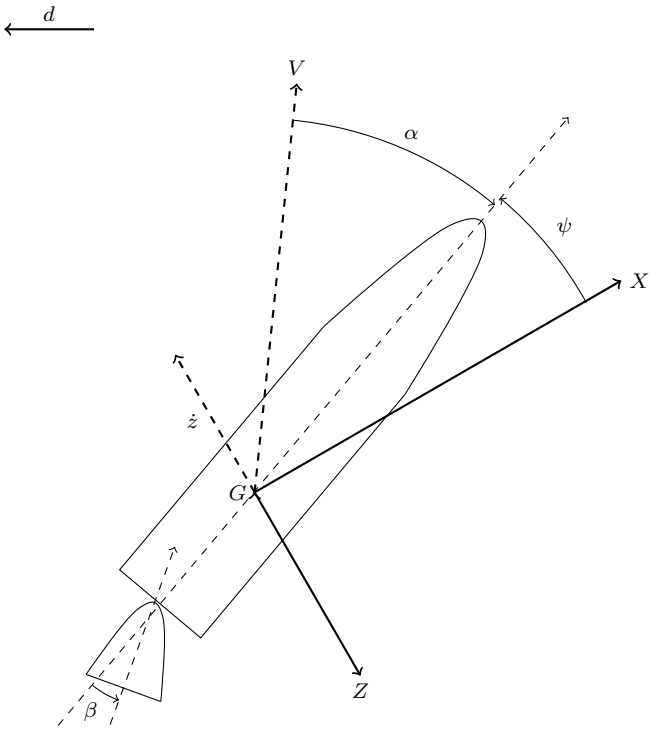

Figure 6.1: Simplified representation of the considered launch vehicle (longitudinal motion).

6.1.1 Notations and non-linear modelling of the rigid body dynamics

Only the longitudinal motion of the launch vehicle is considered. Let define the following notations which are also used in Fig. 6.1:

- V denotes the relative velocity of the launch vehicle with respect to the incoming air flow. This is the norm of the corresponding relative velocity vector;
- α denotes the angle of attack, that is the angle between the relative velocity vector and the main axis of the rigid body. Note that this angle value is exaggerated in Fig. 6.1 since it is rarely greater than a few degrees in nominal operation;
- ψ refers to the launch vehicle attitude, that is the angle between the considered frame (G, X)-axis and the main rigid body axis;
- $\dot{z}$ denotes the drift velocity along (G, Z)-axis;
- β is the thruster control angle;
- d is the wind speed norm.

As far as control theory is concerned, the rigid body motion can be described by the dynamic evolution of the state vector $\boldsymbol{x} = \begin{bmatrix} \psi \\ \dot{\psi} \\ \dot{z} \end{bmatrix}$. This motion can be controlled through the thruster angle β and is potentially disturbed by wind gusts of speed d. As stated in further sections, the critical output variable is α which evolution should be constrained.

Using Newton's second law, the dynamic evolution of the launch vehicle attitude ψ is given by:

$$\ddot{\psi} = K_1 \sin(\beta) + A_6 \sin(\alpha) \tag{6.1}$$

where A_6 is a coefficient evaluating the aerodynamic efficiency and K_1 a coefficient describing thrust efficiency. Both coefficients are uncertain with their values respectively lying in $\Omega_{A_6} = \left[\underline{A_6}, \overline{A_6}\right]$ and $\Omega_{K_1} = \left[\underline{K_1}, \overline{K_1}\right]$. Their values depend on the considered working point (propulsion and aerodynamic efficiencies vary over time) as well as on the launch vehicle configuration. The dynamic evolution of the transverse drift speed $\dot{z}$ is given by:

$$\ddot{z} = a_1 \sin(\psi) + a_2 (\dot{z} - d) + a_3 \sin(\beta) \tag{6.2}$$

where the coefficients a_1 to a_3 are known and negative. Note that the launch vehicle attitude depends on the angle of attack α. Its expression is made explicit after linearising the model.

6.1.2 Linear rigid body dynamics

By supposing that the attitude and angle of attack remain small during the motion, it is possible to linearise the model in (6.1) and (6.2). Upon linearisation, the attitude evolution is described by:

$$\begin{aligned} \ddot{\psi} &= K_1 \beta + A_6 \alpha \\ &= K_1 \beta + A_6 \left(\psi + \tfrac{\dot{z} - d}{V}\right) \end{aligned} \tag{6.3}$$

where it has been noted that the angle of attack can be expressed as follows in the linear case:

$$\alpha = \psi + \frac{\dot{z} - d}{V} \tag{6.4}$$

where the relative speed norm V is fixed and known for a given working point. In a similar way, the linearised drift velocity dynamics is given by:

$$\ddot{z} = a_1 \psi + a_2 (\dot{z} - d) + a_3 \beta \tag{6.5}$$

This can be formalised using the state-space representation which describes the dynamic evolution of the rigid body state vector $\boldsymbol{x}^1 = \begin{bmatrix} \psi \\ \dot{\psi} \\ \dot{z} \end{bmatrix}$ with respect to time.

$$(\mathbf{G}) \begin{cases} \dot{\boldsymbol{x}}^1 = \begin{bmatrix} 0 & 1 & 0 \\ A_6 & 0 & \frac{A_6}{V} \\ a_1 & 0 & a_2 \end{bmatrix} \boldsymbol{x}^1 + \begin{bmatrix} 0 & 0 \\ -\frac{A_6}{V} & K_1 \\ -a_2 & a_3 \end{bmatrix} \begin{bmatrix} d \\ \beta \end{bmatrix} \\ \boldsymbol{z} = \begin{bmatrix} 1 & 0 & \frac{1}{V} \\ 0 & 0 & 1 \end{bmatrix} \boldsymbol{x}^1 + \begin{bmatrix} -\frac{1}{V} & 0 \\ 0 & 0 \end{bmatrix} \begin{bmatrix} d \\ \beta \end{bmatrix} \\ \boldsymbol{y} = \begin{bmatrix} 1 & 0 & 0 \\ 0 & 1 & 0 \end{bmatrix} \boldsymbol{x}^1 \end{cases} \tag{6.6}$$

where $\boldsymbol{y} = \begin{bmatrix} \psi \\ \dot{\psi} \end{bmatrix}$ is the measurements vector and $\boldsymbol{z} = \begin{bmatrix} \alpha \\ \dot{z} \end{bmatrix}$.

However, due to the presence of the uncertain parameters A_6 and K_1, the state-space representation in (6.6) is the representation of an uncertain system. To simplify modelling for controller synthesis purposes, this state-space representation can be made parameter-independent

using an appropriately defined LFR $\mathbf{M}$. Then, uncertain models are obtained through $\mathbf{M}$-$\boldsymbol{\Delta}$ interconnection where the block $\boldsymbol{\Delta}$ is representative of a given vector of uncertainties $\boldsymbol{\theta} = \begin{bmatrix} A_6 \\ K_1 \end{bmatrix}$. An example of such LFR is given by:

$$(\mathbf{M}) \begin{cases} \dot{\boldsymbol{x}}^1 = \begin{bmatrix} 0 & 1 & 0 \\ A_6^n & 0 & \frac{A_6^n}{V} \\ a_1 & 0 & a_2 \end{bmatrix} \boldsymbol{x}^1 + \begin{bmatrix} 0 & 0 & 0 & 0 \\ p_{A_6} A_6^n & p_{K_1} K_1^n & -\frac{A_6^n}{V} & K_1^n \\ 0 & 0 & -a_2 & a_3 \end{bmatrix} \begin{bmatrix} \boldsymbol{w}_1 \\ \boldsymbol{w}_2 \\ d \\ \beta \end{bmatrix} \\ \begin{bmatrix} \boldsymbol{z}_1 \\ \boldsymbol{z}_2 \\ \alpha \\ \dot{z} \end{bmatrix} = \begin{bmatrix} 1 & 0 & \frac{1}{V} \\ 0 & 0 & 0 \\ 1 & 0 & \frac{1}{V} \\ 0 & 0 & 1 \end{bmatrix} \boldsymbol{x}^1 + \begin{bmatrix} 0 & 0 & -\frac{1}{V} & 0 \\ 0 & 0 & 0 & 1 \\ 0 & 0 & -\frac{1}{V} & 0 \\ 0 & 0 & 0 & 0 \end{bmatrix} \begin{bmatrix} \boldsymbol{w}_1 \\ \boldsymbol{w}_2 \\ d \\ \beta \end{bmatrix} \\ \begin{bmatrix} \psi \\ \dot{\psi} \end{bmatrix} = \begin{bmatrix} 1 & 0 & 0 \\ 0 & 1 & 0 \end{bmatrix} \boldsymbol{x}^1 \end{cases} \tag{6.7}$$

where $A_6^n = \underline{A_6} + \frac{\overline{A_6} - \underline{A_6}}{2}$ and $K_1^n = \underline{A_6} + \frac{\overline{K_1} - \underline{K_1}}{2}$ are called the *nominal* parameters values and $p_{A_6} = \frac{A_6^n - \underline{A_6}}{A_6^n}$, $p_{K_1} = \frac{K_1^n - \underline{K_1}}{K_1^n}$. The rigid body dynamics state matrix is denoted $\mathbf{A_n^1}$. Note that this model does not depend on the uncertain parameters A_6 and K_1 anymore but rather on the known nominal values A_6^n and K_1^n and on new known parameters p_{A_6} and p_{K_1}.

The new inputs and outputs highlighted in red in the *nominal* model in (6.7) are used to inject uncertainties through a conventional $\mathbf{M} - \boldsymbol{\Delta}$ LFT interconnection:

$$\begin{aligned} \boldsymbol{w}_1 &= \boldsymbol{\Delta}_{A_6} \boldsymbol{z}_1 \\ \boldsymbol{w}_2 &= \boldsymbol{\Delta}_{K_1} \boldsymbol{z}_2 \end{aligned} \tag{6.8}$$

where $\boldsymbol{\Delta}_{A_6}$ and $\boldsymbol{\Delta}_{K_1}$ are in $[-1, 1]$. A more general way of writing this interconnection is through using the LFT notation:

$$\mathbf{G}(\boldsymbol{\theta}, s) = \mathcal{F}_u \left(\mathbf{M}(s), \boldsymbol{\Delta} \right) \tag{6.9}$$

where $\boldsymbol{\Delta} = \text{diag} \left(\boldsymbol{\Delta}_{A_6}, \boldsymbol{\Delta}_{K_1} \right)$ for values of $\boldsymbol{\Delta}_{A_6}$ and $\boldsymbol{\Delta}_{K_1}$ which are representative of the current value of the vector of uncertainties $\boldsymbol{\theta} = \begin{bmatrix} A_6 \\ K_1 \end{bmatrix}$. Using such interconnection, the whole family of uncertain models can be obtained from a single known LFR and information on the range of the uncertainties.

6.1.3 Flexible modes

Due to its big dimensions and to the materials used, vibrations can propagate inside the launch vehicle structure. High-frequency modes are naturally attenuated within the vehicle structure. However, low-frequency modes are badly damped. These modes can be destructive if re-injected into the system through a badly designed control law. In this chapter, the first five flexible modes are considered as is usually done in the literature [Alazard 03]. Let $j \in \mathbb{N}^\star$ such that $j \leq 5$. The five flexible modes can be modelled by the following linear dynamics:

$$\ddot{q}_j + 2\phi_j \omega_j \dot{q}_j + \omega_j^2 q_j = -\omega_j^2 P_c h_T(j) \beta \tag{6.10}$$

where:

- q_j is j-th modal coordinate;
- ω_j is the considered flexible mode frequency;
- ϕ_j is a damping coefficient;
- P_c is a parameter related with thrust and is considered constant;

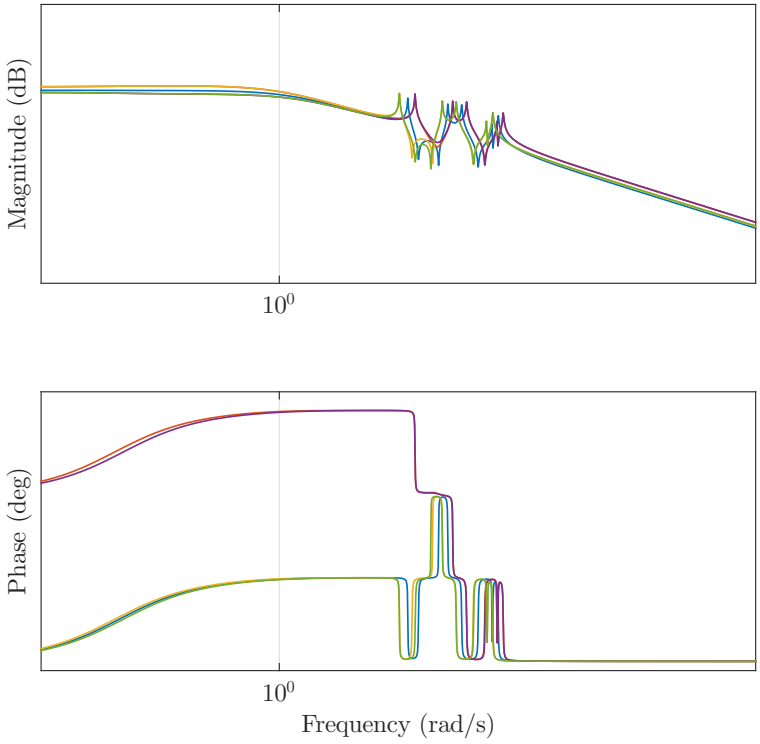

Figure 6.2: Bode diagram of the transfer from β to ψ_f.

- $h_T(j)$ is an uncertain parameter.

These flexible modes interact with the rigid body dynamics through the measurements vector $\boldsymbol{y}$ and thus through the considered control law $\beta = \mathbf{K}(s)\boldsymbol{y}$:

$$\begin{array}{rcl} \psi_f & = & \psi - \sum_{j=1}^{5} h_{cl}(j) q_j \\ \dot{\psi}_f & = & \dot{\psi} - \sum_{j=1}^{5} h_{Gy}(j) \dot{q}_j \end{array} \tag{6.11}$$

where ψ and $\dot{\psi}$ are the corresponding rigid body states and h_{cl} and h_{Gy} are uncertain parameters describing this interaction between the flexible modes and measurements. Let $\boldsymbol{y}_f = \begin{bmatrix} \psi_f \\ \dot{\psi}_f \end{bmatrix}$. In the following, the notation $\boldsymbol{y}$ is used either to refer to the rigid body measurements in case no flexible mode is considered or to $\boldsymbol{y}_f$ in case flexible modes are present. The influence of the flexible modes on the open-loop frequency-response is illustrated in Fig. 6.2 where the Bode diagram of the transfer from β to ψ_f is represented.

The number of uncertainties rises to 27, composed of 2 parametric uncertainties on the rigid body dynamics and 5 uncertainties on each of the 5 considered flexible mode dynamics. Using both the rigid body dynamics (state vector $\boldsymbol{x}^1$) and the flexible modes dynamics (state vector $\boldsymbol{x}^2$), a possible LFR is given by:

$$(\mathbf{M}) \left\{ \begin{array}{rcl} \dot{\boldsymbol{x}} & = & \begin{bmatrix} \mathbf{A_n^1} & \mathbf{0} \\ \mathbf{0} & \mathbf{A_n^2} \end{bmatrix} \boldsymbol{x} + \mathbf{B_{n,\beta}}\beta + \mathbf{B_{n,w}}\boldsymbol{w} \\ \boldsymbol{z} & = & \mathbf{C_z}\boldsymbol{x} + \mathbf{D_{z,\beta}}\beta + \mathbf{D_{z,w}}\boldsymbol{w} \\ \boldsymbol{y} & = & \mathbf{C_y}\boldsymbol{x} + \mathbf{D_{y,\beta}}\beta + \mathbf{D_{y,w}}\boldsymbol{w} \end{array} \right. \tag{6.12}$$

where $\mathbf{A_n^1}$ and $\mathbf{A_n^2}$ are the nominal state matrices related to each dynamics, $\boldsymbol{x} = \begin{bmatrix} \boldsymbol{x}^1 \\ \boldsymbol{x}^2 \end{bmatrix} \in \mathbb{R}^{13}$ in case 5 flexible modes are considered, $\boldsymbol{w} = \begin{bmatrix} \boldsymbol{w}_\Delta \\ d \end{bmatrix} \in \mathbb{R}^{28}$ and $\boldsymbol{z} = \begin{bmatrix} \boldsymbol{z}_\Delta \\ \alpha \\ \dot{z} \end{bmatrix} \in \mathbb{R}^{29}$. Matrices $\mathbf{B_{n,w}}$,

$\mathbf{C_z}$ and $\mathbf{D_{z,w}}$ are obtained in a similar manner than in 6.1.2. For a given vector of uncertainties $\boldsymbol{\theta} \in \mathbb{R}^{27}$ corresponds a diagonal matrix $\boldsymbol{\Delta_\theta} \in \mathbb{R}^{27\times 27}$ which is used to obtain the uncertain model from the LFR in (6.12):

$$\mathbf{G}(\boldsymbol{\theta}, s) = \mathcal{F}_u(\mathbf{M}(s), \boldsymbol{\Delta_\theta}) \tag{6.13}$$

Additional control synthesis inputs and outputs can be eventually appended to the $\boldsymbol{w}$ and $\boldsymbol{z}$ vectors depending on the considered requirements (e.g. requirements on sensitivity functions). Note that the dynamics in (6.12) is reminiscent of the LFR considered in Chapter 2, section 2.3 for structured controller design purposes.

6.1.4 Control system properties

The launch vehicle rigid body dynamics is unstable while the flexible modes dynamics are stable. The rigid body dynamics is observable when considering the output vector $\boldsymbol{y} = \begin{bmatrix} \psi_f \\ \dot{\psi}_f \end{bmatrix}$ and output controllable when considering the control input β.

6.1.5 Constrained output: the angle of attack

The angle of attack is a critical variable when considering the atmospheric flight of the launch vehicle. Indeed, this variable describes the evolution of the angle between the launch vehicle rigid body axis and the incoming air flow. Given the speeds of the launch vehicle which are supersonic and even hypersonic during the atmospheric flight, the angle of attack must remain below a critical value $|\alpha(t)| \leq \overline{\alpha}$, $\forall t$ to minimize the aerodynamic load on the structure. If the controller fails to keep the angle of attack below this critical value, structural damage may occur, leading to the loss of the launch vehicle and its payload.

This motivates considering the angle of attack α as a constrained output on which a time-domain constraint $\mathcal{K}(\Omega_\alpha)$ is set:

$$\alpha(t) \in \Omega_\alpha = [-\overline{\alpha}, \overline{\alpha}], \forall t \tag{6.14}$$

As a reminder, the angle of attack is given by the following expression:

$$\alpha = \psi + \frac{\dot{z} - d}{V} \tag{6.15}$$

where V is the norm of the launcher relative speed with respect to the air flow and d is the unknown wind disturbance. This problem is complex since the constrained output depends on the unknown variable d. Also, due to the presence of flexible modes at rather low frequencies (around 10 rad/s), a careful design of the control law is required using appropriate frequency-domain specifications. These specifications are described in the next section where a structured observer-based controller is designed.

6.2 Nominal observer-based controller synthesis

As detailed in 6.1, the launch vehicle model is subject to some uncertainties on its parameters. The rigid body dynamics depends on two uncertain parameters A_6 and K_1 respectively describing the aerodynamic and thrust efficiency. The flexible modes dynamics depend on 5 uncertain parameters for each of the 5 considered flexible modes. These uncertainties are a real challenge in the determination of a control law fulfilling the expected frequency-domain and time-domain performance.

In Chapter 2, a recent approach to structured controller synthesis based on non-smooth non-convex optimization has been applied to the robust control of a system with uncertainties. Also, the specific observer-based structure has been presented as a possible structure for the robust controller to tune. The use of multiple models to account for different critical values of the vector of uncertainties $\boldsymbol{\theta}$ has been explained.

In this section, the approach detailed in Chapter 2 is applied to the robust atmospheric control of the considered flexible launch vehicle.

6.2.1 Controller structure

The considered controller structure is the observer-based structure described in Chapter 2. The observation stage of the controller is aimed at estimating the rigid body dynamics. A dynamic Youla parameter ($\mathbf{Q}$) is also considered to augment the controller dynamics and offer more degrees of freedom. In this example, the Youla parameter is chosen of order $n_Q = 3$ resulting in a controller of order $n_K = 6$.

The observer-based structure augmented by a dynamics Youla parameters ($\mathbf{Q}$) is recalled here for clarity purposes. Its state-space representation is given by:

$$(\mathbf{K}) \begin{cases} \dot{\begin{bmatrix} \widehat{\boldsymbol{x}_n^1} \\ \boldsymbol{x}_Q \end{bmatrix}} = \begin{bmatrix} \mathbf{A_n^1} - \mathbf{L}\mathbf{C_{n,y}^1} - \mathbf{B_{n,\beta}^1}\mathbf{K_f} - \mathbf{B_{n,\beta}^1}\mathbf{D_Q}\mathbf{C_{n,y}^1} & \mathbf{B_{n,\beta}^1}\mathbf{C_Q} \\ -\mathbf{B_Q}\mathbf{C_{n,y}^1} & \mathbf{A_Q} \end{bmatrix} \begin{bmatrix} \widehat{\boldsymbol{x}_n^1} \\ \boldsymbol{x}_Q \end{bmatrix} \\ \qquad\qquad + \begin{bmatrix} \mathbf{B_{n,\beta}^1}\mathbf{D_Q} + \mathbf{L} \\ \mathbf{B_Q} \end{bmatrix} \boldsymbol{u}_K \\ y_K = \begin{bmatrix} -\mathbf{K_f} - \mathbf{D_Q}\mathbf{C_{n,y}^1} & \mathbf{C_Q} \end{bmatrix} \begin{bmatrix} \widehat{\boldsymbol{x}_n^1} \\ \boldsymbol{x}_Q \end{bmatrix} + \mathbf{D_Q}\boldsymbol{u}_K \end{cases} \tag{6.16}$$

where $\mathbf{A_Q} \in \mathbb{R}^{3\times3}$, $\mathbf{B_Q} \in \mathbb{R}^{3\times2}$, $\mathbf{C_Q} \in \mathbb{R}^{1\times3}$, $\mathbf{D_Q} \in \mathbb{R}^{1\times2}$, $\mathbf{K_f} \in \mathbb{R}^{1\times3}$ and $\mathbf{L} \in \mathbb{R}^{3\times2}$ are the design parameters to tune. The loop is then closed using the relations $\beta = y_K$ and $\boldsymbol{u}_K = \boldsymbol{y}$.

6.2.2 Synthesis models and requirements

In this section, some precisions are brought to describe the models and requirements used for synthesis of the observer-based controller.

Synthesis models Six synthesis models are considered. The first one describes the nominal rigid body dynamics of the launch vehicle and is obtained using an upper-LFT of the model in (6.7) with the null matrix $\mathbf{0}_{2\times2}$. The resulting model is used to constrain the location of the closed-loop poles.

Five models incorporating the flexible modes dynamics are then considered. They are obtained by LFT of the LFR in (6.12) and appropriately defined matrices $\boldsymbol{\Delta} \in \mathbb{R}^{27\times27}$ corresponding to critical values of the vector of uncertainties $\boldsymbol{\theta}$. The first model is the nominal model obtained for $\boldsymbol{\Delta} = \mathbf{0}_{27\times27}$ and the other four models are obtained using diagonal matrices $\boldsymbol{\Delta}$ to select critical values of the uncertain parameters. Constraints related to margins, flexible modes roll-off and disturbance rejections are formulated on these models.

Note that these models were used to draw the Bode diagram in Fig. 6.2. The influence of the flexible modes on the open-loop gain response is clearly visible in this figure, justifying the introduction of a roll-off constraint.

Requirements The following synthesis requirements are stated on the considered synthesis models:

- constraint on the closed-loop dynamics of the rigid model using a statement on the maximal admissible frequency and minimal admissible decay of the poles;
- Closed-loop margins constraint on the nominal and critical flexible launch vehicle models, expressed at the controller output;
- flexible modes roll-off gain constraint on the nominal and critical flexible launch vehicle models, expressed at the controller output:

$$\left\| W(s) T_{w_{y_K} \to z_{y_K}} \right\|_\infty \leq 1 \tag{6.17}$$

where $W(s)$ is an appropriately defined weight and w_{y_K} and z_{y_K} are analysis I/Os injected at the controller output y_K;

- Disturbance rejection constraint on the nominal flexible launch vehicle model:

$$\| W_\alpha(s) T_{d \to \alpha} W_r \|_\infty \leq 1 \tag{6.18}$$

where $W_\alpha(s)$ and W_r are appropriately defined weights.

Additional specifications are often formulated on the launch vehicle control law such as minimizing the cumulated deflection of the thruster or taking amplitude and rate saturations of the thruster into account. These are not considered in the current state of this work as they cannot directly be implemented in the form of a linear problem or they result from time-domain simulations. Additional tools are required to take such specifications into account which is a perspective for future works.

Synthesis The synthesis is performed on the considered synthesis models against the frequency-domain requirements using the `systune` procedure [Apkarian 07, Apkarian 15] from the MATLAB Robust Control Toolbox [MATLAB 14]. All the requirements are considered as objectives, following the terminology used in Chapter 2, or as *soft* constraints, following the terminology in [Apkarian 14]. Two random restarts are used to improve the local minimum reached and the maximum number of iterations is set to 2000. A local solution with a maximum normalized achieved objective (or *soft* constraint) value of 0.98 is obtained in under 140s.

The observer-based controller obtained is tested in the next section both in the frequency- and time-domain.

6.2.3 Frequency-domain and simulation results

In this section, frequency-domain related plots of the obtained results are analysed. The system is also simulated in closed-loop with the obtained controller.

Frequency-domain plots Let consider the following SISO transfer function for a given vector of uncertainties $\boldsymbol{\theta}$:

$$T_{\beta \to y_K}(\boldsymbol{\theta}, s) = -\mathbf{K}(s) \mathbf{G}_{\beta \to \boldsymbol{y}}(\boldsymbol{\theta}, s) \tag{6.19}$$

where $\mathbf{G}_{\beta \to \boldsymbol{y}}(\boldsymbol{\theta}, s)$ is the SIMO transfer from β to $\boldsymbol{y} = \begin{bmatrix} \psi_f \\ \dot{\psi}_f \end{bmatrix}$. The Nichols and Bode diagrams of the open-loop transfer $T_{\beta \to y_K}(\boldsymbol{\theta}, s)$ are represented in Fig. 6.3 for the different critical vectors of uncertainties $\boldsymbol{\theta}$ in Θ_c.

The results shown in the Nichols chart in Fig. 6.3(a) show that the gain and phase margins are respected for all considered critical models. Also, the flexible modes are appropriately damped. It can be noted that the first flexible mode is phase-controlled due to its low frequency while the following modes are gain-controlled. In view of these results, the synthesised controller satisfies to the frequency-domain requirements considered in 6.2.2.

Simulation results The system is simulated over 100s in closed-loop with the observer-based controller synthesized in 6.2.2. In this simulation, the considered disturbance signal is illustrated in Fig. 6.4. This is a typical wind profile used at a given working point to evaluate the influence of a potential wind gust on the atmospheric control of the launch vehicle. The values are hidden for confidentiality purposes but wind speed as high as 40m/s and greater are reached.

The angle of attack and control law obtained in simulation for different values of the vector of uncertainties $\boldsymbol{\theta}$ taken in the critical set Θ_c are shown in Fig. 6.5. Note that the system and

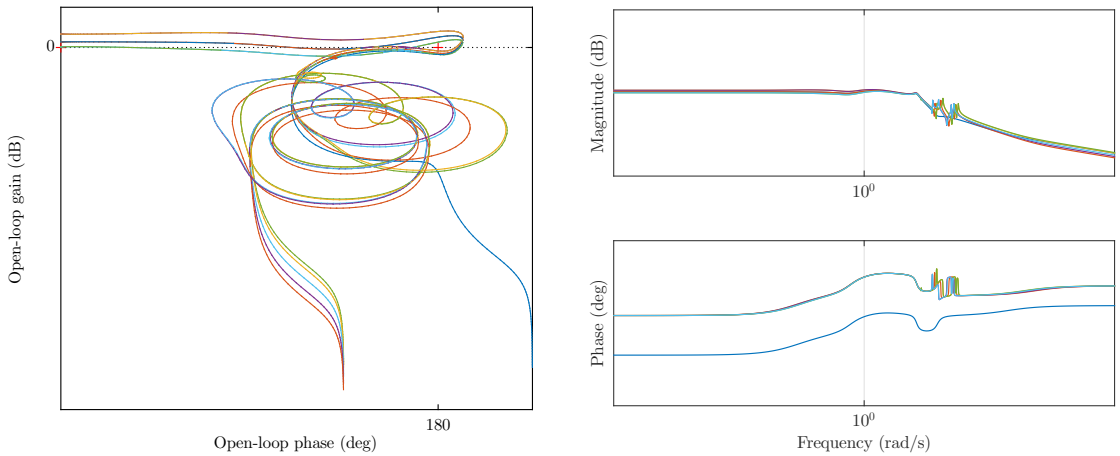

(a) Nichols chart.

(b) Bode diagram.

Figure 6.3: Nichols and Bode diagram of the open-loop transfer $T_{\beta \to y_K}(\boldsymbol{\theta}, s)$ in (6.19). The rigid model frequency responses are represented in blue. Other curves are for critical values of $\boldsymbol{\theta} \in \Theta_c$.

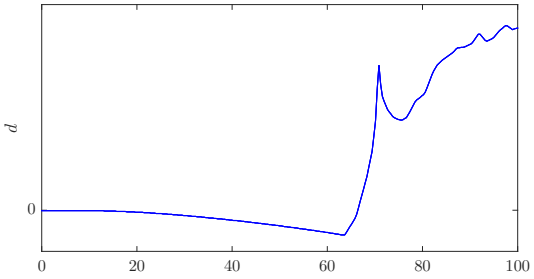

Figure 6.4: Wind profile used in simulation to evaluate the influence of a wind gust (occurring at around $t = 70$s).

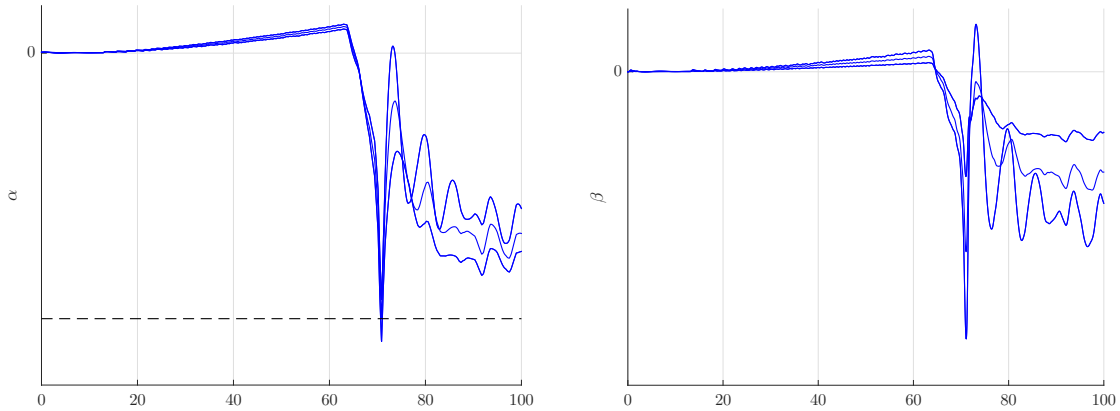

(a) Simulation of the angle of attack for different values of $\boldsymbol{\theta} \in \Theta_c$. A typical time-domain constraint is illustrated in black dashed line.

(b) Control law obtained in simulation for different values of $\boldsymbol{\theta} \in \Theta_c$.

Figure 6.5: Simulation results using the synthesised observer-based controller.

controller states simulation results are not very useful and have been omitted for brevity. The angle of attack is however a critical variable as already highlighted in 6.1.5.

From these simulations results, it can be seen that the considered wind disturbance is well-rejected. The flexible modes are well-attenuated and are not excited by the control law. The angle of attack reaches acceptable maximum values.

The dashed black line in Fig. 6.5(a) illustrates a typical time-domain constraint on the angle of attack as often stated in the specifications. It is thus stated that the absolute value of the angle of attack should remain below a given critical value. Using trial-and-error tuning of the frequency-domain requirements, it is possible to reduce the maximal angle of attack at the cost of gain and phase margins as well as flexible modes damping. Also, as shown in Chapter 4, such trial-and-error-based *cautious* approaches are conservative in the sense that the resulting control law is constrained such that the time-domain constraint is not triggered. Improved performance could be obtained with a control law which would allow the angle of attack to stay on the constraint.

6.2.4 Conclusions

In this section, the synthesis of a structured observer-based controller has been performed for the atmospheric control of an uncertain flexible launch vehicle. The approach proposed in Chapter 4 has been applied to account for the different critical models resulting from the uncertain dynamics. Satisfying results are obtained in both the frequency- and time-domain. The wind disturbance is appropriately rejected to limit the angle of attack.

The controller structure is eventually adapted in the following section which is dedicated to illustrating the methods developed in Chapters 4 and 5 for output-constraint control. The specifications and, consequently, the requirements are however kept identical to achieve similar performance on the rigid and flexible – when considered – dynamics alike.

In the following, application of OIST and OISTeR is considered to enforce a time-domain constraint such as the one illustrated in Fig. 6.5(a).

6.3 Illustration of output-constrained control

In this section, the contributions exposed in Chapters 4 and 5 are applied to simplified models of the launch vehicle. The model used is the one in 6.1 but with some modifications.

It has been stated in the previous section that enforcing a time-domain constraint on the angle of attack α is difficult and relies on tedious trial-and-error tuning of the frequency-domain requirements. In this section, the OIST and OISTeR approaches are applied to avoid such tedious work and to guarantee satisfaction of the time-domain constraint.

Remark 6.1 (Non-minimum phase transfer $T_{\beta\to\alpha}(s)$)**.** Before applying OIST, it appears that the transfer from the control input β to the angle of attack α is non-minimum phase. This transfer indeed has a slow positive zero $z_p \approx 0.05$. As illustrated in 4.6.2, slow zeros are not necessarily a problem as long as the control is not saturated for a long time. In the current state of the approaches, guaranteed stability results can however not be formulated. A practical approach to deal with such case is hinted in 6.3.1. ◇

6.3.1 Application of OIST to the flexible launch vehicle

A model of the flexible launch vehicle with 5 flexible modes and no uncertainty is considered for application of OIST. Satisfying results are obtained using a mixture of OIST and OISTeR to mitigate the conservativeness of some of the expressions.

6.3.1 (a) Considered model: no uncertainty, 5 flexible modes with complete measurements

In this example, no uncertainty is considered and the first 5 flexible modes are included in the model. The combined rigid body and flexible modes dynamics is given by the following state-space representation:

$$(\mathbf{G_2})\begin{cases} \dot{\boldsymbol{x}} &= \begin{bmatrix} \mathbf{A_n^1} & \mathbf{0} \\ \mathbf{0} & \mathbf{A_n^2} \end{bmatrix} \boldsymbol{x} + \mathbf{B_{n,\beta}}\beta + \mathbf{B_{n,d}}d \\ &= \mathbf{A_n}\boldsymbol{x} + \mathbf{B_{n,\beta}}\beta + \mathbf{B_{n,d}}d \\ \boldsymbol{y} &= \boldsymbol{x} \end{cases} \tag{6.20}$$

where $\boldsymbol{x} = \begin{bmatrix} \psi & \dot{\psi} & \dot{z} & q_1 & \dot{q}_1 & \dots & q_5 & \dot{q}_5 \end{bmatrix}^\top \in \mathbb{R}^{13}$ and $\mathbf{B_{n,d}}$ is deduced from $\mathbf{B_{n,w}}$ in (6.12). The state matrix $\mathbf{A}$ is not Hurwitz and has two unstable poles. Note the flexible modes dynamics are stable. It can be noted that $(\mathbf{G_2})$ is controllable.

6.3.1 (b) Considered controller

The following dynamic control law is initially considered:

$$\begin{cases} \beta &= y_K \\ \dot{\boldsymbol{x}}_K &= \mathbf{A_K}\boldsymbol{x}_K + \mathbf{B_K}\boldsymbol{y} \\ y_K &= \mathbf{C_K}\boldsymbol{x}_K + \mathbf{D_K}\boldsymbol{y} \end{cases} \tag{6.21}$$

where $\boldsymbol{x}_K \in \mathbb{R}^5$. For $\boldsymbol{X} = \begin{bmatrix} \boldsymbol{x} \\ \boldsymbol{x}_K \end{bmatrix}$, the closed-loop dynamics is given by:

$$\dot{\boldsymbol{X}} = \begin{bmatrix} \mathbf{A_n} + \mathbf{B_{n,\beta}}\mathbf{D_K} & \mathbf{B_{n,\beta}}\mathbf{C_K} \\ \mathbf{B_K} & \mathbf{A_K} \end{bmatrix} \boldsymbol{X} + \begin{bmatrix} \mathbf{B_{n,d}} \\ \mathbf{0} \end{bmatrix} d \tag{6.22}$$

The controller synthesis is performed under the following frequency-domain requirements:

- the closed-loop poles should lie within $\left[-200, 1.10^{-7}\right]$;
- Appropriate disturbance rejection: $\|W_\alpha T_{d\to\alpha}(s) W_r\|_\infty \leq 1$ for two appropriately defined weights W_α and W_r;
- Gain and phase margins of the feedback loop at y_K should respectively equal 4dB and 20°;
- The flexible modes are appropriately attenuated using a -6dB gain roll-off requirement.

A satisfying controller is obtained. However, as illustrated in dashed blue line in Fig. 6.8(b), the time-domain requirement $\alpha \in [-2.5°, 2.5°]$ is not satisfied using this controller. This motivates using an *evolutionary* approach to output-constrained control such as OIST (see Chapter 4).

6.3.1 (c) OIST application

A time-domain constraint is considered to ensure that the angle of attack remains in a limited interval $[-2.5°, 2.5°]$. In this example, it is considered that the whole state $\boldsymbol{x}$ is known hence the OIST approach as detailed in Chapter 4 can be applied to enforce the considered time-domain constraint. Elements of the OISTeR approach are also used to reduce the conservatism introduced by the bounds on the unknown disturbance.

Output constraint The angle of attack α can be expressed as a linear function of the state $\boldsymbol{x}$ and disturbance input d:

$$\alpha = \mathbf{C_\alpha^1}\boldsymbol{x} + \mathbf{D_\alpha^1}d \tag{6.23}$$

where $\mathbf{C_\alpha^1} = \begin{bmatrix} 1 & 0 & \frac{1}{V} & \mathbf{0}_{1\times 10} \end{bmatrix}$ and $\mathbf{D_\alpha^1} = \frac{1}{V}$. Using this definition, it appears that the quantity $\mathbf{C_\alpha^1}\mathbf{B_{n,\beta}}$ is negative which is a problem in the application of a mixed OIST/OISTeR strategy as explained below and in Remark 5.20. From this point, the following output is considered which corresponds to the opposite of the angle of attack:

$$\tilde{\alpha} = \mathbf{C_\alpha}\boldsymbol{x} + \mathbf{D_\alpha}d \tag{6.24}$$

where $\mathbf{C}_{\boldsymbol{\alpha}} = -\mathbf{C}^{\mathbf{1}}_{\boldsymbol{\alpha}}$ and $\mathbf{D}_{\boldsymbol{\alpha}} = -\mathbf{D}^{\mathbf{1}}_{\boldsymbol{\alpha}}$. Using this new output variable $\tilde{\alpha}$, the quantity $\mathbf{C}_{\boldsymbol{\alpha}}\mathbf{B}_{\mathbf{n},\boldsymbol{\beta}}$ is now (strictly) positive.

Enforcing the output constraint $\tilde{\alpha} \in [-\overline{\alpha}, -\underline{\alpha}]$ using OIST as described in Chapter 4 is equivalent to satisfying:

$$\begin{array}{rcl} \mathbf{C}_{\boldsymbol{\alpha}}\boldsymbol{x} - \mathbf{D}_{\boldsymbol{\alpha}} \max\left(|\underline{d}|, |\overline{d}|\right) & \geq & -\overline{\alpha} \\ \mathbf{C}_{\boldsymbol{\alpha}}\boldsymbol{x} + \mathbf{D}_{\boldsymbol{\alpha}} \max\left(|\underline{d}|, |\overline{d}|\right) & \leq & -\underline{\alpha} \end{array} \tag{6.25}$$

This is particularly conservative due to the null relative degree of $\tilde{\alpha}$ with respect to the disturbance input d. In particular, this would required that $\overline{\alpha} - \underline{\alpha} > 2\mathbf{D}_{\boldsymbol{\alpha}} \max\left(|\underline{d}|, |\overline{d}|\right) > 0$ which is very demanding. To reduce this conservatism, some results presented within Chapter 5 can be used. More particularly, a more precise bounding of $\tilde{\alpha}$ can be used:

$$\mathbf{C}_{\boldsymbol{\alpha}}\boldsymbol{x} + \mathbf{D}_{\boldsymbol{\alpha}}\underline{d} \leq \tilde{\alpha} \leq \mathbf{C}_{\boldsymbol{\alpha}}\boldsymbol{x} + \mathbf{D}_{\boldsymbol{\alpha}}\overline{d} \tag{6.26}$$

where it is used that $\mathbf{D}_{\boldsymbol{\alpha}}$ is a positive real. This is a much less conservative bounding than the one in (6.25). Let define:

$$\begin{array}{rcl} \beta_m & = & \mathbf{C}_{\boldsymbol{\alpha}}\boldsymbol{x} + \mathbf{D}_{\boldsymbol{\alpha}}\underline{d} \\ \beta_p & = & \mathbf{C}_{\boldsymbol{\alpha}}\boldsymbol{x} + \mathbf{D}_{\boldsymbol{\alpha}}\overline{d} \end{array} \tag{6.27}$$

which are reminiscent of quantities involved in the generalized output constraint introduced in Definition 5.15 in Chapter 5 to the exception that the plant state $\boldsymbol{x}$ is known. The corresponding generalized output-constraint is to ensure that

$$\left\{ \begin{array}{rcl} \beta_m & \geq & -\overline{\alpha} \\ \beta_p & \leq & -\underline{\alpha} \end{array} \right. \tag{6.28}$$

which can be achieved under Lemma 5.19 and application of OIST and OISTeR as detailed in Chapters 4 and 5. It can be noted that β_m and β_p are of relative degree 1 with respect to the control input β. The following first derivatives of β_m and β_p are obtained using the original system dynamics in (6.20):

$$\begin{array}{rcl} \dot{\beta}_m & = & \mathbf{C}_{\boldsymbol{\alpha}}\mathbf{A}\boldsymbol{x} + \mathbf{C}_{\boldsymbol{\alpha}}\mathbf{B}_{\mathbf{n},\boldsymbol{\beta}}\beta + \mathbf{C}_{\boldsymbol{\alpha}}\mathbf{B}_{\mathbf{n},\mathbf{d}}d + \mathbf{D}_{\boldsymbol{\alpha}}\dot{\underline{d}} \\ \dot{\beta}_p & = & \mathbf{C}_{\boldsymbol{\alpha}}\mathbf{A}\boldsymbol{x} + \mathbf{C}_{\boldsymbol{\alpha}}\mathbf{B}_{\mathbf{n},\boldsymbol{\beta}}\beta + \mathbf{C}_{\boldsymbol{\alpha}}\mathbf{B}_{\mathbf{n},\mathbf{d}}d + \mathbf{D}_{\boldsymbol{\alpha}}\dot{\overline{d}} \end{array} \tag{6.29}$$

By definition of the relative degree, the quantity $\mathbf{C}_{\boldsymbol{\alpha}}\mathbf{B}_{\mathbf{n},\boldsymbol{\beta}}$ is non-null. Also, due to the new choice of constrained output $\tilde{\alpha} = -\alpha$, this quantity is positive. Note that both $\dot{\beta}_m$ and $\dot{\beta}_p$ depend on the unknown disturbance d. To obtain applicable saturations, the quantity $\mathbf{C}_{\boldsymbol{\alpha}}\mathbf{B}_{\mathbf{n},\mathbf{d}}d$ is bounded as follows:

$$|\mathbf{C}_{\boldsymbol{\alpha}}\mathbf{B}_{\mathbf{n},\mathbf{d}}d| \leq |\mathbf{C}_{\boldsymbol{\alpha}}\mathbf{B}_{\mathbf{n},\mathbf{d}}| \max\left(|\underline{d}|, |\overline{d}|\right) \tag{6.30}$$

Generalized propagated bounds Since a mixed OIST/OISTeR approach is used, the notion of generalized propagated bounds is required as defined in Definition 5.18. Let $\underline{\beta}_0 = -\overline{\alpha}$ and $\overline{\beta}_0 = -\underline{\alpha}$. The relative degree of β_m and β_p with respect to u equals 1 hence, the following is considered:

$$\begin{array}{rcl} \underline{\beta}_1 & = & \kappa_1\left(\underline{\beta}_0 - \beta_m\right) + \dot{\underline{\beta}}_0 \\ \overline{\beta}_1 & = & \kappa_1\left(\overline{\beta}_0 - \beta_p\right) + \dot{\overline{\beta}}_0 \end{array} \tag{6.31}$$

where the design parameter κ_1 is given below. Under Lemma 5.19, the following is satisfied:

$$\left\{ \begin{array}{rcl} \dot{\beta}_m & \geq & \underline{\beta}_1 \\ \dot{\beta}_p & \leq & \overline{\beta}_1 \end{array} \right., \forall t \in \mathbb{R}_+ \Rightarrow \left\{ \begin{array}{rcl} \beta_m & \geq & \underline{\beta}_0 \\ \beta_p & \leq & \overline{\beta}_0 \end{array} \right. \tag{6.32}$$

where the dependence of $\dot{\beta}_m$ and $\dot{\beta}_p$ on β can be used to obtained the OIST saturations on the control input.

Resulting control saturations Using Lemma 5.19, the following saturations on the control input β are obtained:

$$\begin{aligned} \underline{\beta} &= \frac{1}{\mathbf{C_\alpha B_{n,\beta}}}\left[\underline{\beta}_1 - \mathbf{C_\alpha A}\boldsymbol{x} - \mathbf{D_\alpha}\dot{\underline{d}} + |\mathbf{C_\alpha B_{n,d}}| \max\left(|\underline{d}|, |\overline{d}|\right)\right] \\ \overline{\beta} &= \frac{1}{\mathbf{C_\alpha B_{n,\beta}}}\left[\overline{\beta}_1 - \mathbf{C_\alpha A}\boldsymbol{x} - \mathbf{D_\alpha}\dot{\overline{d}} - |\mathbf{C_\alpha B_{n,d}}| \max\left(|\underline{d}|, |\overline{d}|\right)\right] \end{aligned} \tag{6.33}$$

where $\mathbf{C_\alpha B_{n,\beta}} > 0$. The expression of the design coefficient κ_1 is obtained using Theorem 5.22 where the condition to fulfil is $\overline{u} - \underline{u} > 0$. Let $\breve{\kappa}_1 = 0.2$. Saturations overlap is avoided for κ_1 chosen as follows:

$$\kappa_1 = \frac{\breve{\kappa}_1 + 2\,|\mathbf{C_\alpha B_{n,d}}| \max\left(|\underline{d}|, |\overline{d}|\right) + \mathbf{D_\alpha}\left(\dot{\overline{d}} - \dot{\underline{d}}\right)}{\overline{\alpha} - \underline{\alpha} - \mathbf{D_\alpha}\left(\overline{d} - \underline{d}\right)} \tag{6.34}$$

Introduction of an anti-windup The transfer from the control input β to $\tilde{\alpha}$ is non-minimum phase: of the two zeros z_1 and z_2, one is slow unstable with $0 < z_2 \leq 0.5$. When trying to improve the performance using an anti-windup as in Chapter 4, divergence of the saturated system is invariably witnessed. This comes from the fact that Proposition 4.32 is not satisfied. Indeed, when considering the proof of Proposition 4.32 in A.1 it appears that the matrix $\mathbf{A} - \mathbf{B_{n,\beta}}\boldsymbol{K}_{\text{oist}}(t)$ is unstable for the considered non-minimum phase transfer.

In this example, a workaround is used which offers a practical approach to using OIST with non-minimum phase transfers $T_{\beta\to\tilde{\alpha}}(s)$. Let consider the original non-minimum phase transfer $T_{\beta\to\tilde{\alpha}}(s)$:

$$T_{\beta\to\tilde{\alpha}}(s) = \frac{K\,(s+z_1)\,(s-z_2)}{(s-p_1)\,(s-p_2)\,(s-p_3)} \tag{6.35}$$

where $z_1 > 0$ and $z_2 > 0$. Let also consider a slightly modified expression of this transfer such that its zeros are all real negative:

$$T^{mp}_{\beta\to\tilde{\alpha}}(s) = \frac{K\,(s+z_1)\,(s+z_2)}{(s-p_1)\,(s-p_2)\,(s-p_3)} \tag{6.36}$$

Both transfer functions in (6.35) and (6.36) can be expressed as state-space representations in the companion canonical form. In the case of (6.35), a state-coordinate matrix $\mathbf{T}$ is also obtained to retrieve the state-space representation in the original coordinates. Using matrix $\mathbf{T}$, the companion form of the transfer function in (6.36) can be expressed in the original coordinates which leads to the following state-space representation:

$$\begin{cases} \dot{\boldsymbol{\eta}} &= \mathbf{A^1_n}\boldsymbol{\eta} + \mathbf{B^1_{n,\beta}}\beta \\ y_\eta &= \mathbf{C^{mp}_\alpha}\boldsymbol{\eta} \end{cases} \tag{6.37}$$

where $\mathbf{B^1_{n,\beta}}$ is the part of the input matrices impacting the rigid body motion. The resulting equivalent transfer function $\mathbf{C^{mp}_\alpha}\left(s\mathbf{I} - \mathbf{A^1_n}\right)^{-1}\mathbf{B^1_{n,\beta}}$ is minimum phase.

The anti-windup is then designed using the data of this minimum phase transfer. Equations (4.66) and (4.67) are used to obtain the following compensator and updated controller dynamics:

$$\begin{cases} \dot{\boldsymbol{x}}_a &= \mathbf{A_n}\boldsymbol{x}_a + \mathbf{B_{n,\beta}}v_1 - \mathbf{B_{n,\beta}}\left(y_K - \text{sat}^{\overline{\beta}}_{\underline{\beta}}(y_K)\right) \\ \boldsymbol{y}_a &= \boldsymbol{x}_a \\ v_1 &= -\boldsymbol{K}^{mp}_{\text{oist}}(t)\boldsymbol{x}_a \\ \boldsymbol{v}_2 &= \boldsymbol{y}_a \end{cases} \tag{6.38}$$

where $\boldsymbol{x}_a \in \mathbb{R}^{13}$ is the anti-windup compensator state, $\text{sat}^{\overline{\beta}}_{\underline{\beta}}(y_K)$ is the OIST stage output and $\boldsymbol{K}^{mp}_{\text{oist}}$ is defined as:

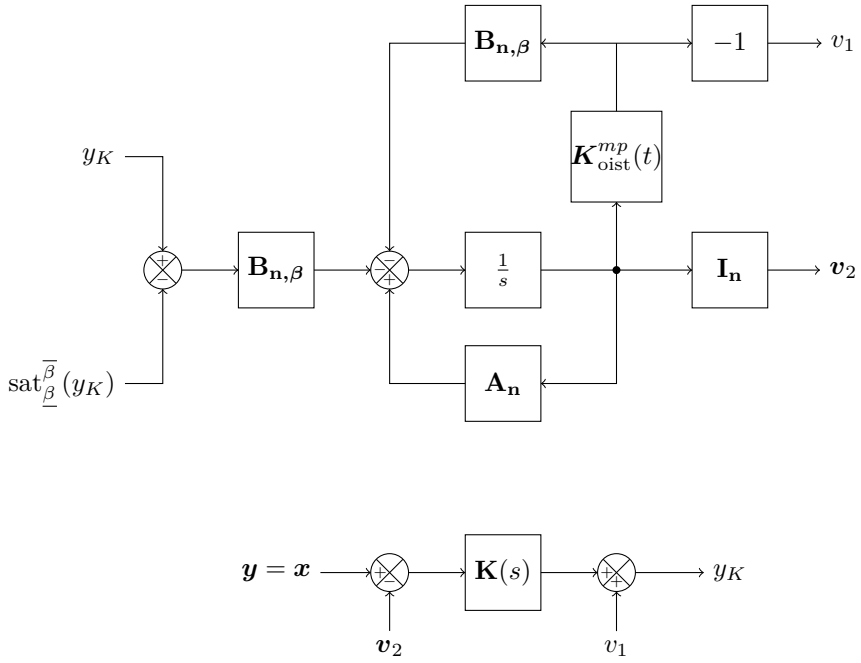

Figure 6.6: Example 6.3.1: considered interconnection of the designed anti-windup (6.38) and controller (6.40).

$$\boldsymbol{K}^{mp}_{\text{oist}}(t) = \frac{\kappa_1(t)\mathbf{C}^{\mathbf{mp}}_{\boldsymbol{\alpha}} + \mathbf{C}^{\mathbf{mp}}_{\boldsymbol{\alpha}}\mathbf{A_n}}{\mathbf{C}^{\mathbf{mp}}_{\boldsymbol{\alpha}}\mathbf{B_{n,\beta}}} \tag{6.39}$$

The controller inputs and outputs are modified consequently to avoid state divergence upon saturations of the system input:

$$(\mathbf{K}) \begin{cases} \dot{\boldsymbol{x}}_K &= \mathbf{A_K}\boldsymbol{x}_K + \mathbf{B_K}\left(\boldsymbol{y} - \boldsymbol{v}_2\right) \\ y_K &= \mathbf{C_K}\boldsymbol{x}_K + \mathbf{D_K}\left(\boldsymbol{y} - \boldsymbol{v}_2\right) + v_1 \end{cases} \tag{6.40}$$

The anti-windup and controller interconnection is illustrated in Fig. 6.6.

6.3.1 (d) Simulation results

The model considered in 6.3.2 (a) is simulated over 500s using the custom wind profile represented in Fig. 6.7 with its known bounds in black lines. The constrained output α is expected to satisfy the constraint $\alpha \in [\underline{\alpha}, \overline{\alpha}]$ where $\overline{\alpha} = -\underline{\alpha} = 2.5°$. This is equivalently translated as a constraint on $\tilde{\alpha}$. The simulations are performed w/ or w/o the OIST stage in the loop (resp. plain and dashed blue line in the figures). With OIST in the loop, two simulations are also performed: w/ or w/o the anti-windup compensator and compensated controller provided in (6.38) and (6.40) (resp. plain blue and plain red line in the figures). The design coefficient κ_1 is chosen as in (6.34) with $\breve{\kappa}_1 = 0.2$ w/o the anti-windup compensator and $\breve{\kappa}_1 = 0.1$ w/ the compensator. These different choices are made to avoid peaking when saturating the control input upon violation of the output constraint. Simulation results are represented in Figs. 6.8 and 6.9. It can be seen in Fig. 6.8(b) that the original controller does not satisfy the considered time-domain requirement (the dashed blue line crosses the constraint which is represented in black).

The results shown in Fig. 6.8 are satisfying. The introduction of OIST saturations in the loop helps to satisfy the considered time-domain constraint on output $\tilde{\alpha}$. Note that the constraint is enforced at the cost of some conservatism as can be seen in Fig. 6.8(b) where the gap between the actual $\tilde{\alpha}$ value and the constraint is caused by the lack of knowledge on the disturbance input d. More precisely, this is due to the difference $\overline{d} - \underline{d}$ which is obviously not null. The introduction of the anti-windup compensator (6.38) in the loop slightly increases the performance. Overall,

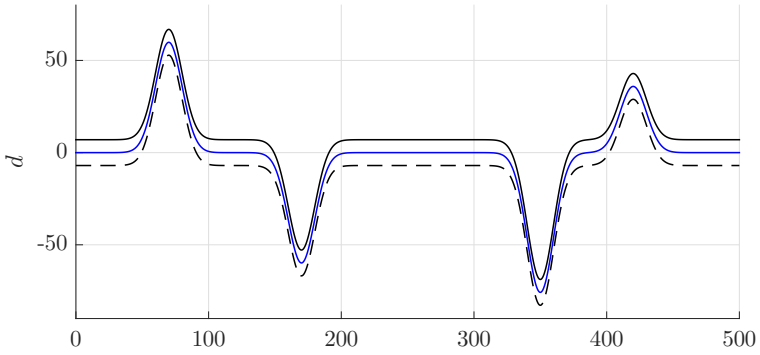

Figure 6.7: Custom wind profile used in simulation for the examples related to output-constrained control.

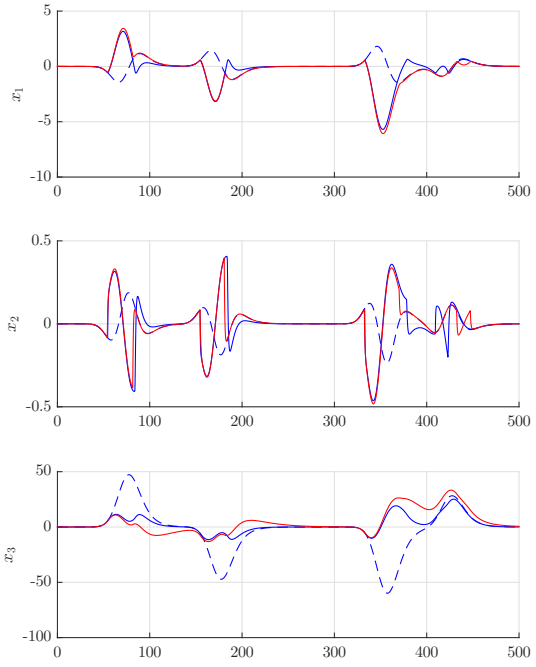

(a) State simulation results w/ (resp. w/o) OISTeR in the loop in plain (resp. dashed) blue. Results with the anti-windup compensator in (6.38) are represented in red.

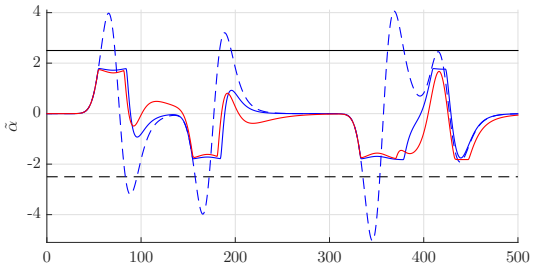

(b) In plain (resp. dashed) blue line: constrained output $\tilde{\alpha}$ simulation results w/ (resp. w/o) OISTeR in the loop. In red: with the anti-windup compensator in the loop.

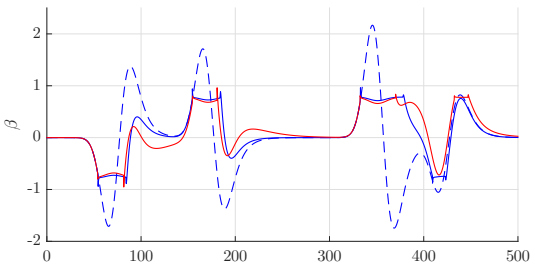

(c) In plain (resp. dashed) blue line: control input u simulation results w/ (resp. w/o) OISTeR in the loop. In red: with the anti-windup compensator.

Figure 6.8: Example 6.3.1: state, constrained output and control input simulation results w/ or w/o OIST in the loop and w/ or w/o an anti-windup compensator in the saturated case.

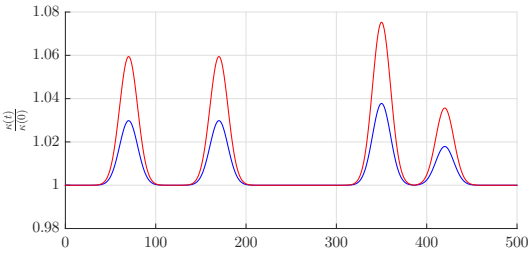

(a) Design coefficient $\frac{\kappa_1(t)}{\kappa_1(0)}$ (6.34) simulation results. In red: when additionally using the anti-windup compensator.

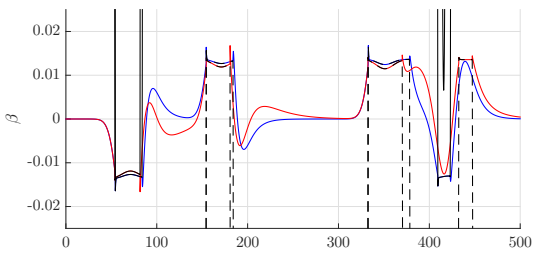

(b) Control input β and OISTeR saturations (in black) when using OISTeR in the loop. In red: when additionally using the anti-windup compensator.

Figure 6.9: Example 6.3.1: design coefficient κ_1 and control input β simulation results.

the control law saturates for shorter periods of time. The practical modification brought to account for the non-minimum phase transfer $T_{\beta\to\tilde{\alpha}}(s)$ is mandatory to avoid divergence upon saturation. Using the original transfer defined by the matrix $\mathbf{C_\alpha}$ in lieu of $\mathbf{C_\alpha^{mp}}$ in the anti-windup compensator definition (6.38) leads to controller and system states divergence. Note that the constant $\breve{\kappa}_1$ is chosen small (< 0.2 in both cases, i.e. w/ or w/o the anti-windup compensator). This helps to avoid peaking upon saturation of the control signal.

The time-varying design coefficient κ_1 and the saturated control input β along with the OIST saturations are represented in Fig. 6.8 in both the w/ and w/o anti-windup compensator cases. The low value chosen for $\breve{\kappa}_1$ helps to avoid peaking of the control law when activation of a saturation upon violation of the output constraint.

6.3.1 (e) Conclusions

In this section, the OIST approach to output-constrained control has been successfully applied to the flexible launch vehicle with no uncertainty and a known state vector $\boldsymbol{x}$. The dynamic controller ($\mathbf{K}$) did not initially satisfy the time-domain requirement on the angle of attack. After application of OIST, this requirement is enforced using the appropriately defined control input signal $\beta = \text{sat}_{\underline{\beta}}^{\overline{\beta}}(y_K)$. Performance is slightly increased using an appropriately defined anti-windup compensator: using a practical modification of the initially non-minimum phase transfer $T_{\beta\to\tilde{\alpha}}(s)$ the matrix $\mathbf{A} - \mathbf{B_{n,\beta}} \boldsymbol{K}_{\text{oist}}^{mp}(t)$ is ensured to be Hurwitz $\forall t$. Also, some elements of OISTeR were used to reduce the conservatism of the original OIST approach for transfers with relative degree 0 with respect to the disturbance input d.

Long-term approaches should focus on a theoretical approach to applying OIST on non-minimum phase transfers so as to obtain a sufficiently wide basin of attraction. In the next section, OISTeR is applied to the output-constrained control of the rigid launch vehicle model with incomplete state measurements.

6.3.2 Application of OISTeR to the rigid launch vehicle model

A model of the rigid launch vehicle with incomplete state measurements is considered for application of OISTeR. In this example, satisfying results are obtained when using a particular reduced-order interval observer which helps reducing the inherent OISTeR conservatism.

6.3.2 (a) Considered model: no uncertainty, rigid with incomplete measurements

In this example, no uncertainty nor flexible mode is considered. The rigid body dynamics is given by the following state-space representation:

$$(\mathbf{G_3}) \begin{cases} \dot{\boldsymbol{x}} &= \mathbf{A}\boldsymbol{x} + \mathbf{B}_{\boldsymbol{\beta}}\beta + \mathbf{B_d}d \\ \boldsymbol{y} &= \mathbf{C}\boldsymbol{x} \end{cases} \tag{6.41}$$

where $\boldsymbol{x} = \begin{bmatrix} \psi \\ \dot{\psi} \\ \dot{z} \end{bmatrix} \in \mathbb{R}^3$ and $\boldsymbol{y} = \begin{bmatrix} \psi \\ \dot{\psi} \end{bmatrix}$. The matrix $\mathbf{A} = \mathbf{A_n^1}$ is not Hurwitz with two unstable real poles. The matrices $\mathbf{B}_{\boldsymbol{\beta}}$ and $\mathbf{B_d}$ are appropriately defined matrices deduced from $\mathbf{B_{n,\beta}}$ and $\mathbf{B_{n,w}}$ in (6.12). As stated in 6.1.4, $(\mathbf{G_3})$ is output controllable. This means there exists a static gain $\boldsymbol{K} \in \mathbb{R}^{1\times 2}$ such that $\mathbf{A} - \mathbf{B}_{\boldsymbol{\beta}}\boldsymbol{K}\mathbf{C}$ is Hurwitz. This is used in the following.

6.3.2 (b) Output-feedback static controller

The system being output controllable, the following control law is considered:

$$\beta = -\boldsymbol{K}\boldsymbol{y} + v \tag{6.42}$$

where $\boldsymbol{K} \in \mathbb{R}^{1\times 2}$ is such that $\mathbf{A} - \mathbf{B}_{\boldsymbol{\beta}}\boldsymbol{K}\mathbf{C}$ is Hurwitz and v is the corrective input introduced with the OISTeR approach in Chapter 5. This results in the following closed-loop dynamics:

$$\begin{cases} \dot{\boldsymbol{x}} &= (\mathbf{A} - \mathbf{B_u}\boldsymbol{K}\mathbf{C})\,\boldsymbol{x} &+ \mathbf{B}_{\boldsymbol{\beta}} v + \mathbf{B_d} d \\ &= \mathbf{M}\boldsymbol{x} &+ \mathbf{B}_{\boldsymbol{\beta}} v + \mathbf{B_d} d \\ \boldsymbol{y} &= \mathbf{C}\boldsymbol{x} & \end{cases} \tag{6.43}$$

It is supposed that bounds $[\underline{d}, \overline{d}]$ are known $\forall t$ on the unknown disturbance d. The following notations are considered for future use:

$$\mathbf{M} = \mathbf{A} - \mathbf{B}_{\boldsymbol{\beta}}\boldsymbol{K}\mathbf{C} = \begin{bmatrix} \mathbf{M}_{11} & \mathbf{M}_{12} \\ \mathbf{M}_{21} & \mathbf{M}_{22} \end{bmatrix} \tag{6.44}$$

where $\mathbf{M}_{11} \in \mathbb{R}^{2\times 2}$, $\mathbf{M}_{12} \in \mathbb{R}^{2\times 1}$, $\mathbf{M}_{21} \in \mathbb{R}^{1\times 2}$ and $\mathbf{M}_{22} \in \mathbb{R}$.

6.3.2 (c) OISTeR application

The objective is still to constrain the angle of attack such that $\alpha \in [\underline{\alpha}, \overline{\alpha}]$, $\forall t$. This time however the problem is more difficult since it is supposed that only $\boldsymbol{y} = \begin{bmatrix} \psi \\ \dot{\psi} \end{bmatrix} = \begin{bmatrix} \boldsymbol{x}_1 \\ \boldsymbol{x}_2 \end{bmatrix}$ is known and not the whole state vector $\boldsymbol{x}$. Especially, the value of the state $\boldsymbol{x}_3 = \dot{z}$ is unknown. This motivates using the OISTeR approach to enforce the time-domain constraint on α.

For similar reasons as those stated in 6.3.1, the actual considered constrained output is $\tilde{\alpha} = -\alpha$. This allows a proper definition of the saturations provided by OISTeR. More details are given on the subject in Remark 5.20.

Reduced-order interval observer Unsatisfying results were obtained when considering an interval observer on the whole state $\boldsymbol{x}$. This resulted from the difficulty to design an interval observer which provided a sufficiently tight interval. A natural workaround is to exploit the knowledge on parts of the state vector $\boldsymbol{x}$ and use a reduced-order interval observer on the remaining state variables. Reduced-order interval observers have been for example considered in [Efimov 13c].

In the considered case, a reduced-order interval observer is designed on $\boldsymbol{x}_3 = \dot{z}$. Let write $(\mathbf{G_3})$ in (6.41) in the following form:

$$(\mathbf{G_3}) \begin{cases} \dot{\boldsymbol{y}} &= \mathbf{M}_{11}\boldsymbol{y} + \mathbf{M}_{12}\boldsymbol{x}_3 + \mathbf{B}_{\boldsymbol{\beta},\mathbf{1}} v + \mathbf{B_{d,1}} d \\ \dot{\boldsymbol{x}}_3 &= \mathbf{M}_{22}\boldsymbol{x}_3 + \mathbf{M}_{21}\boldsymbol{y} + \mathbf{B}_{\boldsymbol{\beta},\mathbf{2}} v + \mathbf{B_{d,2}} d \end{cases} \tag{6.45}$$

where the input matrices are appropriately defined. Noting that $\mathbf{M}_{22} \in \mathbb{R}$ is Hurwitz (by definition of the model) and Metzler[1], the following system is an interval observer of $\boldsymbol{x}_3$:

$$\begin{array}{rcl} \dot{\underline{\boldsymbol{x}_3}} &=& \mathbf{M}_{22}\underline{\boldsymbol{x}_3} + \mathbf{M_{21}}\boldsymbol{y} + \mathbf{B}_{\boldsymbol{\beta},\mathbf{2}} v + \mathbf{B_{d,2}}\underline{d} \\ \dot{\overline{\boldsymbol{x}_3}} &=& \mathbf{M}_{22}\overline{\boldsymbol{x}_3} + \mathbf{M_{21}}\boldsymbol{y} + \mathbf{B}_{\boldsymbol{\beta},\mathbf{2}} v + \mathbf{B_{d,2}}\overline{d} \end{array} \tag{6.46}$$

[1] A real number is a degenerated form of Metzler matrix.

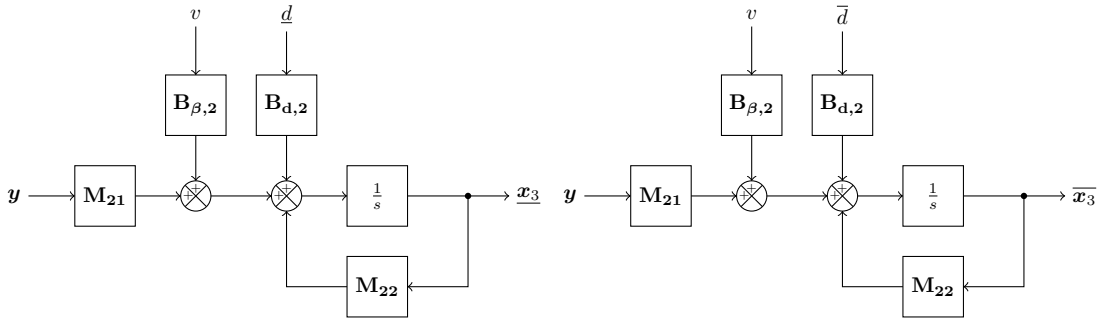

Figure 6.10: Example 6.3.2 reduced-order interval observer of state $\boldsymbol{x}_3$. The input vector $\boldsymbol{y}$ is the measurements vector $\begin{bmatrix}\boldsymbol{x}_1\\ \boldsymbol{x}_2\end{bmatrix} = \begin{bmatrix}\psi\\ \dot{\psi}\end{bmatrix}$.

where it is used that $\mathbf{B_{d,2}} \in \mathbb{R}_+$. It is supposed in simulation that the initial state $\boldsymbol{x}_3(0)$ is known and $\underline{\boldsymbol{x}_3}(0) = \overline{\boldsymbol{x}_3}(0) = \boldsymbol{x}_3(0) = 0$. The reduced-order interval observer block diagram is represented in Fig. 6.10.

Generalized output-constraint The original constraint $\mathcal{K}(\Omega_\alpha)$ is expressed on the angle of attack α and can be easily transposed to the update constrained output $\tilde{\alpha}$. Using (6.4), $\tilde{\alpha} = -\alpha$ depends on $\boldsymbol{y}$ and $\boldsymbol{x}_3$ in the following manner:

$$\alpha = \mathbf{C_{\alpha,1}}\boldsymbol{y} + \mathbf{C_{\alpha,2}}\boldsymbol{x}_3 + \mathbf{D_\alpha} d \tag{6.47}$$

where $\mathbf{C_{\alpha,1}} = \begin{bmatrix}-1 & 0\end{bmatrix}$, $\mathbf{C_{\alpha,2}} = -\frac{1}{V}$ and $\mathbf{D_\alpha} = \frac{1}{V}$. Using the interval observer state $\begin{bmatrix}\boldsymbol{x}_3\\ \overline{\boldsymbol{x}_3}\end{bmatrix}$, the constrained output in (6.47) can be bounded by the two following quantities:

$$\begin{array}{rcl} \beta_m & = & \mathbf{C_{\alpha,1}}\boldsymbol{y} + \mathbf{C_{\alpha,2}}\overline{\boldsymbol{x}_3} + \mathbf{D_\alpha}\underline{d} \\ \beta_p & = & \mathbf{C_{\alpha,1}}\boldsymbol{y} + \mathbf{C_{\alpha,2}}\underline{\boldsymbol{x}_3} + \mathbf{D_\alpha}\overline{d} \end{array} \tag{6.48}$$

where it is used that $\mathbf{C_{\alpha,2}} < 0$ and $\mathbf{D_\alpha} > 0$. The generalized output-constraint is thus to ensure that

$$\left\{ \begin{array}{rcl} \beta_m & \geq & -\overline{\alpha} \\ \beta_p & \leq & -\underline{\alpha} \end{array} \right. \tag{6.49}$$

which can be achieved under Lemma 5.19 and application of OISTeR as detailed in Chapter 5. In the present case, the relative degree of β_m and β_p with respect to v is equal to 1. The following first derivatives are obtained using the reduced-order interval observer dynamics in (6.46) and the original system dynamics in (6.45):

$$\begin{array}{rcl} \dot{\beta}_m & = & \mathbf{C_{\alpha,1}M_{11}}\boldsymbol{y} + \mathbf{C_{\alpha,2}M_{22}}\overline{\boldsymbol{x}_3} + \mathbf{C_{\alpha,2}M_{21}}\boldsymbol{y} + \mathbf{C_{\alpha,2}B_{\beta,2}}v + \mathbf{C_{\alpha,2}B_{d,2}}\overline{d} + \mathbf{D_\alpha}\dot{\underline{d}} \\ \dot{\beta}_p & = & \mathbf{C_{\alpha,1}M_{11}}\boldsymbol{y} + \mathbf{C_{\alpha,2}M_{22}}\underline{\boldsymbol{x}_3} + \mathbf{C_{\alpha,2}M_{21}}\boldsymbol{y} + \mathbf{C_{\alpha,2}B_{\beta,2}}v + \mathbf{C_{\alpha,2}B_{d,2}}\underline{d} + \mathbf{D_\alpha}\dot{\overline{d}} \end{array} \tag{6.50}$$

where it has been noted that $\mathbf{C_{\alpha,1}M_{12}} = 0$ and $\mathbf{C_{\alpha,1}B_{d,1}} = 0$. Also, by definition of the relative degree, the quantity $\mathbf{C_{\alpha,2}B_{\beta,2}}$ is non-null.

Generalized propagated bounds The generalized propagated bounds are defined as in Definition 5.18. Let $\underline{\beta}_0 = -\overline{\alpha}$ and $\overline{\beta}_0 = -\underline{\alpha}$. The relative degree of β_m and β_p with respect to v equals 1 hence, the following is also used:

$$\begin{array}{rcl} \underline{\beta}_1 & = & \kappa_1\left(\underline{\beta}_0 - \beta_m\right) + \dot{\underline{\beta}}_0 \\ \overline{\beta}_1 & = & \kappa_1\left(\overline{\beta}_0 - \beta_p\right) + \dot{\overline{\beta}}_0 \end{array} \tag{6.51}$$

where κ_1 is a design parameter defined later. Under Lemma 5.19, the following is satisfied:

$$\left\{ \begin{array}{rcl} \dot{\beta}_m & \geq & \underline{\beta}_1 \\ \dot{\beta}_p & \leq & \overline{\beta}_1 \end{array} \right. , \forall t \in \mathbb{R}_+ \Rightarrow \left\{ \begin{array}{rcl} \beta_m & \geq & \underline{\beta}_0 \\ \beta_p & \leq & \overline{\beta}_0 \end{array} \right. \tag{6.52}$$

where the dependence of $\dot{\beta}_m$ and $\dot{\beta}_p$ on v can be used to obtained the OISTeR saturations on the corrective signal v.

Resulting control saturations Using Lemma 5.19, the following saturations on the corrective input signal v are obtained:

$$\begin{array}{rcl} \underline{v} & = & \frac{1}{\mathbf{C_{\alpha,2}B_{\beta,2}}} \left[\underline{\beta}_1 - (\mathbf{C_{\alpha,1}M_{11}} + \mathbf{C_{\alpha,2}M_{21}})\, \boldsymbol{y} - \mathbf{C_{\alpha,2}M_{22}} \overline{\boldsymbol{x}}_3 - \mathbf{C_{\alpha,2}B_{d,2}} \overline{d} - \mathbf{D_\alpha} \dot{\underline{d}} \right] \\ \overline{v} & = & \frac{1}{\mathbf{C_{\alpha,2}B_{\beta,2}}} \left[\overline{\beta}_1 - (\mathbf{C_{\alpha,1}M_{11}} + \mathbf{C_{\alpha,2}M_{21}})\, \boldsymbol{y} - \mathbf{C_{\alpha,2}M_{22}} \underline{\boldsymbol{x}}_3 - \mathbf{C_{\alpha,2}B_{d,2}} \underline{d} - \mathbf{D_\alpha} \dot{\overline{d}} \right] \end{array} \tag{6.53}$$

where $\mathbf{C_{\alpha,2}B_{\beta,2}} > 0$. The expression of the design coefficient κ_1 is obtained using Theorem 5.22. The condition is that $\overline{v} - \underline{v} > 0$. Let $\breve{\kappa}_1 = 0.1$. Saturations overlap is mitigated for κ_1 chosen as follows:

$$\kappa_1 = \frac{\breve{\kappa}_1 - \mathbf{C_{\alpha,2}M_{22}} \left(\overline{\boldsymbol{x}}_3 - \underline{\boldsymbol{x}}_3 \right) - \mathbf{C_{\alpha,2}B_{d,2}} \left(\overline{d} - \underline{d} \right) + \mathbf{D_\alpha} \left(\dot{\overline{d}} - \dot{\underline{d}} \right)}{\overline{\alpha} - \underline{\alpha} + \mathbf{C_{\alpha,2}} \left(\overline{x}_3 - \underline{x}_3 \right) - \mathbf{D_\alpha} \left(\overline{d} - \underline{d} \right)} \tag{6.54}$$

6.3.2 (d) Simulation results

The model considered in 6.3.2 (a) is simulated over 500s using the same disturbance input d as in the previous example (see Fig. 6.7). The initial condition is set to $\boldsymbol{x}_0 = \mathbf{0}$. The constrained output α is expected to satisfy the constraint $\alpha \in [\underline{\alpha}, \overline{\alpha}]$ where $\overline{\alpha} = -\underline{\alpha} = 3°$. This is equivalently translated into a constraint on $\tilde{\alpha}$. The design coefficient κ_1 is chosen as in (6.54) with $\breve{\kappa}_1 = 0.1$. Simulation results are represented in Figs. 6.11 and 6.12 for both the unconstrained system (dashed blue line) and the system in closed-loop with the OISTeR saturations (plain blue line). It can be seen in Fig. 6.11(b) that the original controller $\beta = -\boldsymbol{K}\boldsymbol{x}$ does not satisfy the considered time-domain requirement.

The results shown in Fig. 6.11 are highly satisfactory. Despite the lack of knowledge on $\boldsymbol{x}_3$ the output constraint is enforced thanks to using a reduced-order interval observer. As visible in Fig. 6.11(b), this results in some conservatism which adds to the lack of knowledge on the disturbance. However, using the information on ψ and $\dot{\psi}$ given by the measurements vector $\boldsymbol{y}$, this conservatism is reduced in comparison with using a full-order interval observer on the complete state vector $\boldsymbol{x}$. Note that the constant $\breve{\kappa}_1 = 0.1$ is chosen small such that the saturated corrective input signal variations are smoother than for greater values (e.g. $\breve{\kappa}_1 = 1$).

The time-varying design coefficient κ_1 and the corrective input v along with the OISTeR saturations $\underline{v}$ and $\overline{v}$ are represented in Fig. 6.12.

As mentioned previously, the low value chosen for $\breve{\kappa}_1$ helps to obtain a quite smooth corrective input signal v. For greater values of $\breve{\kappa}_1$, peaking artefacts can be observed at the times of saturation. This illustrates the challenges faced by the control designer when tuning the design coefficients in $\boldsymbol{\kappa}$ as already mentioned in Chapters 4 and 5.

6.3.2 (e) Conclusions

In this section, OISTeR has been successfully applied to the rigid body dynamics of the considered launch vehicle. The static controller $\boldsymbol{K}$ initially used did not satisfy the time-domain requirement on the angle of attack. After application of OISTeR, this requirement is enforced using the appropriately defined corrective input signal $v = \mathrm{sat}_{\underline{v}}^{\overline{v}}(0)$.

However, the considered model does not take any uncertainty into account. A short-term perspective is thus to apply a similar approach to the uncertain rigid body dynamics of the launch vehicle. The coefficients A_6 and K_1 respectively describing aerodynamic and thrust efficiency

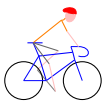

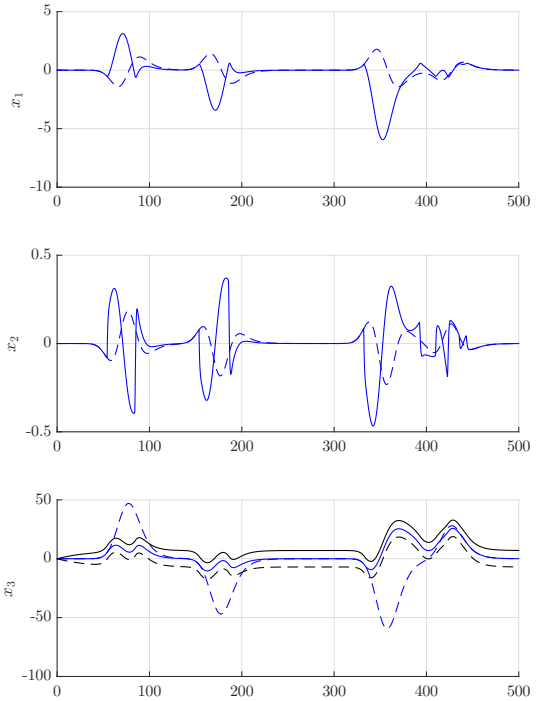

(a) State simulation results w/ (resp. w/o) OISTeR in the loop in plain (resp. dashed) blue. The reduced-order interval observer on $\boldsymbol{x}_3$ output is represented in black lines.

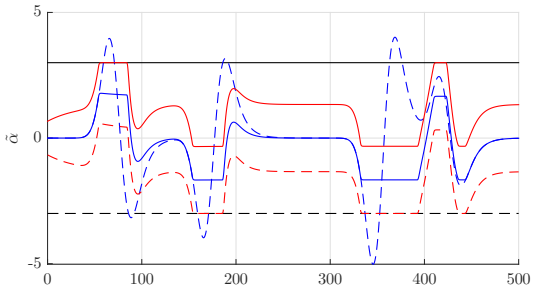

(b) In plain (resp. dashed) blue line: constrained output $\tilde{\alpha}$ simulation results w/ (resp. w/o) OISTeR in the loop. Bounds on $\tilde{\alpha}$ are represented in red as provided by the interval observer.

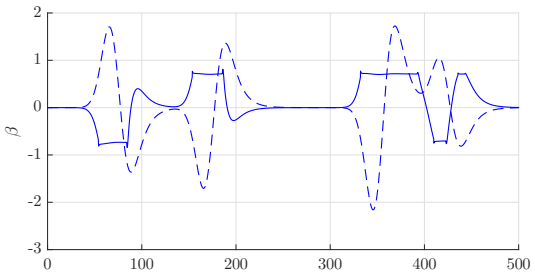

(c) In plain (resp. dashed) blue line: control input u simulation results w/ (resp. w/o) OISTeR in the loop. In the OISTeR case, the control input is given by $\beta = -\boldsymbol{K}\boldsymbol{x} + v$.

Figure 6.11: Example 6.3.2: state, constrained output and control input $\beta = -\boldsymbol{K}\boldsymbol{x}+v$ simulation results.

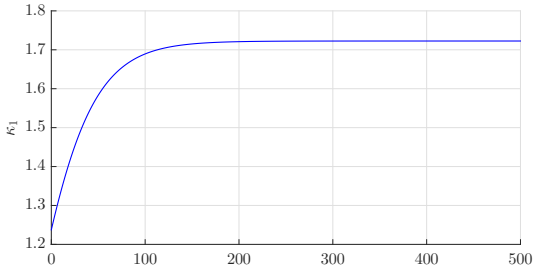

(a) Design coefficient κ_1 (6.54) simulation results.

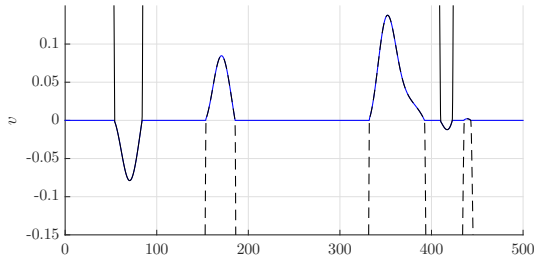

(b) Corrective input v and OISTeR saturations (in black) when using OISTeR in the loop.

Figure 6.12: Example 6.3.2: design coefficient κ_1 and corrective input v simulation results.

would be the uncertain parameters in that case. Also, it can be noted that a specific approach has been used to reduce OISTeR conservatism and use the available data in $\boldsymbol{y}$. A reduced-interval observer has been implemented and produces satisfying results. A medium-term perspective is to generalize such approach and update the conservative expressions obtained in Chapter 5. On the long term, extension of the OISTeR to LPV/LTV systems could be applied to multiple working points of the launch vehicle model.

6.4 Conclusions and perspectives

The main contributions of this thesis work have been successfully applied to different simplified models of the launch vehicle. As far as the output-constrained control problem is concerned, satisfying results have been obtained when considering the OIST and OISTeR approaches. Practical approaches have also been proposed to answer for the non-minimum phase property of the transfer between the control input β and the constrained output describing the evolution of the angle of attack α.

However, as already underlined in the different sections, the considered models are simplified to allow application of the OIST and OISTeR methods which are still conservative in their current forms. Future works should focus on reducing this conservatism so as to apply these methods on more complex models. Also, the extension of OISTeR to the LPV and LTV cases should allow to consider multiple working points for the launch vehicle model. A gain-scheduled approach of the OISTeR saturations could be an option to take into account the variation of the model parameters over time.

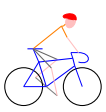

Chapter 7

Development of a non-smooth optimization-based approach to design linear interval observers

The theory of linear interval state-observers has been used in Chapter 5 without much details on the design approaches. For a given system, as far as the design of such interval observers is considered, they are often deduced from a provisional cooperative system. For any dynamical system, its cooperative representation can be obtained by considering a state-coordinate transformation (SCT). Two strategies exist: the SCT is chosen either time-varying or time-invariant. In the time-invariant case, determining an appropriate SCT remains difficult. Also, the existing approaches rely on parameters which selection impact the obtained solution. This motivates considering a new method to determine a time-invariant SCT such that the studied system is cooperative in the new coordinates. This method is called SCorpIO. This chapter is based on results presented in [Chambon 15b, Chambon 16] and [Chambon a].

Existing time-invariant SCT determination methods are presented in 7.1 along with their drawbacks. This motivates the development of a new determination method called SCorpIO. This new approach is introduced in 7.2 based on the reformulation of the original SCT determination problem into a control design problem. Application of the new method is illustrated in 7.3 where comparisons with the existing techniques are also proposed. In 7.4 it is shown that this new approach can be used to simultaneously stabilize a system and design an interval observer on the closed-loop as required in Chapter 5. Conclusions and perspectives are then drawn in 7.5.

7.1 Motivations for a new interval observer design method

The field of research dedicated to linear interval state-observers has been very active in the past few years. The unfamiliar reader may refer to Chapter B for detailed information on the subject. The objective of such dynamical systems is to provide a non-statistical estimate of the interval in which the state $\boldsymbol{x}$ of the studied system $(\mathbf{G})$ lies. This is particularly useful in the case where the system is disturbed by an unknown signal $\boldsymbol{d}$ on which bounds $\underline{\boldsymbol{d}}$ and $\overline{\boldsymbol{d}}$ are known.

Theoretically speaking, a definition of a linear interval observer is given in [Cacace 15, Definition 4, p. 1667][1]. This is a quite general definition which makes no assumption on the original system dynamics. In particular, $(\mathbf{G})$ could be non-cooperative and unstable. An interval observer is defined as a stable system and its property is to keep ordering of the estimated bounds $\underline{\boldsymbol{x}}$ and $\overline{\boldsymbol{x}}$ on the state $\boldsymbol{x}$. A practical solution to design an interval observer[2] is first to obtain a stable dynamics through using a Luenberger observer with gain $\mathbf{L}$ and then to design the interval observer on the inherent observation error $\boldsymbol{e} = \boldsymbol{x} - \widehat{\boldsymbol{x}}$. In the worst case, the observation error dynamics is not cooperative but cooperativity[3] can be enforced using an appropriate state-coordinate transformation defined by a matrix $\mathbf{P}$.

Methods to determine appropriate matrices $\mathbf{P}$ (SCT matrix) and $\mathbf{L}$ (classical observer gain) are listed in B.4. Two main strategies can be identified: either the SCT is chosen time-varying [Mazenc 11] or time-invariant [Raïssi 12].

In this section, the time-invariant strategy is recalled. The different methods are presented and their main limitations are identified. This motivates the development of a new time-invariant SCT determination method.

7.1.1 Notations and main concepts reminder

In this chapter, linear systems are considered both in the continuous-time and discrete-time frameworks. In the first case, systems are referred to using $(\mathbf{G})$ while the notation $(\mathbf{F})$ is used in the second case. The state-space representations of the considered systems are given by:

$$(\mathbf{G}) \begin{cases} \dot{\boldsymbol{x}}(t) &= \mathbf{A}\boldsymbol{x}(t) + \mathbf{B_u}\boldsymbol{u}(t) + \mathbf{B_d}\boldsymbol{d}(t) \\ \boldsymbol{y}(t) &= \mathbf{C}\boldsymbol{x}(t) + \mathbf{D_u}\boldsymbol{u}(t) + \mathbf{D_d}\boldsymbol{d}(t) \\ \boldsymbol{x}(0) &= \boldsymbol{x}_0 \\ t &\in \mathbb{R}^+ \end{cases} \tag{7.1}$$

$$(\mathbf{F}) \begin{cases} \boldsymbol{x}(t+1) &= \mathbf{A}\boldsymbol{x}(t) + \mathbf{B_u}\boldsymbol{u}(t) + \mathbf{B_d}\boldsymbol{d}(t) \\ \boldsymbol{y}(t) &= \mathbf{C}\boldsymbol{x}(t) + \mathbf{D_u}\boldsymbol{u}(t) + \mathbf{D_d}\boldsymbol{d}(t) \\ \boldsymbol{x}(0) &= \boldsymbol{x}_0 \\ t &\in \mathbb{N} \end{cases} \tag{7.2}$$

where $\boldsymbol{x} \in \mathbb{R}^n$, $\boldsymbol{y} \in \mathbb{R}^m$, $\boldsymbol{u} \in \mathbb{R}^l$ is the control input and $\boldsymbol{d} \in \mathbb{R}^k$ is an unknown input. It is supposed that two vectors $\underline{\boldsymbol{x}_0}$ and $\overline{\boldsymbol{x}_0}$ are known such that $\underline{\boldsymbol{x}_0} \leq \boldsymbol{x}_0 \leq \overline{\boldsymbol{x}_0}$. Also, it is supposed that bounds $\underline{\boldsymbol{d}}$ and $\overline{\boldsymbol{d}}$ on the unknown input signal $\boldsymbol{d}$ are known. No assumption is made on $\mathbf{A}$. The worst case where $\mathbf{A}$ is non-Hurwitz non-Metzler is thus considered.

In the continuous-time case, considering the interval observer definition in [Cacace 15], the system composed of

- the Luenberger observer with observer gain $\mathbf{L}$;
- The interval observer on the observation error expressed in new coordinates $\boldsymbol{e}_z = \mathbf{P}\boldsymbol{e}$;

[1] It is also recalled in Definition B.11.
[2] As also detailed in B.3.
[3] See Definition B.3.

- and the following reverse state-coordinate transformation:

$$\begin{cases} \underline{\boldsymbol{e}}(t) &= \mathbf{T}^{+}\underline{\boldsymbol{e}_z}(t) - \mathbf{T}^{-}\overline{\boldsymbol{e}_z}(t) \\ \overline{\boldsymbol{e}}(t) &= \mathbf{T}^{+}\overline{\boldsymbol{e}_z}(t) - \mathbf{T}^{-}\underline{\boldsymbol{e}_z}(t) \\ \underline{\boldsymbol{x}}(t) &= \widehat{\boldsymbol{x}}(t) + \underline{\boldsymbol{e}}(t) \\ \overline{\boldsymbol{x}}(t) &= \widehat{\boldsymbol{x}}(t) + \overline{\boldsymbol{e}}(t) \end{cases} \tag{7.3}$$

is an interval observer for $(\mathbf{G})$[4]. The notion of cooperative system is used to formulate this result. A similar result can be obtained in the discrete-time case. However, this result is obtained at the cost of the following assumption:

Assumption 7.1 (Known state-coordinate transformation)**.**
Let $\mathbf{A} \in \mathbb{R}^{n\times n}$ and $\mathbf{C} \in \mathbb{R}^{m\times n}$. $\exists \mathbf{P} \in \mathbb{R}^{n\times n}$ and $\mathbf{L} \in \mathbb{R}^{n\times m}$ such that $\mathbf{P}\left(\mathbf{A} - \mathbf{LC}\right)\mathbf{P}^{-1}$ is *Hurwitz Metzler* (*Schur non-negative* in the discrete-time case).

To determine appropriate matrices $\mathbf{P}$ and $\mathbf{L}$, different methods have been proposed. In case $\mathbf{P}$ and $\mathbf{L}$ are chosen time-invariant, these methods are recalled in 7.1.2.

Using the interval observer in (B.22), two additional dynamical systems are defined to describe the dynamics of the two following quantities:

$$\begin{aligned} \boldsymbol{E}_d &= \tfrac{1}{2}\left(\overline{\boldsymbol{e}_z} - \underline{\boldsymbol{e}_z}\right) \\ \boldsymbol{E}_m &= \tfrac{1}{2}\left(\overline{\boldsymbol{e}_z} + \underline{\boldsymbol{e}_z}\right) \end{aligned} \tag{7.4}$$

which are used to define what can informally be called as the "quality" of the interval observer. The vector $\boldsymbol{E}_d$ is used to quantify the tightness of the interval $\left[\underline{\boldsymbol{e}_z}, \overline{\boldsymbol{e}_z}\right]$ around the actual trajectory $\boldsymbol{e}_z$ of the interval observer of the observation error expressed in the new coordinates. The quantity $\boldsymbol{E}_m$ refers to the mean of the interval. These quantities are characterized by the following dynamics:

$$\begin{aligned} \dot{\boldsymbol{E}}_d &= \mathbf{M}\boldsymbol{E}_d + \tfrac{1}{2}\left\{\left[\mathbf{P}\left(\mathbf{B_w} - \mathbf{LD_w}\right)\right]^{+} + \left[\mathbf{P}\left(\mathbf{B_d} - \mathbf{LD_d}\right)\right]^{-}\right\}\left(\overline{\boldsymbol{d}} - \underline{\boldsymbol{d}}\right) \\ \boldsymbol{E}_d(0) &= \tfrac{1}{2}\left(\overline{\boldsymbol{e}_z}(0) - \underline{\boldsymbol{e}_z}(0)\right) \\ \dot{\boldsymbol{E}}_m &= \mathbf{M}\boldsymbol{E}_m + \tfrac{1}{2}\mathbf{P}\left(\mathbf{B_d} - \mathbf{LD_d}\right)\left(\overline{\boldsymbol{d}} + \underline{\boldsymbol{d}}\right) \\ \boldsymbol{E}_m(0) &= \tfrac{1}{2}\left(\overline{\boldsymbol{e}_z}(0) + \underline{\boldsymbol{e}_z}(0)\right) \end{aligned} \tag{7.5}$$

7.1.2 Time-invariant strategy to interval observer design

As underlined in Assumption 7.1, the objective is to find two constant matrices $\mathbf{P}$ and $\mathbf{L}$ such that $\mathbf{M} = \mathbf{P}\left(\mathbf{A} - \mathbf{LC}\right)\mathbf{P}^{-1}$ is Hurwitz Metzler. In this section, three methods are presented to determine these matrices in the continuous-time case. They are either trivial or were proposed in the literature.

7.1.2 (a) Real-constrained pole placement (trivial solution)

This trivial approach is motivated by noticing that diagonal matrices satisfy to the definition of a Metzler matrix[5]. Let consider the following assumption:

Assumption 7.2 (Real-constrained pole placement: observability condition)**.**
The pair $(\mathbf{A}, \mathbf{C})$ is either:

- observable;

[4] See Proposition B.24.
[5] See Definition B.1.

- or detectable with real unobservable eigenvalues.

Note that the mentioned form of detectability is stronger than pure detectability for which the unobservable stable modes can be complex. Then, the matrix $\mathbf{L}$ is chosen such that $\mathbf{A} - \mathbf{LC}$ only has negative real eigenvalues. This can be obtained using any usual pole placement technique where the targeted poles are real negative. Choosing $\mathbf{P}$ as the matrix of the right-hand eigenvectors leads to $\mathbf{M} = \mathbf{P}(\mathbf{A} - \mathbf{LC})\mathbf{P}^{-1}$ being diagonal. Consequently, $\mathbf{M}$ is a Metzler matrix.

Lemma 7.3 (Real-constrained pole placement method)**.**
Let $\mathbf{L} \in \mathbb{R}^{n\times m}$ such that $\mathbf{A} - \mathbf{LC}$ is Hurwitz and $eig(\mathbf{A} - \mathbf{LC}) \in \mathbb{R}^n$. Let $\mathbf{P}$ the matrix of right-hand eigenvectors of $\mathbf{A} - \mathbf{LC}$. Then

$$\mathbf{M} = \mathbf{P}(\mathbf{A} - \mathbf{LC})\mathbf{P}^{-1} \tag{7.6}$$

is diagonal Hurwitz hence is Metzler.

A detailed procedure on how to apply Lemma 7.3 is given in Fig. 7.1.

7.1.2 (b) Resolution of a Sylvester equation

This approach is presented in B.4.2 as an example of a time-invariant SCT determination method and is recalled here. It comes from rewriting the following equality

$$\mathbf{M} = \mathbf{P}(\mathbf{A} - \mathbf{LC})\mathbf{P}^{-1} \tag{7.7}$$

in the form of a Sylvester equation:

$$-\mathbf{MP} + \mathbf{PA} = \mathbf{PLC} = \mathbf{QC} \tag{7.8}$$

where $\mathbf{M}$ and $\mathbf{Q} = \mathbf{PL}$ are user-defined parameters and $\mathbf{P}$ is the variable.

Lemma 7.4 (Sylvester equation resolution method)**.**
Let $\mathbf{M} \in \mathbb{R}^{n\times n}$ such that it is Hurwitz Metzler and has no common eigenvalues with $\mathbf{A}$. Let $\mathbf{Q} \in \mathbb{R}^{n\times m}$. Then the following Sylvester equation

$$-\mathbf{MP} + \mathbf{PA} = \mathbf{QC} \tag{7.9}$$

has a unique solution $\mathbf{P} \in \mathbb{R}^{n\times n}$. Choosing $\mathbf{L} = \mathbf{P}^{-1}\mathbf{Q}$, $\mathbf{M} = \mathbf{P}(\mathbf{A} - \mathbf{LC})\mathbf{P}^{-1}$ is Hurwitz Metzler by construction.

As already mentioned in Chapter B, Sylvester equations can be solved using algorithms described in [Golub 79] or [Bartels 72]. A detailed procedure on how to apply Lemma 7.4 is given in Fig. 7.2.

7.1.2 (c) Constructive lemma based on the Sylvester equation

In [Raïssi 12] a constructive lemma was proposed to find a solution to the Sylvester equation in (7.8) without actually solving it:

Lemma 7.5 (Constructive method to solve the Sylvester equation, inspired by [Raïssi 12])**.**
Let $\mathbf{M} \in \mathbb{R}^{n\times n}$ a Metzler matrix and $\mathbf{L} \in \mathbb{R}^{n\times m}$ such that $\mathbf{A}-\mathbf{LC}$ have the same eigenvalues. If there exists two vectors $\boldsymbol{e}_1$ and $\boldsymbol{e}_2$ such that the pairs $(\mathbf{A} - \mathbf{LC}, \boldsymbol{e}_1)$ and $(\mathbf{M}, \boldsymbol{e}_2)$ are observable then

$$\mathbf{P} = \mathbf{O_2}^{-1}\mathbf{O_1} \text{ and } \mathbf{Q} = \mathbf{PL} \tag{7.10}$$

satisfy the Sylvester equation in (7.8) where

$$\mathbf{O_1} = \begin{bmatrix} \boldsymbol{e}_1 \\ \vdots \\ \boldsymbol{e}_1 (\mathbf{A} - \mathbf{LC})^{n-1} \end{bmatrix}, \mathbf{O_2} = \begin{bmatrix} \boldsymbol{e}_2 \\ \vdots \\ \boldsymbol{e}_2 \mathbf{M}^{n-1} \end{bmatrix} \tag{7.11}$$

Proof. See [Raïssi 12, Lemma 1, p. 261]. □

Contrary to the method proposed in 7.1.2 (b), the eigenvalues of $\mathbf{M}$ need to be precisely placed on the same location than the eigenvalues of $\mathbf{A} - \mathbf{LC}$. Typical structures to construct $\mathbf{M}$ include the one presented in the following example.

Example 7.6 (Metzler matrix $\mathbf{M}$ construction example, inspired by [Raïssi 12])**.** Let consider matrices $\mathbf{A} \in \mathbb{R}^{3\times3}$, $\mathbf{L} \in \mathbb{R}^3$ and $\mathbf{C} \in \mathbb{R}^{1\times3}$ such that

$$\text{eig}\,(\mathbf{A} - \mathbf{LC}) = \begin{bmatrix} -1 & -4 + \sqrt{3}\text{j} & -4 - \sqrt{3}\text{j} \end{bmatrix}$$

Then the following matrix $\mathbf{M}$ is Metzler and has the same eigenvalues than $\mathbf{A} - \mathbf{LC}$:

$$\mathbf{M} = \begin{bmatrix} -3 & 2 & 0 \\ 0 & -3 & 2 \\ 2 & 0 & -3 \end{bmatrix} \tag{7.12}$$

♣

A detailed procedure on how to apply Lemma 7.5 is given in Fig. 7.3.

7.1.2 (d) A note on the discrete-time case

In the discrete-time case, the methods described above can still be applied as long as the differing properties of the matrix $\mathbf{M}$ are respected. In particular, this matrix must be chosen Schur non-negative which further restricts the set of admissible eigenvalues of $\mathbf{A} - \mathbf{LC}$.

7.1.3 Limitations of the time-invariant SCT determination methods

In the previous section, strategies were presented to compute an appropriate time-invariant state-coordinate transformation such that a given dynamics is cooperative (and stable) in the new coordinates. These strategies are based on pole placement techniques as well as on specific equation resolution methods. Some limitations to these techniques can be identified:

1. the real-constrained pole placement approach 7.1.2 (a) is a bit too trivial. Placing poles on real negative quantities can result in very large observation gains $\mathbf{L}$ which are inappropriate in most cases;
2. The Sylvester-equation based approach 7.1.2 (b) relies too much on the definition of the expected Metzler matrix $\mathbf{M}$ (and eventually the additional parameter $\mathbf{Q}$), the selection of which is left to the control theorist. Designing a Metzler matrix with prescribed eigenvalues is difficult in the general case especially when the eigenvalues should be complex conjugates;
3. The requirement for the dynamics to be cooperative in the new coordinates is entirely left to an appropriate choice for $\mathbf{P}$. The simultaneous design of $\mathbf{P}$ and $\mathbf{L}$ could spread this constraint on both matrices to achieve better results;
4. Absolutely no consideration is given to the rejection of disturbances or additional control requirements other than pole placement whatsoever.

These limitations do not mean these techniques are not viable ones, their power relying on their ease of use. However, in more complex cases where precise control requirements should also be considered on the observer dynamics, these approaches may fail to return appropriate results. There comes the SCorpIO design method which, although being more complex to implement, provides a solution to this kind of problem and overcomes the identified limitations of the existing techniques. This new method is introduced and detailed in the next section. Detailed examples of application are presented in 7.3 and a comparison in simulation with the existing techniques is provided.

Input: observable matrices $(\mathbf{A}, \mathbf{C})$, vector $\boldsymbol{p} \in \mathbb{R}^n_-$ of targeted poles.
Output: matrices $\mathbf{P}$ and $\mathbf{L}$ such that $\mathbf{M} = \mathbf{P}(\mathbf{A} - \mathbf{LC})\mathbf{P}^{-1}$ is Hurwitz diagonal (hence Metzler)
Procedure:

1. *Pole placement*: compute $\mathbf{L}$ such that $\text{eig}(\mathbf{A} - \mathbf{LC}) = \boldsymbol{p}$;
2. *Right-hand eigenvectors*: compute the right-hand eigenvectors or $\mathbf{A} - \mathbf{LC}$;
3. *Stacking*: stack the eigenvectors in the matrix $\mathbf{P}$;
4. *Conclusion*: $\mathbf{M}$ is Hurwitz diagonal hence is Hurwitz Metzler.

Figure 7.1: Procedure to obtain a Hurwitz Metzler matrix by using real pole placement

Input: observable matrices $(\mathbf{A}, \mathbf{C})$, targeted Hurwitz Metzler matrix $\mathbf{M}$ such that $\text{eig}(\mathbf{M}) \neq \text{eig}(\mathbf{A})$, and unconstrained matrix $\mathbf{Q} \in \mathbb{R}^{n \times m}$.
Output: matrices $\mathbf{P}$ and $\mathbf{L}$ such that $\mathbf{M} = \mathbf{P}(\mathbf{A} - \mathbf{LC})\mathbf{P}^{-1}$ is Hurwitz Metzler
Procedure:

1. *Sylvester equation*: given $\mathbf{M}$ and $\mathbf{Q}$, solve $-\mathbf{MP} + \mathbf{PA} = \mathbf{QC}$ in $\mathbf{P}$;
2. *Observer gain*: let $\mathbf{L} = \mathbf{P}^{-1}\mathbf{Q}$;
3. *Conclusion*: $\mathbf{M}$ is Hurwitz Metzler by construction.

Figure 7.2: Procedure to obtain a Hurwitz Metzler matrix by solving a Sylvester equation

Input: observer gain $\mathbf{L}$ and targeted Hurwitz Metzler matrix $\mathbf{M}$ such that $\text{eig}(\mathbf{M}) = \text{eig}(\mathbf{A} - \mathbf{LC})$.
Output: matrix $\mathbf{P}$ such that $\mathbf{M} = \mathbf{P}(\mathbf{A} - \mathbf{LC})\mathbf{P}^{-1}$ is Hurwitz Metzler
Procedure:

1. *Pole placement*: determine the observer gain $\mathbf{L}$ such that $\mathbf{A} - \mathbf{LC}$ has the desired eigenvalues;
2. *Metzler matrix determination*: choose a Metzler matrix $\mathbf{M}$ such that it has the same eigenvalues than $\mathbf{A} - \mathbf{LC}$;
3. *Observability*: find $\boldsymbol{e}_1$ and $\boldsymbol{e}_2$ such that $(\mathbf{A} - \mathbf{LC}, \boldsymbol{e}_1)$ and $(\mathbf{M}, \boldsymbol{e}_2)$ are observable;
4. *Transformation*: let $\mathbf{P} = \mathbf{O_2}^{-1}\mathbf{O_1}$ where $\mathbf{O_1}$ and $\mathbf{O_2}$ are defined in (D.57);
5. *Conclusion*: $\mathbf{M}$ is Hurwitz Metzler by construction.

Figure 7.3: Procedure to obtain a Hurwitz Metzler matrix by using the constructive Lemma 7.5

7.2 Introduction to SCorpIO: a new time-invariant SCT-based design method

According to the previous section, the main criticism addressed to the existing time-invariant SCT-based methods is the lack of an automated method. Hence, choosing appropriate parameters for these methods is critical. Also, the design of $\mathbf{P}$ and $\mathbf{L}$ is never simultaneous which could restrict the set of admissible solutions.

In this section, a new method is introduced to determine a time-invariant SCT. It is called SCorpIO for *State-Coordinate Transformation Optimization for Interval Observers*. Using this approach, the matrices $\mathbf{P}$ and $\mathbf{L}$ are simultaneously computed and the involved parameters are easier to choose. Interestingly enough, control-oriented requirements can also be formulated to constrain the observer dynamics through appropriate tuning of the observer gain $\mathbf{L}$.

The original problem is first presented. It is then reformulated into a control design problem in 7.2.2. Using a non-smooth optimization-based approach inspired by the structured controller design field, a solution to this problem is proposed in 7.2.3.

7.2.1 Problem statement

The problem of designing an interval observer was tackled in Chapter B. It involves determining an appropriate state-coordinate transformation. In this case, a time-invariant state-coordinate transformation is considered. The original problem statement is recalled here:

Problem 7.7 (Time-invariant SCT determination problem (continuous-time))**.** Considering $(\mathbf{G})$ in (7.1), let suppose the pair $(\mathbf{A}, \mathbf{C})$ is detectable. Find $\mathbf{P} \in \mathbb{R}^{n\times n}$ and $\mathbf{L} \in \mathbb{R}^{n\times m}$ such that

$$\mathbf{M} = \mathbf{P}\left(\mathbf{A} - \mathbf{LC}\right)\mathbf{P}^{-1} \tag{7.13}$$

is Hurwitz Metzler.

Remark 7.8. In the discrete-time case, the matrix $\mathbf{M}$ must be Schur non-negative. ◇

Using the definition of a Metzler matrix, a first reformulation of Problem 7.7 into a conditional problem on the coefficients of $\mathbf{M}$ is proposed:

Problem 7.9 (Coefficients-based formulation of Problem 7.7 (continuous-time))**.** Considering $(\mathbf{G})$ in (7.1), let suppose the pair $(\mathbf{A}, \mathbf{C})$ is detectable. Find $\mathbf{P} \in \mathbb{R}^{n\times n}$ and $\mathbf{L} \in \mathbb{R}^{n\times m}$ such that

$$-\mathbf{M}_{ij} = -\left[\mathbf{P}\left(\mathbf{A} - \mathbf{LC}\right)\mathbf{P}^{-1}\right]_{ij} \leq 0, \forall\,(i,j) \text{ s.t. } 1 \leq i \neq j \leq n \tag{7.14}$$

and $\mathbf{A} - \mathbf{LC}$ is Hurwitz.

Remark 7.10. In the discrete-time case, the inequality in matrix (7.14) must be satisfied $\forall\,(i,j)$ and $\mathbf{A} - \mathbf{LC}$ should be Schur stable. ◇

In terms of control theory, the $n\,(n-1)$ inequalities in (7.14) are reminiscent of the stabilisation conditions on $n\,(n-1)$ "fictitious" unidimensional systems with their unique real pole located at $-\mathbf{M}_{ij}$ or, equivalently, their state-matrix equal to $-\mathbf{M}_{ij}$. This motivates the following reformulation into a structured control design problem.

7.2.2 Reformulation into a structured control design problem

It appears that enforcing the structural property for $\mathbf{M}$ to be Metzler can be viewed as a structured control design problem as hinted by the inequalities in (7.14). This is highlighted in the following proposition:

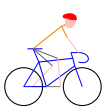

Proposition 7.11 (Equivalent control design problem (continuous-time))**.**
Considering $(\mathbf{G})$ *in* (7.1)*, let suppose the pair* $(\mathbf{A}, \mathbf{C})$ *is detectable. Let denote* $\forall (i,j) \in (\mathbb{N}^\star)^2$, $\forall \mathbf{P} \in \mathbb{R}^{n\times n}$ *and* $\forall \mathbf{L} \in \mathbb{R}^{n\times m}$

$$\mathbf{M}_{ij}(\mathbf{P}, \mathbf{L}) = \left[\mathbf{P}(\mathbf{A} - \mathbf{LC})\mathbf{P}^{-1}\right]_{ij} \tag{7.15}$$

If the system defined by the following dynamics

$$(\mathbf{G_m}) \begin{cases} \dot{\boldsymbol{x}}_l &= (\mathbf{A} - \mathbf{LC})\boldsymbol{x}_l \\ \dot{x}_{ij} &= -\mathbf{M}_{ij}(\mathbf{P}, \mathbf{L})\, x_{ij} \quad \forall i \neq j \end{cases} \tag{7.16}$$

is Hurwitz stable for a pair $(\mathbf{P_s}, \mathbf{L_s})$ *then* $\mathbf{M} = \mathbf{P_s}(\mathbf{A} - \mathbf{L_sC})\mathbf{P_s}^{-1}$ *is Hurwitz Metzler.*

Proof. The proof of this proposition is straightforward when considering the Definition B.1 of a Metzler matrix. Obviously, enforcing the stability of system $(\mathbf{G_m})$ in (7.16) is equivalent to

- determining $\mathbf{L}$ such that $\mathbf{A} - \mathbf{LC}$ is Hurwitz;
- *and* determining $\mathbf{P}$ and $\mathbf{L}$ such that $-\mathbf{M}_{ij}(\mathbf{P}, \mathbf{L})$ is negative $\forall i \neq j$.

If a solution is found to this stabilization problem then $\mathbf{M}$ is definitely Hurwitz Metzler. □

The $n(n-1)$ states $x_{ij} \in \mathbb{R}$ are informally called "fictitious" states since they do not have any physical meaning.

Remark 7.12. In the discrete-time case, n^2 "fictitious" states are considered since the diagonal elements of matrix $\mathbf{M}$ should also be positive to comply with the Definition B.2 of a non-negative matrix. However, due to the Definition of Schur stability, using Proposition 7.11 would result in $-\mathbf{M}_{ij}(\mathbf{P}, \mathbf{L})$ lying in $[-1, 1]$, $\forall (i,j)$ which does not comply with the definition of non-negativity. In that case, $(\mathbf{G_m})$ in (7.16) is replaced by the following dynamics, $\forall t \in \mathbb{N}$:

$$(\mathbf{F_m}) \begin{cases} \boldsymbol{x}_l(t+1) &= (\mathbf{A} - \mathbf{LC})\boldsymbol{x}_l(t) \\ x_{ij}(t+1) &= f\left(-\mathbf{M}_{ij}(\mathbf{P}, \mathbf{L})\right) x_{ij} \quad \forall (i,j) \end{cases} \tag{7.17}$$

where $f : \mathbb{R} \to \mathbb{R}$ is a linear function mapping $\left[-\overline{\mathbf{M_{ij}}}, 0\right]$ onto $[-1, 1]$ with $\overline{\mathbf{M_{ij}}}$ a design parameter:

$$f(x) = \frac{2}{\overline{\mathbf{M}_{ij}}} x + 1 \tag{7.18}$$

Using this function has proved to be effective in practice. From an algorithmic point of view, this means that if $x \notin \left[-\overline{\mathbf{M}_{ij}}, 0\right]$ then $f(x) \notin [-1, 1]$ and reciprocally. Note that an homographic function mapping $]-\infty, 0]$ onto $[-1, 1]$ could be used such as

$$f(x) = \frac{1}{x - \frac{1}{2}} + 1 \tag{7.19}$$

but it is observed in practice that the optimization-based algorithm described below often fails to converge when using such function. This motivated using a mapping function on a finite interval such as (7.18). ◇

7.2.3 Non-smooth optimization-based approach

Using an appropriate reformulation, the original Problem 7.7 of finding a time-invariant SCT such that the observation error dynamics is cooperative in the new coordinates has been formalized as a control design problem in Proposition 7.11.

Hence, the objective is now to find a pair $(\mathbf{P}, \mathbf{L})$ such that the system $(\mathbf{G_m})$ in (7.16) is stable. This is a pure control design problem. Additionally, other constraints can be formalized.

For example, it may be expected that the observation error dynamics[6] satisfies some rejection properties with respect to the disturbance input $\boldsymbol{d}$. Also, it is interesting to constrain the dynamics of the interval observer by enforcing rejection constraints on the dynamics of the interval tightness $\boldsymbol{E}_d$ in (7.5). Note this dynamics depends on the problem variables $\mathbf{P}$ and $\mathbf{L}$ through a non-linear max function which cannot be handled by the considered optimisation technique. Structural constraints like $\mathbf{P}\left(\mathbf{B_d}-\mathbf{LD_d}\right)\in\mathbb{R}_+^{n\times k}$ can raise this limitation.

These informally introduced constraints can be formalized into a multi-models multi-objectives optimization problem. An example of such problem is given below for the described typical requirements. Additional user-defined requirements can however be introduced depending on the considered application.

Problem 7.13 (Typical SCorpIO problem)**.**
Solve the following optimization problem:

$$\begin{aligned}&\min \max_{\mathbf{P},\mathbf{L}} \left\{ \left\| W_e(s) T_{\boldsymbol{d}\to\boldsymbol{e}}\left(s,\mathbf{L}\right)\right\|_2, \left\| W_{E_d}(s) T_{\overline{\boldsymbol{d}}-\underline{\boldsymbol{d}}\to\boldsymbol{E}_d}\left(s,\mathbf{P},\mathbf{L}\right)\right\|_2 \right\} \\ &\text{subject to } \begin{cases} (\mathbf{G_m}) \text{ in (7.16) is Hurwitz stable} \\ \mathbf{P}\left(\mathbf{B_d}-\mathbf{LD_d}\right)\in\mathbb{R}_+^{n\times k} \end{cases}\end{aligned} \tag{7.20}$$

where $W_e(s)$ and $W_{E_d}(s)$ are appropriately defined frequency-dependent weightings and the usual notation for transfer functions is used.

In the following remark, it is explained why this is a multi-models and multi-objectives optimization problem.

Remark 7.14. Since the transfers functions $T_{\boldsymbol{d}\to\boldsymbol{e}}(s)$ and $T_{\overline{\boldsymbol{d}}-\underline{\boldsymbol{d}}\to\boldsymbol{E}_d}(s)$ extracted from the models in (B.18a) and (7.5) respectively and the system $(\mathbf{G_m})$ in (7.16) are defined by different dynamics, this justifies the *multi-models* characterization of the problem. Obviously, multiple requirements are also defined which justifies the *multi-objectives* characterization. ◇

Remark 7.15. In the discrete-time case, the optimization problem in (D.61) becomes

$$\begin{aligned}&\min \max_{\mathbf{P},\mathbf{L}} \left\{ \left\| W_e(z) T_{\boldsymbol{d}\to\boldsymbol{e}}\left(z,\mathbf{L}\right)\right\|_2, \left\| W_{E_d}(z) T_{\overline{\boldsymbol{d}}-\underline{\boldsymbol{d}}\to\boldsymbol{E}_d}\left(z,\mathbf{P},\mathbf{L}\right)\right\|_2 \right\} \\ &\text{subject to } \begin{cases} (\mathbf{F_m}) \text{ in (7.17) is Schur stable} \\ \mathbf{P}\left(\mathbf{B_d}-\mathbf{LD_d}\right)\in\mathbb{R}_+^{n\times k} \end{cases}\end{aligned} \tag{7.21}$$

where the weightings are appropriately redefined. ◇

This kind of problem is reminiscent of the multi-models multi-objectives structured control design problem tackled in Chapter 2. Truly, any optimization algorithm designed to solve (D.61) can be used. In this thesis however, algorithms from the structured control design field were used, more precisely those based on H_∞ techniques. Related works are recalled here for the non-specialised reader only interested in interval observers.

The synthesis of full-order controllers through H_∞ methods has been widely studied and used in the past two decades. Solutions to the problem of H_∞ synthesis in the case of MIMO systems were provided for example in [Doyle 89] and [Scherer 90]. When considering controllers with a fixed order much lower than the original plant, the problem of finding a controller is a non-convex optimization problem. A local solution to this problem was proposed in [Apkarian 06] and implemented in consecutive works [Gahinet 11]. Other implementations for computing fixed-order controllers include [Burke 06]. More recent works [Apkarian 07, Gahinet 12, Apkarian 13, Apkarian 14] consider the case of finding a controller satisfying to multiple requirements on multiple models, eventually on limited frequency ranges. Considering these control-design techniques, it is possible to solve the minimization problems in (D.61).

Remark 7.16. The same techniques can be used in the discrete-time framework to solve the minimization problem in (7.21). ◇

[6] See system $(\mathbf{G_e})$ in (B.18a).

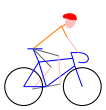

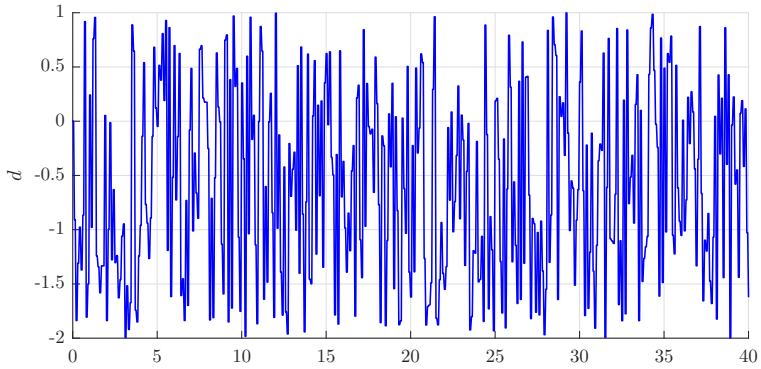

Figure 7.4: Disturbance signal d used in the simulation of (7.22).

The use of these control-design techniques to solve Problem 7.13 is now illustrated on various examples, both from the continuous- and discrete-time frameworks.

7.3 Examples and comparisons

In this section the methods presented both in this chapter and Chapter B are illustrated on various examples. This methods are used to determine a state-coordinate transformation such that a given dynamics is cooperative in the new coordinates. Both the continuous-time and discrete-time frameworks are considered. A comparison of these approaches is also proposed in simulation.

7.3.1 Continuous-time examples

7.3.1 (a) Stable sixth-order system

The SCorpIO approach is first illustrated on a stable sixth-order system inspired by [Mazenc 11].

Model The considered system is given by the following state-space representation:

$$(\mathbf{G}) \begin{cases} \dot{\boldsymbol{x}} &= \mathbf{A}\boldsymbol{x} + \mathbf{B_u} u \\ y &= \mathbf{C}\boldsymbol{x} + d \end{cases} \tag{7.22}$$

where $\boldsymbol{x} \in \mathbb{R}^6$, $u = \sin(t)$ and d is an unknown measurements disturbance with known bounds:

$$\underline{d} = -2 \leq d(t) \leq 1 = \overline{d},\ \forall t \in \mathbb{R}_+ \tag{7.23}$$

In simulation, a random number generator with limited range is used to simulate the disturbance as illustrated in Fig. 7.4. The system state-space matrices are given by:

$$\mathbf{A} = \begin{bmatrix} -1 & 1 & 0 & 0 & -1 & 0 \\ -1 & -2 & 0 & -1 & 0 & 1 \\ -2 & 0 & -3 & -2 & 0 & 0 \\ -1 & 0 & -2 & -3 & 0 & 1 \\ -1 & 0 & 2 & 0 & -4 & 0 \\ -1 & -1 & 0 & 1 & 0 & -1 \end{bmatrix}, \mathbf{B_u} = \begin{bmatrix} -18 \\ -13 \\ -5 \\ -4 \\ -10 \\ 22 \end{bmatrix}, \mathbf{C} = \begin{bmatrix} 1 & 0 & 0 & 0 & 0 & 0 \end{bmatrix} \tag{7.24}$$

Matrix $\mathbf{A}$ is Hurwitz hence the system is stable. In simulation, the initial condition is chosen equal to $\boldsymbol{x}_0 = \begin{bmatrix} 20 & 10 & 6 & 20 & 30 & 40 \end{bmatrix}^\top$. In practice, the initial condition is supposed to be unknown but lies in the known interval $\left[\underline{\boldsymbol{x}_0}, \overline{\boldsymbol{x}_0}\right]$ where $\overline{\boldsymbol{x}_0} = 50 \begin{bmatrix} 1 & 1 & 1 & 1 & 1 & 1 \end{bmatrix}^\top$ and $\underline{\boldsymbol{x}_0} = -\overline{\boldsymbol{x}_0}$.

The objective is to design an interval observer on this system. In [Mazenc 11], a time-varying SCT was considered to obtain a cooperative observation error in the new coordinates. Here, a time-invariant SCT is considered first. As detailed in Chapter B, a classical observer is used. It is initialised at $\widehat{\boldsymbol{x}_0} = \mathbf{0}_6$. The observation error dynamics is thus defined by:

$$(\mathbf{G_e}) \begin{cases} \dot{\boldsymbol{e}} &= (\mathbf{A} - \mathbf{LC})\,\boldsymbol{e} - \mathbf{L}d \\ \boldsymbol{e}_0 &= \boldsymbol{x}_0 - \widehat{\boldsymbol{x}_0} \end{cases} \tag{7.25}$$

where $\mathbf{L} \in \mathbb{R}^6$ is the observer gain and $\boldsymbol{e}_0$ lies in $\left[\underline{\boldsymbol{e}_0}, \overline{\boldsymbol{e}_0}\right] = \left[\underline{\boldsymbol{x}_0} - \widehat{\boldsymbol{x}_0}, \overline{\boldsymbol{x}_0} - \widehat{\boldsymbol{x}_0}\right]$. Note the dynamics in (7.25) is not cooperative whatever the choice of $\mathbf{L}$ since $\mathbf{A}$ is not Metzler.

Similarly to Assumption 7.1, let suppose there exists $\mathbf{P} \in \mathbb{R}^{6\times 6}$ such that $\mathbf{M} = \mathbf{P}\,(\mathbf{A} - \mathbf{LC})\,\mathbf{P}^{-1}$ is Metzler. Then, the following system is an interval observer for the observation error dynamics (7.25) in the new coordinates $\boldsymbol{e}_z = \mathbf{P}\boldsymbol{e}$:

$$(\mathbf{G_e^{z,\sharp}}) \begin{cases} \dot{\underline{\boldsymbol{e}_z}} &= \mathbf{M}\underline{\boldsymbol{e}_z} + (\mathbf{PL})^+\,\underline{d} - (\mathbf{PL})^-\,\overline{d} \\ \dot{\overline{\boldsymbol{e}_z}} &= \mathbf{M}\overline{\boldsymbol{e}_z} + (\mathbf{PL})^+\,\overline{d} - (\mathbf{PL})^-\,\underline{d} \\ \underline{\boldsymbol{e}_z}(0) &= \mathbf{P}^+\underline{\boldsymbol{e}_0} - \mathbf{P}^-\overline{\boldsymbol{e}_0} \\ \overline{\boldsymbol{e}_z}(0) &= \mathbf{P}^+\overline{\boldsymbol{e}_0} - \mathbf{P}^-\underline{\boldsymbol{e}_0} \end{cases} \tag{7.26}$$

Bounds on the state vector $\boldsymbol{x}$ are then easily determined using the relations in (7.3). The next paragraphs are dedicated to the determination of matrices $\mathbf{P}$ and $\mathbf{L}$.

SCorpIO The objective is to find $\mathbf{P}$ and $\mathbf{L}$ such that matrix $\mathbf{A} - \mathbf{LC}$ is Hurwitz (i.e. $(\mathbf{G_e})$ in (7.25) is stable) and $\mathbf{M} = \mathbf{P}\,(\mathbf{A} - \mathbf{LC})\,\mathbf{P}^{-1}$ is Metzler. To do so, the approach presented in 7.2.3 is applied and the problem is reformulated in the form of the typical SCorpIO optimization Problem 7.13. The following requirements are considered:

(1) *transformation matrices maximum elements value*: $|\mathbf{P}_{ij}| \leq 4$, $|\mathbf{T}_{ij}| \leq 4$, $\forall\,(i,j)$. This is used to avoid ill-conditioned matrices especially for the matrix $\mathbf{T}$ which is used to get back in the original coordinates;

(2) *Metzler matrix condition*: $\mathbf{M}_{ij} \geq 0$, $\forall i \neq j$;

(3) *Maximum* $\mathbf{M}$ *elements value*: $\mathbf{M}_{ij} \leq 200 = \overline{\mathbf{M}_{ij}}$, $\forall\,(i,j)$. This reduces the set of admissible solutions. In practice, it is observed that introducing this constraint helps the considered optimization algorithm[7] to converge;

(4) *Closed-loop stability*: the system (7.25) should be stable when $d = 0$ with the following constraint on the state matrix eigenvalues: $\mathrm{Re}\,(\mathrm{eig}\,(\mathbf{A} - \mathbf{LC})) \in [-100, -0.5]$;

(5) *Interval tightness*: $\left\| \frac{1}{0.7} T_{\overline{d}-\underline{d}\to \boldsymbol{E}_d}\,(s, \mathbf{P}, \mathbf{L}) \right\|_2 \leq 1$;

(6) $\boldsymbol{E}_d$ *linear dependence in* $\mathbf{PL}$ *condition*: $\mathbf{PL} \in \mathbb{R}^n_+$.

Note that conditions **(1)** to **(4)** can easily be expressed as a stabilizing condition on an augmented fictitious system similar to (7.16):

$$(\mathbf{G_m}) \begin{cases} \dot{\boldsymbol{x}}_l &= (\mathbf{A} - \mathbf{LC})\,\boldsymbol{x}_l & \\ \dot{x}^1_{ij} &= -\,(\mathbf{T}_{ij} + 4)\,x^1_{ij} & \forall\,(i,j) \\ \dot{x}^2_{ij} &= -\,(\mathbf{T}_{ij} - 4)\,x^2_{ij} & \forall\,(i,j) \\ \dot{x}^3_{ij} &= -\mathbf{M}_{ij}x^3_{ij} & \forall i \neq j \\ \dot{x}^4_{ij} &= -\,(\mathbf{M}_{ij} - 200)\,x^4_{ij} & \forall\,(i,j) \end{cases} \tag{7.27}$$

[7] In this memoir, the `systune` function from the Robust Control Toolbox [MATLAB 14] is used.

These constraints are translated in the *Robust Control Toolbox* [MATLAB 14] framework and the optimization Problem 7.13 is locally solved using `systune`. The code sample for this example is given in C.2.1. The following numerical results are obtained:

$$\mathbf{L} = \begin{bmatrix} 1.0592 \\ -1.3366 \\ -1.2349 \\ 0.2844 \\ -1.1056 \\ -0.5405 \end{bmatrix}, \mathbf{P} = \begin{bmatrix} -0.0639 & -0.2526 & -0.0267 & 0.1132 & -0.0068 & 0.0152 \\ -0.7485 & 0.1513 & -0.7132 & 0.6471 & 0.3764 & -0.6409 \\ 0.1596 & 0.0721 & 0.0259 & -0.1766 & -0.1214 & 0.2299 \\ 1.2550 & -0.7795 & 1.4395 & 2.0105 & 1.1983 & -0.2951 \\ 0.4576 & -0.5743 & -0.7134 & 0.5622 & 2.1349 & -0.1253 \\ -0.5726 & 0.0851 & -0.2180 & -0.3714 & -0.5836 & 0.1634 \end{bmatrix} \tag{7.28}$$

Note that $\mathbf{PL} \in \mathbb{R}^6_+$ hence it satisfies **(6)**. The resulting matrix is Hurwitz Metzler:

$$\mathbf{M} = \begin{bmatrix} -1.4526 & 0.2863 & 0.2218 & 0.0000 & 0.0002 & 0.0004 \\ 0.0001 & -2.1836 & 0.1270 & 0.1011 & 0.0614 & 0.2945 \\ 0.0568 & 0.2193 & -0.8111 & 0.2328 & 0.0486 & 0.4070 \\ 0.0265 & 0.0358 & 0.0005 & -3.6816 & 0.0004 & 2.8285 \\ 0.0333 & 0.2929 & 0.0001 & 1.5194 & -4.8914 & 0.8313 \\ 0.7067 & 0.0003 & 0.0920 & 0.2071 & 0.6954 & -2.0389 \end{bmatrix} \tag{7.29}$$

Other time-invariant SCT determination methods In this example, the matrix $\mathbf{M}$ is expected to have poles at these locations:

$$\boldsymbol{p}_M = \begin{bmatrix} -4.7 & -4.6 & -2.1 & -1.2 & -1.1 & -0.3 \end{bmatrix} \tag{7.30}$$

1. *Sylvester equation resolution*: see B.5.2 for the numerical results;
2. *Real-constrained pole placement*: as explained in 7.1.2 (a), this technique is based on the diagonalization of $\mathbf{A} - \mathbf{LC}$. The following numerical results are obtained:

$$\mathbf{L} = \begin{bmatrix} -0.0000 \\ -1.2981 \\ -1.1800 \\ -1.0496 \\ -0.0981 \\ -0.3113 \end{bmatrix}, \mathbf{P} = \begin{bmatrix} -2.5932 & 1.9801 & -9.9547 & -12.1661 & -3.7046 & 2.7530 \\ -2.8007 & 2.1553 & -9.4734 & -12.2466 & -4.6679 & 2.8031 \\ 1.6458 & -0.1905 & 1.6282 & -1.5989 & -0.8662 & 1.6268 \\ -20.6249 & -16.3609 & -11.6690 & 17.8681 & 7.3660 & -7.5362 \\ 19.8606 & 16.2310 & 10.4293 & -16.7563 & -6.8485 & 5.2526 \\ 0.0250 & 0.4350 & 0.6878 & -0.9352 & -0.0068 & -0.7146 \end{bmatrix} \tag{7.31}$$

   and $\mathbf{M} = \operatorname{diag}(\boldsymbol{p}_M)$ up to numerical errors.

3. *Lemma 7.5-based approach*: the constructive Lemma 7.5 is used. The observability condition is satisfied with the following vectors:

$$\boldsymbol{e}_1 = \begin{bmatrix} 1 & 0 & 0 & 0 & 0 & 0 \end{bmatrix}, \boldsymbol{e}_2 = \begin{bmatrix} 1 & 1 & 0 & 0 & 0 & 0 \end{bmatrix} \tag{7.32}$$

   The following matrix $\mathbf{M}$ is chosen:

$$\mathbf{M} = \begin{bmatrix} -4.7000 & 1.0000 & 1.0000 & 1.0000 & 1.0000 & 1.0000 \\ 0 & -4.6000 & 1.0000 & 1.0000 & 1.0000 & 1.0000 \\ 0 & 0 & -2.1000 & 1.0000 & 1.0000 & 1.0000 \\ 0 & 0 & 0 & -1.2000 & 1.0000 & 1.0000 \\ 0 & 0 & 0 & 0 & -1.1000 & 1.0000 \\ 0 & 0 & 0 & 0 & 0 & -0.3000 \end{bmatrix} \tag{7.33}$$

   and the poles of the classical observer are placed at $\boldsymbol{p}_M$ using the following observer gain:

$$\mathbf{L} = \begin{bmatrix} -0.0000 \\ -1.2981 \\ -1.1800 \\ -1.0496 \\ -0.0981 \\ -0.3113 \end{bmatrix} \tag{7.34}$$

Then, using the definitions of $\mathbf{O_1}$ and $\mathbf{O_2}$ and $\mathbf{P} = \mathbf{O_2}^{-1}\mathbf{O_1}$, the following numerical results are obtained:

$$\mathbf{P} = \begin{bmatrix} 0.5183 & 0.0135 & -0.2614 & -0.2652 & 0.0159 & 0.0607 \\ 0.4817 & -0.0135 & 0.2614 & 0.2652 & -0.0159 & -0.0607 \\ 0.7678 & -0.0868 & 0.1875 & -0.2260 & -0.3072 & 0.1648 \\ 0.0183 & 0.0676 & -0.5454 & 0.4758 & 0.0920 & -0.5624 \\ 0.8023 & 0.5856 & 0.3072 & -0.5223 & -0.2770 & 0.3342 \\ -0.0034 & -0.0589 & -0.0931 & 0.1266 & 0.0009 & 0.0967 \end{bmatrix} \tag{7.35}$$

Time-varying SCT determination, for comparison Please refer to B.4.1 for a detailed explanation of the method and to B.5.1 for the numerical results.

Simulations The system in (7.22) is simulated over 40s along with the interval observer designed using the techniques presented in both this chapter and Chapter B. The simulation results are shown in Fig. 7.5. The system state is represented in plain blue while the interval observer state is represented in plain red when using the SCorpIO design method. The bounds obtained using existing techniques are represented in black.

These simulations show that the proposed technique is a viable interval observer design approach. In comparison with the existing techniques which produce time-invariant SCTs, our technique provides better results. This is closely related to the fact that control-oriented requirements can actually be enforced using the considered optimization-based approach: the obtained interval is tighter thanks to appropriate disturbance rejection and constraints on the transformation matrices elements. Also, the poles of the classical observer can be constrained to accelerate the dynamics. Of course, better results could be obtained when using the existing techniques by choosing a more appropriate vector $\boldsymbol{p}_M$. This shows however that the ability to simultaneously tune $\mathbf{P}$ and $\mathbf{L}$ is interesting since this reduces the need to use trial-and-error-based studies.

When compared to the method presented in [Mazenc 11], our approach performs slightly worse especially in terms of convergence speed. This could be improved by setting stricter constraints on the pole location at the cost of a bigger interval. In terms of interval tightness, both approaches are comparable with a small advantage to the time-varying SCT-based one. However, this does not contradict our objective to design an efficient time-invariant SCT determination method.

7.3.1 (b) Unstable third-order system

The same study is now performed on an unstable third-order system inspired by [Raïssi 12]. Contrary to the previous example where the disturbance was a measurements disturbance, a state disturbance is now considered.

Model The considered system is given by the following state-space representation:

$$(\mathbf{G}) \begin{cases} \dot{\boldsymbol{x}} &= \mathbf{A}\boldsymbol{x} + \mathbf{B_d}d \\ y &= \mathbf{C}\boldsymbol{x} \end{cases} \tag{7.36}$$

where $\boldsymbol{x} \in \mathbb{R}^3$ and d is an unknown yet bounded state disturbance with known bounds:

$$\underline{d} = -1 \leq d(t) \leq 1 = \overline{d},\ \forall t \in \mathbb{R}_+ \tag{7.37}$$

The signal $d(t) = \sin(2t)$ is used in simulation. The system state-space matrices are given by:

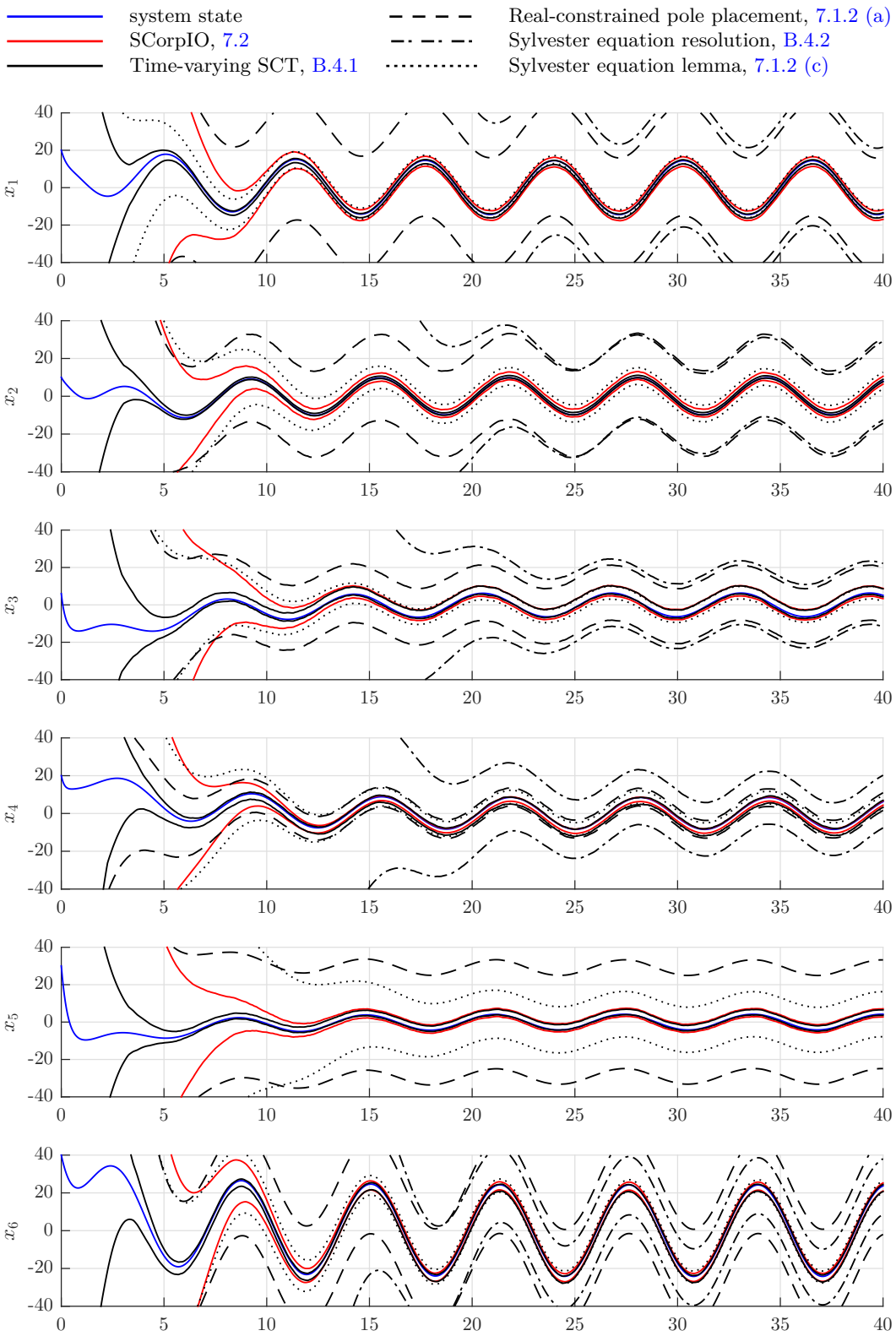

Figure 7.5: System (7.22) simulation with a comparison of bounds obtained using various interval observer design methods.

$$\mathbf{A} = \begin{bmatrix} 2 & 0 & 0 \\ 1 & -4 & \sqrt{3} \\ -1 & -\sqrt{3} & -4 \end{bmatrix}, \mathbf{B_d} = \begin{bmatrix} -1 \\ 0 \\ 1 \end{bmatrix}, \mathbf{C} = \begin{bmatrix} 1 & 0 & 0 \end{bmatrix} \tag{7.38}$$

Matrix $\mathbf{A}$ has the following eigenvalues $\left[2, -4 \pm \sqrt{3}\mathrm{j}\right]$. Hence, the system $(\mathbf{G})$ is unstable. Moreover, the system is detectable only since the couple of complex eigenvalues is not observable although stable. In simulation, the initial condition is chosen equal to $\boldsymbol{x}_0 = \begin{bmatrix} -2 & 1.5 & -1 \end{bmatrix}^\top$. In practice, the initial condition is supposed to be unknown but it is known to lie in the interval $\left[\underline{\boldsymbol{x}_0}, \overline{\boldsymbol{x}_0}\right]$ where $\underline{\boldsymbol{x}_0} = -2 \begin{bmatrix} 1 & 1 & 1 \end{bmatrix}$ and $\overline{\boldsymbol{x}_0} = -\underline{\boldsymbol{x}_0}$.

Once again, the theory of linear interval state-observers presented in Chapter B is applied. A classical observer is used and initialised at $\widehat{\boldsymbol{x}_0} = \mathbf{0}_3$. The observation error dynamics is given by the following representation:

$$(\mathbf{G_e}) \begin{cases} \dot{\boldsymbol{e}} &= (\mathbf{A} - \mathbf{LC})\,\boldsymbol{e} + \mathbf{B_d} d \\ \boldsymbol{e}_0 &= \boldsymbol{x}_0 - \widehat{\boldsymbol{x}_0} \end{cases} \tag{7.39}$$

where $\mathbf{L} \in \mathbb{R}^3$ is the observer gain and $\boldsymbol{e}_0$ lies in $\left[\underline{\boldsymbol{e}_0}, \overline{\boldsymbol{e}_0}\right] = \left[\underline{\boldsymbol{x}_0} - \widehat{\boldsymbol{x}_0}, \overline{\boldsymbol{x}_0} - \widehat{\boldsymbol{x}_0}\right]$. Similarly to the previous example, note that the dynamics in (7.39) is not cooperative whatever the choice of $\mathbf{L}$.

Under Assumption 7.1, there exists $\mathbf{P} \in \mathbb{R}^{3\times3}$ such that $\mathbf{M} = \mathbf{P}\,(\mathbf{A} - \mathbf{LC})\,\mathbf{P}^{-1}$ is Metzler. Consequently, the following system is an interval observer for the observation error dynamics (7.39) in the new coordinates $\boldsymbol{e}_z = \mathbf{P}\boldsymbol{e}$:

$$\left(\mathbf{G_e^{z,\sharp}}\right) \begin{cases} \underline{\dot{\boldsymbol{e}_z}} &= \mathbf{M}\underline{\boldsymbol{e}_z} + (\mathbf{PB_d})^+ \underline{d} - (\mathbf{PB_d})^- \overline{d} \\ \dot{\overline{\boldsymbol{e}_z}} &= \mathbf{M}\overline{\boldsymbol{e}_z} + (\mathbf{PB_d})^+ \overline{d} - (\mathbf{PB_d})^- \underline{d} \\ \underline{\boldsymbol{e}_z}(0) &= \mathbf{P}^+\underline{\boldsymbol{e}_0} - \mathbf{P}^-\overline{\boldsymbol{e}_0} \\ \overline{\boldsymbol{e}_z}(0) &= \mathbf{P}^+\overline{\boldsymbol{e}_0} - \mathbf{P}^-\underline{\boldsymbol{e}_0} \end{cases} \tag{7.40}$$

Bounds on the state vector $\boldsymbol{x}$ are then easily determined using the reverse SCT in (7.3). The next paragraphs are dedicated to the determination of matrices $\mathbf{P}$ and $\mathbf{L}$.

SCorpIO Similarly to the previous example, the problem of finding appropriate matrices $\mathbf{P}$ and $\mathbf{L}$ is reformulated in the form of the typical SCorpIO optimization Problem 7.13. In this case, the following requirements are considered:

(1) *transformation matrices maximum elements value*: $|\mathbf{P}_{ij}| \leq 2$, $|\mathbf{T}_{ij}| \leq 2$, $\forall\,(i,j)$;

(2) *Metzler matrix condition*: $\mathbf{M}_{ij} \geq 0$, $\forall i \neq j$;

(3) *Maximum* $\mathbf{M}$ *elements value*: $\mathbf{M}_{ij} \leq 5 = \overline{\mathbf{M}_{ij}}$, $\forall\,(i,j)$;

(4) *Closed-loop stability*: the system (7.39) should be stable when $d = 0$ with the following constraint on the state matrix eigenvalues: $\mathrm{Re}\left(\mathrm{eig}\left(\mathbf{A} - \mathbf{LC}\right)\right) \in [-\infty, -0.9]$;

(5) *Interval tightness*: $\left\| \frac{1}{0.1} T_{\underline{d}-\underline{d}\to\boldsymbol{E}_d}(s, \mathbf{P}, \mathbf{L}) \right\|_2 \leq 1$;

(6) $\boldsymbol{E}_d$ *linear dependence in* $\mathbf{PB_d}$ *condition*: $\mathbf{PB_d} \in \mathbb{R}^3_-$. This time, better results are obtained when looking for a negative matrix $\mathbf{PB_d}$.

Once again, the optimization Problem 7.13 is locally solved using `systune`. The following numerical results are obtained:

$$\mathbf{L} = \begin{bmatrix} 2.9804 \\ -0.1465 \\ -0.4002 \end{bmatrix}, \mathbf{P} = \begin{bmatrix} 0.1422 & -0.1322 & -0.3850 \\ 0.3617 & 0.9009 & 0.2673 \\ 0.3271 & -0.2566 & 0.2634 \end{bmatrix} \tag{7.41}$$

Note that $\mathbf{PB_d} \in \mathbb{R}^3_-$ hence **(6)** is satisfied. The resulting matrix $\mathbf{M}$ is Hurwitz Metzler:

$$\mathbf{M} = \begin{bmatrix} -2.7655 & 0.9214 & 0.0000 \\ 0.0000 & -3.0898 & 5.0000 \\ 1.7529 & 0.0000 & -3.1251 \end{bmatrix} \tag{7.42}$$

Other time-invariant SCT determination methods

1. *Sylvester equation resolution*: in this case, the basic `lyap` function fails to provide a solution due to $\mathbf{A}$ and $\mathbf{M}$ sharing identical eigenvalues (cf. detectability hypothesis);
2. *Real-constrained pole placement*: since the complex eigenvalues are unobservable, this means that the observer gain $\mathbf{L}$ cannot be used to obtain real negative eigenvalues. Hence, this trivial method is not applicable in that case;
3. *Lemma 7.5-based approach*: the constructive Lemma 7.5 is used. The observability condition is satisfied with the following vectors:

$$\boldsymbol{e}_1 = \begin{bmatrix} 1 & 0 & 1 \end{bmatrix}, \boldsymbol{e}_2 = \begin{bmatrix} 1 & 1 & 0 \end{bmatrix} \tag{7.43}$$

Similarly to what is proposed in [Raïssi 12], the following matrix $\mathbf{M}$ is chosen:

$$\mathbf{M} = \begin{bmatrix} -3 & 2 & 0 \\ 0 & -3 & 2 \\ 2 & 0 & -3 \end{bmatrix} \tag{7.44}$$

and the poles of the classical observer are placed at $\left[-1, -4 \pm \sqrt{3}\mathrm{j}\right]$ using the following observer gain:

$$\mathbf{L} = \begin{bmatrix} 3 \\ 0 \\ 0 \end{bmatrix} \tag{7.45}$$

Then, using the definitions of $\mathbf{O_1}$, $\mathbf{O_2}$ and $\mathbf{P} = {\mathbf{O_2}}^{-1}\mathbf{O_1}$, the following numerical results are obtained:

$$\mathbf{P} = \begin{bmatrix} 0.4085 & 0.8660 & 0.5000 \\ 0.5915 & -0.8660 & 0.5000 \\ -0.0915 & 0.0000 & -1.0000 \end{bmatrix} \tag{7.46}$$

Time-varying SCT determination, for comparison To determine a time-varying SCT, the approach presented in B.4.1 is applied. Let consider the observer gain (7.45). The following Jordan form $\mathbf{J}$ is obtained for $\mathbf{A} - \mathbf{LC}$ such that $\boldsymbol{\mathcal{P}}\left(\mathbf{A} - \mathbf{LC}\right)\boldsymbol{\mathcal{P}}^{-1} = \mathbf{J}$ where

$$\mathbf{J} = \begin{bmatrix} -4.0000 & 1.7321 & 0 \\ -1.7321 & -4.0000 & 0 \\ 0 & 0 & -1.0000 \end{bmatrix}, \boldsymbol{\mathcal{P}} = \begin{bmatrix} 0.5577 & 0 & 1.4142 \\ 0.1494 & -1.4142 & 0 \\ 1.0801 & 0 & 0 \end{bmatrix} \tag{7.47}$$

Let $\omega = 1.7321$. Then, the matrix $\boldsymbol{\eta}(t)$ is given by

$$\boldsymbol{\eta}(t) = \begin{bmatrix} \cos(\omega t) & -\sin(\omega t) & 0 \\ \sin(\omega t) & \cos(\omega t) & 0 \\ 0 & 0 & 1 \end{bmatrix} \tag{7.48}$$

which leads to the time-varying SCT matrix $\mathbf{P}(t) = \boldsymbol{\eta}(t)\boldsymbol{\mathcal{P}}$ and

$$\boldsymbol{\Xi} = \begin{bmatrix} -4 & 0 & 0 \\ 0 & -4 & 0 \\ 0 & 0 & -1 \end{bmatrix} \tag{7.49}$$

where $\boldsymbol{\Xi} = \mathbf{P}\left(\mathbf{A} - \mathbf{LC}\right)\mathbf{P}^{-1} + \dot{\mathbf{P}}\mathbf{P}^{-1}$, see Proposition B.26.

Simulations The system in (7.36) is simulated over 15s along with the interval observer designed using the techniques presented above. Since the system is unstable, the state is not represented. However, the simulations results for the observation error and its bounds obtained for each technique are shown in Fig. 7.6. The observation error is represented in blue in each case and the bounds are either represented in red when using the matrices obtained with SCorpIO or in black for the other methods.

This example shows that SCorpIO is still a viable solution even in this quite particular case where the system is unstable and part of its dynamics is unobservable. The results obtained in terms of interval tightness and rapidity are comparable to the ones obtained by applying Lemma 7.5. In this case also, the time-varying SCT based on [Mazenc 11] remains more efficient.

In short, our objective to design a viable solution for the simultaneous design of time-invariant matrices $\mathbf{P}$ and $\mathbf{L}$ against both mathematical and control requirements is fulfilled in the continuous-time framework.

7.3.2 Discrete-time application example

An illustration of the SCorpIO approach is now proposed in the discrete-time framework. The following example is inspired by [Efimov 13e].

Model The considered discrete-time system is given by the following state-space representation:

$$(\mathbf{F}) \begin{cases} \boldsymbol{x}_{t+1} &= \mathbf{A}\boldsymbol{x}_t + \mathbf{B_d} d \\ \boldsymbol{y}_t &= \mathbf{C}\boldsymbol{x}_t \end{cases} \tag{7.50}$$

where the time sampling equals $T_s = 1$, $\boldsymbol{x}_t \in \mathbb{R}^5$, $\boldsymbol{y}_t \in \mathbb{R}^2$ and d is an unknown disturbance lying in $[-1, 1]$. In simulation, a random number generator with limited range and sampling time T_s is used as illustrated in Fig. 7.7. The system state-space matrices are given by:

$$\mathbf{A} = \begin{bmatrix} -0.54 & 0.45 & 0.36 & 0 & 0 \\ 0.63 & 0.45 & 0.18 & 0.36 & 0 \\ 0.09 & 0.45 & 0.27 & 0.09 & 0.18 \\ 0 & 0 & 0.25 & 0.25\sqrt{2} & -0.25\sqrt{2} \\ 0 & 0 & 0 & 0.25\sqrt{2} & 0.25\sqrt{2} \end{bmatrix}, \mathbf{B} = \begin{bmatrix} -1 \\ 0 \\ 0 \\ 0 \\ 1 \end{bmatrix}, \mathbf{C} = \begin{bmatrix} 1 & 0 & 0 & 0 & 0 \\ 0 & 0 & 0 & 1 & 0 \end{bmatrix} \tag{7.51}$$

Matrix $\mathbf{A}$ is Schur hence the system is Schur stable. In simulation, the initial condition is chosen equal to $\boldsymbol{x}_0 = \begin{bmatrix} -0.3 & -0.5 & 0.6 & 0.9 & -0.2 \end{bmatrix}^\top$. In practice, the initial condition is supposed to be unknown but lies in the known interval $\left[\underline{\boldsymbol{x}_0}, \overline{\boldsymbol{x}_0}\right]$ where $\overline{\boldsymbol{x}_0} = \begin{bmatrix} 1 & 1 & 1 & 1 & 1 \end{bmatrix}$ and $\underline{\boldsymbol{x}_0} = -\overline{\boldsymbol{x}_0}$. Following the conventional interval observer design approach, the observation error dynamics is characterized by:

$$(\mathbf{F_e}) \begin{cases} \boldsymbol{e}_{t+1} &= (\mathbf{A} - \mathbf{LC})\, \boldsymbol{e}_t + \mathbf{B_d} d \\ \boldsymbol{e}_0 &= \boldsymbol{x}_0 - \widehat{\boldsymbol{x}_0} \end{cases} \tag{7.52}$$

where $\mathbf{L} \in \mathbb{R}^{5\times 2}$ is the observer gain and $\boldsymbol{e}_0$ lies in $\left[\underline{\boldsymbol{e}_0}, \overline{\boldsymbol{e}_0}\right] = \left[\underline{\boldsymbol{x}_0} - \widehat{\boldsymbol{x}_0}, \overline{\boldsymbol{x}_0} - \widehat{\boldsymbol{x}_0}\right]$.

Let suppose there exists $\mathbf{P} \in \mathbb{R}^{5\times 5}$ such that $\mathbf{M} = \mathbf{P}\,(\mathbf{A} - \mathbf{LC})\,\mathbf{P}^{-1}$ is non-negative. Then, the following system is an interval observer for the observation error dynamics (7.52) in the new coordinates $\boldsymbol{e}_z = \mathbf{P}\boldsymbol{e}$:

$$\left(\mathbf{F}_{\mathbf{e}}^{\mathbf{z},\sharp}\right) \begin{cases} \underline{\boldsymbol{e}_z}_{t+1} &= \mathbf{M}\underline{\boldsymbol{e}_z}_t + (\mathbf{PB_d})^+ \underline{d} - (\mathbf{PB_d})^- \overline{d} \\ \overline{\boldsymbol{e}_z}_{t+1} &= \mathbf{M}\overline{\boldsymbol{e}_z}_t + (\mathbf{PB_d})^+ \overline{d} - (\mathbf{PB_d})^- \underline{d} \\ \underline{\boldsymbol{e}_z}_0 &= \mathbf{P}^+\underline{\boldsymbol{e}_0} - \mathbf{P}^-\overline{\boldsymbol{e}_0} \\ \overline{\boldsymbol{e}_z}_0 &= \mathbf{P}^+\overline{\boldsymbol{e}_0} - \mathbf{P}^-\underline{\boldsymbol{e}_0} \end{cases} \tag{7.53}$$

Bounds on the initial state vector $\boldsymbol{x}_t$ are then determined using the reverse SCT (7.3). The determination of matrices $\mathbf{P}$ and $\mathbf{L}$ is tackled in the next section.

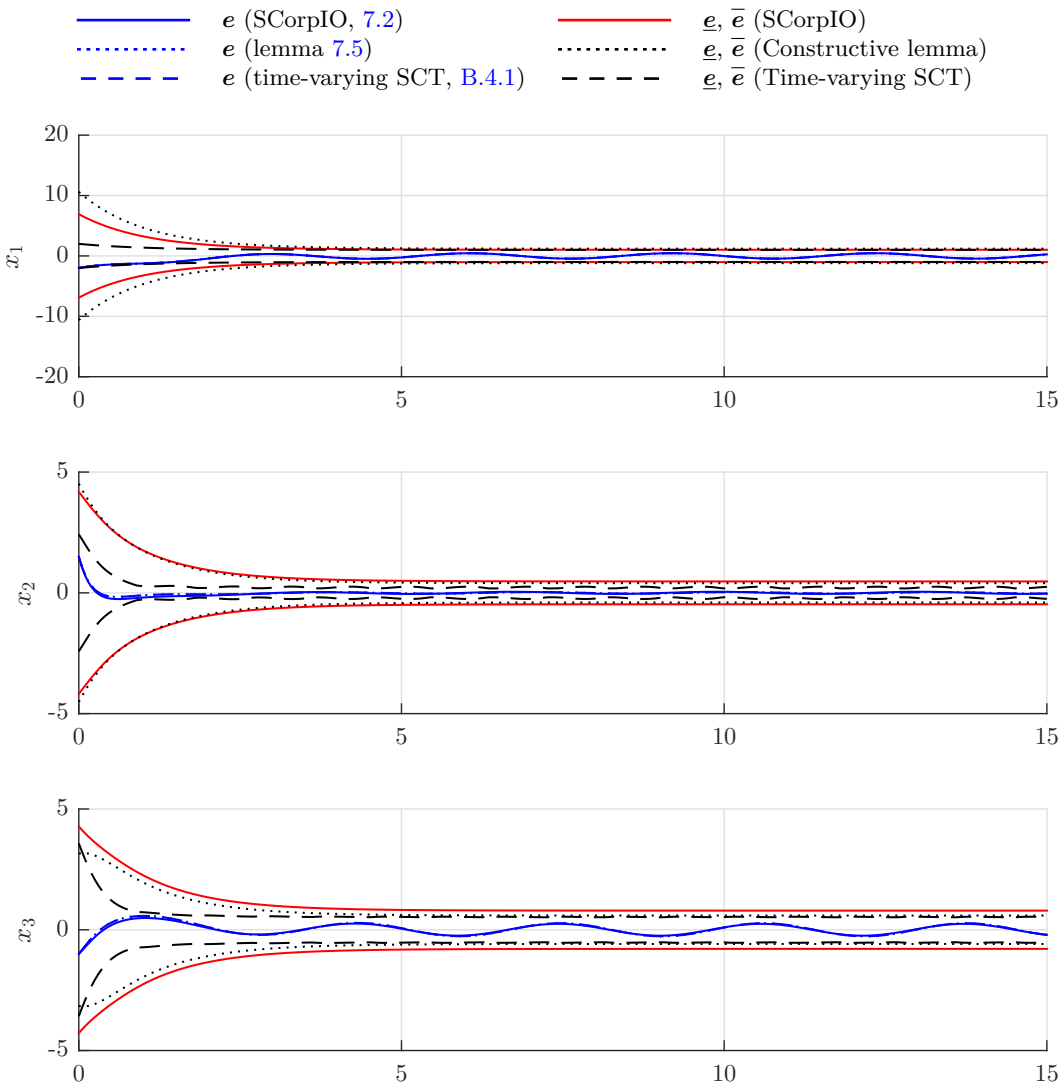

Figure 7.6: System (7.39) simulation with a comparison of estimates and bounds obtained using various interval observer design methods.

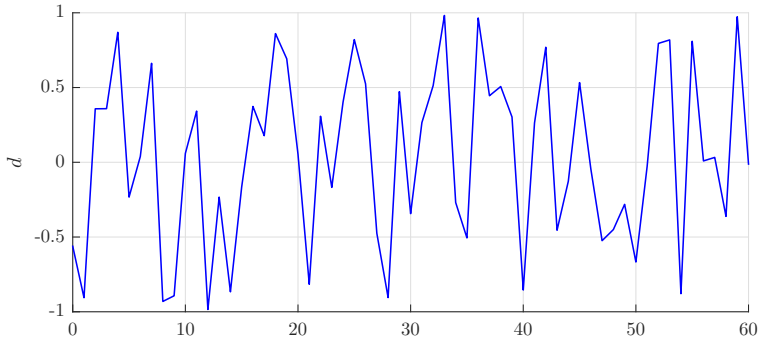

Figure 7.7: Disturbance signal d used in the simulation of (7.50).

SCorpIO The same approach is repeated once again to determine both matrices $\mathbf{P}$ and $\mathbf{L}$. This time however, since the synthesis models are discrete-time, the modification of the approach proposed in Remark 7.12 is applied. That is, the matrix $\mathbf{M}$ is ensured to be Schur-stable and non-negative by stabilizing[8] the fictitious system $(\mathbf{F_m})$ in (7.17). The following constraints are considered in the synthesis:

(1) *transformation matrices maximum elements value*: $|\mathbf{P}_{ij}| \leq 1$, $|\mathbf{T}_{ij}| \leq 1$, $\forall\,(i,j)$;

(2) *Non-negativity condition*: $\mathbf{M}_{ij} \geq 0$, $\forall\,(i,j)$;

(3) *Maximum* $\mathbf{M}$ *elements value*: $\mathbf{M}_{ij} \leq 100 = \overline{\mathbf{M}_{ij}}$, $\forall\,(i,j)$;

(4) *Schur stability*: the system (7.52) should be Schur-stable when $d = 0$;

(5) *Interval tightness*: $\left\| \frac{1}{0.1} T_{\overline{d}-\underline{d}\to \boldsymbol{E}_d}(z,\mathbf{P},\mathbf{L}) \right\|_2 \leq 1$;

(6) $\boldsymbol{E}_d$ *linear dependence in* $\mathbf{PB_d}$ *condition*: $\mathbf{PB_d} \in \mathbb{R}^5_+$.

The resulting optimization problem is locally solved using `systune`. The following numerical results are obtained:

$$\mathbf{L} = \begin{bmatrix} -0.5883 & -0.2396 \\ 0.5828 & 0.1432 \\ -0.0946 & -0.1807 \\ 0.2500 & 0.4680 \\ -0.2729 & 0.2966 \end{bmatrix}, \mathbf{P} = \begin{bmatrix} 0.5337 & -0.0263 & -0.8468 & 0.2105 & 0.6709 \\ -0.4339 & 0.4129 & 0.0089 & -0.3391 & 0.0108 \\ -0.8118 & -0.4898 & 0.8313 & 0.0561 & -0.3900 \\ -0.5149 & -0.9126 & -0.0566 & -0.5979 & -0.5149 \\ 0.1910 & -0.8036 & -0.0500 & -0.5300 & 0.1936 \end{bmatrix} \tag{7.54}$$

It is observed that $\mathbf{PB_d} \in \mathbb{R}^5_+$. The resulting matrix $\mathbf{M}$ is Schur-stable and non-negative:

$$\mathbf{M} = \begin{bmatrix} 0.0000 & 0.0025 & 0.0243 & 0.0196 & 0.1543 \\ 0.1948 & 0.0228 & 0.0013 & 0.0100 & 0.0000 \\ 0.1524 & 0.0005 & 0.0000 & 0.2183 & 0.0107 \\ 0.5809 & 0.0001 & 0.0209 & 0.7039 & 0.0000 \\ 0.3599 & 0.0000 & 0.1170 & 0.0064 & 0.2807 \end{bmatrix} \tag{7.55}$$

Other time-invariant SCT determination methods In the following, pole placement is performed considering the following expected eigenvalues vector:

$$\boldsymbol{p}_M = \begin{bmatrix} 0.1 & 0.3 & 0.5 & 0.7 & 0.9 \end{bmatrix} \tag{7.56}$$

Indeed, in the discrete-time case, a matrix is Schur if its eigenvalues are in the unit circle and non-negative if *all* its entries are positive. Choosing real eigenvalues simplifies the selection of the targeted Schur non-negative matrix $\mathbf{M}$. In practice, the following observer gain is obtained using pole placement:

$$\mathbf{L} = \begin{bmatrix} -1.1993 & -0.2234 \\ 0.6217 & 0.2992 \\ -0.0161 & 0.2228 \\ -0.0205 & -0.4136 \\ -0.0333 & 0.4069 \end{bmatrix} \tag{7.57}$$

1. *Real-constrained pole placement*: this method is equivalent to diagonalizing matrix $\mathbf{A}$. The following SCT matrix $\mathbf{P}$ is obtained:

$$\mathbf{P} = \begin{bmatrix} -0.4816 & -1.3788 & -0.8972 & -0.5748 & 0.0763 \\ -0.3375 & -0.5564 & 0.0284 & 0.9356 & -0.9400 \\ -0.1471 & -0.9124 & 0.8567 & 0.2861 & -0.2092 \\ 0.5944 & -1.4806 & -0.7589 & -0.4881 & 0.2457 \\ -0.1690 & 0.0094 & 0.1658 & 0.2565 & 1.1357 \end{bmatrix} \tag{7.58}$$

[8] In the Schur sense.

2. *Lemma 7.5-based approach*: the targeted Schur non-negative matrix $\mathbf{M}$ is chosen as

$$\mathbf{M} = \begin{bmatrix} 0.1000 & 1.0000 & 1.0000 & 1.0000 & 1.0000 \\ 0 & 0.3000 & 1.0000 & 1.0000 & 1.0000 \\ 0 & 0 & 0.5000 & 1.0000 & 1.0000 \\ 0 & 0 & 0 & 0.7000 & 1.0000 \\ 0 & 0 & 0 & 0 & 0.9000 \end{bmatrix} \tag{7.59}$$

The observability condition in Lemma 7.5 is satisfied with the following vectors:

$$\boldsymbol{e}_1 = \begin{bmatrix} 1 & 0 & 0 & 0 & 0 \end{bmatrix}, \boldsymbol{e}_2 = \begin{bmatrix} 1 & 1 & 0 & 0 & 0 \end{bmatrix} \tag{7.60}$$

Using the definitions of $\mathbf{O_1}$ and $\mathbf{O_2}$ and $\mathbf{P} = \mathbf{O_2}^{-1}\mathbf{O_1}$, the following numerical result is obtained:

$$\mathbf{P} = \begin{bmatrix} 0.7205 & -0.0775 & -0.0914 & -0.0533 & -0.0037 \\ 0.2795 & 0.0775 & 0.0914 & 0.0533 & 0.0037 \\ 0.0876 & 0.1087 & 0.0797 & 0.0507 & 0.0016 \\ 0.0203 & 0.0582 & 0.0379 & 0.0242 & -0.0032 \\ 0.0041 & 0.0116 & 0.0076 & 0.0048 & -0.0006 \end{bmatrix} \tag{7.61}$$

In simulation, this method returns inappropriate results and is discarded from now on.

Simulations The system in (7.50) is simulated over 60s along with the interval observer (7.53) where $\mathbf{P}$ and $\mathbf{L}$ are obtained using the presented design techniques. The simulation results are shown in Fig. 7.8. The system state is represented in blue and the bounds are represented in red when using SCorpIO design techniques and in dashed black when using the real-constrained pole placement technique.

This example shows that SCorpIO is an adequate approach to the design of interval observers in the discrete-time framework. The results are satisfying in comparison with other working time-invariant SCT determination approaches.

7.4 Extension to the design of interval observers on closed-loops

Problem 7.13 is entirely dedicated to designing an interval observer on a given system which is the observation error system (B.18a) in the general case. We have shown in 7.2 that solving this problem is possible using a control-oriented optimization technique. This led to the formulation of a new interval observer design technique named *SCorpIO*. However, considering a classical observer to be able to design an interval observer is not a must. This approach was just proposed as a fast and easy technique to ensure stability of the dynamics from which the interval observer dynamics is deduced.

In Chapter 5, we have shown that using the data from an interval observer for a given system in closed-loop with a synthesized controller can be used to enforce a time-domain constraint on this system. This led to an extension of the OIST approach to uncertain systems and systems with partially measured states – a major contribution of this thesis.

The design of an interval observer on such closed-loop systems is critical. In this section, we show that the method introduced in 7.2 can tackle this challenging problem. Only the continuous-time case is considered but application to the discrete-time case is straightforward.

7.4.1 Interval observer of the closed-loop

Let consider the possibly unstable LTI system in (7.1). To stabilize this system, the following dynamical controller is considered:

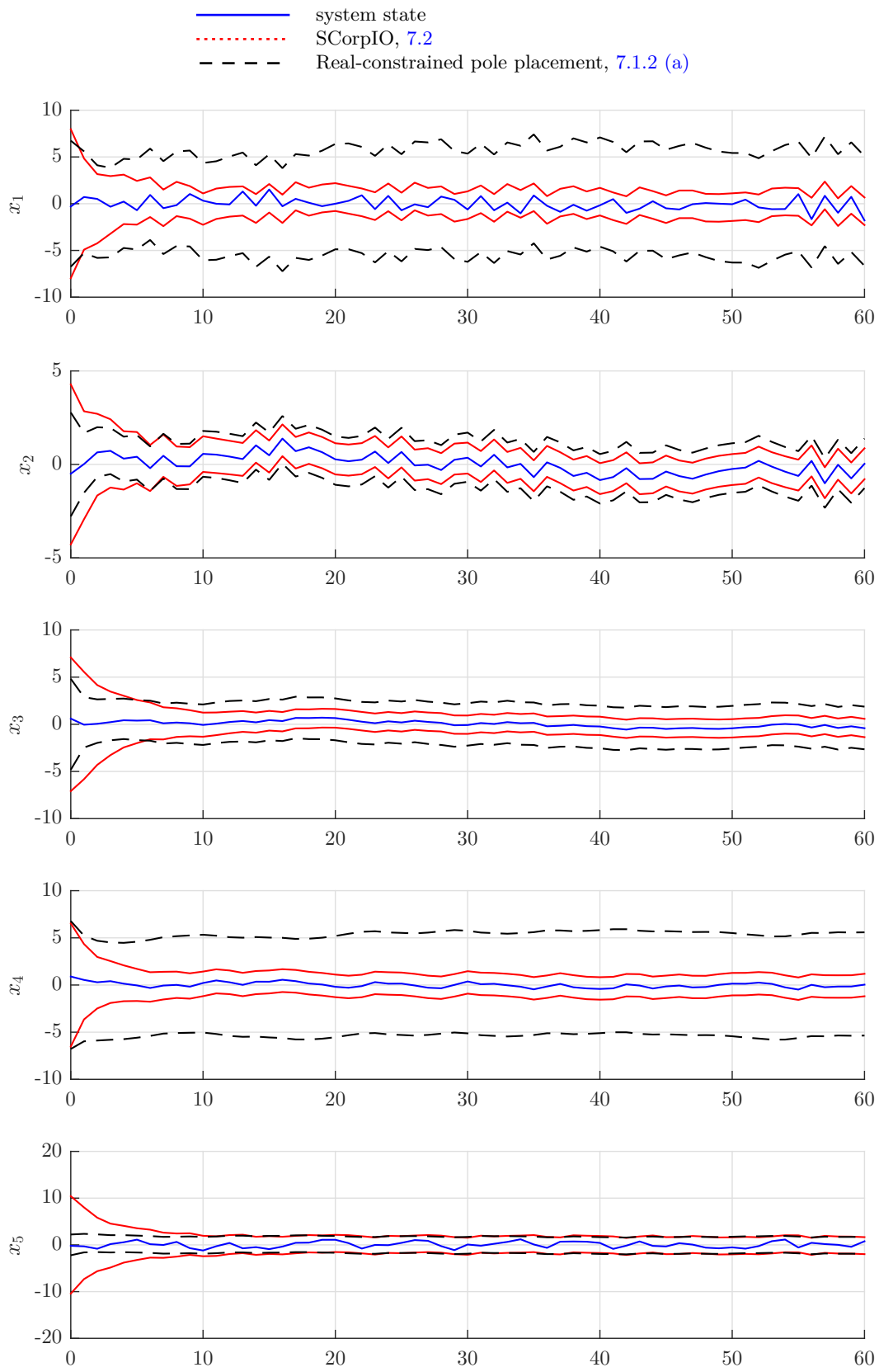

Figure 7.8: System (7.50) simulation with a comparison of estimates and bounds obtained using various interval observer design methods.

$$(\mathbf{K})\begin{cases} \dot{\boldsymbol{x}}_K &= \mathbf{A_K}\boldsymbol{x}_K + \mathbf{B_K}\boldsymbol{u}_K \\ \boldsymbol{y}_K &= \mathbf{C_K}\boldsymbol{x}_K + \mathbf{D_K}\boldsymbol{u}_K \\ \boldsymbol{x}_K(0) &= \mathbf{0} \end{cases} \tag{7.62}$$

where $\boldsymbol{x}_K \in \mathbb{R}^{n_K}$, $\boldsymbol{u}_K \in \mathbb{R}^m$ and $\boldsymbol{y}_K \in \mathbb{R}^l$. This controller is considered in closed-loop with system $(\mathbf{G})$ in (7.1), i.e.:

$$\boldsymbol{u} = \boldsymbol{y}_K + \boldsymbol{v},\ \boldsymbol{u}_K = \boldsymbol{y} \tag{7.63}$$

where $\boldsymbol{v} \in \mathbb{R}^l$ is an exogenous set-point signal. Let suppose the closed-loop is well-posed:

Assumption 7.17 (Closed-loop well-posedness)**.**
It is supposed the closed-loop consisting of system $(\mathbf{G})$ (7.1), controller $(\mathbf{K})$ (7.62) and interconnection (7.63) is well-posed.

The matrix $\mathbf{I}_l - \mathbf{D_K D_u}$ is thus invertible and the closed-loop dynamics is given by:

$$\begin{aligned} \dot{\boldsymbol{X}} &= \begin{bmatrix} \mathbf{A} + \mathbf{B_u}\left(\mathbf{I}_l - \mathbf{D_K D_u}\right)^{-1}\mathbf{D_K C} & \mathbf{B_u}\left(\mathbf{I}_l - \mathbf{D_K D_u}\right)^{-1}\mathbf{C_K} \\ \mathbf{B_K C} + \mathbf{B_K D_u}\left(\mathbf{I}_l - \mathbf{D_K D_u}\right)^{-1}\mathbf{D_K C} & \mathbf{A_K} + \mathbf{B_K D_u}\left(\mathbf{I}_l - \mathbf{D_K D_u}\right)^{-1}\mathbf{C_K} \end{bmatrix} \boldsymbol{X} \\ &\quad + \begin{bmatrix} \mathbf{B_u} & \mathbf{B_d} + \mathbf{B_u}\left(\mathbf{I}_l - \mathbf{D_K D_u}\right)^{-1}\mathbf{D_K D_d} \\ \mathbf{0} & \mathbf{B_K D_d} + \mathbf{B_K D_u}\left(\mathbf{I}_l - \mathbf{D_K D_u}\right)^{-1}\mathbf{D_K D_d} \end{bmatrix} \boldsymbol{W} \\ &= \mathbf{A_X}\boldsymbol{X} + \mathbf{B_{X,v}}\boldsymbol{v} + \mathbf{B_{X,d}}\boldsymbol{d} \end{aligned} \tag{7.64}$$

where $\boldsymbol{X} = \begin{bmatrix} \boldsymbol{x} \\ \boldsymbol{x}_K \end{bmatrix} \in \mathbb{R}^{n+n_K}$ and $\boldsymbol{W} = \begin{bmatrix} \boldsymbol{v} \\ \boldsymbol{d} \end{bmatrix}$. For a stabilizing $(\mathbf{K})$, the matrix $\mathbf{A_X}$ is Hurwitz. Let denote $(\mathbf{G_X})$ the dynamical system in (7.64) with initial condition $\boldsymbol{X}_0 = \begin{bmatrix} \boldsymbol{x}_0 \\ \mathbf{0} \end{bmatrix}$. Considering the definition of an interval observer in [Cacace 15] and supposing the disturbance input $\boldsymbol{d}$ and initial condition $\boldsymbol{X}_0$ are bounded, an interval observer for $(\mathbf{G_X})$ is given in new coordinates $\boldsymbol{X}_Z = \mathbf{P}\boldsymbol{X}$ by

$$\begin{aligned} \dot{\underline{\boldsymbol{X}}_Z} &= \mathbf{P}\mathbf{A_X}\mathbf{P}^{-1}\underline{\boldsymbol{X}_Z} + \left(\mathbf{P}\mathbf{B_{X,d}}\right)^+\underline{\boldsymbol{d}} - \left(\mathbf{P}\mathbf{B_{X,d}}\right)^-\overline{\boldsymbol{d}} + \mathbf{P}\mathbf{B_{X,v}}\boldsymbol{v} \\ \dot{\overline{\boldsymbol{X}}_Z} &= \mathbf{P}\mathbf{A_X}\mathbf{P}^{-1}\overline{\boldsymbol{X}_Z} + \left(\mathbf{P}\mathbf{B_{X,d}}\right)^+\overline{\boldsymbol{d}} - \left(\mathbf{P}\mathbf{B_{X,d}}\right)^-\underline{\boldsymbol{d}} + \mathbf{P}\mathbf{B_{X,v}}\boldsymbol{v} \\ \underline{\boldsymbol{X}_Z}(0) &= \mathbf{P}^+\underline{\boldsymbol{X}_0} - \mathbf{P}^-\overline{\boldsymbol{X}_0} \\ \overline{\boldsymbol{X}_Z}(0) &= \mathbf{P}^+\overline{\boldsymbol{X}_0} - \mathbf{P}^-\underline{\boldsymbol{X}_0} \end{aligned} \tag{7.65}$$

where $\mathbf{P} \in \mathbb{R}^{(n+n_K)\times(n+n_K)}$ is such that $\mathbf{M_X} = \mathbf{P}\mathbf{A_X}\mathbf{P}^{-1}$ is Metzler. Contrary to the original problem, a classical observer is not required here since the interval observer is directly built on a cooperative representation of the closed-loop. This is notably used in Chapter 5 to avoid the dependency of the derivatives of the constrained output α in the measurements vector $\boldsymbol{y}$. The interval tightness $\boldsymbol{E}_d = \frac{1}{2}\left(\overline{\boldsymbol{X}_Z} - \underline{\boldsymbol{X}_Z}\right)$ is then characterized by the following dynamics:

$$\dot{\boldsymbol{E}}_d = \mathbf{M_X}\boldsymbol{E}_d + \frac{1}{2}\left[\left(\mathbf{P}\mathbf{B_{X,d}}\right)^+ + \left(\mathbf{P}\mathbf{B_{X,d}}\right)^-\right]\left(\overline{\boldsymbol{d}} - \underline{\boldsymbol{d}}\right) \tag{7.66}$$

which can be made linear in the design parameter $\mathbf{P}$ by structuring $\mathbf{P}$ such that $\mathbf{P}\mathbf{B_{X,d}} \in \mathbb{R}_+^{(n+n_K)\times k}$. In the next section, the problem of finding $\mathbf{P}$ and $(\mathbf{K})$ such that the system in (7.65) is an interval observer for $(\mathbf{G_X})$ is formally stated.

7.4.2 Problem statement

The Problem 7.7 of finding a time-invariant SCT such that a given system is cooperative in the new coordinates is reformulated in the newly considered case. The decision variables are now $\mathbf{P}$ and the controller $(\mathbf{K})$.

Problem 7.18 (Time-invariant SCT determination problem (closed-loop)).
Considering $(\mathbf{G_X})$ in (7.64) under Assumption 7.17, find $\mathbf{P} \in \mathbb{R}^{(n+n_K)\times(n+n_K)}$ and $(\mathbf{K})$ given in (7.62) such that

$$\mathbf{M_X} = \mathbf{P}\mathbf{A_X}\mathbf{P}^{-1} \tag{7.67}$$

is Hurwitz Metzler where

$$\mathbf{A_X} = \begin{bmatrix} \mathbf{A} + \mathbf{B_u}\left(\mathbf{I}_l - \mathbf{D_K}\mathbf{D_u}\right)^{-1}\mathbf{D_K}\mathbf{C} & \mathbf{B_u}\left(\mathbf{I}_l - \mathbf{D_K}\mathbf{D_u}\right)^{-1}\mathbf{C_K} \\ \mathbf{B_K}\mathbf{C} + \mathbf{B_K}\left(\mathbf{I}_l - \mathbf{D_K}\mathbf{D_u}\right)^{-1}\mathbf{D_K}\mathbf{C} & \mathbf{A_K} + \mathbf{B_K}\mathbf{D_u}\left(\mathbf{I}_l - \mathbf{D_K}\mathbf{D_u}\right)^{-1}\mathbf{C_K} \end{bmatrix} \tag{7.68}$$

Similarly to Proposition 7.11, this problem can be viewed as a stabilization problem on the following system:

$$(\mathbf{G_m}) \begin{cases} \dot{\boldsymbol{x}}_l &= \mathbf{A_X}\boldsymbol{x}_l \\ \dot{x}_{ij} &= -\mathbf{M_X}_{ij}\left(\mathbf{P}, \mathbf{A_K}, \mathbf{B_K}, \mathbf{C_K}, \mathbf{D_K}\right) x_{ij} \quad \forall i \neq j \end{cases} \tag{7.69}$$

where $\mathbf{M_X}_{ij}\left(\mathbf{P}, \mathbf{A_K}, \mathbf{B_K}, \mathbf{C_K}, \mathbf{D_K}\right) = \left[\mathbf{P}\mathbf{A_X}\mathbf{P}^{-1}\right]_{ij}$ with $\mathbf{A_X}$ defined in (7.68) and $1 \leq i \neq j \leq n + n_K$. Again, additional control requirements can be added to enforce specific properties on the considered dynamics, especially disturbance $\boldsymbol{d}$ rejection.

Problem 7.19 (Typical SCorpIO problem (closed-loop)).
Solve the following optimisation problem:

$$\begin{aligned} &\min \max_{\mathbf{P},(\mathbf{K})} \left\{ \left\| W_K(s) T_{\boldsymbol{d}\to\boldsymbol{y}_K}\left(s,(\mathbf{K})\right) \right\|_2, \left\| W_{E_d}(s) T_{\overline{\boldsymbol{d}}-\underline{\boldsymbol{d}}\to\boldsymbol{E}_d}\left(s,\mathbf{P},(\mathbf{K})\right) \right\|_2 \right\} \\ &\text{subject to} \begin{cases} (\mathbf{G_m}) \text{ in (7.69) is Hurwitz stable} \\ \mathbf{P}\mathbf{B_{X,d}} \in \mathbb{R}_+^{(n+n_K)\times k} \end{cases} \end{aligned} \tag{7.70}$$

where $W_K(s)$ and $W_{E_d}(s)$ are appropriately defined frequency-dependent weightings and the usual notations for transfer functions is used.

A local solution to this optimization problem can be obtained using the structured control design techniques mentioned in 7.2.3. This is illustrated in the next section.

7.4.3 Example

The SCorpIO approach for closed-loops in continuous-time as presented in 7.4 is applied on a simple example. Both the controller $(\mathbf{K})$ and state-coordinate transform matrix $\mathbf{P}$ are synthesized to simultaneously stabilize the original system *and* design an interval observer on the resulting closed-loop.

7.4.3 (a) Model

Let consider the LTI system in (7.1) where the state-space matrices are given by:

$$\mathbf{A} = \begin{bmatrix} 1 & -1 \\ 2 & -3 \end{bmatrix}, \mathbf{B} = \begin{bmatrix} \mathbf{B_d} & \mathbf{B_u} \end{bmatrix} = \begin{bmatrix} 0 & 0 \\ 1 & 1 \end{bmatrix}, \mathbf{C} = \begin{bmatrix} 1 & 0 \end{bmatrix}, \mathbf{D} = \mathbf{0}_{1\times 2} \tag{7.71}$$

and $\boldsymbol{x}_0 = \mathbf{0}_2$. A unidimensional state disturbance d is considered. In simulation, the signal represented in Fig. 7.9 is used. Its known upper and lower bounds are represented on the same figure.

The state matrix $\mathbf{A}$ is non-Hurwitz non-Metzler with its eigenvalues equal to $-1 \pm \sqrt{2}\mathrm{j}$. Hence, the considered system is unstable. Also, to build an interval observer on this system, a SCT is

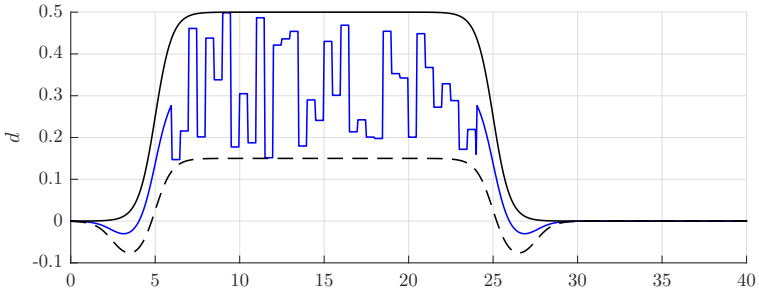

Figure 7.9: Disturbance signal d used in simulation. Known bounds on this signal are represented in black.

required. A controller $(\mathbf{K})$ as in (7.62) is considered with $n_K = 1$ and the loop is closed using the relations in (7.63). We denote $\boldsymbol{X} = \begin{bmatrix} x_1 & x_2 & x_K \end{bmatrix}^\top$ where $\boldsymbol{x}$ is the system state and x_K is the controller state. Also, $\boldsymbol{X}_z = \mathbf{P}\boldsymbol{X}$. The simultaneous synthesis of $\mathbf{P}$ and $(\mathbf{K})$ is now covered.

7.4.3 (b) Application of SCorpIO

The objective is to find $(\mathbf{K})$ and $\mathbf{P}$ such that the system in (7.71) in closed-loop with $(\mathbf{K})$ is stable and its state-matrix $\mathbf{M_X} = \mathbf{P}\mathbf{A_X}\mathbf{P}^{-1}$ is Metzler in the new coordinates $\boldsymbol{X}_Z = \mathbf{P}\boldsymbol{X}$. Satisfying disturbance d rejection properties are also expected. A complete list of synthesis requirements is now detailed. Then, it is shown that it can be formalized as an optimization problem such as Problem 7.13.

The design variables which are optimized are $\mathbf{P} \in \mathbb{R}^{(n+n_K)\times(n+n_K)}$ and the controller matrices $(\mathbf{A_K}, \mathbf{B_K}, \mathbf{C_K}, \mathbf{D_K})$. All other variables are defined from these two design parameters: $\mathbf{T} = \mathbf{P}^{-1}$ and $\mathbf{M_X} = \mathbf{P}\mathbf{A_X}\mathbf{P}^{-1}$ where $\mathbf{A_X}$ is defined in (7.68).

The following constraints are considered:

(1) *transformation matrices maximum elements value*: $|\mathbf{P}_{ij}| \leq 4$, $|\mathbf{T}_{ij}| \leq 4$, $\forall\,(i,j)$. This is used to avoid ill-conditioned matrices especially for the matrix $\mathbf{T}$ which is used to get back in the original coordinates;

(2) *Metzler matrix condition*: $\mathbf{M_X}_{ij} \geq 0$, $\forall i \neq j$;

(3) *Maximum* $\mathbf{M_X}$ *elements value*: $\mathbf{M_X}_{ij} \leq 50 = \overline{\mathbf{M}_{ij}}$, $\forall\,(i,j)$. This reduces the set of admissible solutions. In practice, it is observed that introducing this constraint helps the considered optimization algorithm[9] to converge;

(4) *Closed-loop stability*: the system (7.71) in closed-loop with controller $(\mathbf{K})$ should be stable with the following constraint on the state matrix eigenvalues: $\mathrm{Re}\left(\mathrm{eig}\left(\mathbf{A_X}\right)\right) \in [-50, -0.01]$;

(5) *Interval tightness*: $\left\| 2T_{\overline{d}-\underline{d}\to \boldsymbol{E}_d}\left(s, \mathbf{P}, (\mathbf{K})\right)\right\|_2 \leq 1$;

(6) *Linear dependence in* $\mathbf{P}$ *condition*: $\mathbf{P}\mathbf{B_{X,d}} \in \mathbb{R}_+^{(n+n_K)}$.

Following a scheme similar to the one described in Proposition 7.11, conditions **(1)** to **(4)** can easily be expressed as a stabilizing condition on a fictitious system:

$$(\mathbf{G_m}) \begin{cases} \dot{\boldsymbol{x}}_l &= \mathbf{A_X}\boldsymbol{x}_l & \\ \dot{x}^1_{ij} &= -\left(\mathbf{T}_{ij} + 4\right) x^1_{ij} & \forall\,(i,j) \\ \dot{x}^2_{ij} &= -\left(\mathbf{T}_{ij} - 4\right) x^2_{ij} & \forall\,(i,j) \\ \dot{x}^3_{ij} &= -\mathbf{M_X}_{ij} x^3_{ij} & \forall i \neq j \\ \dot{x}^4_{ij} &= -\left(\mathbf{M_X}_{ij} - 50\right) x^4_{ij} & \forall\,(i,j) \end{cases} \tag{7.72}$$

This is implemented in C.2.2 and commented with more details.

[9] In this work, the `systune` function from the Robust Control Toolbox [MATLAB 14] is used.

Remark 7.20. In practice, when using MATLAB, $\mathbf{P}$ is of type `realp` on which minimum and maximum values for each elements can be set:

```
> P.Minimum = -4;
> P.Maximum =  4;
```

Also, since $\mathbf{B_{X,d}} = \begin{bmatrix} 0 \\ 1 \\ 0 \end{bmatrix}$ in this example, condition **(6)** can be enforced using:

```
> P.Minimum(:,2) = 0;
```

Code samples for the SCorpIO approach are given in C.2.2. ◇

The resulting optimization problem is now formalized. It appears that it can be solved using the control-oriented non-smooth optimization-based algorithms presented in 7.2.3. The problem being non-smooth non-convex, the solution obtained using [Apkarian 13] is locally optimal.

Problem 7.21 (Example: resulting SCorpIO problem)**.**
Solve the following optimisation problem:

$$\begin{aligned} &\min \max_{\mathbf{P},(\mathbf{K})} \left\{ \left\| 2T_{\bar{\boldsymbol{d}}-\underline{\boldsymbol{d}}\to \boldsymbol{E}_d}\left(s,\mathbf{P},(\mathbf{K})\right) \right\|_2 \right\} \\ &\text{subject to} \begin{cases} (\mathbf{G_m}) \text{ in (7.72) is Hurwitz stable} \\ \mathrm{Re}\left(\mathrm{eig}\left(\mathbf{A_X}\right)\right) \in [-50, -0.01] \\ \mathbf{PB_{X,d}} \in \mathbb{R}_+^{(n+n_K)} \end{cases} \end{aligned} \tag{7.73}$$

7.4.3 (c) Results and simulation

Problem 7.21 is solved using the `systune` function from the Robust Control Toolbox [MATLAB 14] based on [Apkarian 07, Apkarian 13, Apkarian 14]. The following local optimal solution is obtained:

$$\mathbf{A_K} = -6.309,\ \mathbf{B_K} = 0.6664,\ \mathbf{C_K} = -31.42,\ \mathbf{D_K} = 5.796 \tag{7.74}$$

$$\mathbf{P} = \begin{bmatrix} -0.2329 & 0.2500 & -1.8527 \\ -0.2500 & 0.0000 & 0.3383 \\ -0.0000 & 0.0000 & -2.1678 \end{bmatrix} \tag{7.75}$$

This results in the following value for the matrix $\mathbf{M_X}$ which is the resulting interval observer state matrix (7.65):

$$\mathbf{M_X} = \begin{bmatrix} -2.0686 & 0.0000 & 0.0000 \\ 1.0000 & -0.8333 & 0.0000 \\ 0.0001 & 5.7783 & -5.4070 \end{bmatrix} \tag{7.76}$$

As expected, this matrix is Hurwitz Metzler, hence the system in (7.65) is a valid interval observer candidate for the system described by (7.71). Also $\mathbf{PB_{X,d}} \in \mathbb{R}_+^3$ hence the system (7.66) is linear in the design matrix $\mathbf{P}$.

The resulting closed-loop and interval observer are simulated over 40s with the disturbance d in Fig. 7.9 and $v = 0$. The simulation results are represented in Fig. 7.10.

The simulation results are quite satisfactory. Tighter intervals could be obtained in the new coordinates by not constraining the maximum admissible value of the elements of $\mathbf{T} = \mathbf{P}^{-1}$. This is beneficial when getting back in the original coordinates is not required by the application.

Note that in this case, it is not possible to compare the SCorpIO method with the ones presented in 7.1.2 since the latter were not designed for both synthesizing controllers and interval observers on the resulting closed-loops.

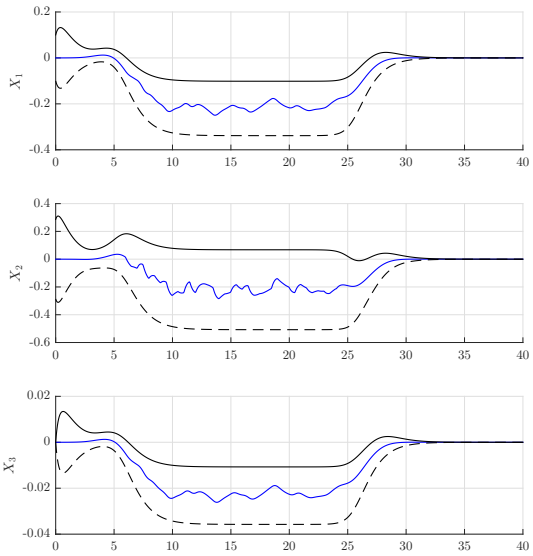

(a) Closed-loop state in the original coordinates (in blue). Bounds obtained using the interval observer are represented in black.

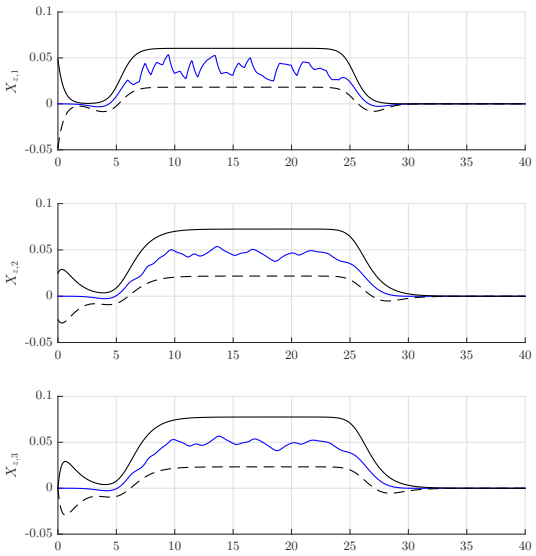

(b) Closed-loop state in the new coordinates $\boldsymbol{X}_z = \mathbf{P}\boldsymbol{X}$ (in blue). Bounds obtained using the interval observer are represented in black.

Figure 7.10: Simulation results for the system (7.71) in closed-loop with (7.74) and the designed interval observer (7.65).

7.5 Conclusions

In this chapter, existing methods to determine time-invariant state-coordinate transformations such that a given system is cooperative in the new coordinates have been recalled. It has been shown that these methods, despite of their ease of use, are not very flexible. They rely on the fine tuning of design parameters on which the obtained solution depends. Also, matrices $\mathbf{L}$ and $\mathbf{P}$ are designed separately which could reduce the set of admissible solutions.

Consequently, a new approach named SCorpIO has been introduced. It relies on the reformulation of the structural Metzler constraint on the state matrix $\mathbf{M}$ into a stabilization problem as presented in Proposition 7.11. The advantage of such reformulation is to allow simultaneous design of $\mathbf{P}$ and $\mathbf{L}$. Also, additional control requirements can be considered in the synthesis for example to enforce disturbance rejection constraints. The reformulation leads to an optimization problem which can be solved using existing control-oriented techniques such as [Apkarian 07] and implemented in [Apkarian 13, Apkarian 14]. With slight modifications, the approach can also be applied in the discrete-time case. Using a similar approach, a solution has been proposed to the simultaneous design of a structured controller and an interval observer on the resulting closed-loop. Examples were presented in both cases.

The main drawback of the method is that it is much more complex to implement than the existing ones. Also, in the presence of high-order models, the amount of models and requirements explodes which can hinder the performance of the optimizing algorithm in terms of computation time and repeatability of the obtained local solution. The development of dedicated algorithms (instead of using approaches specifically dedicated to control design) could help raise these restrictions.

The SCorpIO approach has been used in Chapter 5 to design interval observers on closed-loop. This allowed to extend OIST to the case of systems with partially measured state vectors.

Part IV

Conclusion

Chapter 8

Contributions and perspectives

In this chapter, the main contributions presented in Part III are recalled. It gives a final overview of how the problem of designing a control law satisfying to both frequency-domain and time-domain requirements has been tackled. Of course, the different theories which were presented have their limitations. These are recalled along with some hints for future developments.

8.1 Multi-models multi-objectives robust control design technique

The structured controller synthesis method introduced in [Apkarian 07] and applied to multi-models multi-objectives structured controller synthesis in [Apkarian 14] has been considered in Chapter 2 for the synthesis of a robust observer-based controller. For a given uncertain LTI system, it has been shown how to build synthesis models for critical values of the vector of uncertainties $\boldsymbol{\theta}$. The observer-based controller structure has been detailed. Through using an additional dynamic Youla parameter, it has been shown how to increase the number of degrees of freedom in the structure. The approach is then applied to the synthesis of an observer-based controller. An example of application to the launch vehicle system is proposed in 6.2. The difficulty to enforce a given time-domain constraint is discussed in the same section.

8.2 Linear OIST formulation

In this thesis work, considering our ability to synthesize effective controllers against frequency-domain requirements, it has been decided to consider an *evolutionary strategy* [Goodwin 01] to solve the problem of output-constrained control. More precisely, the OIST approach introduced in [Burlion 12] for non-linear systems and recalled in Chapter 3 has been considered.

This approach is based on the transformation of the output constraint α into saturations on the input. Consequently, the considered output trajectory is forced to satisfy the constraint by limiting the set of admissible input signals. The time-varying and state-dependent input saturations are appropriately defined using information on the relative degree of α with respect to the control input u as well as the notion of propagated bounds. This notion is used in Lemma 4.17 to enforce the time-domain constraint through using the dependence of a derivative of well-defined order of α on u.

The first contribution related the OIST approach is its reformulation in the linear framework for known systems with complete state measurements, leading to Theorem 4.28. Especially, considering linear systems leads to explicit iterative expressions of the propagated bounds and thus of the input saturations. However, as illustrated in 4.3, the output constraint cannot be guaranteed whenever these saturations overlap. Saturations overlap is caused by an inappropriate selection of the OIST design coefficients $\boldsymbol{\kappa}$. Also, the introduction of saturations in the closed-loop can lead to a loss in performance at best and to instability at worst. The following contributions are concerned with both problems.

8.3 OIST saturations overlap mitigation and closed-loop stability analysis

As mentioned previously, saturations overlap is a critical problem when applying OIST. Saturations overlap is due to the presence of unknown disturbances with known bounds. The disturbance input is indeed replaced by its known bounds in the expression of the saturations which leads to some conservatism and, possibly, to saturations overlap. It has been observed that a naive way to avoid saturations overlap is to increase the coefficients values in $\boldsymbol{\kappa}$. A more formal solution was however required.

A major contribution of this work is the formulation of Theorem 4.24 which appropriately defines the OIST design coefficients $\boldsymbol{\kappa}$ such that saturations overlap is avoided at all times. It is based on an appropriate time-dependent selection of these coefficients which are forced to increase whenever saturations overlap could occur.

The second problem was concerned with the possible performance degradation, or worse, destabilisation of the system in closed-loop with the constrained control. Using results from the anti-windup literature [Herrmann 10], the global asymptotic stability of the origin of the system in closed-loop with the saturated nominal controller has been proven in Theorem 4.34, for minimum-phase transfers only. It relies on the introduction of an appropriately defined *Model*

Recovery Anti-Windup (MRAW). It has been observed in simulation that the use of an AW also improves performance, as expected, since the output is allowed to linger on the time-domain constraint.

The contributions presented in Chapter 4 and recalled in 8.2 and 8.3 have been published in [Chambon 15c] and [Chambon b]. However, some limitations to these contributions can be mentioned:

- the considered class of linear systems is quite limited since their dynamics are supposed to be well known and with complete state measurements. This problem is tackled in Chapter 5 as recalled in the following section;
- The results concerned with stability analysis are valid for minimum phase systems only;
- An automated procedure for the tuning of design coefficients could improve the applicability of the method especially in the case of high-dimensional systems.

The contributions to the OIST theory are under implementation in the SMAC toolbox [Onera 16].

8.3.1 Non-minimum phase systems

In the case of minimum phase systems, global asymptotic stability of the origin has been proven in Theorem 4.34. However, in case some zeros of the transfer $T_{u\to\alpha}(s)$ from the control input u to the constrained output α are unstable, it has been observed in 4.6.2 that the origin of the saturated closed-loop is locally stable at best. This is due to the OIST approach itself:

- for minimum phase systems, Proposition 4.32 is applicable;
- For non-minimum phase systems, the system $\dot{\boldsymbol{x}} = [\mathbf{A} - \mathbf{B_u}\boldsymbol{K}_{\text{oist}}(t)]\,\boldsymbol{x}$ is unstable by definition of $\boldsymbol{K}_{\text{oist}}(t)$. Consequently, whenever the saturations are active, the term $\mathbf{B_u}\boldsymbol{K}_{\text{oist}}(t)$ is no longer cancelled in the dynamics and the system diverges.

Informally speaking and depending on the real part of the unstable zero, it may be possible to recover from this diverging behaviour as observed in 4.6.2. However, a formal solution to this problem is not available yet. It is expected that the stability set of such systems may be enlarged by appropriately choosing an anti-windup compensator. Hints on how to synthesise such compensator are given in [Biannic 11].

8.3.2 Automated tuning of the design coefficients

The OIST approach currently suffers from the complexity of the saturations expressions especially in the case of high-order systems for which the relative degree of α with respect to u may be large. In practice, this results in some difficulty to tune the coefficients $\breve{\boldsymbol{\kappa}}$ which influence can be hard to identify but still dramatically influence the simulation results by shaping the control saturations.

In 4.6.1, an example of such automated design procedure was illustrated in the case of a very simple double integrator example. This procedure is based the AMPL environment which allows to formalize non-linear optimization problems. Using an appropriate cost functional and the IPOPT solver, an optimal solution $\breve{\kappa}_{\text{opt}}$ has been obtained on this simple example.

Perspectives include considering more complex examples as well as cost functions. A comparison between different solvers could also be of interest as well as propositions of extensions to the OISTeR approach.

8.4 OIST extension for Robustness

As highlighted in Chapter 4 and 8.2, the OIST approach can only be applied to systems with no uncertainties and with complete state measurements. In Chapter 5, an extension – named OISTeR – of the OIST approach has been proposed for the first time to account for robustness

issues due to the presence of uncertainties. The case of incomplete state measurements has also been treated.

The core of the OISTeR approach is to consider known guaranteed bounds on the possible unknown constrained output α when transforming the constraint into saturations on the input. These bounds are provided by an interval observer. The concepts of generalized output constraint and generalized propagated bounds are then introduced, leading to a reformulation of the propagated bounds lemma in Lemma 5.19. It is interesting to note that this is truly a generalization of the original OIST approach since the original expressions are retrieved whenever it is supposed that the state is completely known.

The OISTeR approach is quite novel and is currently subject to some limitations amongst which even stronger applicability issues than the OIST approach. A more problematic issue is the conservatism of the method. Its implementation in the SMAC toolbox [Onera 16] is however already considered.

8.4.1 Conservatism issues

As illustrated in 5.4, the OISTeR approach is conservative. Especially, it requires both the interval observer to provide a very tight estimation and a good knowledge of the disturbance. This conservatism is also induced by the bounds provided in Lemma 1 [Efimov 13e] which are guaranteed bounds but can overestimate the bounds on the state vector. Different approaches are now hinted to reduce this conservatism.

First, it can be noted that only time-invariant SCT have been used. As illustrated in Chapter 7, interval observers based on time-varying SCT provided tighter intervals in general. The main drawback of using such transformation within the OISTeR theory would be the time-varying aspect of the transformation. This would required rewriting the generalized propagated bounds and saturations expressions to account for the dependency on time. More complex expressions would be obtained as a result.

Second, a stochastic approach to interval estimation could be used. Using approaches based on confidence intervals, it may be possible to reduce the conservatism at the cost of guarantees on the constraint satisfaction, leading to an interesting trade-off in terms of applicability.

8.4.2 Stability issues

The OISTeR approach is very recent and, contrary to the OIST approach in Chapter 4, a formal stability analysis has not yet been conducted. More precisely, the stability of the interval observer $\left(\mathbf{G}^{\mathbf{z},\sharp}\right)$ (5.12) in closed-loop with the OISTeR saturations (5.48) should be analysed. This is particularly critical in the case of non-minimum phase systems where the stability can only be local. Introducing an anti-windup compensator as in Chapter 4 would be an interesting study both to improve the performance and enlarge the stability domain in the case of a non-minimum phase system.

8.5 Non-smooth optimization-based approach to linear interval observer design

It was possible in Chapter 5 to extend the OIST approach to uncertain linear systems by considering guaranteed bounds on the system state as provided by an interval observer. The design of interval observers on linear systems is well-documented as detailed in Chapter B. The most common approaches rely on a state-coordinates transformation (SCT) which is either chosen time-varying or time-invariant. In the time-invariant case, methods have been proposed in the literature to determine an appropriate SCT.

It appears that these methods are easy to implement. The expected result, namely a Metzler state matrix, should however be provided along with other design parameters. Finding a Metzler matrix with given eigenvalues can be hard especially in the complex case. Also, it is not possible to include control-oriented requirements in the determination of the SCT which can lead to very

poor simulation results. For high-order systems, applying these methods is expected to be even harder.

The SCorpIO approach aims at proposing an alternate method to the existing ones. It relies on the reformulation of the mathematical problem of finding $\mathbf{P}$ and $\mathbf{L}$ such that $\mathbf{M} = \mathbf{P}(\mathbf{A} - \mathbf{LC})\mathbf{P}^{-1}$ is Hurwitz Metzler into a control design problem. The problem is then solved using a non-smooth optimization-based approach dedicated to structured controller design. The advantages of the approach is that it allows to formulate control requirements to further constrain the interval observer dynamics. Also, matrices $\mathbf{P}$ and $\mathbf{L}$ are synthesized simultaneously contrary to existing methods. An extension to the design of interval observers on closed-loops is proposed, where the matrices $\mathbf{P}$ and controller ($\mathbf{K}$) are simultaneously tuned.

The main limitation of the SCorpIO method is that it is quite complex to apply with control-oriented requirements rather than pure mathematical ones. The computation time also increases a lot with the system dimension. The contributions presented in Chapter 7 and recalled in this section have been published in [Chambon 15b], [Chambon a] and [Chambon 16].

8.5.1 Dedicated optimization algorithm

The SCorpIO approach relies on the MATLAB procedure `systune` [MATLAB 14] which is dedicated to structured controller synthesis. The reformulation of the Metzler mathematical problem into a control design problem is purely fictitious. The development of a dedicated algorithm eventually based on non-smooth optimization methods to the problem of finding an appropriate SCT could both simplify the application of the method and reduce the computational time. This could be an aside improvement in following versions of the `systune` macro, if manageable.

8.5.2 Non-linear operations on decision variables

In Chapter 7, it is discussed how the tightness $\boldsymbol{E}_d = \frac{1}{2}(\overline{\boldsymbol{x}} - \underline{\boldsymbol{x}})$ of the interval observer can be turned into a control design requirement. However, this requires enforcing $\mathbf{PB_d}$ to be non-negative (or negative) to obtain a dynamics which is linear in the problem variable $\mathbf{P}$. Otherwise, the dynamics would depend non-linearly in $\mathbf{P}$ through the term $\max(\mathbf{PB_d}, \mathbf{0})$. This type of term cannot be considered when using the `systune` procedure which does not implement the max operation on variables of type `realp`.

8.6 Application to the linear flexible launch vehicle

Results from Chapters 2 to 5 are applied to simplified models of the flexible launch vehicle in Chapter 6. Satisfying results are obtained. The transfer from the control input β to the angle of attack α (constrained output) being non-minimum phase, a specific approach is used in the application of OIST, more specifically when considering the addition of an anti-windup compensator to improve performance. A reduced-order interval observer is considered in the application of OISTeR to the rigid launch vehicle so as to reduce the conservatism of the approach. This hints some improvements for future developments of the method.

Future works should focus on further reducing the conservatism. More complex models of the launch vehicle could be considered upon developments of the OIST and OISTeR approaches. More precisely the LPV case could be considered where the model parameters are varied over time to account more faithfully for the evolution of the system.

8.7 Further developments

As far as the OIST approach is concerned, the class of systems considered in Chapter 4 has been extended in Chapter 5 to account for the presence of uncertainties and incomplete state measurements. Further developments should focus on considering LTV and LPV systems. Also, a formulation of OISTeR for non-linear systems would be an interesting addition.

Considering the SCorpIO approach, it could be extended to compute an appropriate SCT such that a given LTV system is cooperative at all times in the new coordinates. An hybrid

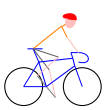

systems approach could be considered where the matrix $\mathbf{P}$ changes at selected instants, the problem being to analyse the cooperativity of the system between those instants. A scheduled approach where the matrix $\mathbf{P}$ is parametrized with respect to the time could also be explored. Such approach would then be integrated within OISTeR to design the required interval observer on the considered LTV system.

Part V

Appendices

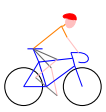

Appendix A

Proofs related to OIST reformulation

A.1 Proof of Proposition 4.32

Considering (4.57) and the system in (4.64), this problem is equivalent to studying the stability of the system $\dot{\boldsymbol{x}}(t) = \mathbf{A}\boldsymbol{x}(t) + \mathbf{B_u}u(t)$ in closed-loop with $v(t) = 0$ or $u(t) = -\boldsymbol{K}_{\text{oist}}(t)\boldsymbol{x}(t)$ (and $\boldsymbol{d}(t) = 0$). The transfer function between u and the regulated variable α is given by

$$\begin{aligned} \alpha &= T_{u\to\alpha}(s) \\ &= \tfrac{s^m + p_1 s^{m-1} + \ldots + p_{m-1}s + p_m}{s^n + d_1 s^{n-1} + \ldots + d_{n-1}s + d_n} u \end{aligned} \tag{A.1}$$

with $k = n - m$ (see Assumption 4.6). Theoretically speaking, a minimum state-space representation of this transfer can be represented in the canonical form which can in turn be expressed as a chain of integrators augmented by the considered transfer zero dynamics, see [Hu 12, Chapter 4]. The chain of integrators is given by

$$\begin{cases} \dot{\widehat{\alpha}} &= \dot{\alpha} \\ &\vdots \\ \dot{\widehat{\alpha^{(k-2)}}} &= \alpha^{(k-1)} \\ \dot{\widehat{\alpha^{(k-1)}}} &= \alpha^{(k)} \\ &= -\boldsymbol{U}^k(t)\boldsymbol{\mathcal{O}}\boldsymbol{x} + \mathbf{C}_{\boldsymbol{\alpha}}\mathbf{A}^k\boldsymbol{x} \end{cases} \tag{A.2}$$

where the last equality is obtained by observing that $u = -K_{\text{oist}}(t)\boldsymbol{x}$ (and $\boldsymbol{d} = 0$). Let $\forall j \in \mathbb{N}$ such that $j \leq k-1$, $\gamma_j = \alpha^{(j)} + \boldsymbol{U}^j(t)\boldsymbol{\mathcal{O}}\boldsymbol{x} - \mathbf{C}_{\boldsymbol{\alpha}}\mathbf{A}^j\boldsymbol{x}$ and $\boldsymbol{\Gamma} = \begin{bmatrix}\gamma_0 & \ldots & \gamma_{k-1}\end{bmatrix} \in \mathbb{R}^k$. Using (4.26) and (4.38) with null disturbances, the chain of integrators in (A.2) can be re-written as

$$\begin{aligned} \dot{\boldsymbol{\Gamma}} &= \begin{bmatrix} -\kappa_1 & 1 & 0 & \ldots & 0 \\ 0 & \ddots & \ddots & \ddots & \vdots \\ \vdots & \ddots & \ddots & \ddots & 0 \\ & & & -\kappa_{k-1} & 1 \\ 0 & & \ldots & 0 & -\kappa_k \end{bmatrix} \boldsymbol{\Gamma} \\ &= \mathbf{A}_{\boldsymbol{\Gamma}}\boldsymbol{\Gamma} \end{aligned} \tag{A.3}$$

This is completed by the zero dynamics as shown in [Hu 12, Chapter 4] which results in the open-loop transfer in (A.1) being equivalent to the following state-space representation

$$\dot{\widehat{\begin{bmatrix}\boldsymbol{\Gamma} \\ \boldsymbol{Z}\end{bmatrix}}} = \begin{bmatrix}\mathbf{A}_{\boldsymbol{\Gamma}} & 0 \\ \mathbf{A}_{\mathbf{Z}\boldsymbol{\Gamma}} & \mathbf{A}_{\mathbf{Z}}\end{bmatrix}\begin{bmatrix}\boldsymbol{\Gamma} \\ \boldsymbol{Z}\end{bmatrix} \tag{A.4}$$

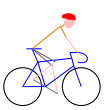

where

$$\mathbf{A_Z} = \begin{bmatrix} 0 & 1 & 0 & \dots & 0 \\ \vdots & \ddots & \ddots & \ddots & \vdots \\ \vdots & & \ddots & \ddots & 0 \\ 0 & \dots & \dots & 0 & 1 \\ -p_m & -p_{m-1} & \dots & -p_2 & -p_1 \end{bmatrix} \tag{A.5}$$

and $\mathbf{A_{Z\Gamma}}$ is the null matrix except for the coefficient $\mathbf{A_{Z\Gamma}}(n-k,1) = 1$. Considering Assumption 4.10, $\mathbf{A_Z}$ eigenvalues are with strictly negative real parts. As far as the dynamics in (A.4) is concerned, the following candidate Lyapunov positive definite function is considered

$$V(\mathbf{\Gamma}, \boldsymbol{Z}) = \frac{1}{2}\mathbf{\Gamma}^\top\mathbf{\Gamma} + \frac{\epsilon}{2}\boldsymbol{Z}^\top\boldsymbol{Z} \tag{A.6}$$

where ϵ is a positive constant. Then

$$\dot{V}(\mathbf{\Gamma}, \boldsymbol{Z}) = \mathbf{\Gamma}^\top\mathbf{A_\Gamma}\mathbf{\Gamma} + \epsilon\boldsymbol{Z}^\top\mathbf{A_Z}\boldsymbol{Z} + \epsilon\boldsymbol{Z}^\top\mathbf{A_{Z\Gamma}}\mathbf{\Gamma} \tag{A.7}$$

where, using the logarithmic function concavity and the fact that $\forall i \in \mathbb{N}^\star$ s.t. $i \leq k$, $\gamma_{i-1}\gamma_i \leq |\gamma_{i-1}\gamma_i|$:

$$\begin{array}{rcl} \mathbf{\Gamma}^\top\mathbf{A_\Gamma}\mathbf{\Gamma} & = & -\sum_{i=0}^{k-1}\kappa_{i+1}\gamma_i^2 + \sum_{i=1}^{k-1}\gamma_{i-1}\gamma_i \\ & \leq & -\sum_{i=0}^{k-1}\kappa_{i+1}\gamma_i^2 + \frac{1}{2}\sum_{i=1}^{k-1}\gamma_i^2 + \frac{1}{2}\sum_{i=0}^{k-2}\gamma_i^2 \\ \mathbf{\Gamma}^\top\mathbf{A_\Gamma}\mathbf{\Gamma} & \leq & -\mathbf{\Gamma}^\top\mathbf{D_{V\Gamma}}\mathbf{\Gamma} \\ & \leq & -\mathbf{\Gamma}^\top\mathrm{diag}\left(\kappa_1 - \frac{1}{2}, \kappa_2 - 1, \dots, \kappa_{k-1} - 1, \kappa_k - \frac{1}{2}\right)\mathbf{\Gamma} \end{array} \tag{A.8}$$

so that $\mathbf{D_{V\Gamma}}$ is a positive definite diagonal matrix upon adapted selection of the positive time-varying coefficients $\kappa_i(t)$. In the same vein

$$\epsilon\boldsymbol{Z}^\top\mathbf{A_{Z\Gamma}}\mathbf{\Gamma} \leq \frac{\epsilon\nu}{2}\left(\mathbf{A_{Z\Gamma}}^\top\boldsymbol{Z}\right)^\top\mathbf{A_{Z\Gamma}}^\top\boldsymbol{Z} + \frac{\epsilon}{2\nu}\mathbf{\Gamma}^\top\mathbf{\Gamma} \tag{A.9}$$

where ν is a positive constant. It comes that

$$\dot{V}(\mathbf{\Gamma}, \boldsymbol{Z}) \leq -\mathbf{\Gamma}^\top\mathbf{D_{V\Gamma}}\mathbf{\Gamma} + \frac{\epsilon}{2\nu}\mathbf{\Gamma}^\top\mathbf{\Gamma} + \epsilon\left(\boldsymbol{Z}^\top\mathbf{A_Z}\boldsymbol{Z} + \frac{\nu}{2}\boldsymbol{Z}^\top\left(\mathbf{A_{Z\Gamma}}\mathbf{A_{Z\Gamma}}^\top\right)\boldsymbol{Z}\right) \tag{A.10}$$

Using the notations $\lambda_{\min}(\mathbf{M})$ and $\lambda_{\max}(\mathbf{M})$ to denote the minimal and maximal real parts of the eigenvalues of the matrix M, it is observed that

$$\boldsymbol{Z}^\top\mathbf{A_Z}\boldsymbol{Z} + \frac{\nu}{2}\boldsymbol{Z}^\top\left(\mathbf{A_{Z\Gamma}}\mathbf{A_{Z\Gamma}}^\top\right)\boldsymbol{Z} \leq \lambda_{\max}(\mathbf{A_Z})\boldsymbol{Z}^\top\boldsymbol{Z} + \frac{\nu}{2}\lambda_{\max}\left(\mathbf{A_{Z\Gamma}}\mathbf{A_{Z\Gamma}}^\top\right)\boldsymbol{Z}^\top\boldsymbol{Z} \tag{A.11}$$

and

$$-\mathbf{\Gamma}^\top\mathbf{D_{V\Gamma}}\mathbf{\Gamma} + \frac{\epsilon}{2\nu}\mathbf{\Gamma}^\top\mathbf{\Gamma} \leq -\lambda_{\min}\left(\mathbf{D_{V\Gamma}}\right)\mathbf{\Gamma}^\top\mathbf{\Gamma} + \frac{\epsilon}{2\nu}\mathbf{\Gamma}^\top\mathbf{\Gamma} \tag{A.12}$$

By choosing $\nu = -\frac{\lambda_{\max}(\mathbf{A_Z})}{\lambda_{\max}\left(\mathbf{A_{Z\Gamma}}\mathbf{A_{Z\Gamma}}^\top\right)} > 0$ (since $\mathbf{A_{Z\Gamma}}\mathbf{A_{Z\Gamma}}^\top$ is positive semi-definite) and $\epsilon = \nu\lambda_{\min}(\mathbf{D_{V\Gamma}}) > 0$ and by observing that the eigenvalues of $\mathbf{A_Z}$ are with strictly negative real parts (see Assumption 4.10) and $\mathbf{D_{V\Gamma}}$ is a positive definite matrix, one obtains

$$\begin{array}{rcl} \dot{V}(\mathbf{\Gamma}, \boldsymbol{Z}) & \leq & -\frac{1}{2}\lambda_{\min}(\mathbf{D_{V\Gamma}})\mathbf{\Gamma}^\top\mathbf{\Gamma} + \frac{1}{2}\lambda_{\max}(\mathbf{A_Z})\boldsymbol{Z}^\top\boldsymbol{Z} \\ & \leq & -\min\left(\lambda_{\min}(\mathbf{D_{V\Gamma}}), -\frac{1}{\epsilon}\lambda_{\max}(\mathbf{A_Z})\right)V(\mathbf{\Gamma}, \boldsymbol{Z}) \\ & \leq & -k_1 V(\mathbf{\Gamma}, \boldsymbol{Z}) \end{array} \tag{A.13}$$

where $k_1 > 0$. Also note that $\dot{V}(0,0) = 0$. As a consequence, the candidate function V is a Lyapunov function and the open-loop system $\dot{\boldsymbol{x}} = [\mathbf{A} - \mathbf{B_u}\boldsymbol{K}_{\text{oist}}(t)]\,\boldsymbol{x}$ is GES.

A.2 Proof of Theorem 4.34

First, considering Proposition 4.31, the origin is a reachable equilibrium of the system in closed-loop with the saturated control signal. Thus, it is of some interest to study the asymptotic stability of this equilibrium. Using (4.3), the state equation in (D.15) can be re-written as

$$\dot{\boldsymbol{x}}(t) = \mathbf{A}\boldsymbol{x}(t) + \mathbf{B_u}\left[-\boldsymbol{K}_{\text{oist}}(t)\boldsymbol{x}_a(t) + \mathbf{C_K}\boldsymbol{x}_K(t) + \mathbf{D_K}\left(\boldsymbol{y}(t) - \boldsymbol{x}_a(t)\right) - \mathrm{Dz}_{\underline{v}(t)}^{\bar{v}(t)}\left(v(t)\right)\right] + \mathbf{B_d}\boldsymbol{d}(t) \tag{A.14}$$

when considering the anti-windup system (4.66) and the modified control law (4.67). Using a similar approach than in [Kapoor 99], let define $\boldsymbol{e}_x(t) := \boldsymbol{x}(t) - \boldsymbol{x}_a(t)$. It follows that

$$\begin{aligned} \dot{\boldsymbol{e}}_x(t) &= \left(\mathbf{A} + \mathbf{B_u}\mathbf{D_K}\right)\boldsymbol{e}_x(t) + \mathbf{B_u}\mathbf{C_K}\boldsymbol{x}_K(t) + \mathbf{B_d}\boldsymbol{d}(t) + \mathbf{B_u}\mathbf{D_K}\mathbf{D_d}\boldsymbol{d}(t) \\ \dot{\boldsymbol{x}}_K(t) &= \mathbf{A_K}\boldsymbol{x}_K(t) + \mathbf{B_K}\boldsymbol{e}_x(t) + \mathbf{B_K}\mathbf{D_d}\boldsymbol{d}(t) \end{aligned} \tag{A.15}$$

Let $\boldsymbol{X} = \begin{bmatrix}\boldsymbol{e}_x & \boldsymbol{x}_K\end{bmatrix}^\top$ and $\boldsymbol{W} = \boldsymbol{d}$, then

$$\begin{aligned} \dot{\boldsymbol{X}} &= \begin{bmatrix}\mathbf{A} + \mathbf{B_u}\mathbf{D_K} & \mathbf{B_u}\mathbf{C_K} \\ \mathbf{B_K} & \mathbf{A_K}\end{bmatrix}\mathbf{X} + \begin{bmatrix}\mathbf{B_d} + \mathbf{B_u}\mathbf{D_K}\mathbf{D_d} \\ \mathbf{B_K}\mathbf{D_d}\end{bmatrix}\boldsymbol{d} \\ &= \mathbf{A_X}\boldsymbol{X} + \mathbf{B_X}\boldsymbol{W} \end{aligned} \tag{A.16}$$

Under Assumptions 4.7 and 4.8, $\|\boldsymbol{W}\|_2$ is finite and $\|\boldsymbol{W}\|$ is bounded. It follows that $\|\boldsymbol{X}\|_2$ is finite and $\|\boldsymbol{X}\|$ converges to zero. In case $\boldsymbol{W} = 0$, the state $\boldsymbol{X}$ converges exponentially to zero. Replacing v in (4.66) by its expression in (4.67), one obtains the following equation:

$$\begin{aligned} &\dot{\boldsymbol{x}}_a(t) = \left[\mathbf{A} - \mathbf{B_u}\boldsymbol{K}_{\text{oist}}(t)\right]\boldsymbol{x}_a(t) \\ &- \mathbf{B_u}\mathrm{Dz}_{\underline{v}(t)}^{\bar{v}(t)}\left(\boldsymbol{K}_{\text{oist}}(t)\boldsymbol{e}_x(t) + \boldsymbol{K}_{\text{oist}}(t)\mathbf{D_d}\boldsymbol{d}(t) + \mathbf{D_K}\boldsymbol{e}_x(t) + \mathbf{D_K}\mathbf{D_d}\boldsymbol{d}(t) + \mathbf{C_K}\boldsymbol{x}_K(t)\right) \end{aligned} \tag{A.17}$$

Considering Proposition 4.32, the open-loop system $\dot{\boldsymbol{x}}_a = \left[\mathbf{A} - \mathbf{B_u}\boldsymbol{K}_{\text{oist}}(t)\right]\boldsymbol{x}_a(t)$ is exponentially stable. Thus, for some positive definite function $V(\boldsymbol{x}_a)$, there exists by the converse Lyapunov theorem, see [Khalil 02], constants α_i, $1 \leq i \leq 4$, such that

$$\begin{aligned} \alpha_1\|\boldsymbol{x}_a\|^2 &\leq V(\boldsymbol{x}_a) \leq \alpha_2\|\boldsymbol{x}_a\|^2 \\ \left\|\tfrac{\partial V(\boldsymbol{x}_a)}{\partial \boldsymbol{x}_a}\right\| &\leq \alpha_3\|\boldsymbol{x}_a\| \\ \tfrac{\partial V(\boldsymbol{x}_a)}{\partial \boldsymbol{x}_a}\left[\mathbf{A}\boldsymbol{x}_a - \mathbf{B_u}\boldsymbol{K}_{\text{oist}}(t)\boldsymbol{x}_a\right] &\leq -\alpha_4\|\boldsymbol{x}_a\|^2 \end{aligned} \tag{A.18}$$

Since, by (A.17):

$$\begin{aligned} &\dot{V}(\boldsymbol{x}_a) = \frac{\partial V(\boldsymbol{x}_a)}{\partial \boldsymbol{x}_a}\left[\mathbf{A}\boldsymbol{x}_a - \mathbf{B_u}\boldsymbol{K}_{\text{oist}}(t)\boldsymbol{x}_a\right] \\ &- \frac{\partial V(\boldsymbol{x}_a)}{\partial \boldsymbol{x}_a}\mathbf{B_u}\mathrm{Dz}_{\underline{v}(t)}^{\bar{v}(t)}\left(\boldsymbol{K}_{\text{oist}}(t)\boldsymbol{e}_x(t) + \mathbf{D_K}\boldsymbol{e}_x(t) + \mathbf{C_K}\boldsymbol{x}_K(t) + \left(\mathbf{D_K} + \boldsymbol{K}_{\text{oist}}(t)\right)\mathbf{D_d}\boldsymbol{d}(t)\right) \end{aligned} \tag{A.19}$$

it comes

$$\begin{aligned} &\dot{V}(\boldsymbol{x}_a) \leq -\alpha_4\|\boldsymbol{x}_a\|^2 \\ &+ \alpha_3\|\boldsymbol{x}_a\|\,\|\mathbf{B_u}\|\left\|\mathrm{Dz}_{\underline{v}(t)}^{\bar{v}(t)}\left(\boldsymbol{K}_{\text{oist}}(t)\boldsymbol{e}_x(t) + \mathbf{D_K}\boldsymbol{e}_x(t) + \mathbf{C_K}\boldsymbol{x}_K(t) + \left(\mathbf{D_K} + \boldsymbol{K}_{\text{oist}}(t)\right)\mathbf{D_d}\boldsymbol{d}(t)\right)\right\| \end{aligned} \tag{A.20}$$

First, using Lemma 4.33 and $\boldsymbol{e}_x := \boldsymbol{x} - \boldsymbol{x}_a$, it is observed that since $\boldsymbol{K}_{\text{oist}}(t)\boldsymbol{x}$ is K_1-Lipschitz then

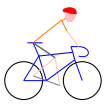

$$\|\boldsymbol{K}_{\text{oist}}(t)\boldsymbol{e}_x\| \leq K_1 \|\boldsymbol{e}_x\|, \forall t \tag{A.21}$$

Second, by property of the deadzone function, $\left\|\text{Dz}_{\underline{v}(t)}^{\overline{v}(t)}(v(t))\right\| \leq \|v(t)\|, \forall t$. It comes that

$$\begin{aligned}\dot{V}(\boldsymbol{x}_a) &\leq -\alpha_4 \|\boldsymbol{x}_a\|^2 + \alpha_3 \|\mathbf{B_u}\| \|\boldsymbol{x}_a\| \{[K_1 + \|\mathbf{D_K}\|] (\|\boldsymbol{e}_x\| + \|\mathbf{D_d}\| \|\boldsymbol{d}\|) + \|\mathbf{C_K}\| \|\boldsymbol{x}_K\|\} \\ &\leq -\alpha_4 \|\boldsymbol{x}_a\|^2 + \alpha_3 \|\mathbf{B_u}\| \|\boldsymbol{x}_a\| \left[K_1 + \left\|\begin{bmatrix}\mathbf{D_K} & \mathbf{C_K}\end{bmatrix}\right\|\right] \|\boldsymbol{X}\| \\ &\qquad + \alpha_3 \|\mathbf{B_u}\| \|\boldsymbol{x}_a\| \left[K_1 + \left\|\begin{bmatrix}0 & \mathbf{D_K}\end{bmatrix}\right\|\right] \|\mathbf{D_d}\| \|\boldsymbol{W}\|\end{aligned} \tag{A.22}$$

Using $k_1 > 0$ and $k_2 > 0$ such that

$$\begin{aligned}k_1 &\geq \alpha_3 \|\mathbf{B_u}\| \left[K_1 + \left\|\begin{bmatrix}\mathbf{D_K} & \mathbf{C_K}\end{bmatrix}\right\|\right] \in \mathbb{R} \\ k_2 &\geq \alpha_3 \|\mathbf{B_u}\| \left[K_1 + \left\|\begin{bmatrix}0 & \mathbf{D_K}\end{bmatrix}\right\|\right] \|\mathbf{D_d}\| \in \mathbb{R}\end{aligned} \tag{A.23}$$

then (A.22) becomes

$$\dot{V}(\boldsymbol{x}_a) \leq -\alpha_4 \|\boldsymbol{x}_a\|^2 + \|\boldsymbol{x}_a\| [k_1 \|\boldsymbol{X}\| + k_2 \|\boldsymbol{W}\|] \tag{A.24}$$

Applying the inequality $2\epsilon \|\boldsymbol{x}_a\| \|\boldsymbol{X}\| \leq \epsilon^2 \|\boldsymbol{x}_a\|^2 + \frac{\|\boldsymbol{X}\|^2}{\epsilon^2}$ for $\epsilon > 0$, (A.24) is re-written as

$$\begin{aligned}\dot{V}(\boldsymbol{x}_a) &\leq -\alpha_4 \|\boldsymbol{x}_a\|^2 + \tfrac{1}{2}k_1^2\epsilon_1^2 \|\boldsymbol{x}_a\|^2 + \tfrac{1}{2}k_2^2\epsilon_2^2 \|\boldsymbol{x}_a\|^2 + \tfrac{k_1^2}{2\epsilon_1^2} \|\boldsymbol{X}\|^2 + \tfrac{k_2^2}{2\epsilon_2^2} \|\boldsymbol{W}\|^2 \\ &\leq \left(-\alpha_4 + \tfrac{1}{2}k_1^2\epsilon_1^2 + \tfrac{1}{2}k_2^2\epsilon_2^2\right) \|\boldsymbol{x}_a\|^2 + \tfrac{k_1^2}{2\epsilon_1^2} \|\boldsymbol{X}\|^2 + \tfrac{k_2^2}{2\epsilon_2^2} \|\boldsymbol{W}\|^2 \\ &\leq -\alpha_5 \|\boldsymbol{x}_a\|^2 + \tfrac{k_1^2}{2\epsilon_1^2} \|\boldsymbol{X}\|^2 + \tfrac{k_2^2}{2\epsilon_2^2} \|\boldsymbol{W}\|^2\end{aligned} \tag{A.25}$$

where $\alpha_5 = \alpha_4 - \frac{1}{2}k_1^2\epsilon_2^2 - \frac{1}{2}k_2^2\epsilon_2^2 > 0$ if the constants ϵ_1 and ϵ_2 are chosen small enough so that $\alpha_4 > \frac{1}{2}k_1^2\epsilon_1^2 + \frac{1}{2}k_2^2\epsilon_2^2$. Using [Isidori 99, Lemma 10.4.2, p. 21], V is thus an ISS-Lyapunov function for the system

$$\dot{\boldsymbol{x}}_a = f_1\left(\boldsymbol{x}_a, \begin{bmatrix}\boldsymbol{X} \\ \boldsymbol{W}\end{bmatrix}\right) \tag{A.26}$$

where f_1 is a non-linear function adequately defined. According to [Isidori 99, Theorem 10.4.1, p. 21], the system in (A.26) is thus ISS. At the beginning of this proof, it has been shown that – for a specific class of bounded finite energy disturbance $\boldsymbol{d}$ – $\|\boldsymbol{X}\|_2$ is finite and $\|\boldsymbol{X}\|$ converges to zero. Using a similar approach to the previous case, there exists V_X and strictly positive constants β_1, β_2 such that $\dot{V}_X(\boldsymbol{X}) \leq -\beta_1 \|\boldsymbol{X}\|^2 + \beta_2 \|\boldsymbol{W}\|^2$. This function is an ISS-Lyapunov function to the following system

$$\dot{\boldsymbol{X}} = f_2(\boldsymbol{X}, \boldsymbol{W}) \tag{A.27}$$

where f_2 is a linear function adequately defined. Using [Isidori 99, Theorem 10.5.2, p. 34], it is possible to conclude that the cascade of systems in (A.28) is ISS. The cascade is illustrated in Fig. A.1. Note that in case $\boldsymbol{d} = 0$ and using [Isidori 99, Corollary 10.5.3, p. 35], the origin $(\boldsymbol{x}_a, \boldsymbol{X}) = (0, 0)$ is GAS for the cascade.

$$\begin{cases}\dot{\boldsymbol{x}}_a &= f_1\left(\boldsymbol{x}_a, \begin{bmatrix}\boldsymbol{X} \\ \boldsymbol{W}\end{bmatrix}\right) \\ \dot{\boldsymbol{X}} &= f_2(\boldsymbol{X}, \boldsymbol{W})\end{cases} \tag{A.28}$$

Using the relation between ISS and CICS property, as stated in [Terrell 09, Theorem 16.4, p. 373], it comes that the cascade in (A.28) is CICS. Hence, using the theorem in [Sontag 89] (where CIBS property is a weaker property than CICS), the origin $(\boldsymbol{x}_a, \boldsymbol{X}) = (0, 0)$ is GAS for the cascade. This concludes the proof.

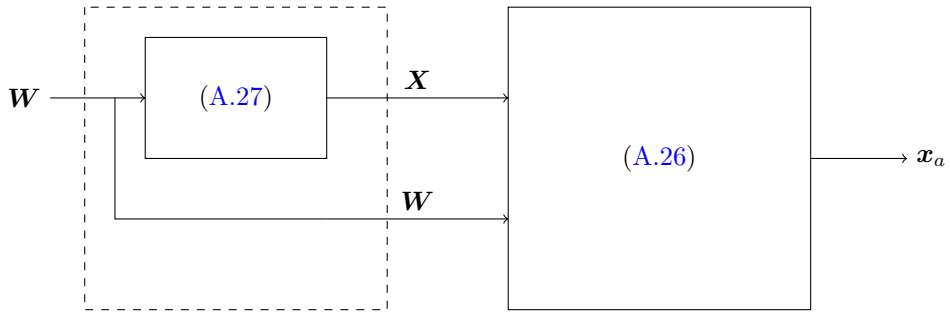

Figure A.1: Illustration of the interconnections in the cascade described by (A.28).

Appendix B

Introduction to linear interval state-observers

Interval state-observers are a recent addition to the class of set-membership methods. They allow the deterministic framing of a disturbed system state in case bounds on the disturbances are known. To qualify as an interval observer, a system should satisfy to some conditions which are difficult to enforce without making choices in the design. More precisely, the design of interval observers is facilitated when the initial system is cooperative. This motivates finding an appropriate state-coordinate transformation such that any non-cooperative system is cooperative in the new coordinates. In this chapter, the linear interval state-observer design based on a classical observer and state-coordinate transformation is presented.

Notations and definitions are recalled in B.1. A non-exhaustive state of the art of interval observers and interval observer design is presented in B.2. Then, linear interval observer design using a classical observer and a state-coordinate transformation (SCT) is tackled in B.3. The two different strategies to enforce cooperativity, namely time-varying and time-invariant SCT, are detailed in B.4 and applied on a simple example in B.5.

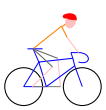

B.1 Notations and definitions

If not otherwise stated, the indices (i, j, k, l, m, n) are integers in $\mathbb{N}$. The ordering operators $<$, $>$, $\leq$ and $\geq$ are understood component-wise, i.e. if $\forall \mathbf{X} \in \mathbb{R}^{m\times n}$, $\forall \mathbf{Y} \in \mathbb{R}^{m\times n}$, $\mathcal{L}(\mathbf{X}, \mathbf{Y})$ stands for one of these comparison operators applied to $\mathbf{X}$ with respect to $\mathbf{Y}$, then:

$$\forall (i,j) \in \mathbb{N}\times\mathbb{N},\ i \leq m,\ j \leq n,\ [\mathcal{L}(\mathbf{X},\mathbf{Y})]_{ij} = \mathcal{L}(\mathbf{X}_{ij}, \mathbf{Y}_{ij}) \tag{B.1}$$

Known time-varying upper- and lower-bound on a possibly unknown time-varying signal $\boldsymbol{x}(t) \in \mathbb{R}^n$ are denoted $\underline{\boldsymbol{x}}(t)$ and $\overline{\boldsymbol{x}}(t)$. These satisfy the following inequalities:

$$\forall t \in \mathbb{R} \text{ (or } \mathbb{N}),\ \underline{\boldsymbol{x}}(t) \leq \boldsymbol{x}(t) \leq \overline{\boldsymbol{x}}(t) \tag{B.2}$$

The maximum and minimum operators are defined component-wise, i.e. if $\mathbf{A} \in \mathbb{R}^{m\times n}$ then:

$$\forall (i,j) \in \mathbb{N}\times\mathbb{N},\ i \leq m,\ j \leq n,\ [\max(\mathbf{A}, \mathbf{0}_{m\times n})]_{ij} = \max(\mathbf{A}_{ij}, 0) \tag{B.3}$$

Let $\mathbf{A} \in \mathbb{R}^{m\times n}$, then the following notations are used: $\mathbf{A}^+ := \max(\mathbf{A}, \mathbf{0}_{m\times n})$ and $\mathbf{A}^- := \mathbf{A}^+ - \mathbf{A}$. Definitions related to linear system dynamics properties are now introduced. They will be useful to design interval observers on linear systems, both in the continuous- and discrete-time cases. This is commented in B.3.

Definition B.1 (Metzler matrix)**.**
Let $\mathbf{A} \in \mathbb{R}^{n\times n}$. The matrix $\mathbf{A}$ is said to be *Metzler* if

$$\forall i \neq j,\ \mathbf{A}_{ij} \geq 0 \tag{B.4}$$

In other words, the off-diagonal elements of a Metzler matrix are positive. In case the diagonal elements are also positive, the matrix is said to be non-negative:

Definition B.2 (Non-negative matrix)**.**
Let $\mathbf{A} \in \mathbb{R}^{n\times n}$. The matrix $\mathbf{A}$ is said to be *non-negative* if

$$\forall (i,j),\ \mathbf{A}_{ij} \geq 0 \tag{B.5}$$

The notion of cooperative system is extensively used when designing interval observers as is shown in B.2. Such systems have interesting properties as far as trajectory ordering is considered. In the two following definitions, an autonomous linear time-invariant system with state matrix $\mathbf{A}$ and state $\boldsymbol{x}$ is considered:

$$(\mathbf{G}) \quad \dot{\boldsymbol{x}}(t) = \mathbf{A}\boldsymbol{x}(t) \quad \forall t \in \mathbb{R}_+ \quad \text{(continuous-time framework)} \tag{B.6a}$$

$$(\mathbf{F}) \quad \boldsymbol{x}(t+1) = \mathbf{A}\boldsymbol{x}(t) \quad \forall t \in \mathbb{N} \quad \text{(discrete-time framework)} \tag{B.6b}$$

Definition B.3 (Cooperative system, continuous-time [Mazenc 11])**.**
The system $(\mathbf{G})$ in (B.6a) is said to be *cooperative* if $\mathbf{A}$ is *Metzler*.

Remark B.4. Let consider the system $(\mathbf{G})$ in (B.6a). Let $\underline{\boldsymbol{x}_0} \leq \overline{\boldsymbol{x}_0}$ two ordered initial conditions and $\underline{\boldsymbol{x}}(t)$ (resp. $\overline{\boldsymbol{x}}(t)$) the two resulting trajectories. Then,

$$\underline{\boldsymbol{x}}(t) \leq \overline{\boldsymbol{x}}(t),\ \forall t \in \mathbb{R}_+ \tag{B.7}$$

$\diamond$

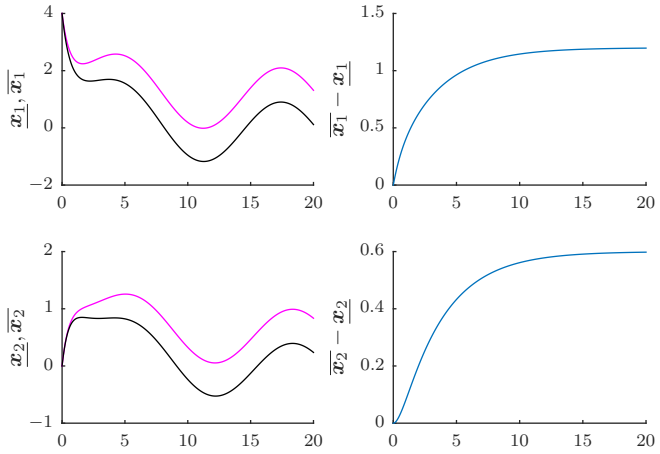

Figure B.1: Simulation results for the cooperative system ($\mathbf{G_1}$) in (B.8a) (*left*) and trajectories comparison (*right*).

Remark B.5. Let consider a continuous-time linear system with n states, m outputs and l inputs. It is said to be cooperative if $\mathbf{A}$ is Metzler, $\mathbf{B} \in \mathbb{R}_+^{n\times l}$, $\mathbf{C} \in \mathbb{R}_+^{m\times n}$ and $\mathbf{D} \in \mathbb{R}_+^{m\times l}$. Note that a cooperative continuous-time system is also a positive system. ◇

To illustrate the notion of cooperativity, a simple example is now introduced where two second-order systems are considered. One of these systems is cooperative while the other is not. This illustrates Remark B.4 where it is stated that a cooperative system preserves ordering of its trajectories with respect to the initial condition and inputs.

Example B.6 (Comparison of second-order cooperative and non-cooperative systems)**.** To illustrate Remark B.4, let consider the two following second-order linear systems:

$$(\mathbf{G_1}) \quad \dot{\boldsymbol{x}} = \begin{bmatrix} -1 & 1 \\ \frac{1}{2} & -1 \end{bmatrix} \boldsymbol{x} + \begin{bmatrix} 1 \\ 0 \end{bmatrix} u \tag{B.8a}$$

$$(\mathbf{G_2}) \quad \dot{\boldsymbol{x}} = \begin{bmatrix} -1 & 1 \\ -\frac{1}{2} & -1 \end{bmatrix} \boldsymbol{x} + \begin{bmatrix} 1 \\ 0 \end{bmatrix} u \tag{B.8b}$$

with initial condition $\boldsymbol{x}_0 = \begin{bmatrix} 4 & 0 \end{bmatrix}^\top$[1]. According to Definition B.1 and Remark B.5, ($\mathbf{G_1}$) is a cooperative system while ($\mathbf{G_2}$) is not. Let consider two ordered inputs $\underline{u}(t)$ and $\overline{u}(t)$ such that $\underline{u}(t) \leq \overline{u}(t)$, $\forall t \in \mathbb{R}_+$. In simulation, the following signals are considered:

$$\begin{array}{rcl} \underline{u}(t) & = & -0.1 + \sin(0.5t) \\ \overline{u}(t) & = & 0.5 + \sin(0.5t) \end{array}, \forall t \tag{B.9}$$

The time-response of both systems in (B.8a) and (B.8b) is then simulated using successively $\underline{u}(t)$ and $\overline{u}(t)$ as the input signal. The state vector is respectively denoted $\underline{\boldsymbol{x}_i}(t)$ (in black color in the figures) and $\overline{\boldsymbol{x}_i}(t)$ (in magenta) for $i \in \{1, 2\}$. The simulation results are shown in Fig. B.1 and B.2. In these figures, the trajectories difference $\overline{\boldsymbol{x}_i}(t) - \underline{\boldsymbol{x}_i}(t)$ has been represented in blue in the right plots. As symbolized by the *red* color in Fig. B.2, system ($\mathbf{G_2}$) does not keep partial ordering of the inputs.

♣

In the discrete-time case, a similar definition of a cooperative system can be formulated. The main difference lies in the nature of the state matrix $\mathbf{A}$:

[1] Note that the initial condition is supposed to be known here. Similar results would be obtained using ordered initial conditions.

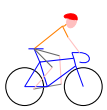

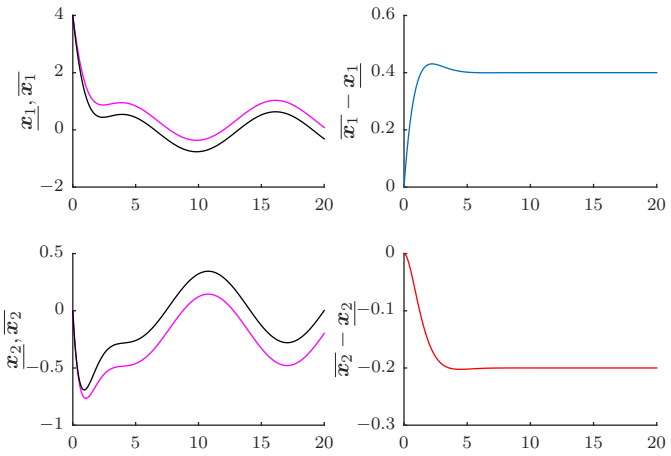

Figure B.2: Simulation results for the non-cooperative system ($\mathbf{G_2}$) in (B.8b) (*left*) and trajectories comparison (*right*).

Definition B.7 (Cooperative system, discrete-time [Efimov 13e])**.**
The system ($\mathbf{F}$) in (B.6b) is said to be *cooperative* if $\mathbf{A}$ is *non-negative*.

Remark B.8. Note that contrary to the continuous-time case, a cooperative discrete-time system is not a positive system. In the discrete-time case, a system is positive if and only if its state-matrix is non-negative *with at least one positive entry* [Germani 07]. ◇

Remark B.9. Similarly to Remark B.5 let consider a discrete-time linear system with n states, m outputs and l inputs. It is said to be cooperative if $\mathbf{A}$ is non-negative, $\mathbf{B} \in \mathbb{R}_+^{n\times l}$, $\mathbf{C} \in \mathbb{R}_+^{m\times n}$ and $\mathbf{D} \in \mathbb{R}_+^{m\times l}$. ◇

The definition of a linear interval observer is now introduced. It is inspired by the definition given in [Cacace 15]. Non-linear formulations are also given for example in [Mazenc 11]. The following linear systems are considered:

$$(\mathbf{G}) \begin{cases} \dot{\boldsymbol{x}}(t) &= \mathbf{A}\boldsymbol{x}(t) + \mathbf{B_u}\boldsymbol{u}(t) + \mathbf{B_d}\boldsymbol{d}(t) \\ \boldsymbol{y}(t) &= \mathbf{C}\boldsymbol{x}(t) + \mathbf{D_u}\boldsymbol{u}(t) + \mathbf{D_d}\boldsymbol{d}(t) \quad , t \in \mathbb{R}_+ \\ \boldsymbol{x}(0) &= \boldsymbol{x}_0 \end{cases} \tag{B.10a}$$

$$(\mathbf{F}) \begin{cases} \boldsymbol{x}(t+1) &= \mathbf{A}\boldsymbol{x}(t) + \mathbf{B_u}\boldsymbol{u}(t) + \mathbf{B_d}\boldsymbol{d}(t) \\ \boldsymbol{y}(t) &= \mathbf{C}\boldsymbol{x}(t) + \mathbf{D_u}\boldsymbol{u}(t) + \mathbf{D_d}\boldsymbol{d}(t) \quad , t \in \mathbb{N} \\ \boldsymbol{x}(0) &= \boldsymbol{x}_0 \end{cases} \tag{B.10b}$$

where $\boldsymbol{x} \in \mathbb{R}^n$, $\boldsymbol{y} \in \mathbb{R}^m$, $\boldsymbol{u} \in \mathbb{R}^l$ is a known input and $\boldsymbol{d}(t) \in \mathbb{R}^k$ is an unknown disturbance input. An interval observer for the system ($\mathbf{G}$) can be designed if some information on the unknown signal $\boldsymbol{d}$ are available. This justifies the following assumption where bounds on the unknown signal and the initial condition are supposed to be known.

Assumption B.10 (Known bounds)**.**

- There exists two known bounds $\underline{\boldsymbol{d}} \in \mathbb{R}^n$ and $\overline{\boldsymbol{d}} \in \mathbb{R}^n$ such that

$$\underline{\boldsymbol{d}}(t) \leq \boldsymbol{d}(t) \leq \overline{\boldsymbol{d}}(t), \forall t \tag{B.11}$$

- The initial condition $\boldsymbol{x}_0$ is supposed to be bounded by two known bounds

$$\underline{\boldsymbol{x}_0} \leq \boldsymbol{x}_0 \leq \overline{\boldsymbol{x}_0} \tag{B.12}$$

The definition of a linear interval observer for linear time-invariant systems is now formally introduced. Note this definition is not constructive and only gives the properties required for a system to qualify as an interval observer of another system.

Definition B.11 (Linear interval observer [Cacace 15, Definition 4, p. 1667])**.**
Consider a system $(\mathbf{G})$ as in (B.10a) (resp. (B.10b)) where $\boldsymbol{u}(t)$ and $\boldsymbol{d}(t)$ are piecewise continuous. Suppose the unknown disturbance input signal $\boldsymbol{d}(t)$ and the initial condition $\boldsymbol{x}_0$ satisfy to Assumption B.10. Then, the dynamical system

$$(\mathbf{G}^\sharp)\begin{cases} \dot{\boldsymbol{z}}(t) &= \mathbf{A}^\sharp \boldsymbol{z}(t) + \mathbf{B}^\sharp_{\mathbf{u}} \boldsymbol{u}(t) + \mathbf{B}^\sharp_{\mathbf{d}} \begin{bmatrix} \underline{\boldsymbol{d}}(t) \\ \overline{\boldsymbol{d}}(t) \end{bmatrix} & \in \mathbb{R}^{2n} \\ \begin{bmatrix} \underline{\boldsymbol{x}}(t) \\ \overline{\boldsymbol{x}}(t) \end{bmatrix} &= \mathbf{C}^\sharp \boldsymbol{z}(t) & \text{where rank}\left(\mathbf{C}^\sharp\right) = 2n \end{cases} \tag{B.13}$$

(resp. $\boldsymbol{z}(t+1) = \ldots$) associated with the initial condition $\boldsymbol{z}_0 = \left(\mathbf{C}^{\sharp\top}\mathbf{C}^\sharp\right)^{-1}\left[\underline{\boldsymbol{x}_0} \quad \overline{\boldsymbol{x}_0}\right]^\top$, where the newly defined matrices are of appropriate dimensions, is a *linear interval observer* for the system $(\mathbf{G})$ in (B.10a) (resp. (B.10b)) if

(1) $\left(\mathbf{G}^\sharp\right)$ is ISS;

(2) For any $\boldsymbol{x}_0$, $\underline{\boldsymbol{x}_0}$, $\overline{\boldsymbol{x}_0}$ in $\mathbb{R}^n$ satisfying to Assumption B.10, the solutions of (B.10a) (resp. (B.10b)) and (B.13) with respectively $\boldsymbol{x}_0$ and $\boldsymbol{z}_0$ as initial conditions are defined $\forall t \in \mathbb{R}_+$ (resp. $\mathbb{N}$) and fulfil

$$\underline{\boldsymbol{x}}(t) \leq \boldsymbol{x}(t) \leq \overline{\boldsymbol{x}}(t), \forall t \tag{B.14}$$

(3) If $\left\|\overline{\boldsymbol{d}}(t) - \underline{\boldsymbol{d}}(t)\right\|$ is uniformly bounded $\forall t \in \mathbb{R}_+$ (resp. $\mathbb{N}$) then $\|\overline{\boldsymbol{x}}(t) - \underline{\boldsymbol{x}}(t)\|$ is also uniformly bounded $\forall t \in \mathbb{R}_+$ (resp. $\mathbb{N}$) and if $\underline{\boldsymbol{d}}(t) = \overline{\boldsymbol{d}}(t)$, $\forall t \in \mathbb{R}_+$ (resp. $\mathbb{N}$) then $\|\overline{\boldsymbol{x}}(t) - \underline{\boldsymbol{x}}(t)\| \to 0$.

It was shown in [Gouzé 00] that cooperative linear systems admit interval observers with a block-diagonal $\mathbf{A}^\sharp$. This means that the bounds dynamics are independent and can be expressed as the states of two independent linear systems:

$$(\mathbf{G}^\sharp)\begin{cases} \dot{\underline{\boldsymbol{x}}}(t) &= \mathbf{A}^\sharp_{\mathbf{1}} \underline{\boldsymbol{x}}(t) + \mathbf{B}^\sharp_{\mathbf{u},\mathbf{1}} \boldsymbol{u}(t) + \mathbf{B}^\sharp_{\mathbf{d},\mathbf{1}} \begin{bmatrix} \underline{\boldsymbol{d}}(t) \\ \overline{\boldsymbol{d}}(t) \end{bmatrix} \\ \dot{\overline{\boldsymbol{x}}}(t) &= \mathbf{A}^\sharp_{\mathbf{2}} \overline{\boldsymbol{x}}(t) + \mathbf{B}^\sharp_{\mathbf{u},\mathbf{2}} \boldsymbol{u}(t) + \mathbf{B}^\sharp_{\mathbf{d},\mathbf{2}} \begin{bmatrix} \underline{\boldsymbol{d}}(t) \\ \overline{\boldsymbol{d}}(t) \end{bmatrix} \end{cases} \tag{B.15}$$

The result is still valid with minor modifications in the discrete-time case. In the case of an original linear system with no uncertain parameter, it is possible to obtain linear interval observers with dynamics as in (B.15) by using an appropriate state-coordinate transformation.

Prior to recalling the common approach to interval observers design in B.3, a state of the art is now presented to suitably recall the origins and main contributions to the interval observer theory.

B.2 State of the art

Interval observer methods belong to the wide class of estimation techniques and to the subclass of *bounded error* or *set-membership* estimation techniques. While estimation techniques often make assumptions on the types of state and measurement noise signals (e.g. Gaussian distributions),

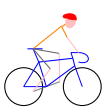

most *set-membership* methods only require assumptions on the bounds of these noises. The consequence is that such methods do not provide an estimate of the state but estimates of bounds on the state. These bounds are guaranteed as long as the modelling bounds on the considered noise signals are satisfied.

The main *set-membership* approaches are mentioned in [Raïssi 10]. To summarize, two main techniques can be identified:

- interval analysis applied to state bounding [Jaulin 02, Raïssi 04, Kieffer 06]. These methods are based on a prediction/correction mechanism similar to the Kalman filter. An enclosure of the state is computed at each time using validated numerical integration. The obtained set is then contracted by discarding inconsistent trajectories. These methods are not used in this thesis. A lot of information on applied interval analysis can be found for example in [Jaulin 01];
- Closed-loop interval observers, which are considered here.

Closed-loop observers are so-called in reference to the measurements of the system being taken into account at each time instant in the determination of the estimate. In the case of interval observers, the measurements as well as the known bounds on the noise signals are used to compute bounds on the considered system state. An interval observer is basically the reunion of two dynamical systems, each one *observing* either the upper or lower bound of the considered system state. This is formalized in Definition B.11. Note that designing reduced-order interval observer to estimate bounds on some components of the state vector is possible using the same definition.

Initial studies [Gouzé 00] (also recalled in [Mazenc 11, Theorem 1, p. 141]) focused on a very particular class of systems, namely cooperative systems. As illustrated in Example B.6, such systems have the interesting property to have ordered trajectories with respect to the initial conditions and forcing input [Smith 95, Farina 00]. This allows straightforward design of interval observers since a copy of the initial system with only minor modifications will qualify. However, only considering the class of cooperative system is a quite restrictive hypothesis: not every dynamical system has its state-matrix being Metzler or non-negative (see Definitions B.3 and B.7).

This motivated more recent studies in which non-cooperative systems are also considered. Two main approaches can be identified to design interval observers on non-cooperative systems:

- an approach based on *Internally Positive Representations* (IPR);
- Approaches based on *State-Coordinate Transformations* (SCT).

The class of positive systems is a subclass of cooperative systems. This is the core of the first approach proposed in [Cacace 15] where the notion of *Internally Positive Representations* [Cacace 12, Cacace 14, Germani 10] of a system is used. The article first describes the design of an IPR-based positive observer using the internally positive representation of the studied system. Then, it is proved in [Cacace 15, Theorem 11] that a reunion of two such observers with adequate inputs is an interval observer for the studied system. More complex designs implying coordinate changes are also discussed in this article when some hypotheses are not satisfied.

The other approaches are based on classical observers and state-coordinate transformations. First, a classical observer is designed to stabilize the system dynamics. This results in an observation error. Then, a state-coordinate transformation is determined such that the observation error dynamics is cooperative in the new coordinates. An interval observer is then designed on this cooperative system. In [Mazenc 11], based on results from [Mazenc 10], the authors proposed a time-varying state-coordinate transformation in the case of time-invariant exponentially stable linear systems. The transformation is based on the real Jordan canonical form determination of the system state matrix. In [Raïssi 12], a time-invariant state-coordinate transformation was proposed for a class of non-linear systems. The problem of finding a transformation such that the state matrix is Metzler is formalized as the solution of a Sylvester equation.

More recently, extensions of these SCT-based approaches have been proposed to accommodate for more complex situations. In [Mazenc 12b], the time-varying SCT is applied to the case of

continuous-time systems with discrete-time outputs. Discrete-time systems are considered for example in [Efimov 13a] where the time-invariant SCT is adapted to this case. The authors also extend the positive representation approach to such systems and show that the resulting design gains can be found using LMIs. In [Mazenc 12a, Mazenc 14], time-varying interval observers are proposed for discrete-time systems. In [Efimov 11, Efimov 13f], it is shown how to achieve stabilization of an uncertain non-linear system using interval observers. The technique can also be applied to LPV and LTV systems. The design of interval observers for continuous-time LPV systems is also tackled in [Chebotarev 15] where the authors consider an additional performance criteria in the design. An LMI-based design is proposed in [Wang 15] for a specific class of LPV systems. As far as LTV systems are concerned, the time-invariant SCT is extended in [Efimov 13d]. As mentioned in [Thabet 14b], the method is however not applicable in most realistic cases. The authors then extend the time-varying SCT approach to LTV systems and propose a methodology for practical implementation. Interval observers are also applied to systems with time-varying delays in [Efimov 13b] and input delay in [Polyakov 13]. Other resources on interval observers for time-delayed systems include [Efimov 13c], [Mazenc 12c] and references therein.

More exotic problems implying interval observers are also reported. In [Moisan 10], a robust interval observer is developed to estimate bounds on the variables of an uncertain chaotic system. In [Briat 16], a method is proposed to design optimal peak-to-peak interval observers both in the continuous- and discrete-time frameworks.

Examples of application of interval observers include fault detection [Raïssi 10, Thabet 14a], bioreactors and bioprocesses monitoring [Alcaraz-Gonzalez 02, Goffaux 09, Moisan 09] and engine air-fuel ratio estimation and control [Efimov 15]. In [Chambon 15d], an interval observer is used in the application of an output-constrained control design method for output-feedback systems. This is a main contribution of this thesis as described in Chapter 5. This work also triggered some new results on how to compute the state-coordinate transformation [Chambon 15b, Chambon 16]. This is another main contribution of this thesis as explained in Chapter 7.

In conclusion, interval observers theory has attracted the research community attention in the past few years. This has resulted in an increasing number of publications with multiple fields of application. The reader interested in finding more information and resources on this active field of research may consult the resources [Dinh 14, Efimov 16].

B.3 Interval observer design

In this section, the design of an interval observer for a given linear time-invariant system is described in details. As briefly mentioned in [Mazenc 10] and recalled in [Efimov 13f] and B.1, there exists various means of defining the structure of an interval observer. Depending on the form of $\mathbf{A}^\sharp$, the dynamics of the two underlying systems may be intertwined. However, as already mentioned, cooperative linear systems admit interval observers with block-diagonal $\mathbf{A}^\sharp$ which is used in the following.

B.3.1 Signal vector ordering: a lemma

The property of cooperative systems is to keep the order of trajectories when ordered inputs are applied to them. Hence, it is first required to order the considered inputs which is done using an existing lemma.

Lemma B.12 (Bounds on $\mathbf{A}\boldsymbol{x}(t)$ knowing bounds on $\boldsymbol{x}(t)$ [Efimov 13d, Lemma 1])**.** *Let $\boldsymbol{x} \in \mathbb{R}^n$ for which bounds are known: $\underline{\boldsymbol{x}}(t) \leq \boldsymbol{x}(t) \leq \overline{\boldsymbol{x}}(t)$, $\forall t$. Let $\mathbf{A} \in \mathbb{R}^{m\times n}$ a constant matrix such that $\mathbf{A} = \mathbf{A}^+ - \mathbf{A}^-$ by definition. Then, $\forall t \in \mathbb{R}_+$ (or $\mathbb{N}$),*

$$\mathbf{A}^+\underline{\boldsymbol{x}}(t) - \mathbf{A}^-\overline{\boldsymbol{x}}(t) \leq \mathbf{A}\boldsymbol{x}(t) \leq \mathbf{A}^+\overline{\boldsymbol{x}}(t) - \mathbf{A}^-\underline{\boldsymbol{x}}(t) \tag{B.16}$$

Proof. As mentioned in [Efimov 13d], the proof is straightforward once noticing that

$$\mathbf{A}\boldsymbol{x}(t) = \left(\mathbf{A}^+ - \mathbf{A}^-\right)\boldsymbol{x}(t)$$

and using the bounds on $\boldsymbol{x}(t)$. □

Remark B.13. In case the matrix $\mathbf{A}$ depends on a set of real parameters Θ bounded by $\underline{\Theta}$ and $\overline{\Theta}$, one may express parameters-free bounds $\underline{\mathbf{A}}$ and $\overline{\mathbf{A}}$ on the matrix $\mathbf{A}(\Theta)$ itself. In this case, Lemma B.12 has a more complex formulation which can be found in [Efimov 13e, Lemma 1] for example. This is however not considered in this chapter where the matrix $\mathbf{A}$ is neither time-varying nor parameter-dependent. ◇

B.3.2 Classical observer and observation error

As seen in Definition B.11, a system must fulfil three conditions to qualify as an interval observer for another dynamical system. Obviously, these conditions are difficult to satisfy without more information on the structure of the system to be observed. In particular, in case the system is unstable, achieving condition (1) or (3) is fanciful. A solution would be to restrict the class of considered systems to stable systems only. To avoid such restrictive assumption, a strategy proposed in [Mazenc 11] amongst other works is to consider a classical observer and to design the interval observer on the resulting observation error dynamics. Using both the classical and interval observers, one then determines bounds on the initial system state as detailed in B.3.5. To be able to stabilize the classical observer dynamics, the following detectability assumption is made:

Assumption B.14 (Initial system detectability)**.**
System $(\mathbf{G})$ in (B.10) is detectable. In case it is observable, then the whole dynamics of the classical observer can be placed.

Let $(\mathbf{G})$ a system with realisation (B.10) and satisfying to Assumptions B.10 and B.14. Let consider a classical observer on system $(\mathbf{G})$ with the following dynamics:

$$\left(\widehat{\mathbf{G}}\right)\begin{cases} \dot{\widehat{\boldsymbol{x}}}(t) &= (\mathbf{A}-\mathbf{LC})\,\widehat{\boldsymbol{x}}(t)+(\mathbf{B_u}-\mathbf{LD_u})\,\boldsymbol{u}(t)+\mathbf{L}\boldsymbol{y}(t) \\ \widehat{\boldsymbol{y}}(t) &= \mathbf{C}\widehat{\boldsymbol{x}}(t)+\mathbf{D_u}\boldsymbol{u}(t) \\ \widehat{\boldsymbol{x}}(0) &= \widehat{\boldsymbol{x}}_0 \end{cases}, t\in\mathbb{R}_+ \tag{B.17a}$$

$$\left(\widehat{\mathbf{F}}\right)\begin{cases} \widehat{\boldsymbol{x}}(t+1) &= (\mathbf{A}-\mathbf{LC})\,\widehat{\boldsymbol{x}}(t)+(\mathbf{B_u}-\mathbf{LD_u})\,\boldsymbol{u}(t)+\mathbf{L}\boldsymbol{y}(t) \\ \widehat{\boldsymbol{y}}(t) &= \mathbf{C}\widehat{\boldsymbol{x}}(t)+\mathbf{D_u}\boldsymbol{u}(t) \\ \widehat{\boldsymbol{x}}(0) &= \widehat{\boldsymbol{x}}_0 \end{cases}, t\in\mathbb{N} \tag{B.17b}$$

where $\mathbf{L}\in\mathbb{R}^{n\times m}$ is the observer gain. Thanks to Assumption B.14, it is possible to find $\mathbf{L}$ such that $\mathbf{A}-\mathbf{LC}$ is Hurwitz. Let choose $\mathbf{L}$ accordingly. Due to the lack of knowledge on the unknown input $\boldsymbol{d}(t)$ the observation of system $(\mathbf{G})$ state by the observer $\left(\widehat{\mathbf{G}}\right)$ in (B.17) results in an observation error $\boldsymbol{e}(t):=\boldsymbol{x}(t)-\widehat{\boldsymbol{x}}(t)$ which dynamics satisfies the following equation.

$$(\mathbf{G_e})\begin{cases} \dot{\boldsymbol{e}}(t) &= (\mathbf{A}-\mathbf{LC})\,\boldsymbol{e}+(\mathbf{B_d}-\mathbf{LD_d})\,\boldsymbol{d}(t) \\ \boldsymbol{e}(0) &= \boldsymbol{x}_0-\widehat{\boldsymbol{x}}_0 \end{cases}, t\in\mathbb{R}_+ \tag{B.18a}$$

$$(\mathbf{F_e})\begin{cases} \boldsymbol{e}(t+1) &= (\mathbf{A}-\mathbf{LC})\,\boldsymbol{e}+(\mathbf{B_d}-\mathbf{LD_d})\,\boldsymbol{d}(t) \\ \boldsymbol{e}(0) &= \boldsymbol{x}_0-\widehat{\boldsymbol{x}}_0 \end{cases}, t\in\mathbb{N} \tag{B.18b}$$

Using such classical observer allows to satisfy condition (1) in Definition B.11. Condition (3) can be enforced through fine selection of the observer gain $\mathbf{L}$.

B.3.3 From the observation error to a cooperative system

In the previous section, a classical observer has been introduced to avoid restrictive assumptions on the initial system dynamics. Designing an interval observer on such stable classical observer is expected to be easier since conditions (1) and (3) in Definition B.11 can be enforced through fine selection of $\mathbf{L}$.

However, the second necessary condition (2) is more challenging. It would be satisfied if $\mathbf{A}-\mathbf{LC}$ was Metzler[2] since any system of the form (B.15) with Metzler state matrix $\mathbf{A}_1^\sharp = \mathbf{A}_2^\sharp = \mathbf{A}-\mathbf{LC}$ satisfies (2). Thus, the question is the following: *is it always possible to choose* $\mathbf{L}$ *such that* $\mathbf{A}-\mathbf{LC}$ *is Hurwitz Metzler*? In the affirmative, then satisfying (2) is straightforward for any classical observer of any detectable system. Finding such matrix $\mathbf{L}$ is however delusive as illustrated in this trivial example:

Example B.15 (Find $\mathbf{L}$ such that $\mathbf{A}-\mathbf{LC}$ is Hurwitz Metzler)**.** Let $\mathbf{A} = \begin{bmatrix} -1 & -1 \\ 0 & -2 \end{bmatrix}$, $\mathbf{C} = \begin{bmatrix} 1 & 0 \end{bmatrix}$ and let parametrize the observer gain $\mathbf{L} = \begin{bmatrix} l_1 \\ l_2 \end{bmatrix}$ where $(l_1, l_2) \in \mathbb{R}^2$. Then,

$$\mathbf{A}-\mathbf{LC} = \begin{bmatrix} -1-l_1 & -1 \\ -l_2 & -2 \end{bmatrix}$$

which is never a Metzler matrix $\forall\,(l_1, l_2)$. ♣

A similar example can be provided in the discrete-time case where this is not possible to find $\mathbf{L}$ such that $\mathbf{A}-\mathbf{LC}$ is non-negative.

As seen in this trivial example, it may not be possible to find a matrix $\mathbf{L}$ such that $\mathbf{A}-\mathbf{LC}$ is Hurwitz Metzler. Two different assumptions are now introduced to allow definition of an interval observer on system $(\mathbf{G_e})$ in (B.18a). Although the resulting interval observers share the same structure, the family of considered systems is reduced in the first case (strong assumption) while additional techniques are required to deal with the second case (weak assumption). Two such techniques are presented in B.4.

Strong assumption In this case, it is supposed that no state-coordinate transformation (SCT) is required to determine a Metzler matrix $\mathbf{M} = \mathbf{A}-\mathbf{LC}$.

Assumption B.16 (Cooperative observation error dynamics: strong assumption)**.**
Let $\mathbf{A} \in \mathbb{R}^{n\times n}$ and $\mathbf{C} \in \mathbb{R}^{m\times n}$. $\exists \mathbf{L} \in \mathbb{R}^{n\times m}$ such that $\mathbf{A}-\mathbf{LC}$ is *Hurwitz Metzler/Schur non-negative.*

This assumption is strong in the sense that all systems may not satisfy it, even trivial ones as in Example B.15. For a system $(\mathbf{G})$ which matrices $\mathbf{A}$ and $\mathbf{C}$ satisfy to Assumption B.16, there exists a cooperative stable observation error dynamics (B.18a).

Weak assumption In this case, it is supposed that a state-coordinate transformation (SCT) has been determined such that $\mathbf{M} = \mathbf{P}\,(\mathbf{A}-\mathbf{LC})\,\mathbf{P}^{-1}$ is Metzler. Existing techniques to determine such SCT are presented in B.4.

Assumption B.17 (Cooperative observation error dynamics: weak assumption)**.**
Let $\mathbf{A} \in \mathbb{R}^{n\times n}$ and $\mathbf{C} \in \mathbb{R}^{m\times n}$. $\exists \mathbf{P} \in \mathbb{R}^{n\times n}$ and $\mathbf{L} \in \mathbb{R}^{n\times m}$ such that $\mathbf{P}\,(\mathbf{A}-\mathbf{LC})\,\mathbf{P}^{-1}$ is *Hurwitz Metzler/Schur non-negative.*

This assumption is weak in the sense that it does not refer to the system dynamics. However, it raises computational problems since an additional matrix $\mathbf{P}$ of size $n \times n$ must be determined.

Remark B.18. The transformation matrix $\mathbf{P}$ is considered to be time-invariant in Assumption B.17. Using a time-varying matrix $\mathbf{P}$, a slightly different formulation is obtained. This is tackled in B.4. ◇

[2] Non-negative in the discrete-time case.

Remark B.19. The considered matrix $\mathbf{P}$ is a state-coordinate transformation matrix. If $\boldsymbol{x}_z = \mathbf{P}\boldsymbol{x}$ then the state-matrix of system $(\mathbf{G_e})$ in (B.18a) equals $\mathbf{P}(\mathbf{A}-\mathbf{LC})\mathbf{P}^{-1}$ in the new coordinates. ◇

For a system $(\mathbf{G})$ whose matrices $\mathbf{A}$ and $\mathbf{C}$ satisfy to Assumption B.17, there exists a cooperative stable observation error dynamics (B.18) *in the new coordinates.*

Example B.20 (Find $\mathbf{P}$ and $\mathbf{L}$ such that $\mathbf{P}(\mathbf{A}-\mathbf{LC})\mathbf{P}^{-1}$ is Hurwitz Metzler)**.** Let $\mathbf{A}$ and $\mathbf{C}$ as defined in Example B.15. We saw that $\nexists \mathbf{L}$ such that $\mathbf{A}-\mathbf{LC}$ is Metzler. Let $\mathbf{P} = \begin{bmatrix} 0 & -1 \\ 1 & 0 \end{bmatrix}$. Then,

$$\mathbf{P}(\mathbf{A}-\mathbf{LC})\mathbf{P}^{-1} = \begin{bmatrix} -2 & l_2 \\ 1 & -1-l_1 \end{bmatrix}$$

and, choosing for example $l_1 = 4$ and $l_2 = 1$, one obtains that $\mathbf{P}(\mathbf{A}-\mathbf{LC})\mathbf{P}^{-1}$ is *Hurwitz Metzler.* ♣

This approach allows to consider systems which do not satisfy to Assumption B.16. However, determining an appropriate matrix $\mathbf{P}$ is rarely as easy as in Example B.20. Existing numerical methods include those presented in B.4 while a new method is introduced in Chapter 7.

B.3.4 Interval observer of the observation error dynamics

In B.3.2, the observation error dynamics (B.18) was expressed both in the discrete- and continuous-time frameworks. An interval observer on the observation error dynamics is now introduced.

Under Assumption B.16 Under Assumptions B.14 and B.16, there exists $\mathbf{L} \in \mathbb{R}^{n\times m}$ such that $\mathbf{A}-\mathbf{LC}$ is Hurwitz Metzler. Let choose this $\mathbf{L}$ which means that the observation error dynamics in (B.18) is cooperative up to its input matrix.

Proposition B.21 (Interval observer of the observation error, Assumption B.16)**.**
Under Assumptions B.10[a], B.14 and B.16, and by Definition B.11, the following system is an interval observer for the system $(\mathbf{G_e})$ *in* (B.18a)*:*

$$(\mathbf{G_e^\sharp}) \begin{cases} \dot{\underline{\boldsymbol{e}}}(t) &= (\mathbf{A}-\mathbf{LC})\,\underline{\boldsymbol{e}}(t) + [\mathbf{B_d}-\mathbf{LD_d}]^+\,\underline{\boldsymbol{d}}(t) - [\mathbf{B_d}-\mathbf{LD_d}]^-\,\overline{\boldsymbol{d}}(t) \\ \dot{\overline{\boldsymbol{e}}}(t) &= (\mathbf{A}-\mathbf{LC})\,\overline{\boldsymbol{e}}(t) + [\mathbf{B_d}-\mathbf{LD_d}]^+\,\overline{\boldsymbol{d}}(t) - [\mathbf{B_d}-\mathbf{LD_d}]^-\,\underline{\boldsymbol{d}}(t) \\ \underline{\boldsymbol{e}}(0) &= \underline{\boldsymbol{e}_0} \\ \overline{\boldsymbol{e}}(0) &= \overline{\boldsymbol{e}_0} \end{cases}, \; t \in \mathbb{R}_+ \tag{B.19}$$

where Lemma B.12 is used to bound the unknown vector $(\mathbf{B_d}-\mathbf{LD_d})\,\boldsymbol{d}(t)$*.*

[a] Which also implies that two vectors $\underline{\boldsymbol{e}_0}$ and $\overline{\boldsymbol{e}_0}$ such that $\underline{\boldsymbol{e}_0} \leq \boldsymbol{e}(0) \leq \overline{\boldsymbol{e}_0}$ are known.

Respectively, in the discrete-time case, the following system is an interval observer for the system $(\mathbf{F_e})$ in (B.18b):

$$(\mathbf{F_e^\sharp}) \begin{cases} \underline{\boldsymbol{e}}(t+1) &= (\mathbf{A}-\mathbf{LC})\,\underline{\boldsymbol{e}}(t) + [\mathbf{B_d}-\mathbf{LD_d}]^+\,\underline{\boldsymbol{d}}(t) - [\mathbf{B_d}-\mathbf{LD_d}]^-\,\overline{\boldsymbol{d}}(t) \\ \overline{\boldsymbol{e}}(t+1) &= (\mathbf{A}-\mathbf{LC})\,\overline{\boldsymbol{e}}(t) + [\mathbf{B_d}-\mathbf{LD_d}]^+\,\overline{\boldsymbol{d}}(t) - [\mathbf{B_d}-\mathbf{LD_d}]^-\,\underline{\boldsymbol{d}}(t) \\ \underline{\boldsymbol{e}}(0) &= \underline{\boldsymbol{e}_0} \\ \overline{\boldsymbol{e}}(0) &= \overline{\boldsymbol{e}_0} \end{cases}, \; t \in \mathbb{N} \tag{B.20}$$

Under Assumption B.17 Under Assumptions B.14 and B.17, there exists two matrices $\mathbf{P} \in \mathbb{R}^{n\times n}$ and $\mathbf{L} \in \mathbb{R}^{n\times m}$ such that $\mathbf{P}\left(\mathbf{A}-\mathbf{LC}\right)\mathbf{P}^{-1}$ is Hurwitz Metzler. Let choose these $\mathbf{P}$ and $\mathbf{L}$ which means that the observation error dynamics in (B.18) are cooperative (up to the input matrix) *in the new coordinates* $\boldsymbol{e}_z = \mathbf{P}\boldsymbol{e}$:

$$\left(\mathbf{G}_{\mathbf{e}}^{\mathbf{z}}\right)\begin{cases}\dot{\boldsymbol{e}}_z(t) &= \mathbf{P}\left(\mathbf{A}-\mathbf{LC}\right)\mathbf{P}^{-1}\boldsymbol{e}_z + \mathbf{P}\left(\mathbf{B_d}-\mathbf{LD_d}\right)\boldsymbol{d}(t)\\ \boldsymbol{e}_z(0) &= \mathbf{P}\boldsymbol{e}(0)\end{cases}, t\in\mathbb{R}_+ \tag{B.21a}$$

$$\left(\mathbf{F}_{\mathbf{e}}^{\mathbf{z}}\right)\begin{cases}\boldsymbol{e}_z(t+1) &= \mathbf{P}\left(\mathbf{A}-\mathbf{LC}\right)\mathbf{P}^{-1}\boldsymbol{e}_z + \mathbf{P}\left(\mathbf{B_d}-\mathbf{LD_d}\right)\boldsymbol{d}(t)\\ \boldsymbol{e}_z(0) &= \mathbf{P}\boldsymbol{e}(0)\end{cases}, t\in\mathbb{N} \tag{B.21b}$$

Proposition B.22 (Interval observer of the observation error, Assumption B.17)**.** *Under Assumptions B.10[a], B.14 and B.17, and by Definition B.11, the following system is an interval observer for system* $\left(\mathbf{G}_{\mathbf{e}}^{\mathbf{z}}\right)$ *in* (B.21a)*:*

$$\left(\mathbf{G}_{\mathbf{e}}^{\mathbf{z},\sharp}\right)\begin{cases}\underline{\dot{\boldsymbol{e}}_z}(t) &= \mathbf{P}\left(\mathbf{A}-\mathbf{LC}\right)\mathbf{P}^{-1}\underline{\boldsymbol{e}_z}(t) + \left[\mathbf{P}\left(\mathbf{B_d}-\mathbf{LD_d}\right)\right]^+\underline{\boldsymbol{d}}(t) - \left[\mathbf{P}\left(\mathbf{B_d}-\mathbf{LD_d}\right)\right]^-\overline{\boldsymbol{d}}(t)\\ \overline{\dot{\boldsymbol{e}}_z}(t) &= \mathbf{P}\left(\mathbf{A}-\mathbf{LC}\right)\mathbf{P}^{-1}\overline{\boldsymbol{e}_z}(t) + \left[\mathbf{P}\left(\mathbf{B_d}-\mathbf{LD_d}\right)\right]^+\overline{\boldsymbol{d}}(t) - \left[\mathbf{P}\left(\mathbf{B_d}-\mathbf{LD_d}\right)\right]^-\underline{\boldsymbol{d}}(t)\\ \underline{\boldsymbol{e}_z}(0) &= \mathbf{P}^+\underline{\boldsymbol{e}_0} - \mathbf{P}^-\overline{\boldsymbol{e}_0}\\ \overline{\boldsymbol{e}_z}(0) &= \mathbf{P}^+\overline{\boldsymbol{e}_0} - \mathbf{P}^-\underline{\boldsymbol{e}_0}\end{cases} \tag{B.22}$$

where Lemma B.12 is used to bound the unknown vector $\mathbf{P}\left(\mathbf{B_d}-\mathbf{LD_d}\right)\boldsymbol{d}(t)$*.*

[a] Which also implies that two signals $\underline{\boldsymbol{e}_z}(0)$ and $\overline{\boldsymbol{e}_z}(0)$ such that $\underline{\boldsymbol{e}_z}(0) \leq \boldsymbol{e}_z(0) \leq \overline{\boldsymbol{e}_z}(0)$ are known.

Respectively, in the discrete-time case, the following system is an interval observer for system $\left(\mathbf{F}_{\mathbf{e}}^{\mathbf{z}}\right)$ in (B.21b):

$$\left(\mathbf{F}_{\mathbf{e}}^{\mathbf{z},\sharp}\right)\begin{cases}\underline{\boldsymbol{e}_z}(t+1) &= \mathbf{P}\left(\mathbf{A}-\mathbf{LC}\right)\mathbf{P}^{-1}\underline{\boldsymbol{e}_z}(t) + \left[\mathbf{P}\left(\mathbf{B_d}-\mathbf{LD_d}\right)\right]^+\underline{\boldsymbol{d}}(t) - \left[\mathbf{P}\left(\mathbf{B_d}-\mathbf{LD_d}\right)\right]^-\overline{\boldsymbol{d}}(t)\\ \overline{\boldsymbol{e}_z}(t+1) &= \mathbf{P}\left(\mathbf{A}-\mathbf{LC}\right)\mathbf{P}^{-1}\overline{\boldsymbol{e}_z}(t) + \left[\mathbf{P}\left(\mathbf{B_d}-\mathbf{LD_d}\right)\right]^+\overline{\boldsymbol{d}}(t) - \left[\mathbf{P}\left(\mathbf{B_d}-\mathbf{LD_d}\right)\right]^-\underline{\boldsymbol{d}}(t)\\ \underline{\boldsymbol{e}_z}(0) &= \mathbf{P}^+\underline{\boldsymbol{e}_0} - \mathbf{P}^-\overline{\boldsymbol{e}_0}\\ \overline{\boldsymbol{e}_z}(0) &= \mathbf{P}^+\overline{\boldsymbol{e}_0} - \mathbf{P}^-\underline{\boldsymbol{e}_0}\end{cases} \tag{B.23}$$

Remark B.23. These formulations are valid only with a time-invariant matrix $\mathbf{P}$. A different formulation is obtained in case of a time-varying SCT. This is tackled in B.4.1. ◇

B.3.5 Interval observer of the initial system state vector

In the previous section, the following were obtained:

(1) $\underline{\boldsymbol{e}}(t)$ and $\overline{\boldsymbol{e}}(t)$ such that $\underline{\boldsymbol{e}}(t) \leq \boldsymbol{e}(t) \leq \overline{\boldsymbol{e}}(t)$, $\forall t$, under Assumptions B.10, B.14 and B.16;

(2) $\underline{\boldsymbol{e}_z}(t)$ and $\overline{\boldsymbol{e}_z}(t)$ such that $\underline{\boldsymbol{e}_z}(t) \leq \boldsymbol{e}_z(t) \leq \overline{\boldsymbol{e}_z}(t)$, $\forall t$, under Assumptions B.10, B.14 and B.17.

This information is now used to determine bounds on the initial system state vector $\boldsymbol{x}$. In the second case (2), it is first necessary to apply the reverse state-coordinate transformation while taking care to keep the signals ordering. To this end, Lemma B.12 is used where $\mathbf{T} = \mathbf{P}^{-1}$:

$$\begin{cases}\underline{\boldsymbol{e}}(t) &= \mathbf{T}^+\underline{\boldsymbol{e}_z}(t) - \mathbf{T}^-\overline{\boldsymbol{e}_z}(t)\\ \overline{\boldsymbol{e}}(t) &= \mathbf{T}^+\overline{\boldsymbol{e}_z}(t) - \mathbf{T}^-\underline{\boldsymbol{e}_z}(t)\end{cases} \tag{B.24}$$

Then, in both cases, the two signals $\underline{\boldsymbol{e}}(t)$ and $\overline{\boldsymbol{e}}(t)$ are such that

$$\underline{\boldsymbol{e}}(t) \leq \boldsymbol{e}(t) \leq \overline{\boldsymbol{e}}(t),\ \forall t \tag{B.25}$$

Using the definition of the observation error $\boldsymbol{e}(t)$ and the estimated state vector $\widehat{\boldsymbol{x}}(t)$, bounds of the initial system state $\boldsymbol{x}$ are obtained, under Assumptions B.10, B.14 and B.16 (or B.17):

$$\widehat{\boldsymbol{x}}(t) + \underline{\boldsymbol{e}}(t) =: \underline{\boldsymbol{x}}(t) \leq \boldsymbol{x}(t) \leq \overline{\boldsymbol{x}}(t) := \overline{\boldsymbol{e}}(t) + \widehat{\boldsymbol{x}}(t),\ \forall t \tag{B.26}$$

Hence the following proposition:

Proposition B.24 (Interval observer of the state vector, Assumption B.17)**.**
Under Assumptions B.10, B.14 and B.17 the reunion of

- *system* $\left(\widehat{\mathbf{G}}\right)$ *in* (B.17a)*;*
- *system* $\left(\mathbf{G}_{\mathbf{e}}^{\mathbf{z},\sharp}\right)$ *in* (B.22)*;*
- *the reverse state-coordinate transformation in* (B.24)*;*
- *the state bounds determination relations in* (B.26)*,*

is an interval observer for the system $(\mathbf{G})$ *in* (B.10a) *if the condition (3) in Definition B.11 is satisfied.*

Note that this interval observer can be written in the following compact form which is reminiscent of the one proposed Definition B.11:

$$(\mathbf{G}^{\sharp}) = \begin{cases} \dot{\begin{bmatrix} \widehat{\boldsymbol{x}}(t) \\ \underline{\boldsymbol{e}_z}(t) \\ \overline{\boldsymbol{e}_z}(t) \end{bmatrix}} = \begin{bmatrix} \mathbf{A}-\mathbf{LC} & \mathbf{0}_n & \mathbf{0}_n \\ \mathbf{0}_n & \mathbf{P}\left(\mathbf{A}-\mathbf{LC}\right)\mathbf{P}^{-1} & \mathbf{0}_n \\ \mathbf{0}_n & \mathbf{0}_n & \mathbf{P}\left(\mathbf{A}-\mathbf{LC}\right)\mathbf{P}^{-1} \end{bmatrix} \begin{bmatrix} \widehat{\boldsymbol{x}}(t) \\ \underline{\boldsymbol{e}_z}(t) \\ \overline{\boldsymbol{e}_z}(t) \end{bmatrix} \\ \qquad + \begin{bmatrix} \mathbf{B_u}-\mathbf{LD_u} & \mathbf{L} & \mathbf{0}_{n\times k} & \mathbf{0}_{n\times k} \\ \mathbf{0}_{n\times l} & \mathbf{0}_{n\times m} & \left[\mathbf{P}\left(\mathbf{B_d}-\mathbf{LD_d}\right)\right]^{+} & -\left[\mathbf{P}\left(\mathbf{B_d}-\mathbf{LD_d}\right)\right]^{-} \\ \mathbf{0}_{n\times l} & \mathbf{0}_{n\times m} & -\left[\mathbf{P}\left(\mathbf{B_d}-\mathbf{LD_d}\right)\right]^{-} & \left[\mathbf{P}\left(\mathbf{B_d}-\mathbf{LD_d}\right)\right]^{+} \end{bmatrix} \begin{bmatrix} \boldsymbol{u}(t) \\ \boldsymbol{y}(t) \\ \underline{\boldsymbol{d}}(t) \\ \overline{\boldsymbol{d}}(t) \end{bmatrix} \\ \begin{bmatrix} \underline{\boldsymbol{x}}(t) \\ \overline{\boldsymbol{x}}(t) \end{bmatrix} = \begin{bmatrix} \mathbf{I_n} & \mathbf{T}^{+} & -\mathbf{T}^{-} \\ \mathbf{I_n} & -\mathbf{T}^{-} & \mathbf{T}^{+} \end{bmatrix} \begin{bmatrix} \widehat{\boldsymbol{x}}(t) \\ \underline{\boldsymbol{e}_z}(t) \\ \overline{\boldsymbol{e}_z}(t) \end{bmatrix} \end{cases} \tag{B.27}$$

A similar proposition is derived under Assumption B.16 for which the reverse state-coordinate transformation is useless. Using the discrete-time formulations of the assumptions and equations, a similar proposition is obtained for discrete-time systems.

B.3.6 Conclusions on interval observer design

This concludes the design of an interval observer for a given system $(\mathbf{G})$ or $(\mathbf{F})$. In this section, two assumptions, B.16 and B.17, were gradually considered to allow for the construction of interval observers as defined in Definition B.11. Indeed, to facilitate the design of interval observers it is often supposed that there exists a matrix $\mathbf{L}$ and eventually a matrix $\mathbf{P}$ such that the considered observation error dynamics – see (B.18a) or (B.18b) – is cooperative.

In most cases, contrary to Example B.20, determining appropriate matrices $\mathbf{P}$ and $\mathbf{L}$ is not trivial and requires specific methods. In the following section, two of these methods are presented. They were introduced along with the interval observer theory. The first method considers a time-varying SCT and was proposed in [Mazenc 11] while the second method proposes a time-invariant SCT and is documented for example in [Raïssi 12]. More methods are presented in Chapter 7 for comparison with the method introduced in the same chapter.

B.4 Two different strategies to enforce cooperativity

In B.3.3, assumptions were made to satisfy (2) in Definition B.11. Both suppose that the design matrices have been finely chosen such that the observation error state matrix in (B.18) is (Hurwitz) Metzler:

- in the first case, Assumption B.16 restricts the class of considered systems to be able to enforce cooperativity by choosing an appropriate observer gain $\mathbf{L}$;
- In the second case, Assumption B.17 proposes that a state-coordinate transformation $\boldsymbol{e}_z = \mathbf{P}\boldsymbol{e}$ can be determined such that the transformed state matrix is Metzler.

Restricting the class of systems is not a good solution since even a trivial system such as in Example B.15 cannot be considered. In the literature, a state-coordinate transformation is thus applied. However, Assumption B.17 gives no constructive rule to determine matrices $\mathbf{P}$ and $\mathbf{L}$ such that $\mathbf{M} = \mathbf{P}\left(\mathbf{A} - \mathbf{LC}\right)\mathbf{P}^{-1}$ is Hurwitz Metzler. It was also suggested in Remark B.18 that the matrix $\mathbf{P}$ may be chosen time-varying. A warning was issued in Remark B.23 on the fact that a different formulation of the interval observer is obtained in that case (see B.4.1).

Two existing techniques are presented in this section to determine $\mathbf{P}$ and $\mathbf{L}$. The aim is not to provide a comparison of these techniques. Variations and comparisons of these methods are rather detailed in Chapter 7.

The first method was introduced in [Mazenc 11] following works in [Mazenc 10]. It is based on a time-varying state-coordinate transformation. The second method is documented in [Raïssi 12] and considers a time-invariant transformation.

B.4.1 Time-varying state-coordinate transformation

In first approach, let consider continuous-time systems only. As mentioned in Remark B.23, the interval observer expression in (B.22) is not valid since $\mathbf{P}$ depends on the time. This comes from the fact that if $\underline{\boldsymbol{e}_z} = \mathbf{P}\underline{\boldsymbol{e}}$ then

$$\begin{aligned} \dot{\underline{\boldsymbol{e}_z}} &= \dot{\mathbf{P}}\underline{\boldsymbol{e}} + \mathbf{P}\dot{\underline{\boldsymbol{e}}} \\ &= \left[\dot{\mathbf{P}}\mathbf{P}^{-1} + \mathbf{P}\left(\mathbf{A} - \mathbf{LC}\right)\mathbf{P}^{-1}\right]\underline{\boldsymbol{e}_z} \end{aligned} \tag{B.28}$$

which is denoted $\dot{\underline{\boldsymbol{e}_z}} = \boldsymbol{\Xi}\underline{\boldsymbol{e}_z}$ later on. The same relation is obtained for the upper bound. This leads to the following formulation of an interval observer in the case where a time-varying state-coordinate transformation is used:

$$\left(\mathbf{G}_{\mathbf{e}}^{\mathbf{z},\sharp}\right)\begin{cases} \dot{\underline{\boldsymbol{e}_z}}(t) &= \boldsymbol{\Xi}\underline{\boldsymbol{e}_z}(t) + \left[\mathbf{P}\left(\mathbf{B_d} - \mathbf{LD_d}\right)\right]^{+}\underline{\boldsymbol{d}}(t) - \left[\mathbf{P}\left(\mathbf{B_d} - \mathbf{LD_d}\right)\right]^{-}\overline{\boldsymbol{d}}(t) \\ \dot{\overline{\boldsymbol{e}_z}}(t) &= \boldsymbol{\Xi}\overline{\boldsymbol{e}_z}(t) + \left[\mathbf{P}\left(\mathbf{B_d} - \mathbf{LD_d}\right)\right]^{+}\overline{\boldsymbol{d}}(t) - \left[\mathbf{P}\left(\mathbf{B_d} - \mathbf{LD_d}\right)\right]^{-}\underline{\boldsymbol{d}}(t) \\ \underline{\boldsymbol{e}_z}(0) &= \mathbf{P}(0)^{+}\underline{\boldsymbol{e}_0} - \mathbf{P}(0)^{-}\overline{\boldsymbol{e}_0} \\ \overline{\boldsymbol{e}_z}(0) &= \mathbf{P}(0)^{+}\overline{\boldsymbol{e}_0} - \mathbf{P}(0)^{-}\underline{\boldsymbol{e}_0} \end{cases} \tag{B.29}$$

The problem of finding the adequate state-coordinate transformation is now formulated.

Problem B.25 (Time-varying state-coordinate transformation determination)**.**
Given $\mathbf{A} \in \mathbb{R}^{n\times n}$ and $\mathbf{C} \in \mathbb{R}^{m\times n}$ such that Assumption B.14 is satisfied, determine $\mathbf{P}(t) \in \mathbb{R}^{n\times n}$, $\forall t \in \mathbb{R}_+$ and $\mathbf{L} \in \mathbb{R}^{n\times m}$ such that

$$\boldsymbol{\Xi} = \mathbf{P}\left(\mathbf{A} - \mathbf{LC}\right)\mathbf{P}^{-1} + \dot{\mathbf{P}}\mathbf{P}^{-1} \tag{B.30}$$

is Hurwitz Metzler.

A solution to this problem was proposed in [Mazenc 11] using a transformation of the initial matrix $\mathbf{A} - \mathbf{LC}$ into its real Jordan canonical form. The following explanation is entirely credited to [Mazenc 11, Theorem 2, p. 142] and its proof.

Supposing that $\dot{\boldsymbol{e}} = (\mathbf{A} - \mathbf{LC})\,\boldsymbol{e}$ with $\mathbf{A}-\mathbf{LC}$ Hurwitz, let consider the change of coordinates $\boldsymbol{Y} = \boldsymbol{\mathcal{P}}\boldsymbol{e}$ such that $\dot{\boldsymbol{Y}} = \mathbf{J}\boldsymbol{Y}$ where $\mathbf{J}$ is the real Jordan canonical form of $\mathbf{A} - \mathbf{LC}$:

$$\mathbf{J} = \begin{bmatrix} \mathbf{J_1} & 0 & \dots & 0 \\ 0 & \mathbf{J_2} & \ddots & \vdots \\ \vdots & \ddots & \ddots & 0 \\ 0 & \dots & 0 & \mathbf{J_s} \end{bmatrix} \in \mathbb{R}^{n\times n} \tag{B.31}$$

where the first r matrices are associated with the r real eigenvalues (of multiplicity n_i):

$$\mathbf{J_i} = \begin{bmatrix} -\mu_i & 1 & \dots & 0 \\ 0 & -\mu_i & \ddots & \vdots \\ \vdots & \ddots & \ddots & 1 \\ 0 & \dots & 0 & -\mu_i \end{bmatrix} \in \mathbb{R}^{n_i\times n_i},\ 1 \le i \le r \tag{B.32}$$

and the last matrices are associated with the complex conjugate eigenvalues (of multiplicity m_i):

$$\mathbf{J_i} = \begin{bmatrix} \mathbf{\Gamma_i} & \mathbf{I_2} & 0 & \dots & 0 \\ 0 & \mathbf{\Gamma_i} & \mathbf{I_2} & \ddots & \vdots \\ \vdots & \ddots & \ddots & \ddots & 0 \\ 0 & & \ddots & \ddots & \mathbf{I_2} \\ 0 & \dots & \dots & 0 & \mathbf{\Gamma_i} \end{bmatrix} \in \mathbb{R}^{2m_i\times 2m_i},\ r+1 \le i \le s \tag{B.33}$$

where $\mathbf{\Gamma_i} = \begin{bmatrix} -\kappa_i & \omega_i \\ -\omega_i & -\kappa_i \end{bmatrix} \in \mathbb{R}^{2\times 2}$ is the real matrix with eigenvalues $-\kappa_i + \mathrm{j}\omega_i$ and $-\kappa_i - \mathrm{j}\omega_i$. Then, let consider the coordinate transformation $\boldsymbol{\xi} = \boldsymbol{\eta}(t)\boldsymbol{Y}$ where

$$\boldsymbol{\eta}(t) = \begin{bmatrix} \mathbf{I_q} & 0 & \dots & 0 \\ 0 & \mathbf{N_{r+1}}(t) & \ddots & \vdots \\ \vdots & \ddots & \ddots & 0 \\ 0 & \dots & 0 & \mathbf{N_s}(t) \end{bmatrix} \tag{B.34}$$

with $q = \sum_{i=1}^{r} n_i$ and

$$\mathbf{N_i}(t) = \begin{bmatrix} \mathbf{\Omega_i}(t) & 0 & \dots & 0 \\ 0 & \mathbf{\Omega_i}(t) & \ddots & \vdots \\ \vdots & \ddots & \ddots & 0 \\ 0 & \dots & 0 & \mathbf{\Omega_i}(t) \end{bmatrix}$$

for $r+1 \le i \le s$ where $\mathbf{\Omega_i}(t) = \begin{bmatrix} \cos(\omega_i t) & -\sin(\omega_i t) \\ \sin(\omega_i t) & \cos(\omega_i t) \end{bmatrix}$. Then $\dot{\boldsymbol{\xi}} = \mathbf{\Xi}\boldsymbol{\xi}$ where $\mathbf{\Xi}$ is Metzler Hurwitz and satisfies (B.30).

Proposition B.26 (Real Jordan canonical form approach)**.**
Let $\mathbf{L} \in \mathbb{R}^{n\times m}$ such that $\mathbf{A} - \mathbf{LC}$ is Hurwitz. Let $\mathbf{P}(t) = \boldsymbol{\eta}(t)\boldsymbol{\mathcal{P}}$ where $\boldsymbol{\eta}(t)$ is defined in (B.34) and $\boldsymbol{\mathcal{P}}$ transforms $\mathbf{A}-\mathbf{LC}$ into $\mathbf{J}$ as defined in (B.31). Then the matrix $\mathbf{\Xi}$ defined as

$$\mathbf{\Xi} = \mathbf{P}\,(\mathbf{A} - \mathbf{LC})\,\mathbf{P}^{-1} + \dot{\mathbf{P}}\mathbf{P}^{-1} \tag{B.35}$$

is Hurwitz Metzler.

A detailed procedure on how to apply Proposition B.26 is given in Fig. B.3.

The main comment that can be made on this method is that it is based on a strong theoretical background. Also, there are not much design parameters since only the observer gain $\mathbf{L}$ must

Input: detectable matrices $(\mathbf{A}, \mathbf{C})$ and stabilizing observer gain $\mathbf{L}$ such that $\mathbf{A}-\mathbf{LC}$ is Hurwitz.
Output: time-varying matrix $\mathbf{P}(t)$ and $\boldsymbol{\Xi}$ such that $\boldsymbol{\Xi} = \mathbf{P}\left(\mathbf{A}-\mathbf{LC}\right)\mathbf{P}^{-1} + \dot{\mathbf{P}}\mathbf{P}^{-1}$ is Hurwitz Metzler
Procedure:

1. *Jordan canonical form*: determine $\boldsymbol{\mathcal{P}}$ such that $\boldsymbol{\mathcal{P}}\left(\mathbf{A}-\mathbf{LC}\right)\boldsymbol{\mathcal{P}}^{-1} = \mathbf{J}$ where $\mathbf{J}$ is the Jordan canonical form in (B.31). Note this can be obtained using usual eigenstructure determination algorithms;
2. *Eigenvalues ordering by type (optional)*: adapt the obtained expressions of $\boldsymbol{\mathcal{P}}$ and $\mathbf{J}$ such that the real eigenvalues come first on the diagonal of $\mathbf{J}$ and the complex eigenvalues come last;
3. *Time-varying Metzler transformation*: construct $\boldsymbol{\eta}(t)$ as in (B.34) using $\mathbf{J}$ eigenvalues;
4. *Resulting transformation matrix*: define $\mathbf{P}(t) = \boldsymbol{\eta}(t)\boldsymbol{\mathcal{P}}$;
5. *Conclusion*: $\boldsymbol{\Xi} = \mathbf{P}\left(\mathbf{A}-\mathbf{LC}\right)\mathbf{P}^{-1} + \dot{\mathbf{P}}\mathbf{P}^{-1}$ is Hurwitz Metzler.

Figure B.3: Procedure to obtain a Hurwitz Metzler matrix through time-varying state-coordinate transformation.

be chosen prior to applying the method. This is done easily for example using pole placement techniques. Complex eigenvalues are also tackled efficiently. However, the method can be hard to implement in practice due to the time-varying property of the transformation. Also, it is based on a transformation into a Jordan canonical form which is known to be numerically unstable in the case of high order or badly-conditioned systems. Application of this method is illustrated in B.5.1.

Remark B.27. In the discrete-time case, the state-coordinate transformation is used to obtain a non-negative observation error dynamics in the new coordinates. A similar transformation to the one presented in this section can be used. This is presented in [Mazenc 12a, Mazenc 14]. ◇

B.4.2 Time-invariant state-coordinate transformation

In the continuous-time case, the following problem is considered when looking for a time-invariant SCT:

Problem B.28 (Time-invariant state-coordinate transformation determination)**.**
Given $\mathbf{A} \in \mathbb{R}^{n\times n}$ and $\mathbf{C} \in \mathbb{R}^{m\times n}$ such that Assumption B.14 is satisfied, determine $\mathbf{P} \in \mathbb{R}^{n\times n}$ and $\mathbf{L} \in \mathbb{R}^{n\times m}$ such that

$$\mathbf{M} = \mathbf{P}\left(\mathbf{A}-\mathbf{LC}\right)\mathbf{P}^{-1} \tag{B.36}$$

is Hurwitz Metzler.

A solution to this problem can be obtained by solving a Sylvester equation. This was documented in [Raïssi 12]. By rewriting (B.36) as

$$-\mathbf{MP} + \mathbf{PA} = \mathbf{PLC}$$

it appears that this is equivalent to a Sylvester equation where $\mathbf{P}$ is the variable if $\mathbf{PL}$ is set to a design value $\mathbf{Q}$:

Proposition B.29 (Sylvester equation resolution approach)**.**
Let $\mathbf{M} \in \mathbb{R}^{n\times n}$ such that it is Hurwitz Metzler and has no common eigenvalues with $\mathbf{A}$. Let $\mathbf{Q} \in \mathbb{R}^{n\times m}$. Then the following Sylvester equation

Input: observable matrices $(\mathbf{A}, \mathbf{C})$, targeted Hurwitz Metzler matrix $\mathbf{M}$ such that $\text{eig}(\mathbf{M}) \neq \text{eig}(\mathbf{A})$, and unconstrained matrix $\mathbf{Q} \in \mathbb{R}^{n\times m}$.
Output: matrices $\mathbf{P}$ and $\mathbf{L}$ such that $\mathbf{M} = \mathbf{P}(\mathbf{A} - \mathbf{LC})\mathbf{P}^{-1}$ is Hurwitz Metzler
Procedure:

1. *Sylvester equation*: given $\mathbf{M}$ and $\mathbf{Q}$, solve $-\mathbf{MP} + \mathbf{PA} = \mathbf{QC}$ in $\mathbf{P}$;
2. *Observer gain*: let $\mathbf{L} = \mathbf{P}^{-1}\mathbf{Q}$;
3. *Conclusion*: $\mathbf{M}$ is Hurwitz Metzler by construction.

Figure B.4: Procedure to obtain a Hurwitz Metzler matrix by solving a Sylvester equation

$$-\mathbf{MP} + \mathbf{PA} = \mathbf{QC} \tag{B.37}$$

has a unique solution $\mathbf{P} \in \mathbb{R}^{n\times n}$ *with* $\mathbf{M} = \mathbf{P}(\mathbf{A} - \mathbf{LC})\mathbf{P}^{-1}$ *where* $\mathbf{L} = \mathbf{P}^{-1}\mathbf{Q}$.

Remark B.30. For Proposition B.29 to be applicable, the couple $(\mathbf{A}, \mathbf{C})$ must be observable. In case it is only detectable then $\mathbf{M}$ and $\mathbf{A}$ share the unobservable eigenvalues. ◇

The Sylvester equation (B.37) can be solved using algorithms such as [Golub 79] or [Bartels 72]. A detailed procedure on how to apply Proposition B.29 is given in Fig. B.4.

Some comments can already be formulated on this method. The main advantage is its ease of use. The main drawback is that its applicability depends on the definition of two design parameters which selection is far from being obvious. In particular, one has to propose $\mathbf{M}$ such that it is Hurwitz Metzler. In case of great dimensions and if specific eigenvalues are targeted, e.g. couples of complex numbers, this is quite a challenge. Moreover, the impact of the choice of $\mathbf{Q}$ is difficult to evaluate. Application of this method is illustrated in B.5.2.

Remark B.31. In the discrete-time case, $\mathbf{M}$ should be chosen Schur non-negative. ◇

B.5 Example of application of the SCT strategies

Let consider the example proposed in [Mazenc 11]. The considered system is represented by a continuous-time linear model with measurement disturbance. Its state space matrices are defined as:

$$\mathbf{A} = \begin{bmatrix} -1 & 1 & 0 & 0 & -1 & 0 \\ -1 & -2 & 0 & -1 & 0 & 1 \\ -2 & 0 & -3 & -2 & 0 & 0 \\ -1 & 0 & -2 & -3 & 0 & 1 \\ -1 & 0 & 2 & 0 & -4 & 0 \\ -1 & -1 & 0 & 1 & 0 & -1 \end{bmatrix}, \mathbf{B} = \begin{bmatrix} -18 & 0 \\ -13 & 0 \\ -5 & 0 \\ -4 & 0 \\ -10 & 0 \\ 22 & 0 \end{bmatrix}, \mathbf{C} = \begin{bmatrix} 1 & 0 & 0 & 0 & 0 & 0 \end{bmatrix}, \mathbf{D} = \begin{bmatrix} 0 & 1 \end{bmatrix} \tag{B.38}$$

and the resulting state-space representation is

$$(\mathbf{G}) \begin{cases} \dot{\boldsymbol{x}} &= \mathbf{A}\boldsymbol{x} + \mathbf{B}\begin{bmatrix} u \\ d \end{bmatrix} \\ y &= \mathbf{C}\boldsymbol{x} + \mathbf{D}\begin{bmatrix} u \\ d \end{bmatrix} \end{cases} \tag{B.39}$$

where $u(t) = \sin(t)$ and $d \in \mathbb{R}$ is an unknown signal such that $\underline{d} = -2 \leq d(t) \leq 1 = \overline{d}$, $\forall t$. In simulation, this disturbance signal will be modelled by a uniform random number generator with bounds $\underline{d}$ and $\overline{d}$. This is illustrated in Fig. B.5. Using the Popov-Belevitch-Hautus Lemma 2.4,

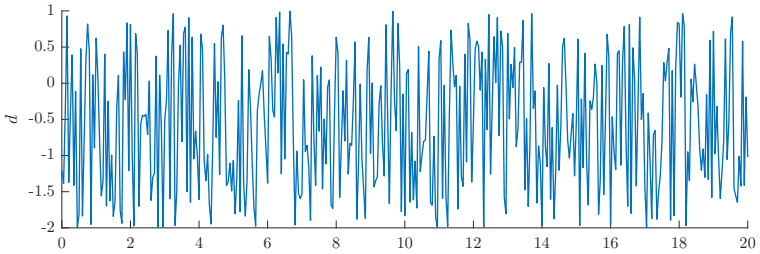

Figure B.5: Disturbance signal used for simulations.

it is observed that the pair $(\mathbf{A}, \mathbf{C})$ is detectable hence Assumption B.14 is satisfied. The initial condition is chosen at $\boldsymbol{x}_0 = \begin{bmatrix} 20 & 10 & 6 & 0 & 30 & 40 \end{bmatrix}^\top$ for simulation purposes. As far as initializing the interval observer, the elements of the initial condition are supposed to belong to the interval $[0, 40]$. Hence,

$$\underline{\boldsymbol{x}_0} = \mathbf{0},\ \overline{\boldsymbol{x}_0} = \begin{bmatrix} 40 & 40 & 40 & 40 & 40 & 40 \end{bmatrix}^\top \tag{B.40}$$

and Assumption B.10 is satisfied. Simulations are run overs 20s. An interval observer is used to determine bounds on the system state. A time-varying and time-invariant SCT are considered. The results obtained using both methods are now detailed.

B.5.1 Time-varying SCT

The approach detailed in B.4.1 is used. Although the initial system is stable, the observer gain proposed in [Mazenc 11] is used to fasten its dynamics:

$$\mathbf{L} = \begin{bmatrix} 0.7397 \\ -0.4220 \\ -1.4424 \\ 1.2362 \\ -0.9692 \\ 1.2417 \end{bmatrix} \tag{B.41}$$

Using the MATLAB `eig` and `cdf2rdf` routines, the real Jordan canonical form is obtained:

$$\mathbf{J} = \begin{bmatrix} -4.6575 & 0.7571 & 0 & 0 & 0 & 0 \\ -0.7571 & -4.6575 & 0 & 0 & 0 & 0 \\ 0 & 0 & -1.1170 & 0.8945 & 0 & 0 \\ 0 & 0 & -0.8945 & -1.1170 & 0 & 0 \\ 0 & 0 & 0 & 0 & -1.0000 & 0 \\ 0 & 0 & 0 & 0 & 0 & -2.1906 \end{bmatrix},$$

$$\boldsymbol{\mathcal{P}} = \begin{bmatrix} 0.3777 & -0.3009 & -0.2765 & 0.2941 & 1.1237 & -0.0641 \\ 1.1645 & -0.4724 & 1.5862 & 1.6869 & 0.4770 & -0.3188 \\ -1.7446 & -2.5520 & -0.6411 & 1.5977 & 0.8470 & -1.5023 \\ 3.0045 & 2.2481 & -0.3290 & -0.7563 & -0.7794 & -1.2633 \\ 3.1327 & 2.6106 & 1.5664 & -2.6106 & -1.0442 & 0.5221 \\ 1.1655 & -0.2357 & 1.1227 & -1.0985 & -0.6441 & 1.1206 \end{bmatrix} \tag{B.42}$$

Let $\omega_1 = 0.7571$ and $\omega_2 = 0.8945$. Then, the matrix $\boldsymbol{\eta}(t)$ is given by

$$\boldsymbol{\eta}(t) = \begin{bmatrix} \cos(\omega_1 t) & -\sin(\omega_1 t) & 0 & 0 & 0 & 0 \\ \sin(\omega_1 t) & \cos(\omega_1 t) & 0 & 0 & 0 & 0 \\ 0 & 0 & \cos(\omega_2 t) & -\sin(\omega_2 t) & 0 & 0 \\ 0 & 0 & \sin(\omega_2 t) & \cos(\omega_2 t) & 0 & 0 \\ 0 & 0 & 0 & 0 & 1 & 0 \\ 0 & 0 & 0 & 0 & 0 & 1 \end{bmatrix} \tag{B.43}$$

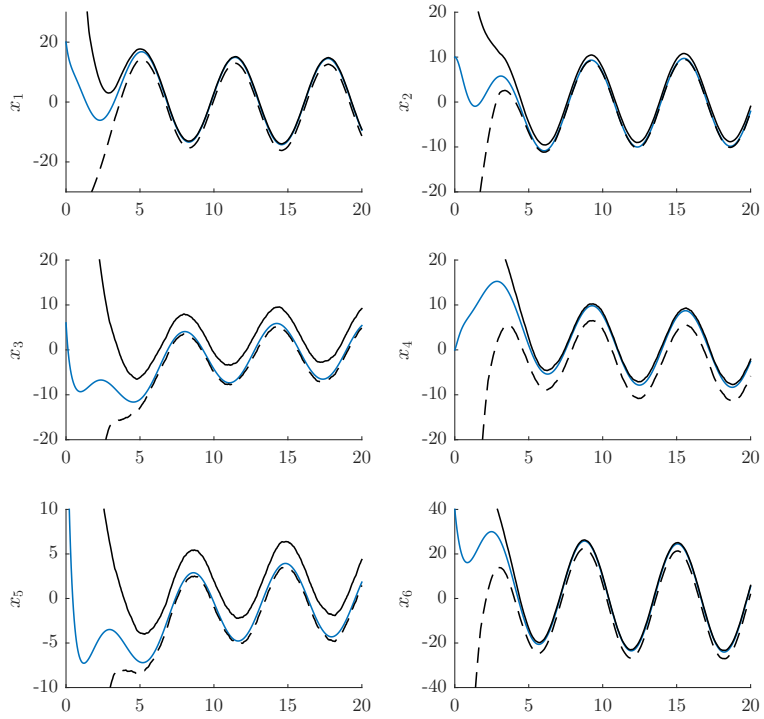

Figure B.6: State simulation (in blue) and bounds (in black) obtained using a time-varying SCT. The lower bound is represented in dashed line.

which results in the following state-coordinate transformation matrix:

$$\mathbf{P} = \boldsymbol{\eta}(t)\boldsymbol{\mathcal{P}}$$

and

$$\boldsymbol{\Xi} = \begin{bmatrix} -4.6575 & 0 & 0 & 0 & 0 & 0 \\ 0 & -4.6575 & 0 & 0 & 0 & 0 \\ 0 & 0 & -1.1170 & 0 & 0 & 0 \\ 0 & 0 & 0 & -1.1170 & 0 & 0 \\ 0 & 0 & 0 & 0 & -1.0000 & 0 \\ 0 & 0 & 0 & 0 & 0 & -2.1906 \end{bmatrix}$$

This concludes the procedure. Using these results, the system and interval observer are simulated. Simulation results are shown in Fig. B.6.

The results show that the obtained interval observer is very efficient. The initial interval size is due to the lack of knowledge on the initial condition $\boldsymbol{x}_0$ and the conservativeness of the coordinate change. The observation error does not reduce to zero after convergence due to the lack of knowledge on the disturbance signal $\boldsymbol{d}$.

B.5.2 Time-invariant SCT

The approach detailed in B.4.2 is used. Following the procedure in Fig. B.4, two matrices $\mathbf{M}$ and $\mathbf{Q}$ are defined first:

$$\mathbf{M} = \begin{bmatrix} -5 & 1 & 1 & 1 & 1 & 1 \\ 0 & -4.5 & 1 & 1 & 1 & 1 \\ 0 & 0 & -2 & 1 & 1 & 1 \\ 0 & 0 & 0 & -1.5 & 1 & 1 \\ 0 & 0 & 0 & 0 & -1.2 & 1 \\ 0 & 0 & 0 & 0 & 0 & -1 \end{bmatrix}, \mathbf{Q} = \begin{bmatrix} 2.0 \\ -1.0 \\ 1.5 \\ -1.5 \\ 1.0 \\ -2.0 \end{bmatrix} \tag{B.44}$$

Note that $\mathbf{M}$ is chosen with real eigenvalues which are simpler to consider.

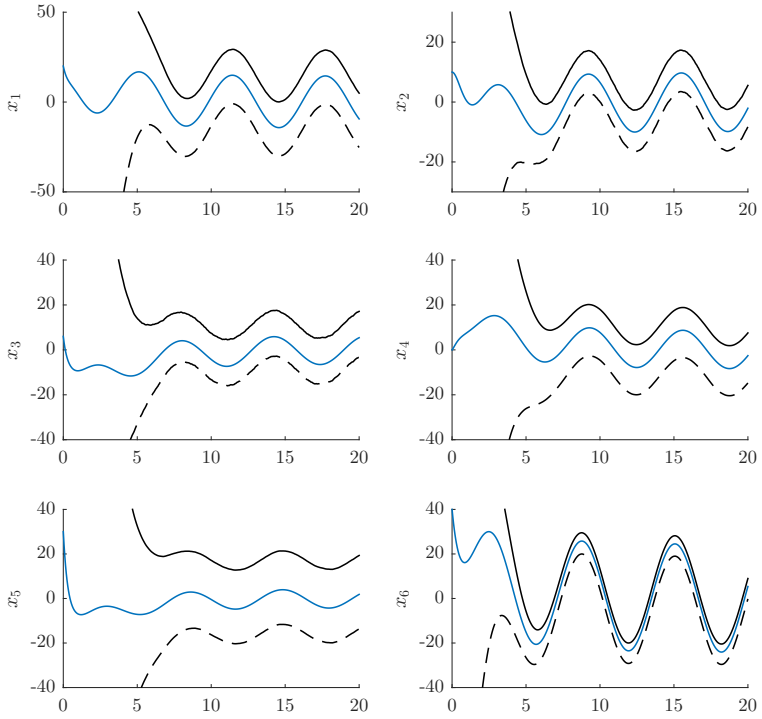

Figure B.7: State simulation (in blue) and bounds (in black) obtained using a time-invariant SCT. The lower bound is represented in dashed line.

Remark B.32. The choice of both $\mathbf{M}$ and $\mathbf{Q}$ is quite sensitive. Different values, for example $\mathbf{Q} = \begin{bmatrix}1 & 2 & 3 & 4 & 5 & 6\end{bmatrix}^\top$ may result in very poor interval observers. ◇

Then, the Sylvester equation (B.37) is solved using the MATLAB `lyap` routine. The following transformation matrix is obtained:

$$\mathbf{P} = \begin{bmatrix} -3.3968 & -0.0833 & -3.7396 & 2.8355 & 2.6310 & -5.0547 \\ -2.8800 & -0.0916 & -2.1429 & 3.3640 & 2.0985 & -4.6087 \\ -8.5216 & -0.0935 & -7.4180 & 7.4651 & 4.5924 & -10.1148 \\ 1.2569 & -0.3391 & 1.6531 & -1.6455 & -0.3959 & -0.5058 \\ -0.6916 & -0.0677 & -1.1805 & 0.9952 & 0.5327 & -2.6374 \\ 2.4000 & 2.0000 & 1.2000 & -2.0000 & -0.8000 & 0.4000 \end{bmatrix} \tag{B.45}$$

which results in the following observer gain $\mathbf{L} = \mathbf{P}^{-1}\mathbf{Q}$:

$$\mathbf{L} = \begin{bmatrix} 1.2000 \\ -1.4668 \\ -2.3973 \\ -0.2509 \\ -0.4168 \\ 0.2381 \end{bmatrix} \tag{B.46}$$

This concludes the procedure. Using these results, the system and interval observer are simulated. Simulation results are shown in Fig. B.7.

In comparison with the time-varying state-coordinate transformation, one can observe that the interval obtained is bigger. However, the result is satisfactory as far as Definition B.11 is concerned. Also, this example shows that initializing the method described in B.4 is more challenging than expected. Indeed, the fine selection of the two design matrices $\mathbf{M}$ and $\mathbf{Q}$ is crucial to obtain satisfying results.

B.6 Conclusion

In this appendix, the theory and design of linear interval state-observers for linear systems have been recalled for the reader who is unfamiliar with these notions. In the chosen approach, a classical observer is used to stabilize the potentially unstable dynamics of the original system. Then, a state-coordinate transformation is applied to transform the resulting observation error system into a cooperative system. These choices allow the design of a system complying with Definition B.11. As far as the state-coordinate transformation is concerned, two different transformations were presented, based on existing results: time-varying transformation [Mazenc 11] or time-invariant transformation [Raïssi 12]. Both transformations were illustrated on a simple example.

Appendix C

Code samples

C.1 Chapter 4

AMPL/IPOPT code.

```
####################
### PARAMETERS ###

param N = 2000;

param x10 = 1; param x20 = 0;
param x1f = 0; param x2f = 0;

param alpmin = -0.3; param alpmax = 0.3;

param weightuco = 1;
param weightalp = 1;

# Final time
param tf = 20;

# dmin and dmax, deul is a signal modelling the disturbance in the Euler
    integration scheme
param dmin {0..N}; # data
param dmax {0..N}; # data
param deul {0..N}; # data

####################
### VARIABLES ###

# States (unconstrained then constrained)
var x1un {0..N}; #, default x10;
var x2un {0..N}; #, default x20;
var x1co {0..N}; #, default x10;
var x2co {0..N}; #, default x20;

# Kappa
var kb1, >=0, <= 1000, default 1;
var kappa {0..N};

# Unconstrained/constrained control
var uco {0..N-1};

```

```
38 ####################
39 ### OBJECTIVE ###
40 minimize cout: weightalp * tf/N * sum {i in 0..N-1} (x1co[i]-x1un[i])^2 +
       weightalp * tf/N * sum {i in 0..N-1} (x2co[i]-x2un[i])^2 + weightuco * tf/N
        * sum {i in 0..N-1} uco[i]^2;
41
42 ######################
43 ### CONSTRAINTS ###
44 subject to x1uninit: x1un[0] = x10;
45 subject to x2uninit: x2un[0] = x20;
46 subject to x1coinit: x1co[0] = x10;
47 subject to x2coinit: x2co[0] = x20;
48
49 ### DYNAMICAL CONSTRAINTS: Euler Scheme
50 subject to x1undyn {i in 0..N-1}: x1un[i+1] = x1un[i] + tf/N*x2un[i];
51 subject to x2undyn {i in 0..N-1}: x2un[i+1] = x2un[i] - tf/N*(x1un[i]+x2un[i])
       + tf/N*deul[i];
52
53 subject to x1codyn {i in 0..N-1}: x1co[i+1] = x1co[i] + tf/N*x2co[i];
54 subject to x2codyn {i in 0..N-1}: x2co[i+1] = x2co[i] + tf/N*uco[i] + tf/N*deul
       [i];
55
56 ### KAPPA CONSTRAINTS
57 subject to kappadyn {i in 0..N}: kappa[i] = (kb1 + 2*max(abs(dmin[i]),abs(dmax[
       i]))) / (alpmax - alpmin);
58
59 ### CONTROL CONSTRAINTS
60 subject to ucosat {i in 0..N-1}: uco[i] = max(min(kappa[i]*(alpmin-x2co[i]) +
       max(abs(dmin[i]),abs(dmax[i])),kappa[i]*(alpmax-x2co[i]) - max(abs(dmin[i])
       ,abs(dmax[i]))),min(-x1co[i]-x2co[i],max(kappa[i]*(alpmin-x2co[i]) + max(
       abs(dmin[i]),abs(dmax[i])),kappa[i]*(alpmax-x2co[i]) - max(abs(dmin[i]),abs
       (dmax[i])))));
61
62 subject to ucodyn {i in 0..N-2}: -10 <= (uco[i+1] - uco[i])*N/tf <= 10;
63
64 ####################
65 ### DATA ###
66
67 data;
68
69 for {i in 0..N} {
70 let dmin[i] := -exp(-0.25*i*tf/N);
71 let dmax[i] := exp(-0.25*i*tf/N);
72 let deul[i] := exp(-0.25*i*tf/N)*sin(2*i*tf/N);
73 }
74
75 ####################
76 ### SOLVE ###
77
78 ############# SOLVING OPTIONS ##############
79
80 #option solver ipopt;
81
82 option ipopt_options "max_iter=10000";
83
84 solve;
```

```
85
86
87  ######  OUTPUT SCREEN
88
89  display x1uninit, x2uninit, x1coinit, x2coinit;
90  #display x1unfin, x2unfin, x1cofin, x2cofin;
91
92  printf: " # cout = %24.16e\n", cout;
93  printf: " # N = %d\n", N;
94  printf: " # kb1 = %24.16e\n", kb1;
95  printf: " # tf = %24.16e\n", tf;
96  printf: " # Data\n";
97  printf{i in 0..N-1}: " %24.16e %24.16e %24.16e %24.16e %24.16e %24.16e %24.16e
        %24.16e %24.16e %24.16e %24.16e %24.16e %24.16e %24.16e %24.16e\n",
98  i*tf/N, x1un[i], x2un[i], x1co[i], x2co[i], -x1un[i]-x2un[i], uco[i], dmin[i],
        dmax[i], deul[i], kappa[i], x1undyn[i], x2undyn[i], x1codyn[i], x2codyn[i];
99  printf: " %24.16e %24.16e %24.16e %24.16e %24.16e %24.16e %24.16e %24.16e
        %24.16e %24.16e %24.16e\n",
100 tf, x1un[N], x2un[N], x1co[N], x2co[N], -x1un[N]-x2un[N], uco[N-1], dmin[N],
        dmax[N], deul[N], kappa[N];#, x1unfin, x2unfin, x1cofin, x2cofin;
101
102 end;
```

C.2 Chapter 7

C.2.1 Example 7.3.1 (a) SCorpIO Matlab code

This code illustrates the application of the SCorpIO approach as presented in 7.2 to the continuous-time example introduced in 7.3.1 (a), as inspired by [Mazenc 11].

```
1  %% Model
2  A   = [-1  1   0   0 -1  0;
3         -1 -2   0 -1   0   1;
4         -2   0 -3 -2   0   0;
5         -1   0 -2 -3   0   1;
6         -1   0   2   0 -4   0;
7         -1 -1   0   1   0 -1];
8  Bu  = [-18;-13;-5;-4;-10;22];
9  B   = [zeros(6,1) Bu];
10 C   = [1 0 0 0 0 0];
11 D   = [1 0];
12 Dw  = D(:,1);
13
14 % State-space representation
15 sys = ss(A,B,C,D);
16
17 % Dimensions
18 nx = length(A);
19 ny = size(C,1);
20 nu = size(Bu,2);
21 nw = 1;
22
23 % Controller dimension configuration
24 nk = 1;
25
26 % M_ij maximum value
```


```
mvmax = 2e2;

% |P_ij| and |T_ij| maximum value
PTmax = 4;

%% Tunable parameters
% Observer gain definition with preliminary initialisation
L0  = place(A,C,-abs(real(eig(A)))+1i*imag(eig(A)))./;
L   = realp(L ,L0);

% SCT matrix
P   = realp(P ,eye(nx));

% Maximum element condition on P
if PTmax > 0
    P.Minimum = -PTmax;
    P.Maximum = PTmax;
end

% Additional definitions
T   = eye(nx)/P;
M   = P*(A-L*C)/P;
PL  = P*L;

%% Synthesis models
% Observation error dynamics (new coordinates)
Gsyn(:,:,1) = ss(M,-P*L*Dw,eye(nx),zeros(nx,nw));

% Ed dynamics
Gsyn(:,:,2) = ss(M,0.5*P*L*Dw,eye(nx),zeros(nx,nw));

% PL non-negativity condition
kk = 3;
for ii = 1:nx
    for jj = 1:ny
        Gsyn(:,:,kk) = ss(-PL(ii,jj),zeros(1,nw),zeros(nx,1),zeros(nx,nw));
        kk = kk + 1;
    end
end

% Metzler condition
for ii = 1:nx
    for jj = 1:nx
        if ii ~= jj
            Gsyn(:,:,kk) = ss(-M(ii,jj),zeros(1,nw),zeros(nx,1),zeros(nx,nw));
            kk = kk + 1;
        end

        % M_ij maximum value condition
        if mvmax > 0
            Gsyn(:,:,kk) = ss(M(ii,jj)-mvmax,zeros(1,nw),zeros(nx,1),zeros(nx,nw
                ));
            kk = kk + 1;
        end

        % T_ij maximum value condition
```

```
82          if PTmax > 0
83              Gsyn(:,:,kk)   = ss(-T(ii,jj)-PTmax,zeros(1,nw),zeros(nx,1),zeros(nx,
                    nw));
84              Gsyn(:,:,kk+1) = ss( T(ii,jj)-PTmax,zeros(1,nw),zeros(nx,1),zeros(nx
                    ,nw));
85              kk = kk + 2;
86          end
87      end
88  end
89
90  % Renaming I/Os for clarity
91  Gsyn.InputName = {w };
92  Gsyn.OutputName = {Ed};
93
94  %% Requirements
95  % Metzler condition
96  reqMetzlerEtAl        = TuningGoal.Poles();
97  reqMetzlerEtAl.Models = 3:kk-1;
98
99  % Disturbance rejection (Ed dynamics)
100 reqRejEd              = TuningGoal.Variance(w,Ed ,0.7);
101 reqRejEd.Models       = 2;
102
103 % Observation error dynamics stability
104 reqStab               = TuningGoal.Poles();
105 reqStab.MinDecay      = 0.5;
106 reqStab.MaxFrequency  = 1e2;
107 reqStab.Models        = 1;
108
109 % Stacking requirements
110 Soft = [reqRejEd];
111 Hard = [reqMetzlerEtAl reqStab];
112
113 %% Synthesis
114 options = systuneOptions(MaxIter,500,RandomStart,5,UseParallel,true);
115 [CL,fSoft,gHard] = systune(Gsyn,Soft,Hard,options);
116 fSoft, gHard,
117
118 %% Results
119 P   = getValue(P,CL);
120 L   = getValue(L,CL);
121
122 M   = P*(A-L*C)/P,
123 T   = eye(nx)/P,
```

C.2.2 Example 7.4.3 SCorpIO Matlab code

This code illustrates the application of the SCorpIO approach to the simultaneous design of a stabilizing controller and an interval observer of the closed-loop for the example introduced in 7.4.3.

```
1  %% Model
2  A   = [1 -1;2 -3]; eig(A),
3  B   = [0 0;1 1];
4  Bu  = B(:,2); Bw = B(:,1);
5  C   = [1 0];
```

```
D   = [0 0];

% State-space representation
G = ss(A,B,C,D,InputName,{w , u }, OutputName, y );

% Dimensions
nx = length(A);
ny = size(C,1);
nu = size(Bu,2);
nw = size(Bw,2);

% Controller dimension configuration
nk = 1;

% M_ij maximum value
mvmax = 5e1;

%% First synthesis to initialize stabilizing controller
K0  = ltiblock.ss(K0 ,nk,nu,ny);
CL0 = lft(G,K0);

% Stability requirement
reqStab = TuningGoal.Poles();
reqStab.MinDecay = 1e-3;
reqStab.MaxFrequency = 1e1;

% Synthesis
CL = systune(CL0,reqStab);
K0 = getValue(K0,CL);

%% Tunable elements
% Controller state-space matrices
Ak  = realp(Ak ,K0.a);
Bk  = realp(Bk ,K0.b);
Ck  = realp(Ck ,K0.c);
Dk  = realp(Dk ,K0.d);
K   = ss(Ak,Bk,Ck,Dk);

% SCT matrix
P   = realp(P ,eye(nx+nk));

% Constraint such that P*BXw is positive
P.Minimum([4 5 6]) = 0;

% Closed-loop matrices
AX  = [A+Bu*Dk*C Bu*Ck;Bk*C Ak];
BXv = [Bu;zeros(nk,nu)];
BXw = [Bw;zeros(nk,nw)];

% Expected Hurwitz Metzler matrix
MX  = P*AX/P;

%% Synthesis models
% Original closed-loop
Gsyn(:,:,1) = ss(AX,[BXv BXw],eye(nx+nk),zeros(nx+nk,nu+nw),...
                    InputName,{ v , w },...
```

```
62                      OutputName, X );
63
64 % Ed dynamics
65 Gsyn(:,:,2) = ss(MX,[zeros(nx+nk,nu) 0.5*P*BXw],eye(nx+nk),zeros(nx+nk,nu+nw));
66
67 % Metzler condition models
68 kk = 3;
69 for ii = 1:nx+nk
70     for jj = 1:nx+nk
71         if ii ~= jj
72             Gsyn(:,:,kk) = ss(-MX(ii,jj),zeros(1,nu+nw),zeros(nx+nk,1),zeros(nx+
                   nk,nu+nw));
73             kk = kk+1;
74         end
75
76         % M_ij maximum value condition
77         if mvmax > 0
78             Gsyn(:,:,kk) = ss(MX(ii,jj)-mvmax,zeros(1,nu+nw),zeros(nx+nk,1),
                   zeros(nx+nk,nu+nw));
79             kk = kk+1;
80         end
81     end
82 end
83
84 %% Requirements
85 % Metzler condition
86 reqMetzler            = TuningGoal.Poles();
87 reqMetzler.Models     = 3:kk-1;
88
89 % Disturbance rejection (Ed dynamics)
90 reqRejEd = TuningGoal.Variance(w,X,1);
91 reqRejEd.Models = 2;
92
93 % Closed-loop stability
94 reqStab               = TuningGoal.Poles();
95 reqStab.MinDecay      = 1e-2;
96 reqStab.MaxFrequency  = 5e1;
97 reqStab.Models        = 1;
98
99 % Stacking requirements
100 Soft = [reqRejEd];
101 Hard = [reqMetzler reqStab];
102
103 %% Synthesis
104 options = systuneOptions(MaxIter,500,RandomStart,2,UseParallel,true);
105 [CL,fSoft,gHard] = systune(Gsyn,Soft,Hard,options);
106
107 %% Results
108 Ak  = getValue(Ak,CL);
109 Bk  = getValue(Bk,CL);
110 Ck  = getValue(Ck,CL);
111 Dk  = getValue(Dk,CL);
112 P   = getValue(P,CL);
113 K   = ss(Ak,Bk,Ck,Dk);
114
115 AX  = [A+Bu*Dk*C Bu*Ck;Bk*C Ak];
```


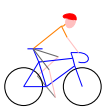

```
116 MX  = P*AX/P, eig(MX),
```

Part VI

Résumé de thèse en français

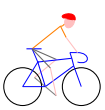

Appendix D

Commande de systèmes linéaires sous contraintes fréquentielles et temporelles Application au lanceur flexible

La synthèse de loi de commande sous contraintes fréquentielles et temporelles en présence de perturbations extérieures inconnues est un problème complexe. Par exemple, les techniques de synthèse H_∞ de contrôleur structuré ne permettent pas de formuler directement les contraintes temporelles dans le problème de minimisation. Il en résulte la nécessité de modifier les réglages des contraintes fréquentielles par essais-erreurs pour espérer les satisfaire et ce, sans garantie théorique. Dans cette thèse, nous explorons et enrichissons l'application d'une méthode de commande sous contraintes dite *évolutionnaire* utilisée en complément de la synthèse H_∞ dans le but de satisfaire une collection de contraintes fréquentielles et temporelles de manière garantie.

Ce chapitre reprend de manière fidèle l'organisation du manuscrit écrit en langue anglaise à l'exception des chapitres de pré-requis et annexes qui ne rentrent pas dans les contributions de la thèse. Des références aux chapitres de la Partie II peuvent donc apparaître par la suite. Le problème du contrôle sous contraintes temporelles *et* fréquentielles est introduit dans la section D.1. L'approche dite *évolutionnaire* choisie pour résoudre ce problème est ensuite présentée dans les sections D.2 et D.3. Elle est appliquée à un ensemble de modèles plus ou moins simplifiés du lanceur dans la section D.4. Une contribution annexe requise à terme pour l'extension OISTeR est présentée à la section D.5. Les conclusions de l'étude sont exposées dans la section D.6.

Table des matières

D.1 Introduction

La complexité croissante des systèmes industriels a conduit à la nécessité de développer des algorithmes de contrôle fiables et efficaces tout au long des phases de vie de ces systèmes. Dans le cas des lanceurs de véhicules spatiaux, la phase atmosphérique du vol est particulièrement critique. En raison des vitesses atteintes par le lanceur, dans le but d'atteindre la vitesse orbitale nécessaire à la satellisation et accessoirement de s'extraire rapidement des couches denses de l'atmosphère, les structures de celui-ci sont soumises à des forces aérodynamiques très importantes et potentiellement destructives si la loi de commande n'en tient pas compte.

La mise en place d'une stratégie de commande efficace repose sur une modélisation fidèle des phénomènes physiques à l'œuvre ainsi que sur la formulation d'un cahier des charges précis de contraintes à satisfaire. En pratique, dans le cas des problèmes de contrôle, ces contraintes sont de deux ordres : soit il s'agit de contraintes fréquentielles de sorte que le comportement fréquentiel du système en boucle fermée est adapté ; soit il s'agit de contraintes temporelles qui concernent les signaux temporels du système au cours de son évolution dynamique. Dans le cas du lanceur, une contrainte temporelle est ainsi spécifiée sur l'angle d'incidence α. En minimisant cet angle, les forces aérodynamiques sont minimisées et la destruction du lanceur où sa sortie de trajectoire optimale (dans le meilleur des cas) est évitée. Quant aux contraintes fréquentielles, elles concernent principalement la stabilité en boucle fermée mais également l'atténuation des modes souples présents à basse fréquence et qui ne doivent pas être excités par la loi de commande obtenue.

Dans cette thèse, nous considérons le problème de synthèse d'une loi de commande pour un système linéaire en présence de contraintes fréquentielles et temporelles. Certains paramètres du modèle linéaire considéré peuvent également être considérés comme incertains. Du fait de la nature différentes des contraintes considérées, une stratégie appropriée est développée dans ce travail. Dans un premier temps, une loi de commande, dite nominale, est synthétisée dans le but de satisfaire les contraintes fréquentielles. Dans notre cas, nous utilisons la synthèse H_∞. Dans un second temps, la loi de commande obtenue est modifiée de manière appropriée afin de satisfaire la contrainte temporelle sur la sortie considérée. En conclusion, la loi de commande nominale est active tant que la contrainte temporelle est satisfaite. Dès que cette contrainte est violée, la sortie du contrôleur est saturée de manière appropriée afin de restreindre l'ensemble admissible d'évolution de la sortie contrainte. Une telle stratégie de commande est appelée stratégie *évolutionnaire* dans la littérature associée au contrôle sous contraintes sur les sorties [Goodwin 01].

En ce qui concerne l'état de l'art des différentes notions évoquées et utilisées dans ce manuscrit de thèse, nous référons le lecteur intéressé à l'état de l'art de la version complète du manuscrit (en anglais), disponible dans la section 1.2.

En terme de contributions, ce travail de thèse a proposé des améliorations de la stratégie *évolutionnaire* considérée, à savoir l'approche OIST, introduite dans [Burlion 12] et rappelée en détails dans le Chapitre 3. Ces contributions sont les suivantes :

- formulation de l'approche OIST dans le cas des systèmes linéaires (voir section D.2). Une solution au problème de chevauchement des saturations ainsi qu'une preuve de stabilité asymptotique globale dans le cas des transferts à minimum de phase sont proposées, pour la première fois ;
- Extension OISTeR de l'approche OIST à la classe des systèmes incertains et/ou avec mesures partielles de l'état. Cette contribution repose sur l'utilisation d'observateurs par intervalles. La solution d'évitement de chevauchement des saturations est étendue à ce cas plus complexe ;
- Application des approches OIST et OISTeR à des modèles plus ou moins simplifiés (notamment : avec ou sans modes flexibles) de lanceur ;
- Proposition d'une nouvelle méthode de construction d'un observateur par intervalles avec changement de coordonnées à temps invariant. Cette méthode repose sur la formulation du problème mathématique d'origine en problème de stabilisation d'un système linéaire dit *fictif* (puisque ne modélisant pas la dynamique d'un système réel).

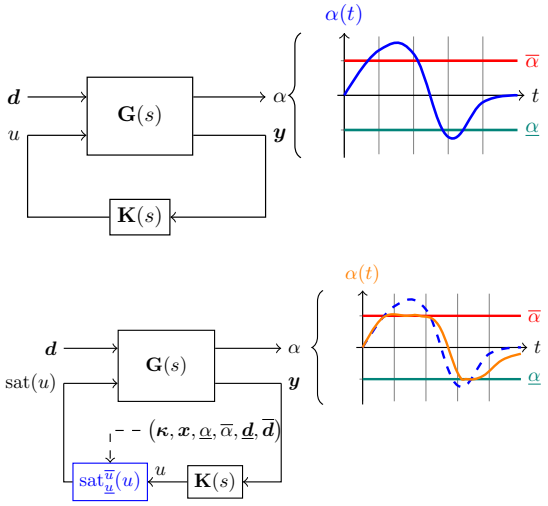

Figure D.1: Illustration de l'approche OIST. *Gauche* : contrôleur nominal (avant application des saturations OIST); *Droite* : après application de l'approche OIST, la contrainte est vérifiée (en orange).

Ces contributions sont présentées en détails dans la partie anglaise du manuscrit, à savoir la Partie III. Dans ce résumé en langue française, ces contributions sont présentées rapidement, sans rentrer dans les détails. Le résumé est organisé comme suit. La formulation de l'approche OIST dans le cas des systèmes linéaires est présentée dans la section D.2 ainsi que les contributions concernant l'évitement de chevauchement des saturations obtenues. L'extension OISTeR de cette approche au cas des systèmes incertains et à mesures d'état partielles est présentée dans la section D.3. Ces contributions sont appliquées au contrôle d'un lanceur sous contrainte temporelle sur l'angle d'incidence dans la section D.4. L'approche OISTeR faisant appel à un observateur par intervalles, une nouvelle méthode de construction de tels observateurs, intitulée SCorpIO, est proposée et détaillée dans la section D.5 avant de conclure dans la section D.6.

D.2 Formulation dans le cadre linéaire de l'approche OIST

Un certain nombre de techniques de synthèse de loi de commande existe afin de satisfaire aux exigences d'un cahier des charges. Par exemple, dans le cas où des contraintes fréquentielles sont formulées au sein du problème de commande et que le contrôleur est structuré afin de restreindre son nombre d'états ou d'utiliser une structure éprouvée, la technique de synthèse H_∞ telle que présentée dans le Chapitre 2 de pré-requis peut être utilisée. Avec ce type de technique, la prise en compte de contraintes temporelles sur l'état ou les sorties est plus complexe à gérer et nécessite une approche par essais-erreurs pour les satisfaire. Un exemple de contrainte temporelle qui peut être considérée est la contrainte d'appartenance à un intervalle : étant donnée une variable d'état ou de sortie $\alpha \in \mathbb{R}$, celle-ci doit satisfaire $\alpha \in \Omega_\alpha(t)$ où $\Omega_\alpha(t) = [\underline{\alpha}(t), \overline{\alpha}(t)]$ est un intervalle pré-défini.

L'approche OIST (*Output to Input Saturation Transformation*) introduite dans [Burlion 12] et rappelée dans le Chapitre 3 consiste à transformer cette contrainte sur une sortie α en saturations sur l'entrée de commande u dans le but de restreindre la trajectoire du système et donc l'ensemble d'évolution de α. La loi de commande, dite nominale, reste inchangée tant que la contrainte est satisfaite. Dans le cas contraire, la sortie du contrôleur est saturée de manière adéquate, les bornes de la saturation étant fournies par OIST. Ceci est illustré dans la Fig. D.1.

Comme présenté dans la section D.2.1, OIST se classe dans la famille des méthodes de contrôle sous contraintes dites *évolutionnaires*. Cela signifie qu'elle repose sur une loi de commande nominale (le contrôleur synthétisé en utilisant des techniques H_∞ par exemple) qui est modifiée (dans notre cas, elle est saturée) par une structure additionnelle dès que la contrainte temporelle

sur la variable α n'est plus vérifiée. L'approche OIST a été initialement introduite dans le cadre des systèmes non-linéaires. Dans ce manuscrit, nous considérons sa formulation dans le cadre des systèmes linéaires. Cette formulation nous permet également d'obtenir des solutions théoriques intéressantes aux problèmes de chevauchement des saturations[1] et d'analyse de stabilité[2]. Cette section repose sur les résultats présentés dans les articles [Chambon 15c] et [Chambon b].

Cette section est organisée comme suit : dans un premier temps, un état de l'art succinct des techniques de commande sous contraintes est présenté dans la section D.2.1. L'approche OIST telle qu'introduite dans [Burlion 12] est rappelée dans la section D.2.2 en l'appliquant à un système linéaire. Des limites aux résultats actuels sont alors identifiées. Ces limites sont levées dans le cadre des systèmes linéaires sous le forme de contributions présentées dans la section D.2.3. L'application au contrôle d'une bille sous contrainte temporelle sur sa position sur un rail inclinable est considérée avant de conclure dans la section D.2.4.

D.2.1 État de l'art succinct de la commande sous contraintes

Un état de l'art de la commande sous contraintes temporelles sur les sorties est présenté dans la section 3.2.2 du Chapitre 3. Il est brièvement rappelé dans cette section.

Les techniques de contrôle sous contraintes temporelles sur les sorties sont nombreuses et variées de part l'importance de ces contraintes destinées à assurer la bonne marche des systèmes en définissant les zones de fonctionnements nominal et dégradé. Dans les ressources documentaires [Goodwin 01, Rojas 02] et [De Dona 02], ces stratégies de commande sont divisées en trois familles :

- les méthodes dites *prudentes* qui consistent à faire en sorte que les signaux de sortie n'atteignent jamais les contraintes (et donc ne les violent pas). Ces méthodes sont souvent considérées comme peu performantes car les signaux de sortie sont forcés de ne jamais stationner sur les contraintes, ce qui est obtenu en utilisant une commande conservatrice qui sous-estime le domaine admissible ;

- Les approches dites *évolutionnaires*[3] qui reposent sur une loi de commande nominale existante qui est modifiée par un signal supplémentaire seulement lorsque les contraintes temporelles sont violées. Un exemple d'approche évolutionnaire est l'utilisation d'un compensateur anti-windup qui ne modifie la dynamique de la boucle fermée que lorsqu'une saturation s'active sur la commande ;

- Les méthodes dites *tactiques* qui prennent en compte les contraintes temporelles au sein d'un problème de contrôle optimal. La commande prédictive est un exemple bien connu d'approche tactique pour la commande.

Dans chaque famille, des exemples documentés d'approches sont renseignés dans la section 3.2.2. Veuillez vous y référer pour plus de détails.

D.2.2 Présentation de l'approche OIST

Dans cette section, les notions développées dans [Burlion 12] et décrites dans le Chapitre 3 sont brièvement rappelées dans le cas d'un système linéaire. L'approche OIST est utilisée afin de satisfaire une contrainte sur une sortie α du système considéré lorsque le contrôleur nominal existant ne le permet pas. Cela est formellement présenté dans le Problème 4.11. Des limites à l'approche actuelle sont identifiées sur un exemple déjà introduit dans le Chapitre 4.

D.2.2 (a) Principe

Une réalisation possible du système linéaire considéré dans cette section est donnée par :

[1] Pour la première fois, les coefficients de la méthode sont choisis variants avec le temps.

[2] Un compensateur anti-windup est considéré afin d'obtenir un certificat sur la stabilité asymptotique de la boucle fermée avec saturations.

[3] A ne pas confondre avec les algorithmes évolutionnaires en optimisation.

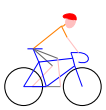

$$(\mathbf{G}) \begin{cases} \dot{\boldsymbol{x}} &= \mathbf{A}\boldsymbol{x} &+ \mathbf{B_u}u &+ \mathbf{B_d}\boldsymbol{d} \\ \boldsymbol{y} &= \boldsymbol{x} & &+ \mathbf{D_d}\boldsymbol{d} \end{cases} \tag{D.1}$$

où $\boldsymbol{x} \in \mathbb{R}^n$ est le vecteur d'état, $u \in \mathbb{R}$ est l'entrée de commande, $\boldsymbol{d} \in \mathbb{R}^{m-1}$ est une entrée de perturbation inconnue et $\boldsymbol{y} \in \mathbb{R}^n$ est la sortie de mesure qui est équivalente au vecteur d'état bruité par les perturbations de sortie présentes au sein du vecteur $\boldsymbol{d}$. Un contrôleur nominal $(\mathbf{K})$ de réalisation :

$$(\mathbf{K}) \begin{cases} \dot{\boldsymbol{x}}_K &= \mathbf{A_K}\boldsymbol{x}_K + \mathbf{B_K}\boldsymbol{u}_K \\ \boldsymbol{y}_K &= \mathbf{C_K}\boldsymbol{x}_K + \mathbf{D_K}\boldsymbol{u}_K \end{cases} \tag{D.2}$$

est supposé connu et assure que la boucle fermée $(u = y_K, \boldsymbol{u}_K = \boldsymbol{y})$ satisfait aux contraintes fréquentielles du cahier des charges.

Contrainte temporelle sur une sortie Considérons le signal de sortie $\alpha = \mathbf{C_\alpha}\boldsymbol{y} \in \mathbb{R}$. Imaginons que nous souhaitions que cette sortie satisfasse la contrainte temporelle suivante :

$$\mathcal{K}(\Omega_\alpha) = \{\alpha \in \Omega_\alpha(t) = [\underline{\alpha}(t), \overline{\alpha}(t)], \forall t\} \tag{D.3}$$

où $\underline{\alpha}(t)$ et $\overline{\alpha}(t)$ sont des paramètres connus dépendants du temps. Il est également supposé que le contrôleur (D.2) ne permette pas de satisfaire la contrainte $\mathcal{K}(\Omega_\alpha)$. L'approche OIST propose de saturer la sortie du contrôleur nominal $(\mathbf{K})$ afin de satisfaire la contrainte de sortie $\mathcal{K}(\Omega_\alpha)$. La manière dont sont déterminées les bornes de la saturation est exposée dans la suite et repose sur la notion de degré relatif de la sortie par rapport à l'entrée de commande u. Une définition plus formelle de la contrainte de sortie est proposée dans la Définition 3.9.

Notons que la fonction de transfert entre la sortie α et l'entrée de commande u est supposée être à minimum de phase à partir de maintenant. Les raisons de ce choix sont expliquées plus tard conjointement à l'analyse de stabilité du système avec saturation.

Degré relatif La notion de degré relatif de la sortie α par rapport à l'entrée de commande u est introduite, en anglais, dans la Définition 3.4. Le degré relatif est un entier désigné par k dans cet exposé. Il quantifie l'ordre de la dérivée de α qui dépend de l'entrée de commande u. Par exemple, en supposant que $\mathbf{D_d} = \mathbf{0}$ et que α soit de degré relatif k par rapport à u, alors les dérivées de α d'ordre j tel que $j < k$ ne dépendent pas de l'entrée de commande u et, pour $j = k$, on a :

$$\alpha^{(k)}(t) = \mathbf{C_\alpha}\mathbf{A}^k\boldsymbol{x}(t) + \mathbf{C_\alpha}\mathbf{A}^{k-1}\mathbf{B_u}u(t) \tag{D.4}$$

En d'autres termes, $\mathbf{C_\alpha}\mathbf{A}^j\mathbf{B_u} = 0$, $\forall j$ s.t $j < k-1$ et $\mathbf{C_\alpha}\mathbf{A}^{k-1} \neq 0$. Dans le cas où $\mathbf{D_d} \neq \mathbf{0}$ et en supposant que l'Hypothèse 4.5 soit satisfaite, une expression plus complexe de la dérivée k-ième de α est obtenue (4.23).

L'hypothèse du degré relatif de α par rapport à u est utilisée dans la suite pour obtenir les saturations à appliquer à u de sorte à ce que α satisfasse la contrainte temporelle $\mathcal{K}(\Omega_\alpha)$. Ceci est possible notamment en introduisant la notion de bornes propagées grâce auxquelles le lemme central de l'approche OIST peut être énoncé.

Bornes propagées et lemme La notion de bornes propagées est détaillée, en anglais, dans la Définition 3.14. Elle repose sur l'introduction de paramètres de réglage $\boldsymbol{\kappa}$ choisis constants dans un premier temps et est utilisée au sein du lemme suivant :

Lemma D.1 (Lemme des bornes propagées)**.**
Supposons que les Hypothèses 3.13 et 3.15 soient satisfaites. En définissant les bornes propagées comme dans la Définition 3.14 pour $i \in \mathbb{N}$ tel que $i \leq k$, alors :

$$\alpha^{(k)}(t) \in [\underline{\alpha}_k(t), \overline{\alpha}_k(t)] = \Omega_\alpha^k(t),\ \forall t \in \mathbb{R}_+ \Rightarrow \alpha(t) \in [\underline{\alpha}(t), \overline{\alpha}(t)] = \Omega_\alpha(t),\ \forall t \in \mathbb{R}_+ \quad \text{(D.5)}$$

Ce lemme, dont la preuve est donnée dans la section 3.3.3, montre qu'en satisfaisant une contrainte temporelle (donnée par les bornes propagées) sur la dérivée k-ième de la sortie contrainte α alors la contrainte temporelle sur α est satisfaite. Comme la dérivée k-ième de α dépend de u par définition du degré relatif, la contrainte temporelle correspondante est facile à satisfaire en choisissant l'entrée de commande u de façon appropriée. En particulier, cela est possible si cette entrée est saturée par des signaux bien définis.

Saturations Toujours en supposant que $\mathbf{D_d} = \mathbf{0}$ et en utilisant le Lemme D.1, la contrainte temporelle sur $\alpha^{(k)}$ est satisfaite si le signal de commande u est choisi égal à $u = \text{sat}_{\underline{u}}^{\overline{u}}(y_K)$ où $\underline{u}(t)$ et $\overline{u}(t)$ sont donnés par :

$$\underline{u}(t) = \frac{\underline{\alpha}_k(t) - \mathbf{C_\alpha A}^k \boldsymbol{x}(t)}{\mathbf{C_\alpha A}^{k-1}\mathbf{B_u}},\ \overline{u}(t) = \frac{\overline{\alpha}_k(t) - \mathbf{C_\alpha A}^k \boldsymbol{x}(t)}{\mathbf{C_\alpha A}^{k-1}\mathbf{B_u}} \quad \text{(D.6)}$$

où on notera que $\mathbf{C_\alpha A}^{k-1}\mathbf{B_u} \neq 0$ par définition du degré relatif. Des expressions plus complexes de ces signaux sont obtenues dans le cas $\mathbf{D_d} \neq \mathbf{0}$, voir les sections 4.4.3 (c) et 4.4.3 (d). Dans la section 4.4.3 (d), il est également expliqué que la définition des bornes propagées doit être adaptée en présence de perturbations à bornes connues. En effet, pour garantir la différentiabilité des bornes propagées, les valeurs absolues et fonctions max doivent être remplacées par des fonctions approchantes différentiables. Il en résulte des expressions plus conservatrices des bornes propagées (4.41) et des saturations (4.43).

D.2.2 (b) Limites

L'approche OIST telle que présentée ici est appliquée à un modèle linéaire de bille en déplacement sur un rail tel que présenté en introduction de la section 4.3 et illustré dans la Fig. 4.2. Une perturbation d peut affecter la dynamique de la position de la bille. En simulation, le signal illustré sur la Fig. 4.3(a) est utilisée. L'objectif est de garantir que la bille ne tombe pas du rail ce qui est formalisé par une contrainte sur la sortie $\alpha = r$ où r est la position de la bille sur le rail. Un contrôle par retour d'état avec action intégrale est implémenté. On observe en pointillés rouge sur la Fig. D.2(a) que cette loi de commande ne permet pas seule de satisfaire la contrainte temporelle telle qu'illustrée sur le même graphique.

L'approche *évolutionnaire* OIST est donc utilisée afin de saturer la sortie du contrôleur de manière appropriée afin de contraindre l'ensemble d'évolution acceptable de la position r de la balle. Dans un premier temps, les paramètres $\boldsymbol{\kappa}$ des bornes propagées sont choisis constants comme le propose la méthode initialement présentée dans [Burlion 12]. Le résultat, en trait plein rouge sur la Fig. D.2(a) semble acceptable à première vue mais un grossissement aux instants proches de $t = 75$s montre que la contrainte temporelle est violée. Ce phénomène s'explique par ce que nous appelons le chevauchement des saturations $\underline{u}$ et $\overline{u}$, notion définie dans la Définition 3.19. En d'autres termes, il est visible sur la Fig. D.2(b) que les saturations se croisent aux alentours de $t = 75$s. Ce croisement est dû à une mauvaise définition des paramètres $\boldsymbol{\kappa}$ de la méthode OIST qui autorise les bornes propagées et donc les saturations à se croiser : $\exists t$ t.q. $\overline{\alpha}_k(t) < \underline{\alpha}_k(t)$. En pratique, cela signifie que la satisfaction de la contrainte temporelle n'est pas garantie pour toutes les valeurs des paramètres $\boldsymbol{\kappa}$.

Pour éviter ce chevauchement, deux approches sont possibles : soit les paramètres restent constants mais sont choisis plus grands (voir Fig. 4.5), ce qui peut conduire à l'apparition de pics dans le signal de commande dus à une saturation plus brutale de celui-ci, soit les paramètres sont choisis variants avec le temps et cela de manière appropriée. Cette dernière solution est sélectionnée. La méthode de construction des paramètres variants est une contribution de ce travail.

D'autre part, l'introduction de saturations au sein de la boucle de contrôle peut être problématique en ce qui concerne la stabilité de la boucle fermée résultante. Une analyse de stabilité est nécessaire. Elle constitue une autre contribution de ce travail de thèse.

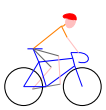

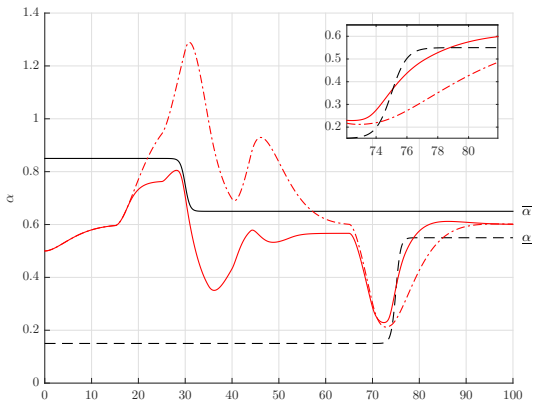

(a) Résultats de simulation de la sortie contrainte α (en rouge) et, en noir, contrainte temporelle considérée. Sans utiliser OIST, la courbe en trait pointillé rouge est obtenue (le contrôleur nominal ne satisfait pas la contrainte) tandis que la courbe en trait plein rouge est obtenue en utilisant OIST avec $\boldsymbol{\kappa}$ constant, tel que proposé dans [Burlion 12] et le Chapitre 3.

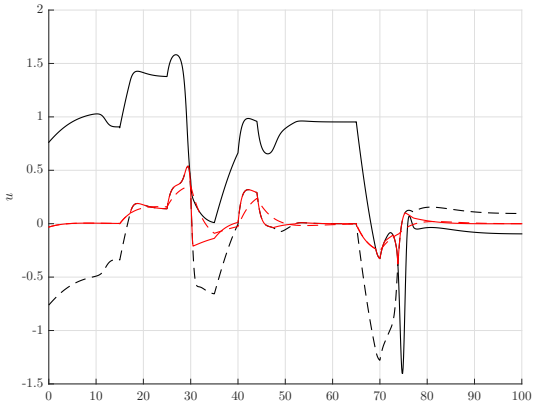

(b) Résultats de simulation du signal de commande (en rouge) et saturations obtenues en utilisant la méthode OIST telle que présentée dans [Burlion 12] et le Chapitre 3. Le chevauchement des saturations débute aux alentours de $t_1 = 73$s.

Figure D.2: Illustration du chevauchement: résultats de simulation avec (trait plein rouge) ou sans (trait pointillé rouge) les saturations issues de OIST, pour $\kappa_1 = 1$ and $\kappa_2 = 0.6$.

D.2.3 Contributions à OIST dans le cadre des systèmes linéaires

Dans cette section, les contributions de la thèse à l'amélioration de l'approche OIST sont présentées. Il est notamment question du problème de chevauchement des bornes propagées et des saturations ainsi que de l'analyse de stabilité de la boucle fermée en présence des saturations OIST.

D.2.3 (a) Solution au problème du chevauchement des bornes propagées et des saturations

Comme expliqué ci-dessus, le chevauchement des saturations illustré dans l'étude de cas de la section 4.3 est dû à une mauvaise définition des coefficients $\boldsymbol{\kappa}$. Si ces coefficients sont choisis trop petits, il peut en résulter un croisement des bornes propagées et des saturations notamment à cause du conservatisme des bornes $\underline{\boldsymbol{d}}$ et $\overline{\boldsymbol{d}}$ supposées encadrer la perturbation $\boldsymbol{d}$. Afin de remédier à ce problème, une étude des quantités $\Delta_j(t) = \overline{\alpha}_j(t) - \underline{\alpha}_j(t)$ pour $0 \leq j \leq k-1$ et $\overline{u} - \underline{u}$ est nécessaire. En particulier, ces quantités doivent être strictement positives comme souligné dans le Lemme 4.23. En remarquant que $\kappa_j(t)$ peut être factorisé dans l'expression de $\Delta_j(t)$, on aboutit au théorème suivant pour la sélection de coefficients $\boldsymbol{\kappa}(t)$ dépendant du temps :

Theorem D.2 (Sélection de paramètres OIST dépendant du temps afin d'éviter le chevauchement des signaux $\underline{u}(t)$ et $\overline{u}(t)$)**.**
Soit $\breve{\boldsymbol{\kappa}} = \begin{bmatrix}\breve{\kappa}_1 & \dots & \breve{\kappa}_k\end{bmatrix}^\top \in \mathbb{R}_+^{\star k}$ *un vecteur de constantes strictement positives. Le chevauchement des bornes propagées et des saturations est évité si :*

- $\underline{\alpha} < \overline{\alpha}$, $\forall t$ *(comme supposé dans le Problème 4.11) et* $\lambda_1^d \neq 0$, $\forall t$ *;*
- $\forall j \in \mathbb{N}^\star$ *tel que* $j \leq k-1$*, la condition* $\widehat{\Delta}_j > 0$ *est satisfaite en choisissant,* $\forall t$ *:*

$$\kappa_j = \frac{\breve{\kappa}_j - \lambda_j^n}{\lambda_j^d} \tag{D.7}$$

où $\breve{\kappa}_j$ *est tel que* $\kappa_1 > \frac{1}{2}$, $\forall j > 1$ *:* $\kappa_j > 1$ *et* $\lambda_{j+1}^d \neq 0$, $\forall t$ *;*

- *Pour $j = k$, l'inéquation $\overline{u} - \underline{u} > 0$ est garantie en choisissant, $\forall t$:*

$$\kappa_k = \frac{1}{\lambda_k^d}\left[\breve{\kappa}_k - \lambda_k^n + 2\sum_{i=1,l_i=0}^{q} |\mathbf{D}_{\boldsymbol{\alpha}i}| \max\left(\left|\underline{d_i^{(k)}}\right|, \left|\overline{d_i^{(k)}}\right|\right) + 2\sum_{i=1,l_i\neq 0}^{q}\sum_{j=l_i}^{k} \left|\mathbf{C}_{\boldsymbol{\alpha}}\mathbf{A}^{j-1}\mathbf{B}_{\mathbf{d}i}\right| \max\left(\left|\underline{\boldsymbol{d}_i^{(k-j)}}(t)\right|, \left|\overline{\boldsymbol{d}_i^{(k-j)}}(t)\right|\right)\right] \tag{D.8}$$

où $\breve{\kappa}_k$ est sélectionné tel que $\kappa_k > \frac{1}{2}$, $\forall t$.

Les quantités λ_j^d et λ_j^n utilisées dans ce théorème sont définies dans (4.47) et sont donc différentiables. En pratique, on observe que la valeur numérique des coefficients augmente dès qu'un chevauchement des bornes propagées ou des saturations est imminent. Le choix de coefficients variant avec le temps permet de formuler une solution garantie au Problème 4.11 :

Theorem D.3 (Solution garantie au Problème 4.11 par la méthode OIST)**.**
Soit le système (**G**) *tel que donné dans* (D.1) *en boucle fermée avec le contrôleur* (**K**) *dans* (D.2)*. Soit α la sortie contrainte considérée et $\mathcal{K}(\Omega_\alpha)$ la contrainte temporelle sur cette sortie. Supposons que les hypothèses 4.4 à 4.10 sont satisfaites.*

Si la loi de commande u est sélectionnée telle que

$$u = sat_{\underline{u}}^{\overline{u}}(y_K)\,,\ \forall t \tag{D.9}$$

où

- *$\underline{u}$ et $\overline{u}$ sont données dans* (4.43)*;*
- *Les bornes propagées sont choisies égales à* (4.41)*;*
- *Les paramètres $\boldsymbol{\kappa}$ de la méthode sont choisis en fonction du Théorème D.2,*

alors $\alpha \in \Omega_\alpha$, $\forall t$.

Ce théorème garantit la satisfaction de la contrainte temporelle formulée sur la sortie α. En revanche, rien ne garantit que l'état interne du système en boucle fermée converge. Une analyse de stabilité est donc nécessaire. Dans le cas d'un transfert $T_{u\to\alpha}(s)$ à minimum de phase, la stabilité asymptotique peut être démontrée en considérant un compensateur anti-windup.

D.2.3 (b) Analyse de stabilité pour un transfert $T_{u\to\alpha}(s)$ à minimum de phase

L'étude de la boucle fermée en présence de la saturation obtenue par l'application de l'approche OIST repose sur la transformation suivante, qui consiste à remarquer que les signaux de saturation $\underline{u}$ et $\overline{u}$ dépendent de la même manière de l'état $\boldsymbol{x}$ du système :

$$u = \mathrm{sat}_{\underline{u}}^{\overline{u}}(y_K) = \mathrm{sat}_{\underline{u}+\boldsymbol{K}_{\mathrm{oist}}\boldsymbol{y}}^{\overline{u}+\boldsymbol{K}_{\mathrm{oist}}\boldsymbol{y}}(y_K + \boldsymbol{K}_{\mathrm{oist}}\boldsymbol{y}) - \boldsymbol{K}_{\mathrm{oist}}\boldsymbol{y} \tag{D.10}$$

où $\boldsymbol{K}_{\mathrm{oist}}$ est défini dans (4.54). En notant $v = \mathrm{sat}_{\underline{v}}^{\overline{v}}(y_K + \boldsymbol{K}_{\mathrm{oist}}\boldsymbol{y})$ où $\underline{v} = \underline{u} + \boldsymbol{K}_{\mathrm{oist}}\boldsymbol{y}$ et $\overline{v} = \overline{u} + \boldsymbol{K}_{\mathrm{oist}}\boldsymbol{y}$, une réalisation de la boucle fermée en présence des saturations OIST est donnée par :

$$\begin{cases} \dot{\boldsymbol{x}}(t) &= \left[\mathbf{A} - \mathbf{B_u}\boldsymbol{K}_{\text{oist}}(t)\right]\boldsymbol{x}(t) + \mathbf{B_u}v(t) + \left(\mathbf{B_d} - \mathbf{B_u}\boldsymbol{K}_{\text{oist}}(t)\mathbf{D_d}\right)\boldsymbol{d}(t) \\ \boldsymbol{y}(t) &= \boldsymbol{x}(t) + \mathbf{D_d}\boldsymbol{d}(t) \\ \dot{\boldsymbol{x}}_K(t) &= \mathbf{A_K}\boldsymbol{x}_K(t) + \mathbf{B_K}\boldsymbol{y}(t) \\ y_K(t) &= \mathbf{C_K}\boldsymbol{x}_K(t) + \mathbf{D_K}\boldsymbol{y}(t) \\ v(t) &= \text{sat}_{\underline{v}(t)}^{\overline{v}(t)}\left(y_K(t) + \boldsymbol{K}_{\text{oist}}(t)\boldsymbol{y}(t)\right) \\ \alpha(t) &= \mathbf{C_\alpha}\boldsymbol{x}(t) + \mathbf{D_\alpha}\boldsymbol{d}(t) \end{cases} \tag{D.11}$$

L'objectif est de montrer que l'origine de cette boucle fermée (que l'on suppose atteignable, voir 4.4.4 (a)) est asymptotiquement stable dans le cas où le transfert $T_{v\to\alpha}(s)$ est à minimum de phase. Cette analyse de stabilité est inspirée par les travaux présentés dans [Herrmann 10]. Dans un premier temps, l'hypothèse d'un transfert à minimum de phase permet de démontrer la proposition suivante.

Proposition D.4 (Stabilité "boucle ouverte" ($v = 0$, $\boldsymbol{d} = 0$))**.**
Le système boucle ouverte suivant

$$\dot{\boldsymbol{x}} = \left[\mathbf{A} - \mathbf{B_u}\boldsymbol{K}_{oist}(t)\right]\boldsymbol{x} \tag{D.12}$$

est GES (Globalement Exponentiellement Stable).

A noter que cette proposition n'est pas satisfaite dans le cas d'un transfert à non-minimum de phase puisque dans ce cas, il peut être montrer que la matrice $\mathbf{A} - \mathbf{B_u}\boldsymbol{K}_{\text{oist}}(t)$ n'est pas Hurwitz $\forall t$ (voir A.1). Sur le modèle de l'article [Herrmann 10], un compensateur anti-windup est introduit :

$$(G_a)\begin{cases} \dot{\boldsymbol{x}}_a(t) &= \mathbf{A}\boldsymbol{x}_a(t) + \mathbf{B_u}u_a(t) \\ \boldsymbol{y}_a(t) &= \boldsymbol{x}_a(t) \\ u_a(t) &= -\boldsymbol{K}_{\text{oist}}(t)\boldsymbol{y}_a(t) - \text{Dz}_{\underline{v}(t)}^{\overline{v}(t)}\left(y_K(t) + \boldsymbol{K}_{\text{oist}}(t)\boldsymbol{y}(t)\right) \\ \dot{\boldsymbol{x}}_K^1(t) &= \mathbf{A_K}\boldsymbol{x}_K^1(t) + \mathbf{B_K}\boldsymbol{y}_a(t) \\ v_1(t) &= -\mathbf{C_K}\boldsymbol{x}_K^1(t) - \left[\mathbf{D_K} + \boldsymbol{K}_{\text{oist}}(t)\right]\boldsymbol{y}_a(t) \end{cases} \tag{D.13}$$

On modifie alors l'entrée de commande v de la manière suivante :

$$\begin{aligned} v(t) &= \text{sat}_{\underline{v}(t)}^{\overline{v}(t)}\left(u(t) + \boldsymbol{K}_{\text{oist}}(t)\boldsymbol{y}(t) + v_1(t)\right) \\ &= \text{sat}_{\underline{v}(t)}^{\overline{v}(t)}\left(\mathbf{C_K}\boldsymbol{x}_K^2(t) + \mathbf{D_K}\left(\boldsymbol{y}(t) - \boldsymbol{y}_a(t)\right) + \boldsymbol{K}_{\text{oist}}(t)\left(\boldsymbol{y}(t) - \boldsymbol{y}_a(t)\right)\right) \end{aligned} \tag{D.14}$$

Le théorème suivant peut ainsi être formulé :

Theorem D.5 (Analyse de stabilité en boucle fermée, Problème 4.13)**.**
Si les Hypothèses 4.4 à 4.10 sont satisfaites[a] *(ce qui assure la validité du Théorème D.2 et de la Proposition D.4), l'origine du système boucle fermé composé du système suivant :*

$$\dot{\boldsymbol{x}} = \left[\mathbf{A} - \mathbf{B_u}\boldsymbol{K}_{oist}\right]\boldsymbol{x} + \mathbf{B_u}v + \left[\mathbf{B_d} - \mathbf{B_u}\boldsymbol{K}_{oist}\mathbf{D_d}\right]\boldsymbol{d} \tag{D.15}$$

(où les signaux $\underline{v}$ et $\overline{v}$ sont donnés dans (4.55)), de la loi de commande v définie dans (D.14) et du compensateur anti-windup donné par (D.13) est GAS (Globalement Asymptotiquement Stable).

[a] En excluant le cas pathologique où le signal $\boldsymbol{d}$ est une distribution non convergente d'énergie finie.

La démonstration de ce théorème est rapportée dans A.2. La boucle fermée obtenue est illustrée dans la Fig. 4.6.

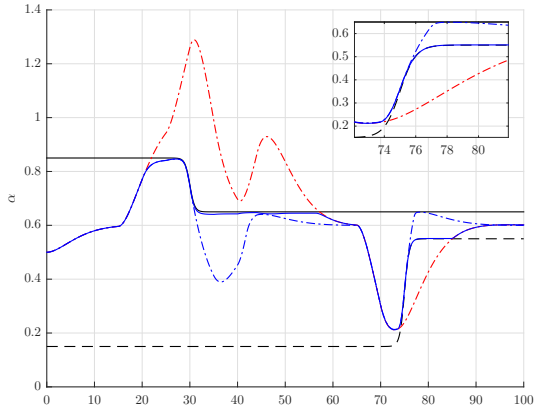

(a) Résultats de simulation de la variable de sortie contrainte.

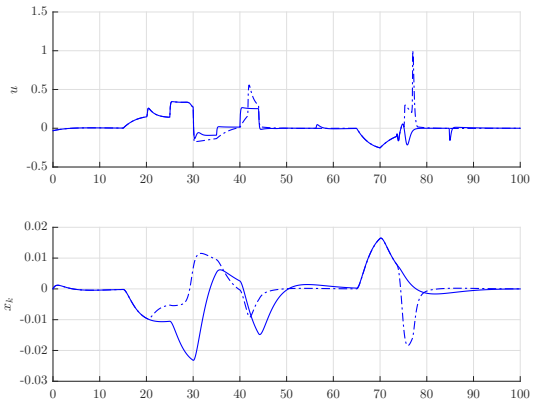

(b) Résultats de simulation du signal de commande u et de l'état du contrôleur dynamique x_K.

Figure D.3: Comparaison des résultats de simulation avec (en bleu, trait plein) ou sans (en bleu, trait pointillé) compensateur anti-windup.

D.2.4 Remarques et conclusion

L'approche OIST telle que présentée ainsi que les contributions initiées dans ce travail sont appliquées au modèle de la bille sur le rail déjà utilisé pour identifier les limites de la méthode OIST initiale. Les détails de l'implémentation sont disponibles dans la section 4.5. Les résultats de simulation sont illustrés dans les Figs. 4.7 et 4.8 et sont très satisfaisants. Dans cet exemple, l'utilisation d'un compensateur anti-windup n'est pas nécessaire pour obtenir la stabilité asymptotique de l'origine. En revanche, on observe que l'utilisation d'un tel compensateur améliore la performance de la boucle fermée. Ceci est illustré dans la Fig. D.3.

On constate qu'en présence du compensateur anti-windup, la variable de sortie est "autorisée" à stationner sur la contrainte. L'écart entre la valeur nominale de la sortie (sans OIST, en rouge) et la valeur contrainte (en trait plein bleu) est minimisé dans ce cas et l'ensemble du domaine admissible du signal de sortie est utilisé. La performance est ainsi améliorée. Grâce aux contributions proposées dans cette thèse, on constate bien entendu que la contrainte n'est plus violée à $t = 75$s de part l'utilisation de coefficients $\boldsymbol{\kappa}$ variants avec le temps.

Des remarques concernant l'optimisation des coefficients $\boldsymbol{\kappa}$ de la méthode OIST ainsi que la considération de transferts $T_{u\to\alpha}(s)$ à non-minimum de phase sont détaillées dans la section 4.6. Nous invitons le lecteur désireux d'en apprendre plus sur ces sujets à consulter cette section.

Dans cette section, les contributions du Chapitre 4 ont été évoquées. Elles concernent l'amélioration de la méthode OIST ainsi que sa formulation dans le cadre des systèmes linéaires. Grâce à une définition appropriée des coefficients $\boldsymbol{\kappa}$ de la méthode, les bornes $\underline{u}$ et $\overline{u}$ de la saturation sont assurées de ne plus se chevaucher ce qui donne une garantie à la satisfaction de la contrainte temporelle sur la sortie α. Par ailleurs, grâce à l'introduction d'un compensateur anti-windup, la stabilité asymptotique de l'origine a été démontrée.

Malgré des résultats très satisfaisants sur des exemples académiques, OIST reste complexe a mettre en œuvre. A court terme, des perspectives d'amélioration concernent une automatisation de la méthode, éventuellement accompagnée d'une étape d'optimisation des coefficients $\check{\boldsymbol{\kappa}}$ par rapport à un critère de coût à définir. Une étude plus détaillée du cas d'un transfert à non-minimum de phase est également planifiée. Le cas des systèmes linéaires incertains avec mesures d'état partielles est considéré dans la section suivante, qui fait écho au Chapitre 5.

D.3 Extension de OIST au cas incertain et en présence de variables d'état non mesurées

La méthode OIST a été présentée dans la section D.2 pour un système linéaire sans incertitude et avec connaissance complète de son vecteur d'état $\boldsymbol{x}$. Il s'agit d'une classe plutôt limitée

de systèmes linéaires. Dans cette section, l'approche OIST, dédiée à la prise en compte d'une contrainte temporelle sur une sortie, est étendue aux systèmes linéaires incertains et dont l'état n'est pas entièrement mesuré : $\boldsymbol{y} \neq \boldsymbol{x}$.

L'extension de la méthode OIST à cette classe plus large de systèmes est appelée OISTeR. Elle est présentée de manière non exhaustive dans cette section. Pour des détails supplémentaires, veuillez vous reporter au Chapitre 5, en anglais. Les résultats présentés dans cette section sont basés sur les résultats préliminaires présentés dans [Chambon 15d].

D.3.1 Classe de systèmes et problème considérés

Classe de systèmes Dans cette section, nous considérons les systèmes linéaires ayant pour réalisation possible :

$$(\mathbf{G}) \begin{cases} \dot{\boldsymbol{x}} &= \mathbf{A}(\boldsymbol{\theta})\,\boldsymbol{x} + \mathbf{B_u} u + \mathbf{B_d}(\boldsymbol{\theta})\,\boldsymbol{d} \\ \boldsymbol{y} &= \mathbf{C}(\boldsymbol{\theta})\,\boldsymbol{x} + \mathbf{D_u}(\boldsymbol{\theta})\,u + \mathbf{D_d}(\boldsymbol{\theta})\,\boldsymbol{d} \\ \boldsymbol{x}(0) &= \boldsymbol{x}_0 \end{cases} \tag{D.16}$$

où $\boldsymbol{x} \in \mathbb{R}^n$, $\boldsymbol{y} \in \mathbb{R}^l$ ($\boldsymbol{y} \neq \boldsymbol{x}$), $u \in \mathbb{R}$ est l'entrée de commande et $\boldsymbol{d} \in \mathbb{R}^{m-1}$ est une entrée inconnue servant à injecter les perturbations dans le système. Le vecteur $\boldsymbol{\theta} \in \mathbb{R}^q$ est le vecteur d'incertitudes où on suppose que celles-ci sont bornées : $\boldsymbol{\theta} \in \Theta$ où Θ est un sous-ensemble de $\mathbb{R}^q$. Les bornes du vecteur d'incertitudes sont supposées connues et sont dénotées $\underline{\boldsymbol{\theta}}$ et $\overline{\boldsymbol{\theta}}$ telles que $\underline{\boldsymbol{\theta}} \leq \boldsymbol{\theta} \leq \overline{\boldsymbol{\theta}}$ (voir Hypothèse 5.1). La condition initiale, potentiellement inconnue, est également supposée appartenir à un intervalle connu $\left[\underline{\boldsymbol{x}_0}, \overline{\boldsymbol{x}_0}\right]$.

En utilisant les bornes sur le vecteur d'incertitudes, il est possible de définir des matrices qui bornent les matrices inconnues dans la réalisation du système ($\mathbf{G}$) :

$$\begin{array}{rcccl} \underline{\mathbf{A}} & \leq & \mathbf{A}(\boldsymbol{\theta}) & \leq & \overline{\mathbf{A}} \\ \underline{\mathbf{B_d}} & \leq & \mathbf{B_d}(\boldsymbol{\theta}) & \leq & \overline{\mathbf{B_d}} \\ \underline{\mathbf{C}} & \leq & \mathbf{C}(\boldsymbol{\theta}) & \leq & \overline{\mathbf{C}} \\ \underline{\mathbf{D_u}} & \leq & \mathbf{D_u}(\boldsymbol{\theta}) & \leq & \overline{\mathbf{D_u}} \\ \underline{\mathbf{D_d}} & \leq & \mathbf{D_d}(\boldsymbol{\theta}) & \leq & \overline{\mathbf{D_d}} \end{array}, \forall \boldsymbol{\theta} \in \left[\underline{\boldsymbol{\theta}}, \overline{\boldsymbol{\theta}}\right] \tag{D.17}$$

Comme le système ($\mathbf{G}$) peut être potentiellement instable, on suppose qu'un contrôleur ($\mathbf{K}$) de réalisation ($\mathbf{A_K}, \mathbf{B_K}, \mathbf{C_K}, \mathbf{D_K}$) a été synthétisé de sorte à stabiliser ($\mathbf{G}$) pour toute valeur $\boldsymbol{\theta}$ de Θ. En pratique, un tel contrôleur robuste peut être synthétisé sur un ensemble de modèles critiques, voir l'Appendice 2. La boucle fermée, supposée bien posée, est obtenue en reliant le système et le contrôleur (d'entrée $\boldsymbol{u}_K$ et de sortie y_K) de la manière suivante :

$$\begin{cases} \boldsymbol{u}_K &= \boldsymbol{y} \\ u &= y_K + v \end{cases} \tag{D.18}$$

Le signal v est utilisé dans l'approche OISTeR pour modifier le signal d'entrée dans le cas où la contrainte temporelle sur la sortie considérée est violée. Une réalisation de la boucle fermée est donnée par :

$$\begin{aligned} \dot{\boldsymbol{X}} &= \begin{bmatrix} \mathbf{A}(\boldsymbol{\theta}) + \mathbf{B_u}\Delta_u(\boldsymbol{\theta})\,\mathbf{D_K}\mathbf{C}(\boldsymbol{\theta}) & \mathbf{B_u}\Delta_u(\boldsymbol{\theta})\,\mathbf{C_K} \\ \mathbf{B_K}\mathbf{C}(\boldsymbol{\theta}) + \mathbf{B_K}\mathbf{D_u}(\boldsymbol{\theta})\,\Delta_u(\boldsymbol{\theta})\,\mathbf{D_K}\mathbf{C}(\boldsymbol{\theta}) & \mathbf{A_K} + \mathbf{B_K}\mathbf{D_u}(\boldsymbol{\theta})\,\Delta_u(\boldsymbol{\theta})\,\mathbf{C_K} \end{bmatrix} \boldsymbol{X} \\ &\quad + \begin{bmatrix} \mathbf{B_u} & \mathbf{B_d}(\boldsymbol{\theta}) + \mathbf{B_u}\Delta_u(\boldsymbol{\theta})\,\mathbf{D_K}\mathbf{D_d}(\boldsymbol{\theta}) \\ \mathbf{0} & \mathbf{B_K}\mathbf{D_d}(\boldsymbol{\theta}) + \mathbf{B_K}\mathbf{D_u}(\boldsymbol{\theta})\,\Delta_u(\boldsymbol{\theta})\,\mathbf{D_K}\mathbf{D_d}(\boldsymbol{\theta}) \end{bmatrix} \begin{bmatrix} v \\ \boldsymbol{d} \end{bmatrix} \\ &= \mathbf{A_X}(\boldsymbol{\theta})\,\boldsymbol{X} + \mathbf{B_{X,v}} v + \mathbf{B_{X,d}}(\boldsymbol{\theta})\,\boldsymbol{d} \end{aligned} \tag{D.19}$$

où $\boldsymbol{X} = \begin{bmatrix} \boldsymbol{x} \\ \boldsymbol{x}_K \end{bmatrix}$ et $\Delta_u(\boldsymbol{\theta}) = [1 - \mathbf{D_K}\mathbf{D_u}(\boldsymbol{\theta})]^{-1}$. En utilisant l'approche SCorpIO, il est possible de synthétiser un observateur par intervalles de l'état $\boldsymbol{X}$ de la boucle fermée.

Problème considéré De manière totalement similaire à OIST, l'objectif ici est de satisfaire une contrainte temporelle $\mathcal{K}(\Omega_\alpha)$ sur une sortie $\alpha = \mathbf{C_{X\alpha}} \boldsymbol{X}$ de sorte que $\alpha(t) \in \Omega_\alpha(t) = [\underline{\alpha}(t), \overline{\alpha}(t)]$. Dans le cas où le contrôleur (**K**) ne permet pas de satisfaire cette contrainte, la méthode OISTeR peut être utilisée en modifiant la commande (via le signal v) de sorte que la sortie contrainte reste dans le domaine admissible Ω_α. De manière formelle, la méthode OISTeR permet d'obtenir une solution au problème suivant :

Problem D.6 (Contrôle du système (D.16) sous contrainte temporelle de sortie)**.**
Trouver deux signaux $[\underline{v}(t), \overline{v}(t)]$ et un domaine $\mathcal{C}_0$ tels que pour deux signaux $\underline{\alpha}(t)$ et $\overline{\alpha}(t)$ avec $\underline{\alpha}(t) \leq \overline{\alpha}(t)$, $\forall t \in \mathbb{R}_+$ alors la sortie α satisfait la contrainte $\mathcal{K}(\Omega_\alpha)$:

$$\alpha(t) \in \Omega_\alpha(t) = [\underline{\alpha}(t), \overline{\alpha}(t)], \forall t \in \mathbb{R}_+ \tag{D.20}$$

dans le cas d'un système (**G**) (D.16) en boucle fermée bien posée avec un contrôleur dynamique (**K**) saturé :

$$\begin{cases} \dot{\boldsymbol{x}}(t) &= \mathbf{A}(\boldsymbol{\theta})\boldsymbol{x}(t) + \mathbf{B_u} u(t) + \mathbf{B_d}(\boldsymbol{\theta})\boldsymbol{d}(t) \\ \boldsymbol{y}(t) &= \mathbf{C}(\boldsymbol{\theta})\boldsymbol{x}(t) + \mathbf{D_u}(\boldsymbol{\theta})u(t) + \mathbf{D_d}(\boldsymbol{\theta})\boldsymbol{d}(t) \\ \alpha(t) &= \mathbf{C_\alpha}\boldsymbol{x}(t) \\ \dot{\boldsymbol{x}}_K(t) &= \mathbf{A_K}\boldsymbol{x}_K(t) + \mathbf{B_K}\boldsymbol{y}(t) \\ y_K(t) &= \mathbf{C_K}\boldsymbol{x}_K(t) + \mathbf{D_K}\boldsymbol{y}(t) \\ u(t) &= y_K(t) + v(t) \\ v(t) &= \mathrm{sat}_{\underline{v}(t)}^{\overline{v}(t)}(0) \\ \boldsymbol{x}_0 &\in \mathcal{C}_0 \end{cases} \tag{D.21}$$

où l'on suppose que les Hypothèses 4.4 à 4.10 et dans la section 5.2.1 sont satisfaites.

L'approche utilisée pour construire les signaux $\underline{v}(t)$ et $\overline{v}(t)$ est décrite dans la suite. A noter que la stabilité de la boucle fermée n'est pas garantie par l'approche OISTeR, comme cela a également été constaté pour OIST. Dans l'état actuel de ce travail novateur, la stabilité de la boucle fermée n'est pas considérée. L'analyse de stabilité est laissée en perspective de ce travail. Dans le cas d'un modèle linéaire sans incertitude mais avec mesures incomplètes du vecteur d'état, cette analyse ainsi que sa preuve ne devraient cependant pas trop différer des résultats obtenus pour OIST dans le cas des systèmes à minimum de phase. La méthode de construction de $\underline{v}(t)$ et $\overline{v}(t)$ est maintenant présentée.

D.3.2 Présentation de l'extension : OISTeR

Dans cette section, l'approche OISTeR est décrite afin d'obtenir les signaux saturants $\underline{v}(t)$ et $\overline{v}(t)$ permettant de satisfaire la contrainte temporelle sur la sortie $\alpha = \mathbf{C_{X\alpha}} \boldsymbol{X}$. Une version plus détaillée de cette description est disponible dans la section 5.3 du Chapitre 5.

Contrainte temporelle généralisée La contrainte temporelle considérée concerne la sortie $\alpha = \mathbf{C_{X\alpha}} \boldsymbol{X}$. Comme mentionné précédemment, l'état $\boldsymbol{X}$ du système en boucle fermée n'est pas supposé connu. L'approche proposée est de considérer des bornes connues et garanties du signal de sortie α et de garantir la contrainte temporelle sur ces bornes. En utilisant par exemple un observateur par intervalles bien construit de l'état $\boldsymbol{X}$, il est possible de borner α par les quantités suivantes :

$$\mathbf{C_{X\alpha}}^+ \underline{\boldsymbol{X}} - \mathbf{C_{X\alpha}}^- \overline{\boldsymbol{X}} \leq \mathbf{C_{X\alpha}} \boldsymbol{X} \leq \mathbf{C_{X\alpha}}^+ \overline{\boldsymbol{X}} - \mathbf{C_{X\alpha}}^- \underline{\boldsymbol{X}} \tag{D.22}$$

La contrainte temporelle est alors spécifiée sur les bornes du signal α plutôt que sur le signal lui-même. Ceci conduit à introduire la notion de contrainte de sortie généralisée, dans le sens où elle concerne les bornes plutôt que le signal lui-même.

Definition D.7 (Contrainte de sortie généralisée $\mathcal{K}(\Omega_\alpha)$)**.**
Soit $\alpha = \mathbf{C_{X\alpha}} \boldsymbol{X}$ la sortie à contraindre du système (D.16). Soit $\Omega_\alpha(t) = [\underline{\alpha}(t), \overline{\alpha}(t)]$ où $\underline{\alpha}(t)$ et $\overline{\alpha}(t)$ sont des signaux unidimensionnels suffisamment différentiables tels que

$$\underline{\alpha}(t) \leq \overline{\alpha}(t),\ \forall t \in \mathbb{R}_+ \tag{D.23}$$

Supposons que des bornes sur l'état du système soient connues telles que $\boldsymbol{X} \in \left[\underline{\boldsymbol{X}}, \overline{\boldsymbol{X}}\right]$. La sortie $\alpha = \mathbf{C_{X\alpha}} \boldsymbol{X}$ satisfait la contrainte $\mathcal{K}(\Omega_\alpha)$ si

$$\begin{cases} \mathbf{C_{X\alpha}}^+ \underline{\boldsymbol{X}} - \mathbf{C_{X\alpha}}^- \overline{\boldsymbol{X}} & \geq & \underline{\alpha} \\ \mathbf{C_{X\alpha}}^+ \overline{\boldsymbol{X}} - \mathbf{C_{X\alpha}}^- \underline{\boldsymbol{X}} & \leq & \overline{\alpha} \end{cases},\ \forall t \in \mathbb{R}_+ \tag{D.24}$$

Grâce à cette réécriture de la contrainte sur des bornes garanties du signal de sortie α, les quantités en jeu sont désormais connues. Toutefois, il peut être constaté que cette réécriture est conservatrice puisqu'on doit satisfaire l'inégalité suivante :

$$\overline{\alpha} - \underline{\alpha} \leq \left(\mathbf{C_{X\alpha}}^+ + \mathbf{C_{X\alpha}}^-\right)\left(\overline{\boldsymbol{X}} - \underline{\boldsymbol{X}}\right) \tag{D.25}$$

Un observateur par intervalles de bonne qualité ou l'utilisation d'un observateur par intervalles d'ordre réduit(voir Chapitre 6) permet toutefois d'assurer un conservatisme minimal. Dans la section suivante, la façon de déterminer les bornes de l'état $\boldsymbol{X}$ est discutée.

Observateur par intervalles de l'état de la boucle fermée La théorie des observateurs par intervalles a été étudiée de manière extensive ces dernières années. Un observateur par intervalles permet de fournir des bornes sur l'état d'un système, dans notre cas, nous sommes intéressés par des bornes sur l'état $\boldsymbol{X}$ de la boucle fermée, notamment lorsque le système considéré est perturbé par un signal d'entrée $\boldsymbol{d}$ inconnu mais à bornes $\underline{\boldsymbol{d}}(t)$ et $\overline{\boldsymbol{d}}(t)$ connues. Des extensions ont notamment été proposées dans le cas des systèmes incertains en utilisant des bornes sur les matrices d'état telles que définies dans D.17.

L'observateur par intervalles considéré au sein de l'approche OISTeR est décrit en détails dans la section 5.3.1. Sa construction repose sur la réécriture du système incertain d'origine (D.16) sous la forme suivante :

$$\begin{aligned} \dot{\boldsymbol{X}} &= \mathbf{A_{X,n}} \boldsymbol{X} + \boldsymbol{\Delta}\mathbf{A_X}(\boldsymbol{\theta})\boldsymbol{X} + \mathbf{B_{X,v}} v + \mathbf{B_{X,d}}(\boldsymbol{\theta})\boldsymbol{d} \\ &= \mathbf{A_{X,n}} \boldsymbol{X} + \mathbf{B_{X,v}} v + \boldsymbol{f}(\boldsymbol{X}, \boldsymbol{d}, \theta) \end{aligned} \tag{D.26}$$

qui utilise le vecteur nominal $\boldsymbol{\theta}_n = \frac{\overline{\boldsymbol{\theta}} - \underline{\boldsymbol{\theta}}}{2}$ pour définir la matrice $\mathbf{A_{X,n}} = \mathbf{A_X}(\boldsymbol{\theta}_n)$ et où $\boldsymbol{\Delta}\mathbf{A_X}(\boldsymbol{\theta}) = \mathbf{A_X}(\boldsymbol{\theta}) - \mathbf{A_{X,n}}$. On définit également $\boldsymbol{f}(\boldsymbol{X}, \boldsymbol{d}, \theta) = \boldsymbol{\Delta}\mathbf{A_X}(\boldsymbol{\theta})\boldsymbol{X} + \mathbf{B_{X,d}}(\boldsymbol{\theta})\boldsymbol{d}$, quantité qui peut être bornée de la manière suivante en utilisant le Lemme 1 dans [Efimov 13e] :

$$\underline{\boldsymbol{f}}\left(\underline{\boldsymbol{X}}, \overline{\boldsymbol{X}}, \underline{\boldsymbol{d}}, \overline{\boldsymbol{d}}\right) \leq \boldsymbol{f}(\boldsymbol{X}, \boldsymbol{d}, \theta) \leq \overline{\boldsymbol{f}}\left(\underline{\boldsymbol{X}}, \overline{\boldsymbol{X}}, \underline{\boldsymbol{d}}, \overline{\boldsymbol{d}}\right) \tag{D.27}$$

La dynamique du système (D.26) n'étant pas coopérative, on considère un changement de coordonnées $\boldsymbol{Z} = \mathbf{P}\boldsymbol{X}$ de sorte que la matrice $\mathbf{P}\mathbf{A_{X,n}}\mathbf{P}^{-1}$ soit (Hurwitz) Metzler dans les nouvelles coordonnées. A noter que la synthèse simultanée du contrôleur et de ce changement de coordonnées peut être effectuée en utilisant l'approche SCorpIO présentée dans la section D.5 et, de manière plus complète, dans le Chapitre 7. Moyennant quelques hypothèses rappelées dans la section 5.3.1, le système suivant est un observateur par intervalles candidat de la boucle fermée (D.16) :

$$\begin{aligned}
\dot{\underline{\boldsymbol{Z}}} &= \mathbf{M}_{\mathbf{Z}}\underline{\boldsymbol{Z}} + \mathbf{P}\mathbf{B}_{\mathbf{X},\mathbf{v}}v + \underline{\boldsymbol{g}}\left(\underline{\boldsymbol{Z}}, \overline{\boldsymbol{Z}}, \underline{\boldsymbol{d}}, \overline{\boldsymbol{d}}\right) \\
\dot{\overline{\boldsymbol{Z}}} &= \mathbf{M}_{\mathbf{Z}}\overline{\boldsymbol{Z}} + \mathbf{P}\mathbf{B}_{\mathbf{X},\mathbf{v}}v + \overline{\boldsymbol{g}}\left(\underline{\boldsymbol{Z}}, \overline{\boldsymbol{Z}}, \underline{\boldsymbol{d}}, \overline{\boldsymbol{d}}\right) \\
\underline{\boldsymbol{Z}_0} &= \mathbf{P}^{+}\underline{\boldsymbol{X}_0} - \mathbf{P}^{-}\overline{\boldsymbol{X}_0} \\
\overline{\boldsymbol{Z}_0} &= \mathbf{P}^{+}\overline{\boldsymbol{X}_0} - \mathbf{P}^{-}\underline{\boldsymbol{X}_0} \\
\underline{\boldsymbol{X}} &= \mathbf{T}^{+}\underline{\boldsymbol{Z}} - \mathbf{T}^{-}\overline{\boldsymbol{Z}} \\
\overline{\boldsymbol{X}} &= \mathbf{T}^{+}\overline{\boldsymbol{Z}} - \mathbf{T}^{-}\underline{\boldsymbol{Z}}
\end{aligned} \tag{D.28}$$

où $\mathbf{T} = \mathbf{P}^{-1}$, $\underline{\boldsymbol{X}_0} = \begin{bmatrix} \boldsymbol{x}_0 \\ \mathbf{0} \end{bmatrix}$, $\overline{\boldsymbol{X}_0} = \begin{bmatrix} \overline{\boldsymbol{x}_0} \\ \mathbf{0} \end{bmatrix}$ et les bornes $\underline{\boldsymbol{g}}\left(\underline{\boldsymbol{Z}}, \overline{\boldsymbol{Z}}, \underline{\boldsymbol{d}}, \overline{\boldsymbol{d}}\right)$ et $\overline{\boldsymbol{g}}\left(\underline{\boldsymbol{Z}}, \overline{\boldsymbol{Z}}, \underline{\boldsymbol{d}}, \overline{\boldsymbol{d}}\right)$ sont définies dans (5.18). Le principal problème de cette formulation est que les bornes $\underline{\boldsymbol{g}}$ et $\overline{\boldsymbol{g}}$ ne sont pas différentiables. Or, dans l'application de OISTeR, celles-ci devront potentiellement être dérivées. L'approche choisie est d'approcher ces quantités par des quantités différentiables bien que plus conservatrices. Ceci est détaillé dans la Proposition 5.11 et appliqué aux bornes $\underline{\boldsymbol{g}}$ et $\overline{\boldsymbol{g}}$. Il en résulte la Proposition 5.12 où un observateur par intervalles candidat de l'état $\boldsymbol{X}$ de la boucle fermée est proposé, avec une dynamique différentiable.

Bornes propagées généralisées et lemme La considération de bornes sur la sortie α conduit à redéfinir les bornes propagées, de manière asymétrique. Ainsi, on définit :

$$\begin{aligned}
\beta_m &= \mathbf{C}_{\mathbf{X}\boldsymbol{\alpha}}{}^{+}\underline{\boldsymbol{X}} - \mathbf{C}_{\mathbf{X}\boldsymbol{\alpha}}{}^{-}\overline{\boldsymbol{X}} \\
\beta_p &= \mathbf{C}_{\mathbf{X}\boldsymbol{\alpha}}{}^{+}\overline{\boldsymbol{X}} - \mathbf{C}_{\mathbf{X}\boldsymbol{\alpha}}{}^{-}\underline{\boldsymbol{X}}
\end{aligned} \tag{D.29}$$

Dans le cas où l'observateur par intervalles a été construit de sorte à ce que sa dynamique soit différentiable, ces quantités sont différentiables. D'autre part, il est possible de définir un degré relatif de ces quantités par rapport à l'entrée de commande v, tel que cela est fait dans l'Hypothèse 5.17. On les utilise pour introduire la notion de bornes propagées généralisées qui sont utiles pour redéfinir le Lemme D.1.

Definition D.8 (Bornes propagées généralisées)**.**
Soit un vecteur de signaux temporels positifs suffisamment dérivables

$$\boldsymbol{\kappa}(t) = \begin{bmatrix} \kappa_1(t) & \dots & \kappa_k(t) \end{bmatrix} \in \mathbb{R}_{+}^{k}$$

et supposons que les bornes $(\underline{\alpha}(t), \overline{\alpha}(t))$ de la contrainte temporelle sont de classe $\mathcal{C}^k\left(\mathbb{R}_+, \mathbb{R}\right)$. Soit $\underline{\beta}_0(t) = \underline{\alpha}(t)$, $\overline{\beta}_0(t) = \overline{\alpha}(t)$ et, $\forall i \in \mathbb{N}^{\star}$ s.t. $i \leq k$:

$$\begin{aligned}
\underline{\beta}_i(t) &= \kappa_i(t)\left(\underline{\beta}_{i-1}(t) - \beta_m^{(i-1)}(t)\right) + \dot{\widehat{\underline{\beta}_{i-1}}}(t) \\
\overline{\beta}_i(t) &= \kappa_i(t)\left(\overline{\beta}_{i-1}(t) - \beta_p^{(i-1)}(t)\right) + \dot{\widehat{\overline{\beta}_{i-1}}}(t)
\end{aligned} \tag{D.30}$$

où β_m et β_p sont définis dans (D.29). On appelle ces quantités des bornes propagées généralisées dans le sens où elles généralisent la Définition D.8 au cas d'un vecteur d'état $\boldsymbol{X}$ inconnu à bornes connues.

La notion de bornes propagées généralisées est utilisée dans le lemme suivant, qui est lui-même une généralisation du Lemme D.1 :

Lemma D.9 (Lemme des bornes propagées généralisées)**.**
Considérons la Définition D.8 des bornes propagées généralisées. Supposons que l'Hypothèse 5.17 est satisfaite et que $\forall i \in \mathbb{N}$ *tel que* $i \leq k$, $\beta_m^{(i)}(0) \geq \underline{\beta}_i(0)$ *et* $\beta_p^{(i)}(0) \leq \overline{\beta}_i(0)$. *Alors,*

$$\left\{\begin{array}{rcl}\beta_m^{(k)} & \geq & \underline{\beta}_k \\ \beta_p^{(k)} & \leq & \overline{\beta}_k\end{array}\right., \forall t \in \mathbb{R}_+ \Rightarrow \left\{\begin{array}{rcl}\beta_m & \geq & \underline{\beta}_0 = \underline{\alpha} \\ \beta_p & \leq & \overline{\beta}_0 = \overline{\alpha}\end{array}\right., \forall t \in \mathbb{R}_+$$
$$\Rightarrow \underline{\alpha} \leq \mathbf{C}_{\mathbf{X}\boldsymbol{\alpha}}\boldsymbol{X} \leq \overline{\alpha},\ \forall t \in \mathbb{R}_+ \Rightarrow \alpha(t) \in \Omega_\alpha(t),\ \forall t \in \mathbb{R}_+ \quad \text{(D.31)}$$

Pour référence, les expressions de $\beta_m^{(k)}$ et $\beta_p^{(k)}$ sont détaillées dans (5.45). Une preuve de ce lemme est décrite dans le Chapitre 5. Le cheminement est clairement identique a ce qui a été proposé dans OIST mais appliqué aux bornes propagées généralisées, à savoir le degré relatif k des quantités β_m et β_p est utilisé pour en déduire les expressions des bornes $\underline{v}$ et $\overline{v}$ de la saturation permettant de satisfaire la contrainte. En effet, par l'Hypothèse 5.17, les quantités $\beta_m^{(k)}$ et $\beta_p^{(k)}$ dépendent de v. De la même manière que précédemment, il faut alors éviter tout chevauchement de ces saturations afin d'obtenir des garanties sur la satisfaction de la contrainte temporelle sur α.

Saturations et évitement de chevauchement En utilisant le Lemme D.9 et les expressions des dérivées k-ième de β_m et β_p, nous pouvons en déduire les bornes $\underline{v}$ et $\overline{v}$ de la saturation OISTeR :

$$\begin{array}{rcl}\underline{v} & = & \frac{1}{\mathcal{L}_{\mathbf{B_z},\mathbf{v}}\mathcal{L}_{\boldsymbol{h}_1}^{k-1}\sigma_m(\boldsymbol{\zeta})}\left[\underline{\beta}_k - \mathcal{L}_{\boldsymbol{h}_1}^k\sigma_m(\boldsymbol{\zeta}) - \sum_{j=0}^{k-1}\frac{\mathrm{d}^j}{\mathrm{d}t^j}\left(\mathcal{L}_{\mathbf{I}}\mathcal{L}_{\boldsymbol{h}_1}^{k-1-j}\sigma_m(\boldsymbol{\zeta})\,\boldsymbol{h}_2(\boldsymbol{\mathcal{D}})\right)\right] \\ \overline{v} & = & \frac{1}{\mathcal{L}_{\mathbf{B_z},\mathbf{v}}\mathcal{L}_{\boldsymbol{h}_1}^{k-1}\sigma_p(\boldsymbol{\zeta})}\left[\overline{\beta}_k - \mathcal{L}_{\boldsymbol{h}_1}^k\sigma_p(\boldsymbol{\zeta}) - \sum_{j=0}^{k-1}\frac{\mathrm{d}^j}{\mathrm{d}t^j}\left(\mathcal{L}_{\mathbf{I}}\mathcal{L}_{\boldsymbol{h}_1}^{k-1-j}\sigma_p(\boldsymbol{\zeta})\,\boldsymbol{h}_2(\boldsymbol{\mathcal{D}})\right)\right]\end{array} \quad \text{(D.32)}$$

Comme signalé dans 5.3.3 (c), ces expressions sont valides seulement si les quantités

$$\mathcal{L}_{\mathbf{B_z},\mathbf{v}}\mathcal{L}_{\boldsymbol{h}_1}^{k-1}\sigma_m(\boldsymbol{\zeta}) \text{ et } \mathcal{L}_{\mathbf{B_z},\mathbf{v}}\mathcal{L}_{\boldsymbol{h}_1}^{k-1}\sigma_p(\boldsymbol{\zeta})$$

sont positives. Dans le cas contraire, le plus simple est de redéfinir la sortie contrainte en $\tilde{\alpha} = -\alpha$ ainsi que la contrainte de manière appropriée. Ceci est illustré dans l'application au lanceur de la section 6.3.2. Les quantités $\underline{v}$ et $\overline{v}$ sont utilisées afin de modifier la sortie du contrôleur (donc l'entrée du système) dès que la contrainte temporelle sur α est violée, en choisissant $v = \mathrm{sat}_{\underline{v}}^{\overline{v}}(0)$.

De la même manière que dans l'approche OIST, le problème du chevauchement des saturations se pose. Il est appréhendé identiquement en considérant les quantités $\Delta_j = \beta_p^{(j)} - \beta_m^{(j)}$ pour j tel que $1 \leq j \leq k$ et en définissant le coefficient $\kappa_j(t)$ correspondant de manière appropriée de sorte que cette quantité soit positive strictement. Les résultats concernant cette condition sont reportés dans le Lemme 5.21 et le Théorème 5.22.

Conclusion Dans cette section, nous avons présenté les différentes étapes de l'application de l'approche OISTeR afin de satisfaire une contrainte temporelle sur une sortie α du système considéré. Moyennant l'utilisation de bornes sur l'état $\boldsymbol{X}$ de la boucle fermée, fournies par un observateur par intervalles, la contrainte temporelle peut être satisfaite en corrigeant la sortie du contrôleur par un signal v défini de manière appropriée, dès que cette contrainte est violée. Le problème de chevauchement des saturations, déjà rencontré pour l'approche OIST, a été résolu de manière similaire en définissant les coefficients $\boldsymbol{\kappa}(t)$ de manière appropriée.

Du fait de la nouveauté des résultats, l'analyse de stabilité de la boucle fermée en présence du signal de correction v déterminé à partir d'un observateur par intervalles n'a pu être menée. Il s'agit d'une perspective d'amélioration à court terme de l'approche OISTeR.

D.3.3 Exemples

L'approche OISTeR est appliquée à deux exemples dans la section 5.4. Le premier exemple considéré est un système linéaire du second ordre avec une seule composante de l'état mesurée. Dans le second exemple, un système linéaire coopératif incertain du second ordre est considéré.

Dans les deux cas, on constate que l'approche OISTeR permet de satisfaire la contrainte temporelle spécifiée sur la sortie contrainte α. En revanche, ceci est obtenu au prix d'une connaissance précise des bornes sur la perturbation d et sur le vecteur d'incertitudes $\boldsymbol{\theta}$ dans le cas incertain. OISTeR est une approche conservatrice qui repose sur la nécessité d'utiliser un observateur par intervalles qui renvoie un intervalle plutôt précis autour de la valeur exacte du vecteur d'état $\boldsymbol{X}$. Ceci laisse présager de perspectives d'amélioration de l'approche. Dans l'application au lanceur flexible (voir section D.4), des approches pratiques sont utilisées afin de réduire ce conservatisme.

D.3.4 Conclusions et perspectives

Dans cette section, nous avons présenté l'extension de OIST aux classes de systèmes linéaires incertains et avec mesures incomplètes de l'état. Cette extension repose sur l'utilisation d'un observateur par intervalles sur l'état du système en boucle fermée avec un correcteur dynamique ($\mathbf{K}$). Cet observateur permet ainsi d'obtenir des bornes garanties sur la valeur de la variable de sortie α. La contrainte temporelle initiale est alors formulée sur ces bornes plutôt que sur la variable α et, moyennant l'utilisation du Lemme D.9, les bornes $\underline{v}$ et $\overline{v}$ de la saturation définissant le signal $v = \text{sat}_{\underline{v}}^{\overline{v}}(0)$ peuvent être déterminées. Ces bornes permettent de modifier la valeur du signal de contrôle dès que la contrainte temporelle sur α n'est plus satisfaite.

En terme de perspectives, une preuve de la stabilité asymptotique de la boucle fermée corrigée par le signal v dans le cas des systèmes à minimum de phase est une priorité. A plus long terme, il serait intéressant de réduire le conservatisme de la méthode, notamment en formalisant l'approche pratique utilisée dans la section 6.3.2, à savoir l'utilisation d'un observateur par intervalles d'ordre réduit. Une telle approche permet d'utiliser la connaissance de certaines variables d'état dans la phase d'application de OISTeR. D'autres approches pourraient également être imaginées comme l'utilisation de techniques stochastiques dans l'estimation de l'intervalle de définition de $\boldsymbol{X}$. A plus long terme encore, la considération de systèmes LTV et LPV serait une amélioration intéressante de la méthode.

D.4 Application des contributions au contrôle atmosphérique d'un lanceur flexible

Dans cette section, les différentes contributions proposées dans ce travail de thèse sont appliquées au contrôle atmosphérique d'un modèle linéaire de lanceur flexible sous contraintes fréquentielles et temporelles. Les résultats présentés dans cette section sont inspirés du Chapitre 6 et des articles [Chambon 15a] et [Chambon 15d] (en anglais) et y font fréquemment référence.

D.4.1 Modèle linéaire de la dynamique longitudinale du lanceur

Dans cette section, nous considérons la dynamique longitudinale du lanceur. Les notations utilisées sont identiques à celles de la Fig. 6.1 du Chapitre 6. En particulier, on note α l'angle d'incidence qui est la variable critique dans ce problème. La dynamique rigide du lanceur est décrite par l'angle d'attitude ψ, sa dérivée $\dot{\psi}$ ainsi que la vitesse de dérive $\dot{z}$ sur l'axe (G, Z). L'entrée de commande du système est l'angle de braquage β de la tuyère. Seule l'attitude ψ et sa dérivée $\dot{\psi}$ sont mesurées. On verra ci-dessous que ces mesures sont perturbées par la présence de modes souples. La norme de la vitesse relative du lanceur par rapport au flux d'air est notée V. Le vent, de vitesse de norme d, agit comme une perturbation sur le système. La dynamique du lanceur peut être découpée en deux parties : la dynamique rigide qui décrit l'évolution du corps du lanceur au cours du temps, et la dynamique flexible qui décrit l'évolution des modes souples. L'évolution temporelle de la dynamique rigide est décrite par les équations suivantes :

$$\begin{aligned} \ddot{\psi} &= K_1\beta + A_6\alpha \\ \ddot{z} &= a_1\psi + a_2\left(\dot{z} - d\right) + a_3\beta \end{aligned} \tag{D.33}$$

où K_1 et A_6 sont des paramètres incertains évaluant respectivement l'efficacité de propulsion et l'efficacité aérodynamique. L'angle d'incidence est défini par la relation suivante :

$$\alpha = \psi + \frac{\dot{z} - d}{V} \tag{D.34}$$

On constate qu'il dépend directement de l'entrée de perturbation d. Ainsi, l'angle d'incidence est particulièrement sensible à la présence de vent et une bourrasque brutale peut faire évoluer cet angle de manière inappropriée. Afin de minimiser la force aérodynamique sur les structures, cet angle d'incidence doit être conservé minimal tout au long du vol atmosphérique du lanceur. En pratique, une contrainte temporelle est considérée :

$$\mathcal{K}\left(\Omega_\alpha\right) = \left\{\alpha(t) \in \Omega_\alpha(t) = \left[-\overline{\alpha}(t), \overline{\alpha}(t)\right], \forall t\right\} \tag{D.35}$$

En raison des matériaux utilisés et des dimensions du lanceur, des modes flexibles sont présents à basse fréquence. Dans le cas du lanceur, la dynamique flexible n'impacte pas la dynamique rigide et agit plutôt comme une dynamique perturbant les sorties. Ainsi, en présence de ces modes, l'attitude mesurée ainsi que sa dérivée ψ_f et $\dot{\psi}_f$ sont des versions bruitées de ψ et $\dot{\psi}$. Dans le modèle utilisé, cinq modes flexibles sont considérés à cause des pics de magnitude qu'ils causent à relativement basse fréquence comme montré sur le diagramme de Bode du transfert de β à ψ_f dans la Fig. 6.2. Une loi de commande mal dimensionnée qui n'atténuerait pas ces modes souples pourrait provoquer leur excitation et mener à terme à la destruction du lanceur. La dynamique du mode souple j pour $j \leq 5$ est décrite par l'équation suivante :

$$\ddot{q}_j + 2\phi_j\omega_j\dot{q}_j + \omega_j^2 q_j = -\omega_j^2 P_c h_T\left(j\right)\beta \tag{D.36}$$

où q_j est la j-ième coordonnée modale, ω_j est la fréquence du mode considérée comme incertaine, ϕ_j est un coefficient d'amortissement, P_c est une constante et $h_T\left(j\right)$ est un paramètre incertain. Les dynamiques flexibles impactent les mesures de la manière suivante :

$$\begin{array}{rcl} \psi_f & = & \psi - \sum_{j=1}^{5} h_{cl}\left(j\right) q_j \\ \dot{\psi}_f & = & \dot{\psi} - \sum_{j=1}^{5} h_{Gy}\left(j\right) \dot{q}_j \end{array} \tag{D.37}$$

où ψ et $\dot{\psi}$ sont des composantes de la dynamique rigide et h_{cl} et h_{Gy} sont des paramètres incertains. En résumé, la dynamique rigide comporte 2 paramètres incertains tandis que chaque dynamique flexible comporte 5 paramètres incertains, ce qui donne un total de 27 paramètres incertains pour le modèle considéré.

En raison de la présence de paramètres incertains, nous utilisons l'approche habituelle pour générer l'ensemble des modèles possibles qui consiste à écrire la dynamique du lanceur sous forme LFR obtenue à partir de la dynamique nominale[4] et en externalisant les incertitudes :

$$(\mathbf{M}) \left\{ \begin{array}{rcccccc} \dot{\boldsymbol{x}} & = & \begin{bmatrix} \mathbf{A_n^1} & \mathbf{0} \\ \mathbf{0} & \mathbf{A_n^2} \end{bmatrix} \boldsymbol{x} & + & \mathbf{B_{n,\beta}}\beta & + & \mathbf{B_{n,w}}\boldsymbol{w} \\ \boldsymbol{z} & = & \mathbf{C_z}\boldsymbol{x} & + & \mathbf{D_{z,\beta}}\beta & + & \mathbf{D_{z,w}}\boldsymbol{w} \\ \boldsymbol{y} & = & \mathbf{C_y}\boldsymbol{x} & + & \mathbf{D_{y,\beta}}\beta & + & \mathbf{D_{y,w}}\boldsymbol{w} \end{array} \right. \tag{D.38}$$

où, dans le cas où on considère 5 modes flexibles, $\boldsymbol{x} \in \mathbb{R}^{13}$, $\boldsymbol{w} = \begin{bmatrix} \boldsymbol{w}_\Delta \\ \boldsymbol{d} \end{bmatrix} \in \mathbb{R}^{28}$ et $\boldsymbol{z} = \begin{bmatrix} \boldsymbol{z}_\Delta \\ \alpha \\ \dot{z} \end{bmatrix} \in \mathbb{R}^{29}$. On note que la matrice d'état est diagonale par blocs par conséquence du découplage des dynamiques rigide et flexible. La LFR peut être obtenue en pratique en utilisant les travaux et outils présents dans [Magni 06, Onera 16]. Pour une valeur fixée $\boldsymbol{\theta} \in \mathbb{R}^{27}$ des paramètres incertains, le modèle correspondant est obtenu à partir de la LFR (D.38) par LFT avec une matrice diagonale $\boldsymbol{\Delta_\theta}$ définie de manière appropriée :

$$\mathbf{G}\left(\boldsymbol{\theta}, s\right) = \mathcal{F}_u\left(\mathbf{M}(s), \boldsymbol{\Delta_\theta}\right) \tag{D.39}$$

[4]La dynamique nominale est obtenue en choisissant une valeur nominale pour les paramètres incertains. Par exemple si un tel paramètre θ est supposé borné par $\underline{\theta}$ et $\overline{\theta}$, une valeur nominale possible est $\frac{\overline{\theta}+\underline{\theta}}{2}$.

Ceci permet d'obtenir les modèles critiques du lanceur pour les valeurs critiques des paramètres incertains $\boldsymbol{\theta}$, lesquelles sont déterminées par exemple par μ-analyse [Roos 10]. En fonction des objectifs de contrôle, les signaux $\boldsymbol{w}$ et $\boldsymbol{z}$ peuvent être enrichis afin de formuler des contraintes de contrôle additionnelles au sein du problème de synthèse.

D.4.2 Synthèse d'un contrôleur robuste nominal

La synthèse d'un contrôleur robuste nominal conformément à un cahier des charges fréquentiel est considérée. Un ensemble de modèles critiques est déterminé et utilisé lors de la synthèse afin de satisfaire plusieurs contraintes fréquentielles. Cette synthèse est réalisée en utilisant l'approche développée dans [Apkarian 07, Apkarian 14]. La satisfaction de la contrainte temporelle sur l'incidence α est assurée du mieux possible par essais-erreurs sur les réglages des critères fréquentiels. Cette section n'apportant pas de contribution théorique majeure, il est recommandé au lecteur intéressé de se reporter au Chapitre 2 et à la section 6.2.

Il apparaît que l'approche par réglage des critères fréquentiels n'est pas infaillible et demande un investissement important dans le temps de réglage. Une approche *évolutionnaire* est envisagée afin de satisfaire la contrainte temporelle sur l'angle d'incidence. La méthode OIST est sélectionnée.

D.4.3 Application de OIST pour le contrôle sous contrainte temporelle

Dans cette section, la méthode OIST (ainsi que son extension OISTeR) est utilisée afin de satisfaire la contrainte temporelle sur l'angle d'incidence du lanceur. En raison des hypothèses nécessaires à l'application de cette méthode, des modèles simplifiées par rapport à celui détaillé dans la section D.4.1 sont utilisés. En outre, il est constaté que le transfert $T_{\beta\to\alpha}(s)$ est à non-minimum de phase. Une approche pratique est utilisée et détaillée dans ce résumé.

D.4.3 (a) Application de OIST au modèle de lanceur flexible

Dans le cadre de l'application de la méthode OIST, le modèle nominal (sans incertitudes) du lanceur flexible est considéré. Il est en effet nécessaire de connaître l'état exact du lanceur pour pouvoir utiliser cette approche :

$$(\mathbf{G_2})\begin{cases} \dot{\boldsymbol{x}} &= \begin{bmatrix} \mathbf{A_n^1} & \mathbf{0} \\ \mathbf{0} & \mathbf{A_n^2} \end{bmatrix} \boldsymbol{x} + \mathbf{B_{n,\beta}}\beta + \mathbf{B_{n,d}}d \\ &= \mathbf{A_n}\boldsymbol{x} + \mathbf{B_{n,\beta}}\beta + \mathbf{B_{n,d}}d \\ \boldsymbol{y} &= \boldsymbol{x} \end{cases} \tag{D.40}$$

où $\boldsymbol{x} \in \mathbb{R}^{13}$ et la matrice $\mathbf{B_{n,d}}$ est définie de manière appropriée à partir de la matrice $\mathbf{B_{n,w}}$. Un contrôleur dynamique structuré avec $n_K = 5$ est synthétisé (voir 6.3.1 (b) pour plus de détails). Dans la suite, nous ne détaillons pas l'application de OIST, qui est disponible dans le Chapitre 6 mais nous insistons sur les détails pratiques de son application.

Changement de sortie contrainte En considérant l'expression initiale de l'angle d'incidence :

$$\alpha = \psi + \frac{\dot{z} - d}{V} = \mathbf{C_\alpha^1}\boldsymbol{x} + \mathbf{D_\alpha^1}d \tag{D.41}$$

il est constaté qu'une telle définition conduit à $\mathbf{C_\alpha^1 B_{n,\beta}} < 0$ ce qui rend complexe l'application de l'approche combinée OIST/OISTeR utilisée par la suite. Il est donc choisi de modifier légèrement la sortie contrainte considérée :

$$\tilde{\alpha} = \mathbf{C_\alpha}\boldsymbol{x} + \mathbf{D_\alpha}d \tag{D.42}$$

où $\mathbf{C_\alpha} = -\mathbf{C_\alpha^1}$ et $\mathbf{D_\alpha} = -\mathbf{D_\alpha^1}$. La contrainte temporelle devient alors $\tilde{\alpha} \in [-\overline{\alpha}, -\underline{\alpha}]$.

Approche combinée OIST/OISTeR pour la réduction du conservatisme Dès les premières étapes de l'approche OIST, on constate que la condition suivante doit être vérifiée :

$$\overline{\alpha} - \underline{\alpha} > 2\mathbf{D}_{\boldsymbol{\alpha}} \max\left(|\underline{d}|, |\overline{d}|\right) \tag{D.43}$$

Il s'agit d'une condition très conservatrice. Afin d'améliorer l'applicabilité de la méthode, il est décidé d'utiliser des éléments de l'approche OISTeR. Notamment, nous pouvons utiliser la notion de borne propagée généralisée en considérant les bornes garanties suivantes sur la sortie contrainte α :

$$\mathbf{C}_{\boldsymbol{\alpha}}\boldsymbol{x} + \mathbf{D}_{\boldsymbol{\alpha}}\underline{d} \leq \tilde{\alpha} \leq \mathbf{C}_{\boldsymbol{\alpha}}\boldsymbol{x} + \mathbf{D}_{\boldsymbol{\alpha}}\overline{d} \tag{D.44}$$

On définit alors :

$$\begin{aligned} \beta_m &= \mathbf{C}_{\boldsymbol{\alpha}}\boldsymbol{x} + \mathbf{D}_{\boldsymbol{\alpha}}\underline{d} \\ \beta_p &= \mathbf{C}_{\boldsymbol{\alpha}}\boldsymbol{x} + \mathbf{D}_{\boldsymbol{\alpha}}\overline{d} \end{aligned} \tag{D.45}$$

et on poursuit avec l'application de la méthode OISTeR. Les détails sont donnés dans la section 6.3.1 (c).

Construction de l'anti-windup Comme déjà signalé, le transfert $T_{\beta\to\tilde{\alpha}}(s)$ est à non-minimum de phase. Cela signifie que si l'approche OIST avec compensateur anti-windup est appliquée sans modifications alors la matrice $\mathbf{A_n} - \mathbf{B}_{\mathbf{n},\boldsymbol{\beta}}\boldsymbol{K}_{\text{oist}}(t)$ n'est pas Hurwitz (cf. preuve de la Proposition D.4) et la boucle fermée avec compensateur ne sera pas stable.

Afin de remédier à ce problème, une solution pratique est de modifier légèrement le transfert $T_{\beta\to\tilde{\alpha}}(s)$ afin qu'il soit à minimum de phase et de concevoir le compensateur sur le transfert modifié. Une diminution de performance sera constatée mais la stabilité de la boucle fermée pourra être obtenue.

La transformation du transfert consiste à changer le signe du zéro positif et à utiliser ce nouveau transfert dans la construction du compensateur. Les transformations successives utilisées sont détaillées dans la section 6.3.1 (c).

Simulation et conclusions Le modèle nominal du lanceur flexible est simulé en boucle fermée avec le contrôleur considéré et le bloc de saturation de la sortie du contrôleur avec les bornes fournies par la méthode OIST. Le signal de perturbation d utilisé est représenté avec ses bornes dans la Fig. 6.7. Dans un premier temps, l'anti-windup n'est pas implémenté dans la boucle puis il est rajouté dans un second temps afin de pouvoir comparer les résultats. Ces derniers sont représentés dans les Figs. 6.8 et 6.9.

Malgré le fait que le transfert $T_{\beta\to\tilde{\alpha}}(s)$ est à non-minimum de phase, on constate que les résultats obtenus sont très satisfaisants. En l'absence actuelle de preuve de convergence, cette observation est justifiée de manière informelle par le fait que le zéro instable de la fonction de transfert est lent, voir les explications de la section 4.6.2. L'ajout d'un compensateur anti-windup basé sur un transfert modifié dans la boucle fermée améliore légèrement les performances. L'utilisation du transfert $T_{\beta\to\tilde{\alpha}}(s)$ non modifié dans la construction de ce compensateur aurait conduit à la non satisfaction de la Proposition D.4 et à l'instabilité de la boucle fermée.

D.4.3 (b) Application de OISTeR au modèle de lanceur rigide

Dans cet exemple, nous considérons le modèle rigide nominal du lanceur mais avec des mesures incomplètes de l'état : $\boldsymbol{y} = \begin{bmatrix}\psi \\ \dot{\psi}\end{bmatrix}$. Le modèle considéré est le suivant :

$$(\mathbf{G_3}) \begin{cases} \dot{\boldsymbol{x}} &= \mathbf{A}\boldsymbol{x} + \mathbf{B}_{\boldsymbol{\beta}}\beta + \mathbf{B}_{\mathbf{d}}d \\ \boldsymbol{y} &= \mathbf{C}\boldsymbol{x} \end{cases} \tag{D.46}$$

où $\boldsymbol{x} = \begin{bmatrix}\psi \\ \dot{\psi} \\ \dot{z}\end{bmatrix} \in \mathbb{R}^3$. En l'absence d'une connaissance complète de l'état, l'approche OIST ne peut être appliquée et nous considérons donc la méthode OISTeR. Le système $(\mathbf{G})$ étant stabilisable

par retour de sortie, nous considérons un retour de sortie statique $\boldsymbol{K} \in \mathbb{R}^{1\times 2}$ de sorte que la matrice $\mathbf{A} - \mathbf{B}_{\boldsymbol{\beta}}\boldsymbol{K}\mathbf{C}$ soit Hurwitz. En boucle fermée, on obtient donc la dynamique suivante, où v est un signal qui va être utilisé par OISTeR pour moduler l'entrée de commande dès que la contrainte temporelle $\mathcal{K}(\Omega_\alpha)$ est violée :

$$\left\{\begin{array}{rcrcl} \dot{\boldsymbol{x}} &=& (\mathbf{A} - \mathbf{B}_{\mathbf{u}}\boldsymbol{K}\mathbf{C})\,\boldsymbol{x} &+& \mathbf{B}_{\boldsymbol{\beta}} v + \mathbf{B}_{\mathbf{d}} d \\ &=& \mathbf{M}\boldsymbol{x} &+& \mathbf{B}_{\boldsymbol{\beta}} v + \mathbf{B}_{\mathbf{d}} d \\ \boldsymbol{y} &=& \mathbf{C}\boldsymbol{x} & & \end{array}\right. \tag{D.47}$$

L'approche OISTeR repose sur la construction d'un observateur par intervalles de l'état du système. Afin de réduire le conservatisme de l'approche et d'améliorer les résultats, il est décidé dans cet exemple d'utiliser un observateur par intervalles réduit sur la variable $\boldsymbol{x}_3 = \dot{z}$ qui est la seule variable d'état non mesurée. De par les propriétés de la matrice $\mathbf{M}$, la construction d'un tel observateur par intervalles est aisée. Écrivons :

$$\mathbf{M} = \mathbf{A} - \mathbf{B}_{\boldsymbol{\beta}}\boldsymbol{K}\mathbf{C} = \begin{bmatrix} \mathbf{M}_{11} & \mathbf{M}_{12} \\ \mathbf{M}_{21} & \mathbf{M}_{22} \end{bmatrix} \tag{D.48}$$

où on constate que $\mathbf{M_{22}} < 0 \in \mathbb{R}$ est Hurwitz et Metzler puisqu'un simple réel est une forme triviale de matrice Hurwitz. Le système $(\mathbf{G_3})$ dans (D.46) peut s'écrire sous la forme suivante :

$$(\mathbf{G_3}) \left\{\begin{array}{rcl} \dot{\boldsymbol{y}} &=& \mathbf{M}_{11}\boldsymbol{y} + \mathbf{M}_{12}\boldsymbol{x}_3 + \mathbf{B}_{\boldsymbol{\beta},\mathbf{1}} v + \mathbf{B}_{\mathbf{d},\mathbf{1}} d \\ \dot{\boldsymbol{x}}_3 &=& \mathbf{M}_{22}\boldsymbol{x}_3 + \mathbf{M}_{21}\boldsymbol{y} + \mathbf{B}_{\boldsymbol{\beta},\mathbf{2}} v + \mathbf{B}_{\mathbf{d},\mathbf{2}} d \end{array}\right. \tag{D.49}$$

où $\boldsymbol{x}_3$ désigne la variable d'état $\dot{z}$ non mesurée et les matrices d'entrées sont définies de manière appropriée. Un observateur par intervalles de cette variable d'état $\boldsymbol{x}_3$ est donné par la dynamique suivante :

$$\begin{array}{rcl} \dot{\underline{\boldsymbol{x}_3}} &=& \mathbf{M}_{22}\underline{\boldsymbol{x}_3} + \mathbf{M}_{\mathbf{21}}\boldsymbol{y} + \mathbf{B}_{\boldsymbol{\beta},\mathbf{2}} v + \mathbf{B}_{\mathbf{d},\mathbf{2}}\underline{d} \\ \dot{\overline{\boldsymbol{x}_3}} &=& \mathbf{M}_{22}\overline{\boldsymbol{x}_3} + \mathbf{M}_{\mathbf{21}}\boldsymbol{y} + \mathbf{B}_{\boldsymbol{\beta},\mathbf{2}} v + \mathbf{B}_{\mathbf{d},\mathbf{2}}\overline{d} \end{array} \tag{D.50}$$

où on a utilisé le fait que la matrice $\mathbf{B_{d,2}}$ est un réel positif. La manière d'implémenter un tel observateur par intervalles réduit est illustrée dans la Fig. 6.6. La méthode OISTeR est alors appliquée en utilisant la mesure $\boldsymbol{y}$ et les bornes $\underline{\boldsymbol{x}_3}$ et $\overline{\boldsymbol{x}_3}$ sur la variable d'état non mesurée. Plus particulièrement, on considère les deux quantités suivantes :

$$\begin{array}{rcl} \beta_m &=& \mathbf{C}_{\boldsymbol{\alpha},\mathbf{1}}\boldsymbol{y} + \mathbf{C}_{\boldsymbol{\alpha},\mathbf{2}}\overline{\boldsymbol{x}_3} + \mathbf{D}_{\boldsymbol{\alpha}}\underline{d} \\ \beta_p &=& \mathbf{C}_{\boldsymbol{\alpha},\mathbf{1}}\boldsymbol{y} + \mathbf{C}_{\boldsymbol{\alpha},\mathbf{2}}\underline{\boldsymbol{x}_3} + \mathbf{D}_{\boldsymbol{\alpha}}\overline{d} \end{array} \tag{D.51}$$

qui sont utilisées dans le lemme de propagation des bornes de l'approche OISTeR. Plus de détails sur la suite de l'implémentation sont exposés dans la section 6.3.2 où sont notamment rapportées les expressions des bornes de la saturation fournies par OISTeR.

Le système en boucle fermée avec le contrôleur statique $\boldsymbol{K}$ et la saturation fournie par OISTeR est alors simulé. Les résultats sont rapportés dans les Figs. 6.11 et 6.12. Ceux-ci sont très satisfaisants. On constate que la contrainte temporelle est satisfaite sur les bornes de la sortie contrainte $\tilde{\alpha}$ lesquelles sont fournies par les mesures ainsi que par l'observateur par intervalles sur la variable d'état $\boldsymbol{x}_3$ non mesurée. Une formalisation théorique précise de l'approche par observateur par intervalles réduit peut être considérée comme perspective de ce travail.

D.4.4 Conclusions

Les approches OIST et OISTeR pour la commande sous contrainte temporelle sur les sorties ont été appliquées dans cette section à des modèles simplifiés de lanceur. Les résultats obtenus en simulation sont encourageants. Des approches pratiques permettant de réduire le conservatisme de ces méthodes et de considérer le cas d'un transfert à non-minimum de phase ont été présentées. Une formalisation théorique de ces approches est planifiée en perspective de ces travaux ainsi que la considération de modèles plus fidèles de lanceurs (avec paramètres incertains, LPV, LTC, etc.).

D.5 SCorpIO : synthèse d'observateurs par intervalles par une approche basée contrôle

La théorie des observateurs par intervalles a fait l'objet de nombreuses études récemment. Cette théorie est présentée de manière exhaustive dans le Chapitre B. De nombreuses ressources documentaires y sont répertoriées pour le lecteur intéressé.

Dans la majorité de ces ressources, l'approche choisie pour la construction d'observateurs par intervalles répond à la nécessité de satisfaire aux 3 conditions de la Définition B.11 proposée dans [Cacace 15]. Par ailleurs, cette approche doit pouvoir s'appliquer à n'importe quel système linéaire détectable, y compris les systèmes instables. Elle consiste donc à suivre les étapes suivantes :

- stabilisation de la dynamique du système par considération d'un observateur classique avec gain $\mathbf{L}$;
- Expression de la dynamique de l'erreur d'observation $\boldsymbol{e} = \boldsymbol{x} - \widehat{\boldsymbol{x}}$;
- Changement de coordonnées $\boldsymbol{e}_z = \mathbf{P}\boldsymbol{e}$ de sorte que $\mathbf{M} = \mathbf{P}\left(\mathbf{A} - \mathbf{LC}\right)\mathbf{P}^1$ soit Metzler (cette matrice est Hurwitz par définition de $\mathbf{L}$) ;
- Déduction de la dynamique de l'observateur par intervalles qui produit des bornes $\underline{\boldsymbol{e}_z}$ et $\overline{\boldsymbol{e}_z}$ sur $\boldsymbol{e}_z$ desquelles sont déduites des bornes $\underline{\boldsymbol{e}}$ et $\overline{\boldsymbol{e}}$ par changement de coordonnées inverse ;
- Déduction de bornes sur $\boldsymbol{x}$: $\underline{\boldsymbol{x}} = \widehat{\boldsymbol{x}} + \underline{\boldsymbol{e}}$ et $\overline{\boldsymbol{x}} = \widehat{\boldsymbol{x}} + \overline{\boldsymbol{e}}$.

D'autres approches sont recensées dans la littérature, comme par exemple celle basée sur les IPR [Cacace 15], mais ne sont pas considérées dans ce travail. Poursuivre sur les méthodes de détermination de $\mathbf{P}$ et $\mathbf{L}$.

D.5.1 Méthodes existantes de construction d'observateurs par intervalles

Au vu de ces remarques, le problème le plus difficile dans la construction d'un observateur par intervalles est le suivant :

Problem D.10 (Détermination d'un changement de coordonnées invariant)**.**
Soi $(\mathbf{G})$ un système de réalisation (7.1). Supposons que la paire de matrices $(\mathbf{A}, \mathbf{C})$ est détectable. Trouver $\mathbf{P} \in \mathbb{R}^{n\times n}$ et $\mathbf{L} \in \mathbb{R}^{n\times m}$ telles que

$$\mathbf{M} = \mathbf{P}\left(\mathbf{A} - \mathbf{LC}\right)\mathbf{P}^{-1} \tag{D.52}$$

est Hurwitz Metzler.

Un ensemble de techniques existe afin de déterminer ces matrices. Celles-ci sont présentées en détail dans la section 7.1.2 du Chapitre 7. Elles sont brièvement rappelées ici.

Placement de pôles réels (solution triviale) Cette approche consiste à constater que les matrices diagonales sont trivialement des matrices Metzler. Ainsi, en plaçant les pôles de la matrice $\mathbf{A} - \mathbf{LC}$ de sorte qu'ils soient réels négatifs alors on obtient $\mathbf{P}\left(\mathbf{A} - \mathbf{LC}\right)\mathbf{P}^{-1}$ diagonale (donc Metzler) par diagonalisation.

Lemma D.11 (Approche par placement de pôles réels)**.**
Soit une matrice $\mathbf{L} \in \mathbb{R}^{n\times m}$ *telle que* $\mathbf{A} - \mathbf{LC}$ *est Hurwitz et* $eig\left(\mathbf{A} - \mathbf{LC}\right) \in \mathbb{R}^n$. *Soit* $\mathbf{P}$ *la matrice des vecteurs propres à droite de* $\mathbf{A} - \mathbf{LC}$. *Alors*

$$\mathbf{M} = \mathbf{P}\left(\mathbf{A} - \mathbf{LC}\right)\mathbf{P}^{-1} \tag{D.53}$$

est Hurwitz diagonale donc Metzler (trivialement).

La procédure de construction est rappelée dans la Fig. 7.1. De par le placement de pôle exigeant, cette approche peut conduire à un gain d'observation $\mathbf{L}$ inapproprié.

Résolution d'une équation de Sylvester En réécrivant l'égalité $\mathbf{M} = \mathbf{P}(\mathbf{A} - \mathbf{LC})\mathbf{P}^{-1}$ sous la forme d'une équation de Sylvester :

$$-\mathbf{MP} + \mathbf{PA} = \mathbf{PLC} = \mathbf{QC} \tag{D.54}$$

il est possible d'obtenir $\mathbf{P}$ et $\mathbf{L}$ pour des matrices $\mathbf{M}$ et $\mathbf{Q}$ fixées par résolution de cette équation [Golub 79, Bartels 72].

Lemma D.12 (Approche par résolution d'une équation de Sylvester)**.**
Soit $\mathbf{M} \in \mathbb{R}^{n\times n}$ une matrice Hurwitz Metzler telle qu'elle n'a aucune valeur propre commune avec $\mathbf{A}$. Soit $\mathbf{Q} \in \mathbb{R}^{n\times m}$ une matrice quelconque. Alors l'équation de Sylvester suivante

$$-\mathbf{MP} + \mathbf{PA} = \mathbf{QC} \tag{D.55}$$

a une unique solution $\mathbf{P} \in \mathbb{R}^{n\times n}$. En choisissant $\mathbf{L} = \mathbf{P}^{-1}\mathbf{Q}$, la matrice $\mathbf{M} = \mathbf{P}(\mathbf{A} - \mathbf{LC})\mathbf{P}^{-1}$ est Hurwitz Metzler par construction.

La procédure de construction est rappelée dans la Fig. 7.2. Cette approche requiert que les matrices $\mathbf{M}$ et $\mathbf{L}$ soient choisies préalablement à la résolution de l'équation. Il apparaît qu'il peut être complexe de construire une matrice $\mathbf{M}$ qui soit Hurwitz Metzler pour un vecteur de valeurs propres donné. Il apparaît également lors de l'application de la méthode que le choix de la matrice $\mathbf{Q}$ est déterminant dans les performances de l'observateur par intervalles. En résumé, les paramètres de la méthode sont difficiles à régler et la solution $(\mathbf{P}, \mathbf{L})$ dépend beaucoup de ceux-ci.

Lemme constructif ([Raïssi 12]) Un lemme constructif a été proposé dans [Raïssi 12] afin de trouver une solution à l'équation de Sylvester sans la résoudre. Ce lemme est rappelé ici.

Lemma D.13 (Méthode constructive de résolution d'une équation de Sylvester [Raïssi 12])**.**
Sot une matrice Hurwitz Metzler $\mathbf{M} \in \mathbb{R}^{n\times n}$ et une matrice $\mathbf{L} \in \mathbb{R}^{n\times m}$ telle que $\mathbf{A} - \mathbf{LC}$ et $\mathbf{M}$ ont les mêmes valeurs propres. S'il existe deux vecteurs $\boldsymbol{e}_1$ et $\boldsymbol{e}_2$ telles que les paires $(\mathbf{A} - \mathbf{LC}, \boldsymbol{e}_1)$ et $(\mathbf{M}, \boldsymbol{e}_2)$ soient observables alors les matrices

$$\mathbf{P} = \mathbf{O_2}^{-1}\mathbf{O_1} \text{ and } \mathbf{Q} = \mathbf{PL} \tag{D.56}$$

satisfont l'équation de Sylvester (D.55) où

$$\mathbf{O_1} = \begin{bmatrix} \boldsymbol{e}_1 \\ \vdots \\ \boldsymbol{e}_1(\mathbf{A} - \mathbf{LC})^{n-1} \end{bmatrix}, \mathbf{O_2} = \begin{bmatrix} \boldsymbol{e}_2 \\ \vdots \\ \boldsymbol{e}_2\mathbf{M}^{n-1} \end{bmatrix} \tag{D.57}$$

La procédure de construction est rappelée dans la Fig. 7.3. De même que dans l'approche précédente, cette méthode nécessite la construction de la matrice $\mathbf{M}$ ce qui est peut être difficile dans le cas où des valeurs propres complexes sont recherchées.

D.5.2 Introduction à SCorpIO

Les méthodes existantes pour la détermination de deux matrices $\mathbf{P}$ et $\mathbf{L}$ telles que la matrice $\mathbf{M} = \mathbf{P}(\mathbf{A} - \mathbf{LC})\mathbf{P}^{-1}$ est Hurwitz Metzler reposent toutes sur la sélection a priori de paramètres dont la sélection est difficile. Par exemple, la construction d'une matrice $\mathbf{M}$ Hurwitz Metzler avec des valeurs propres complexes pré-définies n'est pas aisée. En outre, les résultats fournis

par ces méthode n'intègrent pas directement d'approche de contrôle pour la détermination de la matrice $\mathbf{L}$ dont la valeur conditionne quand même la dynamique de l'observateur classique et donc de l'observateur par intervalles.

Dans cette section, une approche basée contrôle à la détermination de $\mathbf{P}$ et $\mathbf{L}$ est proposée. Elle repose sur la formulation du Problème D.10 comme un problème de stabilisation et à la résolution de ce problème par l'utilisation de technique de synthèse de contrôleur structuré basée H_∞ [Apkarian 07, Apkarian 14]. Dans un premier temps, le Problème D.10 est traduit en un problème impliquant une collection de contraintes inégalités.

Problem D.14 (Formulation basée coefficients du Problème D.10)**.**
Soit le système $(\mathbf{G})$ avec pour réalisation (7.1), supposons que la paire de matrices $(\mathbf{A}, \mathbf{C})$ est détectable. Trouver deux matrices $\mathbf{P} \in \mathbb{R}^{n\times n}$ et $\mathbf{L} \in \mathbb{R}^{n\times m}$ telles que

$$-\mathbf{M}_{ij} = -\left[\mathbf{P}\left(\mathbf{A}-\mathbf{LC}\right)\mathbf{P}^{-1}\right]_{ij} \leq 0,\ \forall\left(i,j\right)\ \text{s.t.}\ 1 \leq i \neq j \leq n \tag{D.58}$$

et $\mathbf{A}-\mathbf{LC}$ est Hurwitz.

Ces $n(n-1)$ inégalités à satisfaire afin d'obtenir une matrice $\mathbf{M}$ Metzler peuvent faire penser à un problème de stabilisation de $n(n-1)$ modèles dynamiques unidimensionnels. Ceci est mis en exergue dans la proposition suivante :

Proposition D.15 (Problème de synthèse de loi de commande équivalent)**.**
Soit le système $(\mathbf{G})$ *ayant pour réalisation* (7.1)*, supposons que la paire de matrices* $(\mathbf{A}, \mathbf{C})$ *est détectable. Soit* $\forall\left(i,j\right) \in \left(\mathbb{N}^\star\right)^2$*,* $\forall \mathbf{P} \in \mathbb{R}^{n\times n}$ *et* $\forall \mathbf{L} \in \mathbb{R}^{n\times m}$

$$\mathbf{M}_{ij}\left(\mathbf{P},\mathbf{L}\right) = \left[\mathbf{P}\left(\mathbf{A}-\mathbf{LC}\right)\mathbf{P}^{-1}\right]_{ij} \tag{D.59}$$

Si le système ayant pour réalisation

$$\left(\mathbf{G_m}\right)\begin{cases} \dot{\boldsymbol{x}}_l &= \left(\mathbf{A}-\mathbf{LC}\right)\boldsymbol{x}_l \\ \dot{x}_{ij} &= -\mathbf{M}_{ij}\left(\mathbf{P},\mathbf{L}\right)x_{ij} \quad \forall i \neq j \end{cases} \tag{D.60}$$

est (Hurwitz) stable pour une paire de matrices $\left(\mathbf{P_s},\mathbf{L_s}\right)$ *alors* $\mathbf{M} = \mathbf{P_s}\left(\mathbf{A}-\mathbf{L_sC}\right)\mathbf{P_s}^{-1}$ *est Hurwitz Metzler.*

Une preuve est disponible dans la section 7.2.2. Le cas des systèmes linéaires à temps discret est également traité dans la même section. Le problème de contrôle équivalent est donc dévoilé. Sous couvert d'un choix approprié de $\mathbf{P}$ et $\mathbf{L}$, le système $(\mathbf{G_m})$ (qui est un système dit "fictif" puisque n'ayant aucune signification physique à proprement parler) peut être stabilisé et donc la matrice $\mathbf{M}$ est Hurwitz Metzler. Afin de déterminer ces matrices, des algorithmes habituellement réservés à la synthèse de loi de commande structurée sont utilisés.

Le problème de détermination de matrices $\mathbf{P}$ et $\mathbf{L}$ telles que $\mathbf{M}$ soit Hurwitz Metzler a été reformulé dans le Problème D.15 comme un problème de stabilisation d'un système linéaire "fictif". En utilisant une approche multi-modèles multi-objectifs de synthèse de contrôleur structuré, il est également possible de formuler des contraintes de contrôle additionnelles. Par exemple, il peut être envisagé de minimiser la norme H_2 des transferts $T_{\boldsymbol{d}\to\boldsymbol{e}(s,\mathbf{L})}$ et $T_{\overline{\boldsymbol{d}}-\underline{\boldsymbol{d}}\to\boldsymbol{E}_d}\left(s,\mathbf{P},\mathbf{L}\right)$ afin d'améliorer la qualité de l'observateur classique et de l'observateur par intervalles. Un problème de synthèse "SCorpIO" ressemble donc typiquement au problème suivant, sachant que des contraintes de contrôle additionnelles peuvent bien entendu être considérées.

Problem D.16 (Problème de synthèse SCorpIO classique)**.**
Résoudre le problème d'optimisation suivant :

$$\begin{aligned} &\min \max_{\mathbf{P},\mathbf{L}} \left\{ \left\| W_e(s) T_{\boldsymbol{d}\to\boldsymbol{e}}(s,\mathbf{L}) \right\|_2, \left\| W_{E_d}(s) T_{\overline{\boldsymbol{d}}-\underline{\boldsymbol{d}}\to\boldsymbol{E}_d}(s,\mathbf{P},\mathbf{L}) \right\|_2 \right\} \\ &\text{tel que} \begin{cases} (\mathbf{G_m}) \text{ dans (D.60) est Hurwitz-stable} \\ \mathbf{P}\left(\mathbf{B_d} - \mathbf{L}\mathbf{D_d}\right) \in \mathbb{R}_+^{n\times k} \end{cases} \end{aligned} \tag{D.61}$$

où $W_e(s)$ et $W_{E_d}(s)$ sont des filtres fréquentiels définis de manière appropriée.

Une formulation du même problème pour les systèmes à temps discret est également possible (voir section 7.2.3). Une solution locale au Problème D.16 peut être obtenue en utilisant des algorithmes d'optimisation non lisse. De tels algorithmes sont utilisés au sein de méthodes de synthèse de contrôleurs structurés telles que [Apkarian 07]. Dans notre cas, la fonction `systune` de la *Robust Control Toolbox* [MATLAB 14, Gahinet 12, Apkarian 14] est utilisée. Ceci est illustré dans les exemples.

D.5.3 Exemples et comparaison

L'approche proposée de formulation du problème original comme un problème de synthèse de loi de commande permet d'utiliser un algorithme de synthèse habituellement réservé à la synthèse "pure" de contrôleur structuré. Cette approche est appliquée à 3 exemples dont un exemple de système à temps discret dans la section 7.3. La méthode proposée est comparée aux autres approches existantes de détermination d'une transformation à temps invariant (telles que présentées au début de cette section) mais également à l'approche basée sur une transformation à temps variant proposée dans [Mazenc 11].

On constate sur ces exemples que l'approche SCorpIO proposée ici permet d'obtenir des résultats comparables, sinon meilleurs, que ceux obtenus en utilisant les méthodes existantes permettant de déterminer $\mathbf{P}$ et $\mathbf{L}$ constantes. En revanche, l'approche par changement de coordonnées à temps variant semble fournir un intervalle plus réduit dans la plupart des cas. Par ailleurs, malgré les avantages en terme de réglage simultané de $\mathbf{P}$ et $\mathbf{L}$ et la possibilité de formuler des contraintes de contrôle, ces contraintes restent complexes à régler et nécessitent des phases de réglage avant de fournir un résultat satisfaisant. Ces limites soulignent les marges d'amélioration actuelles pour la méthode SCorpIO.

D.5.4 Synthèse simultanée contrôleur structuré/observateur par intervalle

Dans cette section, la synthèse simultanée d'un contrôleur dynamique et d'un changement de coordonnées constant de sorte à obtenir une dynamique de boucle fermée coopérative est étudiée. Cette approche est utilisée dans la méthode OISTeR (voir section D.3) afin d'obtenir un observateur par intervalles de l'état de la boucle fermée qui ne dépendent pas des mesures $\boldsymbol{y}$ du système boucle ouverte original. Lors des dérivations successives nécessaires à l'application de OISTeR, ceci permet de ne pas dériver le vecteur de mesures mais bien l'état d'une dynamique connue.

Considérons donc la dynamique boucle fermée suivante, supposée bien posée :

$$\begin{aligned} \dot{\boldsymbol{X}} &= \begin{bmatrix} \mathbf{A} + \mathbf{B_u}\left(\mathbf{I}_l - \mathbf{D_K}\mathbf{D_u}\right)^{-1}\mathbf{D_K}\mathbf{C} & \mathbf{B_u}\left(\mathbf{I}_l - \mathbf{D_K}\mathbf{D_u}\right)^{-1}\mathbf{C_K} \\ \mathbf{B_K}\mathbf{C} + \mathbf{B_K}\mathbf{D_u}\left(\mathbf{I}_l - \mathbf{D_K}\mathbf{D_u}\right)^{-1}\mathbf{D_K}\mathbf{C} & \mathbf{A_K} + \mathbf{B_K}\mathbf{D_u}\left(\mathbf{I}_l - \mathbf{D_K}\mathbf{D_u}\right)^{-1}\mathbf{C_K} \end{bmatrix} \boldsymbol{X} \\ &\quad + \begin{bmatrix} \mathbf{B_u} & \mathbf{B_d} + \mathbf{B_u}\left(\mathbf{I}_l - \mathbf{D_K}\mathbf{D_u}\right)^{-1}\mathbf{D_K}\mathbf{D_d} \\ \mathbf{0} & \mathbf{B_K}\mathbf{D_d} + \mathbf{B_K}\mathbf{D_u}\left(\mathbf{I}_l - \mathbf{D_K}\mathbf{D_u}\right)^{-1}\mathbf{D_K}\mathbf{D_d} \end{bmatrix} \boldsymbol{W} \\ &= \mathbf{A_X}\boldsymbol{X} + \mathbf{B_{X,v}}\boldsymbol{v} + \mathbf{B_{X,d}}\boldsymbol{d} \end{aligned} \tag{D.62}$$

où $\boldsymbol{X} = \begin{bmatrix} \boldsymbol{x} \\ \boldsymbol{x}_K \end{bmatrix}$ est le vecteur d'état de la boucle fermée et $\boldsymbol{W} = \begin{bmatrix} \boldsymbol{v} \\ \boldsymbol{d} \end{bmatrix}$ est le vecteur d'entrée de la boucle fermée (où on a utilisé $\boldsymbol{u} = \boldsymbol{y}_K + \boldsymbol{v}$ en fermant la boucle). Les matrices $\mathbf{A_K}$, $\mathbf{B_K}$, $_K$ et $\mathbf{D_K}$ sont les matrices de réalisation du contrôleur à déterminer. Par ailleurs, on cherche une matrice $\mathbf{P}$ telle que la dynamique de la boucle fermée exprimée dans les nouvelles coordonnées

$\boldsymbol{X}_Z = \mathbf{P}\boldsymbol{X}$ soit coopérative, donc que la matrice $\mathbf{P}\mathbf{A}_\mathbf{X}\mathbf{P}^{-1}$ soit Metzler. Dans le cas où une telle matrice de transformation est obtenue, un observateur par intervalles de l'état $\boldsymbol{X}_Z$ est donné par :

$$\begin{array}{rcl} \dot{\underline{\boldsymbol{X}_Z}} & = & \mathbf{P}\mathbf{A}_\mathbf{X}\mathbf{P}^{-1}\underline{\boldsymbol{X}_Z} + (\mathbf{P}\mathbf{B}_{\mathbf{X},\mathbf{d}})^+ \underline{\boldsymbol{d}} - (\mathbf{P}\mathbf{B}_{\mathbf{X},\mathbf{d}})^- \overline{\boldsymbol{d}} + \mathbf{P}\mathbf{B}_{\mathbf{X},\mathbf{v}}\boldsymbol{v} \\ \dot{\overline{\boldsymbol{X}_Z}} & = & \mathbf{P}\mathbf{A}_\mathbf{X}\mathbf{P}^{-1}\overline{\boldsymbol{X}_Z} + (\mathbf{P}\mathbf{B}_{\mathbf{X},\mathbf{d}})^+ \overline{\boldsymbol{d}} - (\mathbf{P}\mathbf{B}_{\mathbf{X},\mathbf{d}})^- \underline{\boldsymbol{d}} + \mathbf{P}\mathbf{B}_{\mathbf{X},\mathbf{v}}\boldsymbol{v} \\ \underline{\boldsymbol{X}_Z}(0) & = & \mathbf{P}^+\underline{\boldsymbol{X}_0} - \mathbf{P}^-\overline{\boldsymbol{X}_0} \\ \overline{\boldsymbol{X}_Z}(0) & = & \mathbf{P}^+\overline{\boldsymbol{X}_0} - \mathbf{P}^-\underline{\boldsymbol{X}_0} \end{array} \tag{D.63}$$

où les bornes sur l'état initial de la boucle fermée sont définies de manière appropriée. Le problème est donc le suivant :

Problem D.17 (Problème de stabilisation *et* de détermination d'un changement de coordonnées invariant)**.**
Soit le système $(\mathbf{G}_\mathbf{X})$ dans (D.62) où on a supposé que la boucle fermée est bien posée. Trouver $\mathbf{P} \in \mathbb{R}^{(n+n_K)\times(n+n_K)}$ et une réalisation $(\mathbf{A}_\mathbf{K}, \mathbf{B}_\mathbf{K}, \mathbf{C}_\mathbf{K}, \mathbf{D}_\mathbf{K})$ d'un contrôleur $(\mathbf{K})$ tels que :

$$\mathbf{M}_\mathbf{X} = \mathbf{P}\mathbf{A}_\mathbf{X}\mathbf{P}^{-1} \tag{D.64}$$

est Hurwitz Metzler, où

$$\mathbf{A}_\mathbf{X} = \begin{bmatrix} \mathbf{A} + \mathbf{B}_\mathbf{u}\left(\mathbf{I}_l - \mathbf{D}_\mathbf{K}\mathbf{D}_\mathbf{u}\right)^{-1}\mathbf{D}_\mathbf{K}\mathbf{C} & \mathbf{B}_\mathbf{u}\left(\mathbf{I}_l - \mathbf{D}_\mathbf{K}\mathbf{D}_\mathbf{u}\right)^{-1}\mathbf{C}_\mathbf{K} \\ \mathbf{B}_\mathbf{K}\mathbf{C} + \mathbf{B}_\mathbf{K}\left(\mathbf{I}_l - \mathbf{D}_\mathbf{K}\mathbf{D}_\mathbf{u}\right)^{-1}\mathbf{D}_\mathbf{K}\mathbf{C} & \mathbf{A}_\mathbf{K} + \mathbf{B}_\mathbf{K}\mathbf{D}_\mathbf{u}\left(\mathbf{I}_l - \mathbf{D}_\mathbf{K}\mathbf{D}_\mathbf{u}\right)^{-1}\mathbf{C}_\mathbf{K} \end{bmatrix} \tag{D.65}$$

De manière similaire à la Proposition D.15, ce problème peut être formulé comme un problème de stabilisation du système suivant :

$$(\mathbf{G_m}) \begin{cases} \dot{\boldsymbol{x}}_l & = & \mathbf{A}_\mathbf{X}\boldsymbol{x}_l \\ \dot{x}_{ij} & = & -\mathbf{M}_{\mathbf{X}ij}\left(\mathbf{P}, \mathbf{A}_\mathbf{K}, \mathbf{B}_\mathbf{K}, \mathbf{C}_\mathbf{K}, \mathbf{D}_\mathbf{K}\right) x_{ij} \quad \forall i \neq j \end{cases} \tag{D.66}$$

où $\mathbf{M}_{\mathbf{X}ij}\left(\mathbf{P}, \mathbf{A}_\mathbf{K}, \mathbf{B}_\mathbf{K}, \mathbf{C}_\mathbf{K}, \mathbf{D}_\mathbf{K}\right) = \left[\mathbf{P}\mathbf{A}_\mathbf{X}\mathbf{P}^{-1}\right]_{ij}$ avec $\mathbf{A}_\mathbf{X}$ défini dans (D.65) et $1 \leq i \neq j \leq n + n_K$. Comme précédemment, des contraintes de contrôle additionnelles peuvent être considérées sur des modèles supplémentaires afin de contraindre leurs dynamiques. L'approche est illustrée sur un exemple dans la section 7.4.3.

D.5.5 Conclusion

L'approche SCorpIO a été introduite afin de fournir une alternative aux méthodes existantes de détermination d'un changement de coordonnées à temps invariant permet de rendre un système coopératif dans les nouvelles coordonnées. Cela permet ainsi de synthétiser un observateur par intervalles que ce soit sur le système boucle ouverte ou sur une boucle fermée, le contrôleur étant déterminé simultanément au changement de coordonnées. L'approche repose sur la formulation du problème d'origine en problème de stabilisation d'un système fictif. Elle a été illustrée sur des exemples qui ont permis d'illustrer ses performances comparables aux approches existantes.

Une perspective à court terme d'amélioration de SCorpIO est de développer un algorithme dédié qui permettrait notamment de formaliser les contraintes de signe sur les éléments de $\mathbf{M}$ sans passer par une traduction en contraintes sur les pôles d'un système fictif. Ceci permettrait également de simplifier l'application de la méthode qui dépend encore de multiples paramètres de réglage des contraintes de contrôle afin d'obtenir un résultat satisfaisant.

D.6 Conclusions et perspectives

Nous avons présenté dans ce résumé, en français et en esquivant les détails, les contributions de ce travail de thèse. Une approche dite *évolutionnaire* a été utilisée afin de proposer une stratégie de

commande en présence d'un cahier des charges spécifiant simultanément des contraintes fréquentielles et temporelles. En raison des natures différentes de ces contraintes, une loi de commande nominale est d'abord construite pour satisfaire les contraintes fréquentielles lorsque la contrainte temporelle sur la sortie considérée est satisfaite. La commande nominale est modifiée de manière appropriée dès que la contrainte temporelle est violée.

Un certain nombre de contributions ont été présentées dans ce mémoire de thèse. Elles sont rappelées ici avec les perspectives majeures d'amélioration.

- L'approche *évolutionnaire* OIST pour la commande de systèmes sous contrainte temporelle sur une sorte a été appliquée au cas d'un système linéaire. Les deux contributions majeures liées à cette application ont été, dans un premier temps, de proposer une définition appropriée des coefficients $\boldsymbol{\kappa}$ de la méthode afin d'éviter tout chevauchement des bornes $\underline{u}$ et $\overline{u}$ de la saturation du signal de commande nominale et, dans un second, de proposer une analyse de stabilité de la boucle fermée saturée résultante. Dans le cas des transferts $T_{u\to\alpha}(s)$ à minimum de phase, il a été prouvé que l'origine du système est globalement asymptotiquement stable. Les perspectives d'amélioration liées à ces contributions concernent l'optimisation des coefficients $\boldsymbol{\kappa}$ en vu de satisfaire des objectifs de commande additionnels. Dans cette optique, le formalisme AMPL/IPOPT a été testé sur un système simplifié afin de montrer que les outils de commande optimale peuvent servir un tel but. D'autre part, une analyse plus précise de la stabilité en présence de transferts à non-minimum de phase est requise. L'implémentation d'outils permettant d'appliquer la méthode OIST de manière automatisée à n'importe quel système satisfaisant les hypothèses considérées pourrait également améliorer l'applicabilité de la méthode, qui reste complexe à l'heure actuelle ;

- L'approche OIST a ensuite été étendue à la classe des systèmes linéaires incertains et/ou avec mesures partielles de l'état. Moyennant l'utilisation d'un observateur par intervalles et de la généralisation des concepts utilisés au sein de l'approche OIST, une solution a été proposée au problème de commande d'un système sous contrainte temporelle sur une sortie. L'évitement de chevauchement des saturations, proposé dans la section consacrée à OIST, a été étendu à ce problème. Les perspectives majeures d'amélioration de la méthode concernent la réduction de son conservatisme. En particulier, il serait utile de formaliser l'utilisation des mesures sur les variables d'état, comme illustré dans la section D.4. D'autre part, une analyse de stabilité doit être menée sur le modèle de celle proposée pour OIST, compte tenu du fait qu'une nouvelle structure dynamique est utilisée, à savoir l'observateur par intervalles ;

- L'application des méthodes OIST et OISTeR à des modèles plus ou moins simplifiés du lanceur a été menée dans la section D.4. Des résultats satisfaisants ont été obtenus notamment en utilisant des astuces pratiques pour réduire le conservatisme des méthodes utilisées. Les perspectives d'amélioration concernent la considération de modèles plus complexes, notamment dans le cas de l'application de OISTeR pour laquelle seul le modèle rigide du lanceur a été considéré ;

- L'approche basée contrôle proposée pour la construction d'observateurs par intervalles a été détaillée. Elle permet de déterminer les paramètres du changement de coordonnées à temps invariant en utilisant une approche habituellement réservée à la synthèse de contrôleur structuré. L'avantage de considérer une telle méthode est de pouvoir spécifier des contraintes de commande additionnelles lors de la construction de l'observateur. Notre méthode permet d'obtenir des résultats similaires à ceux obtenus en utilisant les méthodes existantes de détermination d'un changement de coordonnées à temps invariant. Des perspectives d'amélioration de cette méthode incluent le développement d'un algorithme dédié afin de réduire sa complexité d'utilisation. Des améliorations liées à la manipulation des variables à optimiser dans l'algorithme utilisé pourraient également être proposées.

A plus long terme, l'approche *évolutionnaire* considérée pourrait être étendue au cas des systèmes à temps variant (LTV) ou à paramètres variants (LPV). Si une approche similaire à

l'approche OISTeR est choisie, la difficulté principale sera de construire l'observateur par intervalles adapté permettant d'encadrer l'état de tels systèmes de manière suffisamment peu conservatrice. Dans un tel but, les observateurs par intervalles construits à partir d'un changement de coordonnées à temps variant pourraient être utiles.

References

[Abbas-Turki 07] M. Abbas-Turki, G. Duc, B. Clément and S. Theodoulis. *Robust Gain Scheduled Control of a Space Launcher by Introducing LQG/LTR Ideas in the NCF Robust Stabilisation Problem.* In Proc. of the 46th IEEE Conference on Decision and Control, pages 2393–2398, New Orleans, LA, USA, December 2007. [p. 8]

[Alazard 03] D. Alazard, N. Imbert, B. Clément and P. Apkarian. *Launcher attitude control: some additional design and optimization tools.* In CNES/EADS Conference on Launcher Technology, Madrid, Spain, November 2003. [pp. 8, 25, and 114]

[Alcaraz-Gonzalez 02] V. Alcaraz-Gonzalez, J. Harmand, A. Rapaport, J. P. Steyer, V. Gonzalez-Alvarez and C. Pelayo-Ortiz. *Software sensors for highly uncertain WWTPs: a new approach based on interval observers.* Water Research, vol. 36, pages 2515–2524, 2002. [p. 181]

[Antsaklis 05] P. J. Antsaklis and A.N. Michel. Linear systems. Birkhäuser Boston, 2005. [p. 28]

[Apkarian 06] P. Apkarian and D. Noll. *Nonsmooth H_∞ Synthesis.* IEEE Transactions on Automatic Control, vol. 51, no. 1, pages 71–86, 2006. [pp. 15, 22, 24, and 141]

[Apkarian 07] P. Apkarian and D. Noll. *Nonsmooth Optimization for Multiband Frequency-Domain Control Design.* Automatica, vol. 43, no. 4, pages 724–731, 2007. [pp. 10, 15, 22, 23, 24, 29, 118, 141, 157, 158, 162, 225, 230, and 231]

[Apkarian 11] P. Apkarian, L. Ravanbod-Hosseini and D. Noll. *Time domain constrained H_∞-synthesis.* International Journal of Robust and Nonlinear Control, vol. 21, no. 2, pages 197–217, 2011. [pp. 38 and 52]

[Apkarian 13] P. Apkarian. *Tuning controllers against multiple design requirements.* In Proc. of the American Control Conference, pages 3888–3893, Washington, USA, June 2013. [pp. 22, 23, 141, 157, and 158]

[Apkarian 14] P. Apkarian, P. Gahinet and C. Buhr. *Multi-model, multi-objective tuning of fixed-structure controllers.* In Proc. of the European Control Conference, pages 856–861, Strasbourg, France, June 2014. [pp. 10, 15, 22, 23, 29, 118, 141, 157, 158, 162, 225, 230, and 231]

[Apkarian 15] P. Apkarian, M. Ngoc Dao and D. Noll. *Parametric Robust Structured Control Design.* Automatica, vol. 60, no. 7, pages 1857–1869, 2015. [pp. 22, 24, 29, and 118]

[Bartels 72] R. H. Bartels and G. W. Stewart. *Solution of the matrix equation AX+XB=C.* Communications of the Association for Computing Machinery, vol. 15, no. 9, pages 820–826, September 1972. [pp. 136, 189, and 229]

[Biannic 11] J.-M. Biannic and P. Apkarian. *Anti-windup design via nonsmooth multi-objective H_∞ optimization.* In Proc. of the American Control Conference, pages 4457 – 4462, San Francisco, CA, June 2011. [p. 163]

[Boyd 91] S. P. Boyd and C. H. Barratt. Linear controller design : limits of performance. Prentice Hall, 1991. [pp. 16 and 27]

[Boyd 94] S. Boyd, L. El Ghaoui, E. Feron and V. Balakrishnan. Linear matrix inequalities in system and control theory, volume 15 of *Studies in Applied Mathematics.* SIAM, 1994. [p. 21]

[Briat 15] C. Briat. Linear parameter-varying and time-delay systems, volume 3 of *Advances in Delays and Dynamics.* Springer-Verlag Berlin Heidelberg, Berlin, Germany, 2015. [p. 21]

[Briat 16] C. Briat. *Interval peak-to-peak observers for continuous/discrete-time systems with persistent inputs and delays.* Automatica (provisionally accepted), 2016. [p. 181]

[Burke 06] J. V. Burke, D. Henrion, A. S. Lewis and M. L. Overton. *HIFOO – a MATLAB package for fixed-order controller design and H_∞ optimization.* In Proc. of the 5th IFAC Symposium on Robust Control Design, Toulouse, France, August 2006. [pp. 22 and 141]

[Burlion 12] L. Burlion. *A new saturation function to convert an output constraint into an input constraint.* In Proc. of the 20th Mediterranean Conference on Control and Automation, pages 1217–1222, July 2012. [pp. 6, 7, 8, 11, 31, 34, 38, 39, 40, 43, 44, 46, 51, 52, 54, 56, 57, 61, 70, 82, 85, 86, 101, 162, 209, 210, 211, 213, and 214]

[Burlion 13] L. Burlion and H. de Plinval. *Keeping a Ground Point in the Camera Field of View of a Landing UAV.* In Proc. of the IEEE International Conference on Robotics and Automation, pages 5763–5768, May 2013. [p. 38]

[Cacace 12] F. Cacace, L. Farina, A. Germani and C. Manes. *Internally Positive Representation of a Class of Continuous Time Systems.* IEEE Transactions on Automatic Control, vol. 57, no. 12, pages 3158–3163, December 2012. [p. 180]

[Cacace 14] F. Cacace, A. Germani and C. Manes. *Stable Internally Positive Representations of Continuous Time Systems.* IEEE Transactions on Automatic Control, vol. 59, no. 4, pages 1048–1053, April 2014. [p. 180]

[Cacace 15] F. Cacace, A. Germani and C. Manes. *A New Approach to Design Interval Observers for Linear Systems.* IEEE Transactions on Automatic Control, vol. 60, no. 6, pages 1665–1670, June 2015. [pp. 134, 154, 178, 179, 180, and 228]

[Chambon a] E. Chambon, L. Burlion and P. Apkarian. *Détermination de matrice semblable Metzler par optimisation non lisse.* Journal Européen des Systèmes Automatisés (special issue). Accepted, to appear in 2017. [pp. 133 and 165]

[Chambon b] E. Chambon, L. Burlion and P. Apkarian. Time-response shaping using output to input saturation transformation. Accepted, under revision. [pp. 8, 9, 38, 51, 58, 70, 163, and 211]

[Chambon 15a] E. Chambon, P. Apkarian and L. Burlion. *Flexible launch vehicle control using robust observer-based controller obtained through structured H_∞ synthesis.* In J. Bordeneuve-Guibé, C. Roos and A. Drouin, editors, Advances in Aerospace Guidance, Navigation and Control, pages 23–38. Springer, Toulouse, France, 2015. [pp. 9, 10, 15, 111, and 223]

[Chambon 15b] E. Chambon, P. Apkarian and L. Burlion. *Metzler matrix transform determination using a non-smooth optimization technique with an application to interval observers.* In Proc. of the SIAM Conference on Control and its Applications, pages 205–211, Paris, France, July 2015. [pp. 10, 133, 165, and 181]

[Chambon 15c] E. Chambon, L. Burlion and P. Apkarian. *Output to Input Saturation Transformation: Demonstration and Application to Disturbed Linear Systems.* In Proc. of the 54th IEEE Annual Conference on Decision and Control, pages 7566–7571, December 2015. [pp. 8, 9, 38, 51, 58, 70, 85, 101, 163, and 211]

[Chambon 15d] E. Chambon, L. Burlion and P. Apkarian. *Robust output interval constraint using O/I saturation transformation with application to uncertain linear launch vehicle.* In Proc. of the 14th European Control Conference, pages 1796–1801, Linz, Austria, July 2015. [pp. 10, 85, 111, 181, 218, and 223]

[Chambon 16] E. Chambon, L. Burlion and P. Apkarian. *Overview of linear time-invariant interval observer design: towards a non-smooth optimisation-based approach.* IET Control Theory and Applications, vol. 10, no. 11, pages 1258–1268, July 2016. [pp. 10, 91, 101, 133, 165, and 181]

[Chebotarev 15] S. Chebotarev, D. Efimov, T. Raïssi and A. Zolghadri. *Interval Observers for Continuous-Time LPV Systems with L1/L2 Performance.* Automatica, vol. 58, pages 82–89, 2015. [p. 181]

[Chung 95] C. C. Chung and J. Hauser. *Nonlinear Control of a Swinging Pendulum.* Automatica, vol. 31, no. 6, pages 851–862, 1995. [p. 34]

[Clément 01] B. Clément and O. Voinot. *Définition d'un benchmark pour le pilotage robuste des lanceurs.* Rapport technique, Supélec/ONERA, February 2001. [p. 112]

[Colaneri 97] P. Colaneri, J.C. Geromel and A. Locatelli. Control theory and design: An RH_2 and RH_∞ viewpoint. Elsevier Science, 1997. [p. 28]

[Daoutidis 89] P. Daoutidis and C. Kravaris. *Synthesis of feedforward/state feedback controllers for nonlinear processes.* AIChE Journal, vol. 35, no. 10, pages 1602–1616, October 1989. [p. 96]

[De Dona 02] J. De Dona, G. C. Goodwin and M. Seron. Constrained control and estimation. Springer-Verlag, 2002. [pp. 36, 38, 61, 89, and 211]

[Dinh 14] T. D. Dinh. *Observateur par intervalles et observateur positif.* PhD thesis, Université Paris Sud - Paris XI, 2014. [p. 181]

[Doyle 81] J. Doyle and G. Stein. *Multivariable feedback design: concepts for a classical/modern synthesis.* IEEE Transactions on Automatic Control, vol. 26, pages 607–611, 1981. [p. 21]

[Doyle 82] J. Doyle. *Analysis of feedback systems with structured uncertainties.* IEE Proceedings Pt. D (Control Theory and Applications), vol. 129, no. 6, pages 242–250, November 1982. [p. 21]

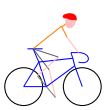

[Doyle 84] J. C. Doyle and G. Stein. *Lecture notes in advances in multivariable control*. ONR/Honeywell Workshop, 1984. [p. 21]

[Doyle 89] J. C. Doyle, K. Glover, P. Khargonekar and B. Francis. *State space solution to standard H_2 and H_∞ control problems*. IEEE Transactions on Automatic Control, vol. 34, no. 8, pages 831–847, 1989. [pp. 21 and 141]

[Dubanchet 12] V. Dubanchet, D. Saussié, C. Bérard, L. Saydy and R. Gourdeau. *Robust Control of a Launch Vehicle in Atmospheric Ascent based on Guardian Maps*. In Proc. of the American Control Conference, pages 938–943, Fairmont Queen Elizabeth, Montréal, Canada, June 2012. [p. 8]

[Efimov 11] D. Efimov, T. Raïssi and A. Zolghadri. *Stabilization of nonlinear uncertain systems based on interval observers*. In Proc. of the 50th Conference on Decision and Control and European Control Conference, pages 8157–8162, December 2011. [p. 181]

[Efimov 13a] D. Efimov, W. Perruquetti, T. Raïssi and A. Zolghadri. *On Interval Observer Design for Time-Invariant Discrete-Time Systems*. In Proc. of the European Control Conference, pages 2651–2656, July 2013. [p. 180]

[Efimov 13b] D. Efimov, W. Perruquetti and J.-P. Richard. *Interval estimation for uncertain systems with time-varying delays*. International Journal of Control, vol. 86, pages 1777–1787, 2013. [p. 181]

[Efimov 13c] D. Efimov, W. Perruquetti and J.-P. Richard. *On reduced-order interval observers for time-delay systems*. In Proc. of the European Control Conference, pages 2116–2121, 2013. [pp. 127 and 181]

[Efimov 13d] D. Efimov, T. Raïssi, S. Chebotarev and A. Zolghadri. *Interval state observer for nonlinear time varying systems*. Automatica, vol. 49, no. 1, pages 200–205, January 2013. [pp. 44 and 181]

[Efimov 13e] D. Efimov, T. Raïssi, W. Perruquetti and A. Zolghadri. *Estimation and control of discrete-time LPV systems using interval observers*. In Proc. of the 52nd IEEE Conference on Decision and Control, pages 5036–5041, Florence, Italy, December 2013. [pp. 90, 107, 149, 164, 178, 182, and 220]

[Efimov 13f] D. Efimov, T. Raïssi and A. Zolghadri. *Control of Nonlinear and LPV Systems: Interval Observer-Based Framework*. IEEE Transactions on Automatic Control, vol. 58, no. 3, pages 773–778, 2013. [pp. 44 and 181]

[Efimov 15] D. Efimov, S. Li, Y. Hu, S. Muldoon, H. Javaherian and V. O. Nikiforov. *Application of Interval Observers to Estimation and Control of Air-Fuel Ratio in a Direct Injection Engine*. In Proc. of the American Control Conference, pages 25–30, 2015. [p. 181]

[Efimov 16] D. Efimov and T. Raïssi. *Design of interval observers for uncertain dynamical systems*. Automation and Remote Control, vol. 77, pages 191–225, 2016. [p. 181]

[El Ghaoui 97] L. El Ghaoui, F. Oustry and M. Ait Rami. *A Cone Complementarity Linearization Algorithm for Static Output-Feedback and Related Problems*. IEEE Transactions on Automatic Control, vol. 42, no. 8, pages 1171–1176, August 1997. [p. 22]

[Farina 00] L. Farina and S. Rinaldi. Positive linear systems: Theory and applications. Wiley, New York, 2000. [p. 180]

[Ferreres 99] G. Ferreres. A practical approach to robustness analysis with aeronautical applications. Springer Verlag, 1999. [p. 24]

[Findeisen 07] R. Findeisen, F. Allgöwer and L. T. Biegler, editors. Assessment and future directions of nonlinear model predictive control. Lecture Notes in Control and Information Sciences. Springer-Verlag, 2007. [p. 38]

[Fourer 02] R. Fourer and B. W. Kernighan. AMPL: A modeling language for mathematical programming. Duxbury Press, 20002. [p. 80]

[Francis 84a] B. A. Francis, J. W. Helton and G. Zames. *H_∞ optimal feedback controllers for linear multivariable systems.* IEEE Transactions on Automatic Control, vol. 29, no. 1, pages 888–900, 1984. [p. 21]

[Francis 84b] B. A. Francis and G. Zames. *On H_∞ optimal sensitivity theory for SISO feedback systems.* IEEE Transactions on Automatic Control, vol. 29, no. 1, pages 9–16, 1984. [p. 21]

[Francis 87] B. A. Francis and J. C. Doyle. *Linear control theory with an H_∞ criterion.* SIAM Journal of Control and Optimization, vol. 25, pages 815–844, 1987. [p. 21]

[Gahinet 94] P. Gahinet and P. Apkarian. *A linear matrix inequality approach to H_∞ control.* International Journal of Robust and Nonlinear Control, vol. 4, no. 4, pages 421–448, 1994. [p. 21]

[Gahinet 11] P. Gahinet and P. Apkarian. *Structured H_∞ synthesis in MATLAB.* In Proc. of the 18th IFAC World Congress, pages 1435–1440, Milan, 2011. [p. 141]

[Gahinet 12] P. Gahinet and P. Apkarian. *Frequency-domain tuning of fixed-structure control systems.* In Proc. of the UKACC International Conference on Control, pages 178–183, Cardiff, United Kingdom, September 2012. [pp. 141 and 231]

[Gahinet 13] P. Gahinet and P. Apkarian. *Automated tuning of gain-scheduled control systems.* In Proc. of the 52nd IEEE Conference on Decision and Control, pages 2740–2745, Florence, Italy, December 2013. [p. 24]

[Ganet 10] M. Ganet and M. Ducamp. *LPV control for flexible launcher.* In Proc. of the AIAA Guidance, Navigation and Control Conference, Toronto, Ontario Canada, August 2010. [pp. 8 and 112]

[Germani 07] A. Germani, C. Manes and P. Palumbo. *State space representation of a class of MIMO Systems via positive systems.* In Proc. of the 46th IEEE Conference on Decision and Control, pages 476–481, 2007. [p. 178]

[Germani 10] A. Germani, C. Manes and P. Palumbo. *Representation of a Class of MIMO Systems via Internally Positive Realization.* European Journal of Control, vol. 3, pages 291–304, 2010. [p. 180]

[Gevers 02] M. Gevers. *A decade of progress in iterative process control design: from theory to practice.* Journal of Process Control, vol. 12, pages 519–531, 2002. [p. 38]

[Gilbert 91] E. G. Gilbert and K. T. Tan. *Linear systems with state and control constraints: the theory and application of maximal output admissible sets.* IEEE Transactions on Automatic Control, vol. 36, no. 9, pages 1008–1019, September 1991. [pp. 37 and 39]

[Gilbert 02] E. Gilbert and I. Kolmanovsky. *Nonlinear tracking control in the presence of state and control constraints: a generalized reference governor.* Automatica, vol. 38, pages 2063–2073, 2002. [p. 38]

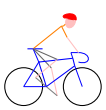

[Glover 88] K. Glover and J. C. Doyle. *State space formulae for all stabilizing controllers that satisfy an H_∞ norm bound and relations to risk sensitivity.* Science and Control Letters, vol. 11, pages 167–172, 1988. [p. 21]

[Goffaux 09] G. Goffaux, A. Vande Wouwer and O. Bernard. *Improving continuous–discrete interval observers with application to microalgae-based bioprocesses.* Journal of Process Control, vol. 19, pages 1182–1190, 2009. [p. 181]

[Golub 79] G. H. Golub, S. Nash and C. Van Loan. *A Hessenberg-Schur method for the problem AX+XB=C.* IEEE Transactions on Automatic Control, vol. 24, no. 6, pages 909–913, December 1979. [pp. 136, 189, and 229]

[Goodwin 01] G. C. Goodwin. *A brief overview of nonlinear control.* In Proc. of the 3rd International Conference on Control Theory and Applications, 2001. [pp. 4, 8, 36, 39, 46, 52, 162, 209, and 211]

[Gouzé 00] J. L. Gouzé, A. Rapaport and M. Z. Hadj-Sadok. *Interval observers for uncertain biological systems.* Ecological Modelling, vol. 133, no. 1-2, pages 45–56, 2000. [pp. 179 and 180]

[Grimm 03] G. Grimm, J. Hatfield, I. Postlethwaite, A. R. Teel, M. C. Turner and L. Zaccarian. *Antiwindup for Stable Linear Systems With Input Saturation: An LMI-Based Synthesis.* IEEE Transactions on Automatic Control, vol. 48, no. 9, pages 1509–1525, September 2003. [pp. 37 and 74]

[Herrmann 10] G. Herrmann, P. P. Menon, M. C. Turner, D. G. Bates and I. Postlethwaite. *Anti-windup synthesis for nonlinear dynamic inversion control schemes.* International Journal of Robust and Nonlinear Control, vol. 20, pages 1465–1482, 2010. [pp. 52, 74, 75, 162, and 216]

[Hu 12] X. Hu, A. Lindquist, J. Mari and J. Sand. Geometric Control Theory. 2012. [p. 169]

[Imbert 01] N. Imbert. *Robustness analysis of a launcher attitude controller via μ-analysis.* In Proc. of the 15th IFAC Symposium on Automatic Control in Aerospace, September 2001. [p. 8]

[Imbert 03] N. Imbert and P. Apkarian. *PIROLA: Bilan.* Rapport technique, ONERA/CNES, December 2003. [p. 112]

[Isidori 95] A. Isidori. Nonlinear control systems. Communications and Control Engineering. Springer-Verlag, 3rd edition, 1995. [pp. 39 and 96]

[Isidori 99] A. Isidori. Nonlinear control systems II. Communications and Control Engineering. Springer London, 1999. [p. 172]

[Iwasaki 94] T. Iwasaki and R. E. Skelton. *All controllers for the general H_∞ control problem: LMI existence conditions and state space formulas.* Automatica, vol. 30, no. 8, pages 1307–1317, 1994. [p. 21]

[Jaulin 01] L. Jaulin, M. Kieffer, O. Didrit and E. Walter. Applied interval analysis. Springer London, 2001. [p. 180]

[Jaulin 02] L. Jaulin. *Nonlinear bounded-error state estimation of continuous time systems.* Automatica, vol. 38, no. 6, pages 1079–1082, June 2002. [p. 180]

[Kapoor 98] N. Kapoor, A. R. Teel and P. Daoutidis. *An Anti-Windup Design for Linear Systems with Input Saturation.* Automatica, vol. 34, no. 5, pages 559–574, May 1998. [p. 74]

[Kapoor 99] N. Kapoor and P. Daoutidis. *An observer-based anti-windup scheme for non-linear systems with input constraints.* International Journal of Control, vol. 72, no. 1, pages 18–29, 1999. [p. 171]

[Khalil 02] H. K. Khalil. Nonlinear systems. Prentice Hall, 3^{rd} edition, 2002. [pp. 21 and 171]

[Kieffer 06] M. Kieffer and E. Walter. *Guaranteed nonlinear state estimation for continuous-time dynamical models from discrete-time measurements.* In Proc. of the 5th IFAC Symposium on Robust Control Design, pages 685–690, 2006. [p. 180]

[Kimura 84] H. Kimura. *Robust stabilizability for a class of transfer functions.* IEEE Transactions on Automatic Control, vol. 29, no. 9, pages 788–793, 1984. [p. 21]

[Knoblauch 12] M. Knoblauch, D. Saussié and C. Bérard. *Structured H_∞ Control for a Launch Vehicle.* In Proc. of the American Control Conference, pages 967–972, Fairmont Queen Elizabeth, Montréal, Canada, June 2012. [p. 7]

[Kučera 80] V. Kučera. Discrete linear control: The polynomial equation approach. John Wiley & Sons, Inc., New York, NY, USA, 1980. [p. 28]

[Kučera 11] V. Kučera. *A Method to Teach the Parameterization of All Stabilizing Controllers.* In Proc. of the 18th IFAC World Congress, pages 6355–6360, Milano, Italy, September 2011. [p. 28]

[Kwakernaak 69] H. Kwakernaak. *Optimal low-sensitivity linear feedback systems.* Automatica, vol. 5, pages 279–285, 1969. [p. 21]

[Lin 93] Z. Lin and A. Saberi. *Semi-global exponential stabilization of linear systems subject to input saturation via linear feedbacks.* Systems and Control Letters, vol. 21, pages 225–239, 1993. [p. 37]

[Lu 97] X.-Y. Lu and S. K. Spurgeon. *Robust sliding mode control of uncertain nonlinear systems.* Systems and Control Letters, vol. 32, no. 2, pages 75–90, November 1997. [p. 21]

[Magni 06] J-F. Magni. *Linear Fractional Representation toolbox for use with Matlab*, February 2006. [pp. 17, 22, and 224]

[MATLAB 14] MATLAB. *Robust Control Toolbox version 5.2 (R2014b).* Natick, Massachusetts, 2014. [pp. 24, 118, 143, 156, 157, 165, and 231]

[Mazenc 10] F. Mazenc and O. Bernard. *Asymptotically Stable Interval Observers for Planar Systems With Complex Poles.* IEEE Transactions on Automatic Control, vol. 55, no. 2, pages 523–527, February 2010. [pp. 180, 181, and 187]

[Mazenc 11] F. Mazenc and O. Bernard. *Interval observers for linear time-invariant systems with disturbances.* Automatica, vol. 47, no. 1, pages 140–147, 2011. [pp. 134, 142, 145, 149, 176, 178, 180, 182, 186, 187, 190, 191, 194, 197, and 231]

[Mazenc 12a] F. Mazenc, T. N. Dinh and S. I. Niculescu. *Interval Observers For Discrete-time Systems.* In Proc. of the 51st Conference on Decision and Control, pages 6755–6760, December 2012. [pp. 181 and 188]

[Mazenc 12b] F. Mazenc, M. Kieffer and E. Walter. *Interval observers for continuous-time linear systems with discrete-time outputs.* In Proc. of the American Control Conference, pages 1889–1894, June 2012. [p. 180]

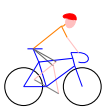

[Mazenc 12c] F. Mazenc, S.-I. Niculescu and O. Bernard. *Exponentially stable interval observers for linear systems with delay.* SIAM Journal on Control and Optimization, vol. 50, no. 1, pages 286–305, 2012. [p. 181]

[Mazenc 14] F. Mazenc, T. N. Dinh and S. I. Niculescu. *Interval observers for discrete-time systems.* International Journal of Robust and Nonlinear Control, vol. 24, pages 2867–2890, 2014. [pp. 181 and 188]

[McFarlane 92] D. McFarlane and K. Glover. *A loop-shaping design procedure using H_∞ synthesis.* IEEE Transactions on Automatic Control, vol. 37, no. 6, pages 759–769, 1992. [p. 21]

[Menon 06] P. P. Menon, G. Herrmann, M. C. Turner, D. G. Bates and I. Postlethwaite. *General Anti-windup synthesis for input constrained nonlinear systems controlled using nonlinear dynamic inversion.* In Proc. of the 45th IEEE Conference on Decision and Control, volume December, pages 5435–5440, 2006. [p. 74]

[Moisan 09] M. Moisan, O. Bernard and J.-L. Gouzé. *Near optimal interval observers bundle for uncertain bioreactors.* Automatica, vol. 45, pages 291–295, 2009. [p. 181]

[Moisan 10] M. Moisan and O. Bernard. *Robust interval observers for global Lipschitz uncertain chaotic systems.* Systems and Control Letters, vol. 59, pages 687–694, 2010. [p. 181]

[Morabito 04] F. Morabito, A. Teel and L. Zaccarian. *Nonlinear antiwindup applied to Euler-Lagrange systems.* IEEE Transactions on Robotics and Automation, vol. 20, no. 3, pages 526–537, June 2004. [p. 37]

[Nett 84] C. N. Nett, C. A. Jacobson and M. J. Balas. *A connection between state-space and doubly coprime fractional representations.* IEEE Transactions on Automatic Control, vol. 29, no. 9, September 1984. [p. 28]

[Olfati-Saber 01] R. Olfati-Saber. *Nonlinear Control of Underactuated Mechanical Systems with Application to Robotics and Aerospace Vehicles.* PhD thesis, Massachusetts Institute of Technology, 2001. [pp. 33 and 34]

[Onera 16] DCSD Onera. *SMAC Systems Modeling, Analysis and Control.* http://w3.onera.fr/smac/, 2016. Webpage consulted on 09/26/2016. [pp. 17, 22, 163, 164, and 224]

[Ortega 01] R. Ortega, A. van der Schaft, I. Mareels and B. Maschke. *Putting energy back in control.* IEEE Control Systems Magazine, vol. 21, pages 18–33, 2001. [p. 21]

[Ortega 02] R. Ortega, A. van der Schaft and B. Maschke. *Interconnection and damping assignment passivity-based control of port-controlled Hamiltonian systems.* Automatica, vol. 38, pages 585–596, 2002. [p. 21]

[Packard 93] A. Packard and J. Doyle. *The complex structured singular value.* Automatica, vol. 29, no. 1, pages 71–109, 1993. [p. 24]

[Polyakov 13] A. Polyakov, D. Efimov, W. Perruquetti and J.-P. Richard. *Output stabilization of time-varying input delay systems using interval observation technique.* Automatica, vol. 49, no. 11, pages 3402–3410, November 2013. [p. 181]

[Poussot-Vassal 08] C. Poussot-Vassal. *Robust LPV multivariable Automotive Global Chassis Control.* PhD thesis, Grenoble INP, Grenoble, France, 2008. [p. 21]

[Qin 03] S. J. Qin and T. A. Badgwell. *A survey of industrial model predictive control technology.* Control Engineering Practice, vol. 11, no. 7, pages 733–764, 2003. [p. 38]

[Raïssi 04] T. Raïssi, N. Ramdani and Y. Candau. *Set membership state and parameter estimation for systems described by nonlinear differential equations.* vol. 40, no. 10, pages 1771–1777, October 2004. [p. 180]

[Raïssi 12] T. Raïssi, D. Efimov and A. Zolghadri. *Interval State Estimation for a Class of Nonlinear Systems.* IEEE Transactions on Automatic Control, vol. 57, no. 1, pages 260–265, January 2012. [pp. 44, 134, 136, 137, 145, 148, 180, 186, 187, 189, 194, and 229]

[Raïssi 10] T. Raïssi, G. Videau and A. Zolghadri. *Interval Observers Design for Consistency Checks of Nonlinear Continuous-Time Systems.* Automatica, vol. 46, pages 518–527, 2010. [pp. 180 and 181]

[Ravanbod 12] L. Ravanbod, D. Noll and P. Apkarian. *An extension of the linear quadratic Gaussian loop transfer recovery procedure.* IET Control Theory and Applications, vol. 6, no. 14, pages 2269–2278, 2012. [p. 21]

[Renault 08] C. Renault and P. Saunois. *Launchers control architecture and synthesis with analytical loop shaping.* In Proc. of the 7th International ESA Conference on Guidance, Navigation and Control Systems, Tralee, County Kerry, Ireland, June 2008. [p. 112]

[Rodríguez 03] H. Rodríguez and R. Ortega. *Stabilization of electromechanical systems via interconnection and damping assignment.* International Journal of Robust and Nonlinear Control, vol. 13, pages 1095–1111, 2003. [p. 21]

[Rojas 02] O. J. Rojas and G. C. Goodwin. *A simple anti-windup strategy for state constrained linear control.* In Proc. of the 15th IFAC World Congress, volume 15, 2002. [pp. 36, 37, and 211]

[Roos 10] C. Roos. *A practical approach to worst-case H_∞ performance computation.* In Proc. of the IEEE International Symposium on Computer-aided Control System Design, pages 380–385, Yokohama, Japan, September 2010. [pp. 23, 24, and 225]

[Saunois 09] P. Saunois. *Comparative analysis of architectures for the control loop of launch vehicles during atmospheric flight.* Aerospace Science and Technology, vol. 13, pages 150–156, 2009. [p. 112]

[Scherer 90] C. Scherer. *The Riccati inequality and state-space H_∞-optimal control.* PhD thesis, University of Würzburg, 1990. [p. 141]

[Scorletti 10] G. Scorletti, V. Fromion, S. De Hillerin, M. Ganet and S. Bennani. *Critère H_∞ pour la commande de lanceurs flexibles.* In Proc. of the 6th Conférence Internationale Francophone d'Automatique, Nancy, France, June 2010. [pp. 8 and 112]

[Smith 95] H. L. Smith. Monotone dynamical systems: an introduction to the theory of competitive and cooperative systems, volume 41 of *Mathematical Surveys and Monographs.* American Mathematical Society, Providence, Rhode Island, 1995. [p. 180]

[Sontag 89] E. D. Sontag. *Remarks on stabilization and input-to-state stability.* In Proc. of the 28th IEEE Conference on Decision and Control, pages 1376 – 1378, Tampa, FL, 1989. IEEE. [p. 172]

[Spong 96] M. W. Spong. *Energy Based Control Of A Class Of Underactuated Mechanical Systems.* In Proc. of the IFAC World Congress, pages 431–435, 1996. [pp. 33 and 34]

[Stein 87] G. Stein and M. Athans. *The LQG-LTR procedure for multivariable feedback control design.* IEEE Transactions on Automatic Control, vol. 32, pages 105–114, 1987. [p. 21]

[Stilwell 97] D. J. Stilwell and W. J. Rugh. *Interpolation of Observer State Feedback Controllers for Gain Scheduling.* The Johns Hopkins University, Technical Report, August 1997. [p. 25]

[Tarbouriech 09] S. Tarbouriech and M. Turner. *Anti-windup design: an overview of some recent advances and open problems.* IET Control Theory and Applications, vol. 3, no. 1, pages 1–19, 2009. [pp. 37 and 74]

[Tarbouriech 11] S. Tarbouriech, G. Garcia, J. M. G. da Silva Jr. and I. Queinec. Stability and stabilization of linear systems with saturating actuators. Springer London, 2011. [p. 71]

[Tee 09] K. P. Tee, S. S. Ge and E. H. Tay. *Barrier Lyapunov Functions for the control of output-constrained nonlinear systems.* Automatica, vol. 45, no. 4, pages 918–927, 2009. [p. 38]

[Teo 09] J. Teo and J. P. How. *Anti-windup compensation for nonlinear systems via gradient projection: application to adaptive control.* In Proc. of the joint 48th IEEE Conference on Decision and Control and 28th Chinese Control Conference, pages 6910–6916, December 2009. [p. 37]

[Terrell 09] W. J. Terrell. Stability and stabilization: an introduction. Princeton University Press, 2009. [p. 172]

[Thabet 14a] R. E. H. Thabet. *Détection de défauts des systèmes non linéaires à incertitudes bornées continus.* PhD thesis, Université de Bordeaux, 2014. [p. 181]

[Thabet 14b] R. E. H. Thabet, T. Raïssi, C. Combastel and D. Efimov. *An effective method to interval observer design for time-varying systems.* Automatica, vol. 50, pages 2677–2684, 2014. [p. 181]

[Turner 02] M. C. Turner and I. Postlethwaite. *Output Violation Compensation for Systems With Output Constraints.* IEEE Transactions on Automatic Control, vol. 47, no. 9, pages 1540–1546, September 2002. [pp. 37 and 52]

[Utkin 92] V. I. Utkin. Sliding modes in control and optimization. Communications and Control Engineering. Springer-Verlag Berlin Heidelberg, 1st edition, 1992. [p. 21]

[Utkin 93] V. I. Utkin. *Sliding Mode Control Design Principles and Applications to Electric Drives.* IEEE Transactions on Industrial Electronics, vol. 40, no. 1, pages 23–36, 1993. [p. 21]

[Voinot 03a] O. Voinot, D. Alazard, P. Apkarian, S. Mauffrey and B. Clément. *Launcher attitude control: discrete-time robust design and gain-scheduling.* Control Engineering Practice, vol. 11, no. 11, pages 1243–1252, November 2003. [p. 25]

[Voinot 03b] O. Voinot, D. Alazard and B. Clément. *Unstationnary control of a launcher using observer-based structures.* In Proc. of the American Control Conference, pages 3466–3471, Denver, United States, June 2003. [pp. 8 and 112]

[Wächter 06] A. Wächter and L. T. Biegler. *On the Implementation of a Primal-Dual Interior Point Filter Line Search Algorithm for Large-Scale Nonlinear Programming.* Mathematical Programming, vol. 106, no. 1, pages 25–57, 2006. [p. 80]

[Wang 15] Y. Wang, D. M. Bevly and R. Rajamani. *Interval observer design for LPV systems with parametric uncertainty.* Automatica, vol. 60, pages 79–85, 2015. [p. 181]

[Youla 76a] D. C. Youla, J. J. Bongiorno Jr. and H. A. Jabr. *Modern Wiener–Hopf design of optimal controllers – Part I: The single-input-output case.* IEEE Transactions on Automatic Control, vol. 21, no. 1, pages 3–13, February 1976. [p. 28]

[Youla 76b] D. C. Youla, H. A. Jabr and J. J. Bongiorno Jr. *Modern Wiener-Hopf design of optimal controllers – Part II: The multivariable case.* IEEE Transactions on Automatic Control, vol. 21, no. 3, pages 319–338, June 1976. [p. 28]

[Zaccarian 01] L. Zaccarian and A. R. Teel. Modern anti-windup synthesis: control augmentation for actuator saturation. Princeton University Press, July 2001. [p. 37]

[Zames 81] G. Zames. *Feedback and optimal sensitivity: Model reference transformations, multiplicative seminorms, and approximate inverses.* IEEE Transactions on Automatic Control, vol. 26, no. 2, pages 301–320, 1981. [p. 21]

[Zasadzinski 07] M. Zasadzinski, H. Souley Ali and M. Darouach. *Robust reduced order H_∞ control via an unbiased observer.* International Journal on Science and Techniques of Automatic Control and Computer Engineering, vol. 1 (special issue), pages 261–275, 2007. [p. 22]

[Zhou 96] K. Zhou, J. Doyle and K. Glover. Robust and optimal control. Prentice-Hall, Inc., Upper Saddle River, NJ, USA, 1996. [p. 21]

Index

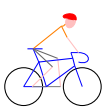

Frequency– and time–domain constrained control of linear systems – Application to a flexible launch vehicle

Abstract In modern control design problems, both frequency- and time-domain requirements are usually considered such that the resulting control law satisfies the specifications. Novel non-smooth optimisation techniques can be used to achieve multiple frequency-domain specifications over a family of linear models. Examples of applications include robust control design where multiple critical models for different values of the uncertain parameters are considered. This is illustrated in this thesis manuscript for a specific observer-based controller structure. However, enforcing time-domain constraints on a given output or state is more challenging since translating them into frequency-domain requirements may be unclear and inaccurate in real-world applications. This motivates the study of a new approach to the aforementioned H_∞ control design techniques. When time-domain constraints are satisfied, the nominal control law reduces to the structured controller synthesized against frequency-domain constraints. Upon violation of the time-domain constraint, an additional tool named *OIST* is used to appropriately saturate the controller output so as to restrict the reachable set of the constrained system output. Satisfying results as well as stability guarantees are obtained for minimum phase systems. Further developments proposed in this thesis allow the consideration of uncertain systems with incomplete state measurements. This is the novel *OISTeR* approach. The method requires the knowledge of certified bounds on the considered system state. Such information is accessible through using interval observers. The theory of interval observers is well-established. In the case of linear systems, the most common approach is to consider an intermediate cooperative system on which the interval observer can be built. For a given linear system, a cooperative representation can be obtained in new coordinates using a time-invariant state-coordinate transformation. The transformation determination methods are easy to use but lack versatility especially when performance guarantees on the interval tightness are required. This motivates the novel *SCorpIO* design method proposed in this work which relies on the reformulation of the original mathematical problem into a structured control-design problem. In this thesis, the considered application is the atmospheric control of a flexible launch vehicle in the presence of wind gusts. It is critical that the angle of attack of the vehicle should remain bounded to limit the aerodynamic load on the structure. Using the techniques developed in this thesis, solutions are proposed for a simplified launch vehicle model. Perspectives are drawn for future developments on more complex problems.

Keywords: output-constrained control, linear systems, uncertain systems, interval observer, structured controller design

Commande de systèmes linéaires sous contraintes fréquentielles et temporelles – Application au lanceur flexible

Résumé Dans la plupart des problèmes de synthèse actuels, la loi de commande obtenue doit répondre simultanément à des critères fréquentiels et temporels en vue de satisfaire un cahier des charges précis. Les derniers développements des techniques de synthèse H_∞ de contrôleurs structurés permettent d'obtenir des lois de commande satisfaisant des critères fréquentiels multiples appliqués à plusieurs modèles de synthèse. Dans ce mémoire, cette approche est appliquée à la synthèse de loi de commande robuste en utilisant une structure de contrôleur basé observateur. En revanche, la synthèse de loi de commande satisfaisant une contrainte temporelle sur une sortie ou un état du système considéré est plus complexe car la formulation d'un équivalent fréquentiel est illusoire dans la plupart des cas. Dans ce travail de thèse, la technique additionnelle *OIST* est considérée pour ce type de contraintes. Elle consiste à saturer la sortie du contrôleur dès que la contrainte n'est plus vérifiée afin de restreindre l'ensemble des sorties admissibles. Des résultats satisfaisants sont obtenus dans le cas des systèmes à minimum de phase. Initialement formulée pour les systèmes linéaires connus dont l'état est mesuré, la technique *OIST* peut être généralisée pour permettre de considérer des systèmes incertains dont seulement une partie de l'état est connue. C'est l'extension *OISTeR* qui est proposée dans ce travail. Elle utilise les données d'un observateur par intervalles pour borner de manière garantie le vecteur d'état. La théorie des observateurs par intervalles a récemment fait l'objet de nombreux travaux. La méthode la plus rapide pour obtenir un observateur par intervalles d'un système donné est de considérer un système intermédiaire coopératif dans de nouvelles coordonnées. Le passage dans ces nouvelles coordonnées s'effectue au moyen d'une matrice de transformation. Les méthodes de détermination actuelles de cette transformation sont faciles à mettre en œuvre mais sont assez peu polyvalentes notamment dans le cas où des contraintes de précision sont spécifiées sur l'observateur par intervalles. Une nouvelle technique de détermination de la transformation, intitulée *SCorpIO* est proposée dans ce mémoire. Elle repose sur la reformulation du problème mathématique sous-jacent en problème de synthèse de loi de commande structurée. L'ensemble des techniques présentées est appliqué au contrôle d'un lanceur flexible durant son vol atmosphérique, en présence de rafales de vent. La difficulté de ce problème repose sur le critère temporel spécifié sur l'angle d'incidence qui doit rester borné afin de minimiser la charge aérodynamique sur les structures. Dans ce mémoire, des solutions sont proposées et illustrées sur un modèle simplifié du lanceur. Des pistes pour la prise en compte de modèles plus complexes sont données.

Mots-clés: contrôle sous contraintes de sortie, systèmes linéaires, systèmes incertains, observateur par intervalles, synthèse de contrôleur structuré